

SYNTHESIS AND CHARACTERIZATION OF POLYAROMATIC HYDROCARBON-BASED FUNCTIONAL MATERIALS

A THESIS

*Submitted in partial fulfilment of the
requirements for the award of the degree*

of

DOCTOR OF PHILOSOPHY

in

CHEMISTRY

by

NEHA KAPOOR



DEPARTMENT OF CHEMISTRY
INDIAN INSTITUTE OF TECHNOLOGY ROORKEE
ROORKEE-247 667 (INDIA)

JULY, 2011

**©INDIAN INSTITUTE OF TECHNOLOGY ROORKEE, ROORKEE-2011
ALL RIGHTS RESERVED**



INDIAN INSTITUTE OF TECHNOLOGY ROORKEE ROORKEE

CANDIDATE'S DECLARATION

I hereby certify that the work which is being presented in the thesis entitled “**SYNTHESIS AND CHARACTERIZATION OF POLYAROMATIC HYDROCARBON-BASED FUNCTIONAL MATERIALS**” in partial fulfilment of the requirements for the award of the degree of **Doctor of Philosophy** and submitted in the **Department of Chemistry, Indian Institute of Technology Roorkee, Roorkee** is an authentic record of my own work carried out during a period from **July, 2007 to July, 2011** under the supervision of **Dr. K. R. Justin Thomas, Assistant Professor, Department of Chemistry, Indian Institute of Technology Roorkee, Roorkee.**

The matter presented in the thesis has not been submitted by me for the award of any other degree of this or any other Institute.

Neha Kapoor
(NEHA KAPOOR)

This is to certify that the above statement made by the candidate is correct to the best of my knowledge.

K. R. Justin Thomas
(K. R. JUSTIN THOMAS)
Supervisor

Date: 22/07/2011

The Ph.D. Viva-Voice Examination of **Ms. NEHA KAPOOR**, Research Scholar, has been held on 19/10/2011

K. R. Justin Thomas
19/10/11
Signature of Supervisor

Justin Thomas
19/10/2011
Signature of External Examiner

Acknowledgement

With great pleasure, I take this opportunity to thank GOD & then all the people who have helped me in one way or the other through the course of my journey towards producing this thesis. First and foremost, I must thank my supervisor, **Dr. K. R. Justin Thomas**, who not only helped me at each and every step of my research as a mentor but also, taught me how to be a good human being apart from being a good chemist. His constructive criticism, excellent guidance and encouragement made me able to bring the present work to conclusion. He is and always will be a huge source of inspiration to me and I sincerely thank him for that.

My sincere thanks to Professor Jiann T. Lin, Institute of Chemistry, Academia Sinica, Taipei, Taiwan and Professor Jwo-Huei Jou, Department of Material Science and Engineering, National Tsing Hua University, Hsinchu, Taiwan for their kind collaboration in OLED device fabrication and characterization.

I am also thankful to Professor K.-C. Ho at the Department of Chemical Engineering, National Taiwan University, Taipei, Taiwan for his insightful contributions to the DSSC fabrication and characterization.

I am grateful to the Head of the Chemistry Department, Indian Institute of Technology, Roorkee, for extending the departmental instruments such as absorption and emission spectrophotometers to carry out my research work.

I am also thankful to the mass spectral facility at the Department of Organic Chemistry, Indian Institute of Science, Bangalore for their timely assistance in recording high resolution mass spectra for several compounds.

I would also like to thank Prof. Ritu Bharthwal, Coordinator, NMR facility at IIC of the Institute for her support.

Also I would like to thank my lab mates Prachi, Payal, Sushil, Dharendra, Prasad, Abhishek, Venkateswararao & other departmental colleagues (Pramod, Sushil, Varun and Rajan) who always inspired me with their dedication toward work, improvised me with their thoughtful criticism and encouraged me in my bad times. I am especially thankful to Sushil and Prasad who helped me a lot in the last one year and made me feel comfortable in the lab.

Also I would like to thank my pals Payal Tyagi and Aarti Agarwal for their love and

support even from long distance. I am thankful to Payal for her support in broaching my career in this field.

I would like to thank Preeti and Karnisha for being there whenever I needed them. Without their emotional support, it would have been a very difficult task and I find myself lucky to have these two pretty girls in my life.

I would also like to thank my friends Jyoti, Rashmi, Manu, Geetu, Nisha and Manali for providing support and friendship that I needed.

Wholeheartedly I would like to thank all the members of Chemistry Department who worked with me with great devotion and showed compassion and empathy like a family.

I would like to record the financial assistance from CSIR and DST in the form of project support to my supervisor and University Grants Commission (UGC), New Delhi for research fellowship (JRF and SRF).

I would like to thank my family especially my mom, for their love and support and more importantly, for believing in me. It was a tough decision of leaving my home against all odds and fighting for my own identity in the field of chemistry and that was the time when my mom supported me and gave me the strength to take this first step to achieve my dream.

Now I would like to thank the most wonderful person in my life, my fiancé, Dr. Vikas Singhal. Without his unconditional love, support and encouragement, it would have been impossible for me to handle the critical situations that came during the thesis writing. I am highly thankful to him for being in my life as my best friend and teaching me how to accept the things and tackle difficulties with a smile.

Finally, I would like to thank all my seniors, colleagues, friends, family and well-wishers who directly or indirectly helped me during this entire journey.

NEHA KAPOOR

Abstract

Polycyclic aromatic hydrocarbons (PAHs) such as anthracene, fluorene, pyrene, perylene, triphenylene, fluoranthene, benzo[*k*]fluoranthene, pentacene, and their derivatives have received immense attention as building blocks for materials suitable for application in optoelectronics due to their unique properties. They exhibit high thermal stability, good charge transporting characteristics and excellent emission properties owing to the structural rigidity and extended π -conjugation. Polymers, dendrimers, oligomers and monomers of PAHs have been reported as functional materials for organic light emitting diodes (OLEDs), photovoltaics including dye sensitized solar cells (DSSC) and thin-film transistors and as nonlinear optical materials (NLO) and optical sensors. PAHs when used as a π -linker in the construction of organic dyes suitable for dye-sensitized solar cells, they effectively assist the charge migration from the donor segment to the acceptor unit. PAHs may also be used as a building block in the triarylamine donor unit which generally helps to modulate the oxidation and dye regeneration propensities. Despite all these advantages, planar PAHs suffer from molecular aggregation which leads to unexpected emission and charge transport characteristics. However, this problem has been often circumvented by introduction bulkier nonplanar groups such as triarylamines or *tert*-butyl groups. Introduction of arylamines on PAHs backbone not only enhances the absorption and emission profiles but also increases the thermal stability, charge transporting ability and amorphous nature.

In this thesis, we have explored the utility of PAHs such as fluoranthene, triphenylene and pyrene in the construction of organic dyes suitable for application in organic light-emitting diodes and dye-sensitized solar cells. We have used these cores as carriers for the functional groups such as arylamines and cyanoacrylic acid segment and studied the effect of the functional group introduction on the optical, electrochemical and thermal properties. The materials can be classified as emitting materials and dyes suitable for DSSC. We have also explored the application of selected compounds in OLED and DSSC.

The thesis contains six chapters. In the first chapter, a review of the literature related to the work of the thesis has been presented. An up-to-date survey of the organic materials developed using PAHs as building block, have been performed. The optical, electrochemical and thermal properties of the known compound were compiled in the form of tables and an attempt to correlate the structure with the properties made. Generally, the PAHs due to their rigidity show enhanced thermal stability and the extended conjugation present in PAHs helps to realize a red-shifted emission. From the literature present in this chapter, it is abundantly

evident that PAHs have not been exploited for applications in electro-optical devices to the fuller extent mainly due to the lack of facile synthetic methodologies and their aggregation characteristics. Though π - π interactions present in aggregated species are beneficial for charge transport, aggregation is detrimental for emission properties. Thus, the molecular materials presented in this thesis were designed with an aim to inhibit the aggregation while exhibiting extended conjugation.

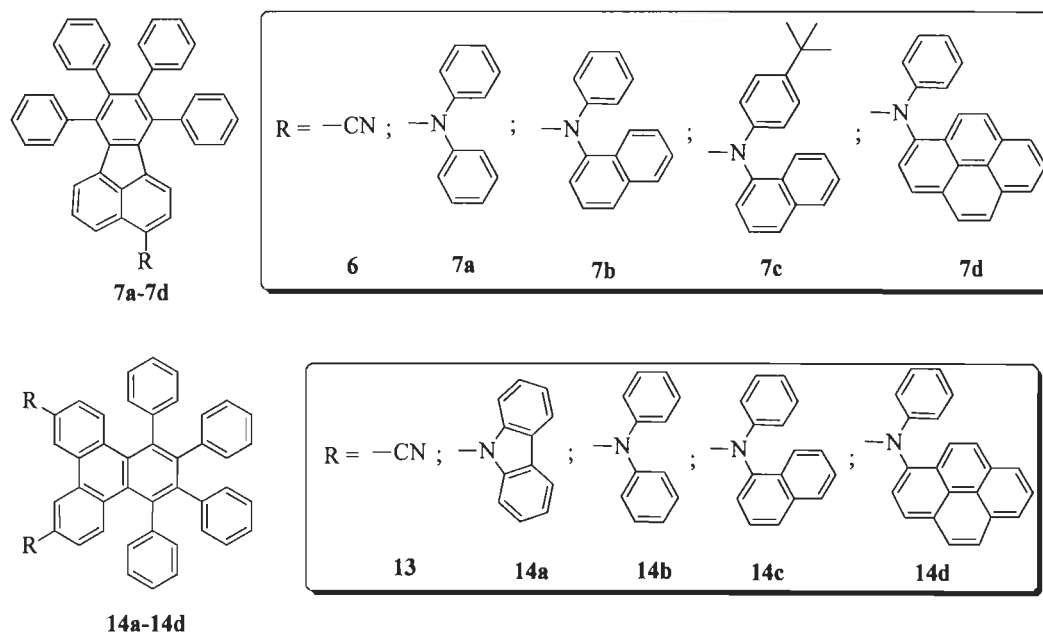


CHART 1. Structures of polyphenylated fluoranthene- (**6**, **7a-7d**) and triphenylene- (**13**, **14a-14d**) based derivatives.

Second chapter describes the synthesis, photophysical, electrochemical and electroluminescent properties of polyphenylated fluoranthene- and triphenylene-based functional materials (CHART 1). The incorporation of diarylamine on the PAH core increases the thermal stability and also red shifts the absorption as well as emission profile. Moreover, the incorporation of diarylamine has been found to suppress the chances of molecular aggregation. Triphenylene derivatives (**14a-14d**) have been found to aggregate in higher concentrations in solutions as well as in solid state while the fluoranthene derivatives resist intermolecular interactions. Due to this fluoranthene derivatives could be used as hole-transporting/emitting molecular layers in OLED devices, on the contrary the triphenylene derivatives gave better results only when they were employed as dopants in suitable host. OLED device fabricated using the pyrenylamine containing derivative, **7d**, displayed promising external quantum efficiency, 1.86% and maximum brightness 36750 cd/m^2 with TPBI as an electron transporting layer. CIE coordinates of the electroluminescence spectra observed for the devices indicate that **7c-7d** based device are yellow emitting while **14a-14d**

based devices are blue emitting. Solvent dependent optical properties of the dyes were also studied and interpreted using Lippert-Mataga, $E_T(30)$ and Kamlett-Taft plots. Theoretical calculations using DFT were performed to rationalize the trends observed in optical and electrochemical properties.

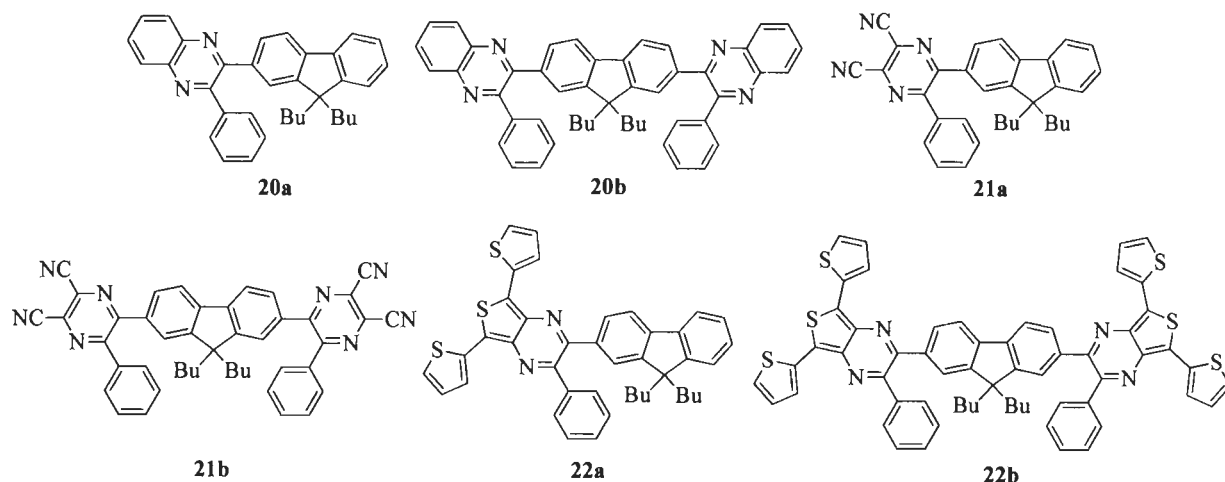


CHART 2. Structures of fluorene-based quinoxaline and pyrazine derivatives.

In the third chapter, synthesis and characterization of fluorene containing quinoxaline, pyrazine and thienopyrazine derivatives have been presented (CHART 2). The optical, thermal and electrochemical properties have been presented with an attempt to correlate the structure-property relationship. Among the compounds, the thienopyrazine derivatives showed the red-shifted absorption due to the built-in dipolar structure. Dicyanopyrazine derivatives, **21a** and **21b** exhibited red shifted absorption/emission profiles when compared to the quinoxalines **20a** and **20b**. Compounds **22a** and **22b** containing thiophene end groups underwent electrochemical polymerization.

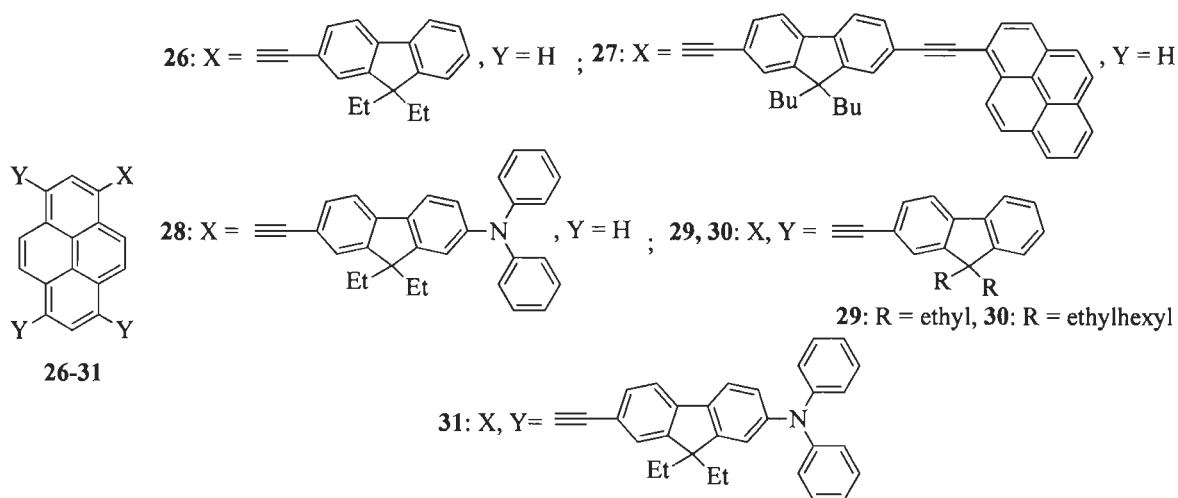


CHART 3. Structures of pyrene-fluorene conjugates with ethynyl linkers.

The fourth chapter presents the organic materials based on pyrene as constituents for organic light-emitting diodes and dye-sensitized solar cells. A series of blue- and yellow-emitting materials have been developed by integrating fluorene and pyrene segments *via* an ethynyl linkage (CHART 3). Both mono-substituted and tetra-substituted derivatives have been synthesized and characterized. The tetra-substituted derivatives displayed red-shifted emission when compared to the mono-substituted derivative indicative of an extended conjugation in the tetra-substituted derivatives. Diphenylamine was incorporated to avoid molecular aggregation. Additionally, the presence of diarylamine end groups exhibited an auxochromic effect on the optical properties. Incorporation of diphenylamine increases the absorption/emission wavelength and thermal stability and lowers the oxidation potential. No significant changes in the optical properties were noticed for the compounds **26**, **27** and **30** due to the variation of solvent polarity; however, the diphenylamine derivatives **28** and **31** displayed solvatochromism in the fluorescence spectra. This indicates that in the excited state the molecules **28** and **31** are more polar due to an efficient charge migration from the diphenylamine donor to the pyrene π -acceptor. The polar excited state may be efficiently solvated by the polar solvents, and this solvent stabilized state may produce a red-shifted emission. These derivatives were employed as emitting dopants in OLED and found to exhibit bright blue or yellow electroluminescence.

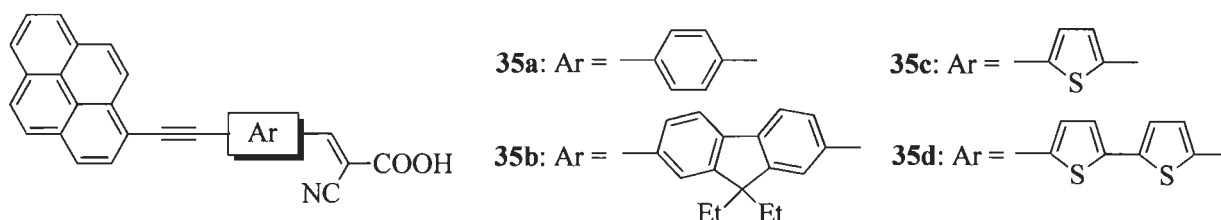


CHART 4. Structures of pyrene ethynyl based organic dyes.

In the fourth chapter, the synthesis and characterization of pyrene-cyanoacrylic conjugates (CHART 4) is also described. The architecture of dyes can be treated approximately as possessing pyrene as a weak π -donor, cyanoacrylic acid as an acceptor and four different spacers in the form of phenyl, fluorene, thiophene or bithiophene. The influence of different spacer on optical and electrochemical properties has been investigated. The rod shaped structure of the dye is useful for the grafting over semiconductor surface and for increasing the charge injection on the TiO_2 surface. Electrochemical studied revealed a favorable HOMO levels which are more positive than the iodide/triiodide redox couple (~ 0.42 V *vs* NHE) and suggest facile dye regeneration by the electrolyte. The excited state oxidation potentials, E_{ox}^* , observed for the dyes (-0.87 to -1.06 V versus NHE) are more

negative than the conduction band edge energy level of the TiO₂ electrode and favor the electron injection into the conduction band of TiO₂ thermodynamically.

In the fifth chapter, we present an alternative strategy for the design of organic dyes using pyrenylamine as a donor segment. A series of dyes derived from diamines with various π -linkers, *N*-phenyl-1-pyrenylamine donors and cyanoacrylic acid acceptors have been synthesized and characterized (CHART 5). The effect of additional donor segment on the optical and electrochemical properties was investigated. Besides the charge transfer transition from the amine to cyanoacrylic acid unit the compounds also exhibited a weak charge transfer transition from the amine to pyrene unit. Introduction of additional donor moiety has been found to be helpful in enhancing the light-harvesting capability and the oxidation propensity of the dyes. Acid-base equilibria of the dyes were also investigated by absorption spectroscopy. The incorporation of another donor system increases the donor strength which makes the proton of carboxylic group less acidic. Due to this there was less chance of deprotonation observed for the dyes with two donor systems. Theoretical investigation revealed that by increasing the spacer length between two amine segments the propensity of charge separation increased as evidenced from the well separated electronic distributions in HOMO and LUMO. The DSSC fabricated using the dyes **43b** and **43c** showed higher overall light-to-electricity conversion efficiencies, η , 4.28% ($J_{sc} = 10.2 \text{ mA cm}^{-2}$, $V_{oc} = 0.595 \text{ V}$, $ff = 0.71$) and 3.89% ($J_{sc} = 9.51 \text{ mA cm}^{-2}$, $V_{oc} = 0.583 \text{ V}$, $ff = 0.70$) respectively.

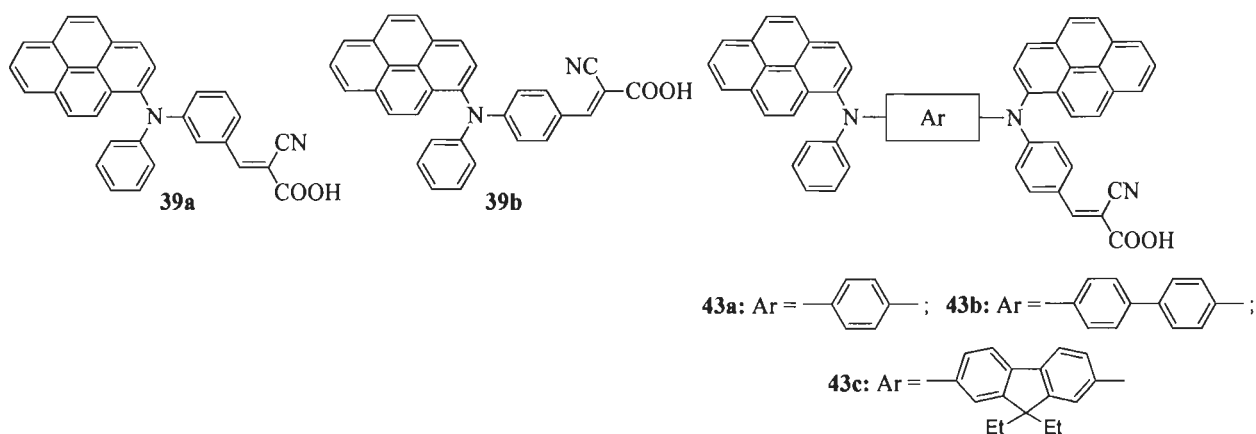


CHART 5. Structure of the *N*-phenyl-1-pyrenylamine-based dyes (**39a-39b** and **43a-43c**).

Summary and future prospects of the work are presented in the final chapter (Chapter 6). PAHs were found as important π -framework for electronic devices. Introduction of diarylamines into the backbone of PAH enhanced their photophysical and electrochemical properties. Suitably designed pyrene-based derivatives have been investigated as promising materials for both OLED and DSSC applications. The success of fluoranthene-based

CONTENTS

	Page No.
<i>Candidate's Declaration</i>	
<i>Acknowledgement</i>	
<i>Abstract</i>	i
<i>List of Schemes</i>	vii
<i>List of Figures</i>	ix
<i>List of Tables</i>	xvii
Chapter 1	1-76
Polyaromatic Hydrocarbon-based Functional Materials for Electroluminescent Application	
1.1	1
1.2	3
1.3	6
1.4	8
1.4.1	8
1.4.2	8
1.4.3	9
1.4.4	9
1.4.5	9
1.4.6	10
1.5	11
1.5.1	11
1.5.2	23
1.5.3	39
1.5.4	44
1.6	60
1.7	62
Chapter 2	77-163
Fluoranthene/Triphenylene-Based Hole Transporting Materials: Synthesis, Optical, Electrochemical and OLED Properties	
2.1	77
2.2	85
2.2.1	85
2.2.2	87
2.2.3	120

2.2.4	Quenching studies	126
2.2.5	Thermal properties	130
2.2.6	Electrochemical properties	133
2.2.7	Electroluminescent characteristics	136
2.2.7.1	OLED performance of fluoranthene derivatives (7a-7d)	136
2.2.7.2	Electroluminescent properties of triphenylene derivatives (14a-14d)	140
2.3	Conclusions	143
2.4	Experimental section	144
2.4.1	Materials	144
2.4.2	Physical methods	144
2.4.3	OLED fabrication and performance evaluation	146
2.4.4	Computational details	146
2.5	References	154
Chapter 3	Synthesis and Characterization of Blue-Emitting Fluorene-Based Pyrazine Derivatives	165-211
3.1	Introduction	165
3.2	Results and discussion	170
3.2.1	Synthesis	170
3.2.2	Optical properties	172
3.2.3	Theoretical investigations	188
3.2.4	Thermal properties	190
3.2.5	Electrochemical properties	192
3.3	Conclusions	198
3.4	Experimental section	198
3.4.1	Materials	198
3.4.2	Physical methods	199
3.5.	References	205
Chapter 4	Synthesis, Photophysical and Electrochemical Properties of Pyrene-Based Functional Materials Containing Acetylene Linkers	213-285
4.1	Introduction	213
4.2	Results and discussion	222
4.2.1	Synthesis	223
4.2.2	Optical properties	225
4.2.3	Thermal properties	259
4.2.4	Electrochemical properties	261
4.2.5	Electroluminescent properties	264
4.3	Conclusions	270

4.4	Experimental section	271
4.4.1	Materials	271
4.4.2	Physical methods	271
4.5	References	278
Chapter 5	Synthesis and Characterization of Pyrenylamine Based- Organic Dyes as Sensitizers for Dye Sensitized Solar Cells	287-346
5.1	Introduction	287
5.2	Results and discussion	295
5.2.1	Synthesis	295
5.2.2	Optical properties	298
5.2.3	Electrochemical properties	315
5.2.4	Theoretical investigations	319
5.2.5	Photovoltaic performance of the dyes	325
5.3	Conclusion	330
5.4	Experimental section	331
5.4.1	Materials	331
5.4.2	Physical methods	331
5.4.3	DSSC fabrication and characterizations	331
5.5	References	340
Chapter 6	Summary and Outlook	347-351

Supporting Information

Publications

List of Schemes

	Page No.
Scheme 1.1	Synthesis of PAH <i>via</i> Diels-Alder reaction. 8
Scheme 1.2	Synthesis of dibenz[<i>a,j</i>]anthracene. 8
Scheme 1.3	Synthesis of dibenzo[<i>a,h</i>]anthracene. 9
Scheme 1.4	Synthesis of corannulene. 9
Scheme 1.5	Synthesis of hexabenzocoronenes. 9
Scheme 1.6	Example of oxidative cyclodehydrogenation leading to large PAH. 10
Scheme 1.7	Synthetic route to fluoranthene from ethyl 9-fluorene-9-carboxylate. 23
Scheme 1.8	Synthesis of fluoranthene from diiodonaphthalene <i>via</i> Sonogashira reaction. 24
Scheme 1.9	Synthesis of fluoranthene <i>via</i> 1,4-Pd migration/arylation process. 24
Scheme 1.10	Synthesis of fluoranthene <i>via</i> a new Suzuki-Heck type coupling cascade. 24
Scheme 1.11	Construction of fluoranthene core using Wilkinson's complex. 25
Scheme 1.12	Synthesis of substituted fluoranthenes. 25
Scheme 1.13	Synthesis of fluoranthene <i>via</i> Diels-Alder reaction. 26
Scheme 2.1	Synthesis of fluoranthene-based triarylamine derivatives (7a-7d). 85
Scheme 2.2	Synthesis of triphenylene-based triarylamine derivatives (14a-14d). 86
Scheme 3.1	Synthesis of quinoxaline (20a, 20b), pyrazine (21a, 21b) and thienopyrazine (22a, 22b) derivatives. 171
Scheme 4.1	Synthetic route of the compounds 26-31 . 224
Scheme 4.2	Synthesis of pyreneethynyl-based cyanoacrylic acid derivatives. 225
Scheme 5.1	Synthetic route of the dyes 39a & 39b . 296
Scheme 5.2	Synthesis of the pyrenylamine-based organic dyes 43a, 43b & 43c containing aromatic linkers. 297

List of Figures

	Page No.
Figure 1.1	Operating mechanism of a multilayer OLED device. 4
Figure 1.2	Working principle of DSSC. 6
Figure 1.3	Fluorene-based multifunctional materials. 12
Figure 1.4	Structures of fluoranthene-based polymers. 27
Figure 1.5	Sulfur-hetero benzo[<i>k</i>]fluoranthene derivatives: organic semiconducting materials for thin film transistors. 28
Figure 1.6	Fluoranthene-based organic dyes suitable for DSSC. 38
Figure 1.7	Structures of hexaalkoxy functionalized triphenylenes used as OLED materials. 40
Figure 1.8	Structures of triphenylene-based polymers. 41
Figure 1.9	Structures of phenylethynyltriphenylenes (A70-A76) and star shaped oligothiophene-substituted triphenylenes (A77-A81). 42
Figure 1.10	Structures of pyrene-based liquid crystalline compounds showing columnar phase. 45
Figure 1.11	Structures of pyrene-based two photon absorbing materials. 46
Figure 1.12	Examples of pyrene derivatives demonstrated to function as efficient materials in OFET. 47
Figure 1.13	Structures of multifunctional pyrene derivatives. 58
Figure 1.14	Structures of pyrenoimidazole-based organic dyes used in DSSC as sensitizer. 60
Figure 2.1	Structures of hole transporting materials. 79
Figure 2.2	Fluoranthene or benzo[<i>k</i>]fluoranthene-based star shaped molecules as emitting or hole-transporting materials. 82
Figure 2.3	Triphenylene-based small molecules. 83
Figure 2.4	Absorption spectra of the compounds 4-7 recorded in toluene. 88
Figure 2.5	Absorption spectra of the compounds 4-7 recorded in dichloromethane. 88
Figure 2.6	Absorption (unfilled) and emission (filled) spectra of triphenylamine (TPA) and pyrene diphenyl amine (PyDPA) recorded in dichloromethane solution. 89
Figure 2.7	Absorption spectra of the compounds 12-14 recorded in toluene. 92
Figure 2.8	Absorption spectra of the compounds 12-14 recorded in dichloromethane. 92
Figure 2.9	Emission spectra of the compounds 4-7 recorded (a) in toluene, (b) 94

	in dichloromethane, (c) emission spectra of 7c and 7d in toluene, dcm and thin solid film.	
Figure 2.10	Emission spectra of the compounds 12-14 recorded in different medium (toluene, dichloromethane and thin solid film).	96
Figure 2.11	Emission spectra of (a) 14a , (b) 14b , (c) 14c and (d) 14d recorded in toluene at different concentration.	98
Figure 2.12	Absorption and emission spectra of 7a (a), (b) & 7b (c), (d) recorded in different solvents.	101
Figure 2.13	Absorption and emission spectra of 7c (a), (b) & 7d (c), (d) recorded in different solvents.	102
Figure 2.14	Absorption and emission spectra of 14a (a), (b) & 14b (c), (d) recorded in different solvents.	104
Figure 2.15	Absorption and emission spectra of 14c (a), (b) & 14d (c), (d) recorded in different solvents.	105
Figure 2.16	Plots for 7a in different solvents (a) Lippert-Mataga plot showing Stokes' shift vs orientation polarizability of the solvents, (b) Stokes' shift vs $E_T(30)$ parameter, (c) emission maxima (in cm^{-1}) vs Kamlet-Taft solvent polarity parameter.	111
Figure 2.17	Plots for 7b in different solvents (a) Lippert-Mataga plot showing Stokes' shift vs orientation polarizability of the solvents, (b) Stokes' shift vs $E_T(30)$ parameter, (c) emission maxima (in cm^{-1}) vs Kamlet-Taft solvent polarity parameter.	112
Figure 2.18	Plots for 7c in different solvents (a) Lippert-Mataga plot showing Stokes' shift vs orientation polarizability of the solvents, (b) Stokes' shift vs $E_T(30)$ parameter, (c) emission maxima (in cm^{-1}) vs Kamlet-Taft solvent polarity parameter.	113
Figure 2.19	Plots for 7d in different solvents (a) Lippert-Mataga plot showing Stokes' shift vs orientation polarizability of the solvents, (b) Stokes' shift vs $E_T(30)$ parameter, (c) emission maxima (in cm^{-1}) vs Kamlet-Taft solvent polarity parameter.	114
Figure 2.20	Plots for 14a in different solvents (a) Lippert-Mataga plot showing Stokes' shift vs orientation polarizability of the solvents, (b) Stokes' shift vs $E_T(30)$ parameter, (c) emission maxima (in cm^{-1}) vs Kamlet-Taft solvent polarity parameter.	115
Figure 2.21	Plots for 14b in different solvents (a) Lippert-Mataga plot showing Stokes' shift vs orientation polarizability of the solvents, (b) Stokes' shift vs $E_T(30)$ parameter, (c) emission maxima (in cm^{-1}) vs Kamlet-Taft solvent polarity parameter.	116
Figure 2.22	Plots for 14c in different solvents (a) Lippert-Mataga plot showing Stokes' shift vs orientation polarizability of the solvents, (b) Stokes'	117

	shift vs $E_T(30)$ parameter, (c) emission maxima (in cm^{-1}) vs Kamlet-Taft solvent polarity parameter.	
Figure 2.23	Plots for 14d in different solvents (a) Lippert-Mataga plot showing Stokes' shift vs orientation polarizability of the solvents, (b) Stokes' shift vs $E_T(30)$ parameter, (c) emission maxima (in cm^{-1}) vs Kamlet-Taft solvent polarity parameter.	118
Figure 2.24	Electronic distribution in the frontier molecular orbitals of the compounds 5a , 6 and 7a .	121
Figure 2.25	Electronic distribution in the frontier molecular orbitals of the compounds 12 , 13 and 14a-14d .	123
Figure 2.26	Emission and Stern-Volmer plots for 5a at different concentration of different quencher (a), (c) diphenylamine and (b), (d) triphenylamine.	128
Figure 2.27	Emission and Stern-Volmer plots for 5a at different concentration of different quencher (a), (c) ferrocene and (b), (d) dimethylaniline.	129
Figure 2.28	TGA curves of (a) fluoranthene derivatives (4-7) and (b) triphenylene derivatives (12-14).	131
Figure 2.29	DSC curves of (a) 7a and (b) 14b showing three heating cycles.	131
Figure 2.30	Cyclic voltammograms recorded (a) for the amine functionalized derivatives (7a-7d) & (b) for (14b-14d) in dichloromethane solutions (concentration: 2.0×10^{-4} M; scan rate: 100 mV/sec; supporting electrolyte: TBA PF ₆)	134
Figure 2.31	I-V-L characteristics of the devices using 7c & 7d as emitting as well as hole transporting layer with (a) TPBI or (b) Alq ₃ as electron transporting layer.	137
Figure 2.32	Energy level diagrams of the four devices fabricated using the dyes 7c and 7d with TPBI and Alq ₃ .	139
Figure 2.33	Comparison of EL spectra observed for the devices with 7c and 7d with the PL spectra recorded for the thin films.	139
Figure 2.34	I-V-L characteristic and power efficiency vs current density curves of devices using 14a-14d as a dopant without (a), (b) and with host material CBP (c), (d).	141
Figure 2.35	EL spectra of the devices using 14a , 14b (a) and using 14c , 14d (b).	142
Figure 3.1	Structures of fluorene-based donor-acceptor systems.	167
Figure 3.2	Structures of quinoxaline-based functional materials.	169
Figure 3.3	Structures of pyrazine derivatives containing fluorene segment.	170
Figure 3.4	Absorption spectra of quinoxalines (20a , 20b) and pyrazines (21a , 21b) recorded (a) in toluene and (b) in dichloromethane solutions.	173
Figure 3.5	Absorption spectra of thienopyrazines (22a , 22b) recorded (a) in	173

	toluene and (b) in dichloromethane.	
Figure 3.6	Emission spectra of quinoxalines (20a , 20b), pyrazines (21a , 21b) and thenopyrazines (22a , 22b) recorded in toluene.	175
Figure 3.7	Emission spectra of the compounds (a) 20a , (b) 21a , (c) 20b and (d) 21b recorded in different medium (toluene, dichloromethane and thin solid film).	176
Figure 3.8	Emission spectra for 20b recorded in cyclohexane (a) and in toluene (b) at different concentration.	177
Figure 3.9	Emission spectra for 21b recorded in toluene at different concentration.	177
Figure 3.10	Emission spectra of 22a and 22b in toluene and dichloromethane.	178
Figure 3.11	Dipolar interactions in 22a and 22b .	179
Figure 3.12	Absorption and emission spectra of 20a (a), (b) and 20b (c), (d) recorded in different solvents.	180
Figure 3.13	Absorption and emission spectra of 21a (a), (b) and 21b (c), (d) recorded in different solvents.	181
Figure 3.14	Plots for 20a in different solvents (a) Lippert-Mataga plot showing Stokes' shift vs orientation polarizability of the solvents, (b) Stokes' shift vs $E_T(30)$ parameter, (c) emission maxima (in cm^{-1}) vs Kamlet-Taft solvent polarity parameter.	184
Figure 3.15	Plots for 20b in different solvents (a) Lippert-Mataga plot showing Stokes' shift vs orientation polarizability of the solvents, (b) Stokes' shift vs $E_T(30)$ parameter, (c) emission maxima (in cm^{-1}) vs Kamlet-Taft solvent polarity parameter.	185
Figure 3.16	Plots for 21a in different solvents (a) Lippert-Mataga plot showing Stokes' shift vs orientation polarizability of the solvents, (b) Stokes' shift vs $E_T(30)$ parameter, (c) emission maxima (in cm^{-1}) vs Kamlet-Taft solvent polarity parameter.	186
Figure 3.17	Plots for 21b in different solvents (a) Lippert-Mataga plot showing Stokes' shift vs orientation polarizability of the solvents, (b) Stokes' shift vs $E_T(30)$ parameter, (c) emission maxima (in cm^{-1}) vs Kamlet-Taft solvent polarity parameter.	187
Figure 3.18	Electronic distribution in frontier molecular orbitals of the compounds 20a , 21a and 22a .	188
Figure 3.19	DSC curves for 20a (a), 21a (b), 20b (c) and 21b (d).	191
Figure 3.20	Cyclic voltamogram recorded for 20a , 21a , 20b and 21b in dichloromethane.	193
Figure 3.21	Differential pulse voltamograms recorded for 22a and 22b in dichloromethane.	193
Figure 3.22	Cyclic voltammograms obtained during potentiodynamic	195

	polymerization of 22a in 0.2M TBAPF ₆ /DCM at different scan rates 20 (a), 100 (b) and 500 mV/s (c) (glassy carbon working electrode, 10 consecutive scans).	
Figure 3.23	Cyclic voltammograms obtained during potentiodynamic polymerization of 22b in 0.2M TBAPF ₆ /DCM at different scan rates 20 (a), 100 (b) and 500 mV/s (c) (glassy carbon working electrode, 10 consecutive scans).	196
Figure 3.24	Proposed structures of the polymers formed during electropolymerization.	197
Figure 4.1	Structures of the basic units used in the construction of functional materials.	214
Figure 4.2	Cruciform pyrene derivatives containing ethynyl linkers.	216
Figure 4.3	Structures of the fluorene- and spirofluorene-containing pyrene derivatives.	217
Figure 4.4	Oligo(2,7-fluorene ethynylene)s and (3,6-carbazole ethynylene)s with pyrene moieties as blue emitters in OLEDs.	218
Figure 4.5	Structure of pyrene-based compounds (D15-D19).	219
Figure 4.6	Structures of pyrene end-capped rigid rod like compounds.	221
Figure 4.7	Structures of pyreneethynyl derivatives (26-31).	222
Figure 4.8	Structures of pyreneethynyl-based dyes (35a-35d).	225
Figure 4.9	Absorption spectra of the compounds 26-31 recorded in toluene.	226
Figure 4.10	Absorption spectra of the compounds 26-31 recorded in dichloromethane solutions.	226
Figure 4.11	Emission spectra of the compounds 26-31 recorded (a) in toluene, (b) in dichloromethane, (c) thin solid film.	231
Figure 4.12	Absorption and emission spectra of the compounds 26 (a), (b) and 27 (c), (d) recorded in different solvents.	234
Figure 4.13	Absorption and emission spectra of the compounds 28 (a), (b) and 30 (c), (d) recorded in different solvents.	235
Figure 4.14	Absorption (a) and emission (at 350 nm excitation wavelength) (b) spectra of 31 recorded in different solvents.	237
Figure 4.15	Emission spectra of 31 at 450 nm excitation wavelength in different solvents (a) and in DMF at different excitation (b).	237
Figure 4.16	Plots for 27 in different solvents (a) Lippert-Mataga plot showing Stokes' shift vs orientation polarizability of the solvents, (b) Stokes' shift vs E _T (30) parameter, (c) emission maxima (in cm ⁻¹) vs Kamlet-Taft solvent polarity parameter.	241
Figure 4.17	Plots for 27 in different solvents (a) Lippert-Mataga plot showing Stokes' shift vs orientation polarizability of the solvents, (b) Stokes'	242

	shift vs $E_T(30)$ parameter, (c) emission maxima (in cm^{-1}) vs Kamlet-Taft solvent polarity parameter.	
Figure 4.18	Plots for 28 in different solvents (a) Lippert-Mataga plot showing Stokes' shift vs orientation polarizability of the solvents, (b) Stokes' shift vs $E_T(30)$ parameter, (c) emission maxima (in cm^{-1}) vs Kamlet-Taft solvent polarity parameter.	243
Figure 4.19	Plots for 30 in different solvents (a) Lippert-Mataga plot showing Stokes' shift vs orientation polarizability of the solvents, (b) Stokes' shift vs $E_T(30)$ parameter, (c) emission maxima (in cm^{-1}) vs Kamlet-Taft solvent polarity parameter.	244
Figure 4.20	Plots for 31 in different solvents (a) Lippert-Mataga plot showing Stokes' shift vs orientation polarizability of the solvents, (b) Stokes' shift vs $E_T(30)$ parameter, (c) emission maxima (in cm^{-1}) vs Kamlet-Taft solvent polarity parameter.	245
Figure 4.21	Absorption spectra of the dyes 35a-35d recorded in THF.	247
Figure 4.22	Comparison of absorption (filled) and emission (line) spectra of (a) 35a , (b) 35b , (c) 35c , (d) 35d with their corresponding aldehydes (34a-35d) recorded in THF.	248
Figure 4.23	Emission spectra of the dyes 35a-35d recorded in THF.	251
Figure 4.24	Absorption and emission spectra of 35a (a), (b) and 35b (c), (d) recorded in different solvents.	252
Figure 4.25	Absorption and emission spectra of 35c (a), (b) and 35d (c), (d) recorded in different solvents.	253
Figure 4.26	Plots for 35a in different solvents (a) Lippert-Mataga plot showing Stokes' shift vs orientation polarizability of the solvents, (b) Stokes' shift vs $E_T(30)$ parameter, (c) emission maxima (in cm^{-1}) vs Kamlet-Taft solvent polarity parameter.	255
Figure 4.27	Plots for 35b in different solvents (a) Lippert-Mataga plot showing Stokes' shift vs orientation polarizability of the solvents, (b) Stokes' shift vs $E_T(30)$ parameter, (c) emission maxima (in cm^{-1}) vs Kamlet-Taft solvent polarity parameter.	256
Figure 4.28	Plots for 35c in different solvents (a) Lippert-Mataga plot showing Stokes' shift vs orientation polarizability of the solvents, (b) Stokes' shift vs $E_T(30)$ parameter, (c) emission maxima (in cm^{-1}) vs Kamlet-Taft solvent polarity parameter.	257
Figure 4.29	Plots for 35d in different solvents (a) Lippert-Mataga plot showing Stokes' shift vs orientation polarizability of the solvents, (b) Stokes' shift vs $E_T(30)$ parameter, (c) emission maxima (in cm^{-1}) vs Kamlet-Taft solvent polarity parameter.	258
Figure 4.30	TGA curves of the compounds 26-31 .	260

Figure 4.31	Cyclic voltammogram (a) and DPV (b) of 26, 27 & 30 recorded in dichloromethane solution ($2 \times 10^{-5}M$) (ferrocene as internal reference).	262
Figure 4.32	Cyclic voltammogram (a) and DPV (b) of 28 & 31 recorded in dichloromethane (ferrocene as internal reference).	262
Figure 4.33	DPV of 34a-34d (a) and 35a-35d (b) recorded in THF (ferrocene as internal reference).	263
Figure 4.34	Energy level diagram of device I and II (A) and compounds 26-31 with TPBI (B).	265
Figure 4.35	Current density vs voltage curve (a), luminance vs voltage curve (b) and current efficiency vs current density curve (c) of device using neat film of 26-31 as hole transporting and emitting layer without CBP .	266
Figure 4.36	Current density vs voltage curve (a), luminance vs voltage curve (b), current efficiency vs current density curve (c) and luminance efficiency vs luminance curve (d) of device using 26-31 as a dopant with host material CBP .	267
Figure 4.37	EL spectra of the devices with 26-31 without CBP at maximum luminescence (a) and with CBP @100 cd/m ² (b), @1000 cd/m ² (c), @50 mA/m ² (d)	269
Figure 5.1	Structures of the Ru-complexes used as photosensitizer for DSSC.	288
Figure 5.2	A general design of organic dyes.	289
Figure 5.3	Structures of organic dyes having different donor-acceptor systems.	290
Figure 5.4	Structures of triarylamine-based organic dyes for DSSC.	291
Figure 5.5	Structures of organic dyes containing two donor systems.	293
Figure 5.6	Structures of the dyes 39a, 39b and 43a-43c .	295
Figure 5.7	Absorption spectra of the dyes 39a, 39b & 43a-43c recorded in dichloromethane.	298
Figure 5.8	Comparison of absorption (filled) and emission (unfilled) spectra of (a) 39b , (b) 43a , (c) 43b , (d) 43c with their corresponding amines (36b, 41a-41c) and aldehydes (38b, 42a-42c) recorded in dichloromethane.	301
Figure 5.9	Absorption spectra of (a) 39a and (b) 39b in toluene, tetrahydrofuran, dichloromethane, acetonitrile and methanol.	304
Figure 5.10	Absorption (a) and emission (b) spectra of 39b in acetonitrile and methanol.	304
Figure 5.11	Absorption spectra of 43a (a), 43b (b) and 43c (c) in toluene, tetrahydrofuran, dichloromethane, acetonitrile and methanol.	305
Figure 5.12	Illustration of acid-base equilibria of the dyes.	307

Figure 5.13	Absorption spectra of 39a (a) and 39b (b) in dichloromethane before and after addition of TFA or TEA.	308
Figure 5.14	Absorption spectra of 39a (a) and 39b (b) in methanol before and after addition of TFA or TEA.	308
Figure 5.15	Absorption spectra of 43a (a), 43b (b) and 43c (c) in dichloromethane before and after addition of TFA or TEA.	309
Figure 5.16	Absorption spectra of 43a (a), 43b (b) and 43c (c) in methanol before and after addition of TFA or TEA.	310
Figure 5.17	Possibility of deprotonation in system having (a) one donor, (b) two donor unit.	312
Figure 5.18	Absorption spectra of the dyes 39a , 39b and 43a-43c on TiO ₂ layer.	312
Figure 5.19	Absorption spectra of dyes 39a , 39b and 43a-43c recorded in dichloromethane before (a), after (b) addition of TFA, (c) in methanol.	314
Figure 5.20	Cyclic voltammogram of (a) the precursor amines (36b , 41a-41c), (b) aldehydes (38b , 42a-42c) and dyes (39a , 39b and 43a-43c) (c) before and (d) after addition of TFA.	316
Figure 5.21	Energy level diagram of the dyes 39a , 39b and 43a-43c .	319
Figure 5.22	Electronic distribution in the frontier molecular orbital diagrams of the dyes 39a and 39b .	321
Figure 5.23	Electronic distribution in the frontier molecular orbital diagrams of the dyes 43a-43c .	322
Figure 5.24	I-V characteristics of the DSSC fabricated using the dyes 39a , 39b and 43a-43c .	326
Figure 5.25	IPCE plots of the DSSC devices fabricated using the dyes 39a , 39b and 43a-43c .	326
Figure 5.26	Nyquist plots of the DSSC fabricated using the dyes 39b , 43a-43c .	328
Figure 5.27	Bode phase plots of the DSSC fabricated using the dyes 39a , 39b and 43a-43c .	329

List of Tables

	Page No.
Table 1.1	Optical, electrochemical and thermal properties of fluorene-based compounds as blue emitting materials. 14
Table 1.2	OLED performance of the compounds A3-A22 . 18
Table 1.3	Properties of fluorene-containing organic dyes for DSSC. 21
Table 1.4	Optical, electrochemical and thermal properties of fluoranthene - based emitting materials. 31
Table 1.5	OLED performance of fluoranthene derivatives A36-A54 . 36
Table 1.6	Optical, electrochemical and DSSC data of the fluoranthene-based organic dyes (A55-A57). 38
Table 1.7	Optical and electrochemical data of the compounds A70-A76 . 43
Table 1.8	Optical and electrochemical data of the compounds A77-A81 . 43
Table 1.9	Optical, electrochemical and thermal properties of pyrene-based blue emitting materials 50
Table 1.10	OLED performance of A90-A105 . 54
Table 1.11	Optical, thermal and electrochemical properties of A106-A113 . 59
Table 2.1	Optical properties of fluoranthene derivatives (4-7). 90
Table 2.2	Optical properties of triphenylene derivatives (12-14). 90
Table 2.3	Absorption data of compounds 7a-7d and 14a-14d in different solvents. 106
Table 2.4	Emission data of compounds 7a-7d and 14a-14d in different solvents. 107
Table 2.5	Stokes' shift observed for the triarylamine derivatives (7a-7d) and (14a-14d) in different solvents and the parameters used for correlation. 107
Table 2.6	Predicted (TDDFT B3LYP/6-31G(d,p)) vertical transitions and their assignments. 125
Table 2.7	Quenching constant for compound 5a in four different quencher. 127
Table 2.8	Thermal data of the compounds 4-7 and 12-14 . 130
Table 2.9	Electrochemical properties of triarylamine derivatives (7a-7d & 14a-14d). 135
Table 2.10	Electroluminescence characteristics for device performance using 7c & 7d as hole transporting and emitting layer. 137
Table 2.11	Electroluminescence characteristics for devices with 14a-14d as hole transporting and emitting layer (neat) and as dopant. 140

Table 3.1	Optical and electrochemical properties of C1 and C2 .	167
Table 3.2	Optical properties of quinoxalines (20a , 20b), pyrazines (21a , 21b) and thienopyrazines (22a , 22b).	174
Table 3.3	Absorption data of the compounds 20a , 20b , 21a and 21b recorded in different solvent.	183
Table 3.4	Emission data of the compounds 20a , 20b , 21a and 21b recorded in different solvent.	183
Table 3.5	Stokes' shift observed for the compounds 20a , 20b , 21a and 21b in different solvents and the parameters used for correlation.	183
Table 3.6	Predicted (TDDFT B3LYP/6-31G(d,p)) vertical transitions and their assignments.	189
Table 3.7	Thermal properties of the compounds 20a-22a and 20b-22b .	192
Table 3.8	Electrochemical data of the compounds 20a-22a and 20b-22b .	194
Table 4.1	Optical and electrochemical properties of D15-D19 .	220
Table 4.2	Optical properties of the compounds 26-31 .	228
Table 4.3	Absorption data of the compounds 26-31 recorded in different solvents.	238
Table 4.4	Emission data of the compounds 26-31 recorded in different solvents.	239
Table 4.5	Stokes' shift observed for the compounds 26-31 in different solvents and the parameters used for correlation.	239
Table 4.6	Optical properties of the dyes 35a-35d recorded in THF.	249
Table 4.7	Comparison of optical and electrochemical properties of 35a , 35c with D25 and D26 .	249
Table 4.8	Absorption data of the dyes 35a-35d recorded in different solvents.	254
Table 4.9	Emission data of the dyes 35a-35d recorded in different solvents.	254
Table 4.10	Stokes' shift observed for the dyes 35a-35d in different solvents and the parameters used for correlation.	254
Table 4.11	Thermal data of the compounds 26-31 .	260
Table 4.12	Electrochemical data of the compounds 26-31 measured in dichloromethane.	261
Table 4.13	Electrochemical data of 34a-34d and 35a-35d measured in THF.	263
Table 4.14	Electroluminescence characteristics of devices I & II based on compounds 26-31 .	268
Table 4.15	Emission and electroluminescence spectral data of the compounds 26-31 .	270
Table 5.1	Optical and device data for the compounds E5-E10 .	292
Table 5.2	Optical data of precursor amines (38a , 41a-41c), aldehydes (38b ,	299

	42a-42c) and dyes (39b , 43a-43c) measured in dichloromethane solution.	
Table 5.3	Absorption data of the dyes 39a , 39b and 43a-43c recorded in different solvents.	306
Table 5.4	Emission properties of the dyes 39a , 39b and 43a-43b .	313
Table 5.5	Electrochemical properties of amines (36b , 41a-41c), aldehydes (38b , 42a-42c) and dyes (39a , 39b , 43a-43c).	318
Table 5.6	Predicted (TDDFT B3LYP/6-31G(d,p)) vertical transitions and their assignments.	323
Table 5.7	Photovoltaic performance and other parameters extracted from EIS of DSSC sensitized by the dyes 39a , 39b and 43a-43c .	327

Polyaromatic Hydrocarbon-Based Functional Materials for Electroluminescent Applications

1.1 Introduction

Polyaromatic or polycyclic aromatic hydrocarbons (PAHs) have received immense attention due to their interesting optical, electrochemical and liquid crystalline properties.¹ PAH-based derivatives have known to construct fullerenes, carbon nanotubes and the assembly of supramolecular architecture² and their use in electronic devices such as organic field effect transistors (OFET), organic light emitting diode (OLED) and dye sensitized solar cells (DSSC) have also been remarkable.³⁻⁵ Both the molecular size and shape of PAHs play very important role on their optical and electronic properties. Molecular systems embedded with multiple functionality are required for electronic devices and functionality of molecule is determined by their optical, thermal and electrochemical properties. In this direction star-shaped conjugated molecules or dendrimers consisting of π -conjugated substituents joined together by a central PAH core, have attracted increasing attention.⁶ The diversity of optical and electronic properties of them can be exploited for a particular application by subtle modification of central PAH core.

PAHs are attracted candidate in the field of optoelectronics due to their unique property of high thermal stability, good charge transporting properties and excellent fluorescence as well as phosphorescence emission properties. PAHs with π -conjugated length, such as anthracene, fluorene, pyrene, perylene, triphenylene, fluoranthene, benzo[*k*]fluoranthene, have been extensively investigated for their potential application as organic nonlinear optical materials

(NLO), fluorescent sensors, photosensitizers and electroluminescent emitters (EL).⁷⁻¹¹ Various polymers, dendrimers, oligomers and monomers of PAHs have been reported as functional materials in organic light emitting devices (OLEDs) and dye sensitized solar cells (DSSC).^{12,13,5} For instance, fluoranthene, triphenylene, fluorene and pyrene comprises an important class of PAHs with π -conjugated length for electroluminescent purpose. The enfeebling problem associated with the planar PAHs is the molecular aggregation which can overcome by incorporating PAHs with bulky nonplanar groups such as di- or triaryl amines or polyphenylated benzene units. Introduction of aryl amines into PAHs not only enhance the absorption and emission profiles but also increase the thermal stability, charge transporting ability and amorphism. Moreover HOMO/LUMO energy levels can also be tuned by inserting aryl amines which are the requisites for efficient OLEDs.

Additionally organic heterocyclic fragments such as thiophenes¹⁴, quinolines¹⁵, 1,3,4-oxadiazoles¹⁶, quinoxalines¹⁷, 1,3,5-triazines¹⁸, etc. also play a major role in the design and synthesis of functional hybrid materials. In particular, thiophene is an electron-rich moiety. Incorporation of thiophene in π -conjugation enhances the optical properties and raises the HOMO of the molecule and decrease the band gap. Moreover thiophene derivatives also undergo electropolymerization. While quinoxaline is electron deficient moiety and embedding quinoxaline in a molecular architecture substantially lowers the LUMO and increases the thermal stability. Introduction of heterocyclic entities in molecules alters the optical and electrochemical properties of the molecules. High thermal stability, promising charge transport and excellent emission observed for these heterocycle-based compounds make them attractive candidates of electronic devices which mandate one or more functions.

Role of PAH backbone, triaryl amines, polyphenylated benzene units and substituted heterocycles on optical, thermal and electrochemical properties of the molecule and their use in electroluminescent devices has been critically reviewed in this work. The present chapter focuses mainly on the progress achieved in utilizing fluorene, pyrene, fluoranthene and triphenylene-based functional materials for the development of electroluminescent devices. Additionally methods of synthesizing PAH backbone and their characterization techniques have also been discussed in brief. An abbreviated description of the electroluminescent device specifically OLED and DSSC has also been given to get the information about the requisite for a material so that it can give better device performance.

1.2 Organic light emitting diodes (OLED)

OLED is a flat light emitting technology which is made by placing a series of organic thin films between two electrodes. On the basis of the materials and fabrication process, OLEDs can be divided into two families. One is based on small molecule which is fabricated by vapor deposition method and other comprises of polymers fabricated by spin coating or inkjet printing. Small molecules based OLEDs are known as SMOLED which was first demonstrated by Ching W. Tang and Steven Van Slyke¹⁹ in 1987 at Eastman Kodak. This device was made up of two layers using AlQ_3 as electron transporting/green emitting layer and a diamine as hole transporting layer. Polymer based OLEDs are named as POLEDs which was first introduced in 1990 by J. H. Burroughes et al.²⁰ at Cavendish laboratory in Cambridge using poly(*p*-phenylene)vinylene.

An OLED device consists of several organic layer such as hole injection layer (HIL), hole transport layer (HTL), emitting layer (EL), and electron transport layer (ETL) sandwiched by two electrodes, the anode and cathode, all deposited on a glass substrate. Organometallic

chelates, polymers, dendrimers and monomer fluorescent or phosphorescent dyes are commonly used as functional materials in OLEDs.^{21-23,12} High work function metal oxide, Indium tin oxide (ITO), was used as anode and the metals such as Mg, Al with low work function acted as cathode.

The operating mechanism of OLED can be demonstrated by its multilayer structure. As shown in Figure 1.1, an electrical potential difference is applied between the anode and the cathode such that the anode is kept at positive electrical potential with respect to the cathode. The electrons move from cathode to anode through device. The movement of holes and electrons in the device and their recombination occurred through the following steps:

Carrier injection: Holes are injected from anode into the HOMO of hole transport layer *via* hole injection layer. Similarly electrons are injected from the cathode into the LUMO of electron-transport layer (ETL) *via* electron injection layer.

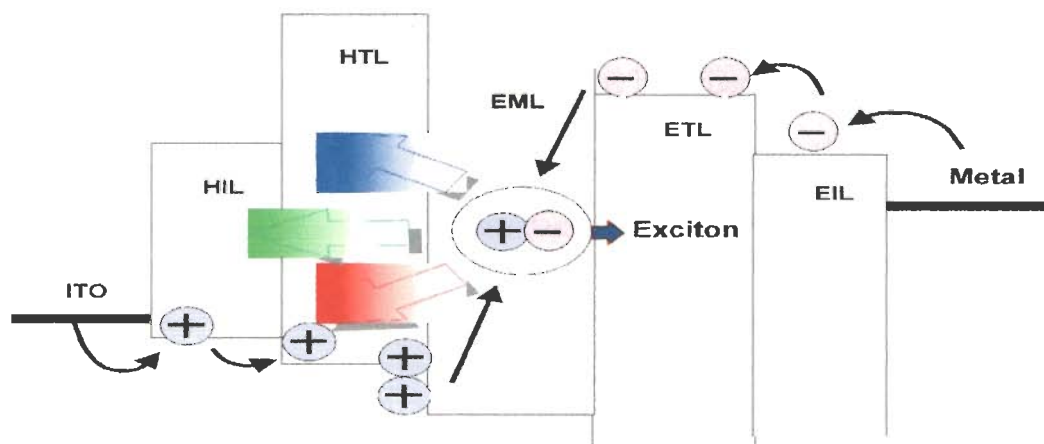


Figure 1.1 Operating mechanism of a multilayer OLED device.

Carrier migration: The injected holes and electrons moves towards oppositely charged electrode by electrostatic force of attraction.

Carrier recombination: The holes and electrons are recombined in the emissive layer to form exciton. An exciton may either be in a singlet or a triplet state depending on the nature of spins in

which holes and electrons have been combined. The decay of this excited state results in a relaxation of the energy levels of the electron, accompanied by emission of radiation whose frequency is in the visible region.

The efficient recombination of holes and electrons in emissive layer is necessary for the better efficiency of device. Therefore, it is essential to balance the injection of holes and electrons into the emitting layer of OLEDs to optimize the electroluminescence (EL) efficiency.

Meanwhile, it is generally accepted that a morphologically stable amorphous organic layer, especially HTL, will lead to a longer lasting OLED. Crystallization or melting of amorphous organic materials caused by joule heat or a short-circuit current due to pinholes in thin films are considered common causes of device degradation. This effect can be reduced using HTL materials with high T_g . Therefore for efficient and stable OLED, a hole transporting materials should have following properties-

- 1) It should be amorphous and should have good film forming properties.
- 2) It should have a moderate hole drift mobility to match the available electron transport material.
- 3) It should have low ionization potential to ensure efficient hole injection.
- 4) It should have high thermal stability.

Triaryl amines being electron rich comprises a class of efficient hole transporting materials. The example of a well known and commonly used hole transporting material is 4,4'-bis(1-naphthylphenylamino)-biphenyl (NPB) having glass transition temperature 98°C. Shirota and Schmidt et al. have reported several starburst aromatic amines with high T_g that are useful as hole transporting materials in OLEDs.²⁴

1.3 Dye Sensitized solar cells (DSSC)

DSSC is a thin film solar cell and comprises a class of low-cost materials. The flexibility in shape, color, transparency and their better performance under diffuse light condition and at higher temperature, make them attractive and promising for commercialization. The dye sensitized solar cell was invented by Michael Grätzel and Brian O'Regan at the Ecole Polytechnique Fédérale de Lausanne in 1991.²⁵ Since the ruthenium-based sensitizers²⁶⁻²⁸ have been intensively investigated for DSSC and the conventional Ru-based dyes have achieved solar-energy to electricity conversion efficiencies up to 11% under AM 1.5 irradiation.²⁹ But due to the rarity and high cost of ruthenium, organic sensitizers came into consideration and have advantages over conventional Ru-complex.

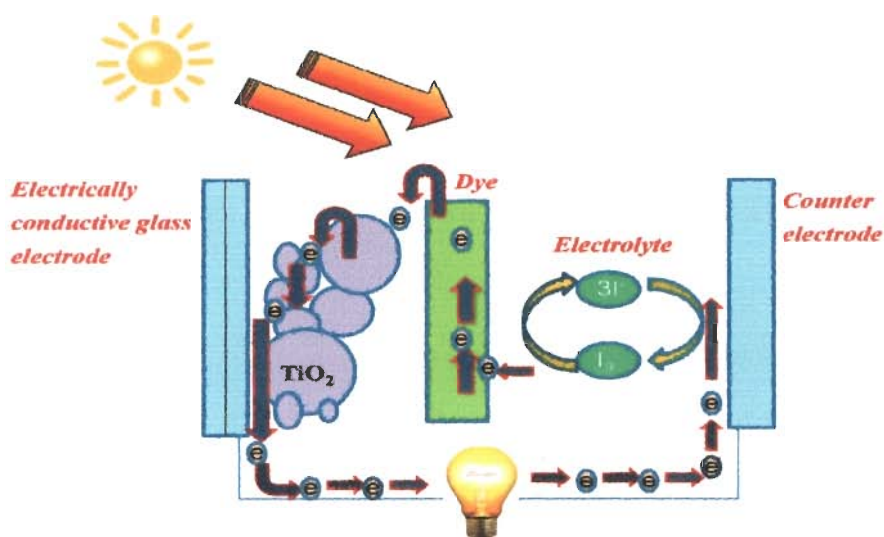


Figure 1.2 Working principle of DSSC.

DSSC consists of a fluorine-doped tin oxide ($SnO_2:F$, FTO) covered glass as anode, a thin mesoporous film of wide-band gap oxide semiconductor, such as TiO_2 , a dye sensitizer which is deposited on the surface of the TiO_2 layer, an electrolyte or hole transport material which fully covers the TiO_2 /dye surface, and a counter electrode (such as platinum on glass for electrolyte-containing DSCs or a silver or gold electrode for cells using organic hole conducting materials).

The working principle of a DSSC device has shown in Figure 1.2. Under light irradiation, an excited dye injects an electron into the conduction band (CB) of the TiO₂ from where the electrons migrate to the counter electrode after traversing the electrical load. The electrolyte or the organic hole conductor serves to regenerate the dye sensitizer and transport the positive charges to the counter electrode, where they recombine with the electrons. Thus, an organic dye plays a very important role for the device performance and it should have the following properties:

1. An ideal sensitizer should absorb all the light below a threshold wavelength of about 920 nm.
2. It must have attachment group such as carboxylate, phosphonate to firmly graft over TiO₂ surface.
3. It should inject the electron to the TiO₂ surface after photoexcitation with unit quantum yield.
4. It should have more negative excited state potential than the energy level of TiO₂ conduction band (-0.5 V vs NHE)
5. The ground state potential of the dye should be more positive than the iodide/ triiodide redox couple (~0.42 V vs NHE).

The photovoltaic performance was determined by several parameters such as overall power conversion efficiency, Incident photon to current conversion efficiency (IPCE), short circuit current (J_{sc}), open circuit voltage (V_{oc}) and fill factor (FF). The formula of overall current conversion efficiency is as follows

$$\eta = \frac{P_{out}}{P_{in}} = FF \frac{V_{oc} J_{sc}}{P_{in}}$$

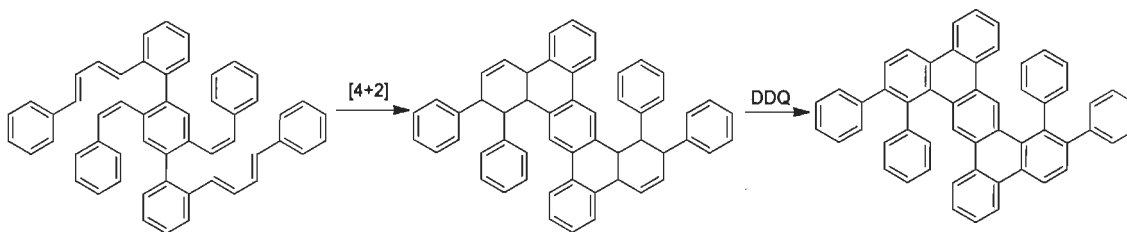
Where P_{out} is the maximum output electrical power (Wm^{-2}) of the device under illumination, P_{in} (Wm^{-2}) is the light intensity incident on the device, V_{oc} is the open circuit voltage, and J_{sc} is the short circuit current in Am^{-2} .

1.4 Synthesis & characterization techniques of PAH

Fundamental contributions to the direct synthesis and characterization of polycyclic aromatics were pioneered by R. Scholl, E. Clar, and M. Zander, who achieved the synthesis of numerous aromatic compounds under drastic conditions at high temperatures with strong oxidation.³⁰ However, only a few selective synthetic methods have been established so far. Some of them are given below:

1.4.1 Intra- and intermolecular Diels-Alder reaction

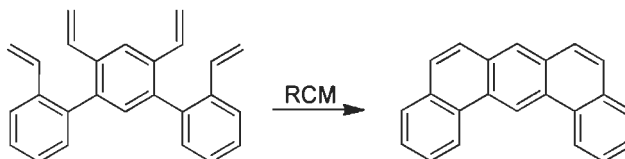
Müller et al. have reported this strategy to synthesize large PAH.³¹ In this method para-terphenyl derivative undergo Diels-Alder reaction to form cyclohexane derivative which was further oxidized by 2,3-dichloro-4,5-dicyanoquinone (DDQ) to form PAH backbone.



Scheme 1.1 Synthesis of PAH *via* Diels-Alder reaction.

1.4.2 Ring-closing olefin metathesis (RCM)

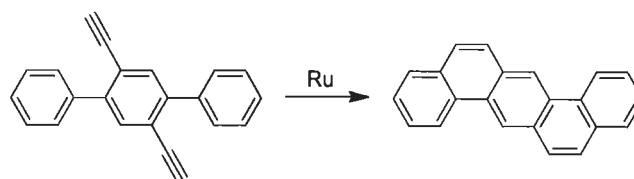
Bonifacio et al. have developed a strategy for the synthesis of PAHs by RCM of pendant olefins on a phenylene backbone.³² RCM of 2,4',6',2''-tetravinyl-[1,1';3',1'']terphenyl in presence of $\text{Cl}_2(\text{PCy}_3)_2\text{Ru}=\text{CHPh}$ and dry CH_2Cl_2 affords dibenz[*a,j*]anthracene in good yield (98%).



Scheme 1.2 Synthesis of dibenz[*a,j*]anthracene.

1.4.3 Benzannulation and electrophilic cyclization

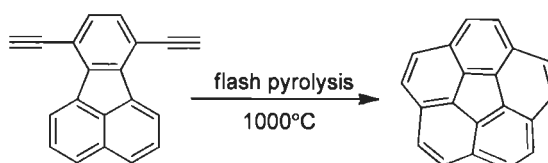
Shen et al. have reported the synthesis of PAH by benzannulation method using $\text{TpRuPPh}_3(\text{CH}_3\text{CN})_2\text{PF}_6$ catalyst.³³ In this method, a mixture of 1,4-Diethynyl-2,5diphenylbenzene, Ru catalyst and 1,2-dichloroethane was heated at 80°C for 24 h to afford dibenzo[*a,h*]anthracene.



Scheme 1.3 Synthesis of dibenzo[*a,h*]anthracene.

1.4.4 Flash vacuum pyrolysis

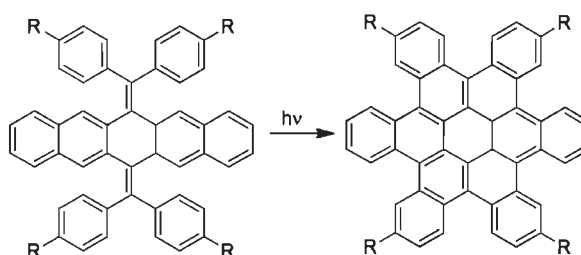
Scott et al.³⁴ have reported thermal cyclization of 7,10-diethynylfluoranthene in the gas phase gives corannulene.



Scheme 1.4 Synthesis of corannulene.

1.4.5 Intramolecular photocyclization

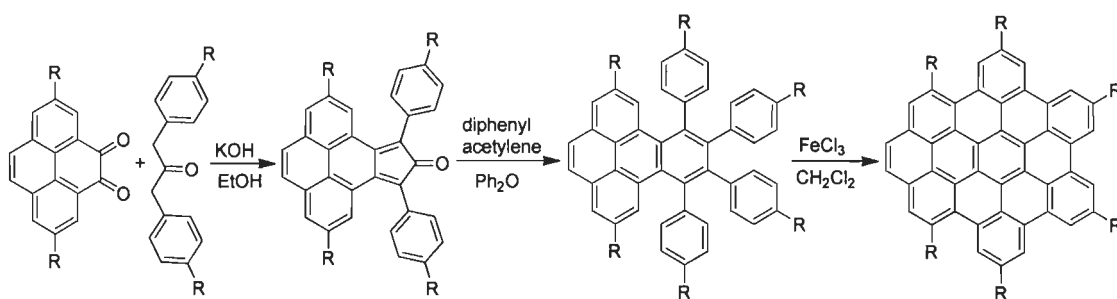
Nuckolls and co-workers have developed a novel approach to synthesize contorted hexabenzocoronenes *via* photocyclization.³⁵



Scheme 1.5 Synthesis of hexabenzocoronenes.

1.4.6 Oxidative cyclodehydrogenation³⁶

This is the most commonly used method for synthesizing extended PAH of different shape and size. In this method, diketone and alkylated diphenylacetone undergo condensation reaction to form cyclopentadienone derivative. The Diels-Alder reaction of cyclopentadienone derivatives, and an alkyne with the subsequent elimination of carbon monoxide afford the PAH backbone incorporated with polyphenylene which planarized *via* oxidative cyclodehydrogenation in the presence of FeCl_3 and dichloromethane. This method does not require any expensive catalytic system and very harsh condition. It is also easy to handle.



Scheme 1.6 Example of oxidative cyclodehydrogenation leading to large PAH.

In general, the characterization of functional materials has been done by various spectroscopic methods. These methods are as follows-

1. ^1H NMR and ^{13}C NMR
2. FT-IR for functional group detection
3. GC-MS spectroscopic methods
4. TGA/DTA/DTG and DSC for thermal analysis
5. UV-vis and fluorescence spectroscopy
6. Single X-ray crystallography
7. CV and DPV for electrochemical analysis

1.5 Optical, thermal, electrochemical and electroluminescent properties of PAH-based functional materials

1.5.1 Fluorene-based functional materials

It is one of the most important active material in organic electronics due to its favorable properties including capability to emit in the blue part of the visible spectrum, chemical and photochemical stability, liquid crystalline properties, two photon absorbing properties³⁷ and easy synthesis with high purity. Fluorene, terfluorenes, spirofluorenes and polyfluorene-based organic compounds comprises the most promising class of blue emitting materials for OLEDs with high quantum efficiencies.^{38,39} But the major drawback with fluorene core is the appearance of an additional undesirable low energy emission band during device operation which reduces the emission efficiency as well as the blue color purity. The emergence of this specific band may be most likely due to the oxidation of fluorene to fluorenone. Hence, the active methylene sites of fluorene are blocked by dialkylation or by preparing spirofluorene derivatives to avoid oxidation. Fluorene act as a bridge to increase the π -conjugation of the molecule.

The structure and electro-optical properties of the blue emitting and hole transporting materials based on fluorene and spirobifluorenes are displayed in Table 1.1 and their device performance compiled in Table 1.2. Fluorene derivatives have also been reported to show multifunctional materials. Chen et al. have reported benzimidazole/amine-based ambipolar compound bridged by 9,9-dialkyl fluorene and spirobifluorene in single layer blue OLED device.³⁸ These materials were also used as host for green and yellow iridium complex for phosphorescent OLED. Jiao et al. have discussed the synthesis, structure, electronic state and luminescent properties of 9,9-di(4-(di-*p*-tolyl)aminophenyl)fluorene derivatives with pyrene, 10-phenylanthracene-9-yl and 10-(4'-diphenylaminophenyl)anthracene-9-yl group as side arm and

also demonstrated that their nonplanar structure reduce the molecular interaction or molecular aggregation.³⁹ K. Kreger and co-workers have developed a star shaped molecule with a triphenylamine core and 3 fluorene as side arm (**A1**) serves as hole transport and emitting layer while the other derivative (**A2**) act as hole blocking layer (Figure 1.3).⁴⁰

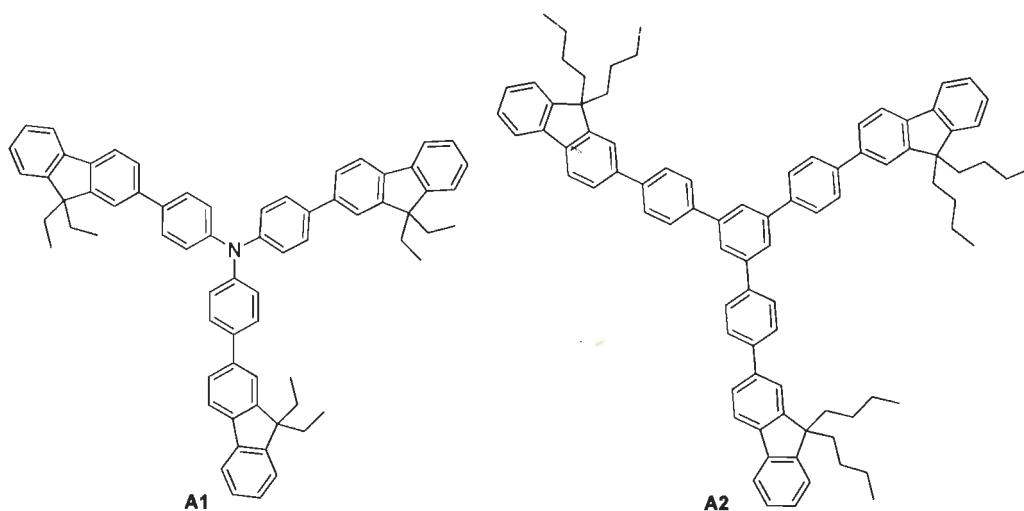


Figure 1.3 Fluorene-based multifunctional materials.

Culligan et al. have reported a class of blue emitting material comprising of anthracene and fluorene (**A3**).⁴¹ The presence of fluorene increases the HOMO/LUMO gap. After that Park et al. have reported the diamine substituted derivative 9,10-Bis-(9',9'-diethyl-7'-diphenylamino-fluoren-2-yl)-anthracene (**A4**).⁷ The incorporation of amine raises the HOMO/LUMO levels which facilitate the hole transporting properties. They have also demonstrated that after the incorporation of amine, the compound become nonplanar which inhibit intramolecular interaction as there was no significant difference in emission wavelength in both solution and thin film.

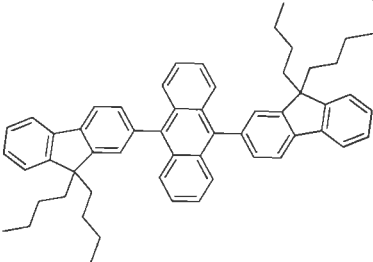
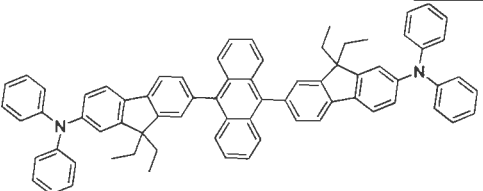
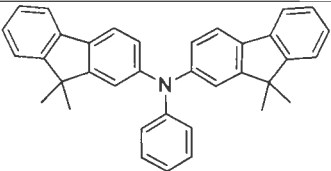
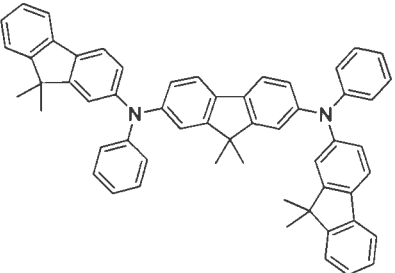
Okumoto et al. have synthesized blue emitting hole transporting materials having amine unit (compound **A5** and **A6**).⁴² They demonstrated that the incorporation of another diphenyl amine donor system red shifts the absorption profile. Additionally it also raises the HOMO/LUMO

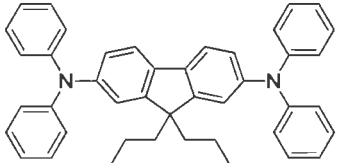
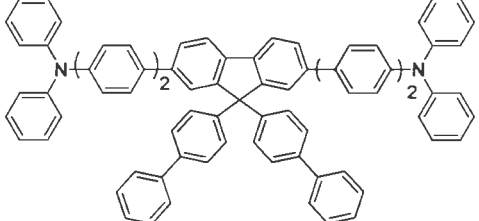
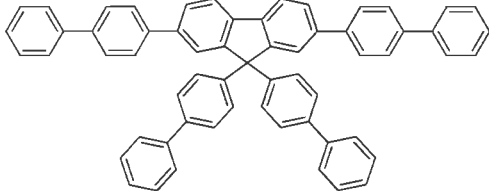
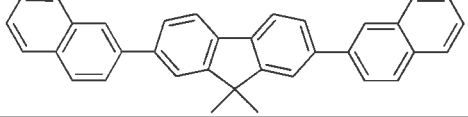
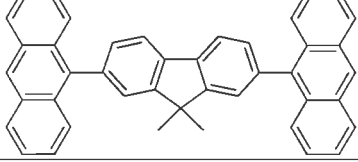
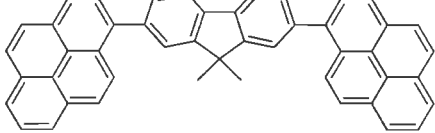
levels, decrease the band gap and increase the thermal stability. Overall the incorporation of another donor system increases the device performance. A blue light emitting OLED device was fabricated using compound **A7** which showed electroluminescence *via* exciplex emission.⁴³ Matsumoto et al. have fabricated a deep blue OLED using compound **A8** as emitter doped with a wide band gap host another fluorene derivative (**A9**) without amine.⁴⁴ Thus, fluorene derivatives can perform multifunction such as as host or as dopant.

Peng et al. have synthesized blue electroluminescent fluorene derivatives and also studied the effect of different substituents on the optical, thermal and electrochemical properties.⁴⁵ The glass transition temperature (T_g) of the fluorene derivatives changes from 85 °C (**A10**), to 164 °C (**A11**), to 145 °C (**A12**) by changing the substituents at the C-2,7 position in fluorene. The reason could be the change the rigidity and planarity of the molecule by diifferent substituents. The absorption /emission profile also red shift by bulky substituents such as anthracene and pyrene. Further the T_g of the derivatives **A10**, **A13**, and **A14** increases from 85 to 136 °C by varying the substitution group at the C-9 position of the fluorene molecule.

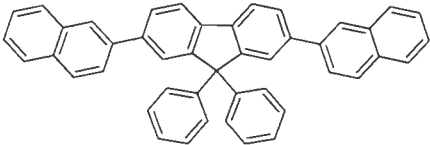
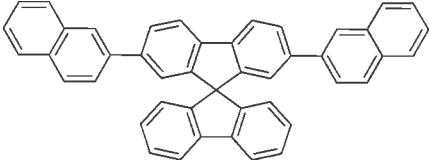
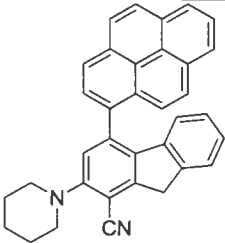
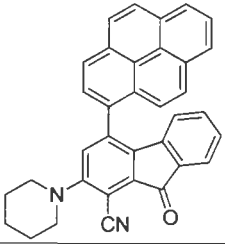
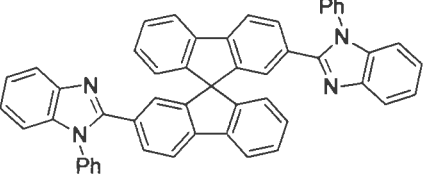
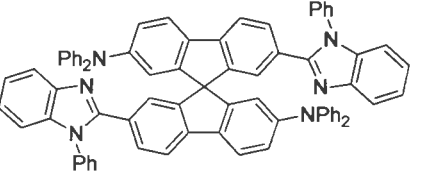
It indicates that C9-aryl substituents and spiro-type group made the molecular structure rather bulky as compared to the C9-methyl substituents and hinders close packing and intermolecular interaction and also increases molecular rigidity. The introduction of a spiro-type linkage leads to the reduction of crystallization tendency and an increase in the glass transition temperature. Thus, the suitable substitution on the fluorene can lead to a good thermal stability with a high T_g value. But there was no significant difference was observed in optical and electrochemical properties in **A10**, **A13** and **A14**.⁴⁵

Table 1.1 Optical, electrochemical and thermal properties of fluorene-based compounds as blue emitting materials.

SN	Compounds	λ_{abs} , nm	λ_{em} , nm (Φ)		E_g	HOMO (eV)	LUMO (eV)	$T_g/T_m/T_d$, °C	Ref.
			Solution	Thin film					
A3		405	N/A	N/A	2.96	5.73	2.77	NA/NA/NA	41
A4		380	454	462	2.89	5.22	2.33	NA/351/NA	7
A5		368	400 (0.56)	NA	3.17	5.31	2.14	82/NA/NA	42
A6		392	414 (0.76)	NA	3.03	5.12	2.09	135/NA/NA	42

A7		360	405	NA	NA	NA	NA	NA/NA/NA	43
A8		NA	NA	NA	NA	NA	NA	NA/NA/NA	44
A9		NA	NA	NA	NA	NA	NA	NA/NA/NA	44
A10		340	381, 399 (0.57)	392, 413	3.20	5.80	2.60	85/NA/357	45
A11		368	414 (0.45)	450	3.00	5.90	2.90	164/NA/367	45
A12		360	418 (0.68)	460	3.00	5.70	2.70	145/NA/457	45

Polyaromatic Hydrocarbon-Based Functional Materials

A13		342	381, 400 (0.66)	395, 414	3.20	5.90	2.70	136/NA/405	45
A14		342	382, 401 (0.68)	394, 414	3.20	5.80	2.60	136/NA/421	45
A15		344	481 (0.35)	NA	3.20	5.80	2.60	NA/NA/NA	46
A16		344	473 (0.39)	NA	3.38	NA	NA	NA/NA/NA	46
A17		331	383	392	3.30	5.73	2.43	154/NA/393	47
A18		386	445	460	2.86	5.46	2.60	165/NA/477	47


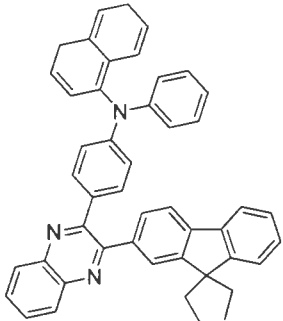
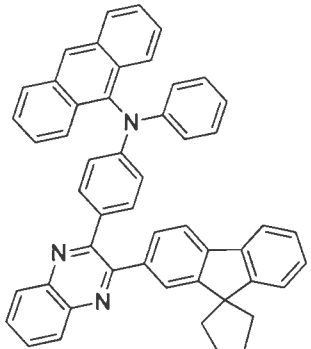
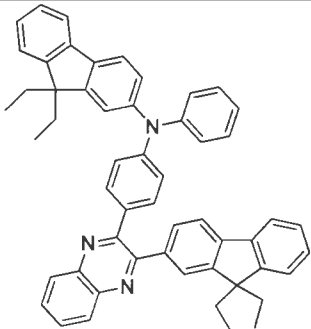
A19		352	394	407	3.17	5.43	2.26	115/NA/370	47
A20		398	547 (0.11)	NA	2.76	5.41	2.65	102/NA/396	17
A21		394	544 (0.21)	NA	2.82	5.45	2.63	126/NA/420	17
A22		405	589 (0.03)	NA	2.59	5.24	2.65	104/NA/399	17

Table 1.2 OLED performance of the compounds A3-A22.

Device	Power efficiency (lm/W)	Current efficiency (Cd/A)	Turn-on voltage	Max. brightness (Cd/m ²)	$\eta_{\text{ext,max}}$, %	EL _{max} (nm)	CIE (x, y)
ITO/CF _x /NPB-Rub/A3/Alq ₃ /Mg:Ag	NA	0.85	NA	NA	NA	460	0.15,0.08
ITO/CuPc/ α -NPD/MADN (A4, 2-3%)/Alq ₃ /LiF/Al	2.1	4.17	4.29	4600	3.3	462	0.14,0.17
ITO/m-MTDATA/A5/TBB/Alq ₃ /Mg:Ag	NA	NA	5.0	2100	1.60	405	NA
ITO/m-MTDATA/A6/TFPB/Alq ₃ /Mg:Ag	NA	NA	3.0	2200	1.08	422	0.16,0.06
ITO/A7/PBD/Alq ₃ /LiF/Al	NA	NA	4.0	400	NA	480	NA
ITO/NPD/TPD/A8:A9/Bphen/Al	NA	NA	NA	NA	3.3	NA	NA
ITO/NPD/NPD/A8:A9/Bphen/Al	NA	NA	NA	NA	3.8	NA	NA
ITO/NPD/DTAFL/A8:A9/Bphen/Al	NA	NA	NA	NA	3.9	NA	NA
ITO/NPD/DPAFL/A8:A9/Bphen/Al	NA	NA	NA	NA	5.0	NA	NA
ITO/NPD/A8/A8:A9/Bphen/Al	NA	NA	NA	NA	5.4	NA	NA
ITO/CuPc/NPB/A11/ Alq ₃ /Mg:Ag	NA	5.0	NA	NA	NA	490	0.19,0.35
ITO/CuPc/NPB/A12/ Alq ₃ /Mg:Ag	NA	4.8	NA	NA	NA	464	0.17,0.24
ITO/CuPc/NPB/A13/ Alq ₃ /Mg:Ag	NA	1.6	NA	NA	NA	452	0.15,0.14
ITO/CuPc/NPB/A14/ Alq ₃ /Mg:Ag	NA	2.0	NA	NA	NA	452	0.16,0.16
ITO/PEDOT:PSS/TPD/A15/BCP/LiF/Al	NA	0.85	3.5	573	NA	476	0.16,0.26
ITO/PEDOT:PSS/ A18/LiF/Al	0.14	0.61	4.0	2800 (19V)	0.52	460	0.15,0.14
ITO/PEDOT:PSS/ A18/A17/LiF/Al	1.10	1.68	3.0	10600 (17V)	1.50	NA	0.16,0.13
ITO/PEDOT:PSS/ A19/A18/A17/LiF/Al	1.55	1.90	2.5	21200(13.5V)	1.57	NA	0.16,0.14
ITO/PEDOT:PSS/ A20/TPBI/LiF/Al	2.44	3.50	3.5	16920	1.43	496	0.16,0.44
ITO/PEDOT:PSS/ A21/TPBI/LiF/Al	1.76	3.44	3.5	30860	1.50	490	0.16,0.38
ITO/PEDOT:PSS/ A22/TPBI/LiF/Al	3.93	6.37	3.5	35160	2.12	506	0.21,0.54

The origin of the low energy emission band produced by the oxidation of fluorene to fluorenone significantly obstruct the commercial scope of fluorene-based blue OLED. Goel et al. have demonstrated the formation of blue emitting fluorene/fluorenone by appropriate positioning of donor-acceptor and chromophoric groups. Compound **A15** and **A16** based device showed stable blue color emission.⁴⁶

Liao and coworkers have reported a series of blue emitting spirobifluorene bearing hole transporting diphenylamino groups and electron transporting phenyl benzimidazole group.⁴⁷ Compound **A18** and **A19** exhibited bathochromic shift in absorption and emission profile and also showed the higher decomposition temperature as compared to **A17**. This indicates that the incorporation of amine red shifts the absorption/emission profile and also increases thermal stability. Moreover it also increases the HOMO/LUMO level due to which the hole transporting properties increases. The glass transition is higher for **A17** than **A19** which show that benzimidazole decrease the chance of crystallization.

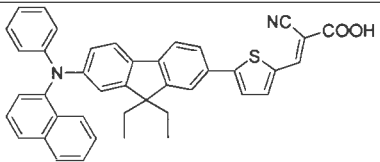
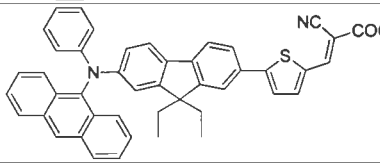
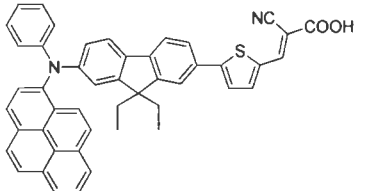
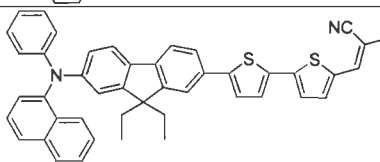
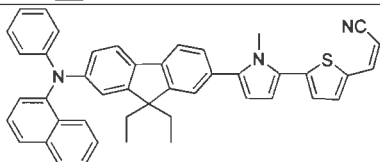
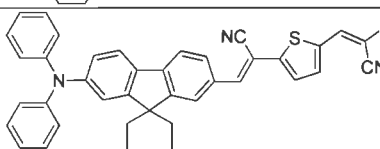
Thomas et al. have reported electroluminescent materials comprised of quinoxaline, diarylamine and additional unit fluorene, anthracene and naphthalene.¹⁷ These derivatives were fabricated as hole transporter and green emitting material. Compound **A22** exhibited red shifted absorption/emission profile as compared to **A20** and **A21**. This indicates that fluorene is increasing the donor strength which also leads to higher HOMO level. **A21** is more thermally stable due to the presence of more rigid phenanthrene.

The above discussion indicates fluorene is a promising candidate for the OLED application. Additionally incorporation of amines make the fluorene derivatives more valuable for hole transport. Moreover fluorene also play a vital role for the photovoltaic application. Recently Wong et al. have reported a fluorene-hexabenzocoronene-based dendrimers in bulk

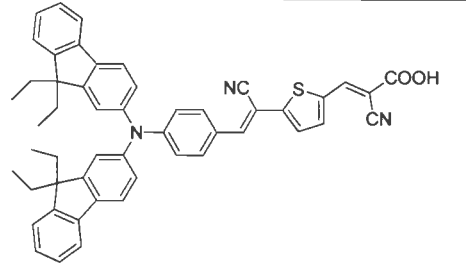
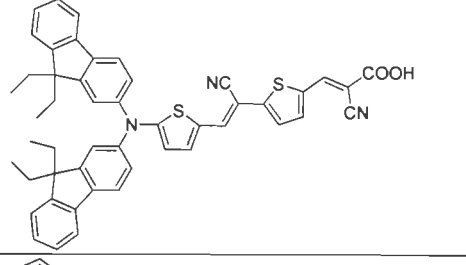
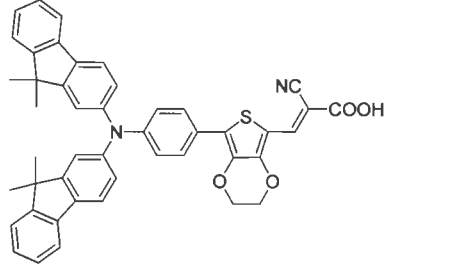
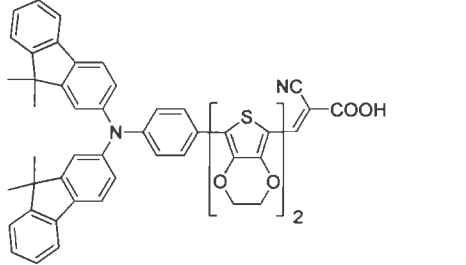
heterojunction solar cell.⁵ In general, fluorene used as a spacer in dye sensitized solar cell. But fluorenylamine unit act as a donor in organic dyes. Various examples of fluorene-based dyes for DSSC have given in Table 1.3 along with their optical properties and device performance. Fluorene was used as a spacer in compound **A23-A27**. Thomas et al. have reported thienylfluorene conjugated dyes (**A23-A25**) in which diarylamine amine with different substituent such as naphthalene, anthracene and pyrene was used as a donor and cyanoacrylic acid was used as acceptor.¹⁴ The substituent on amine did not show much influence on optical properties but the the molar extinction coefficient was found higher for pyrene substituted amine derivative **A25**. The order of the efficiency of the device fabricated using these dyes are **A23>A25>A24**.

A26 exhibited red shifted absorption wavelength (470 nm) as compared to **A23** (421 nm). **A26** also showed cathodically shifted oxidation potential than **A25**. Moreover **A26** (5.70%) displayed higher device efficiency than **A25** (5.23%). This is due to presence of more number of thiophene which is responsible for increasing conjugation. Yen et al. have reported organic dyes with pyrrole as a spacer (**A27**).⁴⁸ Presence of pyrrole increase the efficiency and current density but decrease the V_{oc} . Huang et al.⁴⁹ reported organic dyes (**A28-A30**) with cyanovinyl entity as spacer. **A29** exhibited red shifted absorption/emission profile as compared to **A28**. This indicates that the donor strength increases due to electron richness of fluorene. Thus, **A29** showed higher device efficiency and V_{oc} . Further incorporation of thiophene (**A30**) increase the absorption/emission but decrease the device efficiency. The organic dyes having 3,4-ethylenedioxythiophene as a linker showed a remarkable red shift in V_{oc} and device efficiency (**A31**, 0.76 V, 7.92%) and (**A32**, 0.75 V, 8.32%).⁵⁰

Table 1.3 Properties of Fluorene-containing organic dyes for DSSC.

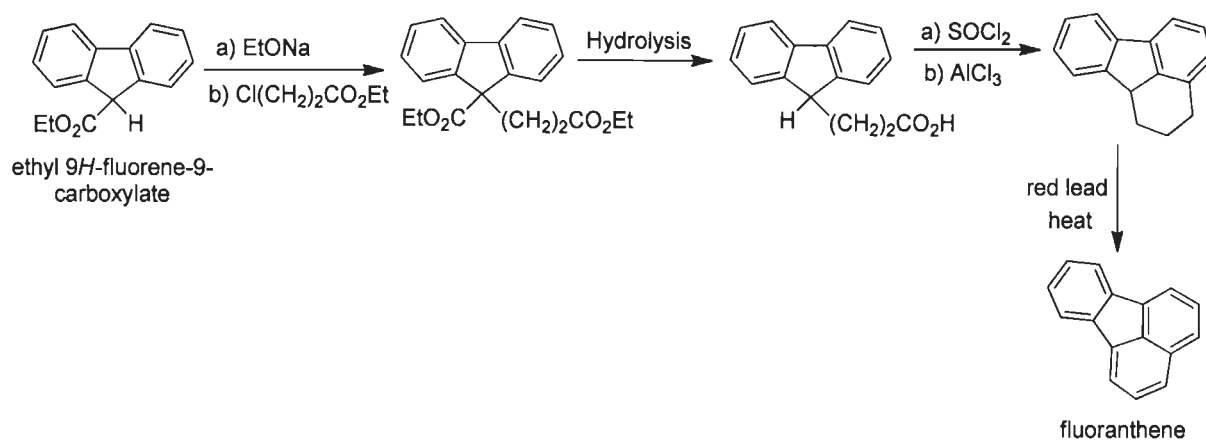
S.N.	Dyes	λ_{abs} , nm ($\epsilon \times 10^3$, $\text{M}^{-1}\text{cm}^{-1}$)	λ_{em} , nm (Φ)	E_{ox} , mV	V_{oc} , V	J_{sc} , mAcm^{-2}	ff	η , %	Ref.
A23		421 (52.9)	538 (0.28)	509	0.65	12.47	0.65	5.23	14
A24		421 (46.3)	536 (0.19)	451	0.57	7.59	0.67	2.86	14
A25		425 (54.5)	537 (0.33)	462	0.60	8.38	0.67	3.35	14
A26		470 (50.0)	NA	464, 747	0.62	13.4	0.63	5.70	48
A27		465 (51.0)	NA	350, 836	0.64	16.79	0.58	6.18	48
A28		482 (70.7)	633	526	0.58	11.0	0.69	4.34	49

Polyaromatic Hydrocarbon-Based Functional Materials

A29		511 (57.0)	654	525	0.61	12.48	0.64	4.81	49
A30		560 (77.8)	672	389	0.58	11.96	0.65	4.51	49
A31		525 (33.5)	688	760	0.76	13.82	0.75	7.92	50
A32		544 (38.5)	697	NA	0.75	15.68	0.71	8.32	50

1.5.2 Fluoranthene-based electroluminescent materials

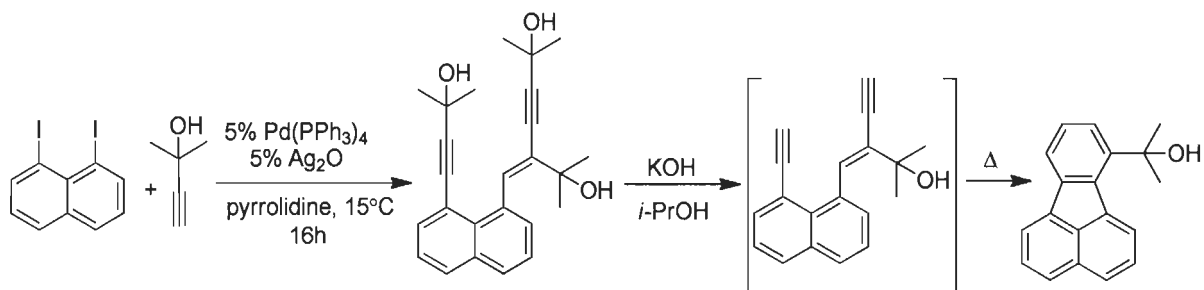
Fluoranthene is a class of non-alternant PAH which consist of naphthalene and a benzene unit connected by a five membered ring. Fluoranthene is one of the U.S. Environmental protection Agency's 16 priority pollutant PAHs and is a carcinogen. The formula of fluoranthene was suggested and established synthetically by following reaction by von Braun and Anton in 1929.⁵¹



Scheme 1.7 Synthetic route to fluoranthene from ethyl 9-fluorencarboxylate.

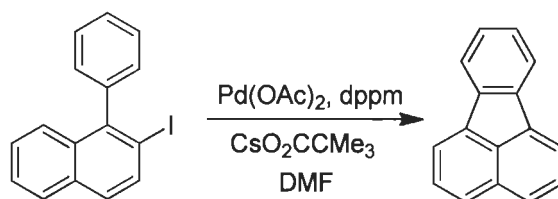
The development of milder methods to synthesize fluoranthene with high regioselectivity and yields are summarized in the following section, indicating the trend of this research field. The further section include the most generally used methods and the most recently developed synthetic methodologies.

González et al. reported a new procedure to synthesize fluoranthene by utilizing sonogashira cross coupling reaction in 1998.⁵² They have treated 1,8-diiodonaphthalene with 2-methylbut-3-yn-2-ol in presence of Pd catalyst. They have used Ag₂O in place of CuI as a co-catalyst and pyrrolidine as a solvent to increase the intermediate yield. After that compound further undergo cleavage by KOH and propanol followed by cycloaddition and aromatization to give fluoranthene with 63% yield.



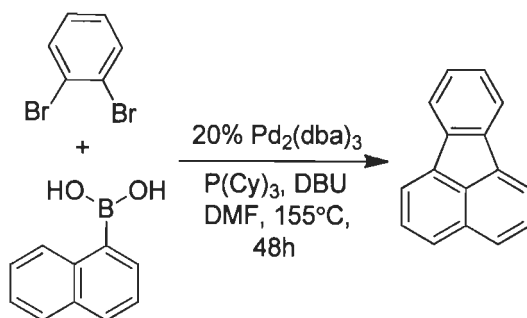
Scheme 1.8 Synthesis of fluoranthene from diiodonaphthalene *via* songashira reaction.

Larock et al. (2002) have developed a procedure to synthesize different polycycles which involves the use of palladium C-H activation to catalyze a 1,4-palladium migration within biaryls generating key aryl palladium intermediates, which subsequently undergo C-C bond formation by intramolecular arylation producing fused polycycles. The following reaction is given for the construction of fluoranthene with 81% yield by the above strategy given by Larock et al.⁵³



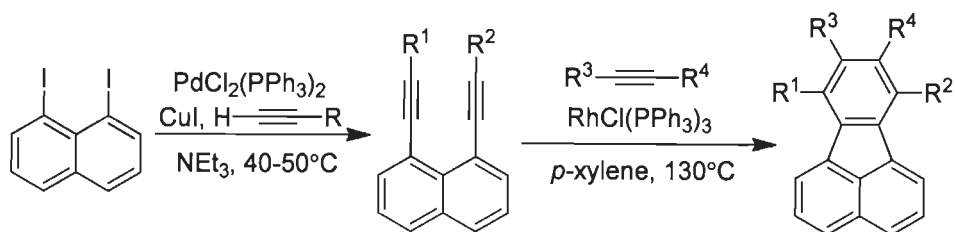
Scheme 1.9 Synthesis of fluoranthene *via* 1,4-Pd migration/arylation process.

Wegner et al. (2003) have demonstrated the reaction between 1-naphthalene boronic acid and 1,2-dibromobenzene using a new Suzuki-Heck type coupling cascade to synthesize fluoranthene with 87% yield.⁵⁴



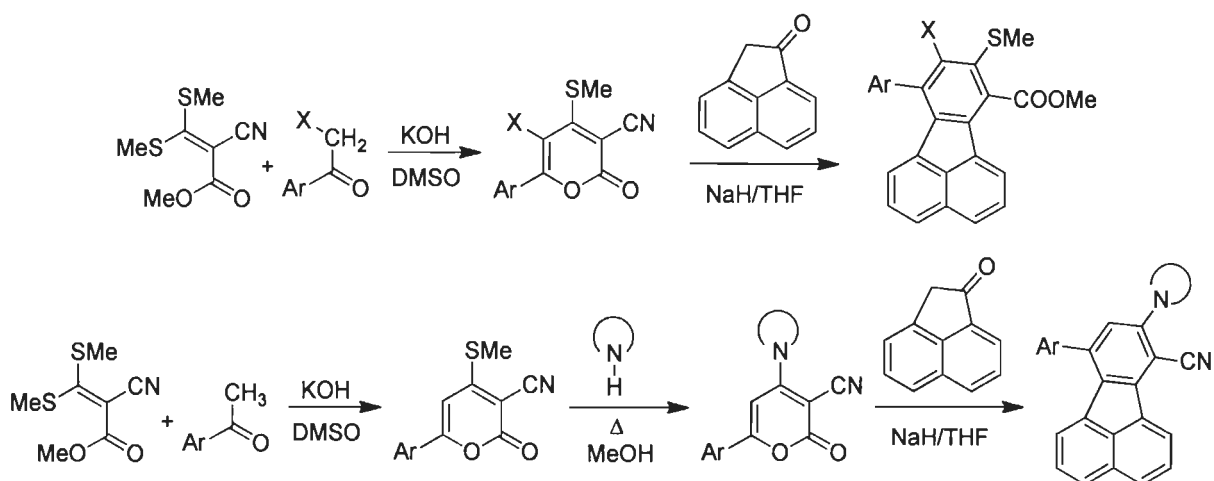
Scheme 1.10 Synthesis of fluoranthene *via* a new Suzuki-Heck type coupling cascade.

Wu et al. (2006) have reported a synthesis of 7,8,9,10-substituted fluoranthenes from the reaction of peri-diyne and alkynes catalyzed by Wilkinson's complex.⁵⁵ For this they started with 1,8-diiodonaphthalene which undergoes Sonogashira cross-coupling with terminal alkynes to obtain diynes. This diyne further reacts with alkyne in the presence of Wilkinson catalyst to produce fluoranthene in good yield.



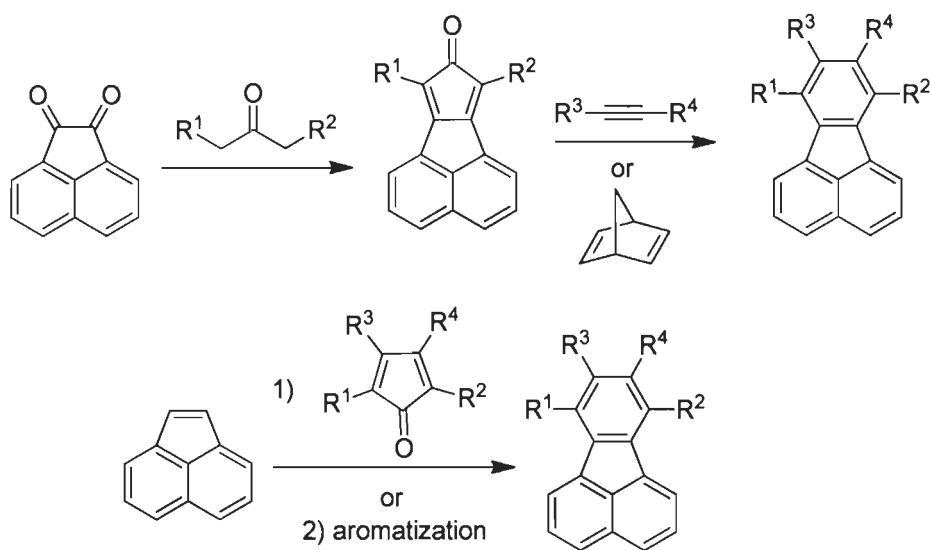
Scheme 1.11 Construction of fluoranthene core using Wilkinson's complex.

Recently Goel et al. (2010) have developed a new strategy to synthesize fluoranthenes with different donor and acceptor.⁵⁶ They reported that the reaction of 2*H*-pyran-2-ones with 2*H*-acenaphthylen-1-one may furnish fluoranthene derivatives *via* carbocation induced ring transformation. Since they have not used the expensive Pd catalyst, this reaction pathway is cheaper as compared to the above procedures.



Scheme 1.12 Synthesis of substituted fluoranthenes.

This is the traditional method for the preparation of fluoranthene. This method proceeds by Diels-Alder reaction of cyclopentadienone derivative with an alkyne or equivalent with the subsequent elimination of carbon mono oxide. Cyclopentadienone derivatives or direct precursors are often generated by the Knoevenagel condensation from a diketone and a ketone. Acenaphthalene undergo (4+2) cycloaddition followed by aromatization to obtain fluoranthenes. This is the simplest method to synthesize fluoranthene skeleton.



Scheme 1.13 Synthesis of fluoranthene *via* Diels-Alder reaction.

As discussed above the optical, electrochemical properties of 9,9-disubstituted fluorenes and polyfluorenes have been intensively studied for electro-optical application. On the other hand its closely related scaffold, fluoranthene have received comparatively less attention. Fluoranthene possess interesting optical, electronic and thermal properties due to its flat π -conjugation framework and rigid skeleton. The oxidatively labile 9-methylene moiety of fluorene is blocked by a 1,9-fused benzene ring in the structure of fluoranthene which make an advantage over fluorene. The absorption spectra of fluoranthene is very complex and contain three groups of bands i) 236 nm, ii) 245-287 nm and iii) 309-359 nm.⁵⁷ Fluoranthene exhibited blue fluorescence

with emission wavelength 444 and 463 nm which make it useful for exploring in electroluminescent devices.

Fluoranthene with π -conjugated system is a promising candidate for making high quality conducting polymers. Xu et al.⁵⁸ synthesized a novel polymer (**A33**) of high quality poly fluoranthene film by direct anodic oxidation of fluoranthene in a middle strong lewis acids boron trifluoride diethyl etherate. These PFA films showed high thermal stability (up to 560 K), good optical and electrochemical properties. Additionally PFA film showed good redox activity and stability even in concentrated sulfuric acid.

Palmaerts et al. have synthesized another polymer namely poly(*p*-fluoranthene vinylene) (**A34**).⁵⁹ This novel conjugated polymer with nonalternant polyaromatic hydrocarbon repeating units, exhibits n-type behavior. Due to their promising redox properties, polymers based on fluoranthene have received interest in optoelectronic device.

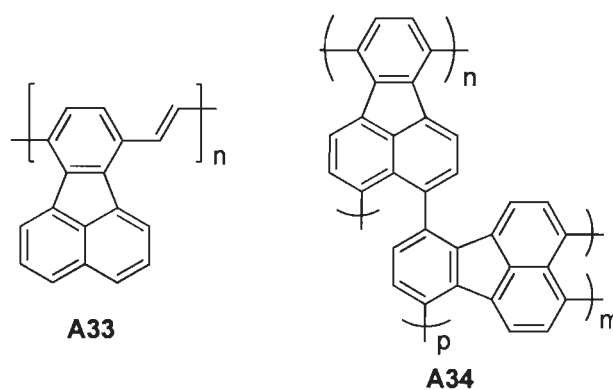


Figure 1.4 Structures of fluoranthene-based polymers.

In one report benzo[*k*]fluoranthene have been used as a side wall in a molecular clip which was used as receptor for electron acceptor molecules.⁶⁰ Sulfur bridged fluoranthene-based organic materials have also been used in developing self assembled microsphere to self-templated nanotubes.⁶¹

Fabrizio et al. have investigated the photophysical, electrochemical and electrogenerated chemiluminescent properties of 9, 10-dimethyl-7,12-diphenyl benzo[*k*]fluoranthene and 9, 10-dimethyl sulfone-7,12-diphenyl benzo[*k*]fluoranthene.⁶²

Yan et al. reported sulfur-hetero fluoranthene and benzo[*k*]fluoranthene organic semiconducting materials (**A35**) which have been used in organic thin film transistors (Figure 1.5).³

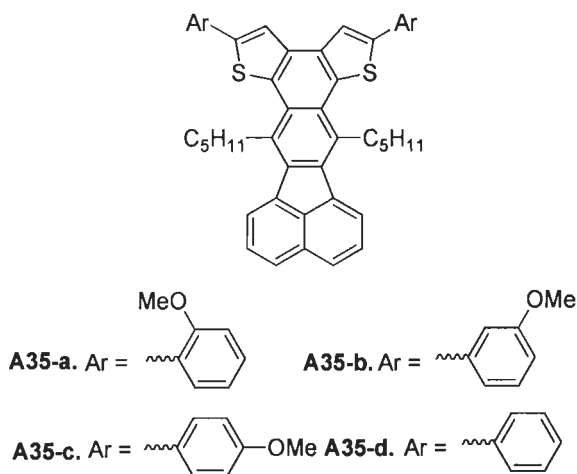


Figure 1.5 Sulfur-hetero benzo[*k*]fluoranthene derivatives: organic semiconducting materials for thin film transistors.

The structure, optical, electrochemical and thermal properties of fluoranthene derivatives (which have been used as function materials in OLED) are summarized in Table 1.4. The data for device fabrication of these derivatives are given in Table 1.5.

Chiechi et al.⁶³ have investigated 7,8,10-triphenyl fluoranthene (**A36**) which is a highly luminescent solid state blue emitting small molecule. The most promising properties of **A36** are its apparent resistance to solid-state quenching/excimer emission (due to twisted peripheral phenyl rings which restrict facial contact) and its high thermal stability for device applications. Electrochemical data reveal that the introduction of three phenyl groups does not significantly change the redox potentials (or HOMO/LUMO gap) from that of fluoranthene. The quantum

yield of **A36** is not the highest among the fluoranthenes. It exhibited quantum yield (Φ) = 0.38 in CH_2Cl_2 and Φ = 0.52 in cyclohexane. The device fabricated using **A36** as emitting layer showed bright blue emission.

Further Kim et al. have reported other 7,8,10-substituted fluoranthene derivative and studied the effect of substituent on photophysical and electrochemical properties.⁶⁴ They have incorporated naphthyl (**A37**) and phenanthrenyl (**A38**) at 8th position of fluoranthene in place of phenyl. In another report⁶⁵ they have studied the effect of electron donating $-\text{CH}_3$ (**A39**) and electron withdrawing $-\text{CN}$ (**A40**) on the para position of phenyl at 8th position. There was no significant difference observed in absorption wavelength by changing the substituent at 8th position of fluoranthene. Only $-\text{CN}$ bearing derivative (**A40**) showed slight red shift which is due to increase in conjugation length due to triple bond of $-\text{CN}$. The emission is also almost similar for all derivatives. The similarity in the HOMO levels reveals that oxidation and reduction is independent of substituents and occurs in fluoranthene. This result can be associated with the results obtained through molecular simulation that indicates the most of electrons on HOMO and LUMO exist in fluoranthene. The electroluminescent data suggests that the EL efficiency can be affected by the side groups as compound **A38** and **A39** showed the better performance. All these derivatives exhibited bright blue emission.

Tong et al. have reported two green emitting fluoranthene derivatives surrounding triphenyl amine or carbazole respectively.^{66,67} Two types of device were fabricated using these derivatives. In one device compound (**A41** & **A42**) act as both hole transporting/emitting layer while in other device it act as emitting layer. **A41**⁶⁶ showed better efficiency when used as hole transporting/emitting layer while **A42**⁶⁷ exhibited higher efficiency when used as emitting layer. Triphenyl amine is stronger donor than carbazole, hence it raises the HOMO/LUMO levels

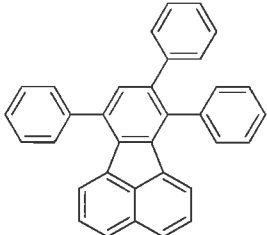
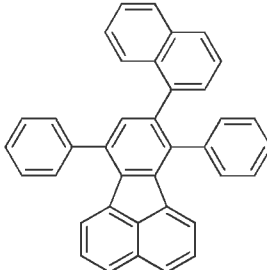
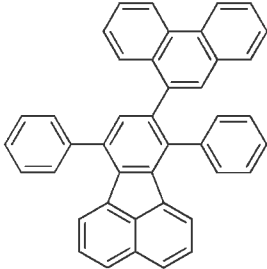
which facilitates the transportation of holes. The devices using these derivatives exhibited green emission.

Recently, Xia et al. have synthesized and characterized a new series of green emitting benzo[*k*]fluoranthene derivatives (**A43-A46**) incorporating with diaryl amine at 3rd position.⁹ These derivatives displayed high thermal stability. These derivatives were employed as hole transporter and green emitter in OLED device. Derivative gave better performance when used as emitting layer and NPB used as hole transporting layer.

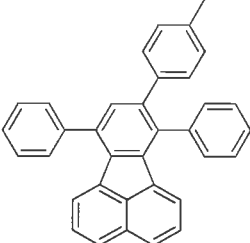
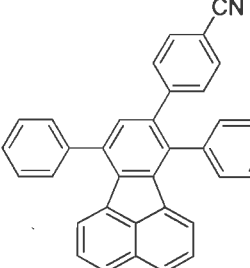
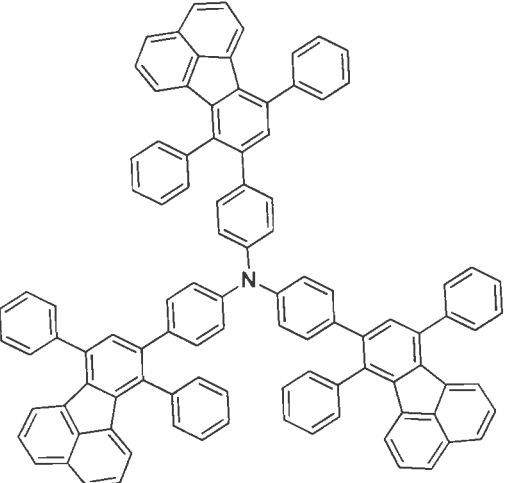
Recently Goel et al.⁵⁶ have synthesized and characterized a novel series of yellow light emitting fluoranthenes (**A47-A49**) with an amine donor (pyrrolidine or piperidine) and nitrile acceptor. All the derivatives are thermally stable. These highly efficient nondoped fluoranthene-based yellow OLEDs exhibited bright yellow fluorescence, high quantum efficiency, and good thermal stability. Thus, the donor/acceptor at 7th and 8th position is responsible for red shift in absorption and emission profile. It also improves the thermal stability and better tunes the HOMO/LUMO levels to explored as yellow emitting material.

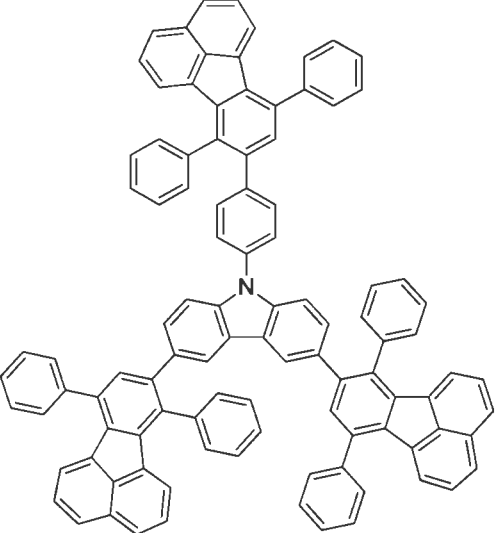
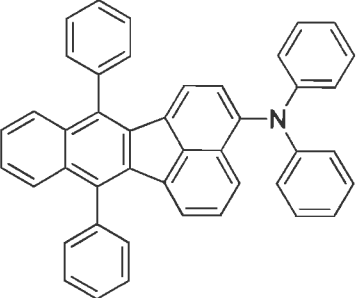
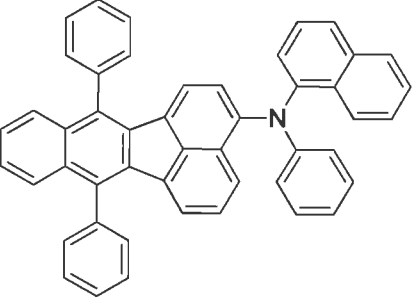
Huang et al.⁶⁸ have reported red emitting benzo[*a*]aceanthrylene derivatives with two peripheral amine donors. The photophysical and electrochemical properties has changed by changing the donor systems. Diphenylamine donor substituted derivative (**A50**) exhibited red shifted absorption/emission (510/638 nm) as compared to carbazole containing derivative (**A51**, 460/572 nm). This is due to the weak donor strength of carbazole as compared to diphenylamine. **A50** showed almost similar absorption/emission as **A52** (510/636 nm). HOMO level increases as the donor strength increases **A51** (5.38 eV) < **A50** = **A54** (5.18 eV), < **A52** (5.13 eV) < **A54** (5.09 eV). Thus, anthracene increases the donor strength more. Additionally **A51** and **A54** showed high thermal stability with high glass transition due to presence of anthracene and carbazole.

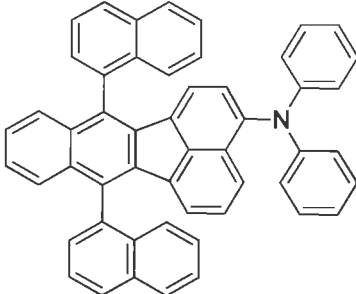
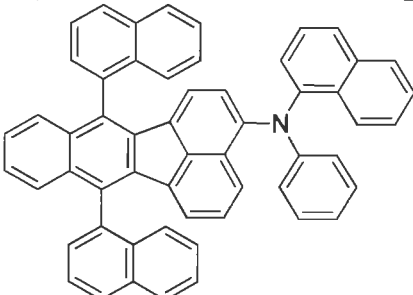
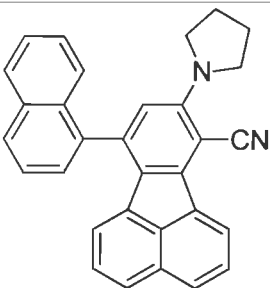
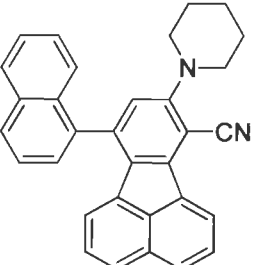
Table 1.4 Optical, electrochemical and thermal properties of fluoranthene-based emitting materials.

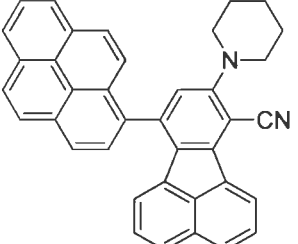
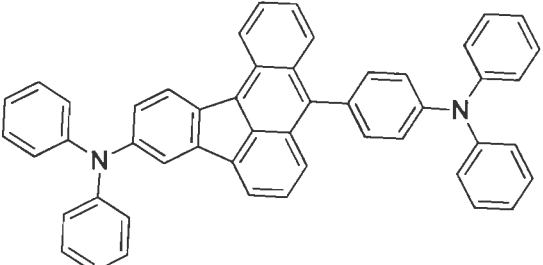
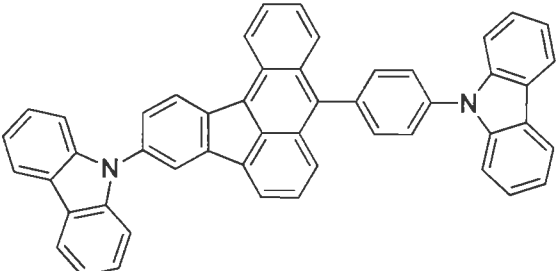
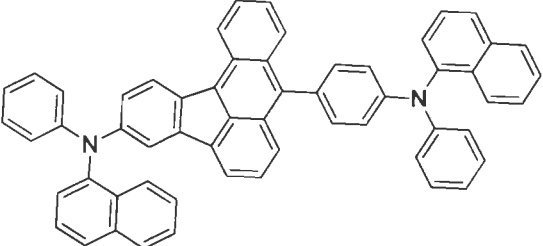
S.N.	Compounds	λ_{abs} , nm	λ_{em} , nm (Φ)		E_g , eV	HOMO, eV	LUMO, eV	$T_g/T_m/T_d$, °C	Ref.
			Solution	Thin film					
A36		381	458	468	3.02	5.84	2.82	NA/199/323	64
A37		380	460	NA	3.03	5.88	2.85	106/228/347	64
A38		380	461	NA	3.01	5.88	2.87	136/303/371	64

Polyaromatic Hydrocarbon-Based Functional Materials

A39		380	461	NA	3.03	5.85	2.82	NA/262/337	65
A40		384	453	NA	2.99	5.89	2.90	NA/236/393	65
A41		NA	NA	494	2.60	5.40	2.80	237/NA/550	66

A42		NA	NA	483	2.70	5.70	3.0	NA/NA/NA	67
A43		259, 312, 439	520, 525 (0.25)		2.58	5.26	2.68	162/NA/468	14
A44		259, 313, 438	516, 521 (0.24)	NA	2.61	5.27	2.66	185/NA/489	9

A45		260, 305, 439	526, 531 (0.24)	NA	2.58	5.28	2.70	191/NA/478	9
A46		258, 306, 436	518, 522 (0.22)	NA	2.61	5.32	2.71	205/NA/514	9
A47		338, 357, 440	550 (0.56)	NA	2.77	5.27	2.77	NA/239/600	56
A48		331	552 (0.36)	NA	2.49	5.34	2.85	NA/206/435	56

A49		332	549 (0.51)	NA	2.46	5.51	2.85	NA/330/470	56
A50		352, 414, 438, 510	638 (0.05)	627 (0.04)	2.03	5.18	3.15	113/224/430	68
A51		331, 460	572 (0.23)	575(sh), 610 (0.16)	2.26	5.38	3.12	178/299/460	68
A52		349, 413, 435, 510	636 (0.07)	623 (0.09)	2.07	5.13	3.06	151/393/420	68

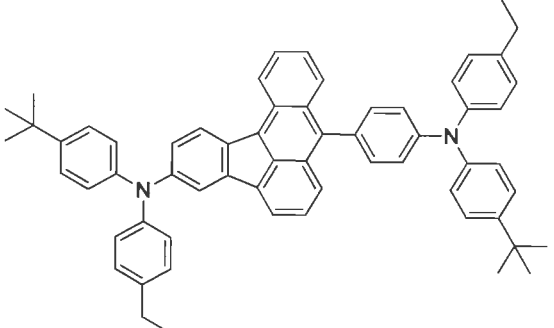
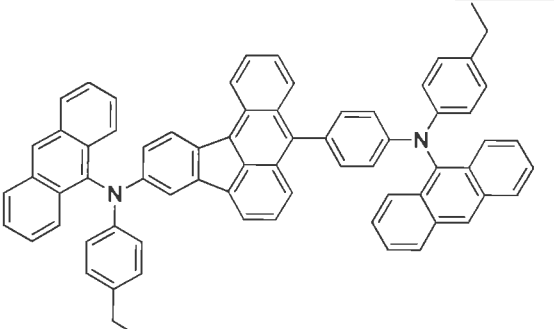
A53		359, 439, 520	661 (0.05)	637 (0.09)	1.89	5.18	3.29	143/NA/440	68
A54		325, 440, 520, 552(sh)	634 (0.09)	636 (0.04), 715 (sh)	1.97	5.09	3.12	202/NA/440	68

Table 1.5 OLED performance of fluoranthene derivatives A36-A54.

Device	Power efficiency (lm/W)	Current efficiency (Cd/A)	Turn-on voltage	Max. brightness (Cd/m ²)	$\eta_{\text{ext,max}}$ %	EL _{max} (nm)	CIE (x, y)
ITO/PEDOT/NPB/CBP/A36/BCP/Ca/Al	1.10	3.02	2.3	5910	1.83	456, 480	(0.18, 0.24)
ITO/2-TNATA/NPB/A36/Alq ₃ /LiF/Al	1.63	3.27	NA	NA	NA	471	0.19, 0.26
ITO/2-TNATA/NPB/A37/Alq ₃ /LiF/Al	1.64	3.24	NA	NA	NA	470	0.19, 0.26
ITO/2-TNATA/NPB/A38/Alq ₃ /LiF/Al	2.11	3.96	NA	NA	NA	478	0.22, 0.33
ITO/2-TNATA/NPB/A39/Alq ₃ /LiF/Al	1.84	3.62	NA	NA	NA	470	0.18, 0.25
ITO/2-TNATA/NPB/A40/Alq ₃ /LiF/Al	0.13	0.28	NA	NA	NA	513	0.28, 0.46

ITO/A41/BPhen/LiF/Al	10.6	9.9	2.65	NA	3.37	504	0.24, 0.54
ITO/NPB/A41/BPhen/LiF/Al	5.6	7.8	2.60	NA	2.64	508	0.24, 0.54
ITO/A42/BPhen/LiF/Al	3.7	3.2	2.68	NA	0.93	524	0.33, 0.55
ITO/NPB/A42/BPhen/LiF/Al	12.1	10.1	2.53	NA	3.57	511	0.25, 0.49
ITO/A43/TPBI/Al	4.7	4.1	2.8	10190	1.6	512	0.28, 0.61
ITO/A44/TPBI/Al	5.7	5.0	2.8	12370	2.0	512	0.26, 0.61
ITO/2-TNATA/A44/TPBI/Al	6.7	10.2	4.7	17840	3.1	512	0.28, 0.61
ITO/A45/TPBI/Al	4.8	4.5	2.9	7957	1.7	516	0.30, 0.61
ITO/A46/TPBI/Al	1.8	2.1	3.0	5703	0.7	516	0.29, 0.61
ITO/PEDOT:PSS/NPB/A47/BCP/Ca/Al	NA	NA	3.0	410	NA	554	NA
ITO/PEDOT:PSS/NPB/A48/BCP/Ca/Al	NA	2.0	2.6	470	NA	557	NA
ITO/PEDOT:PSS/NPB/A49/BCP/Ca/Al	NA	NA	3.0	420	NA	559	NA
ITO/A50/TPBI/Mg:Ag/Ag	0.26	0.50	3.4	5436	0.46	624	0.64, 0.34
ITO/A50/Alq ₃ /Mg:Ag/Ag	0.37	0.91	3.6	9315	0.58	624	0.51, 0.43
ITO/NPB/A50/TPBI/Mg:Ag/Ag	0.33	0.53	3.4	4451	0.48	624	0.63, 0.34
ITO/NPB/A50/BCP/Alq ₃ /Mg:Ag/Ag	0.23	0.52	4.2	4514	0.49	626	0.65, 0.35
ITO/A51/TPBI/Mg:Ag/Ag	0.74	1.70	4.1	15993	0.73	578	0.51, 0.45
ITO/A51/Alq ₃ /Mg:Ag/Ag	2.20	3.90	3.4	31632	1.40	566	0.46, 0.49
ITO/A52/TPBI/Mg:Ag/Ag	0.18	0.42	3.8	4416	0.39	624	0.64, 0.34
ITO/A52/Alq ₃ /Mg:Ag/Ag	0.37	0.97	3.8	8765	0.63	622	0.53, 0.42
ITO/NPB/A52/TPBI/Mg:Ag/Ag	0.38	0.57	3.3	5225	0.51	622	0.64, 0.34
ITO/NPB/A52/BCP/Alq ₃ /Mg:Ag/Ag	0.60	0.77	3.8	4643	0.68	624	0.65, 0.35
ITO/A53/TPBI/Mg:Ag/Ag	0.30	0.53	3.8	3936	0.63	632	0.62, 0.31
ITO/A53/Alq ₃ /Mg:Ag/Ag	0.74	0.99	3.5	7432	0.68	630	0.49, 0.43
ITO/NPB/A53/TPBI/Mg:Ag/Ag	0.33	0.42	3.7	2921	0.49	630	0.59, 0.30
ITO/NPB/A53/BCP/Alq ₃ /Mg:Ag/Ag	0.27	0.31	4.1	2705	0.33	632	0.65, 0.34
ITO/A54/TPBI/Mg:Ag/Ag	0.12	0.28	3.9	1528	0.46	630	0.64, 0.32
ITO/A54/Alq ₃ /Mg:Ag/Ag	0.66	1.02	3.6	6279	0.58	624	0.45, 0.46
ITO/NPB/A54/TPBI/Mg:Ag/Ag	0.30	0.33	3.4	1534	0.48	628	0.64, 0.33
ITO/NPB/A54/BCP/Alq ₃ /Mg:Ag/Ag	0.17	0.36	4.0	1764	0.49	626	0.66, 0.34

Due to its extended π -conjugation, charge transporting properties, fluoranthene unit can also be potential candidate for photovoltaic application. Recently Ma and Wu et al. reported organic dyes for DSSC application which contains fluoranthene as a donor, phenylethynyl or thiophene as a spacer and cyanoacrylic acid or rhodamine-3-acetic acid as an acceptor.^{69,70} The structure of these dyes are shown in Figure 1.6 and related data given in Table 1.6. There was no much difference in absorption wavelength observed for all the dyes but the molar extinction coefficient is higher for **A55**. Moreover **A55** (4.4%) exhibited the best performance than other two dyes (**A56**, 1.6% and **A57**, 3.7%). The V_{oc} is higher for **A57**. The results indicate that the device perform better when thiophene was used as spacer and cyanoacrylic acid was used as acceptor.

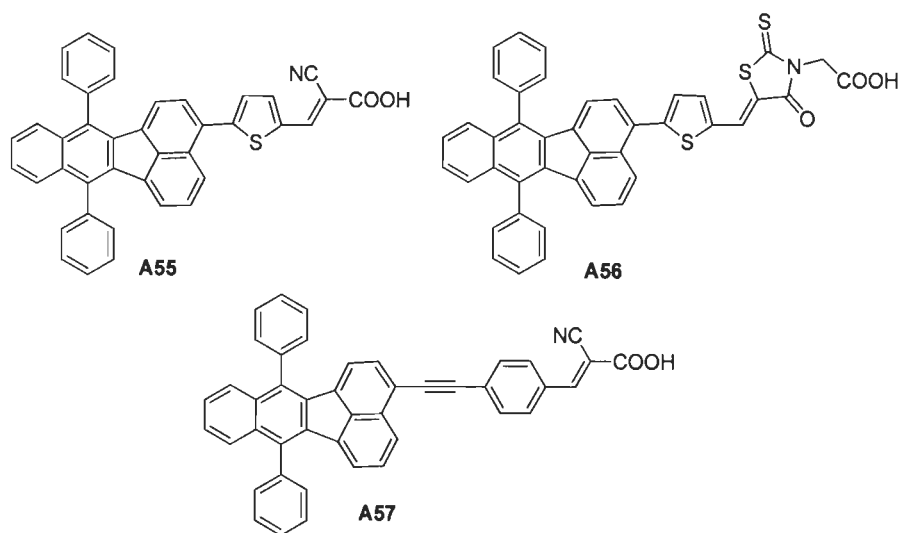


Figure 1.6 Fluoranthene-based organic dyes suitable for DSSC.

Table 1.6 Optical, electrochemical and DSSC data of the fluoranthene-based organic dyes (**A55**-**A57**).

S.N.	λ_{abs} , nm ($\epsilon \times 10^3$, $M^{-1} \text{cm}^{-1}$)	λ_{em} , nm (Φ)	HOMO/LUMO	V_{oc} , V	J_{sc} , mAcm^{-2}	FF	η , %	Ref.
A55	445 (27.0), 354 (18.0), 302 (28.0)	589	5.10/2.80	0.53	14.71	0.54	4.4	69
A56	464 (15.0), 339 (8.0), 301 (16.0)	589	5.06/2.87	0.50	5.02	0.64	1.6	69
A57	433 (19.0), 352 (16.0), 302 (15.0)	589	5.24/2.83	0.59	9.53	0.66	3.7	69

1.5.3 Triphenylene-based organic materials

Triphenylene-based columnar discotic LCs shows great potential as molecular organic materials for optoelectronic devices due to their photoconductivity and high charge carrier mobilities. Rego et al. have reported hexaalkoxy as discotic liquid crystals.⁷¹ Heppke et al. have reported chiral discotic triphenylene derivatives exhibiting a cholesteric blue phase and a ferroelectrically switchable columnar mesophase.⁷² The discotic liquid crystalline materials have been proposed as potential candidate for optoelectronic devices. For instance Bayer et al. have introduced the opto electronic properties of triphenylene-based polymer discotics.⁷³

Christ et al. (1997) have reported hexaalkoxy triphenylenes (**A58**, **A59**) as host material for LED application.⁷⁴ At the same time Bacher et al. (1997) have demonstrated monomer (**A60**), dimer (**A61**) and polymer (**A62**) as hole transporting materials for OLED.⁷⁵ They have also synthesized triphenylene-based polymers from the monomers (**A63-A66**) and demonstrated them as insoluble hole transporter in two layer OLED in their another report.⁷⁶

Freudenmann and co workers⁷⁷ (2001) have synthesized novel-conjugated bridged triphenylene derivative containing cyanomethyl group (**A67**) which is useful for linking two triphenyl system to obtain **A68**. The highly conjugated bridged bistrisphenylenes (**A68**) exhibit strong orange to red photoluminescence ($\lambda_{\text{max}} = 630$ to 660 nm). They show a strong bathochromic shift of more than 250 nm when compared with a single triphenylene system. Moreover **A68** exhibit bright orange to red electroluminescence which is visible in daylight and used as emissive layer in OLED.

Mao et al. (2007) have reported a triphenylene dimer (**A69**) as hole transporting material for OLED.⁷⁸ This dimer exhibited excellent film-forming properties. This compound also showed sufficient charge-carrier mobility and good hole transporting properties. Thus, the hexa-alkoxy

based triphenylenes or bis triphenylenes have proven as potential candidate for OLEDs as hole transporting or emitting material. Recently Yu et al. reported bistriphenylenes as blue emitter in OLED.¹⁰

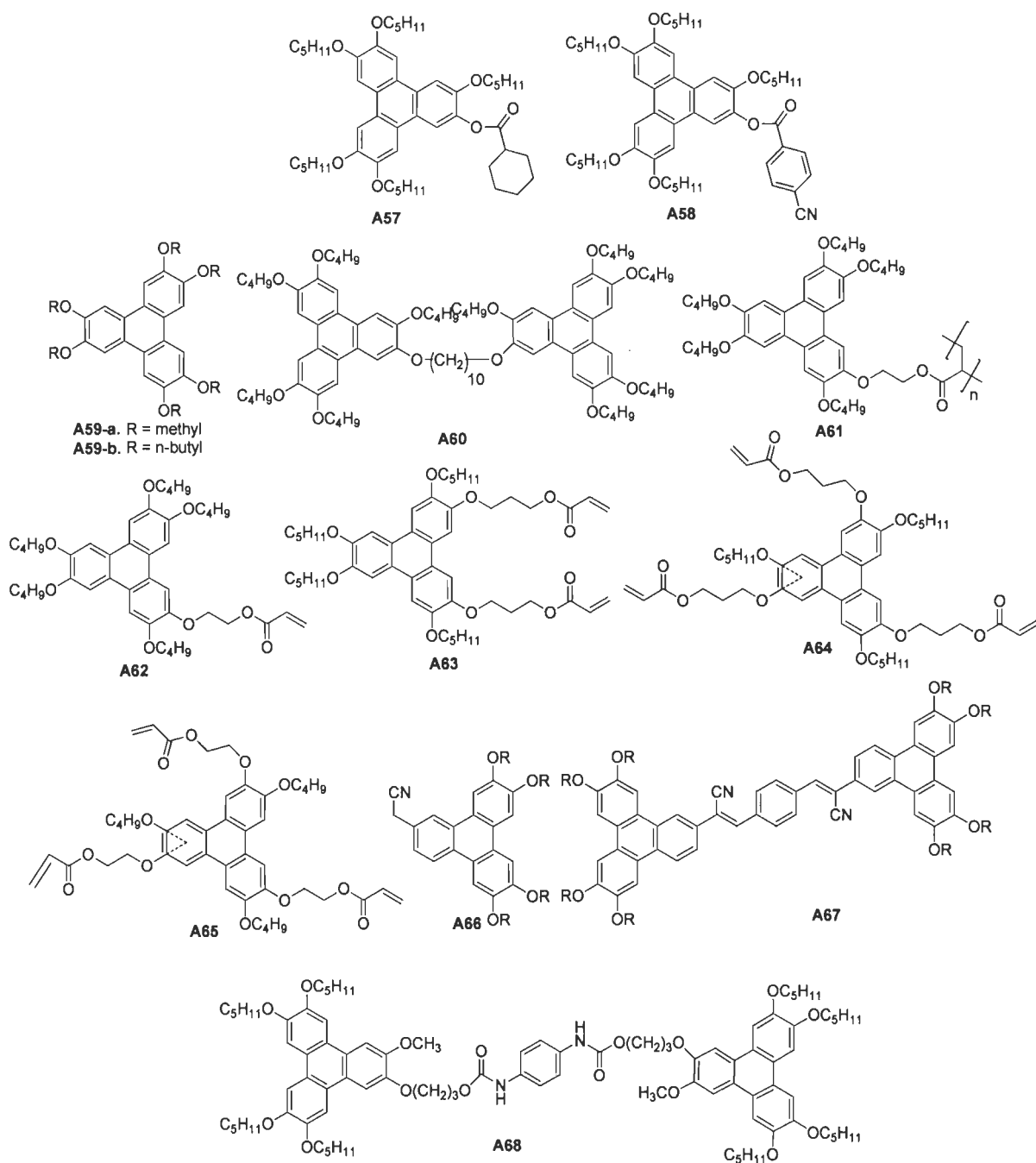


Figure 1.7 Structures of hexaalkoxy functionalized triphenylenes used as OLED materials.

The above discussion indicate that most of the triphenylene monomers have used as hole transporting material in OLED except **A68**. Recently Saleh et al. have synthesized triphenylene based polymers (**A70-a** and **A70-b**) which have been used in blue emitting polymer light emitting diodes.¹² They have demonstrated that the twisted phenyl rings around the triphenylene main core inhibit π - π stacking in the polymers resulting in almost identical photoluminescence (PL) spectra in both solutions and films. These polymers displayed deep blue emission in the range of 430-450 nm.

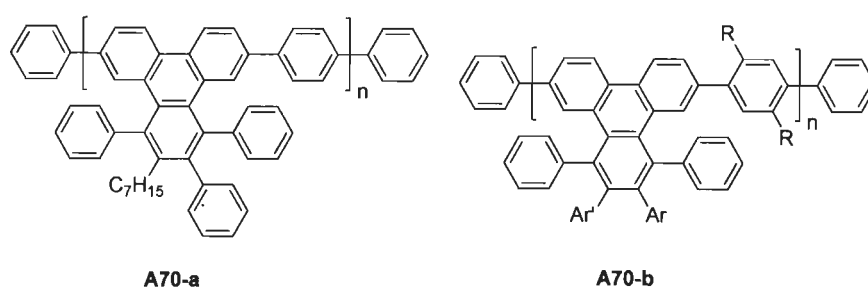


Figure 1.8 Structures of triphenylene-based polymers.

R. Nandy and S. Sankararaman studied absorption/emission, solvatochromism and intramolecular charge transfer of donor-acceptor substituted phenylethynyltriphenylenes (**A70-A76**).⁷⁹ The optical and electrochemical data is given in Table 1.7. All the derivatives exhibited low energy absorption band in the range of 334-367 nm in cyclohexane. The absorption wavelength was found higher than the parent triphenylene due to extended conjugation with phenylethynyl group. **A70** and **A71** showed similar low energy band which a red shift observed for **A72-A76**. The extent of red shift was higher for **A76**. There was no significant difference in absorption wavelength by changing solvent polarity which indicate that ground state is polar irrespective of substituent present over it. There was no change in emission wavelength of **A70** and **A71** by changing the solvent polarity from cyclohexane (CH) to DMSO due to absence of substitution and presence of e- withdrawing group at meta-position. The emission is due to

locally excited state of phenylethynyltriphenylene. **A72-A75** showed slight red shifted emission in DMSO due to presence of e- withdrawing group and **A76** exhibited prominent red shift in DMSO due to ICT from dimethylamine to triphenylene. **A76** showed the highest quantum yield. **A73, A74** exhibited lower quantum yield in ethanol due to hydrogen bonding interaction.

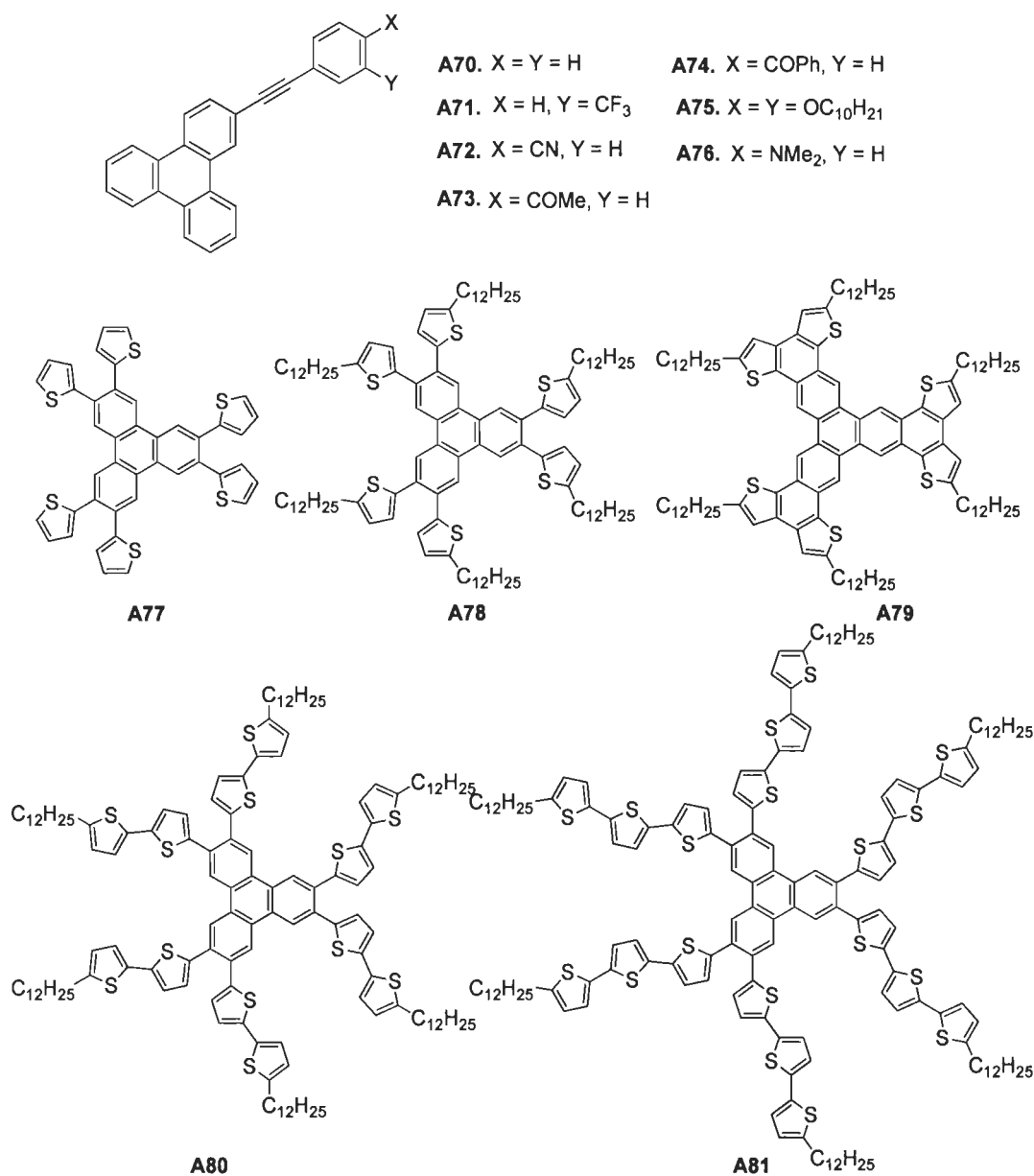


Figure 1.9 Structures of phenylethynyltriphenylenes (**A70-A76**) and star shaped oligothiophene-substituted triphenylenes (**A77-A81**).

Table 1.7 Optical and electrochemical data of the compounds **A70-A76**.

S.N.	Solvent	λ_{abs} , nm	λ_{em} , nm (Φ)	E_g , eV	$E_{p(\text{ox})}$ vs SCE	$E_{p(\text{red})}$ vs SCE	Ref.
A70	CH	334	370 (0.20)	3.42	+1.60	-2.14	79
	DMSO	336	371 (0.28)				
A71	CH	334	368 (0.17)	3.41	+1.65	-2.02	79
	DMSO	337	373 (0.35)				
A72	CH	349	362 (0.60)	3.30	+1.68	-1.85	79
	DMSO	353	412 (0.54)				
A73	CH	351	383 (NA)	3.27	+1.66	-1.70	79
	EtOH	353	434 (0.32)				
A74	CH	354	381 (NA)	3.20	+1.63	-1.63	79
	EtOH	350	490 (0.11)				
A75	CH	343	365 (0.58)	3.19	NA	NA	79
	DMSO	348	421 (0.43)				
A76	CH	367	380 (0.99)	2.97	+0.76	-2.27	79
	DMSO	367	499 (0.36)				

Table 1.8 Optical and electrochemical data of the compounds **A77-A81**.

S.N.	Solvent	λ_{abs} , nm		λ_{em} , nm		E_g , eV	HOMO, eV	LUMO, eV	Ref.
		Solution	Thin film	Solution	Thin film				
A77	CHCl ₃	330	345	430	448	3.14	5.62	2.48	80
A78	CHCl ₃	330	348	430	445	3.14	5.51	2.37	80
A79	CHCl ₃	355	360	435	557	2.82	5.48	2.66	80
A80	CHCl ₃	365	378	483	550	2.85	5.38	2.53	80
A81	CHCl ₃	396	409	500	589	2.65	5.19	2.54	80

Luo et al. reported synthesis, photophysical properties and self assembly of oligothiophene substituted fused triphenylenes (**A77-A81**).⁸⁰ The absorption is due to π - π^* transition. It can be seen that the absorption maxima shows bathochromic shift as the no. of thiophene increases (λ_{max} **A81**, 396 > **A80**, 365 > **A78**, 330 nm). The similar trend was observed for emission wavelength. The absorption/emission is similar for **A77** and **A78** indicating no effect of dodecyl chain. The absorption and emission is broad and red shift when recorded in thin film which suggests the formation of aggregates. The HOMO level raises and band gap decreases with the increasing thiophene unit.

1.5.4 Pyrene-based functional materials

Pyrene is an alternant PAH and consists of four fused benzene rings resulting in a large flat aromatic system. Pyrene is a colorless solid and pyrene forms during incomplete combustion of organic material and therefore can be isolated from coal tar together with a broad range of related compounds. Pyrene has been the subject of tremendous investigation. It exhibits remarkable photophysical and electrochemical properties. Its emission is pure blue which permit it for use as an emissive material in OLEDs. But its tendency to form dimer (excimer) in the excited state obstructs its use. Aggregation leads to an additional emission band at longer wavelength and decrease in electroluminescence. This problem of aggregation can be sorted out by proper substitution on pyrene. Mono-, di-, tri- and tetra derivatives of pyrene have been studied. The substitution is easy on 1, 3, 6 and 8 position of pyrene. 2,7- and 4,5,9,10-substituted derivatives are also known. Hu et al. have found 1,3,6,8-substituted cruciform shaped pyrene derivatives more red shifted absorption and emission profile as compared to 4,5,9,10-substituted derivatives due to the difference in the conjugation pathway.⁸¹

Pyrene derivatives are widely used in various electronic devices due to their unique emission and electronic properties. Pyrene derivatives have wide area of applications. They have been used as biological markers, ion sensors, conformational probes and fluorescent probes in biophysical chemistry. Rathfon et al. have reported pyrene imines incorporated into films and sub-micrometer fibres used for fluorimetric nerve gas sensing.⁸² Pyrene-aza-15-crown ether compounds provide sensitive probes for the detection of metal ions in solution *via* fluorescence and the magnetic field effect.⁸³ Techert et al. have discussed the photophysical characteristics, time-resolved fluorescence and solvatochromism study of pyrene-dimethylamine derivative which is a charge transfer dye laser.⁸⁴

Pyrene derivatives exhibit columnar discotic liquid crystalline nature which also makes them useful for electronic application. de Halleux et al.⁸⁵ have reported tetraphenyl substituted pyrene derivatives (**A82**) for their potential to induce columnar mesophase but none of them showed liquid crystalline properties due to the steric hindrance between the stacked molecules. On the basis of the results they conclude that columnar fluorescent mesophases can be achieved if the size of the rigid pyrene core is extended and peripheral phenyl groups can be replaced by the substituent inducing less steric hindrance between stacked molecules. After that Hayer et al. have reported tetrakis(trisalkoxy-phenylethynyl)pyrene discotic mesogen (**A83**) that forms hexagonal and rectangular columnar mesophases.⁸⁶ These discotics exhibited high fluorescence quantum yield. The excitation energy transfer over large distances is possible with the high efficiency coupled with columnar arrangement generated upon self assembly which might be proven beneficial for optoelectronic application. Thus, the ethynyl linkage is helpful in generating more planar structure and also enhances the extent of conjugation and energy transfer possibility.

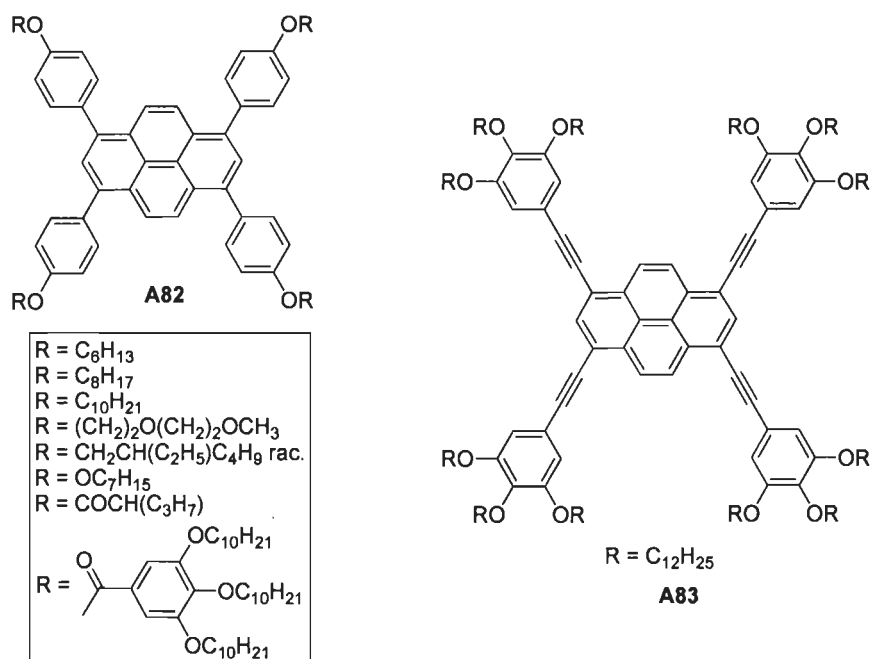


Figure 1.10 Structures of pyrene-based liquid crystalline compounds showing columnar phase.

Gunderson et al.⁸⁷ have been reported the observation of multiple excitation energy transfer (EET) pathways in a covalently linked 20-(4ethynylphenyl)Chl to 1,3,6,8-positions of pyrene. The results indicate that EET contributing pathways may provide greater avenues for designing efficient light harvesting in future artificial photosynthetic systems. Thayumanavan and co-workers⁸⁸ have also reported energy and electron transfer process *via* pyrene phenyl amine donor in the dendritic and linear macromolecular architecture which can be utilized for photovoltaic application due to efficient photoinduced charge separation.

Kim et al. have studied two photon absorption properties of alkynyl substituted pyrene derivatives.⁸⁹ They synthesized a series of pyrene derivatives (**A84**) with 4-(*N,N*-dimethyl amino)phenyl ethynyl group as substituent. The results indicate that pyrene is an efficient π -center for two-photon absorption and its derivative exhibited large TPA cross section (δ) and

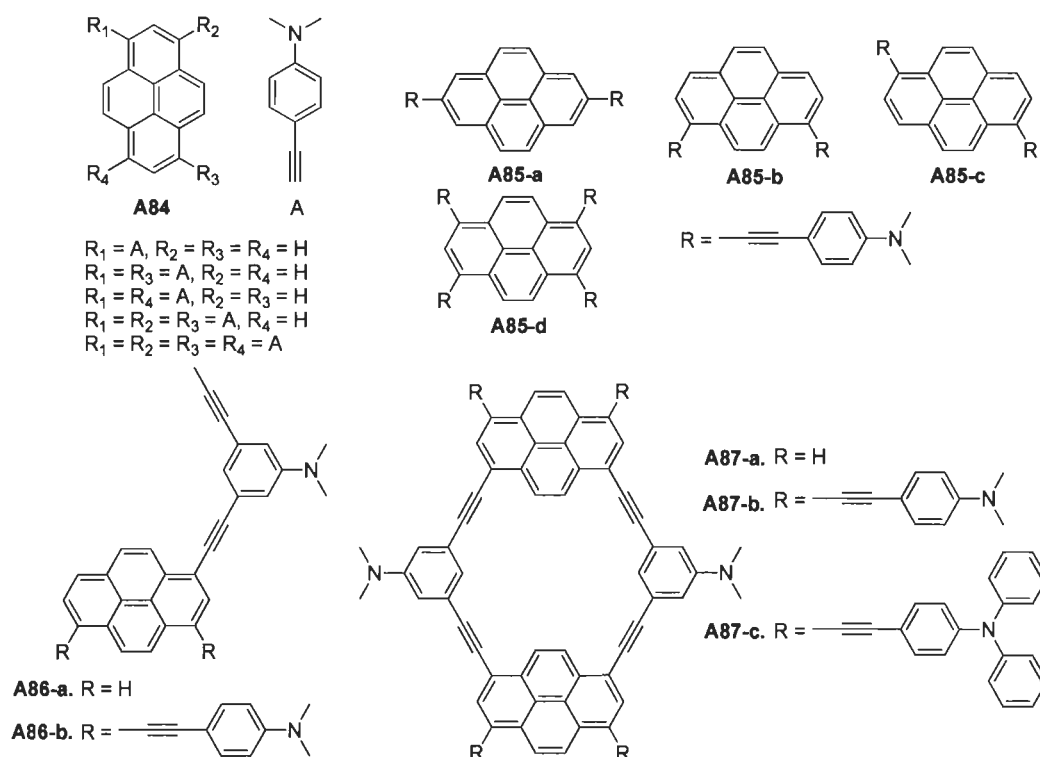


Figure 1.11 Structures of pyrene-based two photon absorbing materials.

high quantum efficiency (Φ) nearly 1.0 which can be comparable with most efficient two photon absorbing materials. Molecular symmetry also play an important role in the design of two photon absorbing materials as they indicate quadrupolar molecules have larger value of δ than those of dipolar molecules.

Recently Zhao et al.⁹⁰ have done the theoretical study on one- or two photon absorption properties of a series of pyrene derivatives (A85-A87) and conclude the following ways to enlarge the TPA cross section 1) by introducing donor group to pyrene, 2) increasing the number of donor group, 3) extending the conjugation length, 4) circular conjugated system is useful for increasing TPA. Position of donor group also affects δ value.

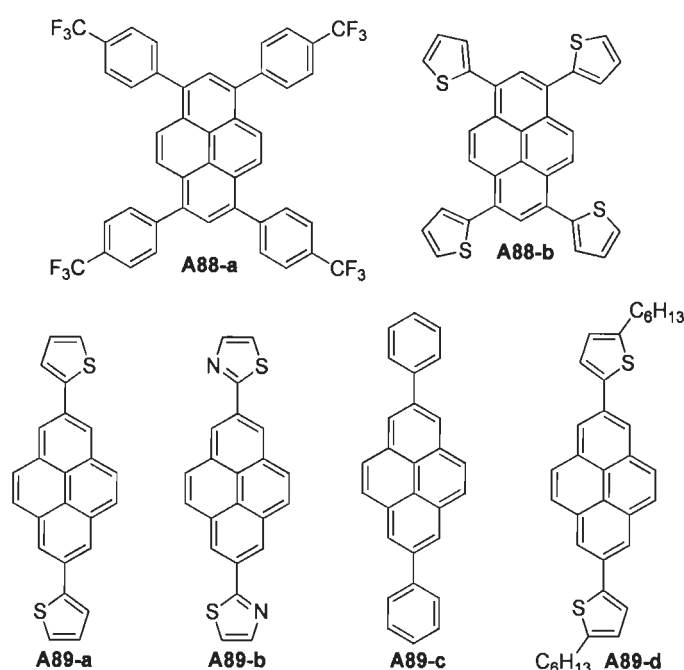


Figure 1.12 Examples of pyrene derivatives demonstrated to function as efficient materials in OFET.

Indeed pyrene derivatives exhibited liquid crystalline behavior and forms columnar phase *via* self assembly. Additionally they also exhibited two photon absorption and charge transporting properties. Thus, pyrene is an important candidate to explore its properties for opto-electronic application. Zhang et al. have synthesized pyrene derivative with trifluoromethylphenyl (A88-a)

and thienyl aromatic substituent (**A88-b**) and showed its performance as *p*-type semiconductor in FET devices.⁹¹ Recently Qiao et al.⁹² have synthesized a series of 2,7-disubstituted pyrene derivatives. All the derivatives displayed thermal and oxidative stability in air. They have explored the molecular structure property relationship by changing the substituent. The planarity of 2,7-dithienylpyrene (**A89-a**) has remarkably improved as compared to previously reported 1,3,6,8-tetrathienyl pyrene which enhance the π - π interaction in the solid state and make them better *p*-type semiconductor for OFET. Thus, variation of substituent and position of substituent both are the key factor in defining properties contributed the molecular structure.

The structure and properties of blue emitting pyrene derivatives are given in Table 1.9 and their OLED performance shown in Table 1.10. Yang et al. have synthesized the simplest two pyrene derivatives 1,1'-dipyrene (**A90**) and 1,4-dipyrenyl benzene (**A91**) and fabricated greenish blue organic diodes using them.⁹³ Both pyrene hydrocarbon based derivatives without heteroatom exhibited high thermal stability and good device performance. **A91** showed better power efficiency (5.18 lm/W) at a voltage, current density, and luminance of 5.2V, 20 mA/cm², and 1714 cd/m², respectively as compared to **A90**. This indicates pyrenyl group is a good luminescent centre and a phenyl group inserting between two pyrenes increase the device performance. These devices showed greenish blue emission. Probably the emission from ETL (Alq₃, which is a green emitting material) is also taking part due to the less difference in the HOMO level of **A90** or **A91** and Alq₃.

Tang et al. have reported fluorene or spirofluorene substituted pyrene derivatives as efficient blue emitters in OLED in their several reports.⁹⁴⁻⁹⁶ Compounds **A92**, **A93** and **A94** exhibited not only high thermal stability but also shown improved hole-injection and hole-transporting ability. The corresponding HOMO energy levels were calculated to be 5.24 and 5.22 eV, indicating that

the electron-rich pyrene derivatives can have an increase in hole efficiency and an improvement in hole-injection ability than conjugated fluorene derivatives. The device performance has improved for **A93** as compared to **A92**, which is due to presence of another pyrene which is in conjugation of fluorene. Other spirofluorene conjugated pyrene derivatives (**A95**, **A96**) have also been proven as promising family of PAHs for opto-electronic applications.

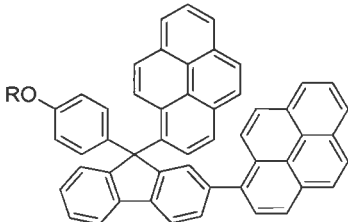
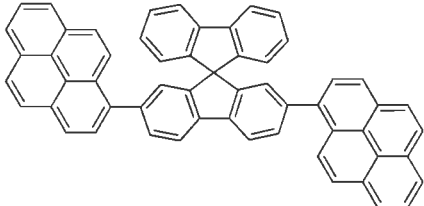
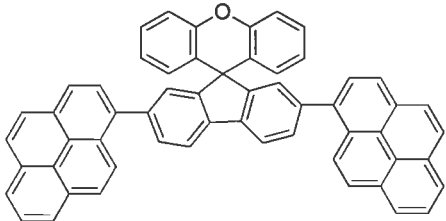
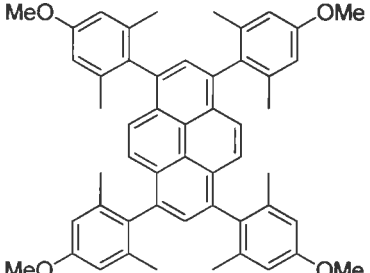
Moorthy⁹⁷ have reported sterically congested tetraarylpyrene **A97** can be readily accessed *via* facile Suzuki coupling and that the 4-fold functionalization manifests in steric inhibition of molecular aggregation in both solution (UV-vis and fluorescence) and solid states (photoluminescence and crystal packing). Thus, the terta substituted derivatives are less prone to molecular aggregation. The arene units so attached impart thermal stability and noncrystalline property to permit the potential of **A97** as emissive materials in OLEDs to be readily explored. The devices fabricated for **A97** lead to pure blue electroluminescence with respectable device performances.

The molecular aggregation or π - π stacking can lowers the device performance by quenching fluorescence emission and electroluminescence. The aggregation can be avoided by acquiring these common methods such as i) incorporation of polyphenyl dendron, ii) incorporation of non planar di- or tri-aryl amines. In short the introduction of the unit (onto PAH backbone) which can make the molecule nonplanar is useful for avoiding aggregation and also helpful in enhancing thermal stability, amorphous nature and thus, device performance.

Recently Lai et al.⁹⁸ have reported triphenylamine incorporated pyrene derivatives (**A98**) which showed red shifted absorption and emission profile as compared to the derivatives without amine. It also increases the HOMO/LUMO levels and decreases the band gap. The triaryl amines unit imparts the dual function to the molecule. Triaryl amine incorporating molecule can act as

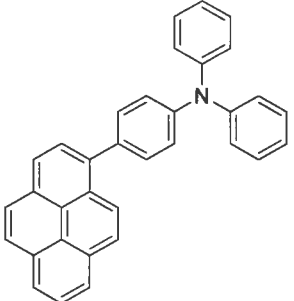
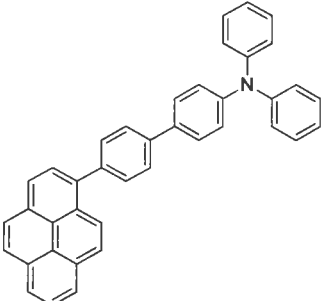
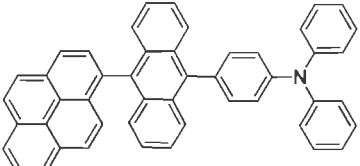
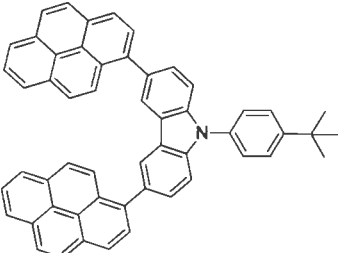
Table 1.9 Optical, electrochemical and thermal properties of pyrene based-blue emitting materials

Sample code	Compound	λ_{abs} , nm	λ_{em} , nm (Φ)		E_g , eV	HOMO, eV	LUMO, eV	$T_g/T_d/T_m$, °C	Ref.
			solution	Film					
A90		280, 330, 349	430 (1.03)	NA	3.14	5.40	2.26	NA/336/417	93
A91		281, 352	426 (1.99)	NA	3.20	5.70	2.50	146/301/466	93
A92		351	408 (0.71)	462	3.05	5.24	2.23	NA/274/459	94
A93		352	424 (0.75)	450	2.88	5.22	2.51	217/359/478	94

A94	 <p>R = 2-ethylhexyl</p>	352	425 (0.74)	459	2.83	5.32	2.49	191/NA/430	95
A95		364	421	NA	2.98	5.55	2.57	NA/NA/NA	96
A96		364	422	NA	2.98	5.59	2.61	NA/NA/NA	96
A97		367	411 (0.38)	442	3.20	5.80	2.60	NA/249/392	97



Polyaromatic Hydrocarbon-Based Functional Materials

A98		374	452 (0.74)	NA	2.82	5.19	2.37	NA/160/416	98
A99		242, 280, 354	469 (0.65)	453	3.0	5.20	2.20	98/278/NA	99
A100		399	444 (0.48)	468	2.70	5.63	2.93	162/NA/NA	100
A101		358 (film)	NA (0.95)	443	2.99	5.57	2.58	NA/293/496	101

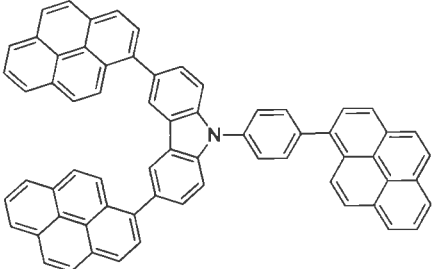
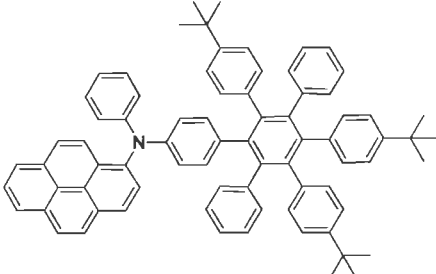
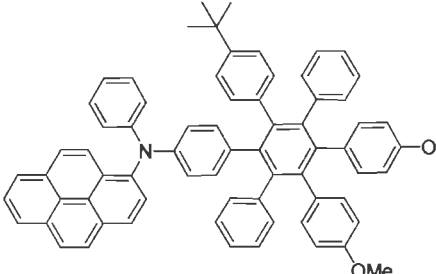
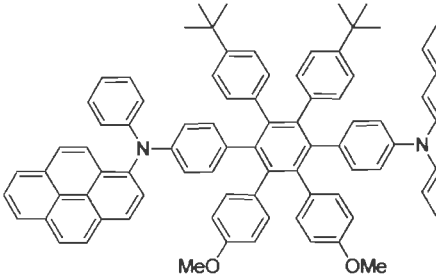
A102		369 (film)	NA (0.95)	465	2.96	5.67	2.71	NA/245/516	101
A103		274, 317, 388, 405	494 (0.27)	474	2.76	5.19	2.43	141/272/449	8
A104		274, 317, 387, 406	494 (0.49)	470	2.79	5.19	2.40	140/240/456	8
A105		274, 317, 327, 387, 406	492 (0.48)	490	2.82	5.19	2.37	151/333/540	8

Table 1.10 OLED performance of A90-A105.

Device	Power efficiency (lm/W)	Current efficiency (Cd/A)	Turn-on voltage	Max. brightness (Cd/m ²)	$\eta_{\text{ext,max}}$, %	EL _{max} (nm)	CIE (x, y)
ITO/NPB/A90/BCP/Alq ₃ /LiF/Al	4.09	7.30 (5.6 V)	NA	1459	NA	488	0.21, 0.35
ITO/NPB/A91/BCP/Alq ₃ /LiF/Al	5.18	8.57 (5.2 V)	NA	1714	NA	468	0.19, 0.25
ITO/TCTA/A92/BCP/Mg:Ag	0.85	2.56	4.0	16664	NA	450	0.17, 0.17
ITO/TCTA/A93/BCP/Mg:Ag	1.17	3.08	3.5	19885	NA	455	0.17, 0.19
ITO/TCTA/A94/BCP/Mg:Ag	NA	3.04	4.0	11620	NA	470	0.18, 0.23
ITO/PEDOT:PSS/A96/CsF/Al	NA	1.10	4.3	2000	NA	422	0.16, 0.08
ITO/NPB/A97/TPBI/LiF/Al	1.03	2.70	4.0	4730	3.26	448	0.14, 0.09
ITO/A98/TPBI/LiF/Al	2.01	1.92	2.8	NA	1.97	462	0.14, 0.11
ITO/NPB/A98/TPBI/LiF/Al	1.85	1.72	NA	NA	1.62	462	0.14, 0.11
ITONPB/A99/ LiF/Al	NA	NA	NA	299 at 22V	NA	446	NA
ITO/A99/F-TBB/Alq ₃ /LiF/Al	NA	0.40 at 19V	8.0	2152 at 24V	NA	453	NA
ITO/NPB/A100/TPBI/LiF/Mg:Ag	6.8	7.9	2.9	NA	NA	480	0.15, 0.30
ITO/A100/TPBI/LiF/Mg:Ag	5.1	6.1	3.0	NA	NA	476	0.15, 0.28
ITO/A101/TPBI/LiF/Al	4.45	4.25	2.7	NA	2.49	475	0.17, 0.25
ITO/NPB/A101/TPBI/LiF/Al	2.72	2.94	2.7	NA	2.21	475	0.15, 0.18
ITO/A102/TPBI/LiF/Al*	3.34	3.76	2.9	NA	2.01	475,558	0.21, 0.26
ITO/NPB/A102/TPBI/LiF/Al*	3.54	6.42	2.8	NA	3.11	475,558	0.22, 0.29
ITO/A103/TPBI/Mg:Ag	NA	3.8 at 6.8V	3.0	21150 at 14V	2.7	474	0.13, 0.21
ITO/A104/TPBI/Mg:Ag	NA	3.5 at 7.0V	3.0	20590 at 14V	2.6	472	0.13, 0.20
ITO/A104/TPBI/Alq ₃ /Mg:Ag	NA	3.4 at 8.7V	3.5	16210 at 15V	2.2	474	0.13, 0.22
ITO/A104/TPOB/Alq ₃ /Mg:Ag	NA	1.9 at 10 V	4.0	7820 at 15V	1.4	476	0.13, 0.23

*yellow emitting device

both hole transporting and emitting materials. This is manifested by diarylamino functionalized pyrene derivatives, **A99** (reported by Jia et al.)⁹⁹ which have been used to perform dual function hole transporter and emitter in blue OLED device.

Tao et al. have reported three anthracene–triphenylamine derivatives for highly efficient non-doped blue OLED device incorporated with phenyl, naphthyl and pyrenyl group respectively.¹⁰⁰ Out of which the pyrene derivative (**A100**) showed highest glass transition temperature. The absorption spectra of **A100** have two major bands. The peak at higher wavelength with the range from 350-400 nm can be attributed to the π - π^* transitions of the middle anthracene core of the compounds. The absorption bands at 300-340 nm come from the combination of the n - π^* transition of triphenylamine moieties and the π - π^* transitions of the substituted pyrene on the anthracene core. **A100**-based device gave good results when used as emitting layer and exhibits highly efficient sky-blue emission with a maximum efficiency of 7.9 cd/A (6.8 lm/W) in a nondoped device structure.

Recently Lai and coworkers¹⁰¹ have synthesized two carbazole-pyrene derivatives (**A101** and **A102**) and designed OLED devices using them as both hole transporting and emitting or only emitting layer. **A102** exhibited bathochromic shift in absorption/emission profile and showed higher decomposition temperature as compared to **A101**. This may be due to the presence of fused polyaromatic pyrene in place of tertiary butyl group which enhances the conjugation and also increases rigidity of the molecule. The device using **A101** as emitting layer showed a single peak of blue emission with CIE coordinates of (0.15, 0.18); whereas **A102**-based devices exhibited two emission peaks at blue and yellow region with CIE coordinates of (0.22, 0.29). The difference in their EL spectra is attributed to the presence of fused polyaromatic pyrene in **A102** in place of tertiary butyl group of **A101**, which effectively increases the electron-

donating property and results in exciplex formation at its interface with the electron-accepting TPBI. Moreover **A102**-based device displayed the higher device efficiency ($\eta = 3.11\%$) with yellow emission.

Thomas et al. have synthesized a series of blue emitting hexaphenylphenylene dendronized pyrenylamine derivatives for OLEDs and compared their photophysical and electrochemical properties.⁸ **A103** and **A104** exhibited almost similar absorption profile and displayed three prominent bands. Out of which the most bathochromically shifted band ascribed to charge transfer state from amine to pyrene. No significant difference was observed in the absorption wavelength of **A105** and **A104** but the molar extinction coefficient was found higher for **A105**. This suggests that most of the transitions are originating from pyrenylamine unit. Presence of hexaphenyl phenylene dendron and diarylamine unit inhibits molecular aggregation. **A105** exhibited high T_g/T_d (151/540 °C) as compared to **A103** and **A104**. This indicates that diarylamine unit is responsible for increasing the thermal stability.

The above examples of pyrene derivatives are blue emitting and some of them which are incorporated with the aryl amines perform both functions like hole transport as well as blue emission. Figure 1.13 displayed some examples of pyrene derivatives which showed variable properties. These can be categorized into 1) green emitting, 2) green emitting with hole transporting properties and 3) electron transporting materials. The low energy absorption band can originate due to increase in the conjugation pathway or due to aggregation/excimer formation. The aggregation may lead to emission quenching of fluorophore.

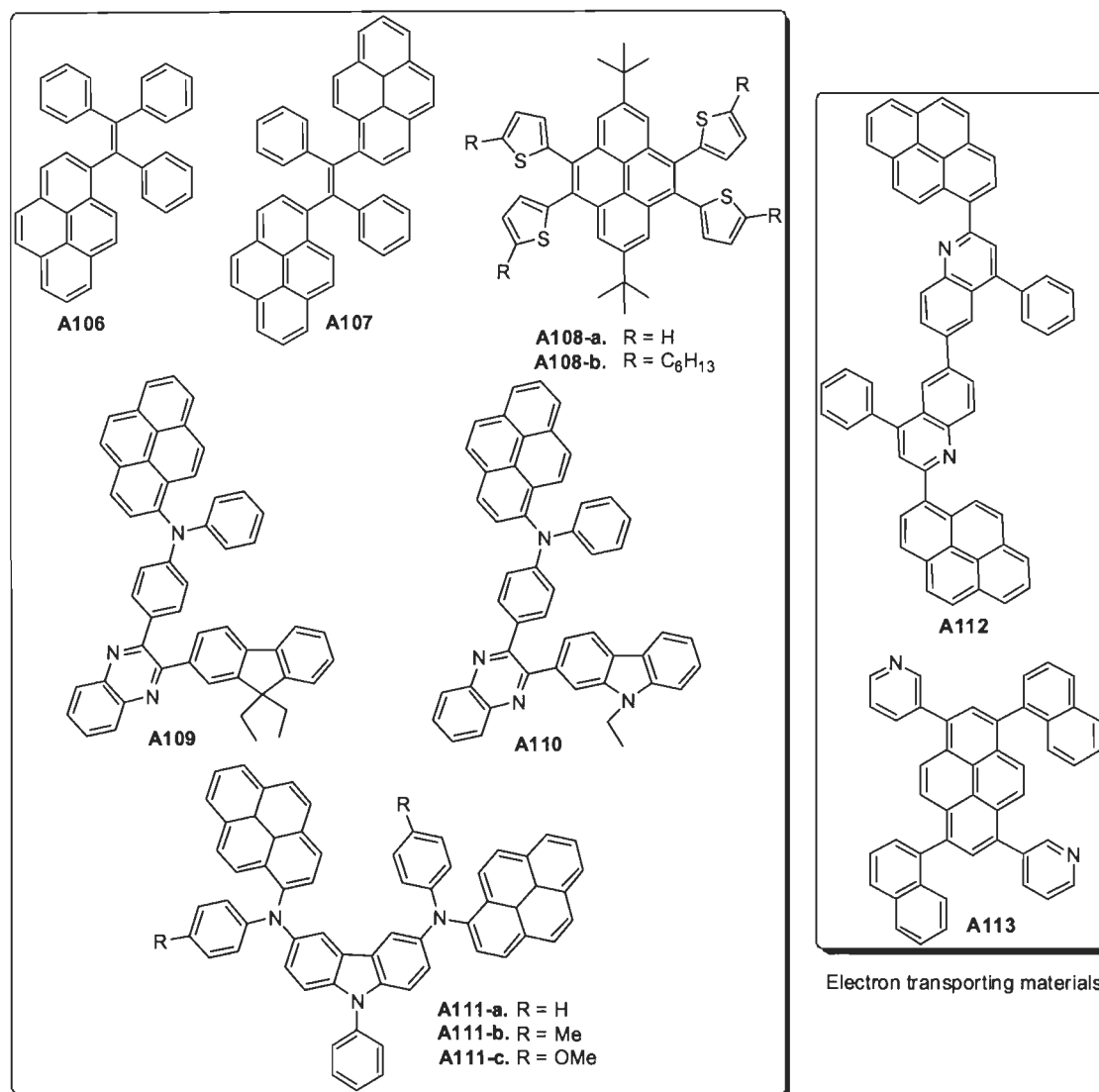
But recently Zhao et al.¹⁰² have reported pyrene-substituted ethenes (**A106**, **A107**) which showed aggregation-enhanced excimer emission with high fluorescence quantum yield and gave highly efficient electroluminescent when fabricated as emitters in OLEDs. The derivatives

reported by them are weakly emissive in solution but become strong emitters when aggregated in condensed phase. They told that The π - π intermolecular interactions between the pyrene rings, coupled with multiple C-H \cdots π hydrogen bonds, efficiently prevent intramolecular rotations, due to which nonradiative energy decay channel block, and hence dye molecules become highly emissive in the solid state. The emission color of the pyrene derivatives can tune by changing the substituent. The multilayer devices using **A106** and **A107** as host emitters exhibit outstanding performances. The **A107**-based devices show low turn-on voltage (3.2 V) with high luminance (149830 cd/m²), and power, current and external quantum efficiencies (9.2 lm/W, 10.2 cd/A and 3.3%, respectively). The obtained results indicate that the present pyrene derivatives are promising materials for the construction of efficient non-doped green OLEDs.

Pyrene derivatives can also show multiple functionality (hole transporting and emitting) in the presence of strong electron donor such as thiophene. Duan et al.¹⁰³ have synthesized and characterized novel pyrene derivatives containing thienyl groups (**A108**). These derivatives showed relatively large band gaps and low HOMO levels which imply that these materials have high stability against photo-degradation, and may be promising candidates for stable hole-transporting materials. Pyrene derivatives can act as hole transporting or electron transporting material. Additionally they have also demonstrated that these derivatives can grow as large-size micro-wires by a simple solution evaporation process due to their good solubility, extended π - π stacking and van der Waals attractions between the alkyl chains.

Thomas et al.¹⁰⁴ have reported several green emitting carbazole derivatives incorporated with diarylamine with pyrene chromophoric unit. The additional group such as methyl and -OMe affect the photophysical and electrochemical properties. The absorption/emission profile increases as the strength of electron donating group increases. Thus, **A111-c** showed red shifted

absorption and emission as compare to **A111-a** and **A111-b**. These three derivatives exhibited high thermal stability. These materials were used as green emitting and hole transporting material with performance.



Green emitting and hole transporting or hole transporting materials

Figure 1.13 Structures of multifunctional pyrene derivatives.

Thomas et al.¹⁷ have further reported a class of green emitting material comprising quinoxaline, triarylamine and fluorophore such as carbazole, pyrene and fluorene. Both the derivatives showed similar absorption wavelength while **A110** show blue shifted emission as

compared to A109. This suggests that incorporation of fluorene and pyrene red shifts the emission profile and also improve brightness of the emission in the devices. The thermal stability is higher for A110 as compared to A109. This indicates that fragments such as carbazole and pyrene enhance the thermal properties like glass transition temperature and decomposition temperature.

Table 1.11 Optical, thermal and electrochemical properties of A106-A113.

Code	λ_{abs} , nm	λ_{em} , nm (Φ)		E_g , eV	HOMO, eV	LUMO, eV	$T_g/T_m/T_d$, °C	Ref.
	solution	Solution	film					
A106	353	388	484	NA	NA	NA	NA/203/269	102
A107	352	391	503	NA	NA	NA	NA/279/370	102
A108-a	359	NA	NA	3.21	5.84	2.63	NA/>300/NA	103
A108-b	362	NA	NA	3.10	5.68	2.58	NA/113/NA	103
A109	317, 401	574 (0.05)	NA	2.76	5.30	2.54	125/NA/410	17
A110	317, 402	567 (0.1)	NA	2.75	5.29	2.54	146/NA/425	17
A111-a	318, 408	539 (0.12)	512	2.76	4.97	2.21	180/355/463	104
A111-b	319, 415	543 (0.11)	529	2.67	4.91	2.24	184/NA/513	104
A111-c	319, 420	553 (0.19)	541	2.62	4.86	2.24	183/NA/455	104
A112	286, 344 (sh), 380	440 (0.91)	491	2.70	5.86	3.16	176/379/NA	105
A113	380	421	NA	3.03	6.14	3.11	172/377/NA	106

Some pyrene derivatives are also reported as electron transporting material. Hancock et al.¹⁰⁵ have reported oligoquinoline bearing pyrenyl end group as efficient blue emitting and electron transporting materials. Further Oh et al.¹⁰⁶ have reported tetra substituted pyrene derivative having two electron deficient quinoline as electron transport material.

Although various OLED devices have been fabricated using pyrene derivatives as functional materials but the pyrene-based organic dyes for DSSC application are limited. Recently Thomas and coworkers¹⁰⁷ have synthesized organic dyes containing pyrenoimidazole as a donor,

cyanoacrylic acid as acceptor and oligothiophene as a π -linker. The trend of red shift in absorption was found as λ_{\max} **A114** (405 nm) < **A115-a** (452 nm) < **A115-b** (464 nm). The absorption shifted towards longer wavelength as the no. of thiophene unit increases. Thiophene also raises the HOMO level of the dye as **A115-b** exhibited the higher HOMO level (5.34 eV) as compared to that of **A114** (5.60 eV) and **A115-a** (5.43 eV). Thus, by changing the conjugation of π -linker, electro-optical properties can be tuned. **A115-b** displayed the higher device performance ($V_{oc} = 543$ mV, $J_{sc} = 15.5$ mA cm⁻², $\eta = 5.65\%$).

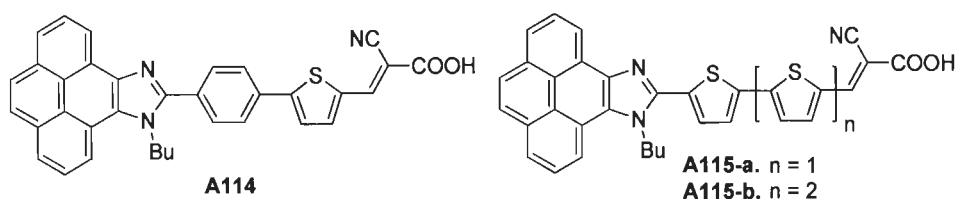


Figure 1.14 Structures of pyrenoimidazole-based organic dyes used in DSSC as sensitizer.

1.6 Conclusions and outlook

The above discussion reveals that the use of PAH-based derivatives in electronic devices such as OFET, OLED and DSSC is noticeable due to their unique optical, charge transporting and liquid crystalline properties. Therefore an acute research has been focused on the optical, thermal and electrochemical properties of materials based on fluorene, fluoranthene, triphenylene and pyrene as a means to improve OLED and DSSC performance through balanced electron and hole injection, transport and stability. The study of photophysical and electrochemical properties of emitting material discussed above reveals that these derivatives can also function as hole or electron transporting material depending on the substituent present over it. In general, electron rich di- or triaryl amine incorporated derivatives act as hole transporting materials while electron deficient such as quinoxaline, oxadiazole, imidazole-bearing derivatives perform as electron

transporter. For instance **A19** with diphenylamine unit acted as hole transporting layer while **A20** with benzimidazole perform electron transporting function.

The effectiveness of an organic material for OLEDs is determined by their molecular structure and properties such as absorption/emission properties, thermal and electrochemical stability. Thermal stability was improved by incorporating polyaromatic backbone and triarylamine such as **A41** displayed very high glass transition (237°C) and high decomposition temperature (550°C). Carbazole derivatives (**A51**, T_g/T_d 178/460°C) showed higher thermal stability as compared to triphenyl amines (**A50**, T_g/T_d 113/430°C) due to fused structure of the former. Presence of di- or tri-aryl amines also enhances the absorption/emission profile and improves the hole transporting ability of molecule by rising the HOMO level as indicated by **A3**, 5.73 eV and **A4**, 5.22 eV. Other than triarylmines, the presence of thiophene improves the optical properties and raises HOMO levels and decreases the band gap. Phenylethynyl also red shifts the absorption/emission profile.

DSSC performance is influenced by various factors such as changing the donor strength, increasing the spacer length, type of acceptor unit which may lead to enhance optical and charge transporting properties. Polyaromatic segments such as pyrene or fluorene with an amine donor increases the donor strength which might lead to high V_{oc} and device efficiency. For instance **A28** showed higher V_{oc} (0.61 V) and η (4.82 %) than **A27** (0.58V, 4.34%) due to presence of fluorene in the former. Thiophene as a spacer increases the charge transporting properties which lead to improved charge injection from dye to TiO_2 layer, and hence increase the device performance. Cyanoacrylic acid is a better acceptor than rhodamine-3-acetic acid for DSSC. As **A55** with thiophene as a spacer and cyanoacrylic acid as acceptor exhibited higher device performance ($J_{sc} = 14.71 \text{ mAcm}^{-1}$, $V_{oc} = 0.53$ and $\eta = 4.4\%$) as compared to **A56** and **A57**.

It was demonstrated without doubt in several studies aggregation of PAH lead to inferior device performance in both OLED and DSSC. From many studies it was found that intermolecular stacking interactions have been avoided by introducing bulkier non planar structural elements such as triarylamine and polyphenylated benzene units.

Our aim of research is to design and synthesize PAHs with different substituent for systematic investigation of their structure property relationship and the tuning of its properties for specific application. The attempts in current research have focused on examining the optical, thermal and electrochemical properties of functional materials based on fluorene, fluoranthene, triphenylene and pyrene PAH backbone and their application in electronic device such as OLED and DSSC. Additionally incorporation with heterocycles such as thiophene and quinoxalines may lead to enhance optical, thermal and charge transporting properties. Thus, the diarylamines and polyphenyl backbone was incorporated to increase the thermal stability. Additionally diarylamine red shifts the absorption and emission profile and also helpful in maintaining amorphism.

1.7 References

1. Debije, M. G.; Piris, J.; de Haas, M. P.; Warman, J. M.; Tomović, Ž.; Simpson, C. D.; Watson, M. D.; Müllen, K. "The optical and charge transport properties of discotic materials with large aromatic hydrocarbon cores" *J. Am. Chem. Soc.* **2004**, *126*, 4641.
2. Cao, X.-Y.; Zi, H.; Zhang, W.; Lu, H.; Pei, J. "Star-shaped and linear nanosized molecules functionalized with hexa-peri-hexabenzocoronene: synthesis and optical properties" *J. Org. Chem.* **2005**, *70*, 3645.

3. Yan, Q.; Zhou, Y.; Ni, B.-B.; Ma, Y.; Wang, J.; Pei, J.; Cao, Y. "Organic semiconducting materials from sulfur-hetero benzo[*k*]fluoranthene derivatives: synthesis, photophysical properties, and thin film transistor fabrication" *J. Org. Chem.* **2008**, *73*, 5328.
4. Zhao, Z.; Li, J.-H.; Chen, X.; Wang, X.; Lu, P.; Yang, Y. "Solution-processable stiff dendrimers: synthesis, photophysics, film morphology, and electroluminescence" *J. Org. Chem.* **2009**, *74*, 383.
5. Wong, W. W. H.; Jones, D. J.; Yan, C.; Watkins, S. E.; King, S.; Haque, S. A.; Wen, X.; Ghiggino, K. P.; Holmes, A. B. "Synthesis, photophysical, and device properties of novel dendrimers based on a fluorene hexabenzocoronene (FHBC) Core" *Org. Lett.* **2009**, *11*, 975.
6. Bernhardt, S.; Kastler, M.; Enkelmann, V.; Baumgarten, M.; Müllen, K. "Pyrene as chromophore and electrophore: encapsulation in a rigid polyphenylene shell" *Chem. Eur. J.* **2006**, *12*, 6117.
7. Park, J.-W.; Kang, P.; Park, H.; Oh, H.-Y.; Yang, J.-H.; Kim, Y.-H.; Kwon, S.-K. "Synthesis and properties of blue-light-emitting anthracene derivative with diphenylamino-fluorene" *Dyes Pigms.* **2010**, *85*, 93.
8. Thomas, K. R. J.; Velusamy, M.; Lin, J. T.; Chuen, C. H.; Tao, Y.-T. "Hexaphenylphenylene dendronised pyrenylamines for efficient organic light-emitting diodes" *J. Mater. Chem.* **2005**, *15*, 4453.
9. Xia, Z.-Y.; Su, J.-H.; Fan, H.-H.; Cheah, K.-W.; Tian, H.; Chen, C. H. "Multifunctional diarylamine-substituted benzo[*k*]fluoranthene derivatives as green electroluminescent emitters and nonlinear optical materials" *J. Phys. Chem. C* **2010**, *114*, 11602.

10. Yu, J.-Y.; Huang, M.-J.; Chen, C. H.; Lin, C.-S.; Cheng, C.-H. "On the improvement of blue emission for all sp^2 -hybridized bistriphenylenyls: incorporating phenylenyl moieties to enhance film amorphism" *J. Phys. Chem. C* **2009**, *113*, 7405.
11. Balaji, G.; Kale, T. S.; Keerthi, A.; Pelle, A. M. D.; Thayumanavan, S.; Valiyaveetil, S. "Low band gap thiophene-perylene diimide systems with tunable charge transport properties" *Org. Lett.* **2011**, *13*, 18.
12. Saleh, M.; Baumgarten, M.; Mavrinskiy, A.; Schäfer, T.; Müllen, K. "Triphenylene-based polymers for blue polymeric light emitting diodes" *Macromolecules* **2010**, *43*, 137.
13. Li, Z. H.; Wong, M. S.; Tao, Y.; Lu, J. "Diphenylamino end-capped oligofluorenes with enhanced functional properties for blue light emission: synthesis and structure–property relationships" *Chem. Eur. J.* **2005**, *11*, 3285.
14. Thomas, K. R. J.; Lin, J. T.; Hsu, Y.-C.; Ho, K.-C. "Organic dyes containing thienylfluorene conjugation for solar cells" *Chem. Commun.* **2005**, 4098.
15. Earmme, T.; Ahmed, E.; Jenekhe, S. A. "Solution-processed highly efficient blue phosphorescent polymer light-emitting diodes enabled by a new electron transport material" *Adv. Mater.* **2010**, *22*, 4744.
16. Fisher, A. L.; Linton, K. E.; Kamtekar, K. T.; Pearson, C.; Bryce, M. R.; Petty, M. C. "Efficient deep-blue electroluminescence from an ambipolar fluorescent emitter in a single-active-layer device" *Chem. Mater.* **2011**, *23*, 1640.
17. Thomas, K. R. J.; Velusamy, M.; Lin, J. T.; Chuen, C.-H.; Tao, Y.-T. "Chromophore-labeled quinoxaline derivatives as efficient electroluminescent materials" *Chem. Mater.* **2005**, *17*, 1860.

18. Ren, S.; Zeng, D.; Zhong, H.; Wang, Y.; Qian, S.; Fang, Q. "Star-shaped donor- π -acceptor conjugated oligomers with 1,3,5-triazine cores: convergent synthesis and multifunctional properties" *J. Phys. Chem. B* **2010**, *114*, 10374.
19. Tang C. W.; Slyke, S. A. V. "Organic electroluminescent diodes" *Appl. Phys. Lett.* **1987**, *51*, 913.
20. Burroughes, J. H.; Bradley, D. D. C.; Brown, A. R.; Marks, R. N.; Mackay, K.; Friend, R. H.; Burn, P. L.; Holmes, A. B. "Light emitting diodes based on conjugated polymers" *Nature* **1990**, *347*, 539.
21. Shunmugam, R.; Tew, G. N. "White-light emission from mixing blue and red-emitting metal complexes" *Polym. Adv. Technol.* **2008**, *19*, 596.
22. Shunmugam, R.; Tew, G. N. "Polymers that contain ligated metals in their side chain: building a foundation for functional materials in opto-electronic applications with an emphasis on lanthanide ions" *Macromol. Rapid Commun.* **2008**, *29*, 1355.
23. Nagesh, K.; Gupta, D.; Kabra, D.; Narayan, K. S.; Ramakrishnan, S. "Tunable two-colour patterning of MEHPPV from a single precursor" *J. Mater. Chem.* **2007**, *17*, 1682.
24. Thelakkat, M.; Schmidt, H.-W. "Synthesis and properties of novel derivatives of 1,3,5-tris(diarylamino)benzenes for electroluminescent devices" *Adv. Mater.* **1998**, *10*, 219.
25. O'Regan, B.; Grätzel, M. "A low-cost, high-efficiency solar cell based on dye-sensitized colloidal TiO₂ films" *Nature* **1991**, *353*, 737.
26. Maruthamuthu, P.; Anandan, S. "Synthesis, characterization and photoconversion study of [Ru(II)(dcbpy)(terpy)Cl]Cl.3H₂O, [Ru(II)(dcbpy)(terpy)SCN]SCN.3H₂O and [Ru(II)(dcbpy)(terpy)CN]CN.3H₂O systems" *Sol. Energy Mater. Sol. Cells* **1999**, *59*, 199.

27. Anandan, S.; Madhavan, J.; Maruthamuthu, P.; Raghukumar, V.; Ramakrishnan, V. T. "Synthesis and characterization of naphthyridine and acridinedione ligands coordinated ruthenium(II) complexes and their applications in dye-sensitized solar cells" *Sol. Energy Mater. Sol. Cells* **2004**, *81*, 419.
28. Anandan, S.; Pitchumani, S.; Muthuraaman, B.; Maruthamuthu, P. "Heteropolyacid-impregnated PVDF as a solid polymer electrolyte for dye-sensitized solar cells" *Sol. Energy Mater. Sol. Cells* **2006**, *90*, 1715.
29. Nazeeruddin, M. K.; Péchy, P.; Renouard, T.; Zakeeruddin, S. M.; Humphry-Baker, P.; Comte, P.; Liska, P.; Cevey, L.; Costa, E.; Shklover, V.; Spiccia, L.; Deacon, G. B.; Bignozzi, C. A.; Grätzel, M. "Engineering of efficient panchromatic sensitizers for nanocrystalline TiO₂-based solar cells" *J. Am. Chem. Soc.* **2001**, *123*, 1613.
30. Clar, E.; Zander, M. "1:2-Benzocoronene and naphtha(2': 3'-1:2)coronene" *J. Chem. Soc.* **1958**, 1577.
31. Müller, M.; Kübel, C.; Müllen; K. "Giant polycyclic aromatic hydrocarbons" *Chem. Eur. J.* **1998**, *4*, 2099.
32. Bonifacio, M. C.; Robertson, C. R.; Jung, J. Y.; King, B. T. "Polycyclic aromatic hydrocarbons by ring-closing metathesis" *J. Org. Chem.* **2005**, *70*, 8522.
33. Shen, H. C.; Tang, J. M.; Chang, H. K.; Yang, C. W.; Liu, R. S. "Short and efficient synthesis of coronene derivatives via ruthenium-catalyzed benzannulation protocol" *J. Org. Chem.* **2005**, *70*, 10113.
34. Scott, L. T.; Cheng, P. C.; Hashemi, M. M.; Bratcher, M. S.; Meyer, D. T.; Warren, H. B. "Corranulene. A three-step synthesis" *J. Am. Chem. Soc.* **1997**, *119*, 10963.

35. Xiao, S. X.; Myers, M.; Miao, Q.; Sanaur, S.; Pang, K. L.; Steigerwald, M. L.; Nuckolls, C. "Molecular wires from contorted aromatic compounds" *Angew. Chem., Int. Ed.* **2005**, *44*, 7390.
36. Fogel, Y.; Kastler, M.; Wang, Z.; Andrienko, D.; Bodwell, G. J.; Müllen, K. "Electron-deficient *N*-heteroaromatic linkers for the elaboration of large, soluble polycyclic aromatic hydrocarbons and their use in the synthesis of some very large transition metal complexes" *J. Am. Chem. Soc.* **2007**, *129*, 11743.
37. Suo, Z.; Drobizhev, M.; Spangler, C. W.; Christensson, N.; Rebane, A. "New fluorophores based on trifluorenylamine with very large intrinsic three-photon absorption cross sections" *Org. Lett.* **2005**, *7*, 4807.
38. Chen, C.-H.; Huang, W.-S.; Lai, M.-Y.; Tsao, W.-C.; Lin, J. T.; Wu, Y.-H.; Ke, T.-H.; Chen, L.-Y.; Wu, C.-C. "Versatile, benzimidazole/amine-based ambipolar compounds for electroluminescent applications: single-layer, blue, fluorescent OLEDs, hosts for single-layer, phosphorescent OLEDs" *Adv. Funct. Mater.* **2009**, *19*, 2661.
39. Jiao, S.; Liao, Y.; Xu, X.; Wang, L.; Yu, G.; Wang, L.; Su, Z.; Ye, S.; Liu, Y. "Synthesis, structure, electronic state and luminescent properties of novel blue-light emitting aryl-substituted 9,9-di(4-(di-*p*-tolyl)aminophenyl)fluorene" *Adv. Funct. Mater.* **2008**, *18*, 2335.
40. Kreger, K.; Bäte, M.; Neuber, C.; Schmidt, H.-W.; Strohriegel, P. "Combinatorial development of blue OLEDs based on star shaped molecules" *Adv. Funct. Mater.* **2007**, *17*, 3456.
41. Culligan, S. W.; Chen, A. C.-A.; Wallace, J. U.; Klubek, K. P.; Tang, C. W.; Chen, S. H. "Effect of hole mobility through emissive layer on temporal stability of blue organic light-emitting diodes" *Adv. Funct. Mater.* **2006**, *16*, 1481.

42. Okumoto, K.; Shirota, Y. "New class of hole-blocking amorphous molecular materials and their application in blue-violet-emitting fluorescent and green-emitting phosphorescent organic electroluminescent devices" *Chem. Mater.* **2003**, *15*, 699.
43. Li, F.; Chen, Z.; Wei, W.; Cao, H.; Gong, Q.; Teng, F.; Qian, L.; Wang, Y. "Blue-light-emitting organic electroluminescence *via* exciplex emission based on a fluorene derivative" *J. Phys. D: Appl. Phys.* **2004**, *37*, 1613.
44. Matsumoto, N.; Miyazaki, T.; Nishiyama, M.; Adachi, C. "Efficient deep-blue organic light-emitting diodes based on 9,9-bis(4-biphenyl)fluorene derivatives" *J. Phys. Chem. C* **2009**, *113*, 6261.
45. Peng, Z.; Tao, S.; Zhang, X.; Tang, J.; Lee, C. S.; Lee, S.-T. "New fluorene derivatives for blue electroluminescent devices: influence of substituents on thermal properties, photoluminescence, and electroluminescence" *J. Phys. Chem. C* **2008**, *112*, 2165.
46. Goel, A.; Chaurasia, S.; Dixit, M.; Kumar, V.; Prakash, S.; Jena, B.; Verma, J. K.; Jain, M.; Anand, R. S.; Manoharan, S. S. "Donor-acceptor 9-uncapped fluorenes and fluorenones as stable blue light emitters" *Org. Lett.* **2009**, *11*, 1289.
47. Liao, Y.-L.; Lin, C.-Y.; Wong, K.-T.; Hou, T.-H.; Hung, W.-Y. "A novel ambipolar spirobifluorene derivative that behaves as an efficient blue-light emitter in organic light-emitting diodes" *Org. Lett.* **2007**, *9*, 4511.
48. Yen, Y.-S.; Hsu, Y.-C.; Lin, J. T.; Chang, C.-W.; Hsu, C.-P.; Yin, D.-J. "Pyrrole-based organic dyes for dye-sensitized solar cells" *J. Phys. Chem. C* **2008**, *112*, 12557.
49. Huang, S.-T.; Hsu, Y.-C.; Yen, Y.-S.; Chou, H. H.; Lin, J. T.; Chang, C.-W.; Hsu, C.-P.; Tsai, C.; Yin, D.-J. "Organic dyes containing a cyanovinyl entity in the spacer for solar cells applications" *J. Phys. Chem. C* **2008**, *112*, 19739.

50. Xu, M.; Wenger, S.; Bala, H.; Shi, D.; Li, R.; Zhou, Y.; Zakeeruddin, S. M.; Grätzel, M.; Wang, P. "Tuning the energy level of organic sensitizers for high-performance dye-sensitized solar cells" *J. Phys. Chem. C* **2009**, *113*, 2966.
51. Tucker, S. H.; Whalley, M. "The chemistry of fluoranthene" *Chem. Rev.* **1952**, *50*, 483.
52. González, J. J.; Francesch, A.; Cárdenas, D. J.; Echavarren A. M. "Steric hindrance facilitated synthesis of enynes and their intramolecular [4 + 2] cycloaddition with alkynes" *J. Org. Chem.* **1998**, *63*, 2854.
53. Campo, M. A.; Larock, R. C. "Novel 1,4-palladium migration in organopalladium intermediates derived from *o*-iodobiaryls" *J. Am. Chem. Soc.* **2002**, *124*, 14326.
54. Wegner, H. A.; Scott, L. T.; de Meijere, A. "A new Suzuki Heck-type coupling cascade: indeno[1,2,3]-annulation of polycyclic aromatic hydrocarbons" *J. Org. Chem.* **2003**, *68*, 883.
55. Wu, Y.-T.; Hayama, T.; Baldrige, K. K.; Linden, A.; Siegel, J. S. "Synthesis of fluoranthenes and indenocorannulenes: elucidation of chiral stereoisomers on the basis of static molecular bowls" *J. Am. Chem. Soc.* **2006**, *128*, 6870.
56. Goel, A.; Kumar, V.; Chaurasia, S.; Rawat, M.; Prasad, R.; Anand, R. S. "Synthesis, electrochemical and optical properties of stable yellow fluorescent fluoranthenes" *J. Org. Chem.* **2010**, *75*, 3656.
57. Amin, S.; Balanikas, G.; Huie, K.; Hussain, N.; Geddie, J. E.; Hecht, S. S. "Synthesis and fluorescence spectra of structural analogues of potential benzo[*b*]fluoranthene-DNA adducts" *J. Org. Chem.* **1985**, *50*, 4642.

58. Xu, J.; Hou, J.; Zhang, S.; Xiao, Q.; Zhang, R.; Pu, S.; Wei, Q. "Electrochemical polymerization of fluoranthene and characterization of its polymers" *J. Phys. Chem. B* **2006**, *110*, 2643.
59. Palmaerts, A.; van Haren, M.; Lutsen, L.; Cleij, T. J.; Vanderzande, D. "Synthesis and properties of poly(*p*-fluoranthenevinylene): a novel conjugated polymer with nonalternant repeating units" *Macromolecules* **2006**, *39*, 2438.
60. Branchi, B.; Balzani, V.; Ceroni, P.; Kuchenbrandt, M. C.; Klärner, F.-G.; Bläser, D.; Boese, R. "Molecular clips with extended aromatic sidewalls as receptors for electron-acceptor molecules. Synthesis and nmr, photophysical, and electrochemical properties" *J. Org. Chem.* **2008**, *73*, 5839.
61. Fang, X.-L.; Deng, S.-L.; Wang, J.; Wang, X.-F.; Chen, C.; Li, Y.; Xie, S.-Y.; Huang, R.-B.; Zheng, L.-S. "From self-assembled microspheres to self-templated nanotubes: morphologies and properties of sulfur-bridged fluoranthene-based organic materials" *Chem. Mater.* **2009**, *21*, 5763.
62. Fabrizio, E. F.; Payne, A.; Westlund, N. E.; Bard, A. J.; Magnus, P. P. "Photophysical, electrochemical, and electrogenerated chemiluminescent properties of 9,10-dimethyl-7,12-diphenylbenzo[*k*]fluoranthene and 9,10-dimethylsulfone-7,12-diphenylbenzo[*k*]fluoranthene" *J. Phys. Chem. A* **2002**, *106*, 1961.
63. Chiechi, R. C.; Tseng, R. J.; Marchioni, F.; Yang, Y.; Wudl, F. "Efficient blue-light-emitting electroluminescent devices with a robust fluorophore: 7,8,10-triphenylfluoranthene" *Adv. Mater.* **2006**, *18*, 325.
64. Kim, S.-K.; Jaung, J.-Y.; Park, J.-W. "New fluoranthene derivatives in electroluminescence" *Mol. Cryst. Liq. Cryst.* **2008**, *491*, 122.

65. Kim, S.-K.; Jaung, J.-Y.; Park, J.-W. "Substituent effect of fluoranthene derivatives in electroluminescence" *Mol. Cryst. Liq. Cryst.* **2009**, *498*, 140.
66. Tong, Q.-X.; Lai, S.-L.; Chan, M.-Y.; Lai, K.-H.; Tang, J.-X.; Kwong, H.-L.; Lee, C.-S.; Lee, S.-T. "Efficient green organic light-Emitting devices with a nondoped dual-functional electroluminescent material" *Appl. Phys. Lett.* **2007**, *91*, 153504.
67. Tong, Q.-X.; Lai, S.-L.; Chan, M.-Y.; Zhou, Y.-C.; Kwong, H.-L.; Lee, C.-S.; Lee, S.-T. "High-efficiency nondoped green organic light-emitting devices" *Chem. Phys. Lett.* **2008**, *455*, 79.
68. Huang, T.-H.; Lin, J. T.; Tao, Y.-T.; Chuen, C.-H. "Benzo[*a*]aceanthrylene derivatives for red-emitting electroluminescent materials" *Chem. Mater.* **2003**, *15*, 4854.
69. Ma, X.; Wu, W.; Zhang, Q.; Guo, F.; Meng, F.; Hua, J. "Novel fluoranthene dyes for efficient dye-sensitized solar cells" *Dyes Pigm.* **2009**, *82*, 353.
70. Wu, W.; Li, J.; Guo, F.; Zhang, L.; Long, Y.; Hua, J. "Photovoltaic performance and long-term stability of quasi-solid-state fluoranthene dyes-sensitized solar cells" *Renewable Energy* **2010**, *35*, 1724.
71. Rego, J. A.; Kumar, S.; Ringsdorf, H. "Synthesis and characterization of fluorescent, low-symmetry triphenylene discotic liquid crystals: tailoring of mesomorphic and optical properties" *Chem. Mater.* **1996**, *8*, 1402.
72. Heppke, G.; Krüerke, D.; Löhning, C.; Löttsch, D.; Moro, D.; Müller, M.; Sawade, H. "New chiral discotic triphenylene derivatives exhibiting a cholesteric blue phase and a ferroelectrically switchable columnar mesophase" *J. Mater. Chem.* **2000**, *10*, 2657.
73. Bayer, A.; Zimmermann, S.; Wendorff, J. H. "Low molar mass and polymer discotics: structure, dynamics and opto-electronic properties" *Mol. Cryst. Liq. Cryst.* **2003**, *396*, 1.

74. Christ, T.; Glösen, B.; Greiner, A.; Kettner, A.; Sander, R.; Stümpflen, V.; Tsukruk, V.; Wendorff, J. H. "Columnar discotics for light emitting diodes" *Adv. Mater.* **1997**, *9*, 48.
75. Bacher, A.; Bleyl, I.; Erdelen, C. H.; Haarer, D.; Paulus, W.; Schmidt, H.-W. "Low molecular weight and polymeric triphenylenes as hole transport materials in organic two-layer LEDs" *Adv. Mater.* **1997**, *9*, 1031.
76. Bacher, A.; Erdelen, C. H.; Paulus, W.; Ringsdorf, H.; Schmidt, H.-W.; Schuhmacher, P. "Photo-cross-linked triphenylenes as novel insoluble hole transport materials in organic LEDs" *Macromolecules* **1999**, *32*, 4551.
77. Freudenmann, R.; Behnisch, B.; Hanack, M. "Synthesis of conjugated-bridged triphenylenes and application in OLEDs" *J. Mater. Chem.* **2001**, *11*, 1618.
78. Mao, H.; He, Z.; Wang, J.; Zhang, C.; Xie, P.; Zhang, R. "A discotic triphenylene dimer as organic hole transporting material for electroluminescence devices" *J. Lumin.* **2007**, *122*, 942.
79. Nandy, R.; Sankararaman, S. "Donor-acceptor substituted phenylethynyltriphenylenes-excited state intramolecular charge transfer, solvatochromic absorption and fluorescence emission" *Beilstein J. Org. Chem.* **2010**, *6*, 992.
80. Luo, J.; Zhao, B.; Chan, H. S. O.; Chi, C. "Synthesis, physical properties and self-assembly of star-shaped oligothiophenes-substituted and fused triphenylenes" *J. Mater. Chem.* **2010**, *20*, 1932.
81. Hu, J. Y.; Era, M.; Elsegood, M. R. J.; Yamato, T. "Synthesis and photophysical properties of pyrene-based light-emitting monomers: highly pure-blue-fluorescent, cruciform-shaped architectures" *Eur. J. Org. Chem.* **2010**, *72*.

82. Rathfon, J. M.; AL-Badri, Z. M.; Shunmugam, R.; Berry, S. M.; Pabba, S.; Keynton, R. S.; Cohn, R. W.; Tew, G. N. "Fluorimetric nerve gas sensing based on pyrene imines incorporated into films and sub-micrometer fibers" *Adv. Funct. Mater.* **2009**, *19*, 689.
83. Takemura, H.; Nakamichi, H.; Sako, K. "Pyrene-azacrown ether hybrid: cation- π interaction" *Tetrahedron Lett.* **2005**, *46*, 2063.
84. Techert, S.; Wiessner, A.; Schmatz, S.; Staerk, H. "Time-resolved fluorescence and solvatochromy of directly linked pyrene DMA derivatives in alcoholic solution" *J. Phys. Chem. B* **2001**, *105*, 7579.
85. de Halleux, V.; Calbert, J.-P.; Brocorens, P.; Cornil, B. J.; Declercq J.-P.; Brédas, J.-L.; Geerts, Y. "1,3,6,8-Tetraphenylpyrene derivatives: towards fluorescent liquid-crystalline columns" *Adv. Funct. Mater.* **2004**, *14*, 649.
86. Hayer, A.; de Halleux, V.; Khler, A.; El-Garouhy, A.; Meijer, E. W.; Barber, J.; Tant, J.; Levin, J.; Lehmann, M.; Gierschner, J.; Cornil, J.; Geerts, Y. H. "Highly fluorescent crystalline and liquid crystalline columnar phases of pyrene-based structures" *J. Phys. Chem. B* **2006**, *110*, 7653.
87. Gunderson, V. L.; Wilson, T. M.; Wasielewski, M. R. "Excitation energy transfer pathways in asymmetric covalent chlorophyll *a* tetramers" *J. Phys. Chem. C* **2009**, *113*, 11936.
88. Nantalaksakul, A.; Mueller, A.; Klaikherd, A.; Bardeen, C. J.; Thayumanavan, S. "Dendritic and linear macromolecular architectures for photovoltaics: a photoinduced charge transfer investigation" *J. Am. Chem. Soc.* **2009**, *131*, 2727.
89. Kim, H. M.; Lee, Y. O.; Lim, C. S.; Kim, J. S.; Cho, B. R. "Two-photon absorption properties of alkynyl-conjugated pyrene derivatives" *J. Org. Chem.* **2008**, *73*, 5127.

90. Zhao, Y.; Guo, J.-F.; Ren, A.-M.; Feng, J.-K. "Theoretical study of one- and two-photon absorption properties of pyrene derivatives" *Theor. Chem. Acc.* **2011**, *128*, 265.
91. Zhang, H.; Wang, Y.; Shao, K.; Liu, Y.; Chen, S.; Qiu, W.; Sun, X.; Ting Qi, T.; Ma, Y.; Yu, G.; Su, Z.; Zhu, D. "Novel butterfly pyrene-based organic semiconductors for field effect transistors" *Chem. Commun.* **2006**, 755.
92. Qiao, Y.; Zhang, J.; Xu, W.; Zhu, D. "Novel 2,7-substituted pyrene derivatives: syntheses, solid-state structures, and properties" *Tetrahedron* **2011**, *67*, 3395.
93. Yang, C.-H.; Guo, T.-F.; Sun, I.-W. "Highly efficient greenish blue-emitting organic diodes based on pyrene derivatives" *J. Lumin.* **2007**, *124*, 93.
94. Tang, C.; Liu, F.; Xia, Y.-J.; Lin, J.; Xie, L.-H.; Zhong, G.-Y.; Fan, Q.-L.; Huang, W. "Fluorene-substituted pyrenes—novel pyrene derivatives as emitters in nondoped blue OLEDs" *Org. Electron.* **2006**, *7*, 155.
95. Tang, C.; Liu, F.; Xia, Y.-J.; Xie, L.-H.; Wei, A.; Li, S.-B.; Fan, Q.-L.; Huang, W. "Efficient 9-alkylphenyl-9-pyrenylfluorene substituted pyrene derivatives with improved hole injection for blue light-emitting diodes" *J. Mater. Chem.* **2006**, *16*, 4074.
96. Liu, F.; Xie, L.-H.; Tang, C.; Liang, J.; Chen, Q.-Q.; Peng, B.; Wei, W.; Cao, Y.; Huang, W. "Facile synthesis of spirocyclic aromatic hydrocarbon derivatives based on *o*-halobiaryl route and domino reaction for deep-blue organic semiconductors" *Org. Lett.* **2009**, *11*, 3850.
97. Moorthy, J. N.; Natarajan, P.; Venkatakrishnan, P.; Huang, D.-F.; Chow, T. J. "Steric inhibition of π -stacking: 1,3,6,8-tetraarylpyrenes as efficient blue emitters in organic light emitting diodes (oleds)" *Org. Lett.* **2007**, *9*, 5215.

98. Lai, S.-L.; Tong, Q.-X.; Chan, M.-Y.; Ng, T.-W.; Lo, M.-F.; Lee, S.-T.; Lee, C.-S. "Distinct electroluminescent properties of triphenylamine derivatives in blue organic light-emitting devices" *J. Mater. Chem.* **2011**, *21*, 1206.
99. Jia, W.-L.; Cormick, T. M.; Liu, Q.-D.; Fukutani, H.; Motala, M.; Wang, R.-Y.; Tao, Y.; Wang, S. "Diaryl amino functionalized pyrene derivatives for use in blue OLEDs and complex formation" *J. Mater. Chem.* **2004**, *14*, 3344.
100. Tao, S.; Zhou, Y.; Lee, C.-S.; Lee, S.-T.; Huang, D.; Zhang, X. "Highly efficient nondoped blue organic light-emitting diodes based on anthracene-triphenylamine derivatives" *J. Phys. Chem. C* **2008**, *112*, 14603.
101. Lai, S. L.; Tong, Q. X.; Chan, M. Y.; Ng, T. W.; Lo, M. F.; Ko, C. C.; Lee, S. T.; Lee, C. S. "Carbazole-pyrene derivatives for undoped organic light-emitting devices" *Org. Electron.* **2011**, *12*, 541.
102. Zhao, Z.; Chen, S.; Lam, J. W. Y.; Wang, Z.; Lu, P.; Mahtab, F.; Sung, H. H. Y.; Williams, I. D.; Ma, Y.; Kwok, H. S.; Tang, B. Z. "Pyrene-substituted ethenes: aggregation-enhanced excimer emission and highly efficient electroluminescence" *J. Mater. Chem.* **2011**, *21*, 7210.
103. Duan, Z.; Hoshino, D.; Yang, Z.; Yano, H.; Ueki, H.; Liu, Y.; Ohuchi, H.; Takayanagi, Y.; Zhao, G.; Nishioka, Y. "Synthesis and characterization of novel pyrene derivatives containing thienyl groups" *Mol. Cryst. Liq. Cryst.* **2011**, *538*, 199.
104. Thomas, K. R. J.; Lin, J. T.; Tao, Y.-T.; Ko, C.-W. "Novel green light-emitting carbazole derivatives: potential electroluminescent materials" *Adv. Mater.* **2000**, *12*, 1949.

105. Hancock, J. M.; Gifford, A. P.; Tonzola, C. J.; Jenekhe, S. A. "High-efficiency electroluminescence from new blue-emitting oligoquinolines bearing pyrenyl or triphenyl endgroups" *J. Phys. Chem. C* **2007**, *111*, 6875.
106. Oh, H.-Y.; Lee, C.; Lee, S. "Efficient blue organic light-emitting diodes using newly-developed pyrene-based electron transport materials" *Org. Electron.* **2009**, *10*, 163.
107. Kumar, D.; Thomas, K. R. J.; Lee, C.-P.; Ho, K.-C. "Novel pyrenoimidazole-based organic dyes for dye-sensitized solar cells" *Org. Lett.* **2011**, *13*, 2622.

Fluoranthene/Triphenylene-Based Hole-Transporting Materials: Synthesis, Optical, Electrochemical and OLED Properties

2.1 Introduction

Molecular materials featuring multiple functional characteristics have been developed in recent years for usage in electronic devices such as organic field effect transistors (OFETs), non-linear optics, solar cells and organic light emitting diodes (OLEDs).¹⁻⁶ Organic light emitting diode in particular, have received significant interest due to their potential application in flat panel and full color range display. Moreover many other factors such as excellent brightness, low energy consumption, high efficient lighting and large view angle, have made OLED as a promising candidate in the evolution of electronic devices. Due to its thin, light weight, flexible and foldable structure, OLEDs have been successfully commercialized in TV screens, computer monitors, mobile phones, palmtop computers, watches, advertising, information and indication/billboards, for space illumination and in large area light emitting elements. OLEDs require no back light and are relatively less expensive to manufacture, indicating its better commercialization over LCDs and is booming in the market.

OLEDs have gained ground after pioneering work by Ching W. Tang and Steven Van Slyke in 1987 at Eastman Kodak⁷ who first demonstrated small molecules based OLEDs which was made up of two layers using AlQ₃ as electron transporting/green emitting layer and a diamine as hole transporting layer. OLED is a solid semiconductor device composed of

thin film of organic molecules that create light with the application of electricity. These organic materials can be divided into three categories 1) hole-transporting materials, 2) electron transporting material, 3) emitting materials.

The efficient recombination of holes and electrons in emissive layer is necessary for the better efficiency of device. The mobility of holes in hole transporting materials is much higher than that of electrons in ETLs. Consequently, holes from the anode tend to transport easily to the ETL and even further to the cathode without recombining efficiently with electrons in the emitting layer. This will largely decrease the current efficiency of the devices. Therefore, a morphologically stable amorphous hole transporting layer displaying moderate hole mobility to match the electron mobility of ETL and a low ionization potential (I_p) for efficient hole injection is required to further achieve highly efficient and stable OLEDs.

Thermal and morphological stability is also required for high performance organic light emitting devices. Compounds having high thermal stability and showing larger glass transition temperature are beneficial to increase the lifetime of the OLED. The simplest way to form amorphous glass is non-planar molecular structure which hampers easy packing of molecules and therefore, crystallization. Di- or tri-arylamines are the preferred agent for this purpose and comprised an important class of hole-transporting materials due to their high glassy state stability and amorphous nature. Many endeavors have been made to develop new amorphous triarylamines with high morphological stability. Shirota et al.⁸ and Schmidt et al.⁹,¹⁰ have reported several families of high T_g starburst aromatic amines which served as hole transporting materials for OLEDs. Triarylamine derivatives have been intensively investigated as hole-transporting or emissive material in OLEDs.^{11,12} Inclusion of rigid polyaromatic segments has also been proven to be beneficial for increasing the thermal properties of the compounds.¹³

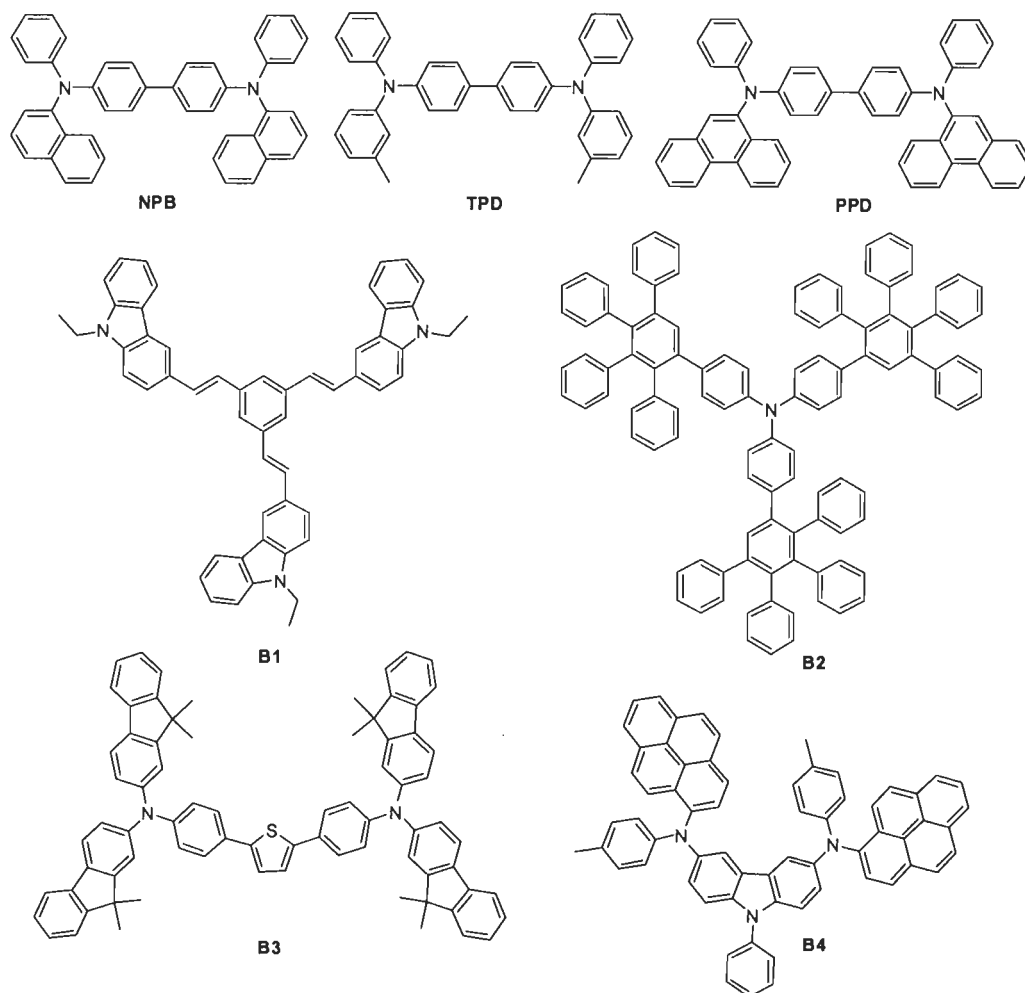


Figure 2.1 Structures of hole transporting materials.

Several materials have been studied as hole-transport materials (HTMs) till date. Among them, *N,N'*-diphenyl-*N,N'*-bis(3-methylphenyl)(1,1'-biphenyl)-4,4'-diamine (**TPD**) and *N,N'*-bis(1-naphthyl)-*N,N'*-diphenyl-1,1'-biphenyl-4,4'-diamine (**NPB**) are well known hole transporters and have been studied extensively.^{14,15} But these materials have low glass transition temperatures 60 and 98°C respectively which affect the morphological stability of the device. Therefore, researchers were focused to develop the HTMs with high thermal stability. The structure of some of the hole-transport materials are shown in Figure 2.1. Compound **B1** and **B2** are the examples of high T_g starburst aromatic amines which served as hole transporting materials in OLED.^{16,17}

Most of the electro-optical devices require materials featuring multiple functionalities. For instance, OLED requires organic materials possessing luminescent and charge

transporting characteristics.^{16,18} Embedding multiple functional entities in a single molecule is synthetically challenging and often leads to molecules dominating one function due to the imbalanced communication between them. Thus, multifunctional molecules are designed, synthesized and evaluated by many groups to diminish the steps in the cumbersome deposition of multi-layers of organic materials and reduce the production cost.¹⁹ Evaluation of structure-property relationship in polyfunctional materials is also beneficial to improve the molecular design understanding for such applications.

Star-shaped conjugated molecules or dendrimers consisting of π -conjugated substituents joined together by a central core, have attracted increasing attention due to their novel structures and new intrinsic electrical, optical and morphological properties.²⁰ Compared with linear organic conjugated oligomers and polymers used in semi-conductors, star-shaped molecules have a number of advantages including better solubility, film-forming properties, structural uniformity and high degree of purity. These unique features render this kind of material rather promising in optoelectronic applications such as light emitting diodes, solar cells, and field-effect transistors.²¹ In the design of star-shaped conjugated materials, two strategies can be used: changing the arm and changing the core. The core is usually made up of polyaromatic hydrocarbon.

Numerous polyaromatic hydrocarbon (PAH) derivatives with π -conjugated length, such as anthracene, fluorene, pyrene, perylene, triphenylene and fluoranthene, have been extensively investigated for their potential application as organic nonlinear optical materials (NLO), fluorescent sensors, and electroluminescent emitters (EL).²²⁻²⁵ Boosted by unique properties of high thermal properties, good transporting properties and excellent fluorescence emission, PAHs have received much interest in organic light emitting diodes (OLEDs) especially in PLEDs.²⁶ In a major breakthrough, Friend et al²⁷ intensively studied PLEDs for their potential applications in a new generation of flat display and lighting technologies. In this direction fluoranthene and triphenylene segment

has attracted a spurge of interest recently as a promising scaffold for making high quality conducting polymers. A conjugated Poly(*p*-fluoranthene vinylene) polymer was found to have optoelectronic properties.²⁸ Phenylene-based polymers such as polytriphenylene are one of the most important class of conjugated wide band gap polymers for blue emitting PLEDs. A series of triphenylene-alt-arylene copolymers and polytriphenylene homopolymers with different alkyl or alkoxy chains as solubilizing units have been used in blue polymeric light emitting diodes.²⁹

Although polymeric fluorophores generally exhibit simple device architecture, good processability and a strong tendency of preserving the amorphism at the operating temperature because of the large molecular weight and high T_g (glass transition temperature). But repeated polymerization steps introduces significant impurities that's a bit hard to deal with. In comparison, small molecules with a low molecular weight have an advantage of easy thin layer fabrication by a high-vacuum deposition technique which enhances the processability and hence the impurities that arise from polymerization steps can be avoided. Moreover, conjugated short-chain model compounds often show similar properties, when compared with the corresponding polymers. So here, we will be dealing with small molecules only.

Fluoranthene and triphenylene cored small molecules were known as effective materials for OLEDs, dye-sensitized solar cells, and field effect transistors. The purpose of choosing fluoranthene and triphenylene as a core is to explore their potential properties due to their extended π -conjugated system, charge transporting and emitting properties. Although various fluoranthene^{30,31} and benzo[*k*]fluoranthene³² derivatives are known but very few fluoranthene-based small molecules have been applied as emitting layer in OLEDs. Some of the fluoranthene-based small molecules are displayed in Figure 2.2 which have been served as hole transporting and emitting material in OLED.³³⁻³⁷

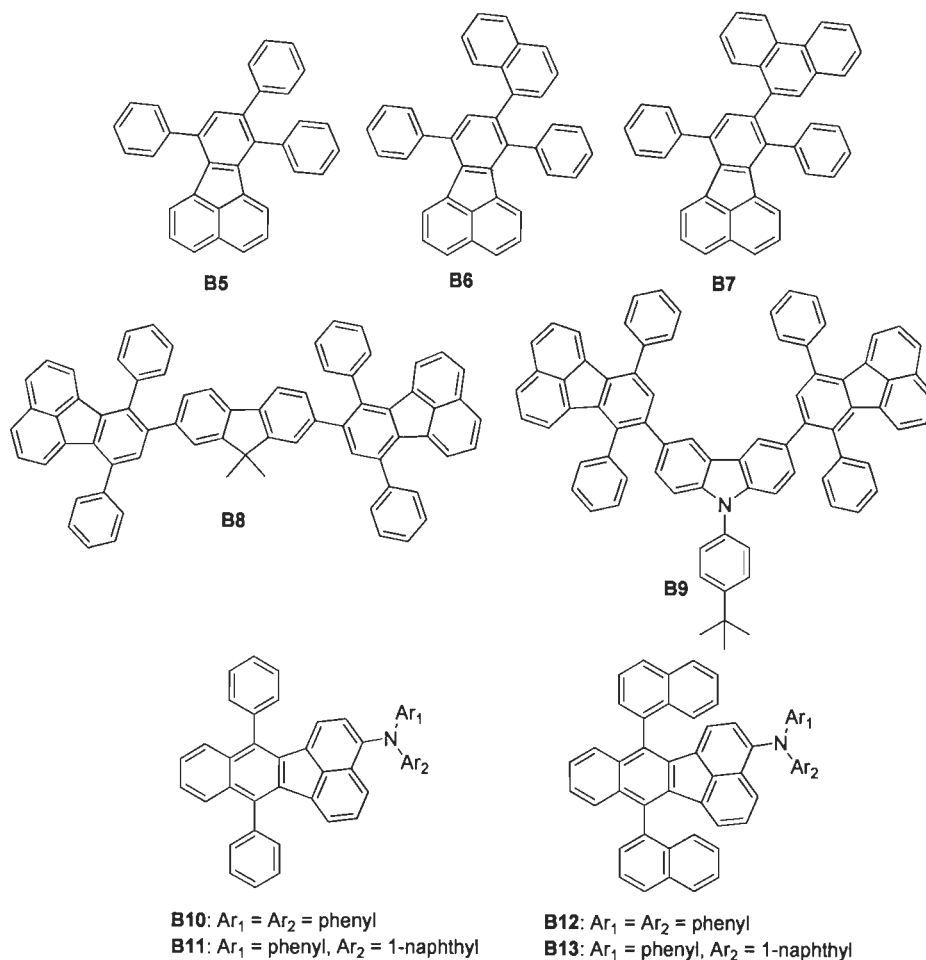


Figure 2.2 Fluoranthene or benzo[*k*]fluoranthene-based star shaped molecules as emitting or hole-transporting materials.

Among small polyaromatic hydrocarbon, Pyrene, a flat aromatic molecule, exhibits excellent fluorescent properties, and the emission is pure blue to permit ready exploitation as an emissive material in organic light emitting diodes (OLEDs). Various pyrene derivatives were used as emitting layer in OLEDs.³⁸ The proper substitution on pyrene can increase the conjugation and tune the emitting properties of the molecule.

Electron-rich triphenylene-based derivatives have been investigated as materials for application in organic field-effect transistors, organic light-emitting diodes (OLED) and dye sensitized solar cells.^{39,40} The triphenylene containing small molecules and oligomers have received considerable attention due to their discotic liquid crystalline nature and their various physical properties including one-dimensional charge migration, one-dimensional energy migration, electro-luminescence, ferroelectric switching, alignment,

and self-assembling behavior on surfaces.⁴¹ A triphenylene dimer have been studied for their discotic as well as hole transporting properties in electroluminescent devices.⁴² Figure 2.3 shows the examples of triphenylene-based small molecules out of which **B14**, **B15**, **B16**, **B17**, **B18** have been used as hole transporting and emitting materials in OLED.⁴³⁻⁴⁶ But the device incorporated with **B14** gave good results only when it was used as only blue emitting material.

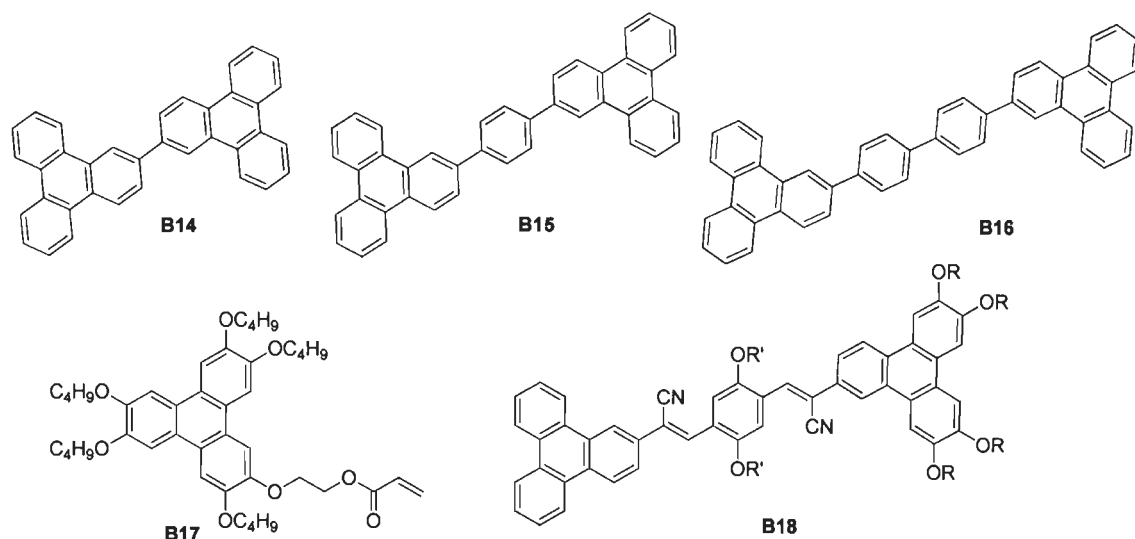


Figure 2.3 Triphenylene-based small molecules.

Blue-emitting organic EL devices have been a subject of current interest because such devices can be utilized to generate light of various colors either by irradiation of luminescent dyes or by excitation-energy transfer to luminescent dopants including emissive phosphors. Based on our research, we have succeeded in making new range of blue emitting materials by replacing the core of molecule by triphenylene. Also, by replacing the core with fluoranthene, we obtained a new range of greenish yellow emitting material. We will be discussing about them as we proceed further.

Since Flat aromatic molecules and linear π -conjugated systems are highly fluorescent and exhibit potential applications in various electronic devices. However, an enfeebling and long standing problem with such systems is the molecular aggregation *via* π - π stacking which can suppress their emission in the solid state. Nonplanarity is the best

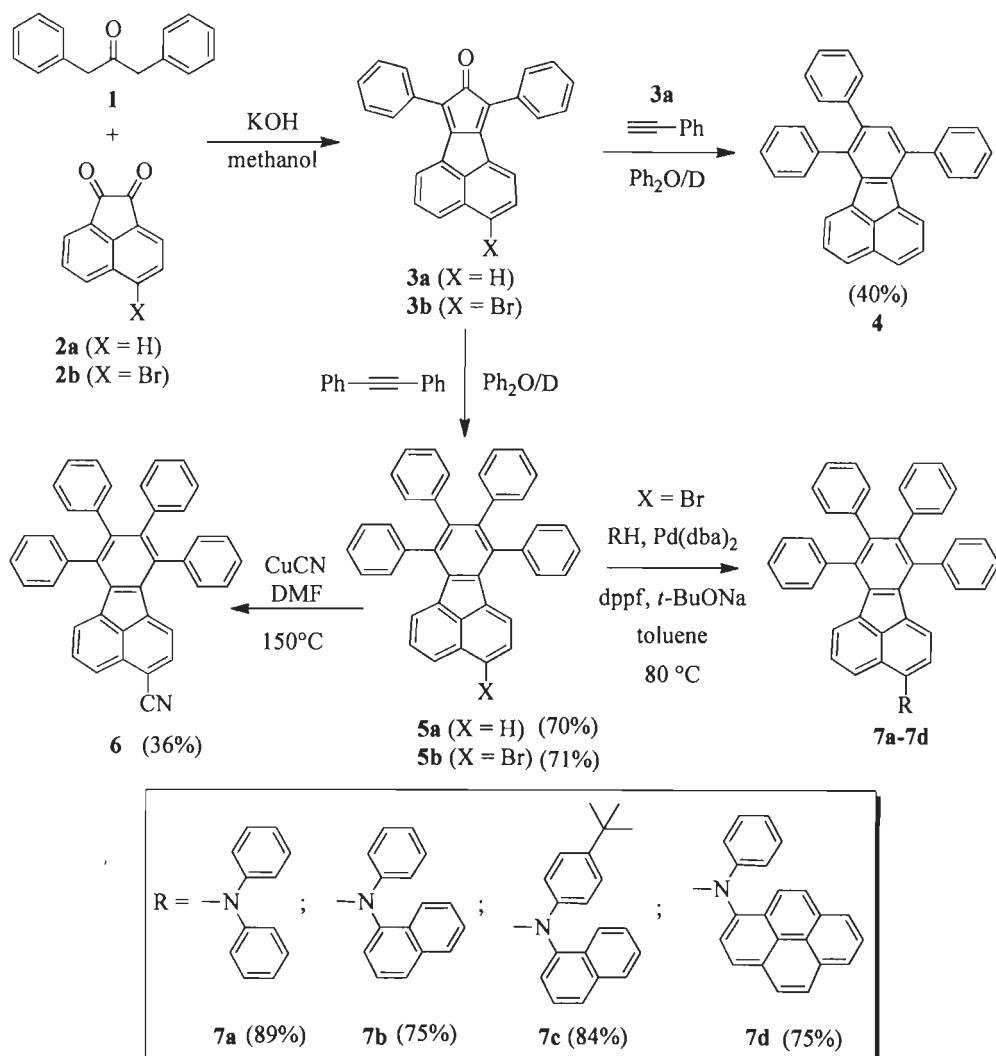
solution to overcome the aggregation and nonplanar configuration can be easily achieved with the use of star shaped molecules or incorporation of bulky trigonal moieties in the molecules.¹⁷ Various molecules incorporated with polyphenyl-based dendrons (Müllen dendrons) have been demonstrated to be detrimental for the molecular aggregation or π - π stacking in the solid state.^{47,48} Thus, conjugated dendrimers incorporating polyaromatics may be potential candidates for applications in electronic devices.

In this Chapter, the synthesis and characterization of two new series of such derivatives by changing their core with Fluoranthene/triphenylene which contains multiple phenyl groups and an amine donor featuring an additional aromatic segment such as pyrene or naphthalene have been discussed. As the newly developed materials contained amine functionality, these were used as emitting hole transporters in OLEDs. Internalization of polyphenyl segments in these derivatives impediment the chance of molecular aggregation or π - π stacking and enhance the thermal stability. All the derivatives were well characterized by ^1H & ^{13}C NMR, and various spectroscopic methods. Additionally solvatochromism study has been done for all triarylamine derivatives. Quenching studies was also done for **5a** in four different quenchers. The comparisons were made between photophysical and electrochemical properties of fluoranthene and triphenylene derivatives. Fluoranthene-based derivatives were found to emit in greenish yellow region while triphenylene-based derivatives were blue emitting.

The parent compounds **4**, **5a**, **12** have also been synthesized for the comparison. Addition to this compounds **6** & **13** and **14a** have been synthesized to see the effect of electron withdrawing $-\text{CN}$ group and carbazole moiety instead of diaryl amine on optical and electrochemical properties respectively. All the triarylamine derivatives exhibit very high thermal stability and display exceptionally high glass transition temperature owing to the presence of rigid structural units.

2.2 Results and discussion

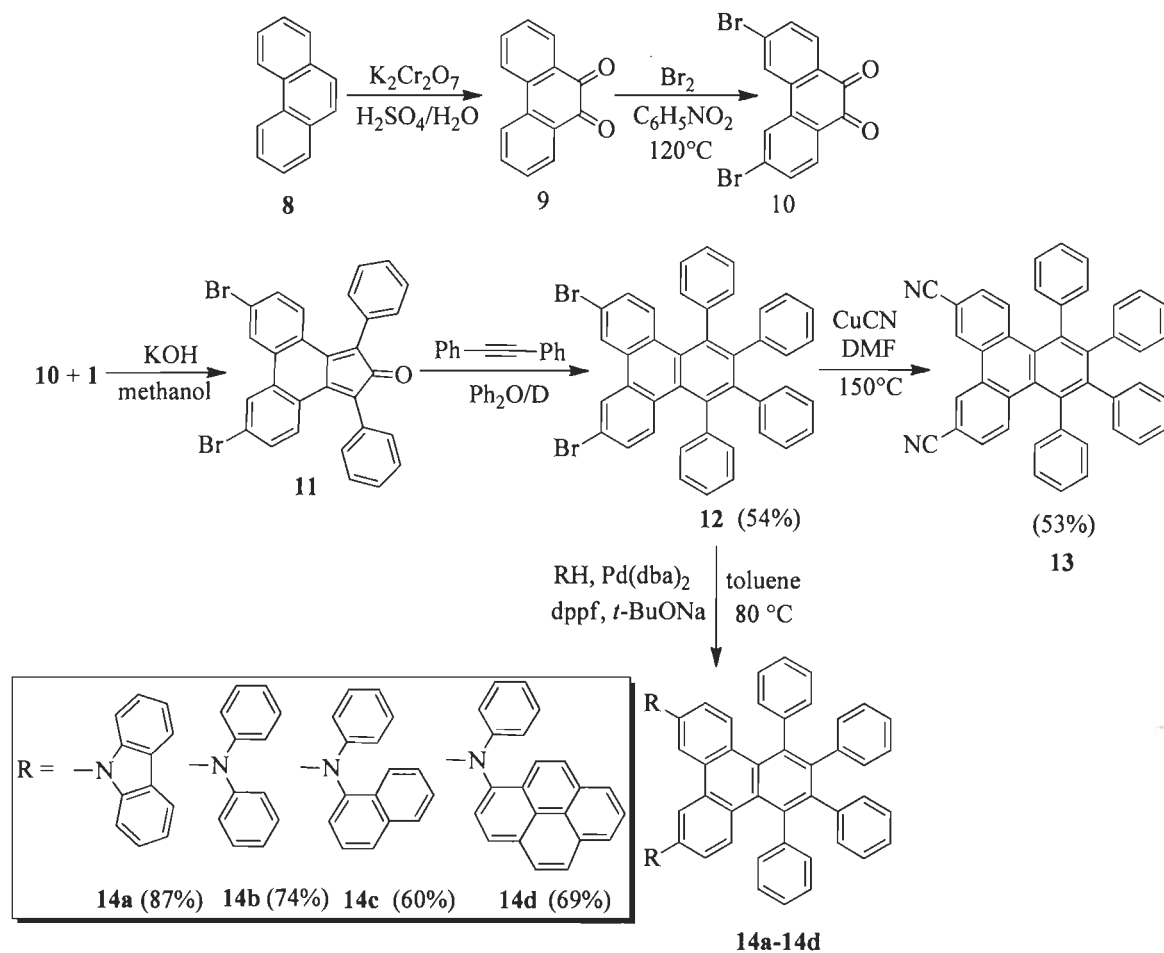
2.2.1 Synthesis



Scheme 2.1 Synthesis of fluoranthene-based triarylamine derivatives (**7a-7d**).

The detailed synthetic routes are shown in Schemes 2.1 & 2.2. The fluoranthene and triphenylene containing bromo derivatives, 3-bromo-7,8,9,10-tetraphenylfluoranthene (**5b**) and 7,10-dibromo-1,2,3,4-tetraphenyltriphenylene (**12**) required for the present study were made by an established route.⁴⁹ In this method 1,3-diphenyl-2-propanone (**1**) was condensed with the appropriate 5-bromoacacenaphthylene-1,2-dione⁵⁰(**2b**) or 3,6-dibromophenanthrene-9,10-dione⁵¹(**10**) to obtain the 3-bromo-7,9-diphenyl-8H-cyclopenta[a]acenaphthylene-8-one or 6,9-dibromo-1,3-diphenyl-2H-cyclopenta[1]phenanthren-2-one respectively. This underwent Diels-Alder reaction with

diphenyl acetylene in refluxing diphenyl ether to generate the desired precursors for both series, 3-bromo-7,8,9,10-tetraphenylfluoranthene (**5b**) and 7,10-dibromo-1,2,3,4-tetraphenyltriphenylene (**12**) respectively.



Scheme 2.2 Synthesis of triphenylene-based triarylamine derivatives (**14a-14d**).

The syntheses of triarylamines of both series (**7a-7d** & **14a-14d**) were accomplished by Pd-catalyzed C-N coupling strategy developed by Hartwig and co-workers⁵². To the best of our knowledge, animation reactions have not been demonstrated for the substrate which we used. For comparison, we have also synthesized 7,8,9,10-tetraphenylfluoranthene-3-carbonitrile (**6**) from 3-bromo-7,8,9,10-tetraphenylfluoranthene (**5b**) and 5,6,7,8-tetraphenyltriphenylene-2,11-dicarbonitrile (**13**) from 7,10-dibromo-1,2,3,4-tetraphenyltriphenylene (**12**) by means of Rossemund van Braun reaction⁵³ in which CuCN was used as reagent and DMF as solvent. This compound has been used in this work to evaluate the role of electron-withdrawing group on the optical and

electrochemical properties. Additionally we have synthesized one more derivative (**14a**) having carbazole as a donor for the comparison. The amine containing compounds are yellow in color and are soluble in common organic solvents.

2.2.2 Optical properties

The absorption spectra of the compounds were recorded in toluene and dichloromethane (2×10^{-5} M) solution. Representative absorption spectra recorded for fluoranthene series are presented in Figures 2.4 & 2.5 along with the parent compounds for comparison. The data are listed in Table 2.1. Here, we are discussing the absorption pattern of both fluoranthene and triphenylene derivatives separately. Among fluoranthene derivatives, the parent compound (**5a**) exhibited two absorption peaks centered at 295 and 373 nm, respectively originating from the π - π^* transitions. It is interesting to note that the data is not significantly different from those observed for the basic unit fluoranthene (289 and 360 nm).⁵⁴ It suggests that outer phenyl rings do not extend the conjugation of the core dramatically. This is possibly due to the twisting of the phenyl groups out of the plane of the aromatic π -system which inhibits an effective π -conjugation with the fluoranthene core (see below for theoretical results).

The absorption spectra were almost similar for **4**, **5a** and **5b**. Though the bromo substituent did not influence the absorption pattern in **5b**, the cyano bearing compound **6** showed bathochromic shift of 13 nm when compared to the parent compound which probably indicates a charge transfer between the π -rich fluoranthene segment and the electron withdrawing cyano unit. Further incorporation of diarylamine red shifts the absorption profile significantly.

All the amine derivatives **7a–7d** showed a new prominent band located at 442–444 nm when compared to that of the parent compound (**5a**). The diarylamine could either act as a strong auxochrome or be involved in a facile charge transfer transition. The appearance of absorption features in the higher wavelength has been noticed earlier for diarylamine substituted pyrene⁵⁵ or anthracene⁵⁶ derivatives. The triphenylamine (TPA), *N,N*-

diphenylnaphthalen-1-amine and *N,N*-diphenylpyren-1-amine (PyDPA) cores show absorption peaks at 303, 294 & 347 and 300 & 395 nm, respectively in dichloromethane solutions (Figure 2.6).^{57,58}

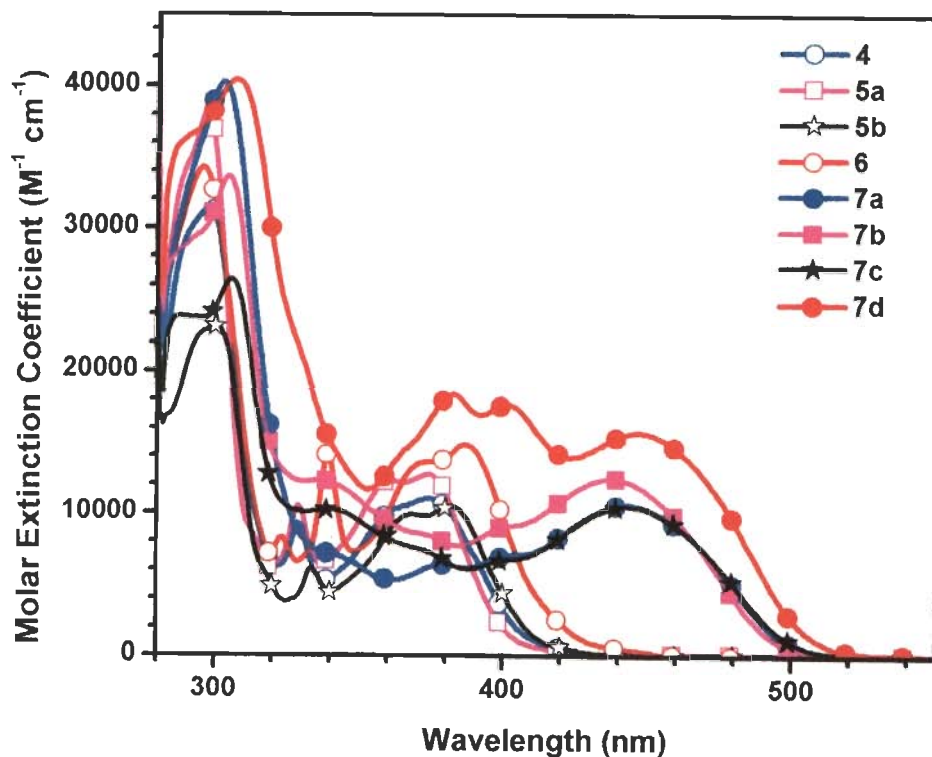


Figure 2.4 Absorption spectra of the compounds 4-7 recorded in toluene.

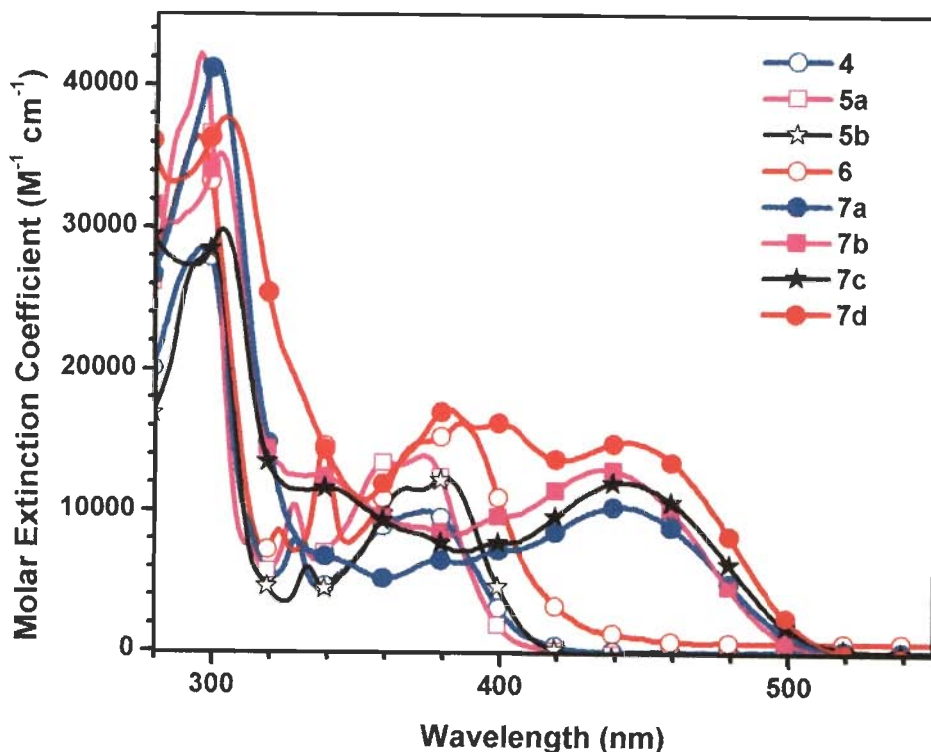


Figure 2.5 Absorption spectra of the compounds 4-7 recorded in dichloromethane.

The common peak at ca. 300 nm in these compounds seems to be originating from the diphenylamine chromophore. The absorptions in the higher wavelength region (347 and 395 nm) are attributed to the weak charge transfer transition from the amine donor to the aromatic acceptor segment. On a similar note the absorption peak appearing at the low energy side of the spectrum in the amine substituted compounds (**7a–7d**) is assigned to the charge transfer transition.

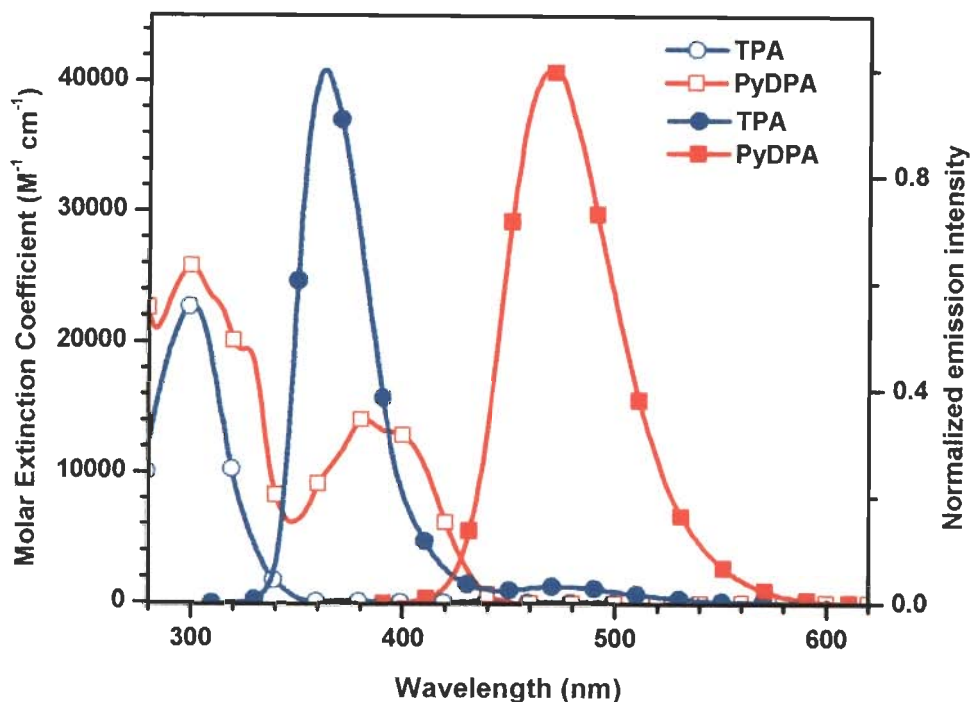


Figure 2.6 Absorption (unfilled) and emission (filled) spectra of triphenylamine (TPA) and pyrenyldiphenylamine (PyDPA) recorded in dichloromethane solution.

On comparing the absorption features of the amine derivatives (**7a–7d**) few salient points emerge: (1) naphthylphenylamine derivative **7b** displays slighter hypsochromic shift (approx. 7 nm) than that of **7a**. This is because of the competitive delocalization of the lone pair of nitrogen by the naphthyl ring, (2) compound **7c** absorbs red-shifted (442 nm) when compared to that of **7b** and approximately the same as **7a** even though it contains a naphthyl unit. The reason for this might be the presence of a *t*-butyl group on the phenyl ring which probably increases the donor strength of the phenyl moiety, (3) absorption spectra of **7b** and **7c** show a hump at 335 nm which is due to the naphthalene unit and similarly two humps at

Table 2.1 Optical properties of fluoranthene derivatives (4-7).

Compound	Toluene			Dichloromethane		
	λ_{\max} , nm (ϵ_{\max} , $M^{-1}cm^{-1}$) $\times 10^3$	λ_{em} , nm (Φ_F , %)	Stoke shift, cm^{-1}	λ_{\max} , nm (ϵ_{\max} , $M^{-1}cm^{-1}$) $\times 10^3$	λ_{em} , nm (Φ_F , %)	Stoke shift, cm^{-1}
4	298.0 (31.4), 329.0 (9.3), 374.0 (11.0)	460.5	4856	297.0 (28.6), 329.0 (7.9), 375.0 (9.9)	460.5 (36)	4880
5a	297.0 (38.3), 329.0 (10.6), 374.5 (12.8)	457 (37)	4987	295.0 (42.2), 328.0 (10.4), 373.0 (13.9)	459 (23)	5094
5b	300.5 (23.1), 334.0 (6.2), 382.5 (10.5)	469.5	4845	299.0 (28.4), 333.0 (5.9), 380.5 (12.3)	474	5184
6	295.5 (34.3), 323.5 (8.3), 339.0 (14.2), 387.5 (14.9)	494.5 (39)	5584	294.0 (36.5), 323.0 (8.7), 339.0 (14.6), 386.0 (16.2)	503 (7)	6026
7a	302.5 (40.3), 443.0 (10.6)	521.5 (41)	3398	300.0 (41.5), 442.0 (10.3)	544.5 (27)	4259
7b	304.0 (33.7), 335.5 (12.3), 437.0 (12.5)	518 (36)	3578	302.0 (35.3), 335.0 (12.5), 435.0 (13.0)	538.5 (26)	4418
7c	305.5 (26.4), 341.5 (10.2), 442.5 (10.5)	524 (37)	3515	303.0 (29.9), 339.5 (11.6), 443.0 (12.0)	549.5 (24)	4375
7d	306.5 (40.5), 382.5 (18.4), 401.0 (17.6), 446.5 (15.7)	530 (28)	3528	304.0 (37.8), 381.0 (17.2), 398.5 (16.2), 444.0 (14.9)	558 (11)	4601

Table 2.2 Optical properties of triphenylene derivatives (12-14).

Compound	Toluene			Dichloromethane			Thin film
	λ_{\max} , nm (ϵ_{\max} , $M^{-1}cm^{-1}$) $\times 10^3$	λ_{em} , nm (Φ_F , %)	Stokes' shift, cm^{-1}	λ_{\max} , nm (ϵ_{\max} , $M^{-1}cm^{-1}$) $\times 10^3$	λ_{em} , nm (Φ_F , %)	Stokes' shift, cm^{-1}	λ_{em} , nm
12	296 (73.3)	399	8721	294 (84.2)	400	9014	-
13	306 (66.9)	416 (33)	8641	304 (67.8)	421 (16)	9142	446, 463
14a	293 (64.2), 331 (46.3)	412	5940	293 (70.7), 328 (53.8)	417	6507	443
14b	350 (56.4)	435 (47)	5583	297 (54.8), 349 (63.0)	444 (37)	6131	471
14c	344 (59.9)	427 (39)	5651	269 (67.2), 342 (72.6)	442 (37)	6615	470
14d	335 (65.7), 407 (31.5)	462 (65)	2925	275 (90.5), 334 (78.4), 403 (34.4)	492 (40)	4489	483

381 and 398 nm in the absorption spectrum of compound **7d** are probably arising due to the pyrene unit. The latter assignments are consistent with the fact that *N,N*-diphenylnaphthalen-1-amine and *N,N*-diphenylpyren-1-amine cores show absorption peaks at 347 and 395 nm, respectively.^{57,58}

It is evident from the data listed in Table 2.9 (Page 135) that the energy gap of these materials can be fine tuned by appropriate substitution on the 3rd position of fluoranthene core. Substitution of electron-withdrawing unit such as cyano widens the band gap while the electron-donating amine segment shrinks it. Among the amines the pyrene derivative **7d** displays the smaller band gap. All these points suggest that the fluoranthene core acts as a π -acceptor and the incorporation of amine functionality renders dipolar character to the structure. Enhanced donor acceptor interaction is expected to decrease the band gap.

The absorption spectra of the triphenylene derivatives were measured in toluene and dichloromethane (2×10^{-5} M) solutions. The spectra are displayed in Figures 2.7 & 2.8 and data are listed in Table 2.2. The parent compound (**12**) showed one absorption band at 294 nm originating from π - π^* transition and red shifted (ca. 37 nm) as compared to the basic core triphenylene (257 nm). This evokes that peripheral phenyl rings are taking part in extending the conjugation length of the molecule. This is contradictory to the statement given for fluoranthene derivative (**5a**) in which the absorption profile was not significantly influenced by peripheral phenyl rings. After the substitution of electron withdrawing group, compound **13** displays a slight bathochromic shift of approx. 10 nm as compared to parent compound **12** which probably due to the presence of -CN chromophore which extends the conjugation.

All the amine derivatives (**14a-14d**) show two absorption bands out of which the high energy band at 269-297 nm arises due to π - π^* transition of the parent core and the second new prominent band at higher wavelength is due to π - π^* transition originating from amine donor which participates in the charge transfer in the molecule and facilitates to increase

the polarity as well as π conjugation length of the molecule. Since carbazole is a weak donor, compound **14a** is showing blue shift as compared to other triarylamine.

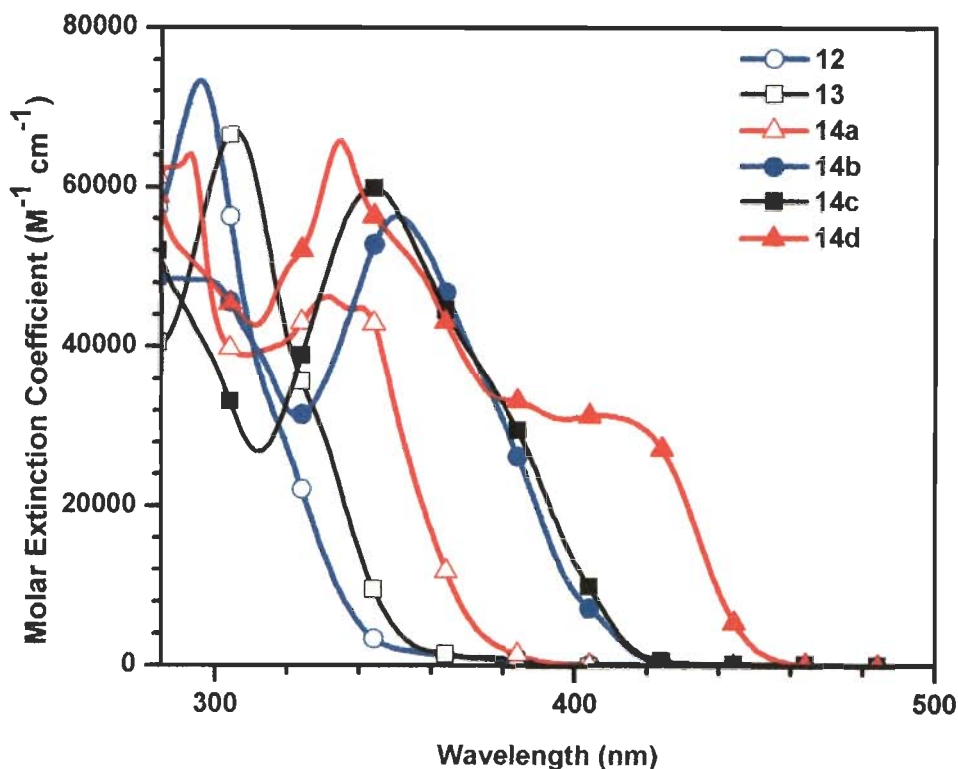


Figure 2.7 Absorption spectra of the compounds 12-14 recorded in toluene.

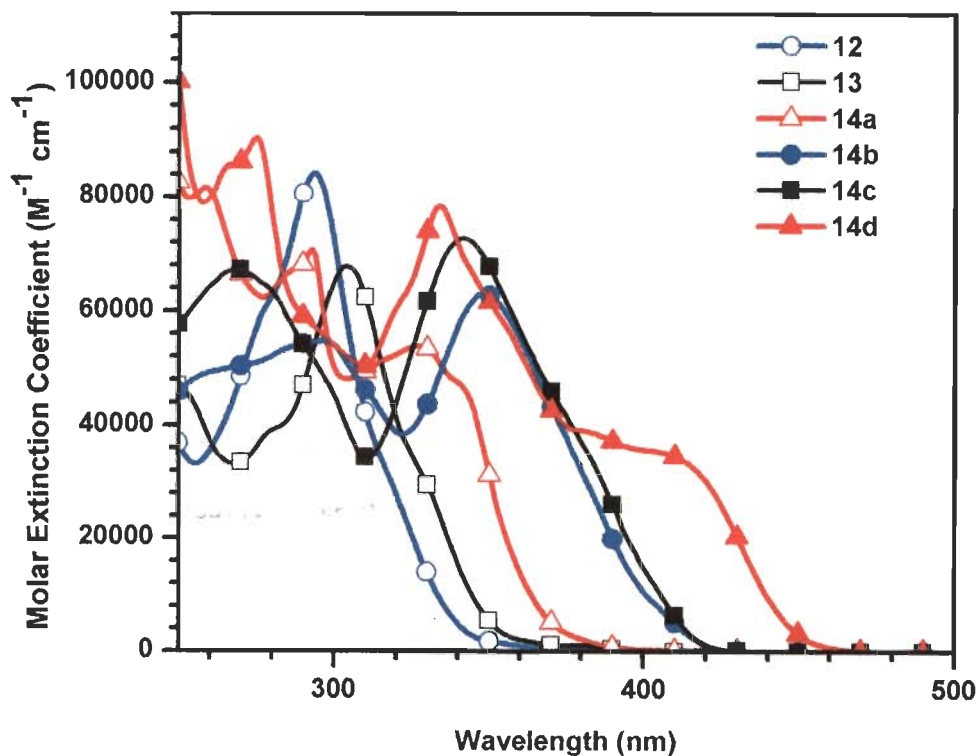


Figure 2.8 Absorption spectra of the compounds 12-14 recorded in dichloromethane.

derivatives. If we compare the absorption features of the amine derivatives, naphthylphenylamine derivative **14c** displays slight hypsochromic shift (approx. 7 nm) than that of **14b**. This is because of competitive delocalization of lone pair of nitrogen by naphthyl ring but in case of **14d**, more blue shift was observed because the lone pair of nitrogen are completely delocalized on pyrene unit instead of triphenylene core in case of **14d** (see theoretical calculation). Thus, compound **14d** showed a hump at 407 nm which arise due to π - π^* transition in pyrene unit with charge transfer character from lone pair of nitrogen to pyrene. The hump at 407 nm in **14d** can be comparable to the absorption spectra of *N,N*-diphenylpyren-1-amine (Figure 2.6).

When the absorption spectra of derivatives of both series i.e. fluoranthene and triphenylene derivatives was compared, the former was found to exhibit red shifted absorption as compared to the later. The reason could be the planarity of the molecule that increases the effective conjugation in the molecule.

The emission spectra were recorded for the fluoranthene derivatives (**4-7**) in toluene and dichloromethane (2×10^{-6} M) solution. The spectra are shown in Figure 2.9. Relevant data are compiled in Table 2.1. The parent compound **5a** exhibited single emission band at 459 nm while unsubstituted fluoranthene showed vibronic bands at 443 and 463 nm.⁵⁴The broadening of emission band in **5a** is due to presence of twisted phenyl rings which tend the molecule towards nonplanarity and lead to more vibrational level. Compound **4** and **5a** displayed almost similar emission band except more broadening in **5a** observed due to the presence of more number of peripheral phenyl rings.

Bromo-substituent (**5b**) slightly red shifts the emission wavelength while -CN bearing derivative (**6**) showed more prominent red shift as compared to **5a**. The red shift in **6** is due

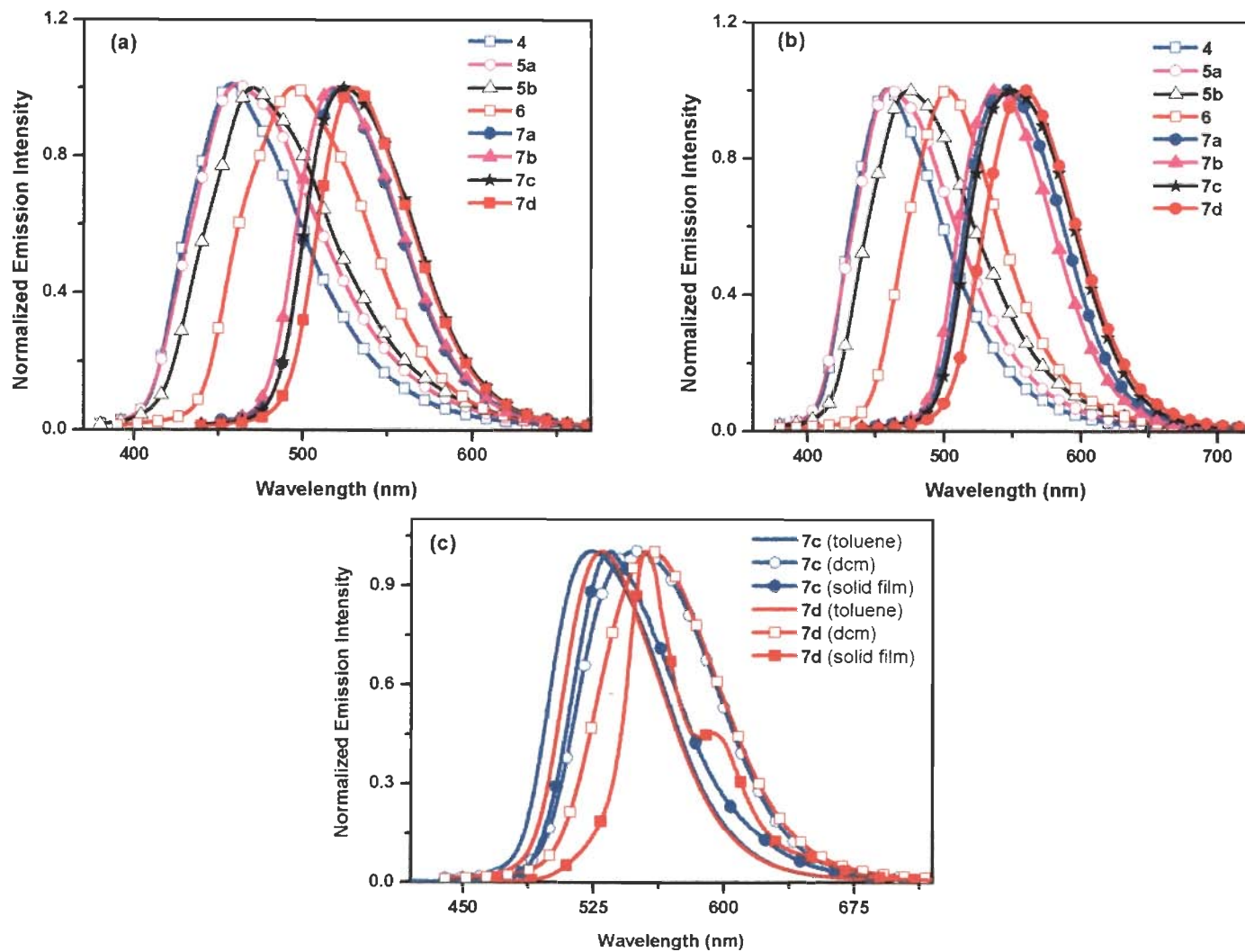


Figure 2.9 Emission spectra of the compounds 4-7 recorded (a) in toluene, (b) in dichloromethane, (c) emission spectra of 7c and 7d in toluene, dcm and thin solid film.

to presence of $-\text{CN}$ chromophore which might have slight charge transfer character in the excited state. This explanation can be predicted by a slight red shift (8 nm) in emission by increasing the solvent polarity from toluene to dichloromethane in case of **6** while no change was observed for parent derivative **5a**.

The amine derivatives showed prominent red shift in emission profile. The emission peak appears in the range 539-558 nm in dichloromethane solution. The emission characteristics were affected by the auxochromes. Emission color of the amine derivatives are greenish yellow or yellow and is dependent on the nature of the diarylamine unit. Pyrene derivative displayed strong yellow emission. We have also recorded the emission of the vapor deposited films of **7c** and **7d** which showed the emission peak at 535 and 555 nm respectively and more clear vibronic fine structure in case of **7d** illustrating the rigidity and retention of the intermolecular segregation (Figure 2.9(c)). The suppression of aggregation in the solid film is attributed to the presence of the twisted polyphenylated chromophore which decreases tendency for molecular aggregation or π - π stacking.

The emission spectra of triphenylene derivatives are recorded in different medium (toluene, dichloromethane solution and thin solid film) and shown in Figure 2.10. Data are collected in Table 2.2. Introduction of diarylamine red shifts the emission profile as compared to bromo parent compound (**12**) due to increase of polar character of molecule in the excited state. Cyano derivative (**13**) shows 21 nm bathochromic shift in dichloromethane as compared to **12** because of bearing strong color imparting cyano chromophore. On the comparison of **13** with **14a**, carbazole derivative exhibits blue shifted emission. The reason either could be the more rigid excited state in case of carbazole derivative or the less polar

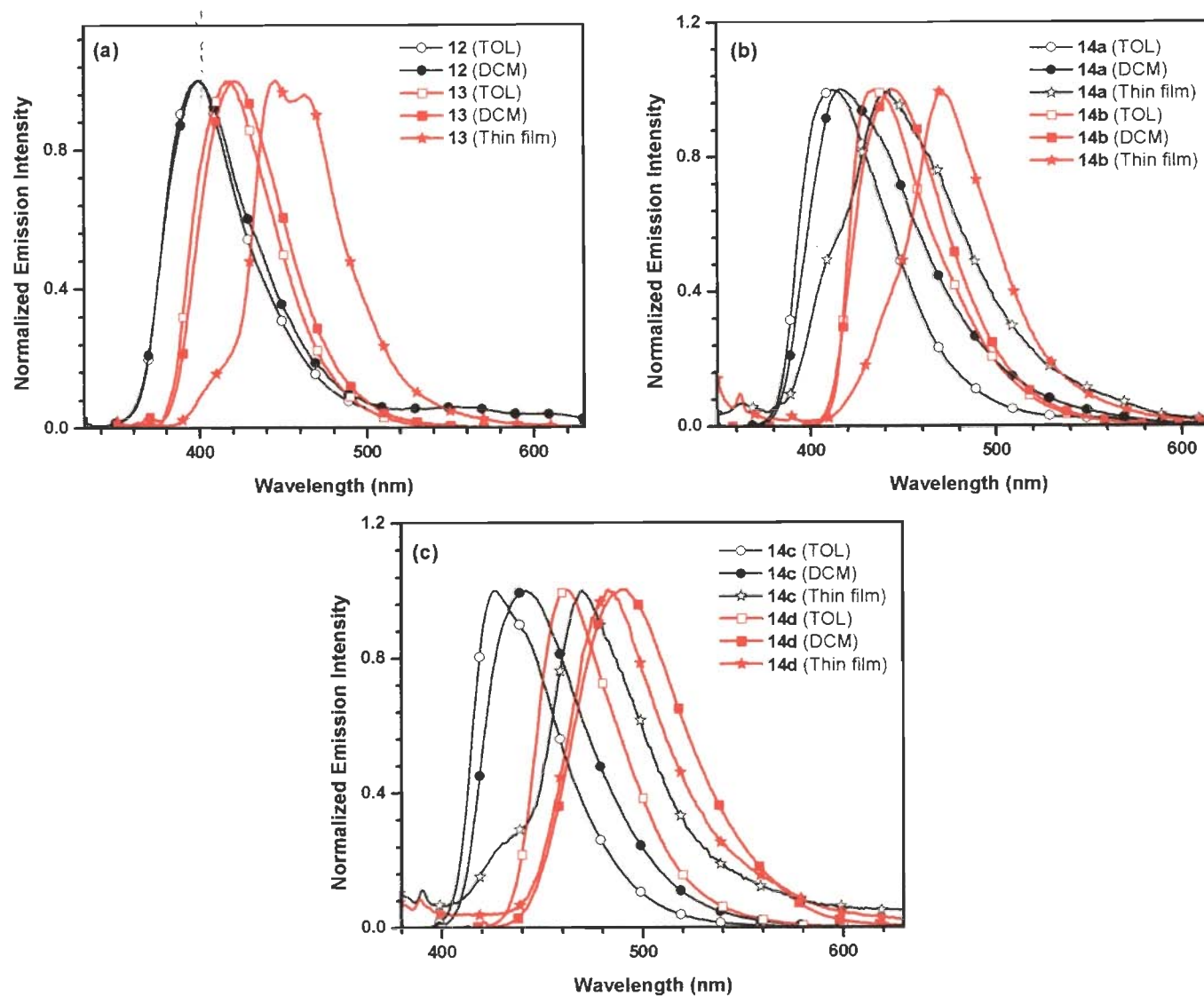


Figure 2.10 Emission spectra of the compounds 12-14 recorded in different medium (toluene, dichloromethane and thin solid film).

character of excited state in **14a** than **13** because of the weak electron donating nature of carbazole. The emission color of amine derivatives lie in the blue region. Among these, pyrene derivative (**14d**) showed larger bathochromic shift as compared to **14a-14c** due to more conjugation or more polar character.

The parent compound (**12**) did not show emission in thin film but the incorporation of electron withdrawing and electron donating group leads to the production of emission in solid state. Cyano containing derivative (**13**) showed two peaks in emission in solid state indicating the molecular aggregation is occurring in the molecule. Compounds **13** and **14a-14c** show red shifted emission as compared to that in solution which may be due to aggregation in solid state. But there was comparatively less difference in emission of thin film and solution in compound **14d**. The emission spectra of **14a-14d** was recorded in toluene at different concentration to confirm the molecular aggregation (Figure 2.11). Compound **14a** show red shifted and broad emission at 1×10^{-3} M concentration. It also show a hump at higher wavelength at higher concentration which is due to the presence of carbazole. All the derivatives show red shifted emission at 10^{-3} M but below 10^{-4} M concentration, there was no change in emission wavelength observed. There is less variation in emission by increasing the concentration in case of diphenylamine and 1-pyrenyl phenyl amine derivatives (**14b** and **14d**). Carbazole and naphthylphenylamine derivatives (**14a** and **14c**) show largest red shift at 10^{-3} M concentration. At this concentration they show two bands out of which the intensity of low energy band continuously decrease with decreasing concentration and finally disappear at 10^{-4} M concentration. In this way only one blue shifted band was observed at low concentration for **14a** and **14c**. This clearly indicates that these molecules are aggregating only at higher concentration.

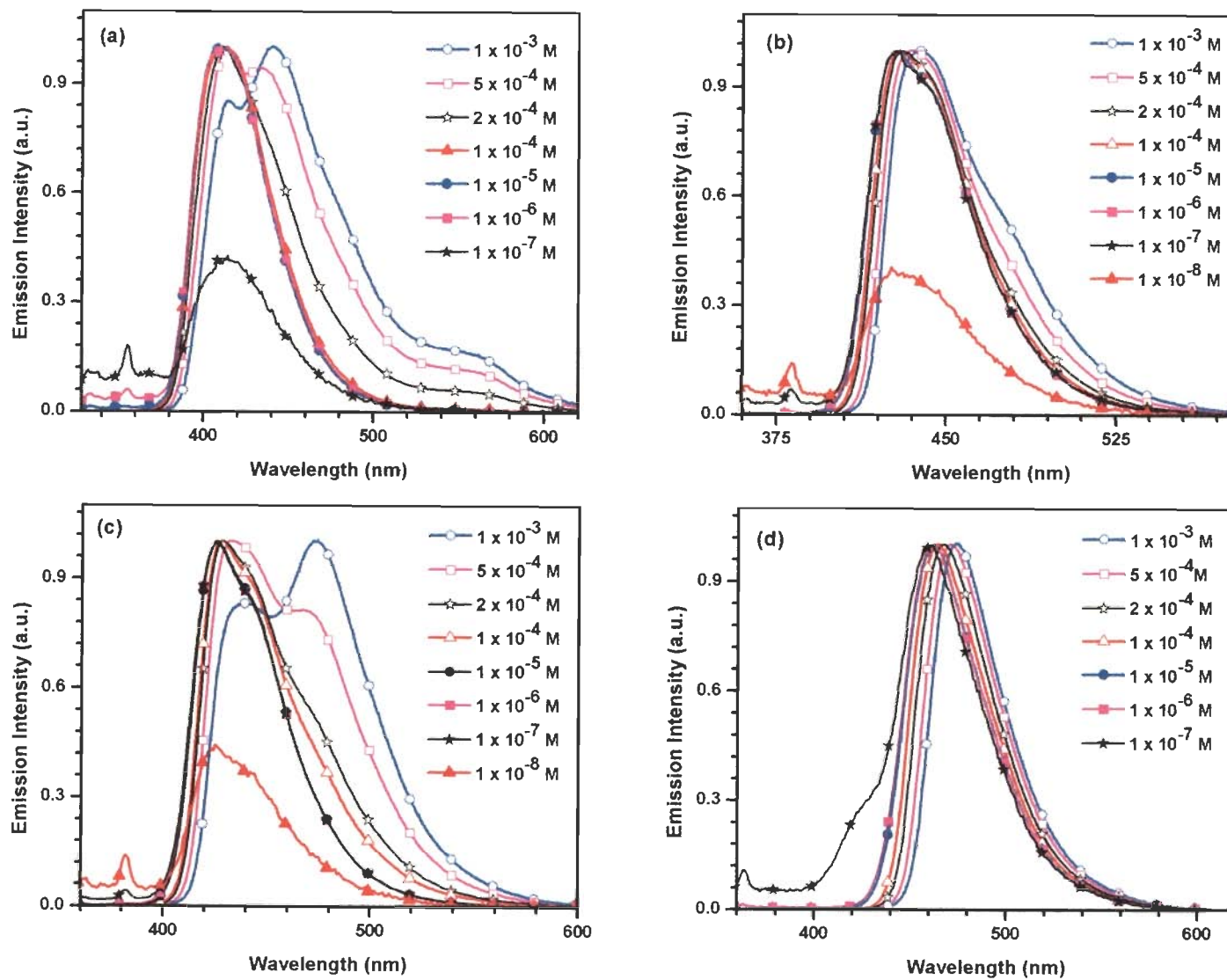


Figure 2.11 Emission spectra of (a) 14a, (b) 14b, (c) 14c and (d) 14d recorded in toluene at different concentration.

Quantum yield was also measured for the compounds of both series in toluene and dichloromethane (see Table 2.1 & 2.2). The fluorescence efficiency of the samples was high in non-polar solvents such as toluene and it decreased in dichloromethane. Quantum yield and solvent polarity dependant emission are mainly determined by the non radiative decay processes in the excited state. Such non radiative decay processes are more pronounced in polar solvents when compared to non polar solvents. Another reason could be the presence of dipole-dipole interaction in the excited state. The intra/intermolecular charge transfer character in excited state facilitates non-radiative decay and thus, diminishes the quantum yield in polar solvents.⁵⁹

It has been noticed that the compounds that display comparatively lower oxidation potential exhibit less quantum yield when recorded in polar solvents. Thus, among amine derivatives (**7a-7d**), pyrene derivative displays relatively lesser quantum efficiency in dichloromethane ($\Phi_F = 11\%$). But the case is reversed in triphenylene derivatives. The compounds having low oxidation potential exhibited high quantum yield. This may be due to rigid nature of molecule which has less possibility to go for more conformational changes. The pyrene substituted derivative **14d** have the highest quantum yield among all derivatives.

A common trend was observed in Stokes' shift value for both the series. The Stokes' shift of the all the amine derivatives (**7a-7d**) & (**14a-14d**) are small when compared to the parent compound **5a** in fluoranthene.scheme and **12** in triphenylene series respectively. Lesser value of Stokes' shift is the indication of the less non-radiative decay of the molecule in the excited state and it is also a measure of rigidity in the ground state and more planarity in the excited state. This proposes that amine derivatives are more rigid and planar in the excited state as compared to their respective parents.

Similarly, bromo derivative (**5b**) and (**12**) has also displayed small Stokes' shift when compared to the cyano derivative (**6**) and (**13**) respectively because of the presence of a heavy bromine atom which make the compound more rigid (Tables 2.1 & 2.2). The value of Stokes' shift is larger for the carbazole (**14a**) derivative as compared to the amine derivatives (**14b-14d**).

Thus, amine functionality made the molecule more rigid and more planar in the excited state and it also decrease the chance of non-radiative decay which is an important factor in increasing the stability of the molecule. This explanation also suggests the diarylamines are more rigid and more planar in the excited state as compared to carbazole derivative. The trend of Stokes' shift values in less polar solvent toluene are $7c < 7d < 7a < 7b$ and $14d < 14b < 14c < 14a$ for fluoranthene and triphenylene respectively. Naphthalene derivative possess larger Stokes' shift than phenyl and pyrene derivatives. Moreover the Stokes' shift values are larger in more polar solvent because of the more solvated excited state or dipole-dipole relaxation of the excited state of molecule. Among all derivatives **14d** show the lesser Stokes' shift.

The solvatochromism has been performed for all the amine derivatives of fluoranthene series as well as triphenylene series. For this the absorption and emission spectra are recorded in different solvents from non polar to polar solvents. The solvents are cyclohexane (CH), carbon tetra chloride (CCl₄), toluene (TOL), chloroform (CHCl₃), dichloromethane (DCM), dimethylformamide (DMF), acetonitrile (ACN) and methanol (MeOH). The absorption and emission spectra in different solvents for amine derivatives of fluoranthene series are shown in Figure 2.12 & 2.13 and that of triphenylene series are presented in Figure 2.14 & 2.15. The absorption and emission data are displayed in Table 2.3 and Table 2.4 respectively. Solubility trend is same for the derivatives of both series. Diphenylamine derivatives of both series **7a** & **14b** are insoluble in methanol and partially soluble in cyclohexane and acetonitrile.

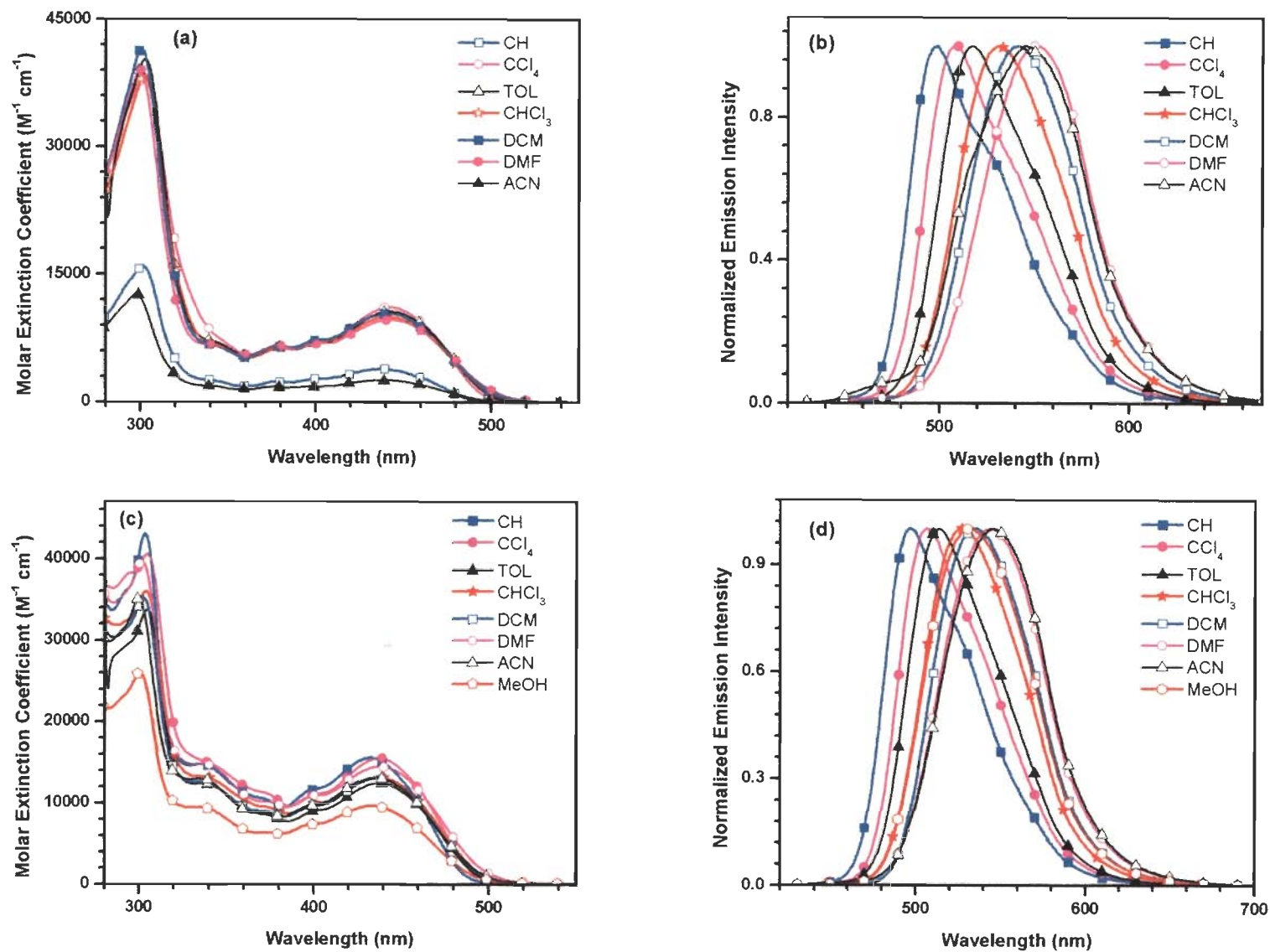


Figure 2.12 Absorption and emission spectra of 7a (a), (b) & 7b (c), (d) recorded in different solvents.

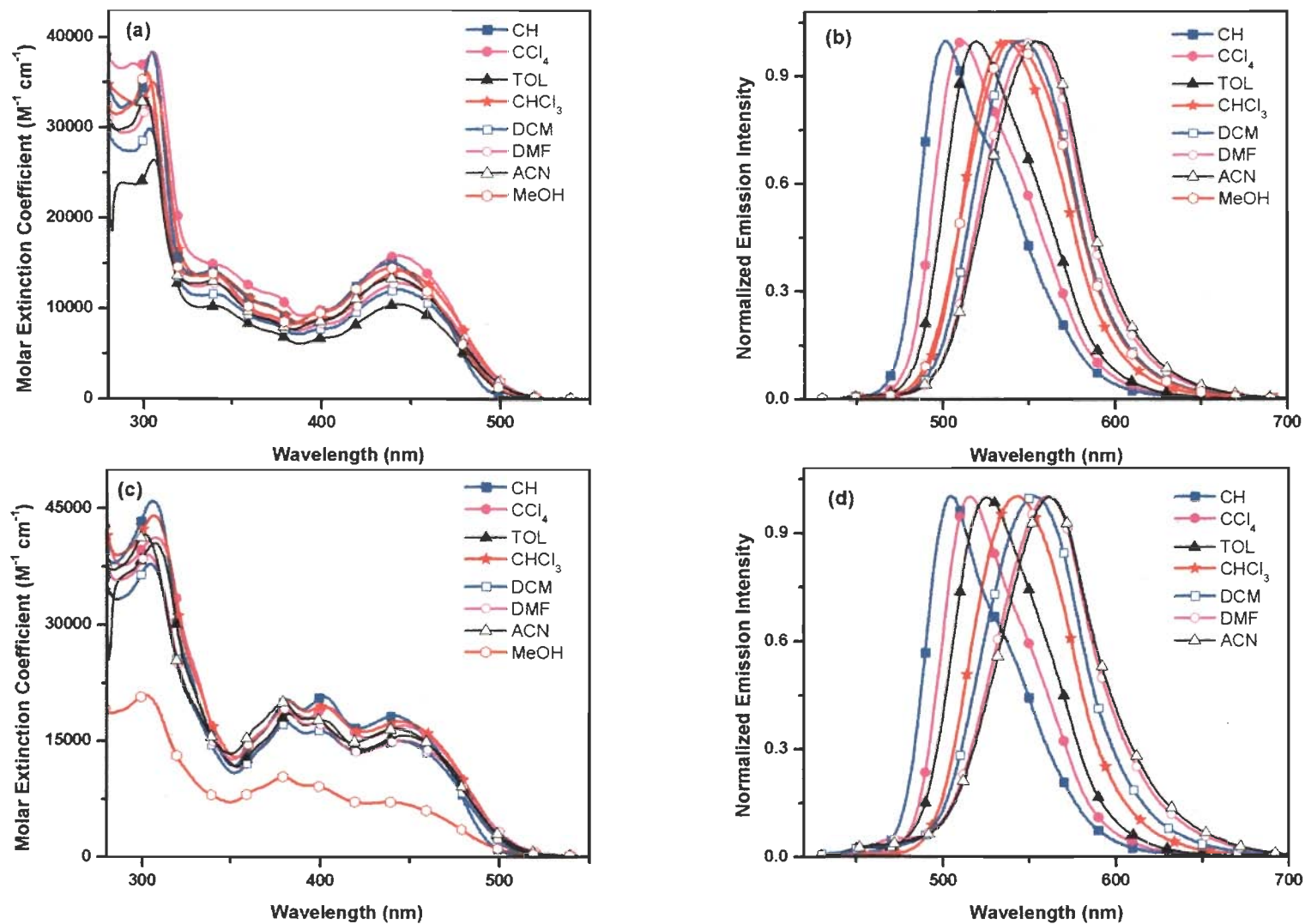


Figure 2.13 Absorption and emission spectra of **7c** (a), (b) & **7d** (c), (d) recorded in different solvents.

Naphthylphenyl and pyrenylphenylamine derivatives (**7b**, **14c** and **7d**, **14d**) are partially soluble in methanol. Compound **7c** showed good solubility in all solvent because of the presence of *t*-butyl group. Carbazole derivative in triphenylene series **14a** is not completely soluble in acetonitrile and methanol. The molar extinction coefficient cannot be measured for the compounds having solubility problem. Therefore, they are showing very less intensity in their absorption spectra.

No significant solvent dependent absorption behavior was observed for the fluoranthene based amine derivatives (**7a-7d**). The lack of solvatochromic shift in the absorption spectra suggests a small difference between dipole moment in the ground state and non polar locally excited state (Franck-Condon excited state). Thus, the ground state is non polar. However, the excited state solvatochromism observed for the compounds is noteworthy. The amine derivatives (**7a-7d**) displayed positive solvatochromism for the emission spectra i.e. a bathochromic shift was observed by increasing the solvent polarity. This is due to more dipole-dipole interaction in the excited state and interaction with a more polar solvent make the higher energy state of the molecule more stable resulting in decrease of energy gap. Some anomalous behavior was observed in emission spectra such as diphenylamine derivative (**7a**) shows blue shift in acetonitrile (Figure 2.12(b)) as compared that in DMF. Similarly a blue shift was observed in methanol for **7b-7d**. (Figure 2.12(d) & 2.13(d))

Among **14a-14d** some abnormal solvent dependant behavior was seen in case of absorption spectra. Compound **14b** & **14c** showed bathochromism and hyperchromism in CCl₄ (Figures 2.14(c) & 2.15(a)). The hump in compound **14d** is shifted towards lower wavelength (Figure 2.15(c)) as the polarity of solvent increases which suggest that ground state of **14d** is interacting with the solvent and is more stable in polar solvent or solvation of molecule occur by polar

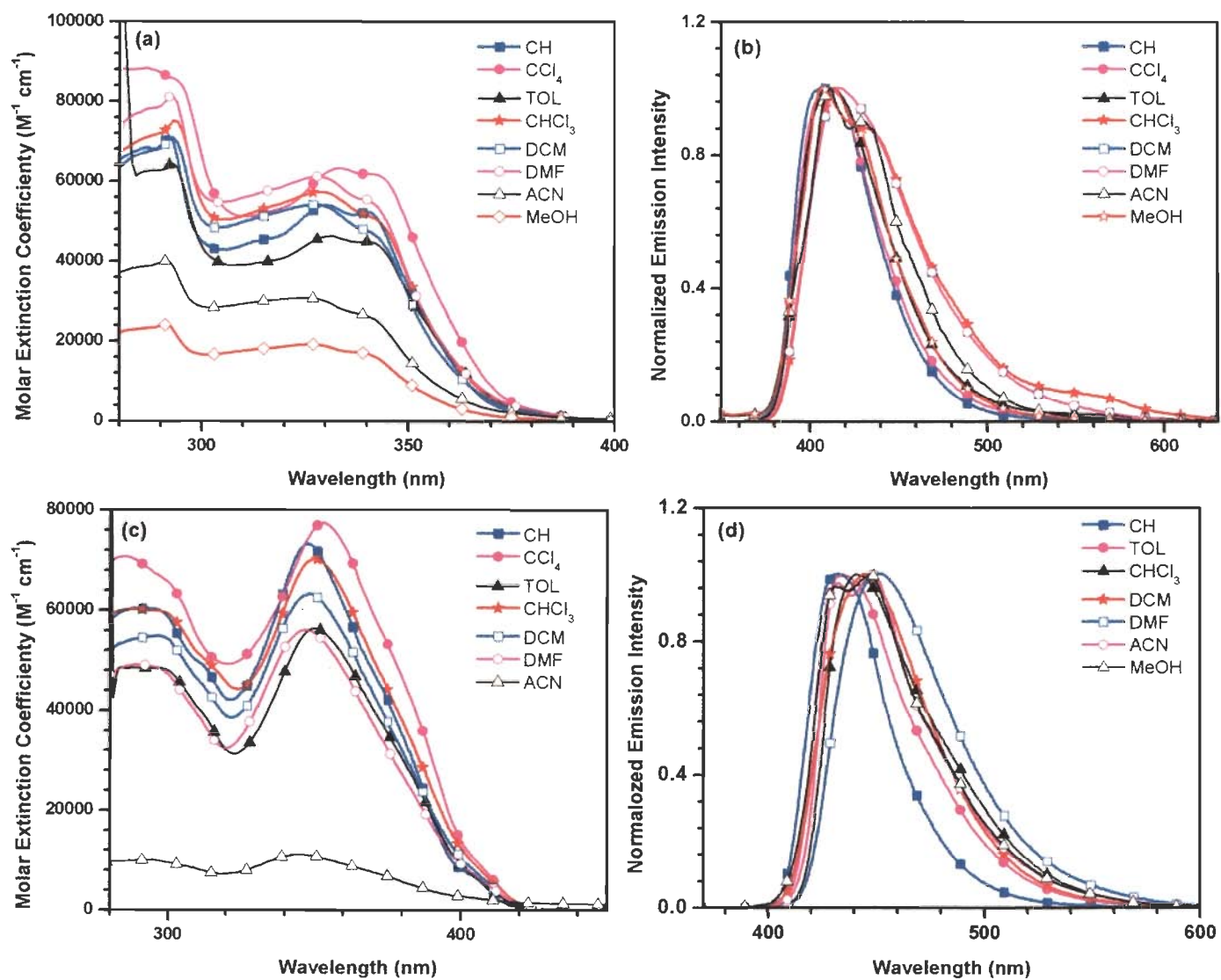


Figure 2.14 Absorption and emission spectra of 14a (a), (b) & 14b (c), (d) recorded in different solvents.

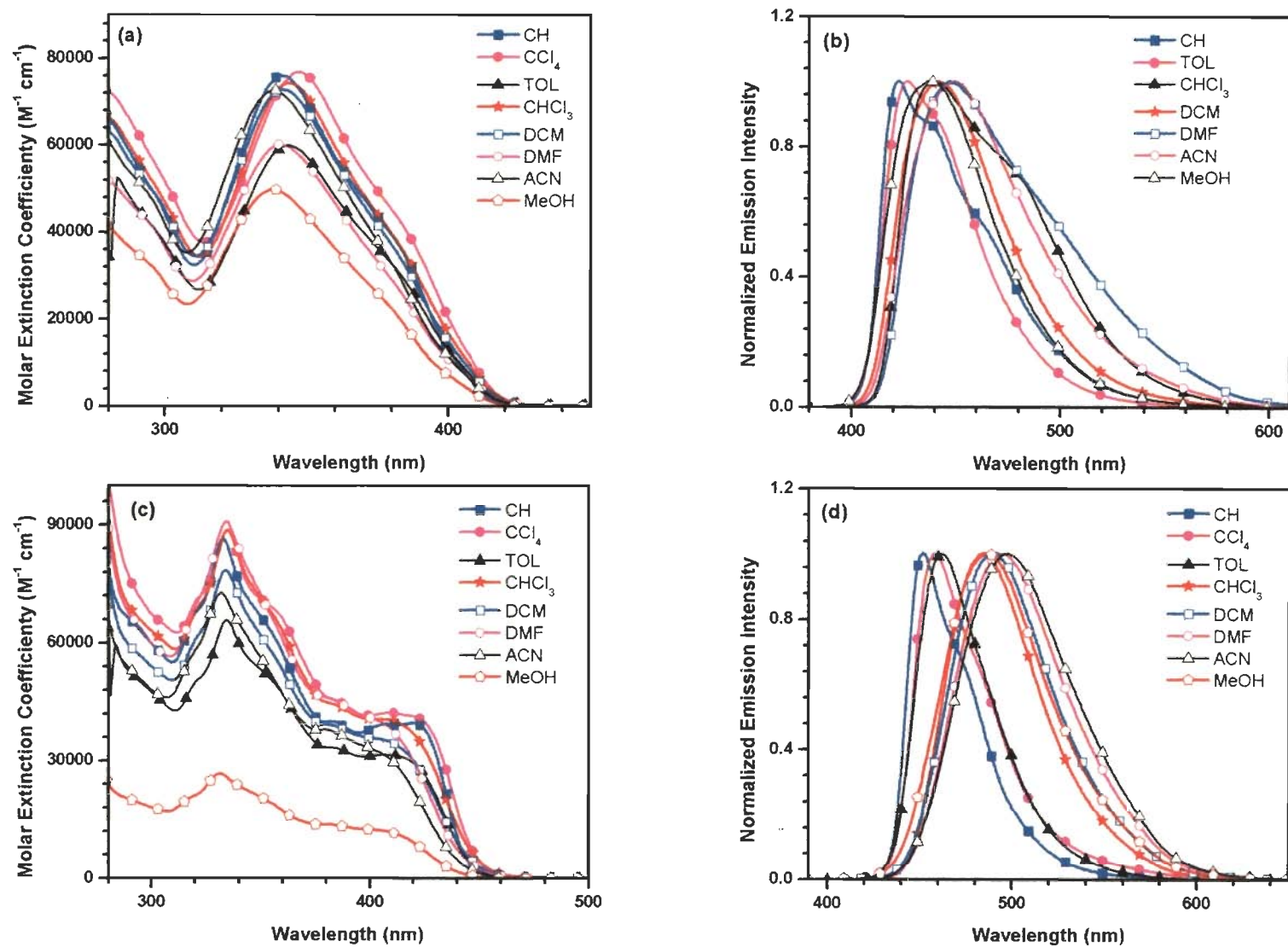


Figure 2.15 Absorption and emission spectra of 14c (a), (b) & 14d (c), (d) recorded in different solvents.

Table 2.3 Absorption data of compounds 7a-7d and 14a-14d in different solvents.

Compound	λ_{\max} , nm (ϵ_{\max} , $M^{-1}cm^{-1}$) $\times 10^3$							
	Cyclohexane	CCl ₄	Toluene	Chloroform	dichloromethane	DMF	acetonitrile	Methanol
7a	301, 437	302 (38.5), 441 (11.1)	303 (40.3), 443 (10.6)	302 (38.4), 443 (9.9)	300 (41.5), 442 (10.3)	300 (39.0), 443 (9.7)	298, 442	-
7b	303 (43.0), 433 (15.5)	304 (40.5), 437 (15.4)	304 (33.7), 437 (12.5)	304 (35.9), 438 (13.2)	302 (35.3), 435 (13.0)	302 (39.6), 438 (14.4)	300 (35.1), 435 (13.1)	300, 432
7c	304 (38.3), 439 (15.0)	305 (38.3), 443 (15.8)	306 (16.4), 443 (10.5)	305 (35.0), 444.0 (14.1)	303 (29.9), 443.0 (12.0)	303 (32.4), 444 (12.8)	301 (33.2), 441 (13.4)	302 (36.1), 439 (14.5)
7d	306 (45.9), 382 (20.2), 402 (20.6), 441 (18.2)	307(41.2), 384 (18.7), 404 (19.2), 447 (16.9)	307(40.5), 383 (18.4), 401 (17.6), 447 (15.7)	306 (44.0), 383 (20.0), 402 (19.4), 444 (17.4)	304 (37.8), 381 (17.2), 399 (16.2), 444 (14.9)	303(38.9), 381 (19.1), 398 (17.1), 446 (15.0)	301 (41.6), 380 (19.9), 396 (17.8), 442 (16.6)	302, 438
14a	292 (71.1), 330 (53.8)	288 (87.8), 333 (63.0)	293 (64.2), 331 (46.3)	293 (75.0), 329 (57.2)	293 (70.7), 328 (53.9)	293 (81.1), 328 (61.0)	291, 325	291, 327
14b	348 (73.0)	353(77.3)	350 (56.4)	350 (70.2)	349 (63.0)	347 (56.1)	345	-
14c	341 (75.9)	347 (76.7)	344 (59.9)	343 (74.3)	342 (72.7)	340 (60.0)	339 (72.6)	338(49.7)
14d	333 (86.4), 420 (39.5)	335 (88.7), 409 (42.0)	335 (65.7), 407 (31.5)	335 (88.6), 404 (40.4)	334 (78.4), 403 (35.4)	334 (90.8), 400 (40.7)	332 (72.8), 397 (33.8)	331, 401

Table 2.4 Emission data of compounds **7a-7d** and **14a-14d** in different solvents.

Compound	λ_{em} , nm							
	cyclohexane	CCl ₄	toluene	chloroform	dichloromethane	DMF	Acetonitrile	Methanol
7a	499	508	517	532	541	550	544	-
7b	497	506	513	525	536	543	545	532
7c	501	512	520	536	547	553	555	539
7d	505	516	525	544	553	561	562	555
14a	410	412	412	415	417	417	411	406
14b	433	-	435	441	444	450	433	431
14c	423	-	427	441	442	447	450	438
14d	452	458	462	485	492	493	498	486

Table 2.5 Stokes' shift observed for the diarylamine derivatives (**7a-7d**) and (**14a-14d**) in different solvents and the parameters used for correlation

Solvent	Orientation polarizability	$E_T(30)$	π^*	Stokes' shift							
				7a	7b	7c	7d	14a	14b	14c	14d
Cyclohexane	-0.001	30.9	0	2843	2974	2819	2874	5913	5641	5685	1686
CCl ₄	0.01143	32.4	0.28	2991	3120	3042	2992	5758	-	-	2616
Toluene	0.0135	33.9	0.54	3231	3390	3343	3324	5940	5583	5651	2925
Chloroform	0.148	39.1	0.58	3776	3783	3866	4140	6299	5896	6479	4134
Dichloromethane	0.219	40.7	0.82	4140	4332	4292	4439	6507	6131	6615	4489
DMF	0.275	43.2	0.88	4392	4415	4439	4596	6507	6596	7040	4716
Acetonitrile	0.306	45.6	0.75	4242	4640	4658	4831	6438	5784	7276	5109
Methanol	0.309	55.4	0.60	-	4351	4226	4813	5950	-	6755	4362

solvent in ground state. Among the emission profiles of **14a-14d**, compound **14a** is not showing significant difference in emission profile by changing the solvent polarity it show blue shift in acetonitrile and methanol (Figure 2.14(b)). **14b** also show blue shifted and vibronic emission in acetonitrile and methanol (Figure 2.14(d)). The reason could be the formation of intramolecular charge transfer state (TICT) in excited state. Thus, the band at 431 nm is due to locally excited state (LE) and the red shifted band at 448 nm is due to ICT state in the emission spectra of **14b** recorded in acetonitrile and methanol. Compound **14b** & **14c** did not show emission in CCl_4 indicating the interaction of these compounds with CCl_4 in the excited state. **14b** and **14c** also deviates from solvatochromism in methanol. **14c** and **14d** follow the proper trend of positive solvatochromism in emission profile (Figure 2.15). The discussion indicates that the excited state of **14d** is the most polar and that of **14a** is the least polar among triphenylene series.

On comparison between fluoranthene and triphenylene-based triarylamine derivatives, the extent of solvatochromism is less for later one. Triphenylene derivatives (**14b** & **14c**) are interacting with the chloro compounds especially in CCl_4 resulting in the fluorescence quenching. While there is no abnormal impact of chloro compound have been seen among fluoranthene derivatives in excited as well as in ground state. All the amine derivatives of both series show blue shift in protic polar solvent methanol which indicates some specific interaction such as hydrogen bonding occurring in excited state. This was confirmed by plotting emission as a function of Kamlet-Taft parameter as discussed later.

The majority of chemical reactions occur in solutions; hence, one of the most important problems is the study of the dependence of the reactivity of molecules on the properties of the medium and the role of the solvent and its interactions with the solute. Intermolecular interactions include two major components: nonspecific (van der Waals interactions

operative for molecules in all cases with no exceptions and electrostatic interactions) and specific (pairwise interactions of the chemical nature determined by individual features of the interacting molecules).

It is possible to estimate the change in dipole moment between ground and excited state by the use of a well-known solvatochromic method. The increase in the dipole moment value in the excited state, $\Delta\mu$, was estimated using the dependence of either the fluorescence wavenumber, ν_f or the Stokes shift, $\Delta\nu$ on some solvent polarisation functions, the Lippert-Mataga model and the $E_T(30)$ solvent parameter given by Reichardt. The difference in frequency of the absorption and fluorescence band maxima, $(\nu_{ab}-\nu_{fl})$, becomes larger with increasing solvent polarity and is a measure of the dipole moment difference, $\Delta\mu_{ge} = \mu_e - \mu_g$. $\Delta\mu_{ge}$ can be estimated from the Lippert-Mataga equation.

$$\nu_{ab} - \nu_{fl} = \frac{2}{hc} \left(\frac{\epsilon - 1}{2\epsilon - 1} - \frac{n^2 - 1}{2n^2 + 1} \right) \frac{(\mu_e - \mu_g)^2}{a^3}$$

Where h is Planck's constant, c is the velocity of light, ν_{ab} and ν_{fl} are the absorption and emission maxima (cm^{-1}), respectively, a (\AA) is the Onsager radius of solutes, Δf represents a measure of the solvent polarity and polarizability defined by the dielectric constant ϵ and refractive index n of solvents, respectively.

$$\Delta f = \frac{\epsilon - 1}{2\epsilon - 1} - \frac{n^2 - 1}{2n^2 + 1}$$

But orientation polarizability only tells about non specific interactions. Therefore, $E_T(30)$ was used to estimate specific interaction such as hydrogen bonding or charge transfer in excited state.

Another parameter Kamlet et al.'s π^* scale takes into account both non-specific as well as specific interactions. Parameters of the Kamlet-Taft solvatochromic relationship which

measure separately the hydrogen bond donor (α), hydrogen bond acceptor (β), and dipolarity/polarizability (π^*) properties of solvents as contributing to overall solvent polarity. Using the π^* , α and β values for the solvents, the multiple linear regression equation for the emission maximum (expressed in 10^3 cm^{-1}) was found to be

$$\bar{\nu}_f^{max} = 23.36 - 6.70\pi^* - 0.64\alpha + 0.54\beta$$

Here we have plotted Stokes' shift vs orientation polarizability or $E_T(30)$ parameter for all amine derivatives of both series (**7a-7d** & **14a-14d**) to know the interaction of molecules with solvent. We have also plotted emission wavelength in terms of wave number vs π^* (Kamlet-Taft parameter). The values of Stokes' shift of amine derivatives along with these three parameters are given in Table 2.5.

Compound **7a** shows a linear relationship in polarizability and Stokes' shift in Lippert-Mataga plots with the increase in polarity up to DMF i.e. Stokes' shift is increasing in a linear trend with increasing polarizability of solvent. It shows the general solvent effect of polarity on fluorophore (Figure 2.16(a)). But in acetonitrile some other interactions are taking part. The linearity also deviates in toluene but the extent of deviation is less as compared to acetonitrile. The possibility of charge transfer in excited state after interaction of solvent was demonstrated by $E_T(30)$ parameter. Now $E_T(30)$ plot of **7a** (Figure 2.16(b)) shows linearity in toluene also. It suggests that specific interaction started with toluene along with the general solvent effect. **7a** also shows deviation from linearity for toluene and acetonitrile in Kamlet-Taft plot (Figure 2.16(c)). Solvatochromism was not done in methanol because of the solubility problem. Naphthylphenylamino derivatives **7b** and **7c** also show the similar trend in Lippert-Mataga and $E_T(30)$ plots as in **7a**. Toluene and acetonitrile are deviating from the linearity in Lippert-Mataga plot (Figure 2.17a & 2.18a) while only acetonitrile shows deviation from linearity in $E_T(30)$ plot.

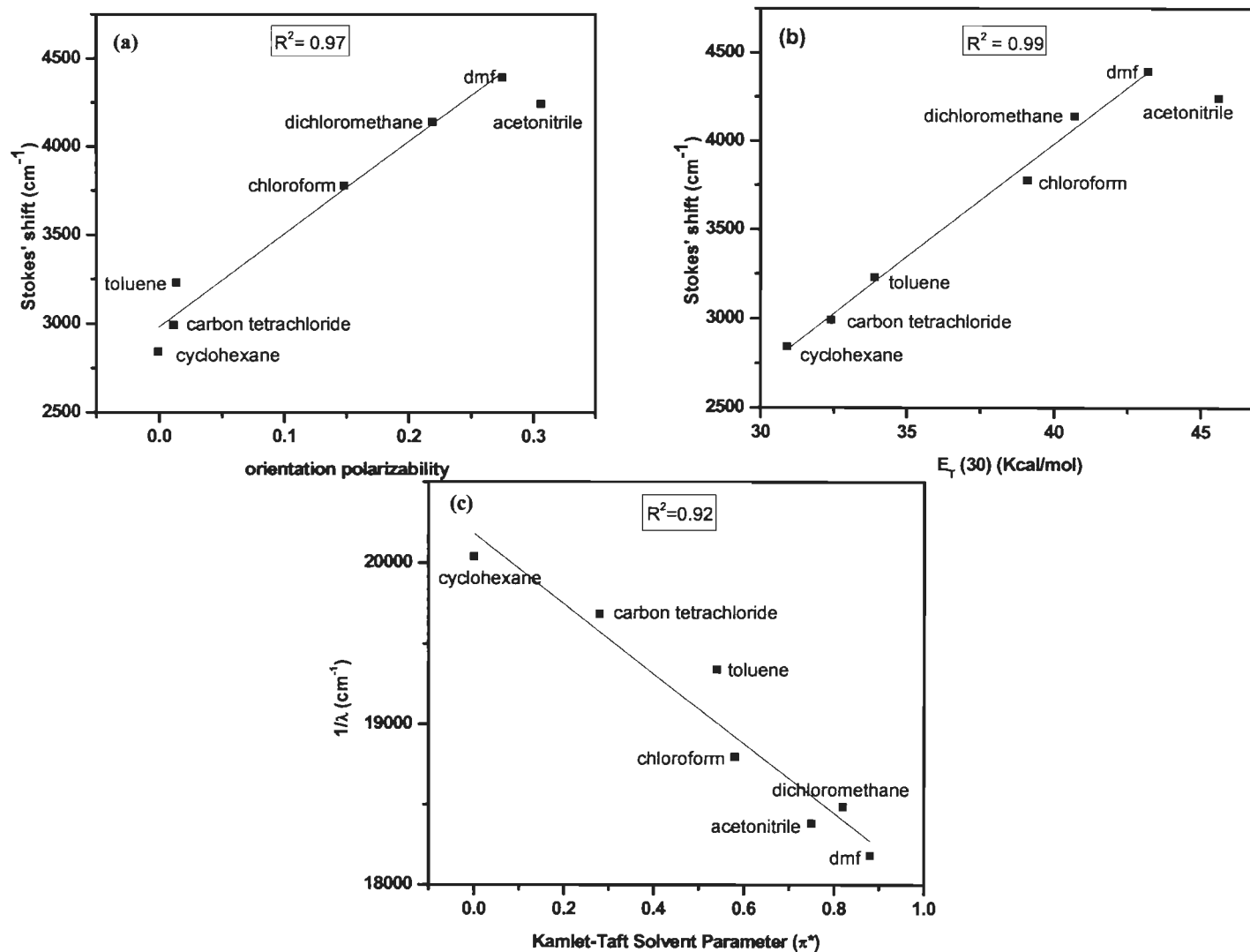


Figure 2.16 Plots for 7a in different solvents (a) Lippert Mataga plot showing Stokes' shift vs orientation polarizability of the solvents, (b) Stokes' shift vs $E_T(30)$ parameter, (c) emission maxima (in cm^{-1}) vs Kamlet-Taft solvent polarity parameter.

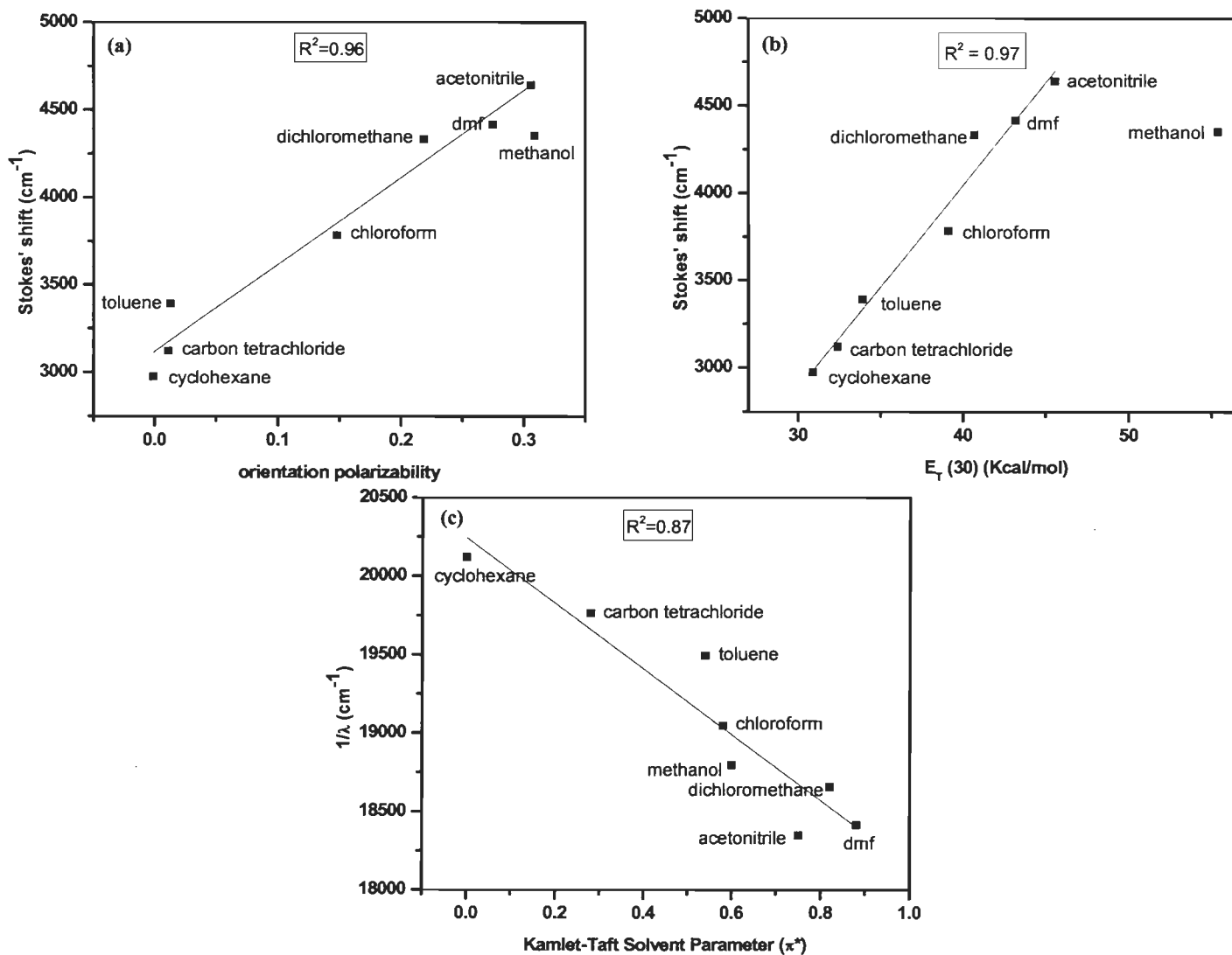


Figure 2.17 Plots for 7b in different solvents (a) Lippert Mataga plot showing Stokes' shift vs orientation polarizability of the solvents, (b) Stokes' shift vs $E_T(30)$ parameter, (c) emission maxima (in cm^{-1}) vs Kamlet-Taft solvent polarity parameter.

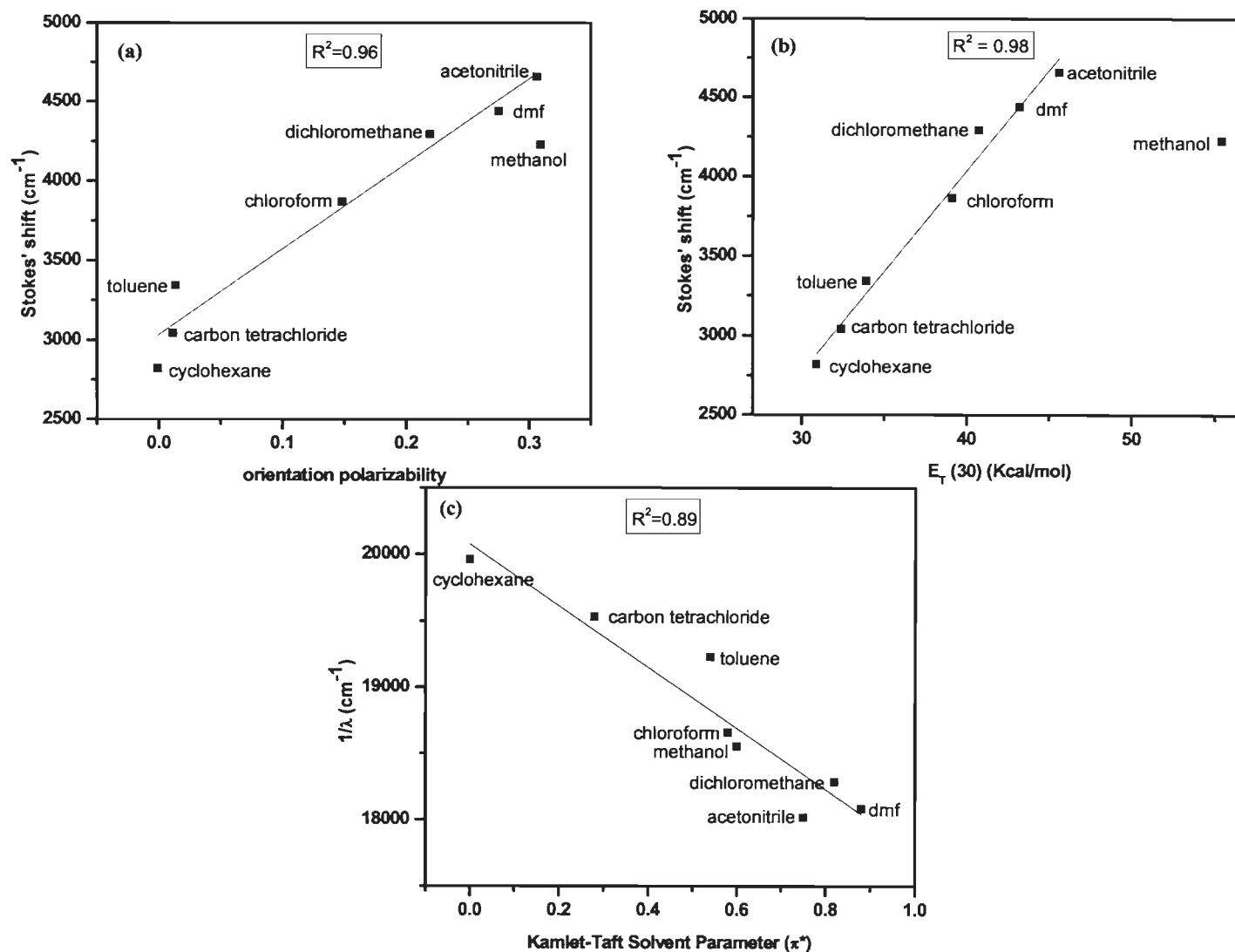


Figure 2.18 Plots for 7c in different solvents (a) Lippert-Mataga plot showing Stokes' shift vs orientation polarizability of the solvents, (b) Stokes' shift vs $E_T(30)$ parameter, (c) emission maxima (in cm^{-1}) vs Kamlet-Taft solvent polarity parameter.

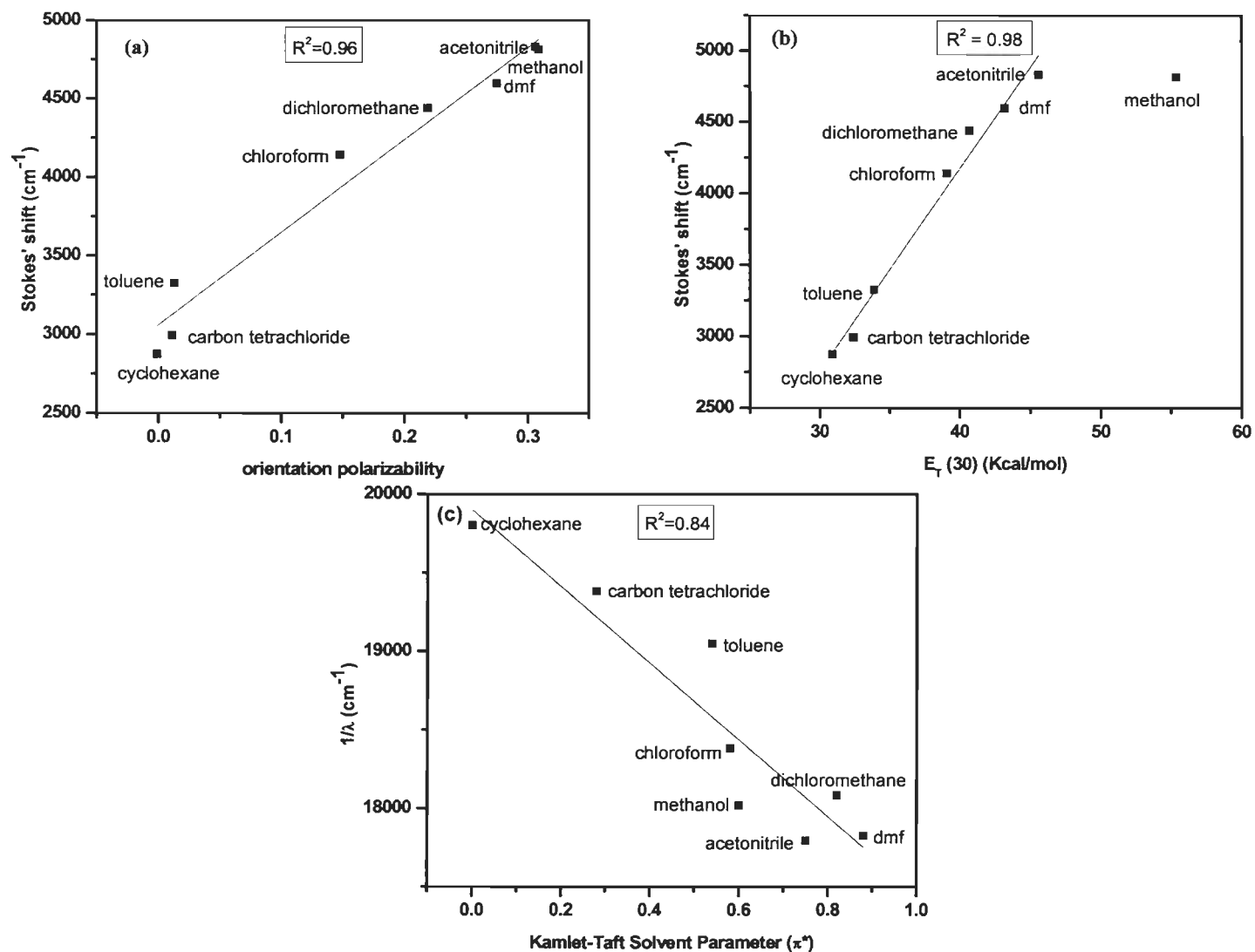


Figure 2.19 Plots for 7d in different solvents (a) Lippert-Mataga plot showing Stokes' shift vs orientation polarizability of the solvents, (b) Stokes' shift vs $E_T(30)$ parameter, (c) emission maxima (in cm^{-1}) vs Kamlet-Taft solvent polarity parameter.

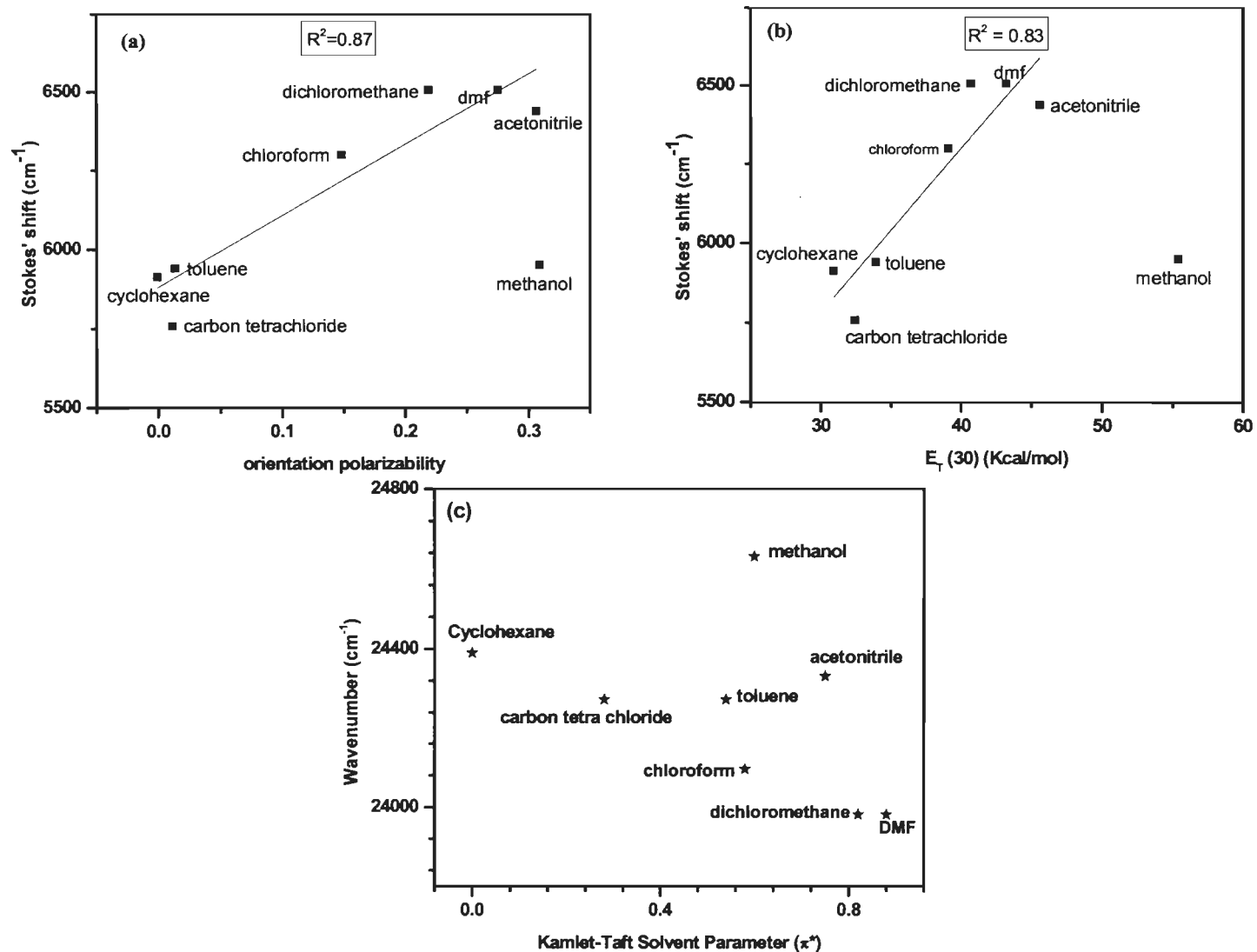


Figure 2.20 Plots for 14a in different solvents (a) Lippert-Mataga plot showing Stokes' shift vs orientation polarizability of the solvents, (b) Stokes' shift vs $E_T(30)$ parameter, (c) emission maxima (in cm^{-1}) vs Kamlet-Taft solvent polarity parameter.

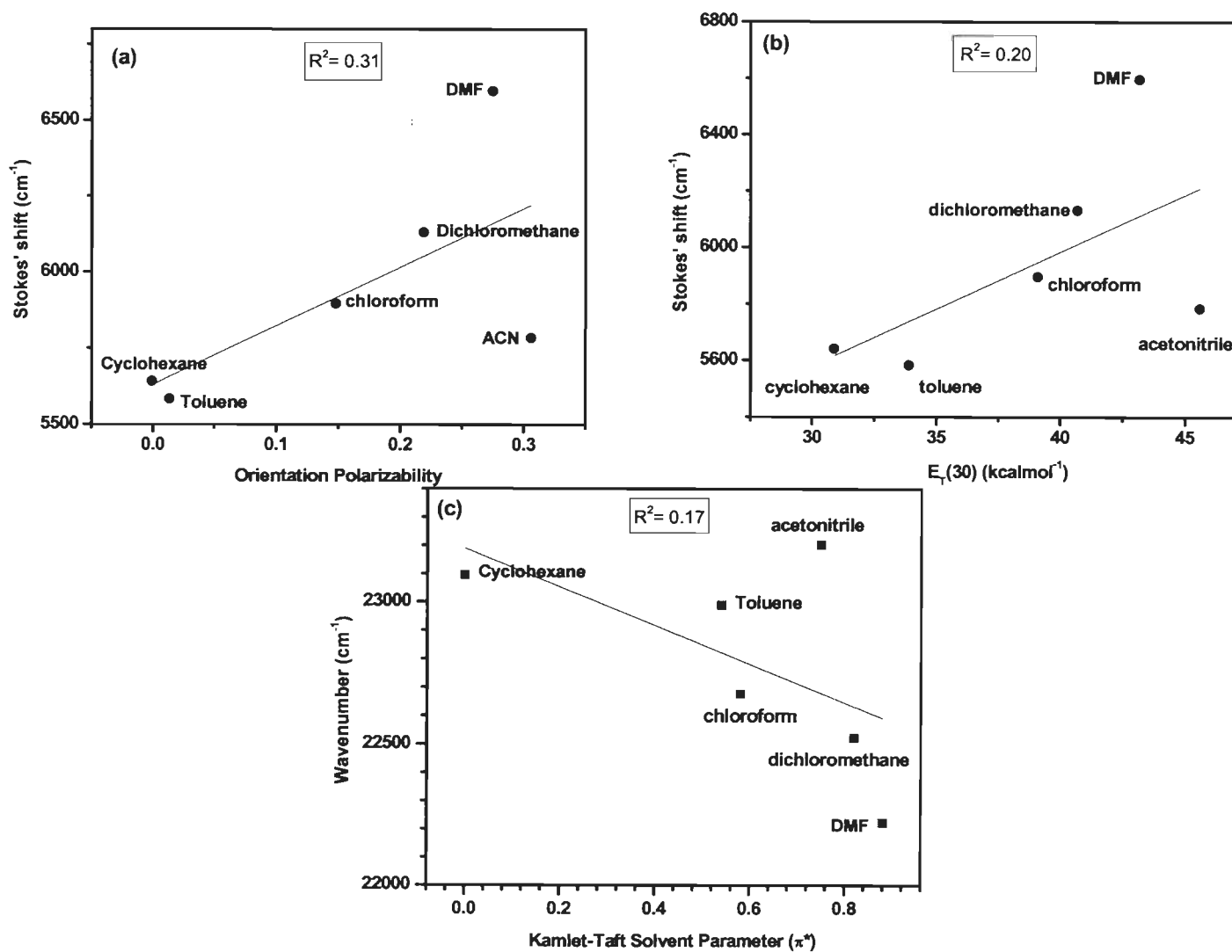


Figure 2.21 Plots for **14b** in different solvents (a) Lippert-Mataga plot showing Stokes' shift vs orientation polarizability of the solvents, (b) Stokes' shift vs $E_T(30)$ parameter, (c) emission maxima (in cm^{-1}) vs Kamlet-Taft solvent polarity parameter.

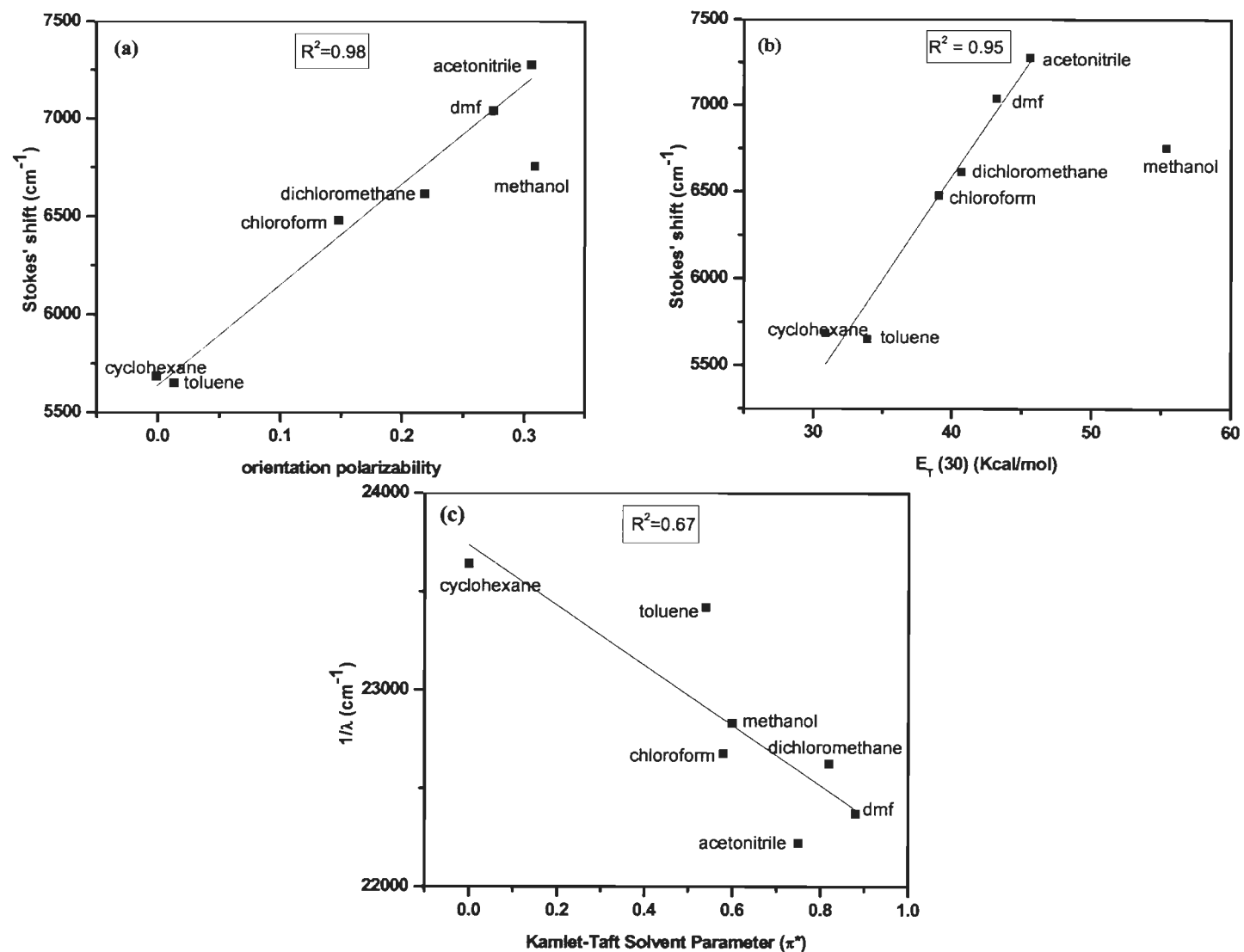


Figure 2.22 Plots for **14c** in different solvents (a) Lippert-Mataga plot showing Stokes' shift vs orientation polarizability of the solvents, (b) Stokes' shift vs $E_T(30)$ parameter, (c) emission maxima (in cm^{-1}) vs Kamlet-Taft solvent polarity parameter.

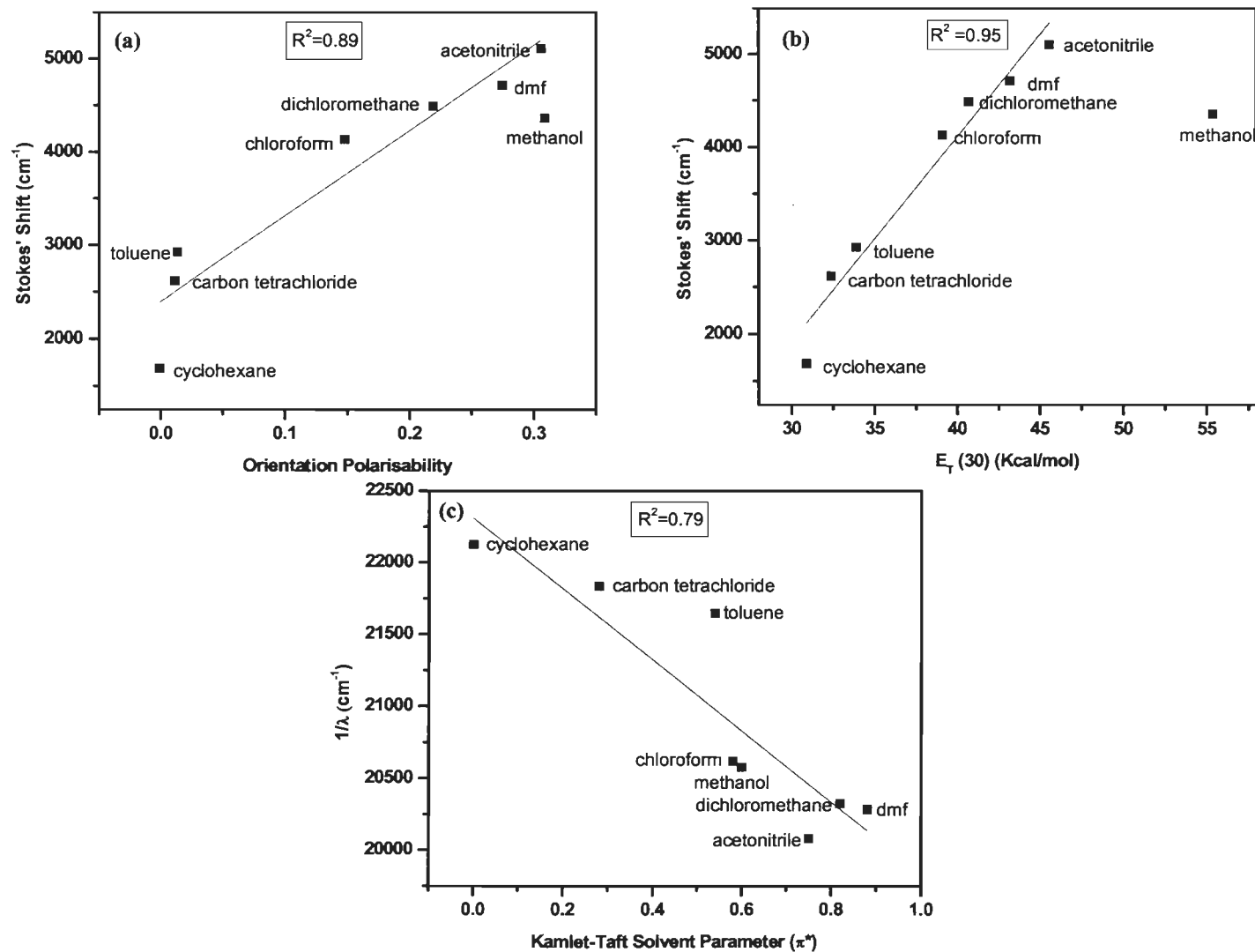


Figure 2.23 Plots for **14d** in different solvents (a) Lippert-Mataga plot showing Stokes' shift vs orientation polarizability of the solvents, (b) Stokes' shift vs $E_T(30)$ parameter, (c) emission maxima (in cm^{-1}) vs Kamlet-Taft solvent polarity parameter.

Toluene has come in line as happened in case of **7a** (Figure 2.17(b) & 2.18(b)). Methanol which is a protic polar solvent show deviation in linearity in Lippert-Mataga and $E_T(30)$ suggesting some specific interaction such as hydrogen bonding occurring in polar protic solvent. These specific interactions were confirmed by Kamlet-Taft in which methanol came closer to linearity (Figure 2.17(c) & 2.18(c)). The solvent effect is similar for **7b** & **7c** showing there is no effect of *t*-butyl on the molecule environment in excited state.

Pyrenylphenylamine derivative (**7d**) follow a linear trend in Lippert-Mataga plot for polar solvents from toluene to methanol while deviating in non polar solvents this suggest that some other specific interaction are also there with general solvent interaction (Figure 2.19(a)). These specific interactions such as charge transfer interaction was seen in $E_T(30)$ plot which show linearity for all solvents except methanol (Figure 2.19(b)). Methanol also shows deviation in Kamlet-Taft showing that in methanol only general solvent effect dominating (Figure 2.19(c)). Other specific interaction like charge transfer and hydrogen bonding did not take part in methanol. Kamlet-Taft show more deviation from linearity in case of **7d** indicating there is less hydrogen bonding interaction occur as compared to naphthylphenylamine derivatives **7b** & **7c**.

The solvatochromism study of all the fluoranthene-based amine derivatives (**7a-7d**) indicates that there was nonspecific as well as specific interaction occurred in excited state by changing the solvent polarity. The donor-acceptor interaction increases with increase in solvent polarity. The hydrogen bonding interactions are more prominent in naphthylphenylamine derivatives (**7b** & **7c**).

Among triphenylene-based amine derivatives, carbazole and diphenylamine derivatives (**14a** and **14b**) did not follow a linear trend in all the three plots (Figures 2.20 & 2.21). While the naphthylphenylamine and pyrenephenylamine derivative (**14c** and **14d**) showed a linear trend in

Lippert-Mataga and $E_T(30)$ plots showing the general solvent as well as specific solvent interaction occurring in the molecules (Figures 2.22 & 2.23). $E_T(30)$ plots is a measure of charge transfer and linearity in these plots indicating the charge transfer in the molecule. The Stokes' shift of **14c** and **14d** increases in linear fashion with increasing the polarity from cyclohexane to acetonitrile. Methanol is deviating from linearity in both the cases. But in Kamlet-Taft plot of **14c**, methanol has come on the linear fit showing specific interaction like hydrogen bonding is occurring in naphthylphenylamine derivative. While these interactions are less prominent in **14d**.

In case of cyclohexane the Stokes' shift is very less for **14d**, it deviates from the linearity in Lippert-Mataga plot. The reason could be the completely non polar nature of cyclohexane but amine derivative (**14d**) is polar in nature, the diffusion rate of fluorophore may high in non polar solvent which induce very less interaction with the solvent. Toluene also shows some deviation in **14d** as calculated Stokes' shift is more than expected value.

2.2.3 Theoretical investigations

In order to understand the absorption characteristics of the dyes we have performed a theoretical calculation for the molecules **5a**, **6** & **7a** in fluoranthene series and **10**, **11** & **12a-12d** in triphenylene series using the density functional theory with the B3LYP functional and 6-31G(d,p) basis set. The prominent higher wavelength vertical transitions and their oscillator strength (f) predicted by the theory is collected in Table 2.6. Among fluoranthene derivatives, the higher wavelength absorption peaks observed for these compounds in toluene agrees well with the theoretically forecast values. A slight discrepancy present for the amine derivative **7a** may be due to the charge transfer nature of the transition. As the red-shifted absorption peaks originated mainly due to the electronic transition from the HOMO to LUMO, the nature of the frontier orbitals were examined. The frontier molecular orbital

diagrams of fluoranthene derivatives are shown in the Figure 2.24.

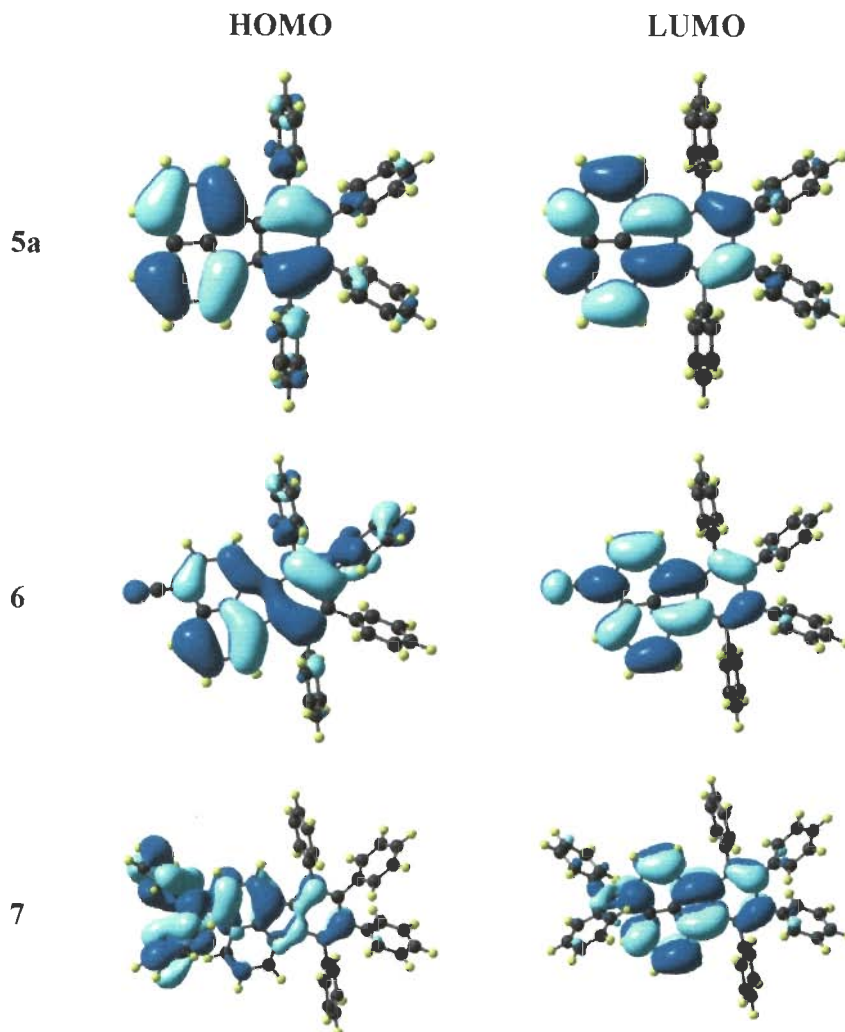


Figure 2.24 Electronic distribution in the frontier molecular orbitals of the compounds **5a**, **6** and **7a**.

From that it is clearly evident that the HOMO and LUMO both are located on the fluoranthene segment in **5a** indicating π - π^* transition among the molecule. In case of **6**, HOMO is located on fluoranthene unit and LUMO is spread upto cyano unit suggesting the transition is π - π^* with very less contribution of charge transfer. It is also evident by the less oscillator strength for low energy transition of compound **6**. The HOMO of amine derivatives spread on amine unit as well on fluoranthene part while its LUMO is situated on fluoranthene unit. From these observations, it may be concluded that the red-shifted absorption in these

compounds are mainly π - π^* transition and with a little contribution from the charge transfer transition from the amine donor to the fluoranthene π -acceptor in the case of amine substituted derivatives **7a-7d**. The extent of charge transfer transition is high as compared to the cyano bearing derivative (**6**).

Figure 2.25 shows the theoretically computed molecular orbitals in the ground states for the representative compounds **12-13**. For **12** and **13**, HOMO and LUMO is located all over the molecule indicating π - π^* transition. The band experimentally found around 296-306 nm in the compounds **12** & **13** appears to be composed of multiple overlapping π - π^* transitions involving HOMO-1 and LUMO+1 orbitals (Table 2.6). After the introduction of amine functionality, HOMO and LUMO become separated indicating the origin of charge transfer character from electron rich amine donors to electron deficient triphenylene core. In amine substituted derivatives (**14a-14d**), HOMO is located on the both diarylamine unit as well as on triphenylene core for all amine derivatives (**14a-14d**) but position for LUMO is different. LUMO is located on triphenylene core for **14a** and **14b** but for **14c** LUMO is spreaded on triphenylene and naphthalene. For **14d** LUMO is completely present on both pyrene unit. In **14a** and **14b**, triphenylene act as an electron acceptor while in **14d** pyrene is acting as an electron acceptor. This observation indicates that the pyrene behaves as a strong electron acceptor as compared to the triphenylene.

The theoretically predicted high energy transition for all amine derivatives (**14a-14d**) is more likely due to HOMO-LUMO transition showing the presence of charge transfer character. Therefore, the frontier molecular orbital diagram revealed that in **14a** and **14b**, the low energy transition is mainly due to π - π^* transition with the contribution of charge transfer character from diarylamine to triphenylene while in **14c** the electrons on nitrogen of amine

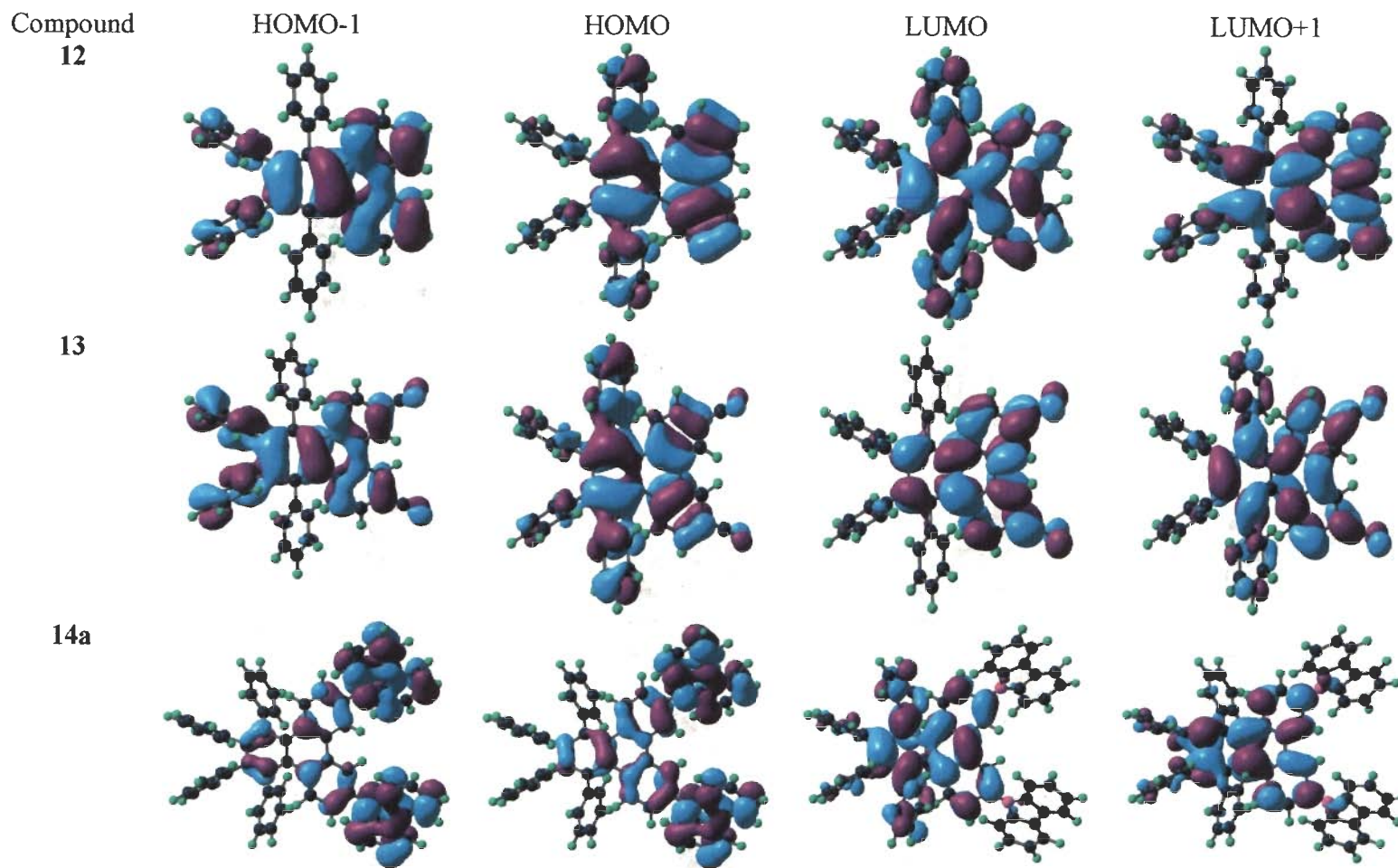


Figure 2.25 Electronic distribution in the frontier molecular orbitals of the compounds 12, 13 and 14a-14d.

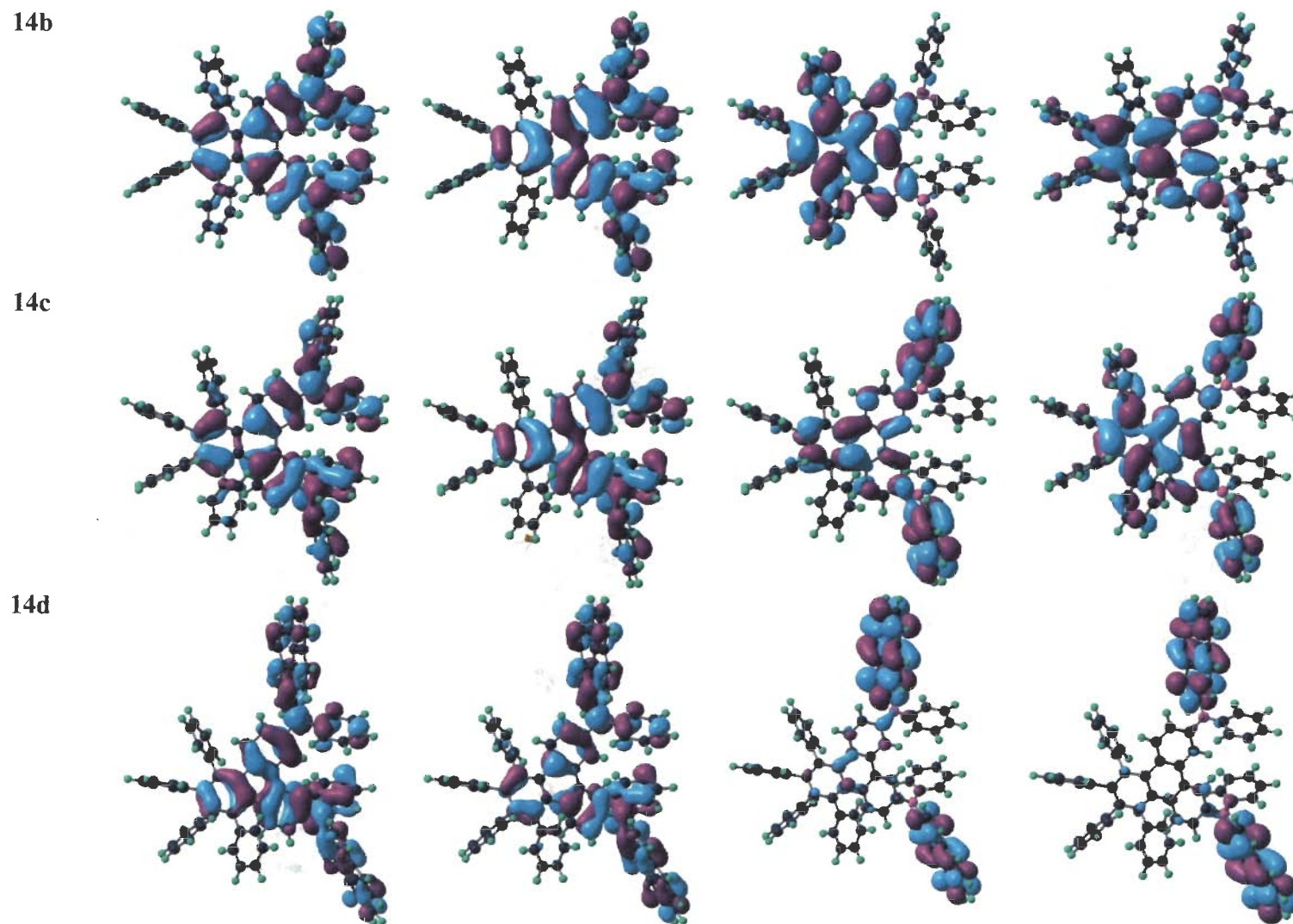


Figure 2.25 Electronic distribution in the frontier molecular orbitals of the compounds 12, 13 and 14a-14d. (continued)

is shared by triphenylene and naphthalene both. The contribution of HOMO-LUMO transition for **14c** is also lesser than **14a** and **14b**. The origin of low energy band of pyrene derivative (**14d**) is due to π - π^* transition in pyrene unit.

Table 2.6 Predicted (TDDFT B3LYP/6-31G(d,p)) vertical transitions and their assignments.

Compound	λ_{abs} (nm)	F	Assignment
5a	375	0.02	HOMO-1→LUMO(+93%)
	360	0.25	HOMO→LUMO (+92%)
6	411	0.02	HOMO→LUMO (53%), HOMO-1→LUMO (40%)
	380	0.31	HOMO-1→LUMO (+54%), HOMO→LUMO (+40%)
7a	469	0.28	HOMO→LUMO (+98%)
	376	0.09	HOMO-1→LUMO (+85%)
12	300	0.3961	HOMO-1→LUMO (+31%), HOMO→LUMO+1 (+28%), HOMO-1→LUMO+2 (+17%), HOMO-2→LUMO+1 (+15%) HOMO-3→LUMO (+5%)
	298.5	0.2631	HOMO-1→LUMO+1 (+57%), HOMO→LUMO (+22%), HOMO→LUMO+2 (+18%)
	296.7	0.2858	HOMO-2→LUMO+1 (+41%), HOMO→LUMO+1 (+20%), HOMO-1→LUMO (+14%), HOMO-1→LUMO+2 (+13%) HOMO-3→LUMO (+7%)
	276.8	0.1035	HOMO→LUMO+2 (+57%), HOMO-2→LUMO (+16%), HOMO-1→LUMO+1 (+9%), HOMO-2→LUMO+2 (+7%)
	326.7	0.2032	HOMO-1→LUMO (+43%), HOMO→LUMO+1 (+39%), HOMO-2→LUMO (+14%)
13	321.8	0.5101	HOMO-1→LUMO+1 (+59%), HOMO→LUMO (+27%), HOMO-2→LUMO+1 (+7%)
	303.8	0.2315	HOMO-2→LUMO+1 (+30%), HOMO-1→LUMO+2 (+24%), HOMO-3→LUMO (+23%), HOMO-2→LUMO+2(+7%)
	375.8	0.0694	HOMO→LUMO(+83%), HOMO-1→LUMO+1 (+8%)
14a	371.7	0.0985	HOMO→LUMO+1 (+56%), HOMO-1→LUMO(+42%)
	359.6	0.3935	HOMO-1→LUMO+1 (+84%), HOMO→LUMO (+11%)
	358.8	0.0718	HOMO-1→LUMO (+55%), HOMO→LUMO+1 (+40%)
	398.1	0.1216	HOMO→LUMO (+84%), HOMO-1→LUMO+1 (+11%)
14b	389.7	0.2191	HOMO→LUMO+1 (+78%), HOMO-1→LUMO (+21%)
	372.8	0.0510	HOMO-1→LUMO (+77%), HOMO→LUMO+1 (+20%)
	365.7	0.7616	HOMO-1→LUMO+1 (+82%), HOMO→LUMO (+13%)
	402.6	0.3192	HOMO→LUMO (+79%), HOMO-1→LUMO+1 (+17%)
14c	396.9	0.1995	HOMO→LUMO+1 (+86%), HOMO-1→LUMO+3 (+6%)
	455.1	0.6188	HOMO→LUMO (+78%), HOMO-1→LUMO+1 (+16%)
14d	447.0	0.1286	HOMO→LUMO+1 (+75%), HOMO-1→LUMO (+19%)
	420.4	0.0196	HOMO-1→LUMO (+73%), HOMO→LUMO+1 (+20%)

2.2.4 Quenching studies

The decrease of fluorescence intensity of a sample is referred as fluorescence quenching. Quenching occurs due to a variety of molecular interactions such as excited state reactions, molecular rearrangements, energy transfer and ground or excited state complex formation. Quenching can be divided into two types. One is the collisional or dynamic quenching, another named as static quenching. In dynamic quenching, quencher diffuses to the fluorophore in the excited state and several interactions occur in the excited state. While in the static quenching, a complex is formed between the fluorophore and the quencher in the ground state and this complex is non-fluorescent. But the requirement of both type of quenching is the molecular contact between the fluorophore and the quencher. For instance, Ravikanth et al. demonstrated that the fluorescence is quenched in directly linked ferrocene to porphyrin through ethyne linkage due to electron transfer from ferrocene to porphyrin unit.⁶⁰

Aromatic and aliphatic amines comprise an important class of quencher for most of unsubstituted aromatic hydrocarbons for example anthracene and perylene are effectively quenched by diethylamine.⁶¹ Hence a variety of quenchers are known for different class of fluorophore. The occurrence of quenching depends upon the chemical properties of fluorophore and quencher and also on the mechanism of quenching. In the mechanism of quenching of amines the excited state fluorophore accepts an electron from the amine by which the formation of excited charge transfer complex takes place. This excited charge transfer complex is known as exciplex. In non polar solvents, the fluorescence was observed from this exciplex. It is called excited state reaction rather than quenching. But in polar solvents, exciplex emission often quenched. Because of the variety of substances that act as quenchers, one can frequently identify fluorophore–quencher combinations for a desired purpose. Here we have done quenching study

of the parent hydrocarbon **5a** of fluoranthene series and we have chosen different amine and ferrocene as a quencher.

Collisional quenching of fluorescence is described by Stern-Volmer equation-

$$\frac{F_0}{F} = 1 + k_q \tau_0 [Q] = 1 + K_D [Q]$$

Where F_0 and F are the intensities of fluorescence in the absence and presence of quencher respectively; k_q is the bimolecular quenching constant; τ_0 is the lifetime of fluorophore in the absence of quencher; and $[Q]$ is the concentration of quencher. The Stern-Volmer quenching constant is given by, $K_D = k_q \tau_0$

In this section we have done quenching study of the parent hydrocarbon (**5a**) of fluoranthene scheme. 1×10^{-4} M solution of **5a** was taken for the study. The quenching study was done with four different quenchers namely triphenylamine, diphenylamine, ferrocene and dimethylaniline. The concentration of 1×10^{-3} M was taken for three quenchers (triphenylamine, diphenylamine and ferrocene) but 1×10^{-5} M was taken for dimethylaniline. The quenching study was done by adding 5 μ L of quencher to the compound in every measurement. The emission plots and Stern-Volmer plots have shown in Figures 2.26 and 2.27. Stern-Volmer plots show a linear trend showing the collisional quenching of parent hydrocarbon but the quenching constant is low as displayed in Table 2.7. The results indicate that the amines are not detrimental to the emission profile. Therefore, the emission would not be affected by the incorporation of diarylamine to the parent hydrocarbon.

Table 2.7 Quenching constant for compound **5a** in four different quencher

Quencher	Triphenylamine	Diphenylamine	Ferrocene	Dimethylaniline
Quenching constant, K_D	10877.8810	11383.4865	19456.3006	1.5228E6

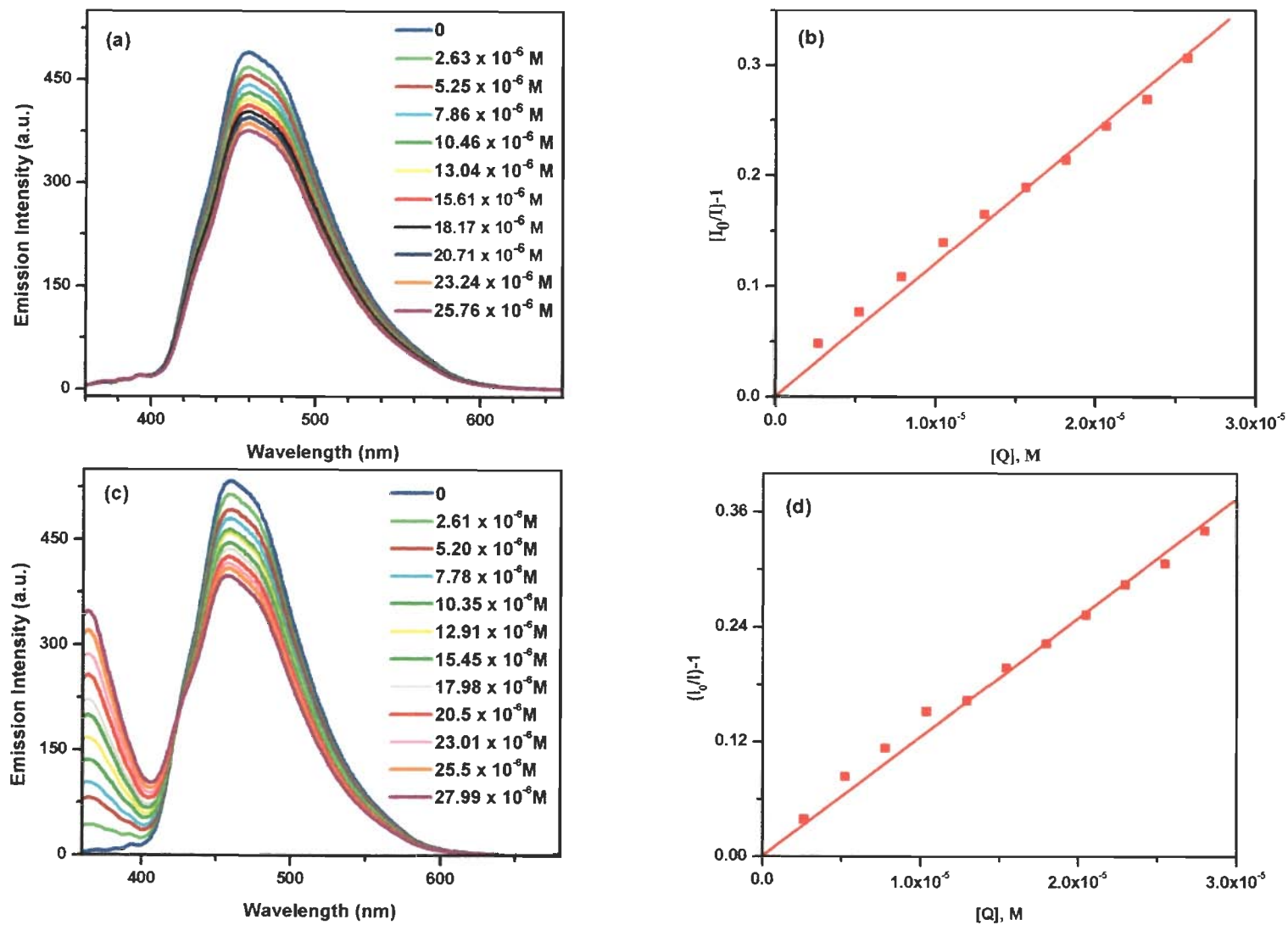


Figure 2.26 Emission and Stern-Volmer plots for 5a at different concentration of different quencher (a), (c) diphenylamine, (b), (d) triphenylamine.

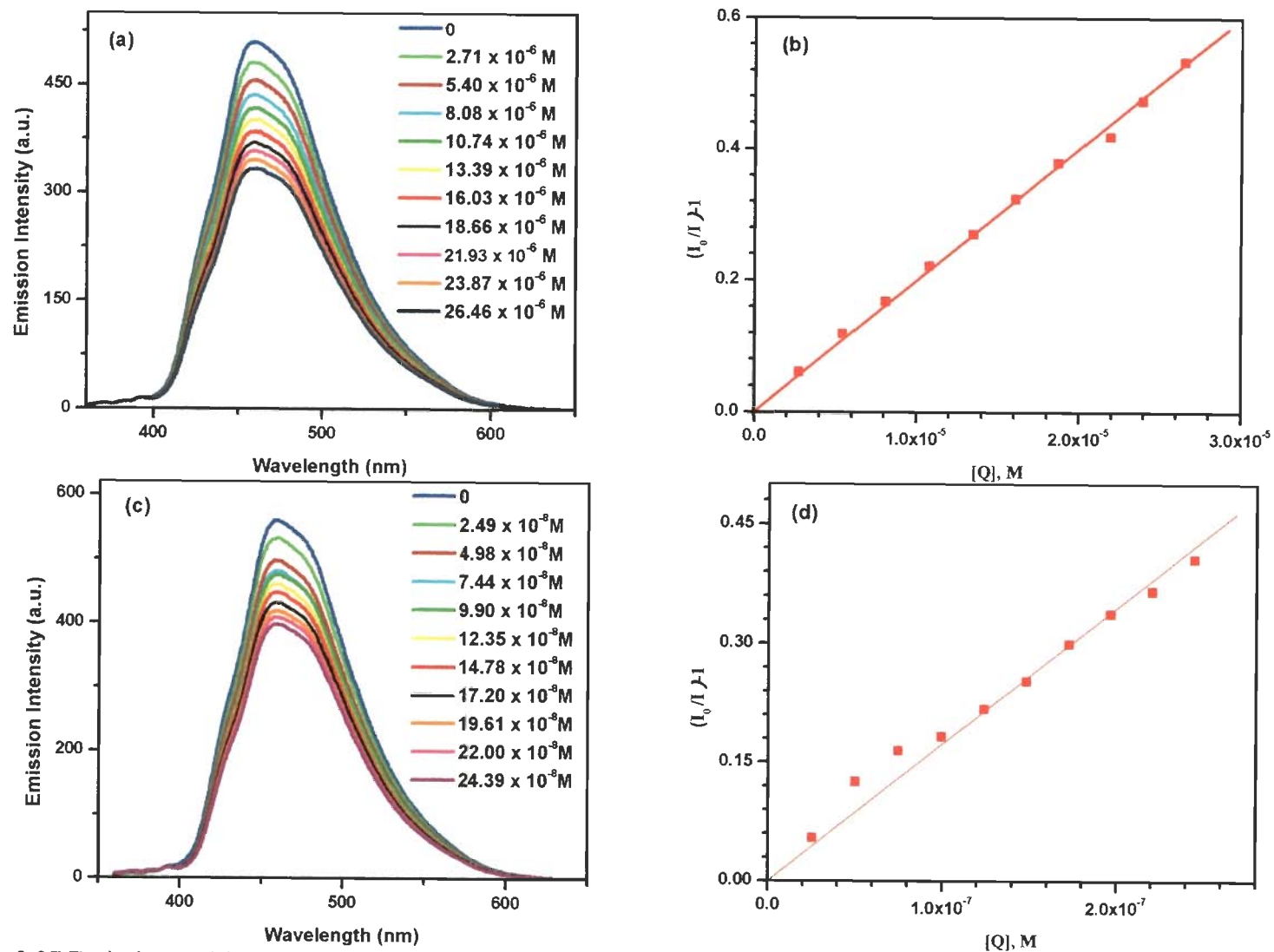


Figure 2.27 Emission and Stern-Volmer plots for **5a** at different concentration of different quencher (a), (c) ferrocene and (b), (d) dimethylaniline.

2.2.5 Thermal properties

The thermal properties of the compounds were studied by both thermogravimetric analysis (TGA) and differential scanning calorimetry (DSC) measurements. (See the Table 2.8 for relevant parameters). All the amine derivatives (**7a-7d** & **14a-14d**) exhibited excellent thermal stability and the decomposition temperatures are in the range of 469-578°C. The marked thermal robustness of the compounds is attributed to the fused polyaromatic architecture and presence of diarylamine. Triphenylene series showed high thermal stability as compared to fluoranthene series due to presence of two substituents which make the compounds more rigid. The thermal stability trend observed for the compounds **4**, **5a**, **5b** and **6** may be assigned to the differences in the number of non-hydrogen atoms and molecular heaviness. But in case of triphenylene derivatives, cyanoderivative (**13**) is more thermally stable than bromo derivative (**12**). This is because of cyano which makes the molecule more rigid due to resonance so that less heating vibrations are possible that resists decomposition.

Table 2.8 Thermal data of the compounds **4-7** and **12-14**.

Compound	T _{onset} (°C)	T _d (°C)	T _m (°C)	T _g (°C)
4	267	366	-	-
5a	310	406	-	-
5b	346	450	-	-
6	345	449	-	-
7a	223	469	345	198
7b	429	519	320	198
7c	395	502	220	192
7d	442	527	401	205
12	127	487	-	-
13	376	509	>360	-
14a	249	578	>360	-
14b	469	555	333	173
14c	473	574	281	183
14d	513	559	278	224

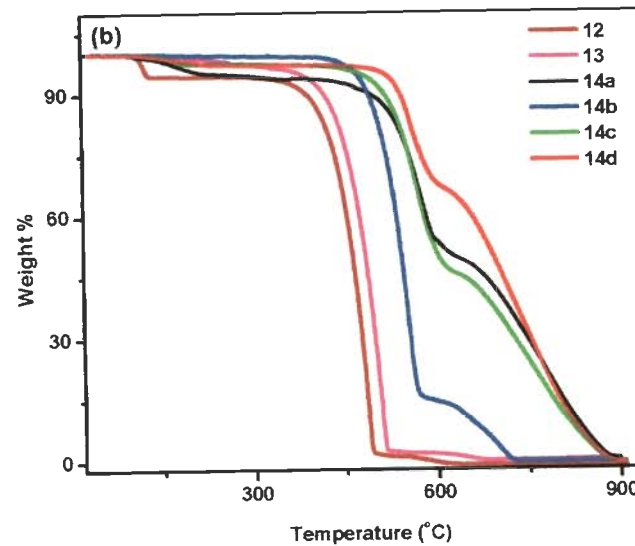
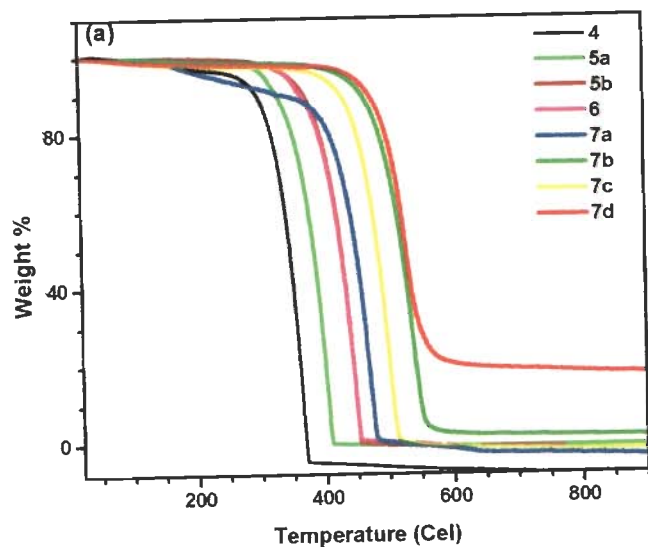


Figure 2.28 TGA curves of (a) fluoranthene derivatives (4-7) and (b) triphenylene derivatives (12-14).

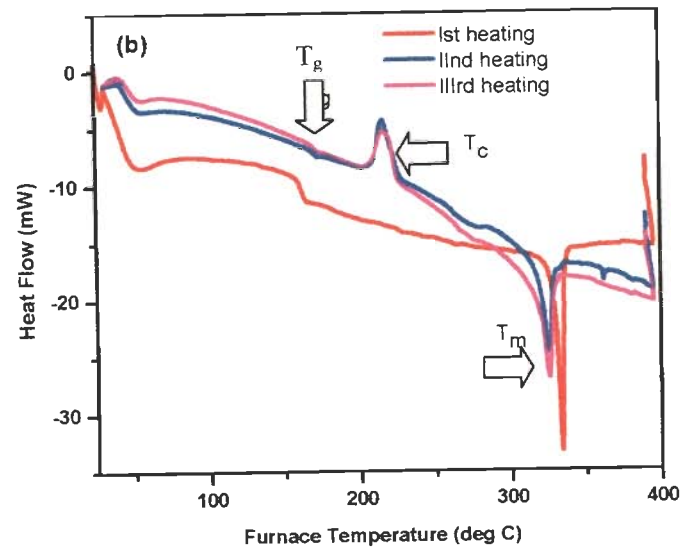
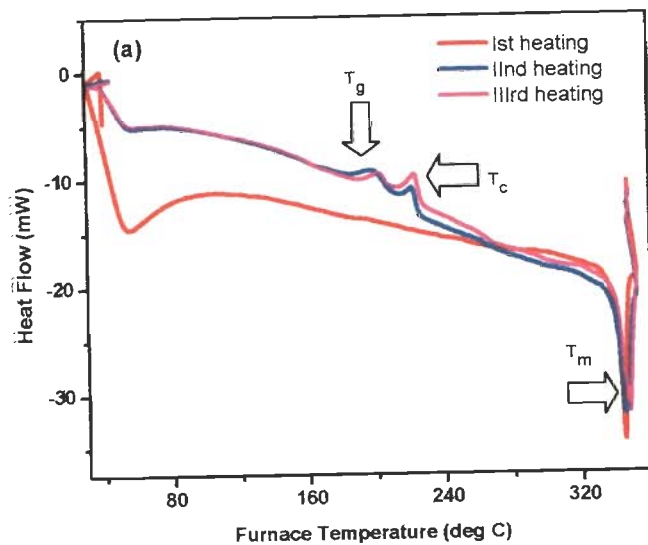


Figure 2.29 DSC curves of (a) 7a and (b) 14b showing three heating cycles.

T_{onset} (5% wt. loss) was calculated from TGA curves which are shown in Figure 2.28. It has been seen that incorporation of amine increase the thermal stability of molecule. Among the naphthylamine derivatives (**7b** and **7c**) improved thermal stability is observed for **7b**. This difference probably arises due to the presence of *tert*-butyl group in **7c** which renders floppiness to the molecule. The stability order realized based on the diarylamine units for both series, diphenylamine (**7a** & **14b**) < 1-pyrenylphenylamine (**14d**) < 1-naphthylphenylamine (**14c**) respectively. **7d** is more thermally stable than **7b**. The carbazole derivative (**14a**) of triphenylene shows exceptionally higher decomposition temperature than triarylamine derivatives (**14b-14d**). This observation is in accordance with the earlier one which unraveled that molecular materials containing flat polyaromatic-extended skeletons were prone to resist thermal degradation.⁶²

The DSC curves of **7a** and **14b** are shown in Figure 2.29. Diphenylamine derivatives **7a** and **14b** melted at 345 and 333 °C to give an isotropic liquid in the first run of the DSC measurement. Upon cooling, the isotropic liquid changed into a glassy state. As the glassy sample was reheated for the second run, a glass transition was observed at 198 & 173 °C, which is defined as the glass transition temperature (T_g) of **7a** and **14b** respectively. Upon further heating beyond T_g , an exothermal peak was observed at 221 and 217 °C for **7a** and **14b** respectively which showed the crystallization of diphenylamine derivatives of both series. Similarly the endothermic peak in first heating run show the melting point of other derivatives. Glass transition temperature of pyrenylphenylamine derivatives (**7d** & **14d**) of both series showed the highest values of 205 °C and 224 °C respectively.

Glass transition and sharp melting of diphenylamine derivatives (**7a** & **14b**) reproduced along with the crystallization temperature at 217 °C in 2nd and 3rd heating cycles. But for naphthyl (**7b** & **14c**) and pyrenylamine (**7d** & **14d**) derivatives there is a broad melting peak was observed

in first heating cycle which disappeared in 2nd and 3rd heating cycles. Moreover no exothermic crystallization peak was observed for 1-naphthylphenyl and 1-pyrenylphenylamine derivatives (**7b** & **14c** and **7d** & **14d**). The results suggest that the glassy and amorphous nature of these derivatives is not destroying at very high temperature. The present amine derivatives (**7a-7d**) were found to show exceptionally higher thermal stability and prolonged glassy state than the reported blue emitting fluoranthene derivatives, 7,10-diphenyl-8-(1-naphthyl) fluoranthene [**B6**] and 7,10-diphenyl-8-(9-phenanthrenyl)fluoranthene [**B7**].³⁴ The thermal properties of triphenylene-based derivatives (**14a-14d**) can be compared to that of thiophene substituted triphenylene derivatives which show liquid crystalline behavior.⁶³ This clearly highlights the importance of amine functionality in improving the thermal properties.

Thus, the results indicate that carbazole unit increase the thermal stability and naphthalene and pyrene inhibit the crystallization and increase the glassy state as compared to diphenylamine. The T_g of all the amine derivatives reported here is much higher than that of commonly used hole transporting material (e.g., 98°C for NPB).¹⁵

2.2.6 Electrochemical properties

The redox propensity of the compounds was examined in 2×10^{-4} M dichloromethane solutions by cyclic and differential pulse voltammetric methods. The cyclic voltammograms recorded for the fluoranthene-based amine derivatives (**7a-7d**) and the triphenylene-based amine derivatives (**14b-14d**) with the internal standard ferrocene are displayed in Figure 2.30. All the amines (**7a-7d**) exhibited one quasi-reversible oxidation couple followed by one irreversible oxidation peak. It is reasonable to assume that the quasi-reversible oxidation wave arises from the amine functionality while the irreversible oxidation may originate from the fluoranthene core. It is interesting to note that this irreversible wave attributable to the

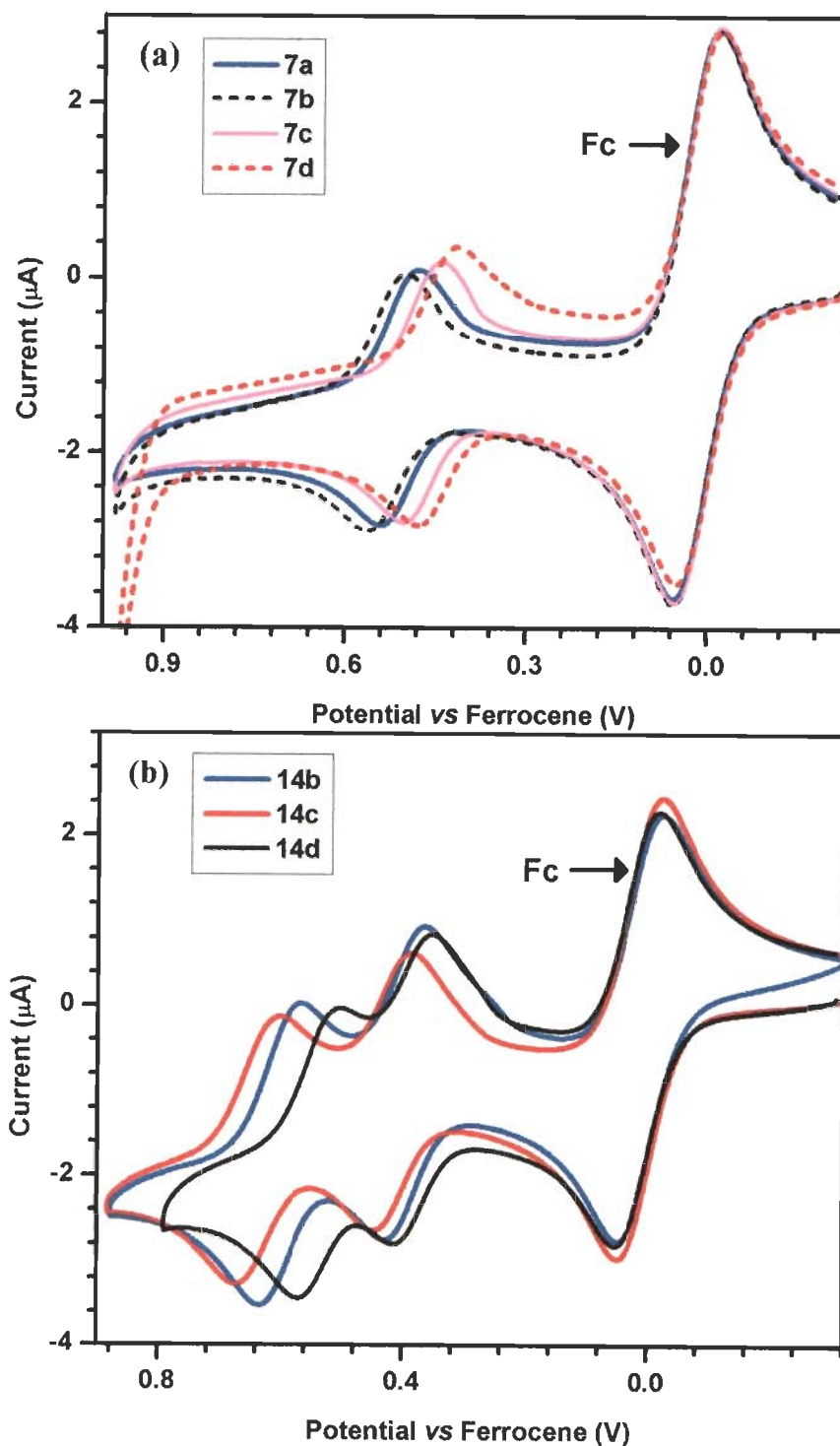


Figure 2.30 Cyclic voltammograms recorded (a) for the amine functionalized derivatives (7a-7d) & (b) for (14b-14d) in dichloromethane solutions (concentration: 2.0×10^{-4} M; scan rate: 100 mV/sec; supporting electrolyte: TBAHP).

fluoranthene core is not observed for the bromo (**5b**) and cyano derivatives (**6**). Probably, the electron attracting nature of these groups either positively shifts this potential and the wave probably appears outside the electrochemical window or makes the core less futile for oxidation. This argument is further supported by the fact that the cyano derivative (**6**) showed a quasi-reversible reduction couple.

The orbital energies, deduced from the oxidation potentials and absorption edge, are listed in Table 2.9. The HOMO energy levels were observed to be 6.66, 5.29, 5.32, 5.26 and 5.23eV for **6**, **7a**, **7b**, **7c**, and **7d** respectively. It revealed that the electron withdrawing substituent lowers the HOMO energy level whereas the electron donating group increases the HOMO energy level and decreases the LUMO energy level resulting in a smaller band gap. The conclusions about the band gap derived from the optical spectra can be corroborated with these findings (*vide supra*). All the amine derivatives show comparable band gap, out of which pyrene derivative (**7d**) show comparatively low band gap, which is evident from the red-shifted absorption profile and cathodically shifted oxidation potential.

Table 2.9 Electrochemical properties of triarylamine derivatives (**7a-7d** & **14a-14d**).

Compound	E_{ox} , mV (ΔE_p , mV)	HOMO, eV	LUMO, eV	E_{0-0} , eV
6	-1864	6.66	3.80	2.86
7a	492 (62)	5.29	2.84	2.45
7b	516 (67)	5.32	2.86	2.46
7c	460 (63)	5.26	2.82	2.44
7d	432 (67)	5.23	2.81	2.42
14a	844	5.64	2.39	3.25
14b	384 (65), 592 (66), 1168	5.18	2.17	3.01
14c	404 (61), 628 (68), 1052	5.20	2.18	3.02
14d	372 (61), 528 (62), 912	5.17	2.38	2.79

The triarylamine derivatives of triphenylene series display two reversible oxidation waves at relatively low oxidation potentials corresponding to the removal of an electron from each triarylamine group and one irreversible oxidation peak at higher potential attributable to the poly phenylated triphenylene core. Significant potential differences between the first reversible oxidation step and the second reversible oxidation step also reveal that the radical cation could efficiently delocalize in the molecule once it is formed. Carbazole derivative (**14a**) displays one irreversible oxidation peak at higher potential than other amine derivative (**14b-14d**) assign for the carbazole moiety. Irrespective of these the bromo and cyano compound do not show any oxidation redox couple due to electron withdrawing nature of bromo and cyano group which cause the more anodic shift. Compounds become prone to oxidize after the incorporation of amines. The energy levels alter by the strength of donor moiety. Strong donor increase the HOMO level and decrease the LUMO level as a result lowers the band gap. The value of HOMO and LUMO energy levels can be compared with the previously reported fluorene derivatives which acted as blue emitting material⁶⁴ in device.

2.2.7 Electroluminescence characteristics

2.2.7.1 OLED performance of fluoranthene derivatives (**7c** and **7d**)

As the amine derivatives have displayed favorable electrochemical, thermal and emission properties, we further examined two selected derivatives (**7c** and **7d**) as hole-transporting emitting materials in double layer OLEDs. We have used both 1,3,5-tris(*N*-phenylbenzimidazol-2-yl)benzene (TPBI) and aluminum tris-8-hydroxyquinoline (Alq₃) as electron transporting material to effect the optimization of charge balance in the devices. The devices had the configuration as ITO/**7c** (40 nm)/TPBI or Alq₃ (40 nm)/LiF (1 nm)/Al (150 nm) [Device I] and ITO/**7d** (40 nm)/TPBI or Alq₃ (40 nm)/LiF (1 nm)/Al (150 nm) [Device II]. Figure 2.31 shows

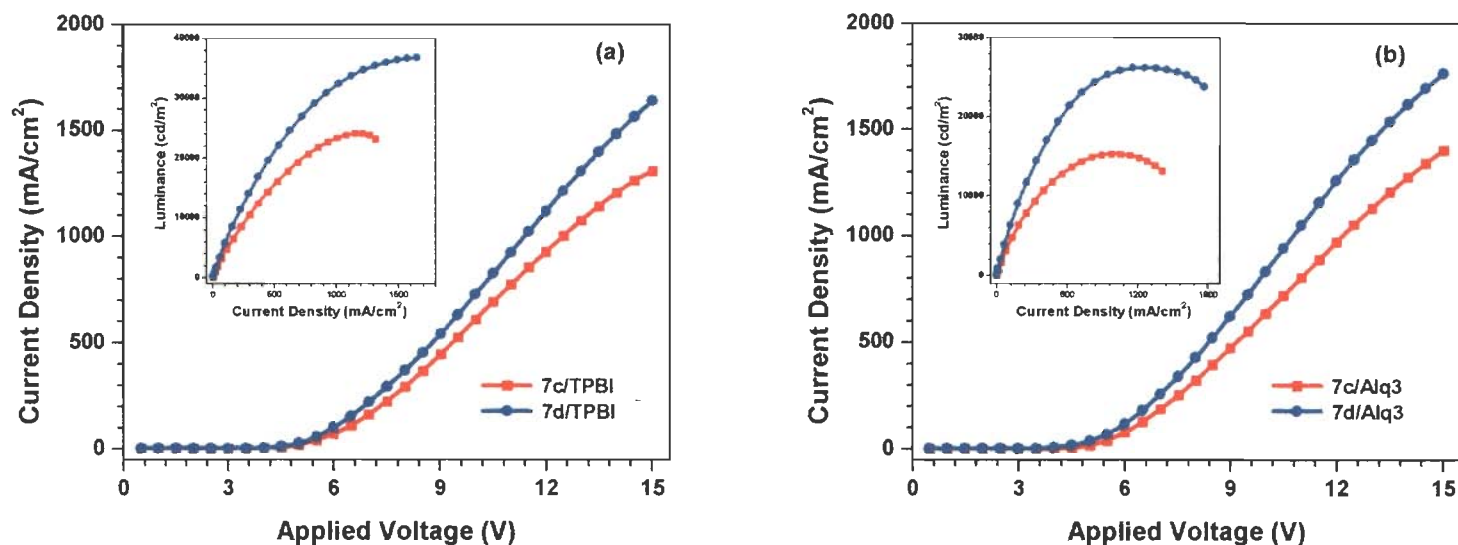


Figure 2.31 I-V-L characteristics of the devices using **7c** & **7d** as emitting as well as hole transporting layer with (a) TPBI or (b) Alq₃ as electron transporting layer.

Table 2.10 Electroluminescence characteristics for device performance using **7c** & **7d** as hole transporting and emitting layer.

	7c		7d	
	TPBI	Alq ₃	TPBI	Alq ₃
λ_{em} (fwhm), nm	534 (70)	534 (74)	558 (56)	558 (62)
Max. brightness (Cd/m ²)	24120	15390	36750	26140
CIE (x, y)	0.34, 0.60	0.34, 0.59	0.42, 0.55	0.41, 0.55
External quantum efficiency (%) at (100/20 mA cm ⁻²)	1.21/1.48	1.09/1.23	1.60/1.86	1.53/1.66
Power efficiency (lm/W) at (100/20 mA cm ⁻²)	2.132/3.300	1.981/2.718	3.026/4.373	2.933/4.010
Current efficiency (Cd/A) at (100/20 mA cm ⁻²)	4.315/5.287	3.904/4.397	5.801/6.733	5.413/5.889
voltage (V) at (100/20 mA cm ⁻²)	6.37/5.04	6.21/5.09	6.03/4.85	5.81/4.62
brightness (Cd/m ²) at (100/20 mA cm ⁻²)	4290/1050	3860/870	5790/1330	5380/1170

the current-voltage-luminance (I-V-L) characteristics of the fabricated devices, and their device characteristics at 100 and 20 mA/cm² are listed in Table 2.10. In general, the TPBI serves as better electron transporting material for these devices than Alq₃, which is clearly evident from the better efficiency and brightness observed for the TPBI based devices. Particularly, the device II with TPBI as electron transporting layer showed the highest external quantum efficiency 1.86%, current efficiency 6.73 cd/A and power efficiency 4.37 lm/W at a voltage of 4.85 V and a current density of 20 mA/cm². Recently, Xia et al. reported diarylamine substituted benzo[*k*]fluoranthene derivatives (**B10-B13**) green emitters and non linear optical materials.³⁷ **B13** show maximum brightness 17840 Cd/m². By replacing the core benzo[*k*]fluoranthene by fluoranthene and by substituting pyrene instead of naphthalene increases the brightness of device. The maximum brightness for fluoranthene derivative **7d** was measured as double (36750 Cd/m²) as compared to that of **B13**.

The improved performance for pyrene containing dye-TPBI device is attributed to the larger barrier for the injection of holes from the dyes (**7d**) to TPBI (0.97 eV) when compared to the corresponding barrier (0.86 eV) at the interface of **7d**-Alq₃ (Figure 2.32). This probably enhances the possibility of recombination and confinement of exciton in the emitting layer. The leaking of holes into the TPBI layer is also confirmed by the residual TPBI based emission observed in the EL (Figure 2.33). EL spectra shows peak at 534 and 558 nm for **7c** and **7d** based devices respectively. CIE coordinates for **7c** and **7d** based devices indicated green and yellow emission respectively. This suggests that the emission is originating from the dye. Though fluorene bridged fluoranthene derivatives have been applied in electroluminescent devices, they were found to be blue emitting in the electroluminescent devices.³⁰ In this work, by using amine functionality we have shown that

the emission color can be tuned to green and yellow depending on the nature of the diarylamine tethered with the fluoranthene core.

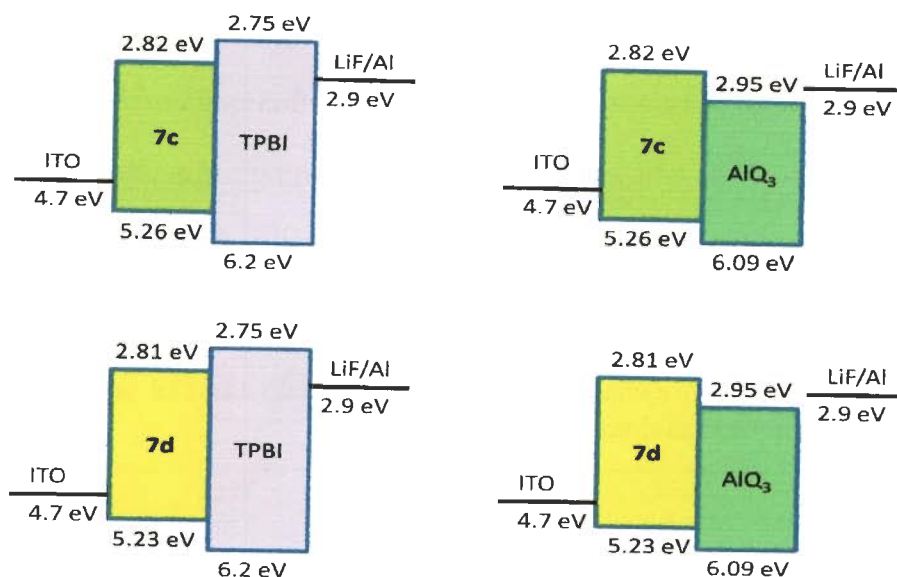


Figure 2.32 Energy level diagrams of the four devices fabricated using the dyes **7c** and **7d** with TPBI and Alq₃.

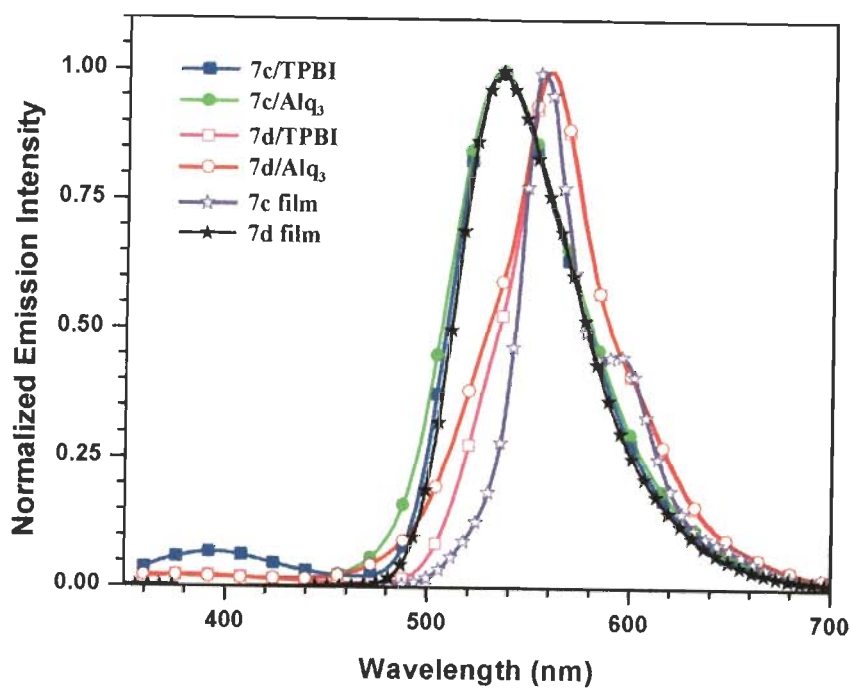


Figure 2.33 Comparison of EL spectra observed for the devices with **7c** and **7d** with the PL spectra recorded for the thin films.

2.2.7.2 Electroluminescent properties of triphenylene derivatives (14a-14d)

Two types of OLED devices were fabricated. In one device **14a-14d** were used as hole-transporting and emitting layer and in the second used as a dopant in CPB layer. Current density vs voltage curve, luminance vs voltage curve, and Power efficiency vs current density curve of device using neat film of **14a-14d** with CBP as hole transporting and emitting layer are shown in Figure 2.34 while that of the device using **14a-14d** as a dopant are displayed in Figure 2.35. The relevant data of both kinds of devices are given in Table 2.11.

Table 2.11 Electroluminescence characteristics for devices with **14a-14d** as hole transporting and emitting layer (neat) and as dopant.

Compound	Driving voltage (V) @ 10 cd/m ²	Power efficiency (lm/W)	Current efficiency (cd/A) @ 100/1,000 cd/m ²	EQE (%)	Max Luminance (cd/m ²)	CIE	EL _{max} , nm
14a	5.4	0.03/–	0.08/--	-	108	(0.16, 0.12)	408
14b	5.3	0.03/–	0.07/--	-	149	(0.15, 0.09)	444
14c	4.4	0.07/–	0.13/--	-	309	(0.15, 0.11)	468
14d	4.9	0.03/–	0.07/--	-	139	(0.15, 0.20)	472
14a + CBP	5.2	0.20/–	0.50/--	1.6	638	(0.16, 0.06)	412
14b + CBP	6.1	0.30/–	0.80/--	1.6	1010	(0.15, 0.06)	452
14c + CBP	4.6	0.6/0.3	1.2/0.8	2.1	1680	(0.16, 0.08)	436
14d + CBP	4.4	1.9/1.0	3.7/2.7	1.6	2660	(0.14, 0.22)	472

The device showed very less efficiency and luminance when **14a-14d** were used as hole transporting and emitting layer. The efficiency and luminance has increased when **14a-14d** used as dopant. Pyrene containing derivative **14d** doped with CBP as hole transporting layer showed the maximum brightness of 2660 cd/m², highest current efficiency 3.7 cd/A and power efficiency

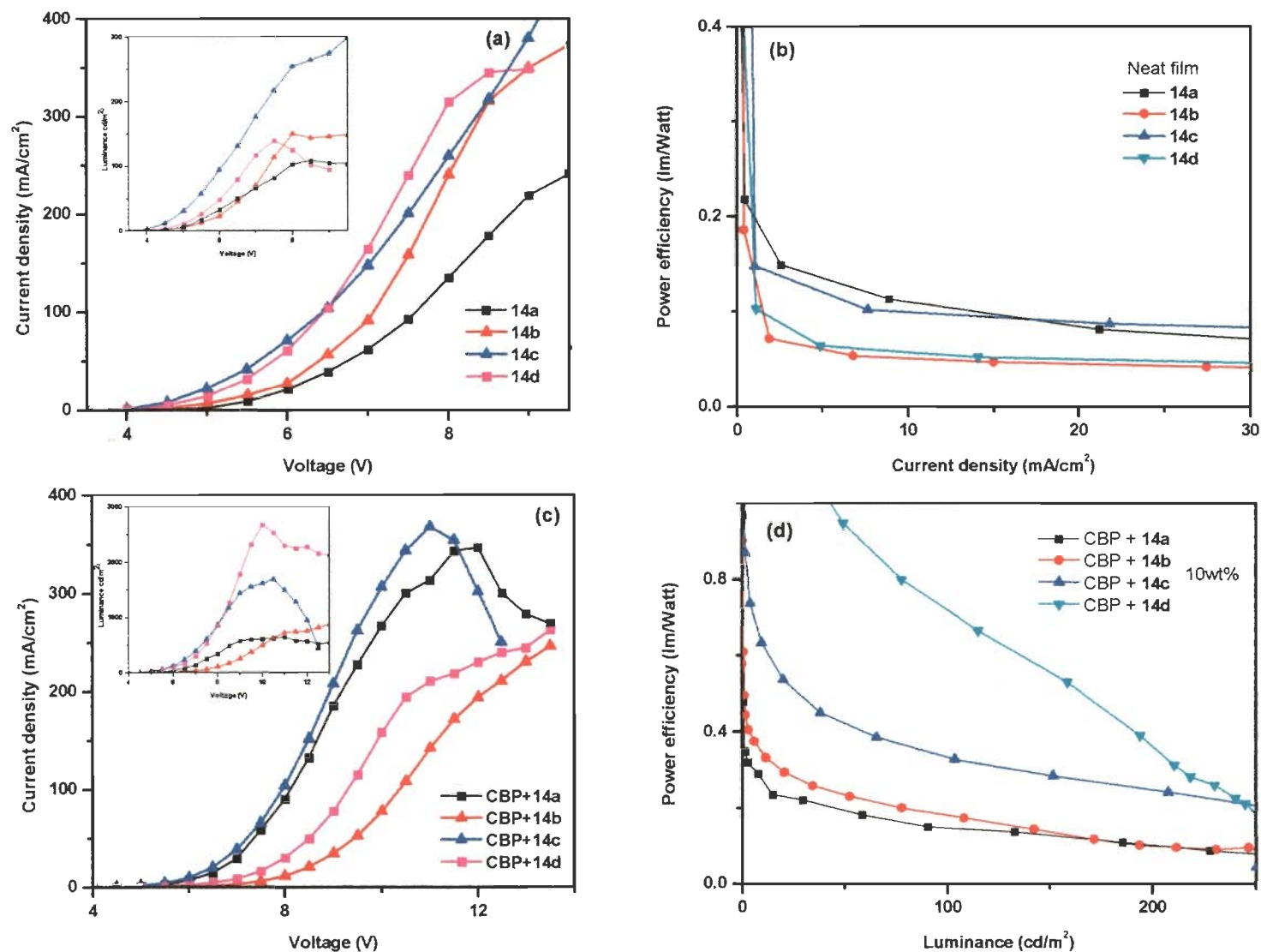


Figure 2.34 I-V-L characteristics and power efficiency vs current density curves of devices using **14a-14d** as a dopant without (a), (b) and with host material **CBP** (c), (d).

1.9 lm/W at a voltage of 4.4 V and a luminance of 100 cd/m². CIE coordinates indicated that all the devices are blue emitting. EL spectra of both type of device are shown in Figure 2.35. Device with **14c** exhibited broad and red shifted EL_{max} when used as neat film which is similar to the PL_{max} in thin film. This indicates that compound (**14c**) aggregates during device performance.

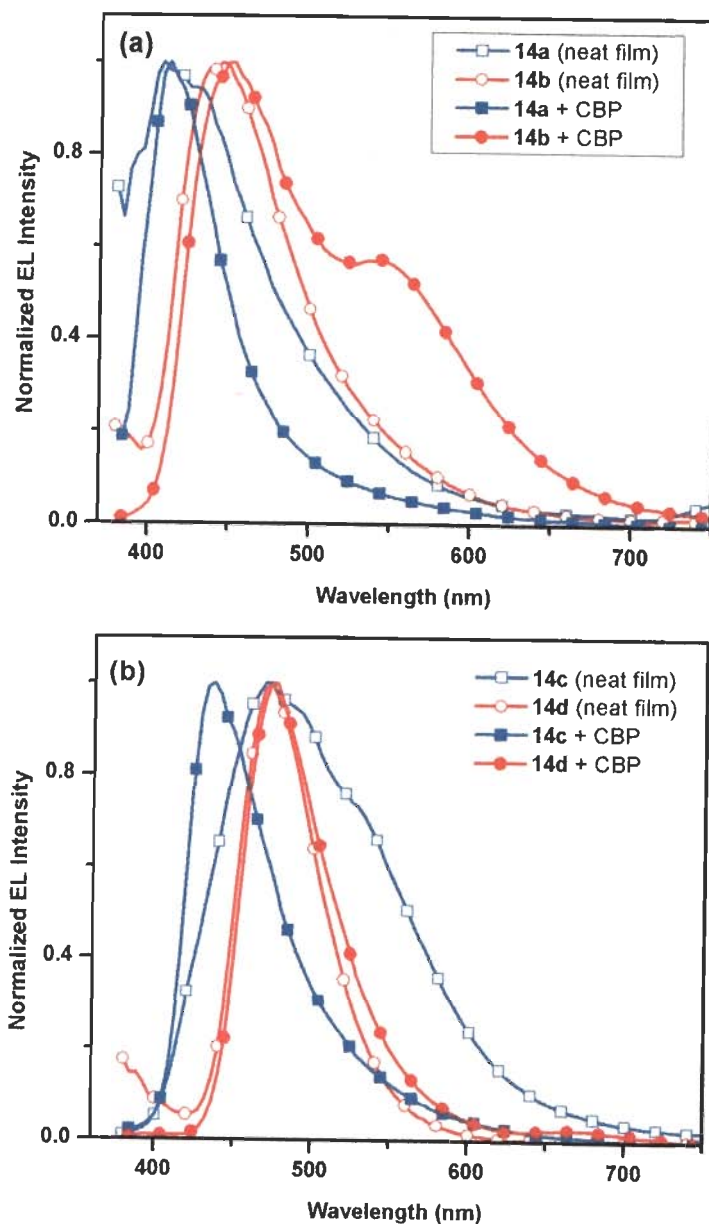


Figure 2.35 EL spectra of the devices with **14a**, **14b** (a) and with **14c**, **14d** (b).

2.3 Conclusions

In summary, we have synthesized electroluminescent materials based on a fluoranthene and triphenylene core integrated with a polyphenylated dendron-like structure. The change in core can alter the photophysical and electrochemical properties. The fluoranthene derivatives show red shifted absorption and emission spectra as compared to that of triphenylene derivatives. Triphenylene derivatives show higher thermal stability than fluoranthene derivatives. Additionally incorporation of diarylamine red shifts the absorption as well as the emission profiles while the effect of electron withdrawing group is not much significant. All the amine derivatives are potential molecular materials displaying unique absorption, emission, thermal and electrochemical properties. The amine derivatives show positive solvatochromism but more significantly in 1-naphthylphenylamine and 1-pyrenylphenylamine derivatives. The solvent dependant emission defining parameters like Lippert-Mataga, $E_T(30)$ and Kamlet-Taft exhibited more linear relationship in case of fluoranthene containing amine derivatives. The results show that both specific and non specific interactions are occurring in the excited state of molecules. The results show that not only the diarylamine but the central core also play an important role in changing the properties of a molecule.

Electrochemical study tells that electron withdrawing group widens the band gap while the electron donating diarylamines shrinks it. Thermal study revealed that pyrenylphenylamine and naphthylphenylamine derivatives are amorphous while diphenylamine derivative have liquid crystalline nature. This suggests that the bulky diarylamine can change liquid crystal to completely amorphous powder which is beneficial for fabrication of OLED. Further quenching study of parent hydrocarbon **5a** of fluoranthene series conclude that the amines are not detrimental to the emission profile. So there could be a nascence of new class of hole-

transporting materials by the incorporation of diarylamine to the parent hydrocarbon without quenching its emission.

Further, these derivatives (**7c** & **7d**) can function as efficient hole-transporting and emitting material in OLEDs. Particularly, the device fabricated using the pyrene containing derivative, **7d**, displayed promising external quantum efficiency 1.86% and maximum brightness 36750 cd/m² with TPBI as an electron transporting layer, which appear to be rather high among the previously reported carbazole based derivatives capable of green or yellow emission and hole transporting.⁶⁵ The OLED device fabrication data for triphenylene derivatives (**14a-14d**) reveal that these derivatives can be served as efficient blue dopant. Moreover pyrene derivative (**14d**) showed better current and power efficiency (3.7 cd/A and 1.9 lm/W) and maximum brightness (2660 cd/m²) as compared to other derivatives (**14a-14c**) of this series when used as a dopant. Therefore, pyrene-based triarylamines can be explored as efficient functional materials in electroluminescent devices.

2.4 Experimental section

2.4.1 Materials

All commercially available materials were used as obtained from their sources. Most of the chemicals were purchased from Sigma Aldrich. Dichloromethane (DCM) and toluene were distilled from phosphorus pentoxide. All chromatographic separations were carried out with hexane:DCM on silica gel (60-120 mesh, Rankem).

2.4.2 Physical methods

¹H and ¹³C NMR spectra were recorded on Bruker AV500 O FT-NMR spectrometer operating at 500 and 125 MHz respectively in CDCl₃ and (CD₃)₂SO (chemical shifts (δ) in ppm and

for CHCl_3 ($^1\text{HNMR}$, $\delta = 7.26$; $^{13}\text{CNMR}$, $\delta = 77,36$ ppm) or DMSO ($^1\text{HNMR}$, $\delta = 2.5$ ppm; $^{13}\text{CNMR}$ $\delta = 40,45$ ppm). IR spectra were measured on NEXUS FT-IR (THERMONICOLET). High-resolution mass spectra were recorded on Esquire4000, Bruker Daltonics using DEF_MS.M method. The electronic absorption spectra were obtained with UV-1800 Shimadzu UV spectrophotometer in dichloromethane and toluene solutions. Emission spectra were recorded in dichloromethane and toluene with Shimadzu RF-5301PC spectrofluorimeter. The fluorescence quantum yields (Φ_F) were determined using the classical formula: $\Phi_s = (\Phi_r \times A_r \times I_s \times \eta_s^2) / (A_s \times I_r \times \eta_r^2)$ where A is the absorbance at the excitation wavelength, I is the integrated area under the fluorescence curve and η the refraction index. Subscripts r and s refer to the reference and to the sample of unknown quantum yield, respectively. Coumarin 6 in ethanol ($\Phi_F=0.78$) and Coumarin 1 in ethyl acetate ($\Phi_F=0.99$) were taken as the reference for fluoranthene and triphenylene derivatives respectively. Cyclic voltammetry experiments were performed with a epsilon electrochemical analyzer. All measurements were carried out at room temperature with a conventional three-electrode configuration consisting of a glassy carbon working electrode, a platinum wire auxiliary, and a nonaqueous acetonitrile Ag/AgNO₃ reference electrode. The $E_{1/2}$ values were determined as $(E_p^a + E_p^c)/2$, where E_p^a and E_p^c are the anodic and cathodic peak potentials, respectively. The potential are quoted against ferrocene internal standard. The solvent in all experiments was dichloromethane and the supporting electrolyte was 0.1 M tetrabutylammonium hexafluorophosphate. Diefferential scanning calorimetry (DSC) and thermogravimetric analysis (TGA) were performed under a nitrogen atmosphere on a SETARAM Instrumentation, KEP technology, DSP131evo differential scanning calorimeter and Perkin-Elmer (Pyris Diamond) at heating rate of 10°C/min.

2.4.3 OLED fabrication and performance evaluation

Prepatterned ITO substrates with an effective individual device area of 3.14 mm² were cleaned as described in a previous report.⁶⁶ The amine derivatives (**7c** or **7d**) acting as hole transporting emitting layers were first deposited (40 nm) on the ITO substrate by vapor deposition. Then 40-nm-thick Alq₃ or a TPBI layer as an electron transport layer was deposited. Finally, a thin layer of LiF (10 Å) followed by aluminium (1500 Å) was deposited as the cathode. The I–V curve was measured on a Keithley 2400 Source meter in an ambient environment. Light intensity was measured with a Newport 1835 optical meter.

The OLED device for triphenylene derivatives (**14a-14d**) was fabricated on the pre-cleaned glass substrate and composed of a 125 nm layer indium tin oxide as anode, 35 nm poly(3,4-ethylene-dioxythiophene)-poly-(styrenesulfonate) (PEDOT:PSS) as hole-injection layer (HIL), emissive layer (EML), a 0.7 nm LiF hole injection layer (HIL), a 150 nm Al layer as cathode. The aqueous solution of PEDOT:PSS was spin coated at 4000 rpm for 20 s to form a 40 nm HIL layer. A series of EMLs, doped in 4,4'-Bis(9H-carbazol-9-yl)biphenyl (CBP), were presented and deposited by spin-coating at 2500 rpm for 20 s. Subsequently, lithium fluoride and aluminum cathode were thermally evaporated at 1.0 x 10⁻⁵ torr.

2.4.4 Computational details

The ground state geometry of the compounds at the gas phase were optimized using the density functional theory method with the B3LYP functional in conjugation with the basis set 6-31G(d,p) as implemented in the Gaussian 09 package. The default options for the self-consistent field (SCF) convergence and threshold limits in the optimization were used. The electronic transitions were calculated using the time-dependent DFT (B3LYP) theory and the 6-31G(d,p) basis set. Even though the time-dependent DFT method less accurately describes the states with

transitions were calculated using the time-dependent DFT (B3LYP) theory and the 6-31G(d,p) basis set. Even though the time-dependent DFT method less accurately describes the states with charge-transfer nature, the qualitative trends in the TDDFT results can still offer correct physical insights. At least 10 excited states were calculated for each molecule.

Synthesis of 7,9-diphenyl-8*H*-cyclopenta[*a*]acenaphthylen-8-one (3a) A mixture of acenaphthylene-1,2-dione (**2a**) (1 g, 5.49 mmol) and diphenyl acetone (**1**) (1.15 g, 5.49 mmol) were suspended in 10 ml of methanol under nitrogen atmosphere. A solution prepared from KOH in 5 ml of methanol was added at 0°C. The mixture was stirred for 6 h. After completion of reaction a greenish black color solid was precipitated which was filtered, washed with methanol and dried. Greenish black. Yield 1.6 g (82%); ¹H NMR (CDCl₃, 500 MHz) δ = 8.07 (d, *J* = 7.0 Hz, 2 H), 7.87 (d, *J* = 8.5 Hz, 2 H), 7.83 (d, *J* = 8.0 Hz, 4 H), 7.59 (t, *J* = 7.5 Hz, 2 H), 7.52 (t, *J* = 7.75 Hz, 4 H), 7.41 (t, *J* = 7.5 Hz, 2 H); IR (KBr, cm⁻¹) ν_{max} 3051, 1696, 1638, 1619.

Synthesis of 7,8,10-triphenylfluoranthene (4) A mixture of 7,9-diphenyl-8*H*-cyclopenta[*a*]acenaphthylen-8-one (**3a**) (1 g, 2.8 mmol) and phenylacetylene (0.31 g, 3.08 mmol) in diphenylether (5 ml) were heated to 220°C and stirred for 7 h. The reaction was performed under nitrogen atmosphere. The reaction was quenched in hexane. A gray color precipitate was formed which was filtered. The obtained solid was dissolved in CH₂Cl₂ and subjected to column chromatography on silica gel. The desired compound was obtained by elution with hexane/dichloromethane. Yellow color solid. Yield: 0.49 g (40%); ¹H NMR (DMSO, 500 MHz): δ = 7.88 (dd, *J* = 8.0 Hz, 4 H), 7.72-7.74 (m, 4 H), 7.57-7.63 (m, 6 H), 7.44-7.50 (m, 8 H), 7.36-7.39 (m, 6 H), 7.17-7.28 (m, 14 H), 6.50 (d, *J* = 7.0 Hz, 2 H); ¹³C NMR (CDCl₃, 125 MHz): δ = 141.0, 140.8, 140.8, 139.4, 138.3, 138.0, 136.6, 136.2, 136.0, 135.7, 133.2, 131.2, 130.4, 130.0, 129.8, 129.2, 128.7, 128.5, 127.8, 127.7, 127.6, 127.3, 126.7, 126.4, 123.4, 123.0.

Synthesis of 7,8,9,10-tetraphenylfluoranthene (5a) A mixture of 7,9-diphenyl-8*H*-cyclopenta[*a*]acenaphthylen-8-one (**3a**) (1 g, 2.8 mmol) and diphenylacetylene (0.55g, 3.08 mmol) in diphenylether (5 ml) were heated to 220°C and stirred for 7 h. The reaction was performed under nitrogen atmosphere. The reaction was quenched by the addition of hexane. A gray color precipitate was formed which was filtered. The desired product was purified by column chromatography on silica gel with hexane/dichloromethane as eluant. Yellow color solid. Yield 1.0 g (70%); ¹H NMR (CDCl₃, 500 MHz) δ 7.72 (d, *J* = 8.0 Hz, 2 H), 7.33-7.27 (m, 12 H), 6.93-6.88 (m, 8 H), 6.86-6.83 (m, 2 H), 6.61 (d, *J* = 7.0 Hz, 2 H); ¹³C NMR (CDCl₃, 125 MHz) δ 140.7, 139.9, 139.8, 137.2, 136.5, 136.5, 133.3, 131.3, 130.1, 129.6, 128.2, 127.6, 126.9, 126.6, 126.5, 125.4, 123.2; IR (KBr, cm⁻¹) *v*_{max} 3056, 1601, 1496, 1428, 778, 701.

Synthesis of 3-bromo-7,8,9,10-tetraphenylfluoranthene (5b) A mixture of 3-bromo-7,9-diphenyl-8*H*-cyclopenta[*a*]acenaphthylen-8-one (**3b**) (1 g, 2.3 mmol) and diphenylacetylene (0.45 g, 2.53 mmol) in diphenylether (5 ml) were heated to 220 °C and stirred for 7 h. After completion of the reaction, it was quenched by adding hexane. A gray precipitate was formed. It was filtered and adsorbed on silica gel for subsequent purification by column chromatography. The desired product was separated by eluting with a 5:1 hexane-dichloromethane mixture as a pale yellow color solid. Yield 0.96 g (71%); ¹H NMR (DMSO, 500 MHz) δ 7.85 (d, *J* = 8.5 Hz, 1 H), 7.69 (d, *J* = 7.5 Hz, 1 H), 7.49 (t, *J* = 7.8 Hz, 1 H), 7.30-7.38 (m, 10 H), 6.96-6.98 (m, 4 H), 6.90 (t, *J* = 7.8 Hz, 4 H), 6.82-6.85 (m, 2 H), 6.42 (d, *J* = 7.5 Hz, 1 H), 6.25 (d, *J* = 7.5 Hz, 1 H); ¹³C (CDCl₃, 125 MHz) δ 141.1, 141.0, 139.7, 139.6, 139.5, 137.4, 137.3, 136.9, 136.4, 136.2, 135.9, 134.5, 131.2, 131.0, 129.9, 129.9, 129.4, 128.9, 128.3, 127.07, 127.05, 126.7, 125.8, 125.5, 123.9, 123.7, 121.9; IR (KBr, cm⁻¹) *v*_{max} 3056, 3021, 1598, 1495, 1441, 1416, 835, 769, 700.

Synthesis of 7,8,9,10-tetraphenylfluoranthene-3-carbonitrile (6) A mixture of 3-bromo-7,8,9,10-tetraphenylfluoranthene (**5b**) (0.73 g, 1.25 mmol) and cuprous cyanide (0.16 g, 1.87 mmol) and dimethylformamide (10 mL) were placed in a round bottom flask and heated at 150 °C with efficient stirring for 48 h. The mixture was poured into 10 ml of ammonia solution to yield a dark yellow precipitate. It was filtered and washed thoroughly with water. This crude product was further purified by column chromatography using a 2: 3 mixture of dichloromethane and hexane to yield a pale yellow solid. Yield 0.24 g (36%); ^1H NMR (CDCl_3 , 500 MHz) δ 7.93 (d, $J = 8.5$ Hz, 1 H), 7.67 (d, $J = 7.5$ Hz, 1 H), 7.41 (t, $J = 7.8$ Hz, 1 H), 7.28-7.35 (m, 10 H), 6.85-6.91 (m, 10 H), 6.61 (d, $J = 7$ Hz, 1H), 6.55 (d, $J = 7.0$ Hz, 1 H); ^{13}C NMR (CDCl_3 , 125 MHz) δ 141.6, 140.7, 138.44, 138.37, 138.2, 138.2, 137.6, 136.9, 136.4, 136.2, 134.4, 133.4, 131.9, 130.2, 130.1, 129.3, 128.9, 128.9, 128.1, 127.6, 127.5, 126.5, 126.4, 125.9, 124.9, 123.7, 123.1, 121.0, 116.9, 107.2; IR (KBr, cm^{-1}) ν_{max} 3050, 3021, 2216 ($\nu_{\text{C}\equiv\text{N}}$), 1603, 1495, 1436, 1383, 766, 699.

Synthesis of *N,N*,7,8,9,10-hexaphenylfluoranthene-3-amine (7a) A mixture of 3-bromo-7,8,9,10-tetraphenylfluoranthene (**5b**) (1.17 g, 2 mmol), diphenylamine (0.41 g, 2.4 mmol), $\text{Pd}(\text{dba})_2$ (0.023 g, 0.04 mmol), dppf (0.022 g, 0.04 mmol), sodium *tert*-butoxide (0.29 g, 3 mmol), and toluene (15 ml) was taken in a pressure tube. The reaction was performed under N_2 atmosphere. The reaction mixture was heated at 80 °C and stirred for 3 d. After completion of reaction, as evidenced by disappearance of 3-bromo-7,8,9,10-tetraphenylfluoranthene, it was quenched by addition of water and extracted with dichloromethane. The combined extract was washed with brine solution and dried over anhydrous Na_2SO_4 followed by evaporation. The product was purified by column chromatography eluting with 30-50% DCM-hexane. Yellow solid. Yield 1.2 g (89%); mp 345 °C; ^1H NMR (CDCl_3 , 500 MHz) δ 7.53 (d, $J = 8.5$ Hz, 1 H),

7.27-7.32 (m, 8 H), 7.21-7.23 (m, 1 H), 7.16 (t, $J = 8.0$ Hz, 4 H), 7.04-7.07 (m, 1 H), 7.01 (d, $J = 7.5$ Hz, 4 H), 6.84-6.96 (m, 14 H), 6.49 (d, $J = 7.0$ Hz, 1 H), 6.46 ppm (d, $J = 7.5$ Hz, 1 H); ^{13}C (CDCl_3 , 125 MHz) δ 149.0, 144.5, 140.7, 140.3, 139.9, 139.8, 137.2, 136.9, 136.8, 136.6, 136.2, 133.7, 131.3, 131.3, 130.1, 130.0, 129.1, 128.2, 127.4, 127.3, 127.0, 126.9, 126.9, 126.6, 125.4, 124.2, 124.1, 123.2, 123.0, 122.2.

Synthesis of *N*-(naphthalen-1-yl)-*N*,7,8,9,10-pentaphenylfluoranthene-3-amine (7b)

Compound **7b** was prepared from **5b** and *N*-phenyl-1-naphthylamine by following a procedure similar to that described above for **7a**. Yellow solid. Yield 75%; mp 320 °C; ^1H NMR (CDCl_3 , 500 MHz) δ 7.98 (d, $J = 9.0$ Hz, 1 H), 7.84 (d, $J = 8.0$ Hz, 1 H), 7.67 (d, $J = 8.5$ Hz, 1 H), 7.61 (d, $J = 8.0$ Hz, 1 H), 7.42 (t, $J = 7.3$ Hz, 1 H), 7.27-7.36 (m, 7 H), 7.17-7.25 (m, 6 H), 7.09-7.12 (m, 2 H), 7.03-7.06 (m, 1 H), 6.79-6.92 (m, 14 H), 6.51 (d, $J = 7.0$ Hz, 1 H), 6.35 (d, $J = 7.5$ Hz, 1 H); ^{13}C (CDCl_3 , 125 MHz) δ 150.7, 145.6, 145.1, 140.7, 140.1, 139.9, 139.9, 139.8, 137.2, 136.9, 136.7, 136.5, 136.2, 135.2, 135.1, 133.0, 131.4, 131.3, 130.3, 130.1, 129.2, 129.0, 128.4, 128.2, 128.1, 127.3, 126.9, 126.8, 126.6, 126.4, 126.3, 126.09, 126.06, 125.9, 125.8, 125.4, 124.7, 124.3, 124.2, 124.1, 123.3, 123.2, 121.5, 121.3.

Synthesis of *N*-(4-*tert*-butylphenyl)-*N*-(naphthalen-1-yl)-7,8,9,10-tetraphenylfluoranthene-3-amine (7c)

Compound **7c** was prepared from **5b** and *N*-(4-*tert*-butylphenyl)-1-naphthyl amine by following a procedure similar to that described above for **7a**. Yellow solid. Yield 84%; mp 220 °C; ^1H NMR (CDCl_3 , 500 MHz) δ 7.99 (d, $J = 8.0$ Hz, 1 H), 7.83 (d, $J = 8.5$ Hz, 1 H), 7.65 (d, $J = 8.0$ Hz, 1 H), 7.59 (d, $J = 8.0$ Hz, 1 H), 7.39-7.42 (m, 1 H), 7.27-7.33 (m, 6 H), 7.21-7.25 (m, 4 H), 7.16-7.17 (m, 2 H), 7.10 (d, $J = 9.0$ Hz, 2 H), 7.02-7.03 (m, 1 H), 6.82-6.91 (m, 11 H), 6.76 (d, $J = 8.0$ Hz, 3 H), 6.49 (d, $J = 7.5$ Hz, 1 H), 6.36 (d, $J = 8.0$ Hz, 1 H), 1.25 (s, 9 H); ^{13}C (CDCl_3 , 125 MHz) δ 148.1, 146.1, 145.5, 144.4, 140.6, 139.94, 139.85, 137.1, 136.8, 136.5,

126.8, 126.6, 126.3, 126.2, 126.04, 125.97, 125.8, 125.7, 125.5, 125.4, 124.4, 124.3, 124.2, 124.1, 123.1, 121.5, 34.1, 31.4; FABMS: m/z 779.2 $[M]^+$.

Synthesis of *N*-(4,6-dihydropyren-1-yl)-*N*,7,8,9,10-pentaphenylfluoranthren-3-amine (7d)

Compound **7d** was prepared from **5b** and 1-pyrenyl-*N*-phenyl amine by following a procedure similar to that described above for **7a**. Orange solid. Yield 75%; mp 401 °C; ^1H NMR (CDCl_3 , 500 MHz) δ 8.18 (d, $J = 9.0$ Hz, 1 H), 8.15 (d, $J = 7.5$ Hz, 1 H), 8.03-8.08 (m, 2 H), 8.01 (d, $J = 4.5$ Hz, 2 H), 7.96 (t, $J = 8.0$ Hz, 1 H), 7.85 (d, $J = 9.5$ Hz, 1 H), 7.73 (d, $J = 8.0$ Hz, 1 H), 7.66 (d, $J = 8.0$ Hz, 1 H), 7.28-7.31 (m, 5 H), 7.19 (t, $J = 7.5$ Hz, 2 H), 7.11-7.14 (m, 3 H), 7.02-7.05 (m, 1 H), 6.81-6.92 (m, 16 H), 6.52 (d, $J = 7.0$ Hz, 1 H), 6.34 (d, $J = 7.5$ Hz, 1 H); ^{13}C (CDCl_3 , 125 MHz) δ 150.9, 145.8, 142.6, 140.7, 140.1, 139.9, 139.84, 139.77, 137.2, 137.0, 136.7, 136.5, 136.2, 135.2, 133.0, 131.34, 131.27, 131.1, 130.1, 130.0, 129.12, 129.09, 128.2, 128.1, 127.9, 127.3, 127.2, 126.90, 126.86, 126.8, 126.6, 126.5, 126.4, 126.3, 126.2, 125.7, 125.4, 125.19, 125.16, 125.0, 124.9, 124.3, 124.1, 123.3, 123.2, 121.6, 121.5; FABMS m/z 797.2 $[M]^+$.

Synthesis of 7,10-dibromo-1,2,3,4-tetraphenyltriphenylene (12) A mixture of 6,9-dibromo-1,3-diphenyl-2*H*-cyclopenta[*b*]phenanthren-2-one (**11**) (8 g, 14.8 mmol) and diphenyl-acetylene (3.16 g, 17.8 mmol) in diphenylether (25 ml) were heated to 220°C and stirred for 7 h. After completion of the reaction, it was quenched by adding hexane. A gray color precipitate was formed. It was filtered and adsorbed on silica gel for subsequent purification by column chromatography. The desired product was separated by eluting with 5:1 hexane/dichloromethane mixture as a pale yellow color solid. Yield 5.5 g (54 %); ^1H NMR (CDCl_3 , 500 MHz) δ 8.45 (d, $J = 2.0$ Hz, 1 H), 7.42 (d, $J = 9.0$ Hz, 1 H), 7.14-7.10 (m, 4 H), 7.09-7.00 (m, 2 H), 6.94-6.87 (m, 3 H), 6.69-6.67 (m, 2 H); ^{13}C NMR (CDCl_3 , 125 MHz) δ 142.3, 141.0, 140.0, 137.3, 132.2, 131.9, 131.6, 131.4, 130.5, 130.0, 129.8, 129.3, 129.1, 128.5, 128.2, 126.7, 126.6, 125.9, 125.5, 123.2,

122.5, 121.0, 118.9. IR (KBr, cm^{-1}) ν_{max} 3050, 3021, 1590, 1490, 1441, 1378, 1026, 864, 816, 770, 698.

Synthesis of 5,6,7,8-tetraphenyltriphenylene-2,11-dicarbonitrile (13) A mixture of 7,10-dibromo-1,2,3,4-tetraphenyltriphenylene (**12**) (2.0 g, 2.89 mmol) and cuprous cyanide (1.8 g, 20.29 mmol) and dimethylformamide (50 mL) were taken in a round bottom flask and heated at 150°C with efficient stirring for 4 d. It was poured into 10 ml of ammonia solution to yield a dark yellow precipitate. It was filtered and washed thoroughly with water. This crude product was further purified by column chromatography using mixture of dichloromethane and hexane (2:3) to yield a pale yellow solid. Yield 0.9 g (53%); mp >360°C; ^1H NMR (CDCl_3 , 500 MHz) δ 8.67 (d, $J = 1.5$ Hz, 1 H), 7.69 (d, $J = 9.0$ Hz, 1 H), 7.29 (dd, $J = 1.5, 7.5$ Hz, 1 H), 7.19-7.12 (m, 3 H), 7.05-7.03 (m, 2 H), 6.97-6.91 (m, 3 H), 6.72-6.69 (m, 2 H); ^{13}C NMR (CDCl_3 , 125 MHz) δ 142.7, 141.4, 139.3, 138.3, 134.6, 131.9, 131.2, 130.7, 130.7, 130.2, 128.50, 128.47, 127.8, 127.1, 126.9, 125.8, 118.8, 110.2; IR (KBr, cm^{-1}) ν_{max} 3050, 3021, 2921, 2228 ($\nu_{\text{C}\equiv\text{N}}$), 1606, 1490, 1449, 1387, 826, 775, 702.

Synthesis of 9,9'-(5,6,7,8-tetraphenyltriphenylene-2,11-diyl)bis(9H-carbazole) (14a) A mixture of 7,10-dibromo-1,2,3,4-tetraphenyltriphenylene (**12**) (0.5 g, 0.73 mmol), carbazole (0.27 g, 1.59 mmol), CuI (61 mg, 0.32 mmol), 1,10 phenanthroline (0.11 g, 0.64 mmol) and K_2CO_3 (0.97 g, 7.0 mmol) was suspended in 5 ml of dimethylformamide. The mixture was refluxed with vigorous stirring under nitrogen atmosphere for 24 h. After this, cool the reaction mixture to ambient temperature. Pour the solution in water and extracted with chloroform, dried over Na_2SO_4 followed by evaporation. The product was purified by column chromatography. Cream color solid. Yield 0.55 g (87%); mp >360°C; ^1H NMR (CDCl_3 , 500 MHz) δ 8.57 (d, $J = 2.5$ Hz, 1 H); 8.09 (d, $J = 7.5$ Hz, 2 H), 7.89 (d, $J = 8.5$ Hz, 1 H), 7.46 (d, $J = 8.0$ Hz, 2 H), 7.37-

7.34 (m, 2 H), 7.29 (dd, $J = 2.0, 7.0$ Hz, 1 H), 7.26-7.13 (m, 7 H), 6.96-6.93 (m, 3 H), 6.81-6.79 (m, 2 H); ^{13}C NMR (CDCl_3 , 125 MHz) δ 142.6, 141.2, 140.8, 140.2, 137.7, 136.0, 132.6, 132.2, 131.9, 131.6, 130.9, 130.3, 128.4, 127.1, 126.9, 126.7, 126.1, 125.6, 124.6, 123.6, 121.2, 120.6, 120.4, 120.2, 109.8.

Synthesis of $N^2, N^2, N^{11}, N^{11}, 5, 6, 7, 8$ -octaphenyltriphenylene-2, 11-diamine (14b) A mixture of 7,10-dibromo-1,2,3,4-tetraphenyltriphenylene (**12**) (1.0 g, 1.45 mmol), diphenylamine (0.59 g, 3.48 mmol), $\text{Pd}(\text{dba})_2$ (0.033 g, 0.058 mmol), dppf (0.032 g, 0.058 mmol), sodium *tert*-butoxide (0.42 g, 4.35 mmol), and toluene (10 ml) was taken in a pressure tube. It was heated at 80°C and stirred for 48 h. After completion of reaction, as evidenced by disappearance of 7,10-dibromo-1,2,3,4-tetraphenyltriphenylene, it was quenched by the addition of water and extracted with dichloromethane. The combined extracts were washed with brine solution and dried over anhydrous Na_2SO_4 . Rotary evaporation of the extracts gave the crude product which on column chromatography purification using 1:4 hexane-dichloromethane mixtures produced a yellow solid. Yield 0.93 g (74 %); mp 333°C ; ^1H NMR (CDCl_3 , 500 MHz) δ 7.58 (s, 1 H), 7.32 (d, $J = 9.0$ Hz, 1 H), 7.18 (t, $J = 7.8$ Hz, 4 H), 7.07-6.98 (m, 11 H), 6.89-6.84 (m, 3 H), 6.71-6.66 (m, 3 H); ^{13}C NMR (CDCl_3 , 125 MHz) δ 147.2, 145.7, 143.1, 140.6, 139.6, 136.6, 132.6, 132.0, 131.6, 130.6, 130.5, 129.2, 128.0, 126.5, 126.1, 125.7, 125.1, 124.8, 123.3, 120.7, 116.1.

Synthesis of N^2, N^{11} -di(naphthalen-1-yl)- $N^2, N^{11}, 5, 6, 7, 8$ -hexaphenyltriphenylene-2, 11-diamine (14c) Compound **14c** was prepared from **12** and *N*-phenyl-1-naphthylamine by following a procedure similar to that described above for **14b**. Yellow solid. Yield 60%; mp 281°C ; ^1H NMR (CDCl_3 , 500 MHz) δ 7.84 (q, $J = 8.5$ Hz, 2 H), 7.72 (d, $J = 8.0$ Hz, 1 H), 7.48 (d, $J = 2.5$ Hz, 1 H), 7.43 (t, $J = 8.0$ Hz, 1 H), 7.37 (t, $J = 7.8$ Hz, 1 H), 7.29-7.22 (m, 2 H), 7.08-7.02

(m, 8 H), 6.98 (d, $J = 7.5$ Hz, 2 H), 6.91-6.84 (m, 4 H), 6.64 (dd, $J = 2.0, 9.0$ Hz, 2 H), 6.58 (dd, $J = 2.5, 7.0$ Hz, 1 H); ^{13}C NMR (CDCl_3 , 125 MHz) δ 147.6, 146.4, 143.1, 142.9, 140.7, 139.4, 136.4, 135.2, 132.6, 132.0, 131.6, 131.3, 130.6, 130.4, 129.04, 128.97, 128.4, 128.3, 127.9, 127.4, 126.7, 126.5, 126.4, 126.3, 126.08, 126.05, 125.0, 124.2, 122.32, 122.26, 119.1, 114.0; HRMS for $\text{C}_{74}\text{H}_{50}\text{N}_2$ [M^+] m/z 966.3936.

Synthesis of $N^2, N^{11}, 5, 6, 7, 8$ -hexaphenyl- N^2, N^{11} -di(pyren-1-yl)triphenylene-2, 11-diamine (14d) Compound **14d** was prepared from **12** and 1-pyrenyl-*N*-phenyl amine by following a procedure similar to that described above for **14b**. Yellow solid. Yellow solid. Yield 69%; mp 278 °C; ^1H NMR (CDCl_3 , 500 MHz) δ 8.19 (d, $J = 7.5$ Hz, 2 H), 8.10 (d, $J = 7.5$ Hz, 2 H), 8.06 (d, $J = 8.5$ Hz, 2 H), 8.01-7.97 (m, 8 H), 7.83 (d, $J = 9.5$ Hz, 2 H), 7.68 (d, $J = 8.0$ Hz, 2 H), 7.54 (d, $J = 2.5$ Hz, 2 H), 7.29-7.27 (m, 2 H), 7.05-6.99 (m, 10 H), 6.94-6.92 (m, 4 H), 6.86-6.82 (m, 10 H), 6.65-6.59 (m, 8 H); ^{13}C NMR (CDCl_3 , 125 MHz) δ 147.7, 146.6, 143.0, 140.7, 140.2, 139.5, 136.5, 132.7, 132.0, 131.6, 131.2, 131.1, 130.7, 130.5, 129.6, 129.1, 128.9, 128.3, 127.9, 127.7, 127.2, 127.1, 126.5, 126.2, 126.2, 126.1, 125.9, 125.2, 125.1, 125.0, 124.8, 123.2, 122.5, 122.2, 119.2, 114.3; HRMS calcd for $\text{C}_{86}\text{H}_{54}\text{N}_2$ [M^+] m/z 1114.4255, found 1114.4262.

2.5 References

1. Dudhe, R. S.; Tiwari, S. P.; Raval, H. N.; Khaderbad, M. A.; Singh, R.; Sinha, J.; Yedukondalu, M.; Ravikanth, M.; Kumar, A.; Rao, V. R. "Explosive vapor sensor using poly(3-hexylthiophene) and Cu^{II} tetraphenylporphyrin composite based organic field effect transistors" *Appl. Phys. Lett.* **2008**, *93*, 263306.

- Gupta, D.; Kabra, D.; Kolishetti, N.; Ramakrishnan, S.; Narayan, K. S. "An efficient bulk-heterojunction photovoltaic cell based on energy transfer in graded-bandgap polymers" *Adv. Funct. Mater.* **2007**, *17*, 226.
- Zhao Z.; Xu, X.; Wang H.; Lu, P.; Yu G.; Liu, Y. "Zigzag molecules from pyrene-modified carbazole oligomers: synthesis, characterization, and application in OLEDs" *J. Org. Chem.* **2008**, *73*, 594.
- Kreger, K.; Bate, M.; Neuber, C.; Schmidt, H.-W.; Strohriegl, P. "Combinatorial development of blue oleds based on star shaped molecules" *Adv. Funct. Mater.* **2007**, *17*, 3456.
- Ananthakrishnan, N.; Padmanaban, G.; Ramakrishnan, S.; Reynolds, J. R. "Tuning polymer light-emitting device emission colors in ternary blends composed of conjugated and nonconjugated polymers" *Macromolecules* **2005**, *38*, 7660.
- Sasabe H.; Kido, J. "Multifunctional materials in high-performance oleds: challenges for solid-state lighting" *Chem. Mater.* **2011**, *23*, 621.
- Tang C. W.; Slyke, S. A. V. "Organic electroluminescent diodes" *Appl. Phys. Lett.* **1987**, *51*, 913.
- Katsuma, K.; Shirota, Y. "A novel class of π -electron dendrimers for thermally and morphologically stable amorphous molecular materials" *Adv. Mater.* **1998**, *10*, 223.
- Thekkat, M.; Schmidt, H.-W. "Synthesis and properties of novel derivatives of 1,3,5-tris(diarylamino)benzenes for electroluminescent devices" *Adv. Mater.* **1998**, *10*, 219.
- Thekkat, M.; Schmitz, C.; Hohle, C.; Strohriegl, P.; Schmitz, H.-W.; Hofmann, U.; Schloter S.; Haarer, D. "Novel functional materials based on triarylamine synthesis and

- application in electroluminescent devices and photorefractive systems” *Phys. Chem. Chem. Phys.* **1999**, *1*, 1693.
11. Tao, S.; Li, L.; Yu, J.; Jiang, Y.; Zhou, Y.; Lee, C.-S.; Lee, S.T.; Zhang, X.; Kwon, O. “Bipolar molecules as an excellent hole-transporter for organic-light emitting devices” *Chem. Mater.* **2009**, *21*, 1284.
 12. Jiao, S.; Liao, Y.; Xu, X.; Wang, L.; Yu, G.; Wang, L.; Su, Z.; Ye, S.; Liu, Y. “Synthesis, structure, electronic state and luminescent properties of novel blue-light-emitting aryl substituted 9,9-di(4-(di-*p*-tolyl)aminophenyl)fluorenes” *Adv. Funct. Mater.* **2008**, *18*, 2335.
 13. Jiang, Z.; Ye, T.; Yang, C.; Yang, D.; Zhu, M.; Zhong, C.; Qin, J.; Ma, D. “Star-shaped oligotriarylamines with planarized triphenylamine core: solution-processable, high-T_g hole-injecting and hole-transporting materials for organic light-emitting diodes” *Chem. Mater.* **2011**, *23*, 771.
 14. Jiang, X.-Y.; Zhang, Z.-L.; Zheng, X.-Y.; Wu, Y.Z.; Xu, S.-H. “A blue organic emitting diode from anthracene derivative” *Thin solid films*, **2001**, *401*, 251.
 15. Chen, L.; Dong, G.; Duan, L.; Wang, L.; Qiao, J.; Zhang, D.; Qiu, Y. “Liquid formed glassy film of *N,N'*-diphenyl-*N,N'*-bis(3-methylphenyl)benzidine: formation, carrier transporting ability, photoluminescence and stability” *J. Phys. Chem. C* **2007**, *111*, 18376.
 16. Li, J.; Liu, D.; Li, Y.; Lee, C.-S.; Kwong, H.-L.; Lee, S. “A high T_g carbazole-based hole-transporting material for organic light-emitting devices” *Chem. Mater.* **2005**, *17*, 1208.
 17. Tong, Q.-X.; Lai, S.-L.; Chan, M.-Y.; Lai, K.-H.; Tang, J.-X.; Kwong, H.-L.; Lee, C.-S.; Lee, S.-T. “High T_g triphenylamine-based starburst hole-transporting materials for organic light-emitting devices” *Chem. Mater.* **2007**, *19*, 5851.

18. Liao, Y.-L.; Hung, W.-Y.; Hou, T.-H.; Lin, C.-Y.; Wong, K.-T. "Hole mobilities of 2,7- and 2,2'-disubstituted 9,9'-spirobifluorene-based triaryldiamines and their application as hole transport materials in OLEDs" *Chem. Mater.* **2007**, *19*, 6350.
19. Wong, W. W. H.; Jones, D. J.; Yan, C.; Watkins, S. E.; King, S.; Haque, S. A.; Wen, X.; Ghiggino, K. P.; Holmes, A. B. "Synthesis, photophysical, and device properties of novel dendrimers based on a fluorene-hexabenzocoronene (FHBC) core" *Org. Lett.* **2009**, *11*, 975.
20. Shirota, Y.; Kageyama, H. "Charge carrier transporting molecular materials and their applications in devices" *Chem. rev.* **2007**, *107*, 953.
21. Gingras, M.; Placide, V.; Raimundo, J.-M.; Bergamini, G.; Ceroni, P.; Balzani, V. "Polysulfurated pyrene-cored dendrimers: luminescent and electrochromic properties" *Chem. Eur. J.* **2008**, *14*, 10357.
22. Debije, M. G.; Piris, J.; Haas, M. P.; Warman, J. M.; Tomovic, Ž.; Simpson, C. D.; Watson, M. D.; Müllen, K. "The optical and charge transport properties of discotic materials with large aromatic hydrocarbon cores" *J. Am. Chem. Soc.* **2004**, *126*, 4641.
23. Walters, R. S.; Kraml, C. M.; Byrne, N.; Ho, D. M.; Qin, Q.; Coughlin, F. J.; Bernhard, S.; Pascal, R. A. "Configurational stable longitudinally twisted polycyclic aromatic compounds" *J. Am. Chem. Soc.* **2008**, *130*, 16435.
24. Edvinsson, T.; Li, C.; Pschirer, N.; Schöneboom, J.; Eickemeyer, F.; Sens, R.; Boschloo, G.; Herrmann, A.; Müllen, K.; Hagfeldt, A. "Intramolecular charge-transfer tuning of perylenes: spectroscopic features and performance in dye-sensitized solar cells" *J. Phys. Chem. C.* **2007**, *111*, 15137.

25. Park, J.-W.; Kang, P.; Park, H.; Oh, H.-Y.; Yang, J.-H.; Kim, Y.-H.; Kwon, S.-K. "Synthesis and properties of blue-light-emitting anthracene derivative with diphenylamino-fluorene" *Dyes Pigm.* **2010**, *85*, 93.
26. Grimsdale, A. C.; Chan, K. L.; Martin, R. E.; Jokisz, P. G.; Holmes, A. B. "Synthesis of light-emitting conjugated polymers for applications in electroluminescent devices" *Chem. Rev.* **2009**, *109*, 897.
27. Burroughes, J. H.; Bradley, D. D. C.; Brown, A. R.; Marks, R. N.; Mackay, K.; Friend, R. H.; Burn, P. L.; Holmes, A. B. "Light emitting diodes based on conjugated polymers" *Nature* **1990**, *347*, 539.
28. Palmaerts, A.; Haren, M.; Lutsen, L.; Cleij, T. J.; Vanderzande, D. "Synthesis and properties of poly(*p*-fluoranthenevinylene): a noble conjugated polymer with nonalternant repeating units" *Macromolecules* **2006**, *39*, 2438.
29. Saleh, M.; Baumgarten, M.; Mavrinskiy, A.; Schäfer T.; Müllen, K. "Triphenylene-based polymers for blue polymeric light emitting diodes" *Macromolecules* **2010**, *43*, 137.
30. Ma, X.; Wu, W.; Zhang, Q.; Guo, F.; Meng, F.; Hua, J. "Novel fluoranthene dyes for efficient dye-sensitized solar cells" *Dyes Pigm.* **2009**, *82*, 353.
31. Fang, X.-L.; Deng, S.-L.; Wang, J.; Wang, X.-F.; Chen, C.; Li, Y.; Xie, S.-Y.; Huang, R.-B.; Zheng, L.-S. "From self-assembled microspheres to self-templated nanotubes: morphologies and properties of sulfur-bridged fluoranthene-based organic materials" *Chem. Mater.* **2009**, *21*, 5763.
32. Branchi, B.; Balzani, V.; Ceroni, P.; Kuchenbrandt, M. C.; Klärner, F.-G.; Bläser, D.; Boese, R. "Molecular clips with extended aromatic sidewalls as receptors for electron-

- acceptor molecules: synthesis and NMR, photophysical, and electrochemical properties” *J. Org. Chem.* **2008**, *73*, 5839.
33. Chiechi, R. C.; Tseng, R. J.; Marchioni, F.; Yang, Y.; Wudl, F. “Efficient blue-light-emitting electroluminescent devices with a robust fluorophore: 7,8,10-triphenylfluoranthene” *Adv. Mater.* **2006**, *18*, 325.
34. Kim, S.-K.; Jaung, J.-Y.; Park, J.-W. “New fluoranthene derivatives in electroluminescence” *Mol. Cryst. Liq. Cryst.* **2008**, *491*, 122.
35. Tong, Q.-X.; Lai, S.-L.; Chan, M.-Y.; Zhou, Y.-C.; Kwong, H.-L.; Lee, C.-S.; Lee, S.-T. “Highly efficient blue organic light-emitting device based on a nondoped electroluminescent material” *Chem. Mater.* **2008**, *20*, 6310.
36. Tong, Q.-X.; Lai, S.-L.; Chan, M.-Y.; Zhou, Y.-C.; Kwong, H.-L.; Lee, C.-S.; Lee, S.-T.; Lee, T.-W.; Noh, T.; Kwon, O. “A high performance nondoped blue organic light-emitting device based on a diphenylfluoranthene-substituted fluorene derivative” *J. Phys. Chem. C.* **2009**, *113*, 6227.
37. Xia, Z.-Y.; Su, J.-H.; Fan, H.-H.; Cheah, K.-W.; Tian, H.; Chen, C. H. “Multifunctional diarylamine-substituted benzo[*k*]fluoranthene derivatives as green electroluminescent emitters and nonlinear optical materials” *J. Phys. Chem. C.* **2010**, *114*, 11602.
38. Sonar, P.; Soh, M. S.; Cheng, Y. H.; Henssler, J. T.; Sellinger, A. “1,3,6,8-Tetrasubstituted pyrenes: solution-processable materials for application in organic electronics” *Org. Lett.* **2010**, *12*, 3292.
39. Hoang, M. H.; Cho, M. J.; Kim, K. H.; Cho, M. Y.; Joo, J.; Choi, D. H. “New semiconducting multibranching conjugated molecules based on π -extended triphenylene and its application to organic field-effect transistor” *Thin solid films* **2009**, *518*, 501.

40. Bagui, M.; Dutta, T.; Chakraborty, S.; Melinger, J. S.; Zhong, H.; Keightley, A.; Peng, Z. "Synthesis and optical properties of triphenylene-based dendritic donor perylene diimide acceptor systems" *J. Phys. Chem. A* **2011**, *115*, 1579.
41. Heppke, G.; Krüerke, D.; Löhning, C.; Löttsch, D.; Moro, D.; Müller, M.; Sawade, H. "New chiral discotic triphenylene derivatives exhibiting a cholesteric blue phase and a ferroelectrically switchable columnar mesophase" *J. Mater. Chem.* **2000**, *10*, 2657.
42. Mao, H.; He, Z.; Wang, J.; Zhang, C.; Xie, P.; Zhang, R. "A discotic triphenylene dimer as organic hole transporting material for electroluminescent devices" *Journal of Luminescence* **2007**, *122*, 942.
43. Shih, H.-T.; Lin, C.-H.; Shih, H.-H.; Cheng, C.-H. "High-performance blue electroluminescent devices based on a biaryl" *Adv. Mater.* **2002**, *14*, 1409.
44. Yu, J.-Y.; Huang, M.-J.; Chen, C.; Lin, C.-S.; Cheng, C.-H. "On the improvement of blue emission for all sp²-hybridized bistriphenylenyls: incorporating phenylenyl moieties to enhance film amorphism" *J. Phys. Chem. C.* **2009**, *113*, 7405.
45. Bacher, A.; Erdelen, C. H.; Paulus, W.; Ringsdorf, H.; Schmidt, H. W.; Schuhmacher, P. "Photo-cross-linked triphenylenes as novel insoluble hole transport materials in organic LEDs" *Macromolecules*, **1999**, *32*, 4551.
46. Freudenmann, R.; Behnisch, B.; Hanack, M. "Synthesis of conjugated-bridged triphenylenes and application in OLEDs" *J. Mater. Chem.* **2001**, *11*, 1618.
47. Thomas, K. R. J.; Velusamy, M.; Lin, J. T.; Chuen, C. H.; Tao, Y. T. "Hexaphenylphenylene dendronized pyrenylamines for efficient organic light-emitting diodes" *J. Mater. Chem.*, **2005**, *15*, 4453.

48. Huang, C.; Zhen, C.-G.; Su, S. P.; Loh, K. P.; Chen, Z.-K. "Solution processable polyphenylphenyl dendron bearing molecules for highly efficient blue light-emitting diodes" *Org. Lett.* **2005**, *7*, 391.
49. Wu, Y.-T.; Hayama, T.; Baldrige, K. K.; Linden, A.; Siegel, J. S. "Synthesis of fluoranthenes and indenocorannulenes: elucidation of chiral stereoisomers on the basis of static molecular bowls" *J. Am. Chem. Soc.* **2006**, *128*, 6870.
50. Qian, X.; Xiao, Y. "4-amino-1,8-dicyanonaphthalene derivatives as novel fluorophore and fluorescence switches: efficient synthesis and fluorescence enhancement induced by transition metal ions and protons" *Tetrahedron Lett.* **2002**, *43*, 2991.
51. Gautrot, J. E.; Hodge, P.; Helliwell, M.; Raftery, J.; Cupertino, D. "Synthesis of electron-accepting polymers containing phenanthra-9,10-quinone units" *J. Mater. Chem.* **2009**, *19*, 4148.
52. Hartwig, J. F. "Transition metal catalyzed synthesis of arylamines and aryl ethers from aryl halides and triflates: scope and mechanism" *Angew. Chem. Int. Ed.* **1998**, *37*, 2046.
53. Wang, Z.; Kim, C.; Facchetti, A.; Marks, T. J. "Anthracenedicarbiximides as air-stable N-channel semiconductors for thin film transistors with remarkable current on/off ratios" *J. Am. Chem. Soc.* **2007**, *129*, 13362.
54. Amin, S.; Balanikas, G.; Huie, K.; Hussain, N.; Geddie, J. E.; Hecht, S. S. "Synthesis and fluorescence spectra of structural analogues of potential benzo[*b*]fluoranthene-DNA adducts" *J. Org. Chem.* **1985**, *50*, 4642.
55. Wee, K.-R.; Ahn, H.-C.; Son, H.-J.; Han, W.-S.; Kim, J.-E.; Cho, D. W.; Kang, S. O. "Emission color tuning and deep blue dopant materials based on 1,6-bis(*N*-phenyl-*p*-(*R*)-phenylamino)pyrene" *J. Org. Chem.* **2009**, *74*, 8472.

56. Yang, B.; Kim, S.-K.; Xu, H.; Park, Y.; Zhang, H.; Gu, C.; Shen, F.; Wang, C.; Liu, D.; Liu, X.; Hanif, M.; Tang, S.; Li, W.; Li, F.; Shen, J.; Park J.-W.; Ma, Y. "The origin of the improved efficiency and stability of triphenylamine-substituted anthracene derivatives for oleds: a theoretical investigation" *ChemPhysChem* **2008**, *9*, 2601.
57. Thomas, K. R. J.; Huang, T.-H.; Lin, J. T.; Pu, S.-C.; Cheng, Y. M.; Hsieh, C. C.; Tai, C. P. Donor-acceptor interactions in red-emitting thienylbenzene-branched dendrimers with benzothiadiazole core" *Chem. Eur. J.* **2008**, *14*, 11231.
58. Thomas, K. R. J.; Thompson, A. L.; Sivakumar, A. V.; Bardeen, C. J.; Thayumanavan, S. "Energy and electron transfer in bifunctional non-conjugated dendrimers" *J. Am. Chem. Soc.* **2005**, *127*, 373.
59. Kosower, E. M.; Dodiuk, H.; Kanety, H. "Intramolecular donor-acceptor systems. 4. solvent effects on radiative and nonradiative processes for the charge-transfer states of *N*-arylamino-naphthalenesulfonates" *J. Am. Chem. Soc.* **1978**, *100*, 4179.
60. Lakshmi, V.; Santosh, G.; Ravikanth, M. "Synthesis and properties of covalently linked thiaporphyrin-ferrocene conjugates" *J. Organomet. Chem.* **2011**, *696*, 925.
61. Bortolus, P.; Camaioni, N.; Flamigni, L.; Mino, F.; Monti, S.; Faucitano, A. "Photostabilization mechanism of imine amine light stabilizers: interaction of singlet and triplet anthracene with piperidine model compounds" *J. Photochem. Photobiol., A* **1992**, *239*.
62. Park, J.-Y.; Jung, S. Y.; Lee, J. Y.; Baek, Y. G. "High efficiency in blue organic light-emitting diodes using an anthracene-based emitting material" *Thin Solid Films* **2008**, *516*, 2917.

63. Luo, J.; Zhao, B., Chan, H. S. O.; Chi, C. "Synthesis, physical properties and self-assembly of star-shaped oligothiophene-substituted and fused triphenylenes" *J. Mater. Chem.* **2010**, *20*, 1932.
64. Okumoto, K.; Shirota, Y. "New class of hole-blocking amorphous molecular materials and their application in blue-violet-emitting fluorescent and green-emitting phosphorescent organic electroluminescent devices" *Chem. Mater.* **2003**, *15*, 699.
65. Thomas, K. R. J.; Lin, J. T.; Tao, Y.-T.; Chuen, C.-H. "Green and yellow electroluminescent dipolar carbazole derivatives: features and benefits of electron-withdrawing segments" *Chem. Mater.* **2002**, *14*, 3852.
66. Balasubramaniam, E.; Tao, Y.-T.; Danel, A.; Tomasik, P. "Blue light-emitting diodes based on dipyrazolopyridine derivatives" *Chem. Mater.* **2000**, *12*, 2788.

Synthesis and Characterization of Blue-Emitting Fluorene-Based Pyrazine Derivatives

3.1 Introduction

The efficient RGB emitters with excellent color purity, good film forming properties and transporting properties are required for full color range displays. Several fluorescent dyes with blue, green, yellow or red emission have been reported so far.¹⁻⁴ They have also been applied as efficient dopants or charge transporting materials for the application in OLEDs.^{5,6} But still the device efficiency and color purity of OLED device is a challenge for the researchers. The efforts are ongoing in developing efficient materials with high color purity, especially blue light emitting materials. It is important to develop blue materials with good stability and high efficiency because these materials are not only the blue light emitters, but are also required as the components for generating white light. These wide band gap materials can also be served as host materials for lower energy dopant materials to generate emission of other colors *via* energy transfer.⁷

Fluorenes comprises an important class of fused polyaromatic system due to their interesting and unique chemical and physical properties. Moreover, fluorene is one of the most promising candidate for efficient and bright pure blue electroluminescence (EL) emission.^{8,9} The major advantage with the fluorene is the facile substitution on 9th position which improves its solubility and also helps to preserve their optical properties in solid state by limiting molecular interactions. Fluorene-based oligomers and polymers constitute an important class of π -

conjugated organic materials because of their excellent optical, thermal, and electrochemical properties.^{10,11} They have been extensively studied and explored for various functional properties including EL, liquid crystalline and two-photon absorption properties for optoelectronic applications in the past few years.^{12,13}

The biggest problem associated with fluorene is the low color stability during device operation i.e. color is changed from blue to bluish green or yellow. The lack of color stability was indicated by the red shift in EL spectra or PL in thin film. This phenomenon has been reported in various polyfluorenes¹⁴ and many hypothesis^{15,16} has been given for its reason. According to them the appearance of low energy band can be due to 1) formation of aggregation or excimers, 2) fluorenone defects by photo-oxidation, thermal oxidation and metal catalyst during operation and 3) interchain interaction and formation of fluorenone-based excimer. This low energy band is undesirable for the color stability. Zhang et al. have reported fluorene based small functional materials for OLEDs and described the long energy emission band during device operation.¹⁷

To overcome this problem, the proper modification is necessary for stable blue color emission. For instance Goel et al. have reported donor-acceptor uncapped fluorene and fluorenone as stable blue emitters.¹⁸ They have demonstrated a strategy to improve blue color purity by appropriate positioning of donor-acceptor and chromophoric groups on fluorene/fluorenone backbone.

Fang et al. have recently demonstrated that electron deficient triazine core incorporated with fluorenyl diphenylamine shows nonlinear and two photon absorption properties and used as emitting materials in OLEDs.¹⁹ They have also demonstrated in their another report that triazine incorporated with phenyl in place of fluorene (C1) is not photoluminescent because of the lack

of donor-acceptor (D-A) structure while electron rich fluorene (**C2**) makes the triazine derivatives photoluminescent.²⁰ Thus combination of electron rich fluorene with electron deficient moiety can be a promising candidate for hole blocking or electron transporting or blue emitting material for OLED. Recently, Fisher et al. have reported diphenylamino fluorene (**C3**) or dicarbazolylamino fluorene (**C4**) derivatives linked with electron deficient oxadiazole unit as efficient deep blue emitter for single layer device.²¹ Structures of **C1-C4** are displayed in Figure 3.1 and the opto-electronic properties of **C1** and **C2** are given in Table 3.1.

Table 3.1 Optical and electrochemical properties of **C1** and **C2**.

Compound	λ_{abs} (nm)	λ_{em} (nm)	HOMO (eV)	LUMO (eV)	E_g (eV)
C1	270	NA	6.51	2.80	3.71
C2	352	385	6.25	2.95	3.30

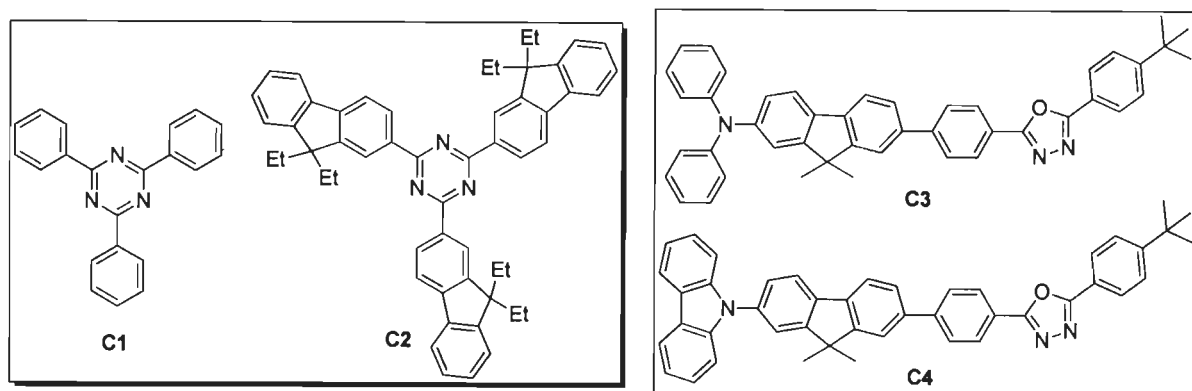


Figure 3.1 Structures of fluorene-based donor-acceptor systems.

Quinoxaline or pyrazines have been explored as a class of electron deficient materials and have been reported as electron transporting materials in OLEDs due to their high thermal stability, outstanding mechanical properties and good film forming properties.^{22,23} Jenekhe et al. have reported polyphenyl quinoxalines as electron transporting polymers for electroluminescent devices in their several reports.^{24,25} Jung et al. have described fluorene based polyquinoxalines as blue emitting polymers and these can be served as efficient electron transporting or hole blocking

materials.²⁶ They have also demonstrated that the polymers exhibited exceptionally high thermal stability due to the presence of quinoxalines.

Various quinoxaline-based polymers have been reported for their electron transporting properties.²⁴ Although polymers generally exhibit simple device architecture, good processability and a strong tendency of preserving the amorphism at the operating temperature because of the large molecular weight and high T_g (glass transition temperature) but repeated polymerization steps introduce significant impurities that are a bit harder to deal with. In comparison, small molecules with a low molecular weight have an advantage of easy thin layer fabrication by a high-vacuum deposition technique which enhances the processability and hence the impurities that arise from polymerization steps can be avoided.

Quinoxaline-based small materials can either act as hole transporting or electron transporting depending on the substituent present on it as shown in Figure 3.2. In many reports, triaryl amine incorporated quinoxalines have applied as hole transporter^{27,28} in OLED while few quinoxalines incorporated with electron withdrawing group are reported as electron transporting material^{29,30}. Molecular systems of donor(D)-acceptor(A) dyads as well as D-A-D/A-D-A triads, based on quinoxaline derivatives, are of current interest due to their potential application in molecular electronic devices and photovoltaic applications.^{31,32} Recently several polymers based on quinoxaline-fluorene-thiophene have been proven as potential candidate for photovoltaic applications.³³ Conjugated thiophene units are known to be good electronic conductors due to their virtue of enhancing π - conjugation and π -delocalization. Idzik et al. have demonstrated the combination of an electron deficient triazine and electron rich thiophene improves the chemical stability of monomer and provides the polymer via electropolymerization with enhanced

mobility of the charge carriers.³⁴ In many reports the electropolymerization of terthienyl systems have been studied.^{35,36}

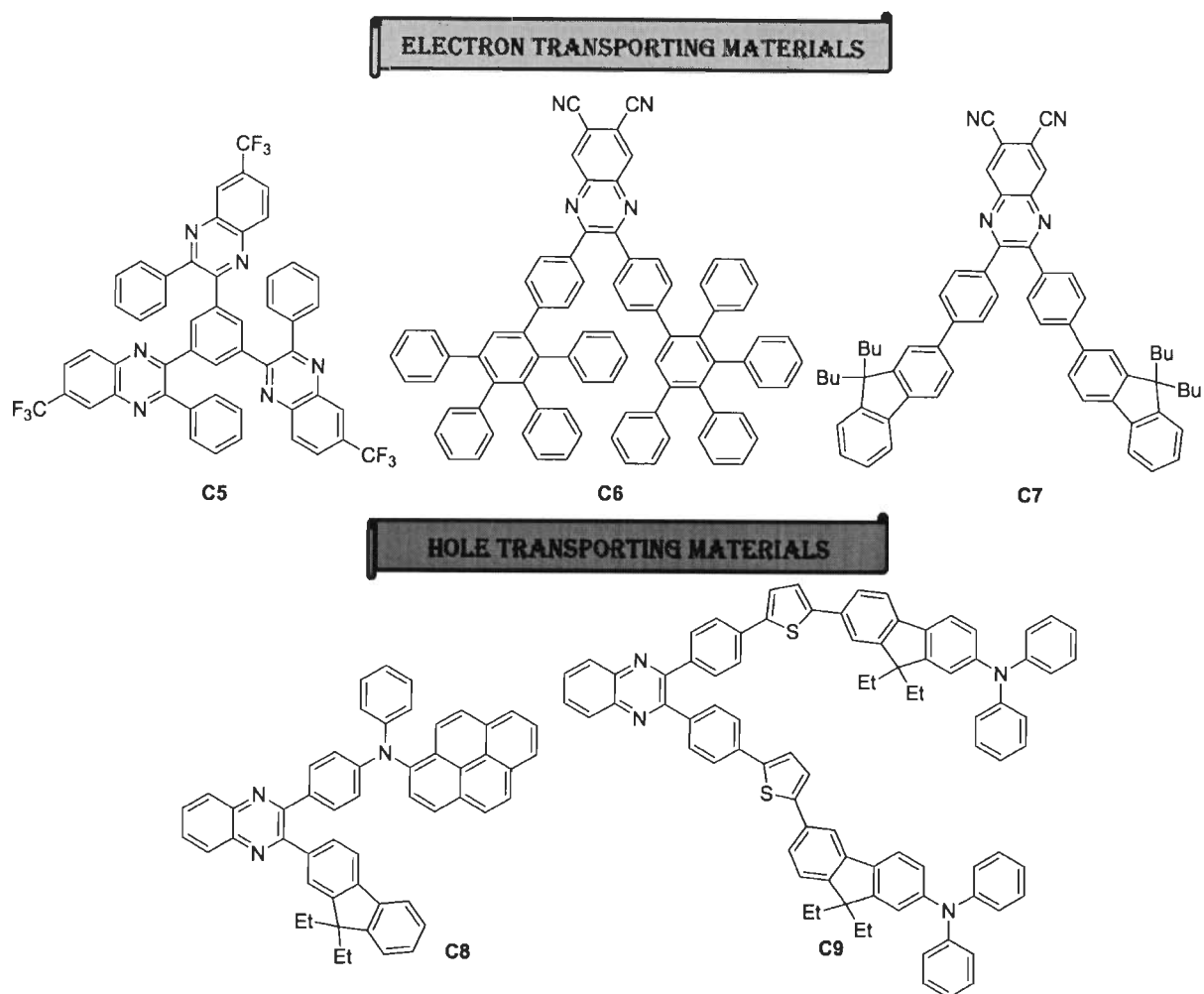


Figure 3.2 Structures of quinoxaline-based functional materials.

In this chapter, we are presenting the synthesis of fluorene-based quinoxalines, pyrazines and thienopyrazines. In our work, fluorene was chosen as electron rich unit and quinoxaline was taken as electron deficient unit. Moreover the incorporation of electron withdrawing $-CN$ group was helpful in increasing the electron mobility by lowering the LUMO energy levels. In other derivatives, we have incorporated fluorene with terthiophene/pyrazine which act as donor/acceptor system. The presence of terthiophene will increase the electron density over the

molecule which will be helpful in increasing the hole carrier mobility and lowering the band gap. The thienopyrazine derivatives can be used as monomer for the polymer based solar cell applications because they exhibited red shifted absorption at 545-556 nm, low band gap and also prone to polymerize during the electrochemical studies.

3.2 Results and discussion

3.2.1 Synthesis

The compounds were synthesized by the following synthetic procedure outlined in Scheme 3.1.

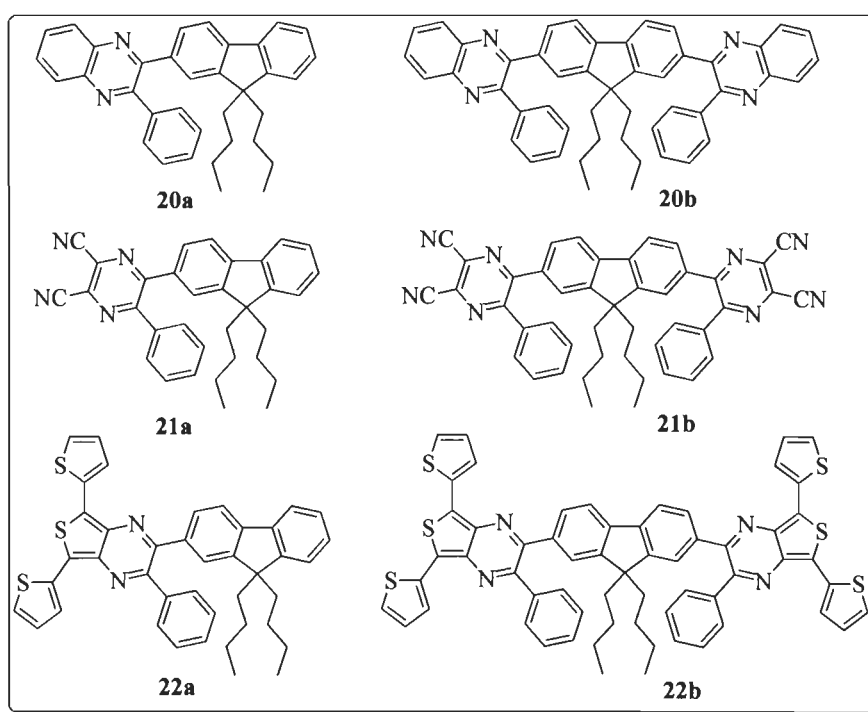
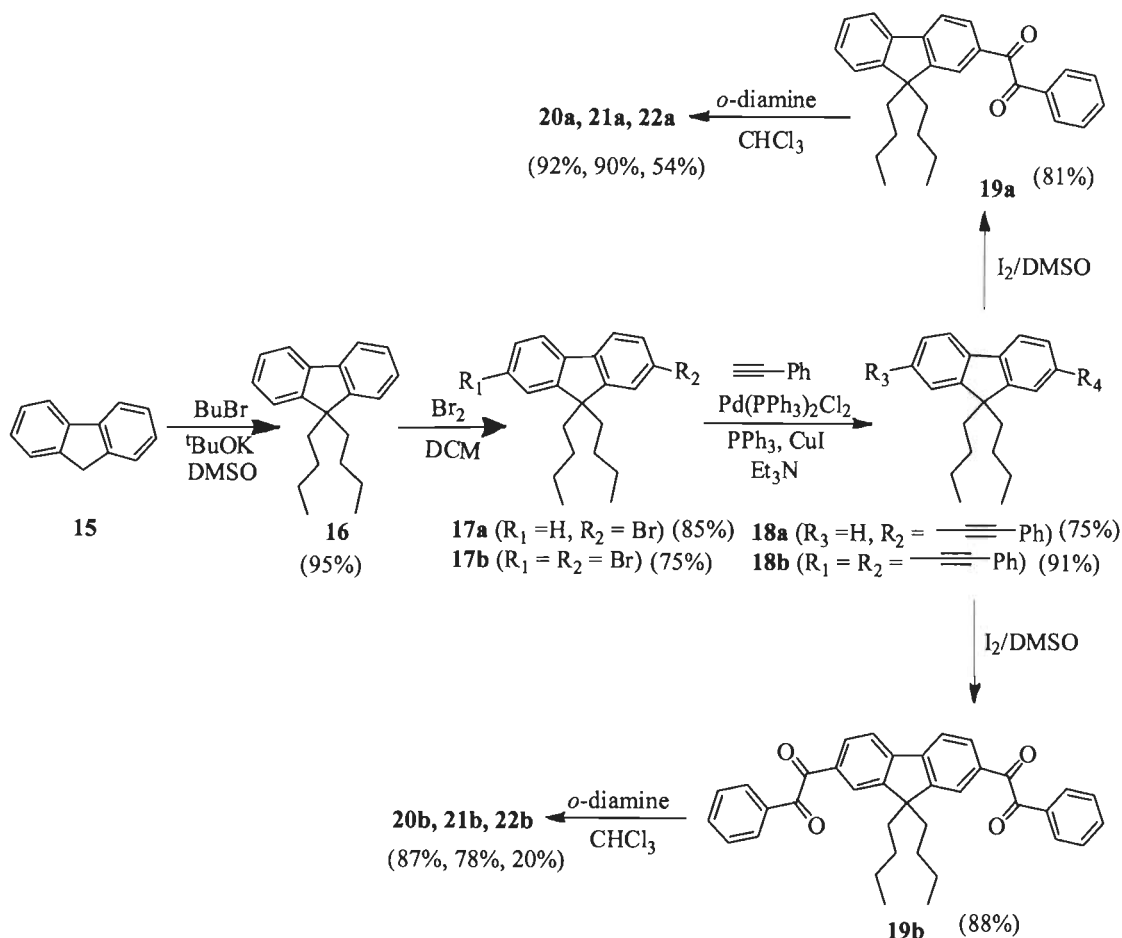


Figure 3.3 Structures of pyrazine derivatives containing fluorene segment.

and the structures of all the synthesized compounds are displayed in Figure 3.3. Although compound **16**, **17a** and **17b** are reported in the literature³⁷ but we have obtained them by following different conditions. The butylation of fluorene was done by butyl bromide using *t*-BuOK in presence of DMSO under nitrogen atmosphere. Further bromination of butylated fluorene was done by bromine and chloroform. Monobromination was done at 0°C to make **17a**

while dibromination was carried out at room temperature to synthesize **17b**. Then compounds **17a** and **17b** were further substituted to Sonogashira cross coupling reactions with phenyl acetylene using $\text{Pd}(\text{PPh}_3)_2\text{Cl}_2/\text{PPh}_3/\text{CuI}$ as catalytic system and Et_3N as a solvent. The ethynyl derivatives **18a** and **18b** were subsequently oxidized by I_2/DMSO to obtain the di- and tetraketone (**19a** and **19b**) respectively.



Scheme 3.1 Synthesis of quinoxaline (**20a**, **20b**), pyrazine (**21a**, **21b**) and thienopyrazine (**22a**, **22b**) derivatives.

The obtained diketone (**19a**) and tetraketones (**19b**) were treated with different *o*-diamines such as *o*-phenylene diamine, 2,3-diaminomaleonitrile or [2,2':5',2''-terthiophene]-3',4'-diamine

to produce the final quinoxalines (**20a** & **20b**), pyrazines (**21a** & **21b**) and thienopyrazines (**22a** & **22b**) respectively.

3.2.2 Optical properties

The optical properties were examined by UV-vis absorption and fluorescence spectroscopic techniques. The absorption spectra for quinoxalines, pyrazines and thienopyrazines were recorded in toluene and dichloromethane and displayed in Figures 3.4 & 3.5. The data were compiled in Table 3.2. In dichloromethane solution, the compounds **20a**, **20b**, **21a** and **21b** showed two absorption bands. The high energy band can be assigned to a π - π^* transition. The low energy band can be ascribed as π - π^* transition having minor charge transfer character from fluorene to electron deficient quinoxaline. The low energy band of **20a** observed at 362 nm is 19 nm red shifted as compared to previously reported 2-(9*H*-fluoren-2-yl)quinoxaline which was observed at 343 nm.³⁸ This indicates that the phenyl ring in **20a** is increasing the conjugation which leads to red shift.

The dicyano containing pyrazine derivative (**21a**) exhibited red shifted absorption as compared to quinoxaline **20a**. The presence of electron withdrawing dicyano unit increases the acceptor strength of pyrazine which results in red shifted absorption. This kind of red shift has been reported previously for pyrazine due to the presence of dicyano unit.³⁹ Molar extinction coefficient is also higher for pyrazines as compared to quinoxalines due to increasing acceptor strength which increases the transition probability. Disubstituted derivatives **20b** and **21b** showed red shifted absorption with high molar extinction coefficient as compared to their corresponding mono substituted derivatives **20a** and **21a** respectively. This is due to the increase in conjugation *via* disubstitution and incrementation in the chromophoric population. Terthiophene bearing derivatives **22a** and **22b** displayed two absorption bands out of which the

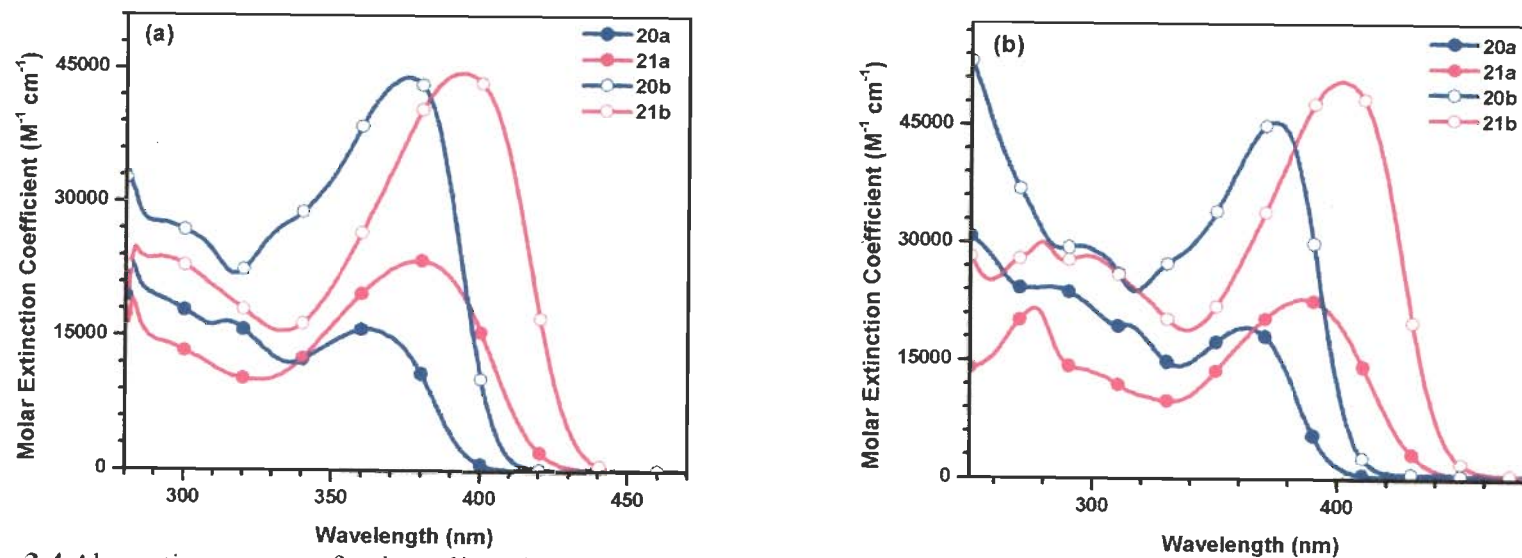


Figure 3.4 Absorption spectra of quinoxalines (20a, 20b) and pyrazines (21a, 21b) recorded (a) in toluene and (b) in dichloromethane solutions.

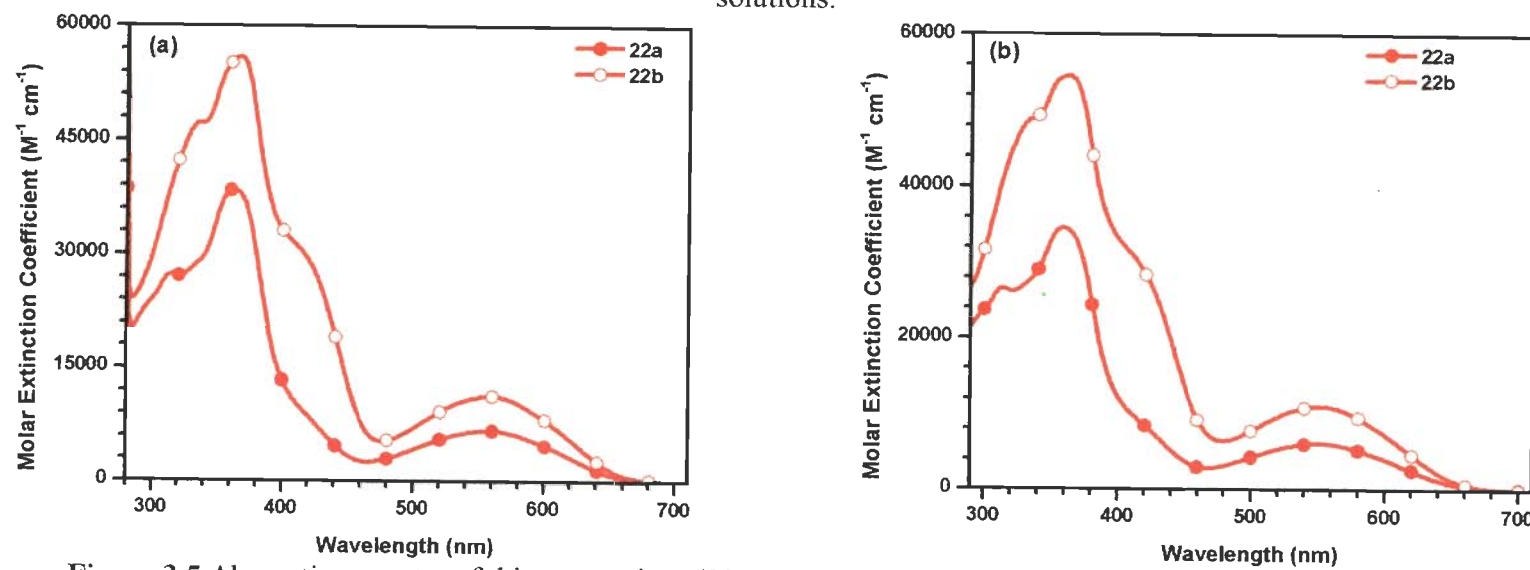


Figure 3.5 Absorption spectra of thienopyrazines (22a, 22b) recorded (a) in toluene and (b) in dichloromethane.

first band at 362 nm is similar to that observed for the compound **20a** while a new band appears at longer wavelength due to charge transfer between electron rich terthiophene and electron deficient pyrazine segments. Thus, terthiophene/pyrazine serves as donor/acceptor system. There is no significant difference in the absorption wavelength of both mono and di-substituted derivatives (**22a** and **22b**) only high molar extinction coefficient was observed in case of di-substituted **22b**. This observation indicates that the another substitution at 7th-position of fluorene is not taking part in increasing the conjugation but it only increases the chromophore density due to the presence of two donor/acceptor system.

Table 3.2 Optical properties of quinoxalines (**20a**, **20b**), pyrazines (**21a**, **21b**) and thienopyrazines (**22a**, **22b**).

Compound	Toluene			Dichloromethane			Thin film λ_{em} , nm
	λ_{max} , nm (ϵ_{max} , $M^{-1}cm^{-1}$) $\times 10^3$)	λ_{em} , nm (Φ_F , %)	Stoke shift, cm^{-1}	λ_{max} , nm (ϵ_{max} , $M^{-1}cm^{-1}$) $\times 10^3$)	λ_{em} , nm (Φ_F , %)	Stoke shift, cm^{-1}	
20a	362 (15.8)	417 (0.04)	3643	282 (24.2), 313 (19.5), 362 (19.2)	443 (0.10)	5051	432
21a	379 (23.4)	451 (0.16)	4212	276 (21.6), 386 (22.8)	486 (0.23)	5331	484
22a	362 (38.4), 556.5 (6.6)	661 (NA)	2841	358 (34.5), 545-556 (6.0)	664 (NA)	2925	-
20b	375.5 (43.9)	415, 431(sh) (0.14)	2535	294 (29.5), 374 (45.4)	440 (0.21)	4011	441
21b	393 (44.5)	445 (0.60)	2973	279 (29.9), 297 (28.2), 401 (50.6)	465 (0.61)	3432	494
22b	366.5 (55.8), 557.5 (11.1)	663 (NA)	2854	363 (54.4), 546-556 (10.8)	666 (NA)	2971	-

The emission spectra of the dyes were recorded in toluene which is shown in Figure 3.6. The data are displayed in Table 3.2. Pyrazine derivatives (**21a**, **21b**) showed red shifted emission as

compared to quinoxaline derivatives (**20a**, **20b**). This suggests that presence of $-\text{CN}$ chromophore is responsible for the red shift. The disubstituted derivatives (**20b**, **21b**) exhibited blue shifted emission profile when compared to the monosubstituted analogues (**20a**, **21a**) due

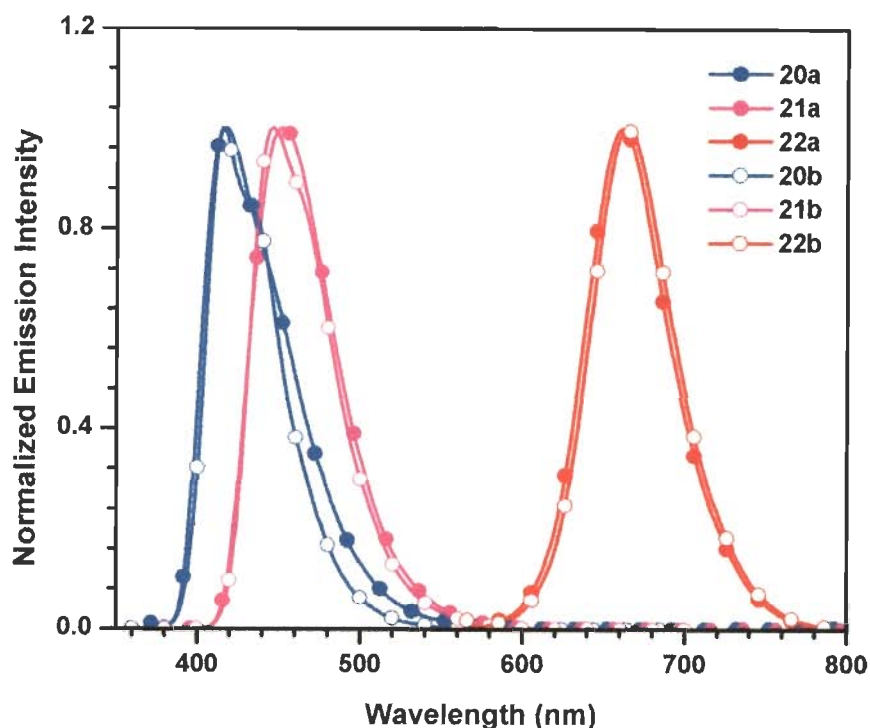


Figure 3.6 Emission spectra of quinoxalines (**20a**, **20b**), pyrazines (**21a**, **21b**) and thenopyrazines (**22a**, **22b**) recorded in toluene.

to the hike in the acceptor strength. Moreover a vibronic pattern was observed for disubstituted derivatives while monosubstituted exhibit a broad emission with the loss of vibronic pattern. The reason could be that the excited state of **20a** and **21a** is more polar or more stabilizes as compared to **20b** and **21b** respectively. The less polar excited state of disubstituted derivative is due to the cancellation of dipolar interaction of two electron deficient unit which cause the competitive acceptance of electron density from fluorene. The dipolar interaction is more in more polar solvent dichloromethane as indicated by broad emission band for quinoxalines and pyrazines as compared to that in less polar toluene (Figure 3.7).

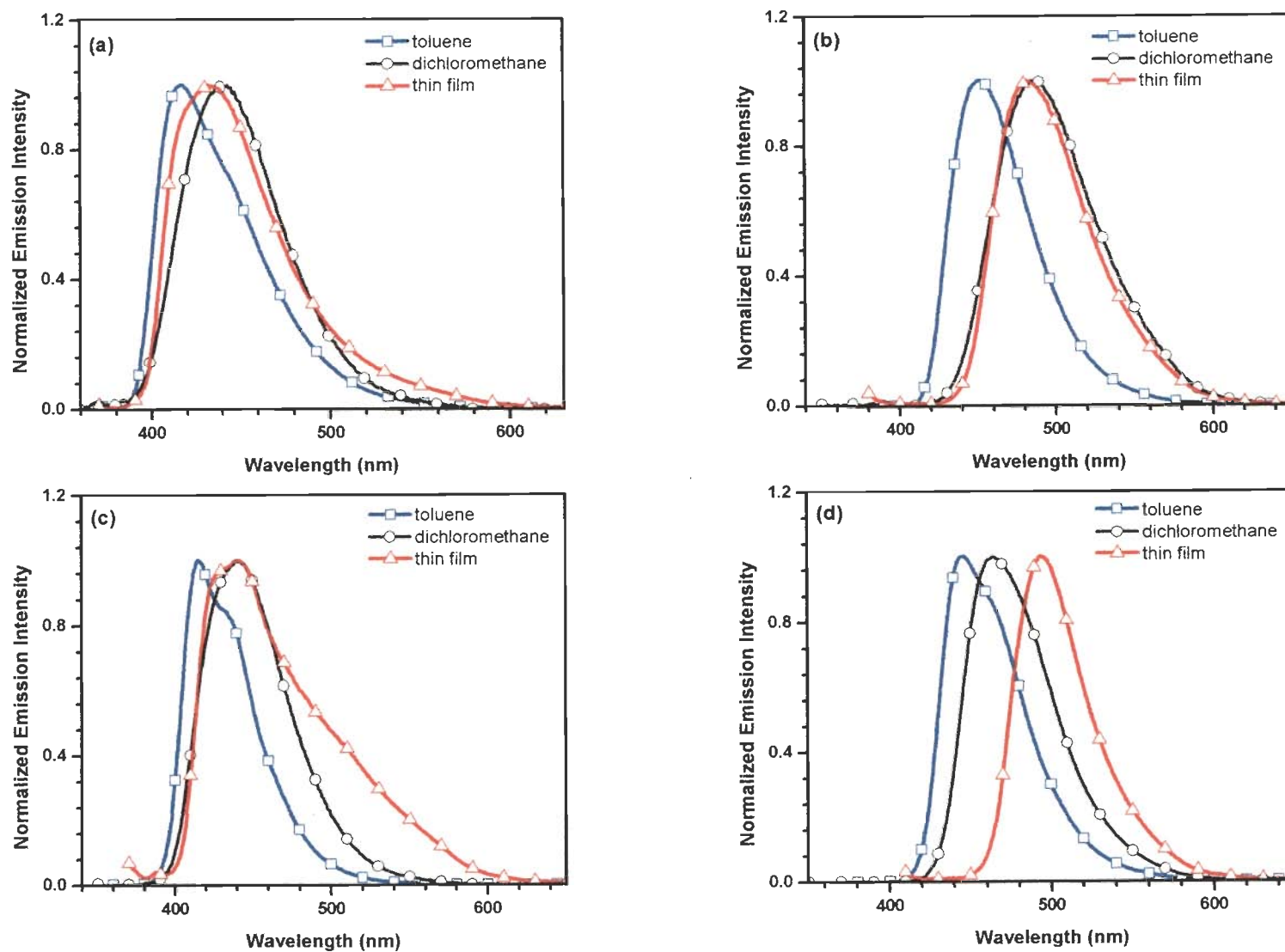


Figure 2.7 Emission spectra of the compounds (a) **20a**, (b) **21a**, (c) **20b** and (d) **21b** recorded in different medium (toluene, dichloromethane and thin solid film).

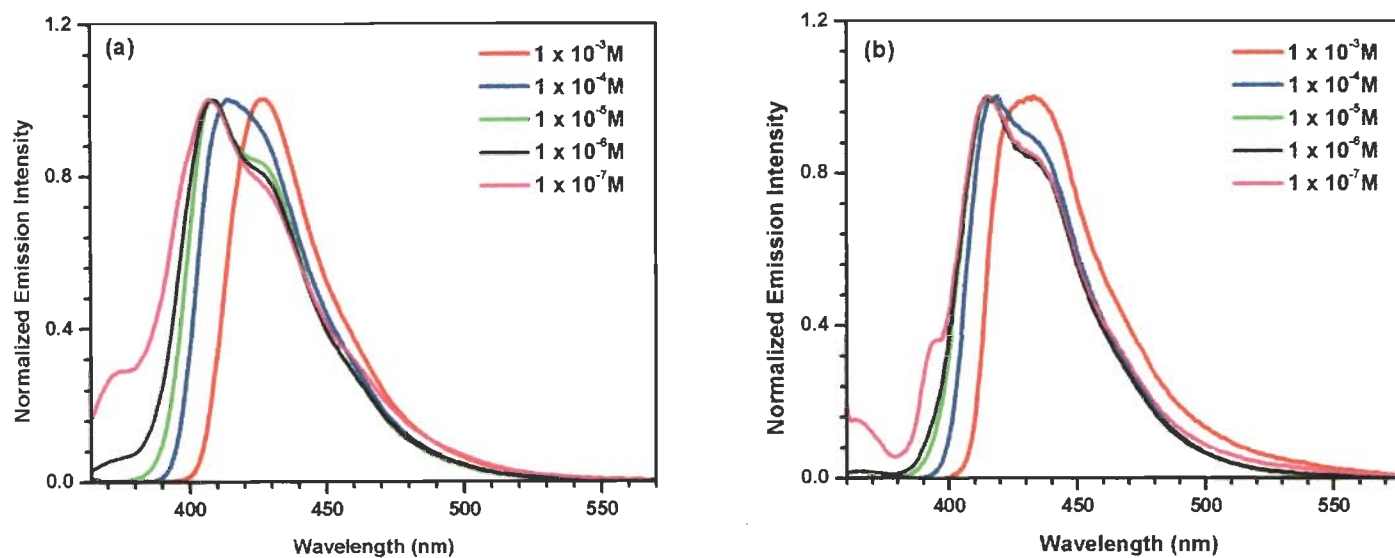


Figure 3.8 Emission spectra for **20b** recorded in cyclohexane (a) and in toluene (b) at different concentration.

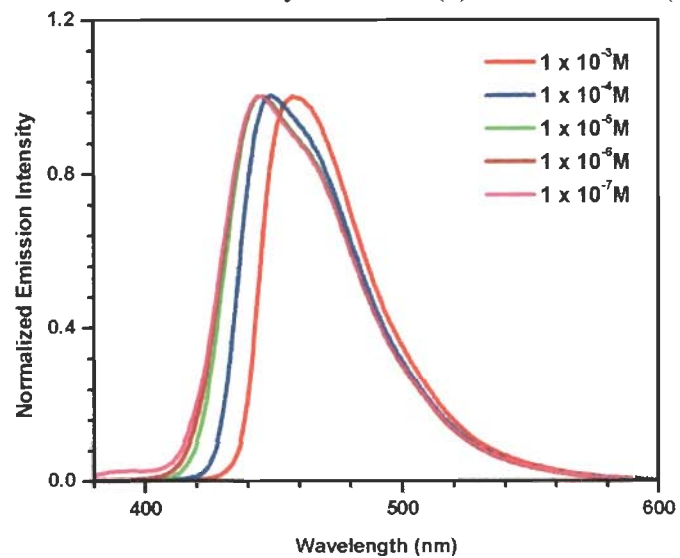


Figure 3.9 Emission spectra for **21b** recorded in toluene at different concentration.

The emission spectra were recorded in thin film and shown in Figure 3.7. Monosubstituted derivatives (**20a** and **21a**) did not show significant change in the emission profile when recorded in thin film as compared to solution. But disubstituted derivatives show broad and red shifted emission in thin film. This could be due to the aggregation in thin film. To confirm the reason, the emission spectra of disubstituted derivatives were recorded in nonpolar solvents at different concentration. Emission spectra of quinoxaline derivative **20b** were recorded in cyclohexane and toluene at different concentration as shown in Figure 3.8. It can be seen that a regular red shift was observed as the concentration increases. There is no change below the concentration 10^{-5} M. It was also observed that compound **20b** showed no significant shift at 10^{-4} M when recorded in toluene. The emission spectra for compound **21b** were not recorded in cyclohexane due to solubility problem. **21b** also show red shifted emission at high concentration in toluene (Figure 3.9). This indicates that disubstituted quinoxaline and pyrazine are aggregating in thin film and high concentrated solution. Thienopyrazine (**22a** and **22b**) did not show emission in thin film.

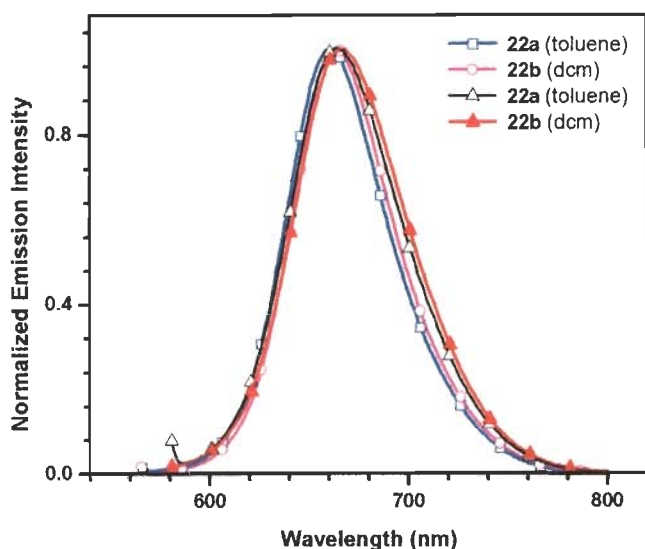


Figure 3.10 Emission spectra of **22a** and **22b** in toluene and dichloromethane.

Thienopyrazine showed emission at longer wavelength than the other derivatives. **22a** and **22b** emit at the same wavelength 663-666 nm (Figure 3.10). Moreover there was no change

observed in the emission wavelength by changing the solvent polarity. This may be due to the same dipole moment in the excited state as illustrated in Figure 3.11. The resultant dipole moment is same for both derivatives.

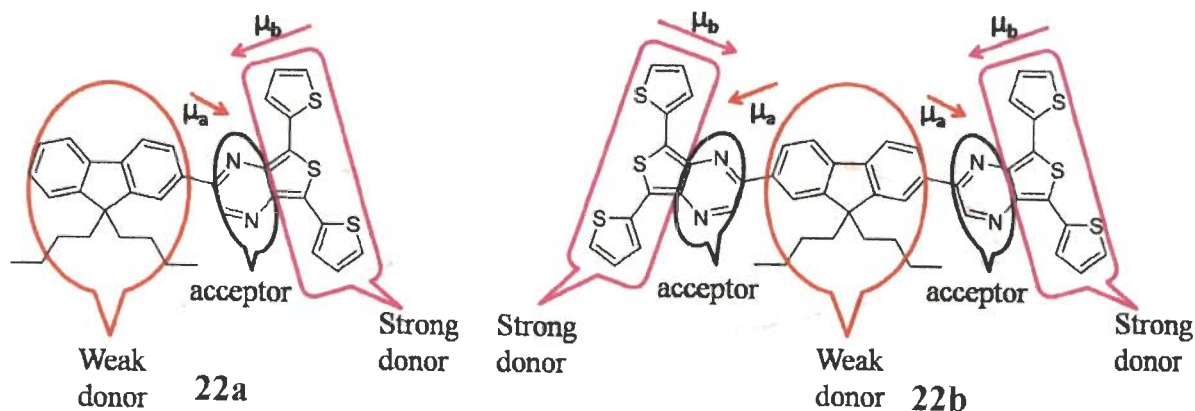


Figure 3.11 Dipolar interactions in **22a** and **22b**.

The presence of five membered thiophene ring made the compound rigid and more planar as compared to six membered phenyl ring.⁴⁰ Thus thienopyrazines are more planar as compared to quinoxalines. The explanation of rigidity and planarity can be confirmed by the value of Stokes' shift which is lesser for **22a** than both **20a** and **21a**. But **22b** exhibited higher value of Stokes' shift as compared to **20b**. This may be due to presence of two donor/acceptor system which causes more stabilization of the excited state. Quantum efficiency of all the dyes is more in polar solvent. The reason could be the viscosity of the medium which can minimize the non radiative decay. The compound **21b** have almost similar value in both solvents. The might be due to the aggregation of molecule **21b** in nonpolar solvent.

The absorption and emission spectra of quinoxalines (**20a**, **20b**) and pyrazines (**21a**, **21b**) were recorded in different solvents to see the effect of polarity of solvents. The absorption and emission data in different solvents are given in Tables 3.3 and 3.4 respectively. The spectra are shown in Figures 3.12, 3.13. There was no significant change observed in absorption spectra of

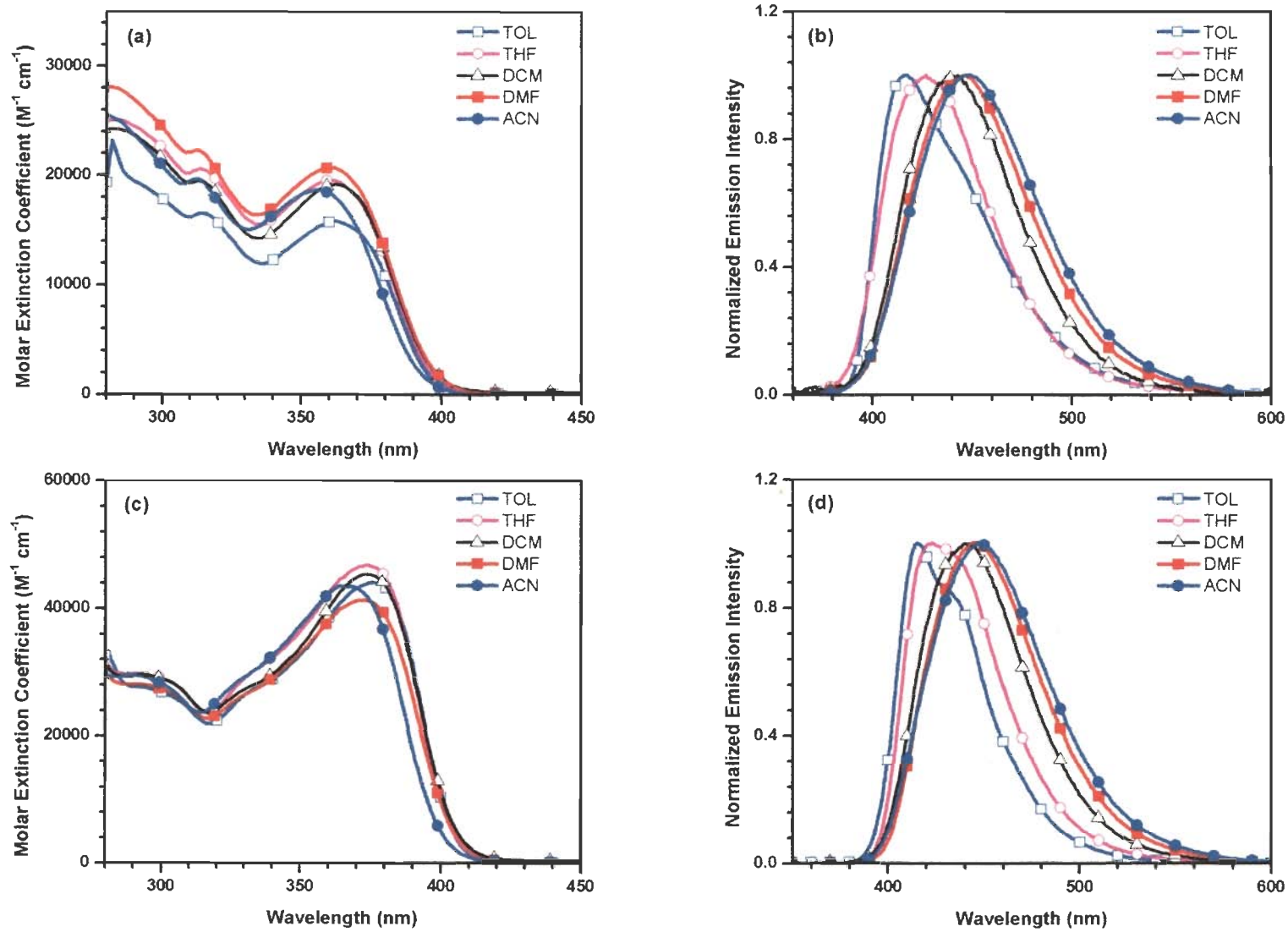


Figure 3.12 Absorption and emission spectra of 20a (a), (b) and 20b (c), (d) recorded in different solvents.

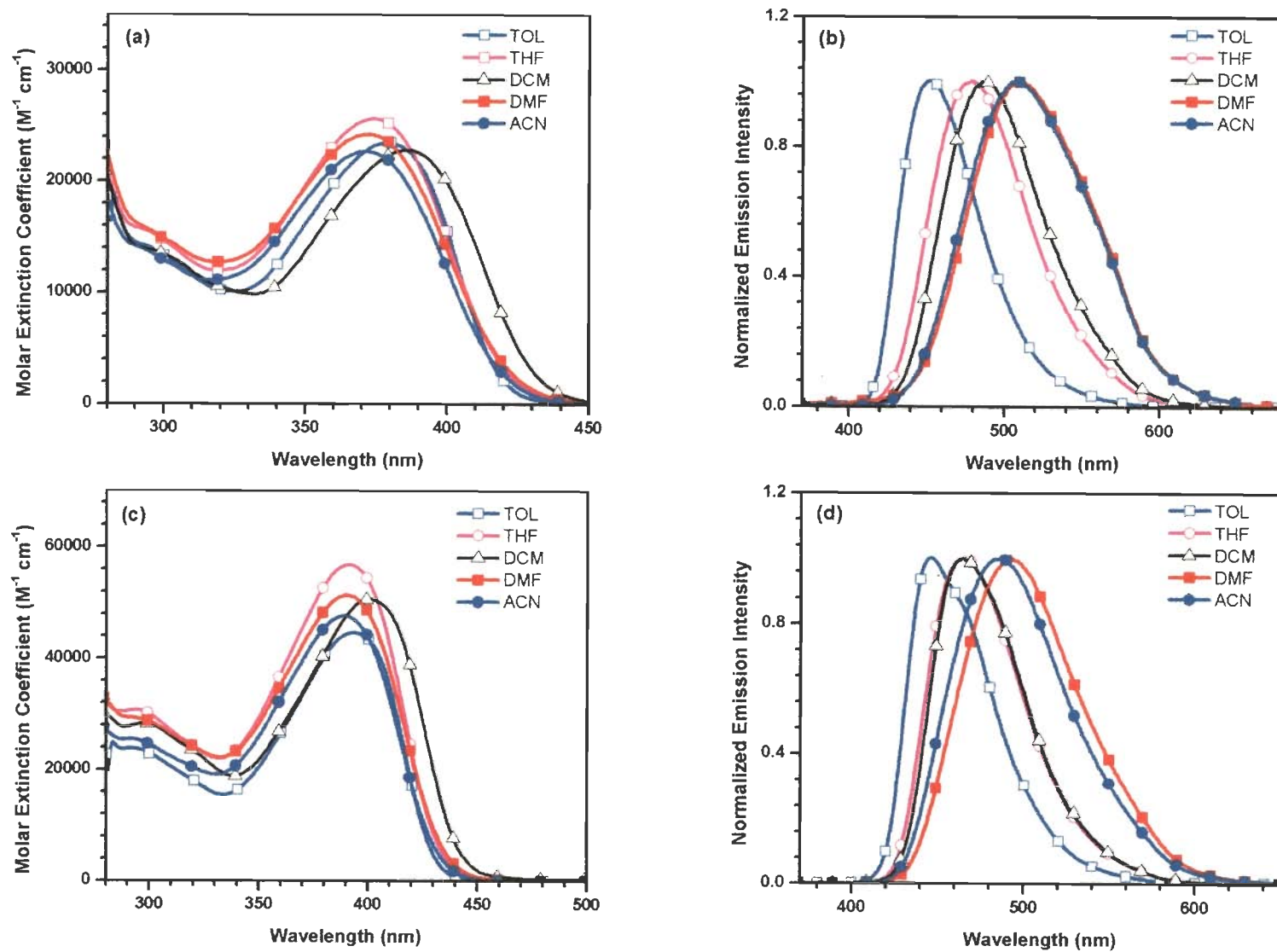


Figure 3.13 Absorption and emission spectra of 21a (a), (b) and 21b (c), (d) recorded in different solvents.

quinoxalines derivatives (**20a**, **20b**) by changing solvent polarity from toluene to acetonitrile (Figures 3.12 (a), (c)). This indicates that the ground state is not polar. But the absorption spectra of pyrazine compounds (**21a**, **21b**) exhibited unusual red shift in dichloromethane solution (Figures 3.13 (a), (c)). This kind of unusual red shift in dichloromethane was previously reported for cationic dyes which attributes that the instant stabilization occurs due to a fast rearrangement of polarizable electrons during excitation.⁴¹

All the compounds (**20a**, **20b** and **21a**, **21b**) exhibited the positive solvatochromism in the emission profile (Figures 3.12 (b), (d) and 3.13 (b), (d)). This suggests the presence of dipolar interactions in the excited state which increases by increasing solvent polarity.

The solvent interaction were further confirmed by the Lippert-Mataga, $E_T(30)$ and Kamlet-Taft plots. The Stokes' shifts observed for the compounds (**20a**, **20b** and **21a**, **21b**) are listed in Table 3.5. Quinoxaline derivatives (**20a**, **20b**) showed both specific and nonspecific interactions. Linearity in Lippert-Mataga plot tells the non specific interactions which arise due to van der Waals and electrostatic interactions (Figure 3.14(a) and 3.15(a)). Linear fit curve of $E_T(30)$ plot in Figures 3.14(b) and 3.15(b), clearly indicates the presence of charge transfer character in the molecule and the deviation of THF in Lippert-Mataga is due to charge transfer interactions

Kamlet-Taft plots describes the hydrogen bonding interactions. Interestingly, the Kamlet-Taft plots showed better linear fit for the quinoxaline derivatives (**20a**, **20b**) as compared to pyrazine derivatives (**21a**, **21b**). It suggests that in quinoxaline derivatives, besides the non specific interaction, other interactions like charge transfer and hydrogen bonding are also taking place. On the contrary the pyrazine derivatives (**21a**, **21b**) showed deviation from linearity in $E_T(30)$ plot in dichloromethane and acetonitrile (Figures 3.16(b) and 3.17(b)) and do not display linearity in Lippert-Mataga and Kamlet-Taft plots.

Thus the above discussion clearly indicates that the non specific interaction between the molecules and the solvents or neighbouring molecules significantly alters the relaxation of the molecule in the excited state.

Table 3.3 Absorption data of the compounds **20a**, **20b**, **21a** and **21b** recorded in different solvents.

Compound	λ_{\max} , nm (ϵ_{\max} , $M^{-1}cm^{-1}$) $\times 10^3$				
	Toluene	THF	dichloromethane	DMF	acetonitrile
20a	362 (15.8)	360 (19.5)	362 (19.2)	360 (20.7)	356 (18.6)
20b	376 (43.9)	374 (46.7)	374 (45.4)	372 (41.2)	364 (43.5)
21a	379 (23.4)	374 (25.6)	386 (22.7)	372 (24.2)	371 (22.7)
21b	393 (44.5)	392 (56.6)	401 (50.6)	390 (51.2)	389 (47.5)

Table 3.4 Emission data of the compounds **20a**, **20b**, **21a** and **21b** recorded in different solvents.

	toluene	THF	dichloromethane	DMF	acetonitrile
20a	417	427	443	447	447
20b	415	423	440	446	448
21a	451	479	486	511	506
21b	446	464	465	492	486

Table 3.5 Stokes' shift observed for the compounds **20a**, **20b**, **21a** and **21b** in different solvents and the parameters used for correlation.

Solvents	Orientation polarizability	$E_T(30)$	π^*	Stokes' Shift			
				20a	20b	21a	21b
Toluene	0.0135	33.9	0.54	3643	2499	4212	3024
THF	0.2096	37.4	0.58	4359	3097	5861	3958
dichloromethane	0.219	40.7	0.82	5051	4011	5331	3432
DMF	0.275	43.2	0.88	5406	4460	7312	5316
Acetonitrile	0.306	45.6	0.75	5719	5151	7191	5131

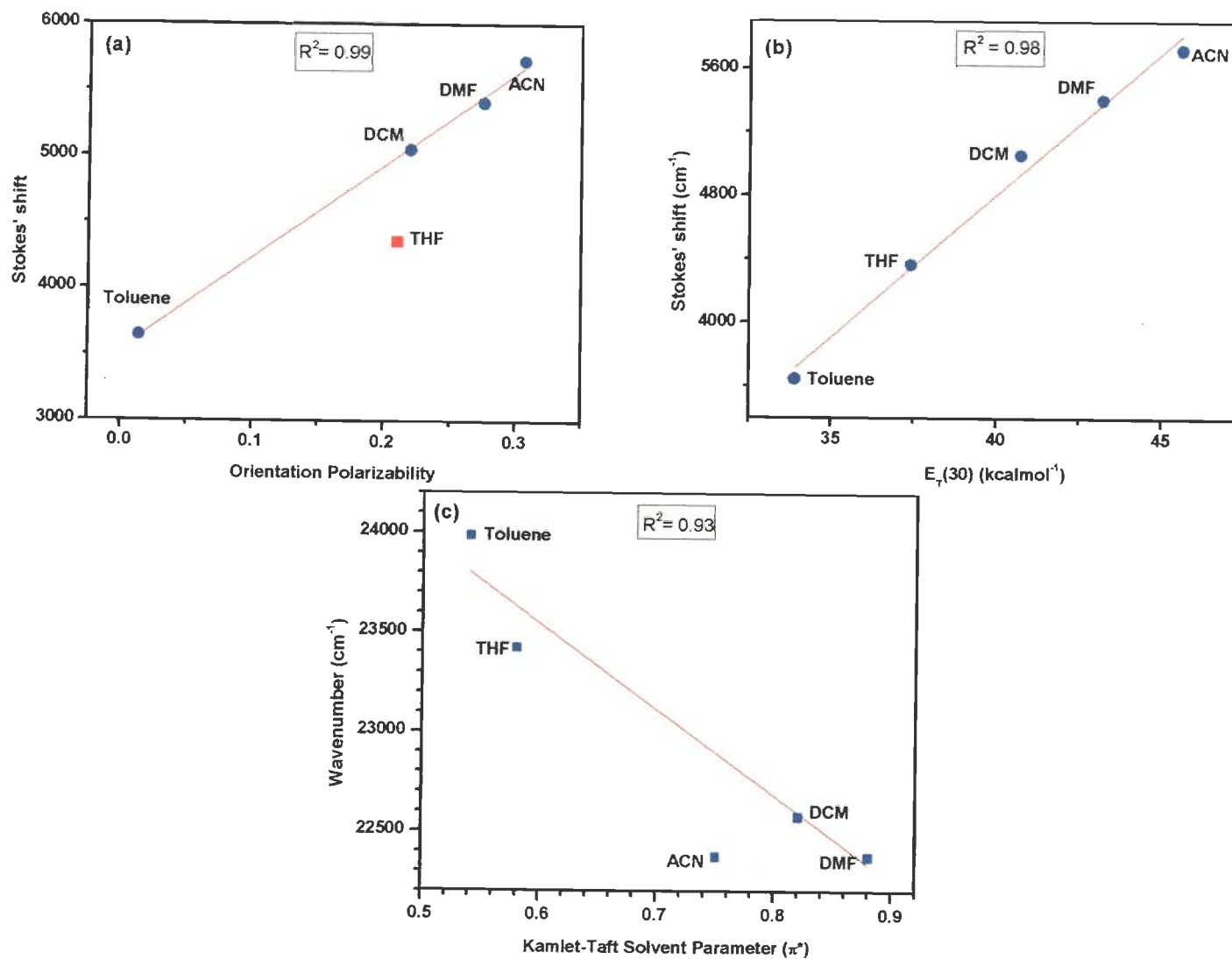


Figure 3.14 Plots for **20a** in different solvents (a) Lippert-Mataga plot showing Stokes' shift vs orientation polarizability of the solvents, (b) Stokes' shift vs $E_T(30)$ parameter, (c) emission maxima (in cm⁻¹) vs Kamlet-Taft solvent polarity parameter.

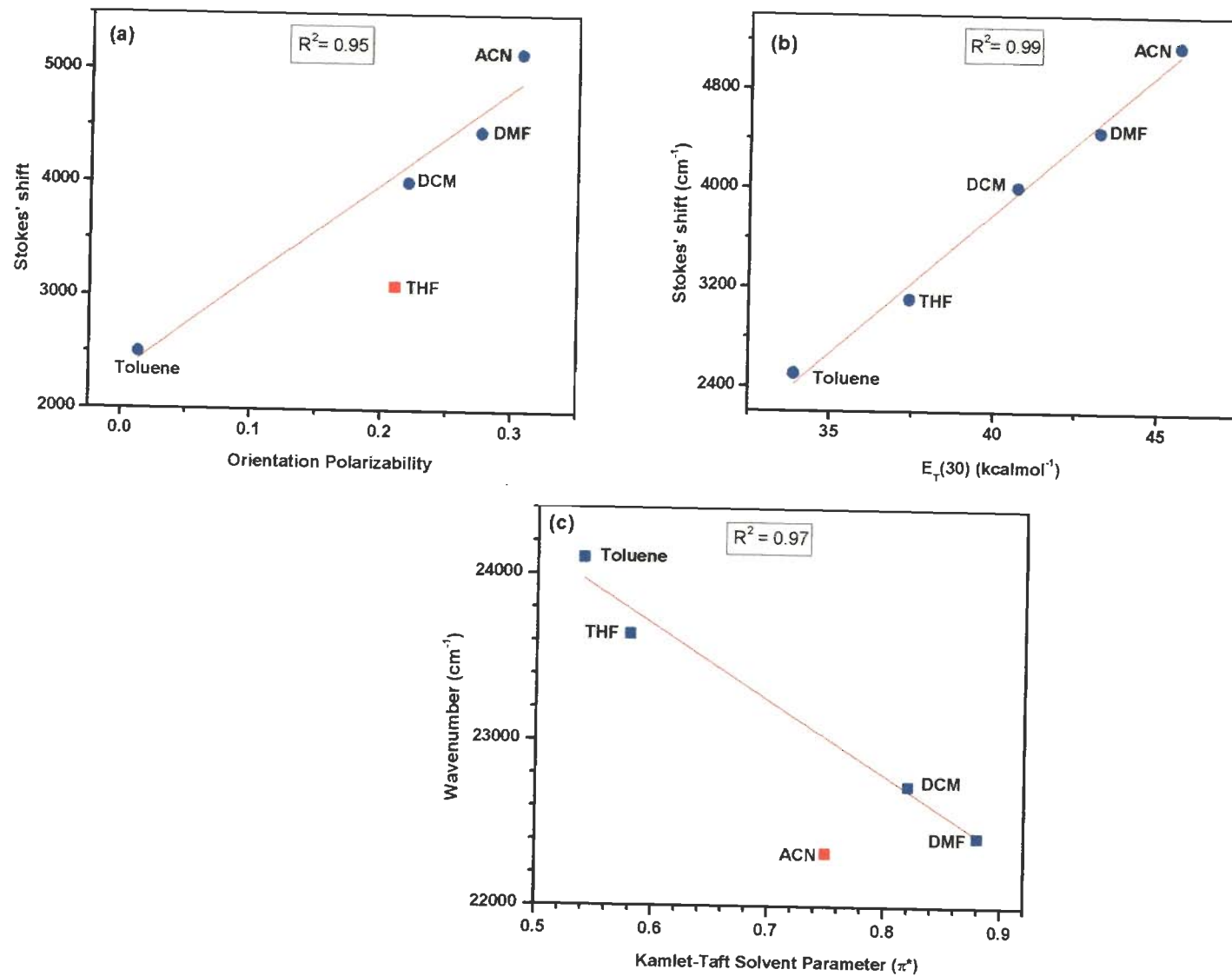


Figure 3.15 Plots for **20b** in different solvents (a) Lippert-Mataga plot showing Stokes' shift vs orientation polarizability of the solvents, (b) Stokes' shift vs $E_T(30)$ parameter, (c) emission maxima (in cm⁻¹) vs Kamlet-Taft solvent polarity parameter.

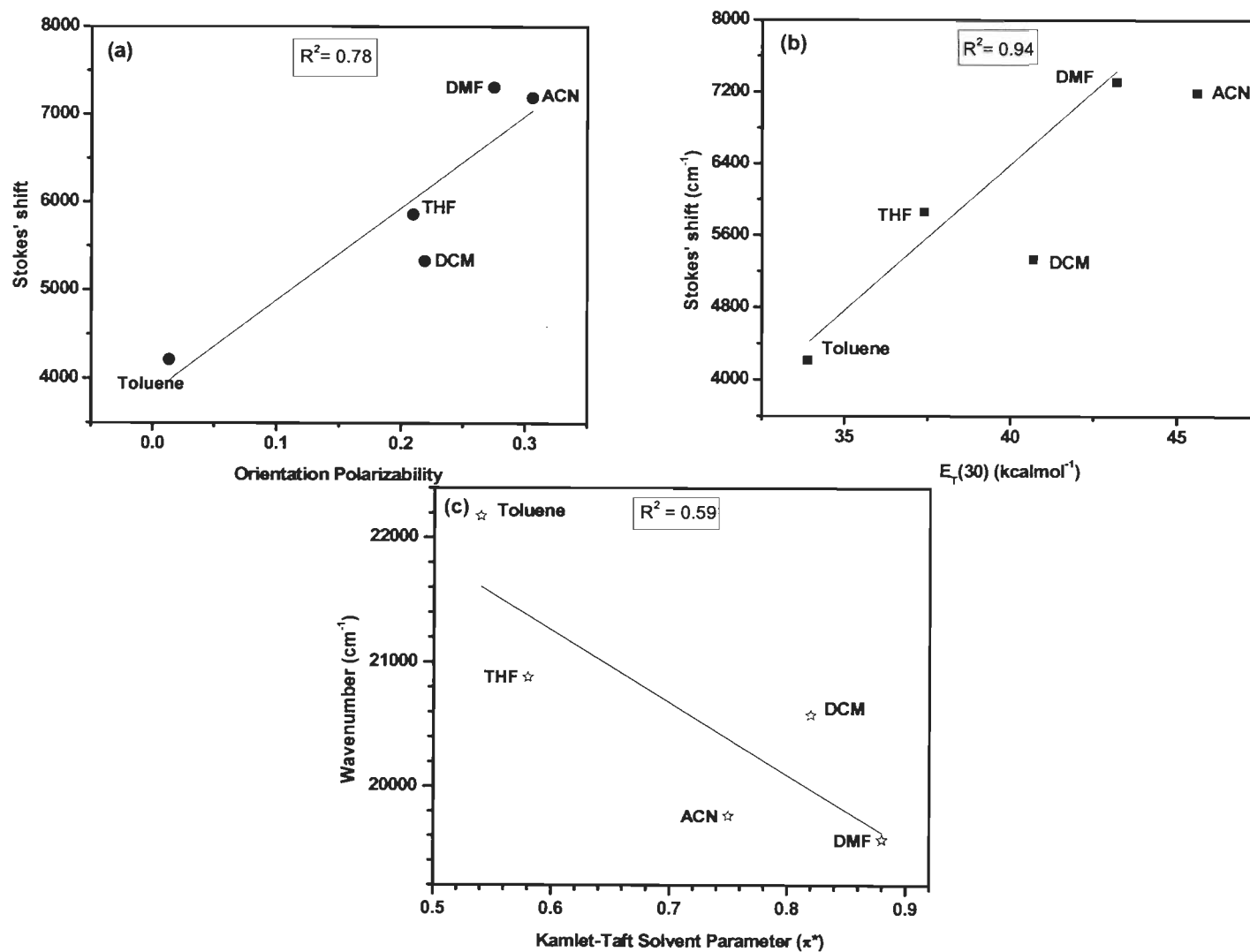


Figure 3.16 Plots for **21a** in different solvents (a) Lippert-Mataga plot showing Stokes' shift vs orientation polarizability of the solvents, (b) Stokes' shift vs $E_T(30)$ parameter, (c) emission maxima (in cm⁻¹) vs Kamlet-Taft solvent polarity parameter.

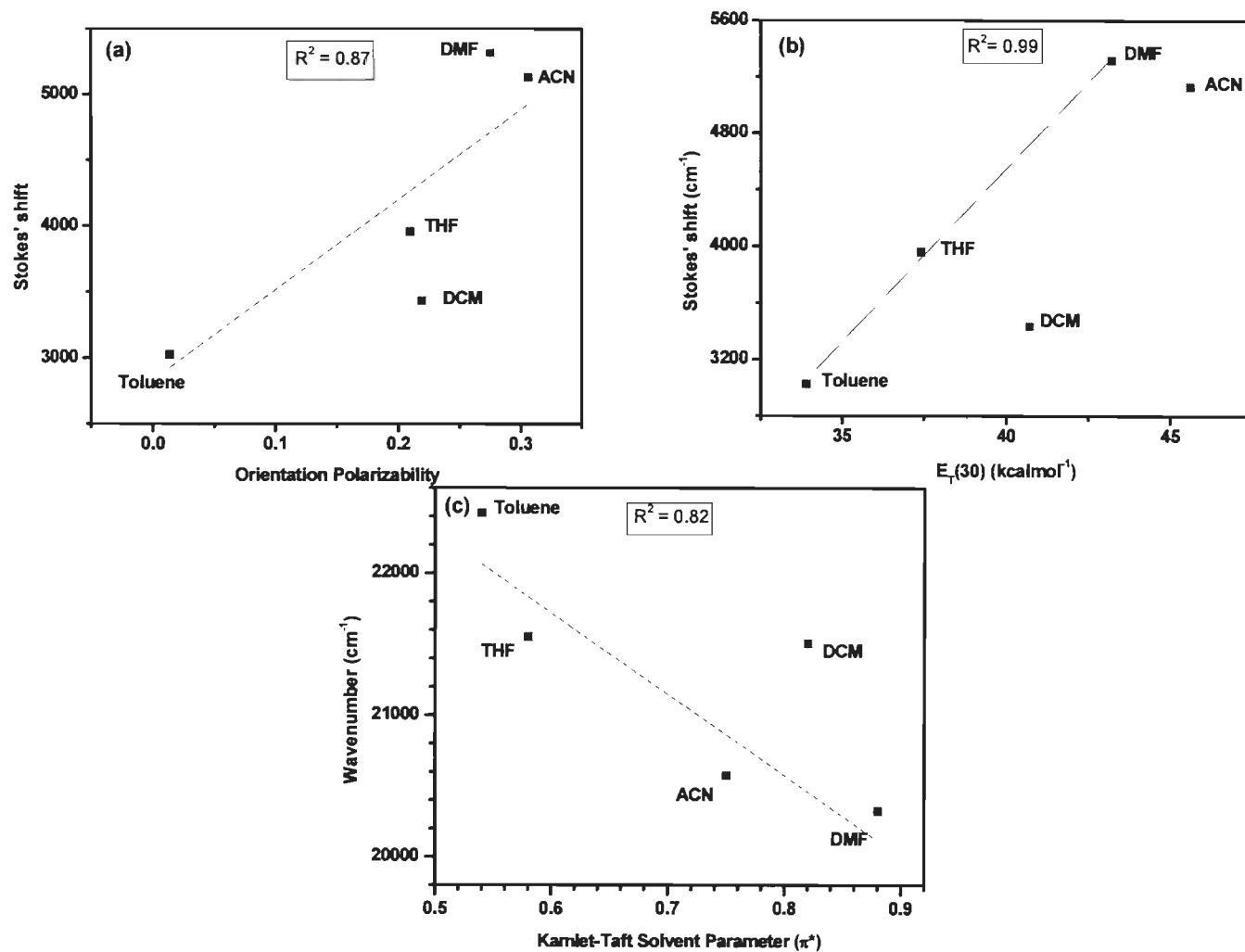


Figure 3.17 Plots for **21b** in different solvents (a) Lippert-Mataga plot showing Stokes' shift vs orientation polarizability of the solvents, (b) Stokes' shift vs $E_T(30)$ parameter, (c) emission maxima (in cm⁻¹) vs Kamlet-Taft solvent polarity parameter.

3.2.3 Theoretical investigations

In order to understand the absorption characteristics of the compounds, we have performed a theoretical calculation for the molecules **20a**, **21a** & **22a** using the density functional theory with the B3LYP functional and 6-31G(d,p) basis set. The prominent higher wavelength vertical transitions, dipole moment (μ) and their oscillator strength (f) predicted by the theory is collected in Table 3.6. The frontier molecular orbital diagrams of the compounds **20a**, **21a** and **22a** are given in Figure 3.18.

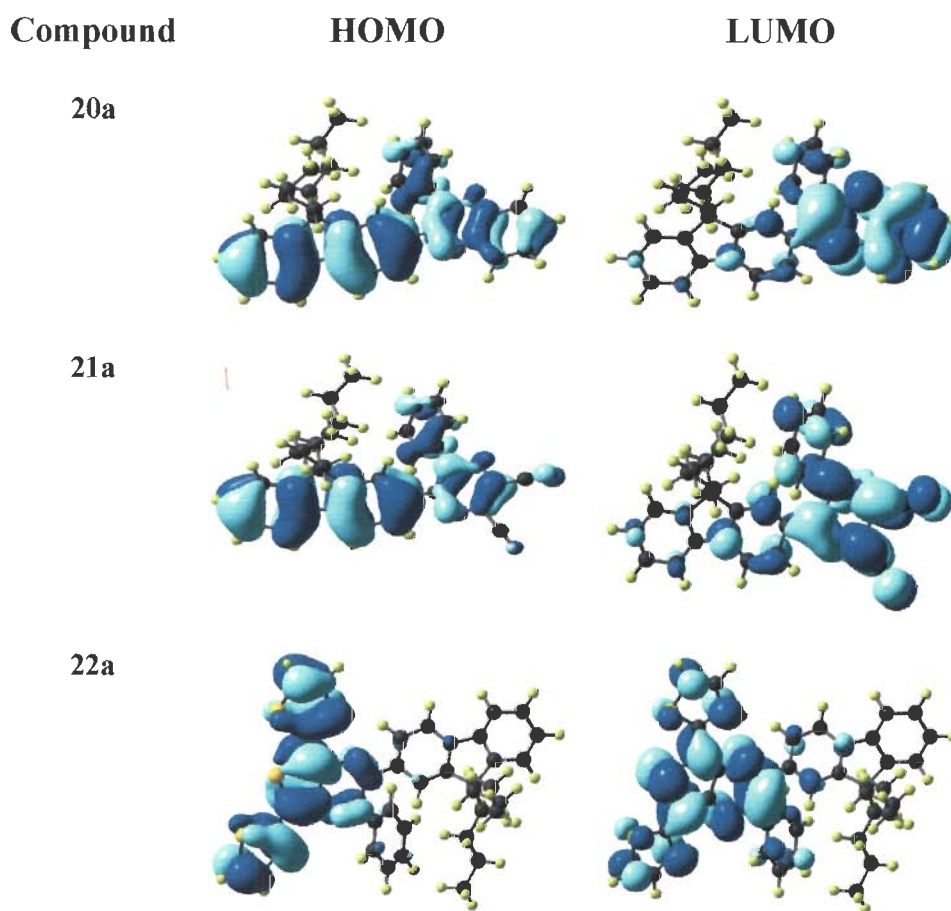


Figure 3.18 Electronic distribution in the frontier molecular orbitals of the compounds **20a**, **21a** and **22a**.

It can be seen that the HOMO of **20a** and **21a** spread over the entire molecule, whereas LUMO is located on the quinoxaline or pyrazine unit respectively. The highest wavelength transition is from HOMO to LUMO (Table 3.6) which suggests that the low energy band of **20a** and **20b** is contributed to a π - π^* transition merged with charge transfer from electron rich fluorene to electron deficient quinoxaline or pyrazine unit.

Table 3.6 Predicted (TDDFT B3LYP/6-31G(d,p)) vertical transitions and their assignments.

compound	λ_{abs} (nm)	μ	f	Assignment
20a	380.2	0.63	0.21	HOMO→LUMO (+96%)
	324.1		0.11	HOMO-1→LUMO (+50%), HOMO→LUMO+1 (+39%), HOMO-2→LUMO (+5%)
	317.1		0.38	HOMO→LUMO+1 (+57%), HOMO-1→LUMO (+34%)
	275.2		0.15	HOMO-1→LUMO+1 (+37%), HOMO→LUMO+3 (13%), HOMO-2→LUMO+1 (+13%), HOMO-3→LUMO+1 (+11%), HOMO-5→LUMO+1 (6%)
21a	421.2	0.63	0.13	HOMO→LUMO (+87%), HOMO→LUMO+1 (+12%)
	400.3		0.32	HOMO→LUMO+1 (+85%), HOMO→LUMO (12%),
	321.7		0.07	HOMO-2→LUMO (+26%), HOMO-1→LUMO (+21%), HOMO-2→LUMO+1 (+20%), HOMO-1→LUMO+1 (+19%), HOMO-3→LUMO (+7%),
	309.5		0.17	HOMO-3→LUMO (+40%), HOMO-4→LUMO (+21%), HOMO-2→LUMO (+13%), HOMO-2→LUMO+1 (+8%), HOMO-5→LUMO (+6%),
22a	602.1	2.77	0.16	HOMO→LUMO (+97%)
	445.4		0.19	HOMO-1→LUMO (+95%)
	389.0		0.21	HOMO→LUMO+1 (+78%), HOMO-2→LUMO (+10%),
	364.0		0.31	HOMO-2→LUMO (+47%), HOMO→LUMO+2 (+38%), HOMO→LUMO+1 (+11%)
	356.1		0.38	HOMO→LUMO+2 (+49%), HOMO-2→LUMO (+35%) HOMO-3→LUMO (+5%)

The HOMO and LUMO of **22a** are located on thienopyrazine unit which clearly indicates that the higher wavelength band of **22a** is due to π - π^* transition arise from thienopyrazine unit, not because of charge transfer transition. That is why there was no change observed in absorption/emission profile by changing the solvent polarity. Moreover, there

was no significant difference in the absorption wavelength of mono- and disubstituted thienopyrazine derivatives.

3.2.4 Thermal properties

The thermal stability and glass forming capability of these materials were investigated by thermogravimetric analysis (TGA) and differential scanning calorimetry (DSC) under a nitrogen atmosphere at a heating rate of 10°C/min., respectively. The relevant data are compiled in Table 3.7. The DSC curves of **20a**, **21a**, **20b** and **21b** were given in Figure 3.19. Compounds **20a**, **20b**, **21a** and **21b** exhibited melting isotherms during the first heating cycle, but rapid cooling of the melt led to the formation of a glassy state which persisted in the subsequent heating cycles. No crystallization exotherm was noticed even if the material was heated above the glass transition temperature (T_g). No glass transition was observed for thienopyrazine derivatives.

All the compounds showed T_g in the range of 59-127°C. The disubstituted derivatives (**20b** and **21b**) exhibited high glass transition temperature as compared to their corresponding mono-substituted one (**20a** and **21a**). This may be due to rigidity of the molecule after incorporation of another quinoxalines. Such type of increase in T_g is reported for fluorene-oxadiazole dyads.⁴² Cyano bearing compound (**21a** and **21b**) showed high glass transition as compared to quinoxaline derivatives (**20a** and **20b**). Such an outcome can be attributed to the presence of polar -CN groups in the former. It should be noted that the nonplanarity facilitates the glassy state in a molecule. The low glass transition of quinoxaline can also be explained on the basis of more planarity than cyano bearing pyrazine. The glass transition temperature was found higher for **21b**.

The decomposition temperature of these materials is also promising. All the compounds show decomposition temperature in the range of 398-457°C. The decomposition temperature

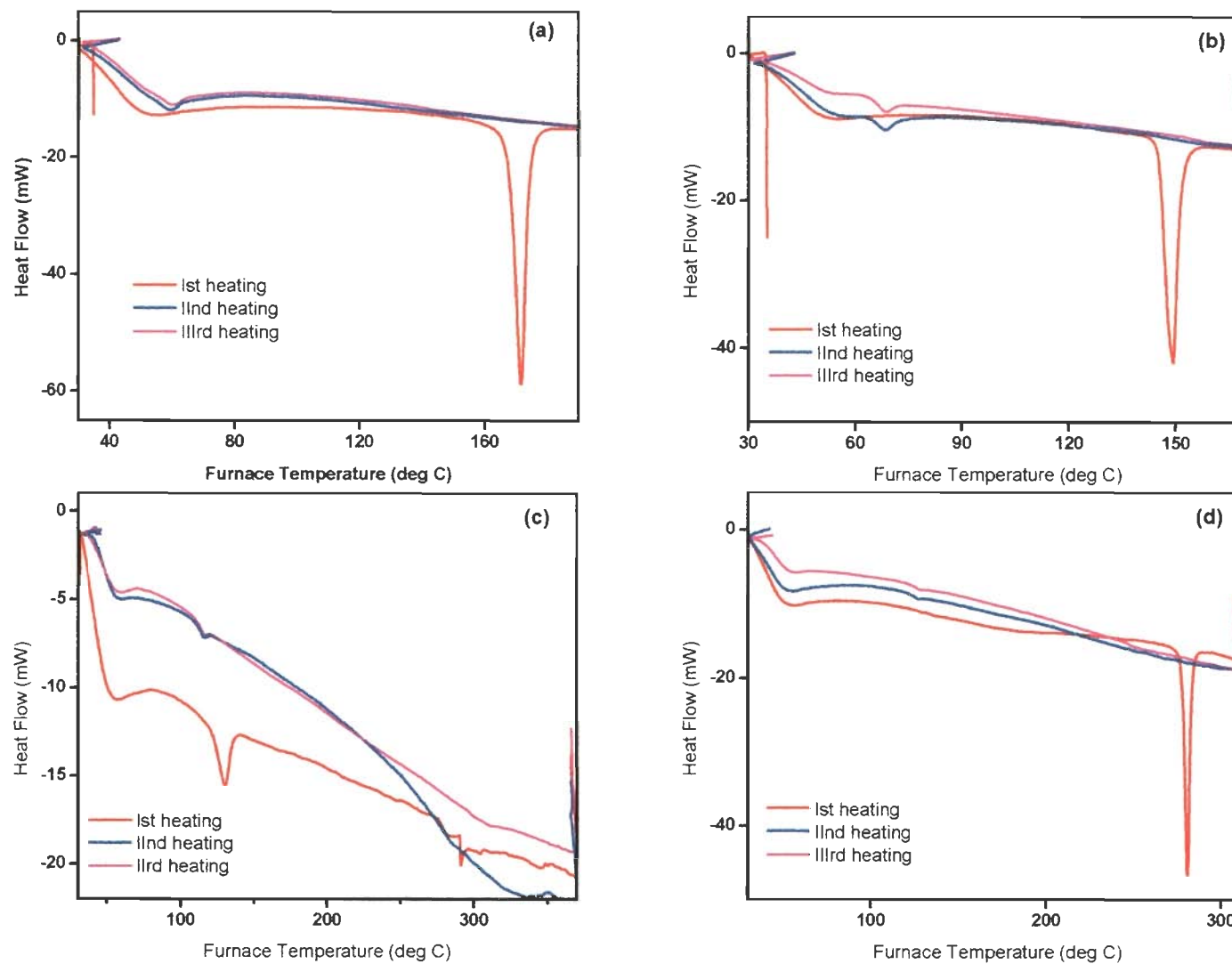


Figure 3.19 DSC curves for 20a (a), 21a (b), 20b (c) and 21b (d).

was found higher than the previously reported dipolar acenaphthopyrazine derivative³⁹ and other quinoxaline derivative containing diphenylamine²⁸. It is also higher than the fluorene-triazine system¹⁹ and naphthalene substituted fluorene derivative⁴³. These derivatives were found more thermally stable than quinoxaline based polymers.⁴⁴

Table 3.7 Thermal properties of the compounds **20a-22a** and **20b-22b**.

Compound	T _m , °C	T _g , °C	T _d , °C	T _{onset} , °C
20a	171	59	420	315
21a	149	68	398	328
22a	229	-	420	380
20b	-	116	457	418
21b	280	127	410	402
22b	-	-	421	375

3.2.5 Electrochemical properties

The redox properties of synthesized compounds were measured by cyclic voltammogram and differential pulse voltammogram in dichloromethane solution ($2 \times 10^{-4} \text{M}$) which shown in Figures 3.20 and 3.21. The pertinent data are listed in Table 3.8. Quinoxalines (**20a** and **20b**) showed one high negative irreversible reduction potential ($>2 \text{ V}$) and one irreversible oxidation peak. The reduction peak is due to the presence of electron deficient quinoxaline and the oxidation peak originates from electron rich fluorene. Both mono and disubstituted derivatives exhibited almost similar reduction potentials. The pyrazines displayed only one quasi reversible reduction peak which occur at less negative potential than that observed for quinoxalines due to the presence of electron withdrawing $-\text{CN}$ group which make the molecule more prone to reduction. The oxidation peak was not observed for **21a** and **21b**. The reason might be the electron attracting nature of these groups which either positively shifts this potential and the

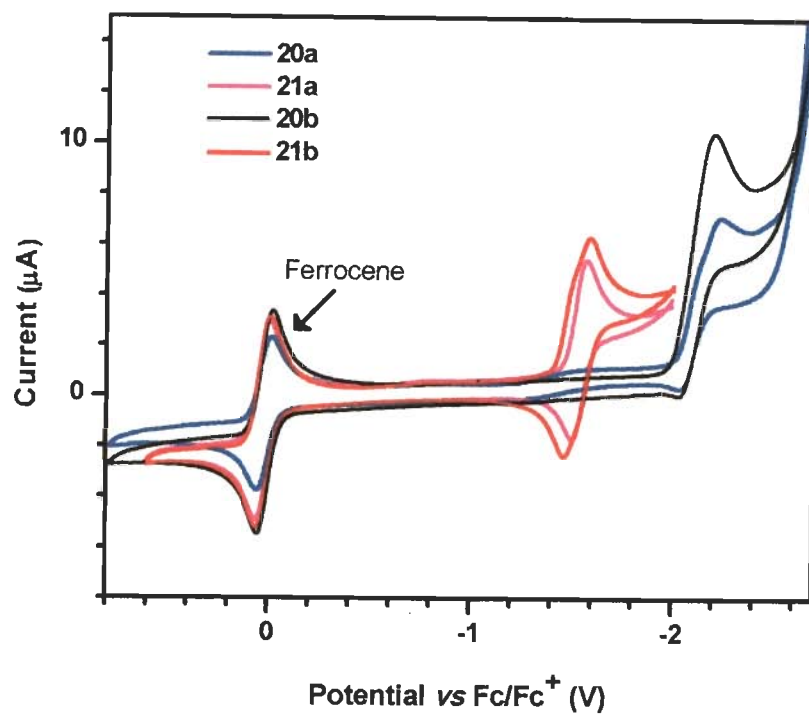


Figure 3.20 Cyclic voltammogram recorded for 20a, 21a, 20b and 21b in dichloromethane.

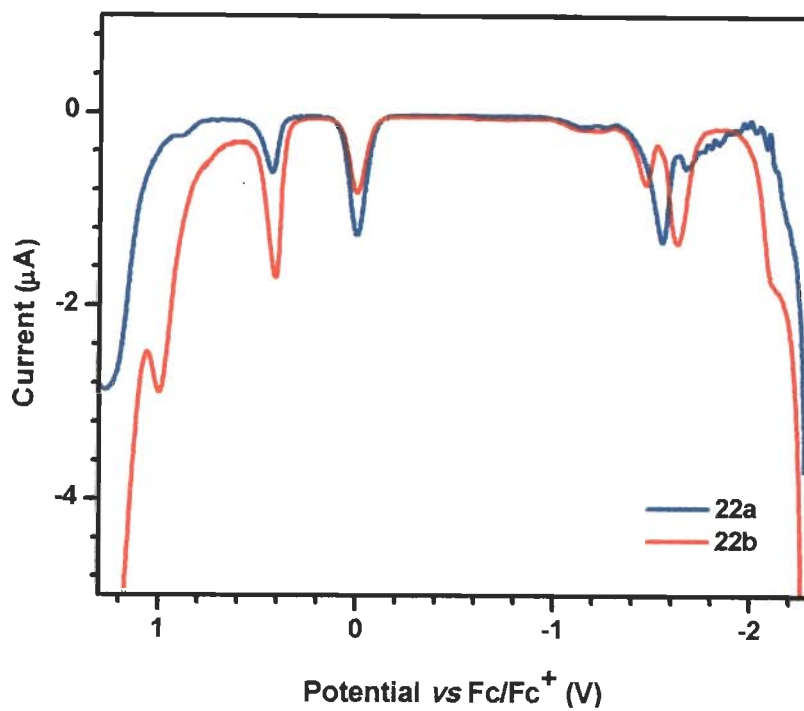


Figure 3.21 Differential pulse voltammograms recorded for 22a and 22b in dichloromethane.

wave probably appears outside the electrochemical window or the core becomes less prone to oxidation.

Thienopyrazine derivatives (**22a**, **22b**) exhibited three oxidation peaks out of which the first two oxidation peaks originate from terthiophene. The first oxidation peak is partly reversible while the second is irreversible. The third oxidation peak at highest potential is also irreversible which arise due to fluorene. The derivatives showed one reversible reduction potential due to presence of electron deficient pyrazine. Introduction of terthiophene decrease the band gap by increasing HOMO level and decreasing LUMO level. The low band gap polymers based on fluorene with terthiophene pyrazine donor/acceptor system have been used in bulk-heterojunction solar cell with power conversion efficiency of 0.8%.⁴⁵

Table 3.8 Electrochemical data of the compounds **20a-22a** and **20b-22b**.

Compound	E_{ox} , mV (ΔE_p , mV)	E_{red} , mV (ΔE_p , mV)	HOMO, eV	LUMO, eV	E_{0-0} (eV)
20a	1180	-2108	5.83	2.69	3.14
21a	-	-1540 (72)	6.11	3.26	2.85
22a	432 (82)	-1548	5.23	3.25	1.98
20b	1168	-2104	5.78	2.70	3.08
21b	-	-1548 (131)	6.09	3.25	2.84
22b	412 (124), 1000	-1624	5.21	3.18	2.03

During cyclic voltametry experiment of **22a** and **22b**, a yellow film was deposited over working electrode which might be due to polymerization. Since electropolymerization of terthiophene-based donor acceptor system have reported previously⁴⁶, the eletropolymerization with the system reported in this work was confirmed by the repeating cyclovoltammetric scans at different scan rates 50, 100, 500 mV/s. In the first cyclovoltammetric scan going to the anodic potentials up to 0.9V vs. Fc/Fc⁺ one irreversible oxidation was observed at scan rate 20 mV/s within the potential region from -0.3V to +0.9V vs Fc/Fc+. Going to the region of the first

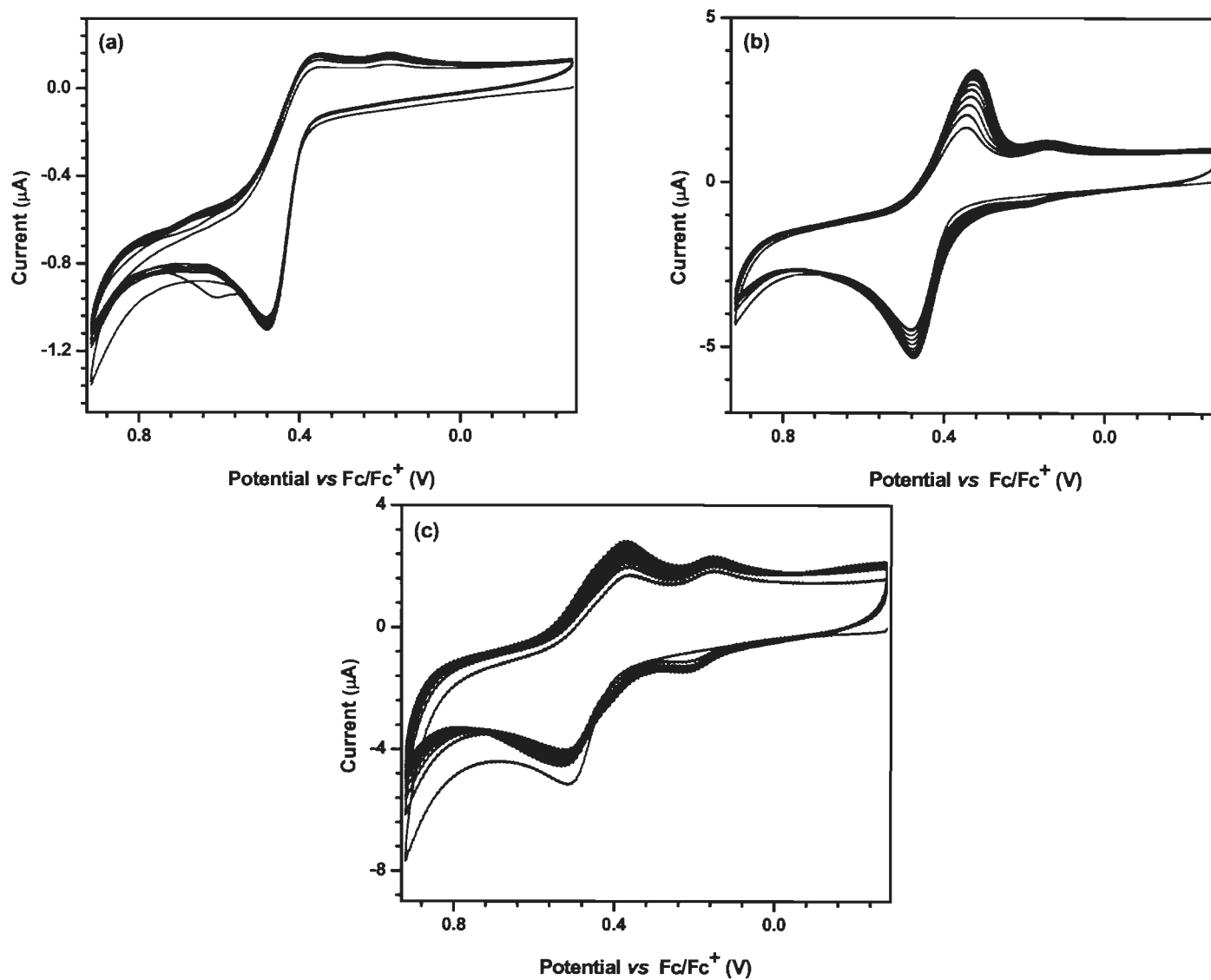


Figure 3.22 Cyclic voltammograms obtained during potentiodynamic polymerization of **22a** in 0.2M TBAPF₆/DCM at different scan rates 20 (a), 100 (b) and 500 mV/s (c) (glassy carbon working electrode, 10 consecutive scans).

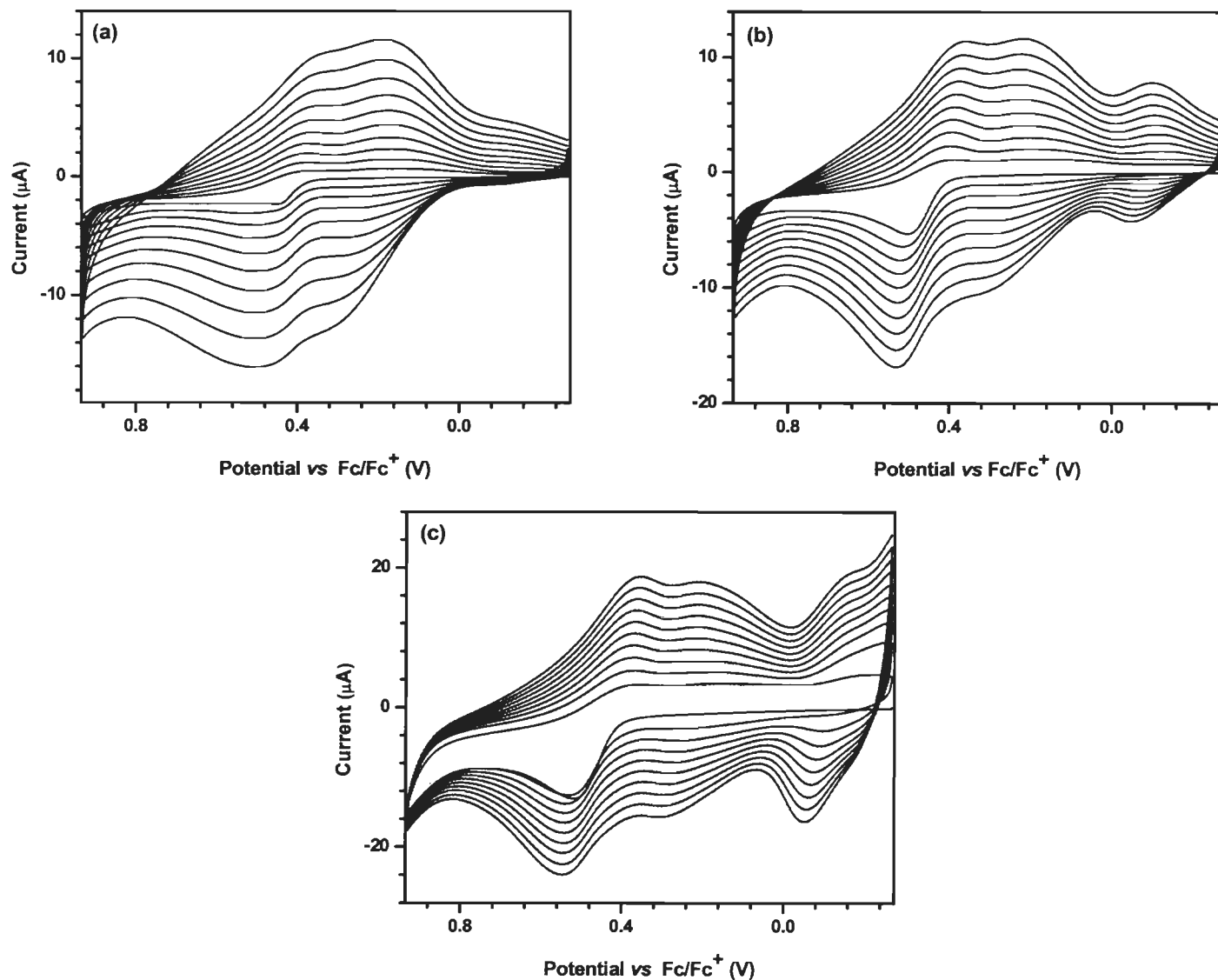


Figure 3.23 Cyclic voltammograms obtained during potentiodynamic polymerization of **22b** in 0.2M $\text{TBAPF}_6/\text{DCM}$ at different scan rates 20 (a), 100 (b) and 500 mV/s (c) (glassy carbon working electrode, 10 consecutive scans).

oxidation peak for **22a** and **22b** new redox processes are observable in the consecutive 10 scans. This suggests the electropolymerisation of these dipolar derivatives and deposition of the polymer films on the electrode surface. However, in the case of **22a** the stability of the electropolymerised films was not very good. Compound **22b** shows good reversibility and reproducibility of the redox processes on cycling. (Figures 3.22 and 3.23) and a fast adsorption on the working electrode takes place. The further electropolymerization process at different scan rate (100, 500 mV/s) made by potential scanning between -0.3V and $+0.9\text{V}$ vs Fc/Fc^+ showed more reversibility of redox processes.

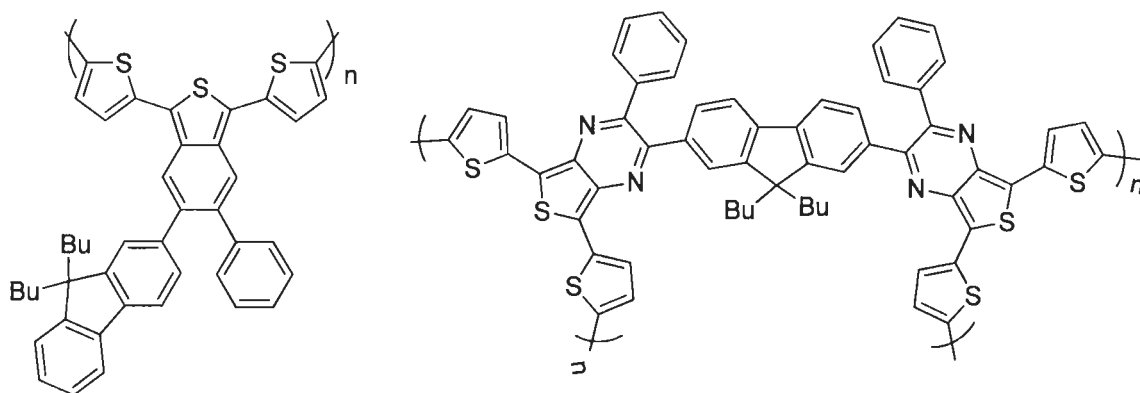


Figure 3.24 Proposed structures of the polymers formed during electropolymerization.

The increase in current with every potential cycle, resulting from the redox processes of the film, indicates a continual growth of conducting material on the electrode. Generally, very complex redox behaviour was observed both during electropolymerization of **22b** and for prepared polymer film on the electrode. This indicates a wide variety of oxidation products. Different chain lengths, regions with various degrees of crystallinity as well as the presence of dimers are expected. The presence of the extra segment of extended effective conjugations can also cause complexity of such electrochemically formed film.³⁵ The assumed structures of products during electropolymerization of both **22a** and **22b** are elucidated in Figure 3.24.

3.3 Conclusions

In summary, a series of fluorene-based quinoxaline, pyrazine and thienopyrazine have been synthesized and well characterized by NMR, IR and Mass spectroscopy. Compounds **20a**, **20b** and **21a**, **21b** absorb light of wavelength in the range of 362-393 nm. These derivatives emit in the blue region (417-451 nm). The presence of electron withdrawing group (-CN) red shifts the absorption and emission profile of pyrazines (**21a**, **21b**) as compared to quinoxalines (**20a**, **20b**). The disubstituted derivatives (**20b** and **21b**) showed aggregation in thin film and in solution (at higher concentration). Thienopyrazine derivatives (**22a**, **22b**) exhibited an additional absorption peak at higher wavelength (ca. 556 nm) corresponds to charge transfer due to presence of donor/acceptor system and emit in the range of 661-663 nm. All the derivatives are thermally stable with decomposition temperature 398-451 °C. Wide band gap blue emitting derivatives (**20a**, **20b** and **21a**, **21b**) can be potential candidate for electronic application. On the other hand presence of terthiophene decreases the band gap of compounds (**22a**, **22b**) dramatically. These derivatives also undergo electropolymerization which can make them suitable monomer for the polymer based bulk heterojunction solar cell.

3.4 Experimental section

3.4.1 Materials

All commercial chemicals were used as received. Fluorene, *t*-BuOK and phenyl acetylene were purchased from Sigma Aldrich. Compound **16**, **17a**, **17b**, are known in the literature but we have used different reagents for making these compounds and the structure of the compounds were confirmed by NMR. Compound **18a**, and **18b** were synthesized by Sonogashira cross coupling reaction reported in the literature. Column chromatography was performed by using

silica gel (Rankem, 100-200 mesh) as stationary phase. All solvents used in synthesis and spectroscopic measurements were distilled over appropriate drying and/or degassing reagents.

3.4.2 Physical methods

Physical methods are similar as written in chapter 2.

Synthesis of 9,9-dibutyl-9H-fluorene (16) A mixture of fluorene (4.98 g, 30 mmol) and *t*-BuOK (10.08 g, 90 mmol) were taken in a round bottom flask and thoroughly mixed under nitrogen atmosphere. On addition of 30 mL of DMSO, the color of reaction mixture changed to red. It was stirred and heated at 65 °C. After 1 h, *n*-butyl bromide (8.07 mL, 75 mmol) was added drop by drop over 20 min. The reaction mixture was stirred and heated at 70 °C until the color become yellow *via* purple. After completion of reaction, it was poured into water and extracted with ethyl acetate and washed three times with brine solution. The combined ethyl acetate extract was dried over Na₂SO₄ and then evaporated to remove the volatiles. Viscous brown syrup obtained was purified by column chromatography to yield a colorless solid. Yield 7.92 g (95%). ¹H NMR (CDCl₃, 500 MHz) δ 7.72-7.71 (m, 2 H), 7.36-7.29 (m, 6 H), 1.99-1.96 (m, 4 H), 1.08 (sextet, *J* = 7.5 Hz, 4 H), 0.68 (t, *J* = 7.3 Hz, 6 H), 0.63-0.57 (m, 4 H); ¹³C NMR (CDCl₃, 125 MHz) δ 150.6, 141.0, 126.9, 126.6, 122.7, 119.5, 54.8, 40.1, 25.8, 23.0, 13.7.

Synthesis of 2-bromo-9,9-dibutyl-9H-fluorene (17a) To a mixture of 9,9-dibutyl-9H-fluorene (8.34 g, 30 mmol) in dichloromethane, bromine (1.7 mL, 33 mmol) was added at 0 °C. The resulting mixture was stirred overnight. After that it was poured into NaHSO₃ solution and the organic layer was collected. Evaporation of the organic layer left a residue. It was purified by column chromatography to afford colorless solid. Yield 9.1 g (85 %); ¹H NMR (CDCl₃, 500 MHz) δ 7.68-7.66 (m, 1 H), 7.56 (dd, *J* = 6.5, 1.0 Hz, 1 H), 7.46-7.44 (m, 2 H), 7.34-7.32 (m, 3 H), 1.97-1.92 (m, 4 H), 1.08 (sextet, *J* = 7.3 Hz, 4 H), 0.68 (t, *J* = 7.5 Hz, 6 H), 0.60-0.55 (m, 4

H); ^{13}C NMR (CDCl_3 , 125 MHz) δ 153.0, 150.3, 140.2, 140.1, 129.9, 127.5, 127.0, 126.2, 122.9, 121.04, 120.99, 119.8, 55.3, 40.1, 25.9, 23.0, 13.8.

Synthesis of 9,9-dibutyl-2-(phenylethynyl)-9H-fluorene (18a) A mixture of 2-bromo-9,9-dibutyl-9H-fluorene (13 g, 36.41 mmol), phenyl acetylene (4.08 g, 40.04 mmol), $\text{Pd}(\text{PPh}_3)_2\text{Cl}_2$ (0.255 g, 0.36 mmol), PPh_3 (0.095 g, 0.36 mmol), and CuI (0.036 g, 0.18 mmol) were dissolved in diisopropylamine (100 mL) under nitrogen atmosphere. The resulting mixture was stirred and heated at 100 °C for 24 h. After completion of the reaction, it was poured into water and extracted with ethyl acetate. The combined organic extract was washed with brine solution then dried over Na_2SO_4 . Evaporation of the volatiles left a yellow residue. It was purified by column chromatography to obtain a yellow solid. Yield 10.3 g (75%); ^1H NMR (CDCl_3 , 500 MHz) δ 7.71-7.67 (m, 2 H), 7.59-7.56 (m, 2 H), 7.54-7.52 (m, 2 H), 7.39-7.32 (m, 6 H), 2.01-1.97 (m, 4 H), 1.09 (sextet, $J = 7.5$ Hz, 4 H), 0.68 (t, $J = 7.5$ Hz, 6 H), 0.65-0.55 (m, 4 H); ^{13}C NMR (CDCl_3 , 125 MHz) δ 151.0, 150.8, 141.5, 140.5, 131.6, 130.7, 128.4, 128.2, 127.5, 126.9, 126.7, 126.0, 123.5, 122.9, 121.4, 120.0, 119.7, 90.6, 89.4, 55.1, 40.2, 25.9, 23.1, 13.9.

Synthesis of 9,9-dibutyl-2,7-bis(phenylethynyl)-9H-fluorene (18b) A mixture of 2,7-dibromo-9,9-dibutyl-9H-fluorene (8.72 g, 20 mmol), phenyl acetylene (4.48 g, 44 mmol), $\text{Pd}(\text{PPh}_3)_2\text{Cl}_2$ (0.28 g, 0.4 mmol), PPh_3 (0.104 g, 0.4 mmol), and CuI (0.04 g, 0.2 mmol) were mixed in triethylamine (80 mL) under nitrogen atmosphere. The resulting mixture was stirred and heated at 100 °C for 24 h. After completion of the reaction, it was poured into water and extracted with ethyl acetate. The organic extract was washed with brine solution and dried over Na_2SO_4 . Finally, the solvent was removed under vacuum to yield a yellow residue. It was purified by column chromatography. Yellow solid. Yield 8.7 g (91%); ^1H NMR (CDCl_3 , 500 MHz) δ 7.69-7.67 (m, 2 H), 7.59-7.52 (m, 8 H), 7.39-7.33 (m, 6 H), 2.02-1.99 (m, 4 H), 1.14-1.07 (m, 4 H),

0.69 (t, $J = 7.3$ Hz, 6 H), 0.64-0.57 (m, 4 H); ^{13}C NMR (CDCl_3 , 125 MHz) δ 151.1, 140.7, 131.6, 130.8, 128.4, 128.3, 126.0, 123.4, 122.0, 120.0, 90.4, 89.8, 55.2, 40.3, 25.9, 23.1, 13.9.

Synthesis of 1-(9,9-dibutyl-9H-fluoren-2-yl)-2-phenylethane-1,2-dione (19a) A mixture of 9,9-dibutyl-2-(phenylethynyl)-9H-fluorene (1.0 g, 2.64 mmol), iodine (0.67 g, 2.64 mmol) and DMSO (10 mL) was taken in round bottom flask. It was stirred and heated at 140°C for 12 h. After completion of reaction, it was quenched by pouring into 10% sodium thiosulfate solution, extracted with ethyl acetate, and dried over Na_2SO_4 . Evaporation of the volatiles left a dark residue, which was purified by column chromatography using hexane/dichloromethane (4:1) as eluent. Light yellow solid. Yield 0.87 g (81%); ^1H NMR (CDCl_3 , 500 MHz) δ 8.04-8.02 (m, 3 H), 7.87 (dd, $J = 6.5, 1.5$ Hz, 1 H), 7.78-7.76 (m, 2 H), 7.68-7.65 (m, 1 H), 7.53 (t, $J = 8.0$ Hz, 2 H), 7.43-7.36 (m, 3 H), 2.02-1.95 (m, 4 H), 1.09-1.03 (m, 4 H), 0.65 (t, $J = 7.5$ Hz, 6 H), 0.58-0.54 (m, 4 H); ^{13}C NMR (CDCl_3 , 125 MHz) δ 195.1, 194.7, 152.3, 151.6, 148.0, 139.4, 134.8, 133.3, 131.6, 130.5, 130.0, 129.1, 129.0, 127.2, 123.5, 123.2, 121.1, 119.9, 55.4, 39.9, 25.9, 23.0, 13.8.

Synthesis of 2,2'-(9,9-dibutyl-9H-fluorene-2,7-diyl)bis(1-phenylethane-1,2-dione) (19b) A mixture of 9,9-dibutyl-2-(phenylethynyl)-9H-fluorene (0.39 g, 0.81 mmol), iodine (0.41 g, 1.62 mmol) and DMSO (10 mL) was taken in round bottom flask. It was stirred and heated at 140 °C for 24 h. After completion of reaction, it was quenched by pouring into 10% sodium thiosulfate solution, extracted with ethyl acetate, and dried over Na_2SO_4 followed by evaporation. The product was purified by column chromatography using hexane/dichloromethane (4:1) as eluent. Yellow solid. Yield 0.38 g (88%); ^1H NMR (CDCl_3 , 500 MHz) δ 8.08 (d, $J = 1.0$ Hz, 2 H), 8.04-8.02 (m, 4 H), 7.92 (dd, $J = 1.5$ Hz, 6.5 Hz, 2 H), 7.86 (d, $J = 8.0$ Hz, 2 H), 7.70-7.67 (m, 2 H), 7.56-7.53 (m, 4 H), 2.06-2.03 (m, 4 H), 1.06 (sextet, $J = 7.5$ Hz, 4 H), 0.65 (t, $J = 7.3$ Hz, 6 H),

0.58-0.51 (m, 4 H); ^{13}C NMR (CDCl_3 , 125 MHz) δ 194.6, 194.3, 153.0, 145.8, 135.0, 133.11, 133.08, 130.4, 130.0, 129.1, 123.8, 121.4, 55.9, 39.6, 26.0, 22.8, 13.7.

Synthesis of 2-(9,9-dibutyl-9H-fluoren-2-yl)-3-phenylquinoxaline (20a) A mixture of 1-(9,9-dibutyl-9H-fluoren-2-yl)-2-phenylethane-1,2-dione (1 g, 2.44 mmol) and benzene-1,2-diamine (0.29 g, 2.68 mmol) was dissolved in 25 mL of chloroform. A pinch of *p*-toluene sulfonic acid was added to the reaction mixture. Then it was stirred and heated to reflux for 8 h. After completion of the reaction, it was quenched by pouring into water and extracted with chloroform. The combined chloroform extract was dried over Na_2SO_4 and evaporated to dryness. The resulting solid was recrystallized from methanol to obtain a yellow solid. Yield 1.1 g (92%); mp 171 °C; ^1H NMR (CDCl_3 , 500 MHz) δ 8.22-8.18 (m, 2 H), 7.85 (dd, $J = 6.5, 1.5$ Hz, 1 H), 7.81-7.77 (m, 3 H), 7.74 (dd, $J = 6.0, 1.0$ Hz, 1 H), 7.58-7.56 (m, 2 H), 7.34-7.29 (m, 6 H), 7.15 (d, $J = 1.0$ Hz, 1 H), 1.82-1.77 (m, 2 H), 1.65-1.59 (m, 2 H), 0.99-0.95 (m, 4 H), 0.64 (t, $J = 7.5$ Hz, 6 H), 0.47-0.42 (m, 4 H); ^{13}C NMR (CDCl_3 , 125 MHz) δ 154.0, 153.7, 151.2, 150.2, 141.9, 141.3, 141.2, 140.4, 139.5, 137.8, 130.0, 129.83, 129.79, 129.23, 129.20, 128.8, 128.7, 128.3, 127.5, 126.8, 124.7, 122.9, 120.13, 120.09, 54.9, 40.1, 25.8, 23.0, 13.8; HRMS $[\text{M}+\text{H}]^+$ m/z calcd for $\text{C}_{35}\text{H}_{34}\text{N}_2$ 483.2800, found 483.2793.

Synthesis of 5-(9,9-dibutyl-9H-fluoren-2-yl)-6-phenylpyrazine-2,3-dicarbonitrile (21a) A mixture of 1-(9,9-dibutyl-9H-fluoren-2-yl)-2-phenylethane-1,2-dione (1 g, 2.44 mmol), 2,3-diaminomaleonitrile (0.29 g, 2.68 mmol) and chloroform (25 mL). Small amount of *p*-toluene sulfonic acid was added to the reaction mixture. Then it was stirred and heated to reflux for 21 h. After completion of reaction, the solvent was evaporated and small amount of methanol was added to it. A yellow solid formed was filtered. Yield 1.0 g (90%); mp 149 °C; ^1H NMR (CDCl_3 , 500 MHz) δ 7.79 (dd, $J = 6.5, 1.5$ Hz, 2 H), 7.76-7.72 (m, 1 H), 7.60-7.58 (m, 2 H), 7.46-7.42

(m, 1 H), 7.38-7.34 (m, 4 H), 7.32-7.29 (m, 1 H), 7.23 (d, $J = 1.0$ Hz, 1 H), 1.85-1.80 (m, 2 H), 1.66-1.63 (m, 2 H), 1.01-0.96 (m, 4 H), 0.65 (t, $J = 7.5$ Hz, 6 H), 0.46-0.41 (m, 4 H); ^{13}C NMR (CDCl_3 , 125 MHz) δ 155.9, 155.3, 151.4, 150.9, 144.4, 139.6, 135.8, 133.5, 131.0, 129.8, 129.7, 129.24, 129.21, 128.9, 128.5, 127.1, 124.3, 123.0, 120.6, 120.5, 113.32, 113.30, 55.1, 40.0, 25.8, 22.9, 13.8; IR (KBr, cm^{-1}) ν_{max} 2958, 2928, 2858, 2237 ($\nu_{\text{C}\equiv\text{N}}$), 1602, 1508, 1376, 1183, 839, 742, 699; HRMS $[\text{M}+\text{H}]^+$ m/z calcd for $\text{C}_{33}\text{H}_{30}\text{N}_4$ 483.2549, found 483.2550.

Synthesis of 2-(9,9-dibutyl-9H-fluoren-2-yl)-3-phenyl-5,7-di(thiophen-2-yl)thieno[3,4-b]pyrazine (22a) 1-(9,9-Dibutyl-9H-fluoren-2-yl)-2-phenylethane-1,2-dione (0.27 g, 0.65 mmol) and 3,4-diamino-2,5-bis(thiophene-2-yl)-thiophene (0.2 g, 0.72 mmol) were dissolved in chloroform (10 mL). A pinch of *p*-toluene sulfonic acid was added to the reaction mixture as a catalyst. Then it was stirred and heated to reflux for 48 h. After completion of reaction, the solvent was evaporated and small amount of methanol was added to it. A black colored precipitate was obtained. It was filtered and washed with methanol. Yield 0.22 g (54%); mp 229 °C; ^1H NMR (CDCl_3 , 500 MHz) δ 7.84 (dd, $J = 6.0, 2.0$ Hz, 1 H), 7.77-7.72 (m, 2 H), 7.69 (dd, $J = 2.5, 1.0$ Hz, 2 H), 7.68-7.67 (m, 2 H), 7.40-7.31 (m, 9 H), 7.14-7.12 (m, 2 H), 1.87-1.81 (m, 2 H), 1.74-1.68 (m, 2 H), 1.03 (sextet, $J = 7.5$ Hz, 4 H), 0.68 (t, $J = 7.5$ Hz, 6 H), 0.58-0.49 (m, 4 H); ^{13}C NMR (CDCl_3 , 125 MHz) δ 153.4, 153.2, 151.4, 150.2, 142.1, 140.4, 139.4, 137.8, 137.6, 137.5, 134.8, 134.7, 130.0, 129.0, 128.9, 128.1, 127.5, 127.3, 127.3, 126.9, 126.6, 124.9, 124.7, 124.6, 122.9, 120.1, 119.7, 54.9, 40.1, 25.9, 23.0, 13.8; HRMS $[\text{M}+\text{H}]^+$ m/z calcd for $\text{C}_{41}\text{H}_{36}\text{N}_2\text{S}_3$ 653.2119, found 653.2126.

Synthesis of 3,3'-(9,9-dibutyl-9H-fluorene-2,7-diyl)bis(2-phenylquinoxaline) (20b) 2,2'-(9,9-Dibutyl-9H-fluorene-2,7-diyl)bis(1-phenylethane-1,2-dione) (0.7 g, 1.29 mmol) and benzene-1,2-diamine (0.31 g, 2.84 mmol) were taken in a mixture chloroform (25 mL) and methanol (5

mL). A small amount of *p*-toluene sulfonic acid was added to the reaction mixture. Then it was stirred and heated to reflux for 8 h. After completion of the reaction, the volatiles were removed and the residue was triturated with methanol (10 mL). A yellow solid obtained was filtered and recrystallized from chloroform-ethanol mixture. Yield 0.77 g (87%); mp 220-222 °C; ¹H NMR (CDCl₃, 500 MHz) δ 8.22-8.17 (m, 4 H), 7.87 (dd, *J* = 6.0, 1.5 Hz, 2 H), 7.85-7.83 (m, 2 H), 7.81-7.76 (m, 4 H), 7.57-7.55 (m, 4 H), 7.33-7.30 (m, 6 H), 7.09 (d, *J* = 1.0 Hz, 2 H), 1.50-1.44 (m, 4 H), 0.86 (sextet, *J* = 7.5 Hz, 4 H), 0.61 (t, *J* = 7.5 Hz, 6 H), 0.32-0.23 (m, 4 H); ¹³C NMR (CDCl₃, 125 MHz) δ 153.8, 153.6, 150.7, 141.24, 141.17, 141.1, 139.4, 138.3, 130.0, 129.9, 129.8, 129.20, 129.18, 128.8, 128.3, 124.7, 120.6, 54.9, 40.1, 25.6, 22.9, 13.8; HRMS [M+H]⁺ *m/z* calcd for C₄₉H₄₂N₄ 687.3488, found 687.3478.

Synthesis of 6,6'-(9,9-dibutyl-9*H*-fluorene-2,7-diyl)bis(5-phenylpyrazine-2,3-dicarbonitrile)

(21b) 2,2'-(9,9-Dibutyl-9*H*-fluorene-2,7-diyl)bis(1-phenylethane-1,2-dione) (0.7 g, 1.29 mmol) and 2,3-diaminomaleonitrile (0.31 g, 2.84 mmol) were dissolved in a mixture of chloroform (25 mL) and methanol (5 mL). A pinch of *p*-toluene sulfonic acid was added to the reaction mixture. Then it was stirred and heated to reflux for 8 h. After completion of the reaction, the solvent was evaporated and a large amount of methanol (15 mL) was added to it. Yellow solid formed was filtered and dried. Yield 0.70 g (78%); mp 280 °C; ¹H NMR (CDCl₃, 500 MHz) δ 7.83 (s, 4 H), 7.60-7.57 (m, 4 H), 7.44 (t, *J* = 7.5 Hz, 2 H), 7.35 (t, *J* = 8.0 Hz, 4 H), 7.19 (s, 2 H), 1.53-1.49 (m, 4 H), 0.93-0.86 (m, 4 H), 0.63 (t, *J* = 7.5 Hz, 6 H), 0.29-0.23 (m, 4 H); ¹³C NMR (CDCl₃, 125 MHz) δ 155.4, 155.3, 151.6, 142.6, 135.5, 135.0, 131.1, 129.8, 129.7, 129.54, 129.51, 128.9, 124.4, 121.4, 113.2, 55.3, 39.8, 25.7, 22.8, 13.8; IR (KBr, cm⁻¹) *v*_{max} 2921, 2855, 2233 (*v*_{C≡N}), 1606, 1510, 1374, 1225, 701; HRMS [M+H]⁺ *m/z* calcd for C₄₅H₃₄N₈ 687.2985, found 687.2992.

Synthesis of 3,3'-(9,9-dibutyl-9H-fluorene-2,7-diyl)bis(2-phenyl-5,7-di(thiophen-2-yl)thieno[3,4 b]pyrazine) (22b) A mixture of 2,2'-(9,9-dibutyl-9H-fluorene-2,7-diyl)bis(1-phenylethane-1,2-dione) (0.30 g, 0.51 mmol), 3,4-diamino-2,5-bis(thiophen-2-yl)-thiophene (0.31 g, 1.12 mmol), TSOH (0.01 g), and chloroform (10 mL) was heated to reflux for 48 h with efficient stirring. After completion of the reaction, the solvent was evaporated under vacuum and the residue was triturated with methanol (10 mL). A black colored precipitate was obtained after ultrasonication which was filtered and washed with methanol. The product was purified by column chromatography to obtain a black solid. Yield: 0.1 g (20%); mp 240-242 °C; ¹H NMR (CDCl₃, 500 MHz) δ 7.83 (dd, *J* = 6.5, 1.5 Hz, 2 H), 7.77 (d, *J* = 8.0 Hz, 2 H), 7.70-7.65 (m, 8 H), 7.40-7.32 (m, 12 H), 7.14-7.12 (m, 4 H), 1.63-1.55 (m, 4 H), 1.01-0.97 (m, 4 H), 0.69 (t, *J* = 7.5 Hz, 6 H), 0.50-0.48 (m, 4 H); ¹³C NMR (CDCl₃, 125 MHz) δ 153.2, 153.1, 150.9, 141.4, 139.4, 138.3, 137.6, 137.4, 134.7, 134.7, 130.0, 129.1, 128.1, 127.4, 127.3, 126.7, 125.0, 124.8, 124.7, 124.6, 120.1, 54.9, 40.0, 25.8, 23.0, 13.9.

3.5 References

1. Tao, Y. T.; Balasubramaniam, E.; Danel, A.; Wisla, A.; Tomasik, P. "Pyrazoloquinoline derivatives as efficient blue electroluminescent materials" *J. Mater. Chem.* **2001**, *11*, 768.
2. Tao, Y. T.; Balasubramaniam, E.; Danel, A.; Jarosz, A.; Tomasik, P. "Organic light-emitting diodes based on variously substituted pyrazoloquinolines as emitting materials" *Chem. Mater.* **2001**, *13*, 1207.
3. Thomas, K. R. J.; Lin, J. T.; Tao, Y.-T.; Ko, C.-W. "Light-emitting carbazole derivatives: potential electroluminescent materials" *J. Am. Chem. Soc.* **2001**, *123*, 9404.

4. Yang, Y.; Zhou, Y.; He, Q.; He, C.; Yang, C.; Bai, F.; Li, Y. "Solution-processable red-emission organic materials containing triphenylamine and benzothiadiazole units: synthesis and applications in organic light-emitting diodes" *J. Phys. Chem. B* **2009**, *113*, 7745.
5. Wee, K.-R.; Ahn, H.-C.; Son, H.-J.; Han, W.-S.; Kim, J.-E.; Cho, D. W.; Kang, S. O. "Emission color tuning and deep blue dopant materials based on 1,6-bis(*N*-phenyl-*p*-(*R*)-phenylamino)pyrene" *J. Org. Chem.* **2009**, *74*, 8472.
6. Moorthy, J. N.; Venkatakrisnan, P.; Huang, D.-F.; Chow, T. J. "Blue light-emitting and hole-transporting amorphous molecular materials based on diarylaminobiphenyl-functionalized bimesitylenes" *Chem. Commun.* **2008**, 2146.
7. Li, W.; Qiao, J.; Duan, L.; Wang, L.; Qiu, Y. "Novel fluorene/carbazole hybrids with steric bulk as host materials for blue organic electrophosphorescent devices" *Tetrahedron* **2007**, *63*, 10161.
8. Matsumoto, N.; Miyazaki, T.; Nishiyama, M.; Adachi, C. "Efficient deep-blue organic light-emitting diodes based on 9,9-bis(4-biphenyl)fluorene derivatives" *J. Phys. Chem. C* **2009**, *113*, 6261.
9. Grisorio, R.; Piliago, C.; Fini, P.; Cosma, P.; Mastroilli, P.; Gigli, G.; Suranna, G. P.; Nobile, C. F. "Influencing the spectral stability and the electroluminescence behavior of new blue-emitting bifluorene-based materials by the 7,7'-functionalization of the core" *J. Phys. Chem. C* **2008**, *112*, 7005.
10. Wong, K.-T.; Chien, Y.-Y.; Chen, R.-T.; Wang, C.-F.; Lin, Y.-T.; Chiang, H.-H.; Hsieh, P.-Y.; Wu, C.-C.; Chou, C. H.; Su, Y. O.; Lee, G.-H.; Peng, S.-M. "Ter(9,9-diarylfluorene)s: highly efficient blue emitter with promising electrochemical and thermal stability" *J. Am. Chem. Soc.* **2002**, *124*, 11576.

11. Setayesh, S.; Andrew C. Grimsdale, A. C.; Weil, T.; Enkelmann, V.; Müllen, K.; Meghdadi, F.; List, E. J. W.; Leising, G. "Polyfluorenes with polyphenylene dendron side chains: toward non-aggregating, light-emitting polymers" *J. Am. Chem. Soc.* **2001**, *123*, 946.
12. Omer, K. M.; Ku, S.-Y.; Wong, K.-T.; Bard, A. J. "Green electrogenerated chemiluminescence of highly fluorescent benzothiadiazole and fluorene derivatives" *J. Am. Chem. Soc.* **2009**, *131*, 10733.
13. Moura, G. L. C.; Simas, A. M. "Two-photon absorption by fluorene derivatives: systematic molecular design" *J. Phys. Chem. C* **2010**, *114*, 6106.
14. Zeng, G.; Yu, W.L.; Chua, S.J.; Huang, W. "Spectral and thermal spectral stability study for fluorene-based conjugated polymers" *Macromolecules* **2002**, *35*, 6907.
15. Montilla, F.; Mallavia, R. "On the origin of green emission bands in fluorene-based conjugated polymers" *Adv. Funct. Mater.* **2007**, *17*, 71
16. Sims, M.; Bradley, D. D. C.; Ariu, M.; Koeberg, M.; Asimakis, A.; Grell, M.; Lidzey, D. G. "Understanding the origin of the 535 nm emission band in oxidized poly(9,9-dioctylfluorene): the essential role of inter-chain/inter-segment interactions" *Adv. Funct. Mater.* **2004**, *14*, 765.
17. Yu, J.; Lou, S.; Qian, J.; Jiang, Y.; Zhang, Q. "Optoelectronic properties of a novel fluorene derivative for organic light-emitting diode" *App. Phys. A* **2009**, *94*, 813.
18. Goel, A.; Chaurasia, S.; Dixit, M.; Kumar, V.; Prakash, S.; Jena, B.; Verma, J. K.; Jain, M.; Anand, R. S.; Manoharan, S. S. "Donor-acceptor 9-uncapped fluorenes and fluorenones as stable blue light emitters" *Org. Lett.* **2009**, *11*, 1289.

19. Ren, S.; Zeng, D.; Zhong, H.; Wang, Y.; Qian, S.; Fang, Q. "Star-shaped donor- π -acceptor conjugated oligomers with 1,3,5-triazine cores: convergent synthesis and multifunctional properties" *J. Phys. Chem. B* **2010**, *114*, 10374.
20. Zhong, H.; Lai, H.; Fang, Q. "New conjugated triazine based molecular materials for application in optoelectronic devices: design, synthesis, and properties" *J. Phys. Chem. C* **2011**, *115*, 2423.
21. Fisher, A. L.; Linton, K. E.; Kamtekar, K. T.; Pearson, C.; Bryce, M. R.; Petty, M. C. "Efficient deep-blue electroluminescence from an ambipolar fluorescent emitter in a single-active-layer device" *Chem. Mater.* **2011**, *23*, 1640.
22. Redecker, M.; Bradley, D. D. C.; Jandke, M.; Strohriegl, P. "Electron transport in starburst phenyl quinoxalines" *Appl. Phys. Lett.* **1999**, *75*, 109.
23. Schmitz, C.; Pösch, P.; Thelakkat, M.; Schmidt, H.-W.; Montali, A.; Feldman, K.; Smith, P.; Weder, C. "*Adv. Funct. Mater.* **2001**, *11*, 41.
24. Cui, Y.; Zhang, X.; Jenekhe, S. A. "Thiophene-linked polyphenylquinoxaline: a new electron transport conjugated polymer for electroluminescent devices" *Macromolecules* **1999**, *32*, 3824.
25. Karastatiris, P.; Mikroyannidis, J. A.; Spiliopoulos, I. K.; Kulkarni, A. P.; Jenekhe, S. A. "Synthesis, photophysics, and electroluminescence of new quinoxaline-containing poly(p-phenylenevinylene)s" *Macromolecules* **2004**, *37*, 7867.
26. Jung, S. H.; Suh, D. H.; Cho, H. N. "New electron-accepting π -conjugated polyquinoxalines with fluorene unit: synthesis and light-emitting properties" *Polym. Bull.* **2003**, *50*, 251.

27. Thomas, K. R. J.; Lin, J. T.; Tao, Y.-T.; Chuen, C.-H. "Quinoxalines incorporating triaryl amines: potential electroluminescent materials with tunable emission characteristics" *Chem. Mater.* **2002**, *14*, 2796.
28. Thomas, K. R. J.; Velusamy, M.; Lin, J. T.; Chuen, C.-H.; Tao, Y.-T. "Chromophore-labeled quinoxaline derivatives as efficient electroluminescent materials" *Chem. Mater.* **2005**, *17*, 1860.
29. Kulkarni, A. P.; Tonzola, C. J.; Babel, A.; Jenekhe, S. A. "Electron transport materials for organic light-emitting diodes" *Chem. Mater.* **2004**, *16*, 4556.
30. Chen, S.; Xu, X.; Liu, Y.; Qiu, W.; Yu, G.; Wang, H.; Zhu, D. "New organic light-emitting materials: synthesis, thermal, photophysical, electrochemical, and electroluminescent properties" *J. Phys. Chem. C* **2007**, *111*, 1029.
31. Bolligarla, R.; Das, S. K. "Synthesis of new intramolecular charge transfer A–D–A tetrathiafulvalene-fused triads exhibiting large solvent sensitive emission behaviour" *Tetrahedron Lett.* **2011**, *52*, 2496.
32. Unver, E. K.; Tarkuc, S.; Baran, D.; Tanyeli, C.; Toppare, L. "Synthesis of new donor–acceptor polymers containing thiadiazoloquinoxaline and pyrazinoquinoxaline moieties: low-band gap, high optical contrast, and almost black colored materials" *Tetrahedron Lett.* **2011**, *52*, 2725.
33. Lindgren, L. J.; Zhang, F.; Andersson, M.; Barrau, S.; Hellström, S.; Mammo, W.; Perzon, E.; Inganäs, O.; Andersson, M. R. "Synthesis, characterization, and devices of a series of alternating copolymers for solar cells" *Chem. Mater.* **2009**, *21*, 3491.
34. Idzik, K. R.; Rapta, P.; Cywinski, P. J.; Beckert, R.; Dunsch, L. "Synthesis and electrochemical characterization of new optoelectronic materials based on conjugated

- donor–acceptor system containing oligo-tri(heteroaryl)-1,3,5-triazines” *Electrochim. Acta* **2010**, *55*, 4858.
35. Jadamiec, M.; Lapkowski, M.; Matlengiewicz, M.; Brembilla, A.; Henry, B.; Rodehüser, L. “Electrochemical and spectroelectrochemical evidence of dimerization and oligomerization during the polymerization of terthiophenes” *Electrochim. Acta* **2007**, *52*, 6146.
36. Asil, D.; Cihaner, A.; Önal, A. M. “A glow in the dark: synthesis and electropolymerization of a novel chemiluminescent terthienyl system” *Chem. Commun.* **2009**, 307.
37. Jung, S.-H.; Kim, D. Y.; Cho, H.-N.; Suh, D. H. “Synthesis and properties of new fluorene-based polyquinoxalines with an ether linkage in the main chain for light-emitting diodes” *J. Polym. Sci., Part A: Polym. Chem.* **2006**, *44*, 1189.
38. Sarkis, G. Y.; Al-Azawe, S. “Synthesis and spectral data for quinoxaline derivatives” *J. Chem. Eng. Data* **1973**, *18*, 102.
39. Huang, T.-H.; Lin, J. T. “Tunable dipolar acenaphthopyrazine derivatives containing diphenylamine” *Chem. Mater.* **2004**, *16*, 5387.
40. Rai, S.; Gayatri, G.; Sastry, G. N.; Ravikanth, M. “Effects of meso-substituents and core-modification on photophysical and electrochemical properties of porphyrin-ferrocene conjugates” *Chem. Phys. Lett.* **2008**, *467*, 179.
41. van den Berg, O.; Jager, W. F.; Picken, S. J. “7-Dialkylamino-1-alkylquinolinium salts: highly versatile and stable fluorescent probes” *J. Org. Chem.* **2006**, *71*, 2666.
42. Kamtekar, K. T.; Wang, C.; Bettington, S.; Batsanov, A. S.; Perepichka, I. F.; Bryce, M. R.; Ahn, J. H.; Rabinal, M.; Petty, M. C. “New electroluminescent bipolar compounds for balanced charge-transport and tuneable colour in organic light emitting diodes: triphenylamine–oxadiazole–fluorene triad molecules” *J. Mater. Chem.* **2006**, *16*, 3823.

43. Peng, Z.; Tao, S.; Zhang, X.; Tang, J.; Lee, C. S.; Lee, S.-T. "New fluorene derivatives for blue electroluminescent devices: influence of substituents on thermal properties, photoluminescence, and electroluminescence" *J. Phys. Chem. C* **2008**, *112*, 2165.
44. Zhang, X.; Shim, J. W.; Tiwari, S. P.; Zhang, Q.; Norton, J. E.; Wu, P.-T.; Barlow, S.; Jenekhe, S. A.; Kippelen, B.; Brédas, J.-L.; Marder, S. R. "Dithienopyrrole–quinoxaline/pyridopyrazine donor–acceptor polymers: synthesis and electrochemical, optical, charge-transport, and photovoltaic properties" *J. Mater. Chem.* **2011**, *21*, 4971.
45. Janietz, S.; Krueger, H.; Schleiermacher, H.-F.; Würfel, U.; Niggemann, M. "Tailoring of low bandgap polymer and its performance analysis in organic solar cells" *Macromol. Chem. Phys.* **2009**, *210*, 1493.
46. Zanardi, C.; Scanu, R.; Pigani, L.; Pilo, M. I.; Sanna, G.; Seeber, R.; Spano, N.; Terzi, F.; Zucca, A. "Synthesis and electrochemical polymerisation of 3-functionalised terthiophenes electrochemical and spectroelectrochemical characterisation" *Electrochim. Acta* **2006**, *51*, 4859.

Synthesis, Photophysical and Electrochemical Properties of Pyrene-Based Functional Materials Containing Acetylene Linkers

4.1 Introduction

In recent years, organic materials with π -conjugated system have received much attention due to their unique photophysical and electronic properties for use in electro-optical applications, such as organic light emitting diodes, organic field effect transistors, solar cells, two photon absorption and nonlinear optics.¹⁻⁴ The molecular systems containing ethylene or ethynyl linkages have been synthesized and extensively studied by many groups. Notable entries are the X-shaped 1,2,4,5-tetravinyl-benzenes reported by Kang et al.⁵ and 1,4-bis(arylethynyl)-2,5-distyrylbenzenes studied by Bunz and co workers.⁶ Ethyne linkages allow the compounds to acquire a planar structure, which induces stronger intramolecular interactions between chromophores and also increases charge transporting properties. Moreover, ethynyl derivatives exhibit higher fluorescence quantum efficiency which makes them useful for organic light emitting devices and photovoltaic applications. For instance, functionalized cruciform shaped conjugated fluorophores are found to display interesting optical and electrochemical properties due to their multiple-conjugation pathway structures. Haley et al. have reported various 1,2,4,5-tetrasubstituted(phenylethynyl)benzenes which showed excellent fluorescent properties with high quantum yield.⁷

Apart from ethylene linkage, photophysical and electrochemical properties of some PAHs such as pyrene, fluorene, carbazole attached directly with alkyne bridging unit have also been extensively investigated as functional materials in organic electronics.^{8,9} Recently Adhikari et al. have reported ethynylphenyl linked carbazoles as single emitting component for white OLED.¹⁰ Additionally, ethyne linkage was also found to be beneficial for increasing charge separation and light harvesting property for solar cell applications. Recently, Teng et al. have explained that introduction of triple bond red shifts the absorption profile and also increases the efficiency of DSSC device.¹¹ Very few ethynyl linked organic dyes have been studied as potential candidate for DSSC application.^{12,13}

In this chapter, we have synthesized and characterized organic materials based on pyrene as constituent for OLED and DSSC applications. The compounds for OLED purpose are made up of four units namely pyrene core, ethyne linkage, fluorene and diphenylamine periphery (Figure 4.1). Further we will discuss the reason for choosing pyrene as a central core attached with fluorene through ethynyl linkage and why diphenylamine was introduced at 7th position of fluorene. We have already discussed above that ethyne linkage is used to increase the conjugation and red shifts the absorption/emission profile.

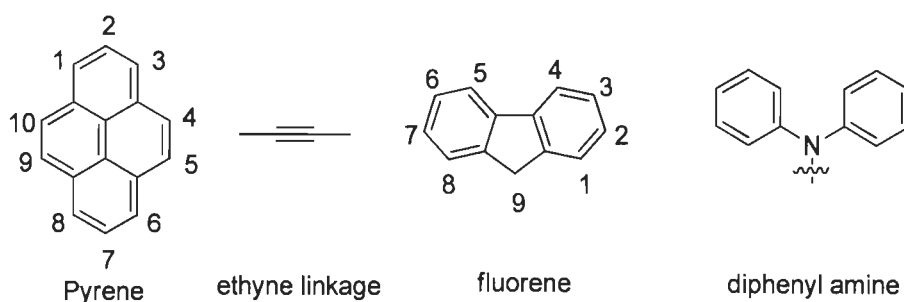


Figure 4.1 Structures of the basic units used in the construction of functional materials.

Pyrene is a versatile fluorophore and has been a subject of numerous investigations due to its interesting optical and electrochemical properties. Moreover, it shows featured

excimer/monomer emission and have exceptionally long fluorescence lifetime. The long-lived S_1 state of pyrene (650 ns in nonpolar media) and favorable redox potentials makes it well-suited for semiconductor sensitization.¹⁴ There are some drawbacks associated with pyrene, for example, its absorption and emission are confined to the UV region, its fluorescence quenching in presence of oxygen and molecular aggregation or π - π stacking. Thus, there is a need to red shift the absorption and emission of pyrene by increasing the π -conjugation which also makes its emission less sensitive to oxygen. Pyrene can be easily substituted at 1,3,6,8 positions. Optical and electrochemical properties of pyrene-based monomer, oligomer, dendrimer and polymers have been extensively studied and found much application in discotic liquid crystals, fluorescence probes, fluorescence sensing and other biological applications.¹⁵⁻¹⁸ Pyrene-based electron transporting materials have also been reported.¹⁹ Some cruciform shaped tetrasubstituted pyrenes have been used as fluorescent liquid crystalline columns and as organic semiconductor for field effect transistors.^{20,21}

Cruciform pyrene fluorophore with extended π -conjugation have been found to show promising optical and electrochemical properties due to their multiple-conjugated pathway structures. Figure 4.2 shows some examples of tetraethynyl-substituted pyrene derivatives. **D1**²² and **D2**²³ have been studied as luminescent liquid crystals and gels for optoelectronic devices. **D3** has been designed to interact with a complementary linear module through triple H bond.²⁴ Although pyrene showed divergent application in the field of biology as remarkable fluorescent probe but its use in OLED and photovoltaics is limited due to its propensity to form molecular aggregates in solid state and concentrated solutions. Sankararaman have investigated the aggregation through π - π and C-H...O interaction in tetraethynyl pyrene octaldehyde derivative (**D4**).²⁵ Venkataramana and Sankararaman have reported the absorption and emission

properties of **D5** and other tetraalkynyl pyrene derivatives.²⁶ Very few tetraethynyl pyrene derivatives were made for application in OLED. Recently Hu et al. have reported the synthesis and photophysical properties of 2,7-di-tert-butyl-4,5,9,10-tetrakis(*p*-*R*-phenylethynyl)pyrenes (**D6**, **D7**) which can be promising blue emitting materials in OLED.²⁷

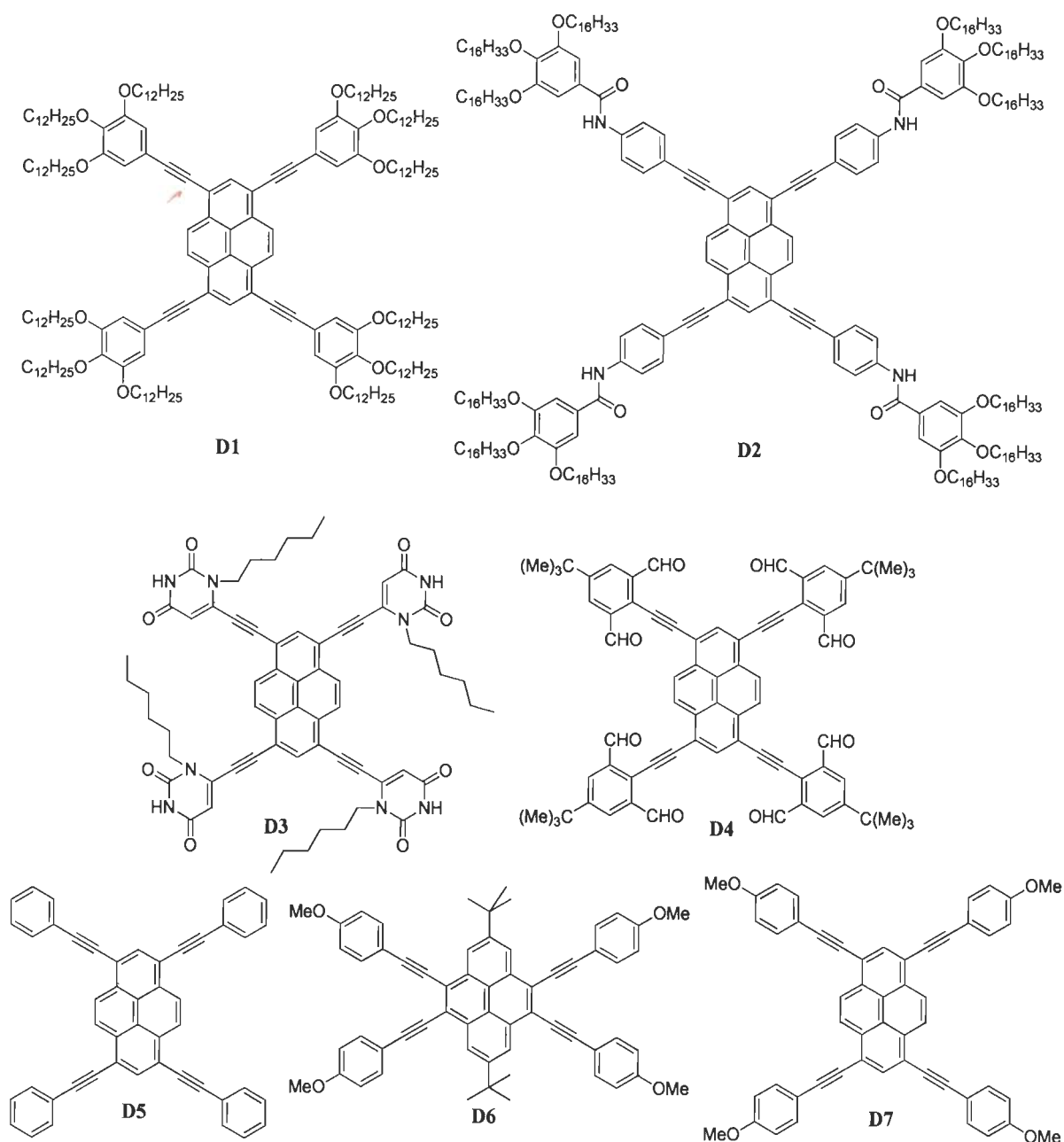


Figure 4.2 Cruciform pyrene derivatives containing ethynyl linkers.

To the best of our knowledge, no OLED device was fabricated using tetraethynyl pyrene derivatives. Although Kim et al. have reported tetraalkynyl conjugated pyrene derivatives incorporated with dimethylamine for its two photon absorption properties.²⁸

Further, fluorene is chosen because its derivatives have been demonstrated to possess interesting and unique chemical and physical properties. The major advantage with the fluorene is the facile substitution on 9th position which improves its solubility and also helps to preserve their optical properties in solid state by limiting molecular interactions. Fluorene-based oligomers and polymers constitute an important class of π -conjugated organic materials because of their excellent optical, thermal, and electrochemical properties.^{29,30} They have been extensively studied and explored for various functional properties including EL, liquid crystalline and two-photon absorption properties for optoelectronic applications in the past few years.^{9,31} Fluorenes are widely used as an important class of blue emitting materials in OLEDs. Tang et al. have reported fluorene- and spirofluorene substituted pyrene derivatives as blue emitters in OLED.³²⁻³⁴ The structures of them are shown in Figure 4.3. Substitution of pyrene with these fluorene derivatives also improve the hole injection. Thus, pyrene-fluorene combination is beneficial for increasing the thermal stability and hole transporting properties of the molecule.

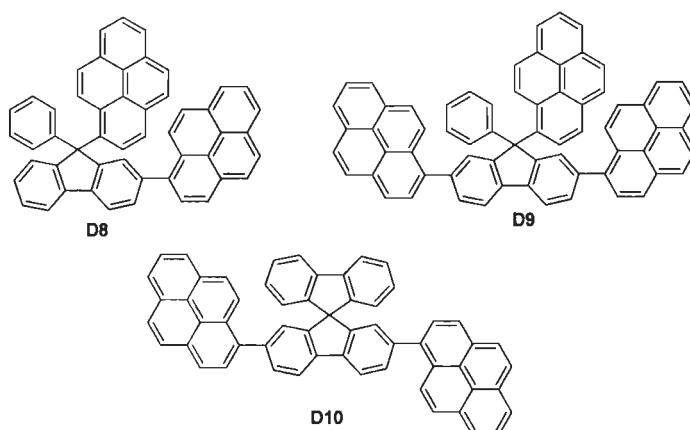


Figure 4.3 Structures of the fluorene- and spirofluorene-containing pyrene derivatives.

Further, introduction of ethyne linkage between fluorene and pyrene not only increases the conjugation but also increase the electronic coupling between pyrene and fluorene which might lead to enhanced charge transporting properties. Zhao et al. have reported light emitting oligomers and dendrimers composed of pyrene, carbazole and fluorene linked by ethynyl linkages in their several reports.³⁵⁻³⁸ The structure of these oligomers (**D11-D14**) are shown in Figure 4.4. The oligomers showed the external quantum efficiency (EQE) 0.41-0.69% and the dendrimer based device exhibited yellow emission with EQE 0.86%.

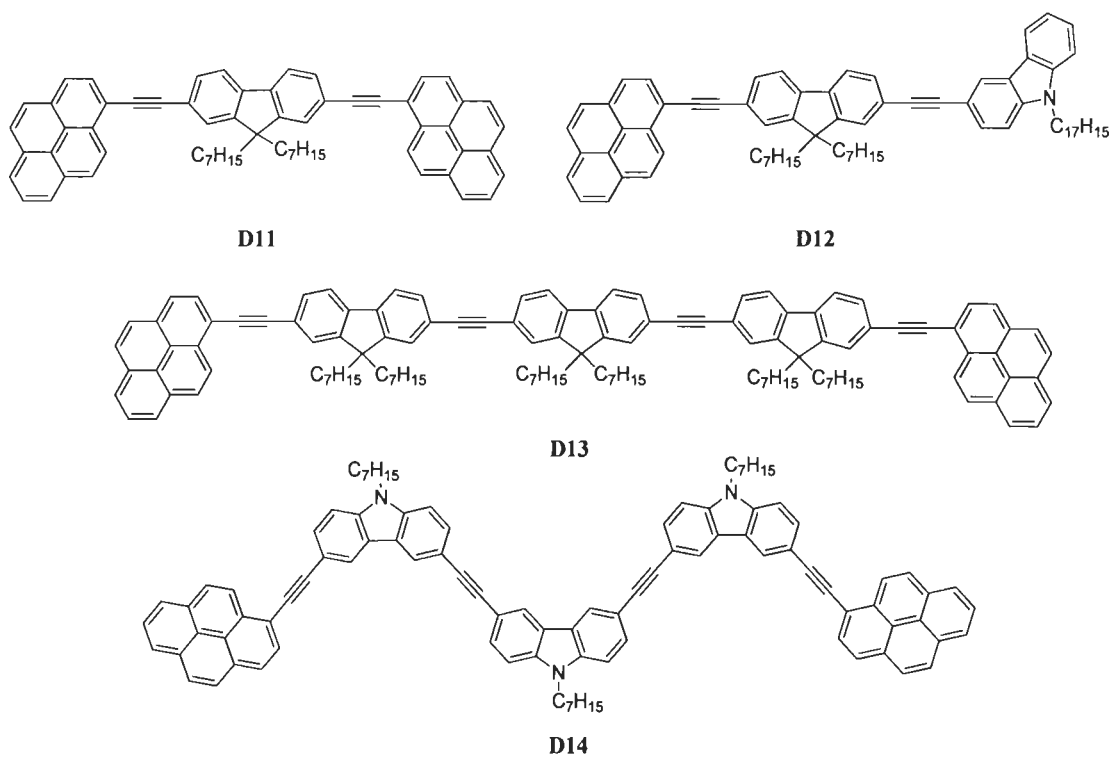


Figure 4.4 Oligo(2,7-fluorene ethynylene)s and (3,6-carbazole ethynylene)s with pyrene moieties as blue emitters in OLEDs.

The major drawback associated with the pyrene-based derivatives is the molecular aggregation or π - π stacking due to its planar nature which makes their use limited in electronic devices. Nonplanarity is the best solution to overcome this problem. Hence, diarylamines are found as the preferred agent due to their non planar structure and amorphous nature.

Incorporation of diarylamine suppresses the chance of molecular aggregation and also increases the thermal stability which might lead to a better efficiency in OLED and good charge transporting properties. To understand the influence of triple bond as a linker and amine on the optical and electrochemical properties, we have shown some examples in Figure 4.5 and compared their optical and electrochemical data, which have been taken from the literature, as shown in Table 4.1.^{39-41, 14}

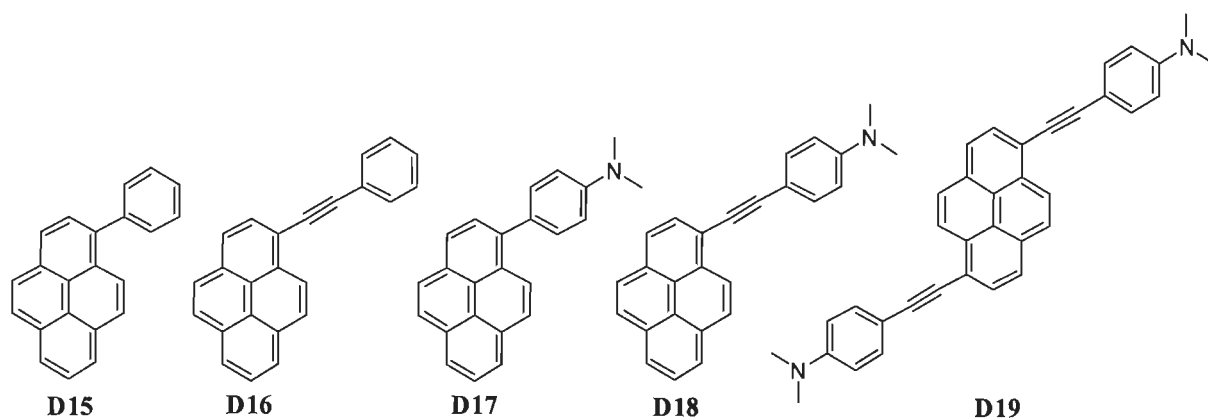


Figure 4.5 Structure of pyrene-based compounds (D15-D19).

The incorporation of ethynyl linkage between pyrene and phenyl red shifts the absorption as well as emission wavelength. Moreover the stokes shift is also decreased which suggest that ethyne linkage makes the compound more planar and rigid resulting in less chances of conformational changes due to which nonradiative decay diminishes in the excited state. The quantum yield also increases by inserting ethyne linkage. The dimethyl amine derivatives **D17**⁴¹ and **D18**⁴⁰ further red shifts the absorption/emission profile as compared to their corresponding parent compounds **D15**³⁹ and **D16**⁴⁰ respectively. Furthermore, the broadening and lacking of structured emission spectra of **D18** as compared to **D16** indicates the absence of excimer formation in **D18**. The incorporation of amino group also tunes the HOMO/LUMO energy

levels. The absorption and emission wavelength showed bathochromic shift by 1,6-substitution on pyrene (**D19**)¹⁴ as compared to **D18** but the fluorescence quantum yield has decreased.

Table 4.1 Optical and electrochemical properties of **D15-D19**.

Compounds	λ_{abs} (nm)	λ_{em} (nm)	Φ_{F}	E_{ox}	HOMO	LUMO	E_{0-0}	Ref.
^a D15	342	382, 398	0.58	-	-	-	-	39
^a D16	381	392, 415	1	1.41	6.21	3.07	3.14	40
^a D17	362	532	0.95	-	-	-	-	41
^a D18	388/388 ^b	540/522 ^b	0.83	0.92	5.72	2.54	3.18	40
^b D19	436	559	0.37	-	-	-	-	14

^arecorded in acetonitrile; ^brecorded in methanol

Thus the above discussion clearly indicates that ethyne linkage and incorporation of amine is enhancing the optical properties and making the compounds more promising for the electronic applications.

Some previous reports have exposed that rod shaped molecules or linkers were found to be beneficial to enhance photoinduced charge transfer and charge separation (**D20-D22**).^{13,42} Additionally pyrene being a versatile fluorophore made these rod shaped linkers more promising for photovoltaic applications. Recently, Thayumanavan and co workers have reported dendritic and linear macromolecular architecture using (diarylamino)pyrene as electron rich moiety for photovoltaic application.⁴³ Figure 4.6 shows some examples of pyreneethynyl-based dyes tested for photovoltaic applications. Out of these, pyrene-thiophene diad system (**D23**) is highly fluorescent and very sensitive to changes in the absorption and emission properties also the metal coordination (**D24**) results in complete fluorescence quenching.⁴⁴ Such type of systems show great potential in the area of molecular sensors. Moreover conjugated thiophene units are known to be good electronic conductors due to their virtue of enhancing π -conjugation and π -delocalization. It also promotes electronic coupling between terminal units.

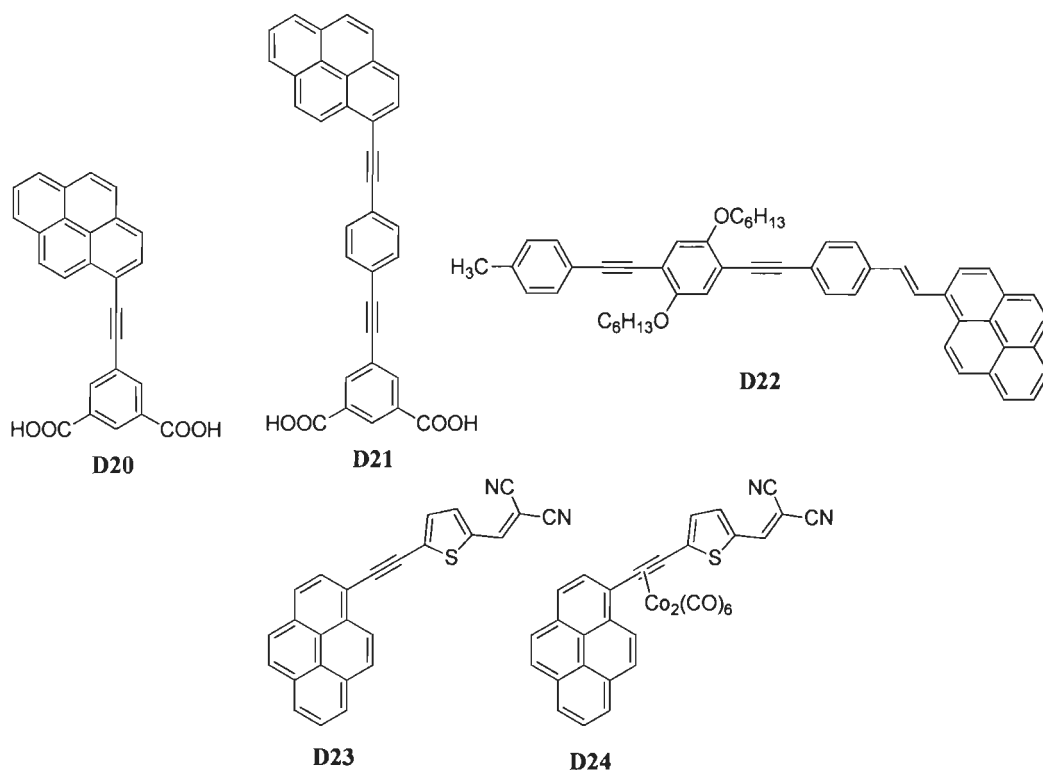


Figure 4.6 Structures of pyrene end-capped rigid rod like compounds.

In this chapter, the organic materials based on pyrene as constituents for OLED and DSSC have been synthesized and characterized. A series of blue and yellow-emitting materials have been developed by integrating fluorene and pyrene segments *via* ethynyl linkage. Both mono-substituted and tetra-substituted derivatives have been synthesized and characterized. The tetra-substituted derivatives displayed red-shifted emission when compared to the analogous mono-substituted derivative indicative of an extended conjugation in the tetra-substituted derivatives. Diphenylamine was incorporated to avoid molecular aggregation. These derivatives were employed as emitting dopants in OLED and found to exhibit bright blue or yellow electroluminescence.

The synthesis and characterization of pyrene-cyanoacrylic conjugates is also described in this chapter. The architecture of dyes can be treated approximately as possessing pyrene as a weak π -donor, cyanoacrylic acid as an acceptor and four different spacers in the form of 1,4-

phenyl, 2,7-(9,9-diethyl-9*H*-fluorene), thiophene or 2,2'-bithiophene. The influence of different spacer on optical and electrochemical properties has been investigated. The rod-like structures of the dyes can be useful for the grafting them over semiconductor surface and for increasing the charge injection on the TiO₂ surface. Electrochemical studies revealed a favorable HOMO/LUMO level for DSSC applications. We will be discussing these in more detail as we will proceed with the chapter.

4.2 Results and discussion

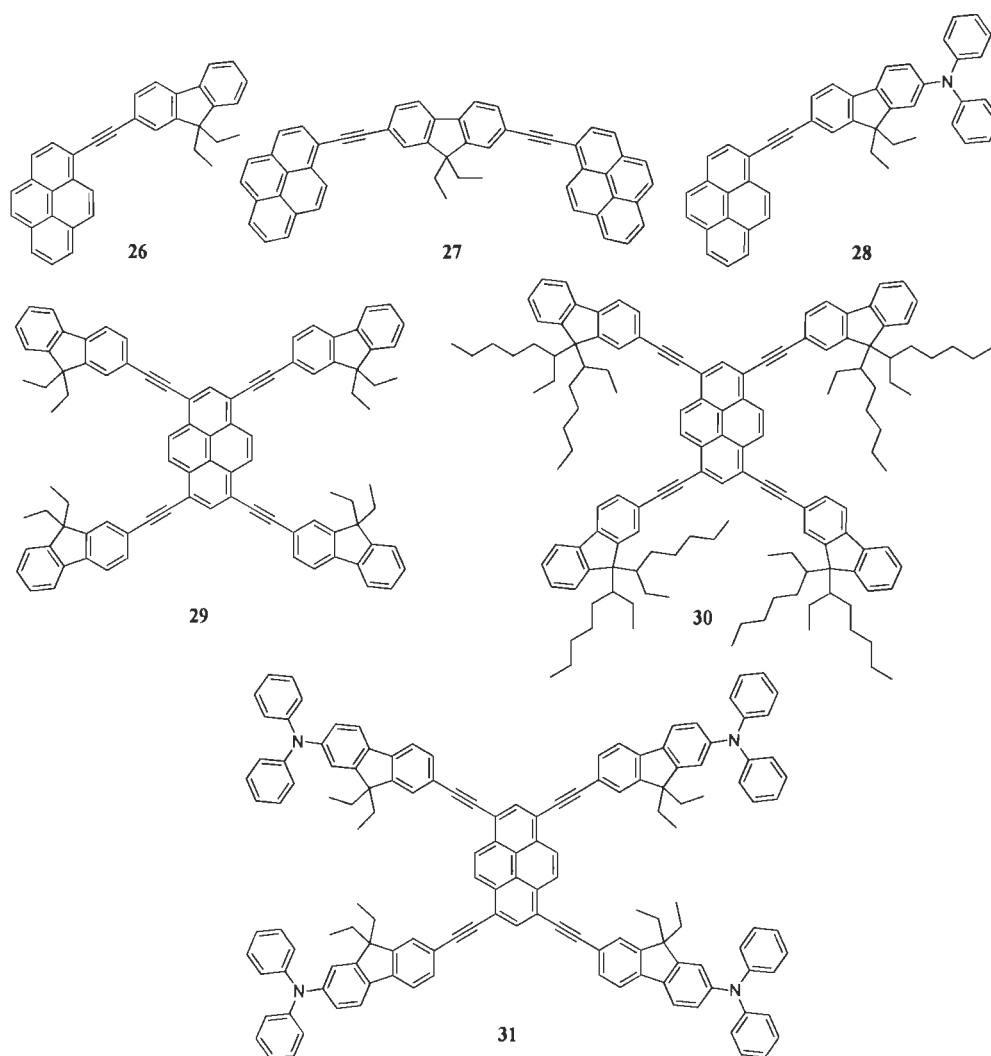


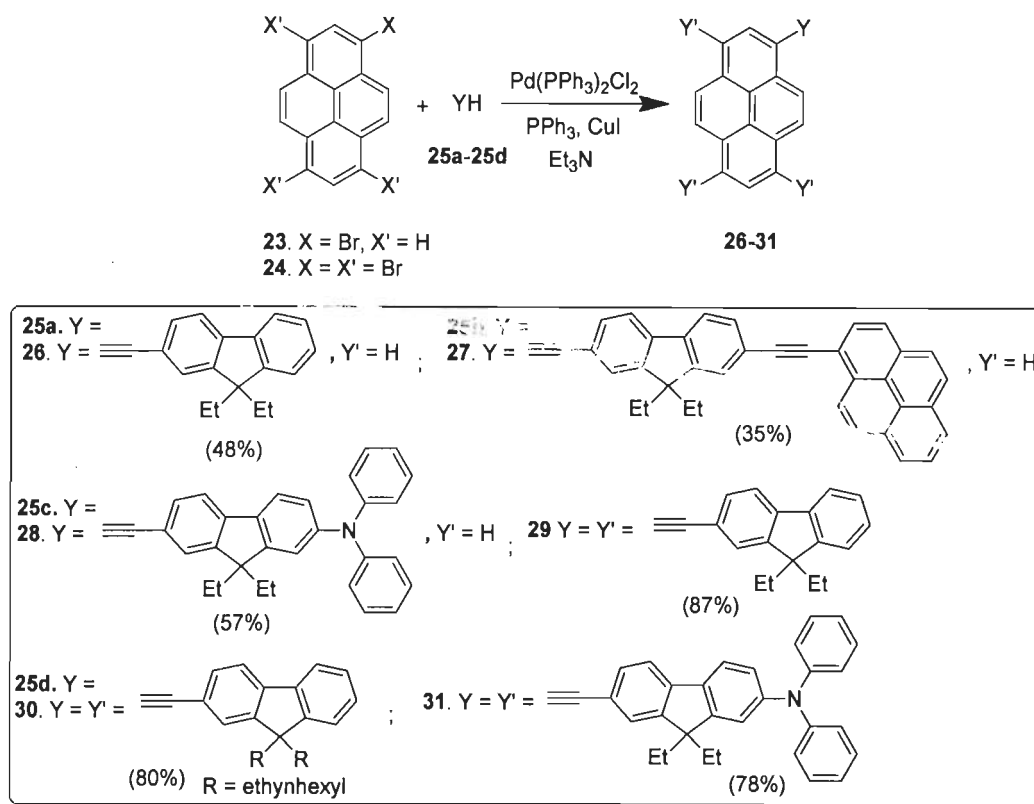
Figure 4.7 Structures of pyreneethynyl derivatives (26-31).

4.2.1 Synthesis

The structures of pyreneethynyl-based functional materials (26-31) developed in this work is given in Figures 4.7 & 4.8. The synthetic route employed for obtaining **26-31** is depicted in Scheme 4.1.

Monobromopyrene (**23**) and 1,3,6,8-tetrabromopyrene (**24**) have been synthesized by reported procedures.⁴⁵ Derivatives **26-28** were made by Sonogashira cross coupling reaction of 1-bromopyrene (**23**) with 9,9-diethyl-2-ethynyl-9*H*-fluorene (**25a**), 9,9-dibutyl-2-ethynyl-9*H*-fluorene (**25b**) and 9,9-diethyl-7-ethynyl-*N,N*-diphenyl-9*H*-fluoren-2-amine (**25c**) respectively using Pd(PPh₃)₂Cl₂/PPh₃/CuI as catalytic system. While derivatives **29-31** were synthesized by Sonogashira cross coupling of 1,3,6,8-tetrabromopyrene (**24**) with **25a**, 2-ethynyl-9,9-di(octan-3-yl)-9*H*-fluorene (**25d**) and **25c** respectively.

Different terminal acetylenes such as 9,9-diethyl-2-ethynyl-9*H*-fluorene (**25a**), 9,9-dibutyl-2-ethynyl-9*H*-fluorene (**25b**), 2-ethynyl-9,9-di(octan-3-yl)-9*H*-fluorene (**25d**) have been synthesized by following known procedures with slight modification. The synthesis involved several steps such as alkylation of fluorene, bromination, Sonogashira cross coupling with 2-methylbut-3-yn-2-ol and finally cleavage by KOH and toluene.^{14,46} While 9,9-diethyl-7-ethynyl-*N,N*-diphenyl-9*H*-fluoren-2-amine (**25c**) has been synthesized by sequential alkylation of fluorene, dibromination, one side C-N cross coupling with diphenylamine, Sonogashira cross coupling with 2-methylbut-3-yn-2-ol and finally cleavage by KOH and toluene. Compound **29** showed solubility problem, thus **30** with long alkyl chain was also made to increase the solubility.



Scheme 4.1 Synthetic route of the compounds **26-31**.

In another part of work we have synthesized four pyreneethynyl containing cyanoacrylic acid derivatives (**35a-35d**) having different spacer unit 1,4-phenyl, 2,7-(9,9-diethyl-9*H*-fluorenyl), thiophenyl, bithiophenyl respectively. The synthetic route of **35a-35d** has given in Scheme 4.2. Pyrene acetylene was made by reported procedure.¹⁴ To synthesize **34a-34d**, pyrene acetylene undergo Sonogashira cross coupling with four different aldehydes 4-bromobenzaldehyde (**33a**), 7-bromo-9,9-diethyl-9*H*-fluorene-2-carbaldehyde (**33b**), 5-bromothiophene-2-carbaldehyde (**33c**) and 5'-bromo-[2,2'-bithiophene]-5-carbaldehyde (**33d**) respectively. Further **34a-34d** undergoes Knoevenagel condensation reaction with cyanoacetic acid in presence of ammonium acetate and acetic acid to obtain the final dyes **35a-35d**.

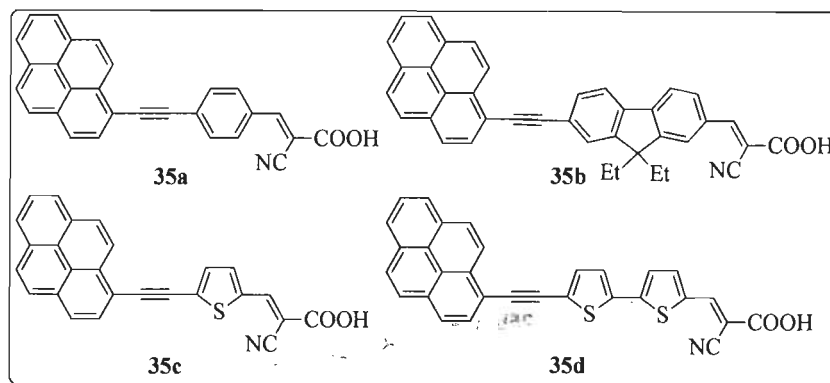
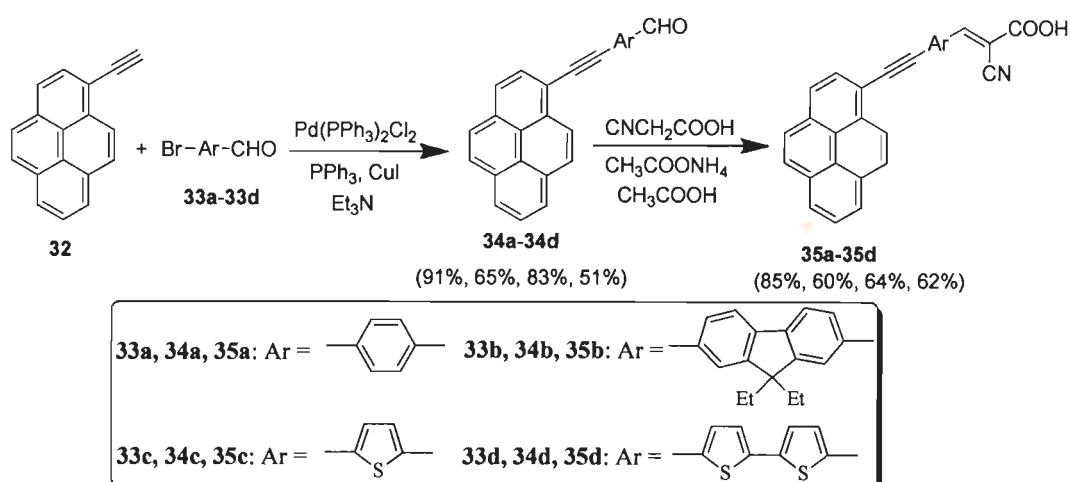


Figure 4.8 Structures of pyreneethynyl-based dyes (35a-35d).



Scheme 4.2 Synthesis of pyreneethynyl-based cyanoacrylic acid derivatives.

4.2.2 Optical properties

The absorption spectra of compounds **26-31** were recorded in toluene and dichloromethane solution ($2 \times 10^{-5} \text{M}$) are shown in Figures 4.9 & 4.10 respectively. The pertinent data are furnished in Table 4.2. The model compound **26** showed vibronic pattern and exhibited absorption bands at two wavelength region 286-322 nm and 381-405 which is due to $\pi-\pi^*$ transition. The vibronic pattern is similar to pyrene but more red shifted as compared to pyrene.⁴⁷ This is due to extended conjugation through ethynyl fluorene. Moreover **26** showed more red shifted absorption with higher molar extinction coefficient as compared to

phenylethynylpyrene which was reported by Yang et al.⁴⁰ This suggests that the presence of electron rich fluorene increases electron density on pyrene as a result π -electron delocalization increases.

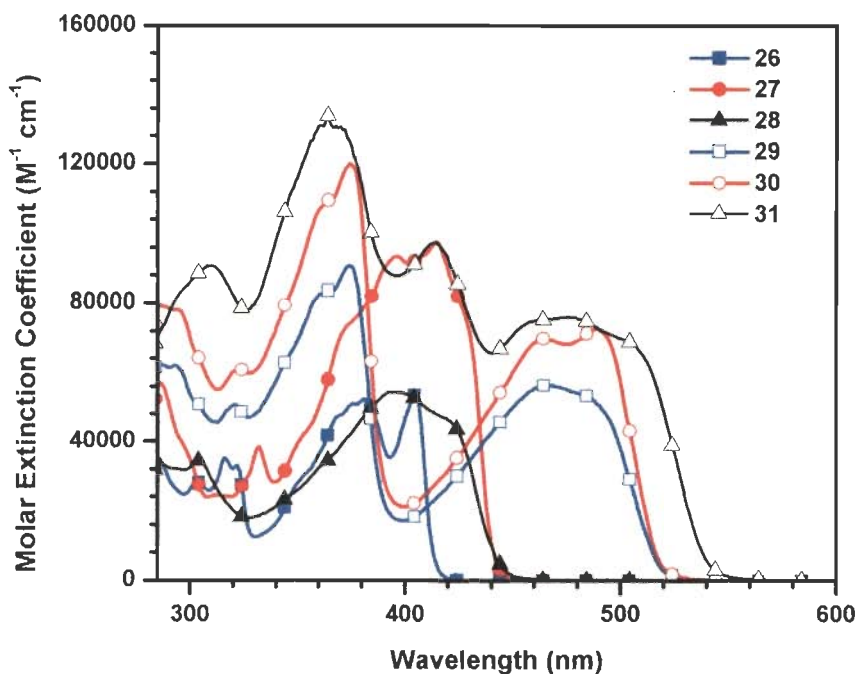


Figure 4.9 Absorption spectra of 26-31 recorded in toluene.

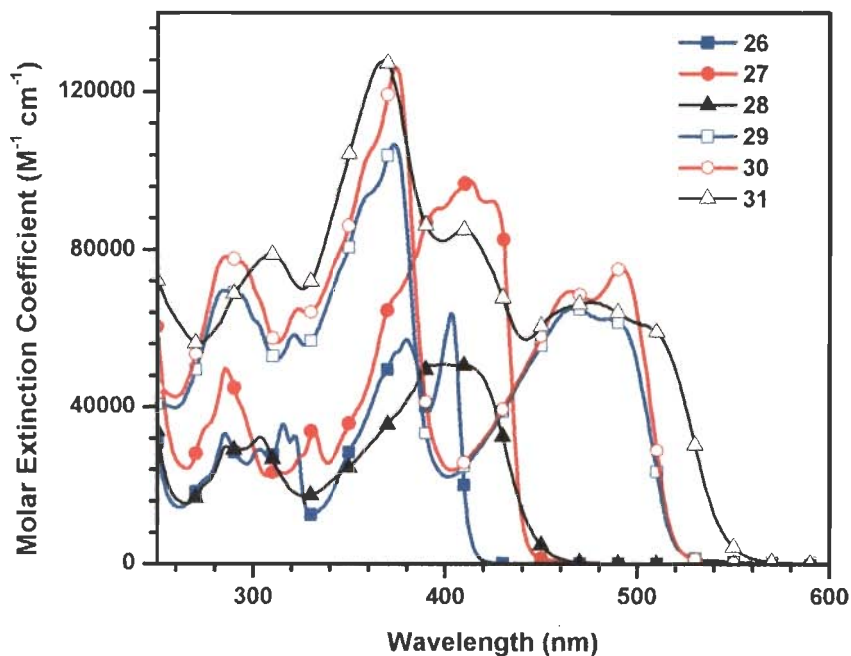


Figure 4.10 Absorption spectra of 26-31 recorded in dichloromethane solutions.

Compound **27** exhibited red shifted (15 nm) and more broad absorption band as compared to **26** due to more conjugation. The molar extinction coefficient is higher for **27** than **26**. This is due to the extended conjugation which increases the chromophore density. The diphenylamine derivative **28** rendered bathochromic shift and more broad absorption as compared to **26**. Introduction of diphenylamine at 7th position of fluorene not only increases the conjugation but also leads to a charge transfer character in the molecule in which diphenylamine act as a π -donor and pyrene act as weak π -acceptor. The peak at 418 nm in the absorption spectra of **28** is due to charge transfer which is merged with π - π^* transition. Thus, the incorporation of amine increases the charge transporting properties in the molecule.

Tetrasubstituted pyrene derivatives (**29-31**) displayed broader absorption and lower energy band than monosubstituted **26** due to more extended conjugation. The compounds **29** & **30** exhibited two bands which are due to π - π^* electronic transition. The absorption band of **30** was found 30 nm red shifted with higher molar extinction coefficient as compared to previously reported tetraphenylethynyl pyrene.²⁵ This is due to the presence of fluorene as described above. Further compound **30** showed red shift (92 nm) as compared to 1,3,6,8-tetrakis(9,9-dihexyl-9H-fluorene-2-yl)pyrene (400nm) in THF.⁴⁸ This indicates that the incorporation of ethyne linkage red shifts the absorption profile. It can be seen that the alkyl chain did not alter the absorption profile as same absorption pattern was observed for both derivatives **29** and **30**. But, we have used the derivative with long alkyl chain (**30**) for all studies of this series which showed better solubility as compared to **29**. The tetrasubstituted derivative with further extended diphenylamine on the periphery (**31**) showed bathochromic shift as compared to **30**. The presence of diphenylamine generates the charge transfer character in the molecule which red shifts the absorption profile.

Table 4.2 Optical properties of the compounds 26-31.

Compound	Toluene			Dichloromethane			Thin solid film
	λ_{\max} , nm (ϵ_{\max} , $M^{-1}cm^{-1}$) $\times 10^3$)	λ_{em} , nm (Φ_F)	Stokes' shift, cm^{-1}	λ_{\max} , nm (ϵ_{\max} , $M^{-1}cm^{-1}$) $\times 10^3$)	λ_{em} , nm (Φ_F , %)	Stokes' shift, cm^{-1}	
26	286 (34.7), 304 (28.2), 316 (35.3), 322 (33.1), 381 (52.3), 405 (53.9)	412, 436 (1)	420	285 (33.2), 303 (29.1), 315 (35.4), 321 (32.5), 380 (57.0), 403 (63.6)	412, 435 (1)	542	496
27	286 (56.9), 332 (38.5), 414 (97.5), 424 (82.1)	438, 463 (1)	754	285 (49.8), 331 (34.7), 412 (97.5), 424 (92.4)	439, 465 (1)	806	486, 505
28	287 (33.5), 304 (34.4), 395 (54.2), 418 (46.8)	449, 475 (sh) (0.98)	1652	286 (29.8), 304 (32.3), 400 (50.8), 410 (50.4)	516 (0.60)	5010	495
29	285, 321, 374, 466, 486	512, 548	1045	284, 321, 373, 467, 485	515, 548	1201	-
30	287(79.3), 374 (120.1), 464 (70.0), 488 (72.5)	513, 549 (0.63)	999	285 (78.2), 374 (126.1), 465 (69.2), 492 (75.1)	514, 551	870	587
31	310 (90.8), 364 (133.8), 413 (97.2), 476 (75.9), 503 (69.0)	535, 568(sh)	1189	310 (78.9), 368 (127.8), 410 (85.1), 476 (66.4), 504 (60.7)	567	2205	581

There was no significant change was observed in absorption profile of all derivatives while going from less polar toluene to more polar dichloromethane solution. This suggests that the ground state is very less polar and show no charge transfer character in the ground state.

The emission spectra of compounds **26-31** were recorded in toluene, dichloromethane and thin film are displayed in Figure 4.11. The emission data along with fluorescence quantum yield and Stokes' shift are given in Table 4.2. Compound **26** exhibited vibronic emission band at 412, 435 nm which is red shifted as compared to pyrene.⁴⁷ This is due to extended conjugation. Further, compound **26** (430 nm) showed red shifted emission (38 nm) in acetonitrile as compared to phenylethynylpyrene (392 nm).⁴⁰ Which confirms that fluorene increases the electron delocalization in the molecule. Compound **27** presented bathochromic shift as compared to **26** due to extended conjugation and presence of two chromophoric units i.e. pyrene.

The derivatives without amine functionality (**26, 27, 29, 30**) showed well resolved vibronic emission band in both toluene and dichloromethane which is a characteristic of monomer emission of pyrene. While the derivatives with diphenylamine (**28, 31**) exhibited a single emission band with minor hump at longer wavelength when recorded in toluene. Red shifted emission and loss of structured emission in **28** and **31** is due to charge transfer from electron donor diphenylamine to π -acceptor pyrene. The polar nature of diphenylamine bearing derivative was confirmed when emission spectra recorded in more polar dichloromethane solution where they exhibited red shift than the emission wavelength recorded in less polar toluene. The red shift is due to pronounced dipolar interaction in more polar solvent which indicate the polar nature of **28** and **31** [Figure 4.11(b)]. There is no significant change in the emission of the compounds **26, 27, 30** by changing the polarity.

Further tetrasubstituted derivatives (**29**, **30**) demonstrated bathochromic shift than that of monosubstituted one (**26**) which is due to increase in the conjugation pathway which shifts the emission profile towards longer wavelength. Moreover there is no significant effect in the emission profile by increasing the alkyl chain length. And there is no significant difference in emission spectra of **29** and **30** (Figure 4.11 (a)).

The emission spectra were recorded in thin film Figure 4.11(c). The values are given in Table 4.2. Compounds **26**, **27** and **30** exhibited red shifted emission in thin film when compared to that observed for dichloromethane solution. Moreover, these derivatives showed broad single peak in thin film with the loss of vibronic pattern. This clearly indicates that the red shifted and broad peak in thin film is due to molecular aggregation or excimer formation in the excited state. Among diphenylamine tethered derivatives **28** & **31** showed no significant change in emission wavelength when recorded in thin film as compared to solution. This demonstrates that molecular aggregation is suppressed due to incorporation of diarylamine. Thus diarylamines are detrimental for molecular aggregation.

The Stokes' shifts of the compounds were relatively small, probably pointing the rigidity of pyrene ethynyl derivatives. For instance, **27** exhibited larger value of Stokes' shift as compared to **26**. The reason could be the more conformational changes in the excited state of **27** due to the presence of two chromophoric unit pyrene. Diphenylamine incorporated derivatives (**28**, **31**) displayed larger Stokes' shift as compared to their parent derivatives **26** and **30** respectively. This is because of the nonplanarity of **28** & **31** which arise due to the incorporation of diarylamine. Thus more conformational changes required to attain planarity in the excited state which results in more non radiative decay in the excited state. Tetrasubstituted derivatives (**30**, **31**) showed higher Stokes' shift than the monosubstituted one **26**. This is due to more vibration

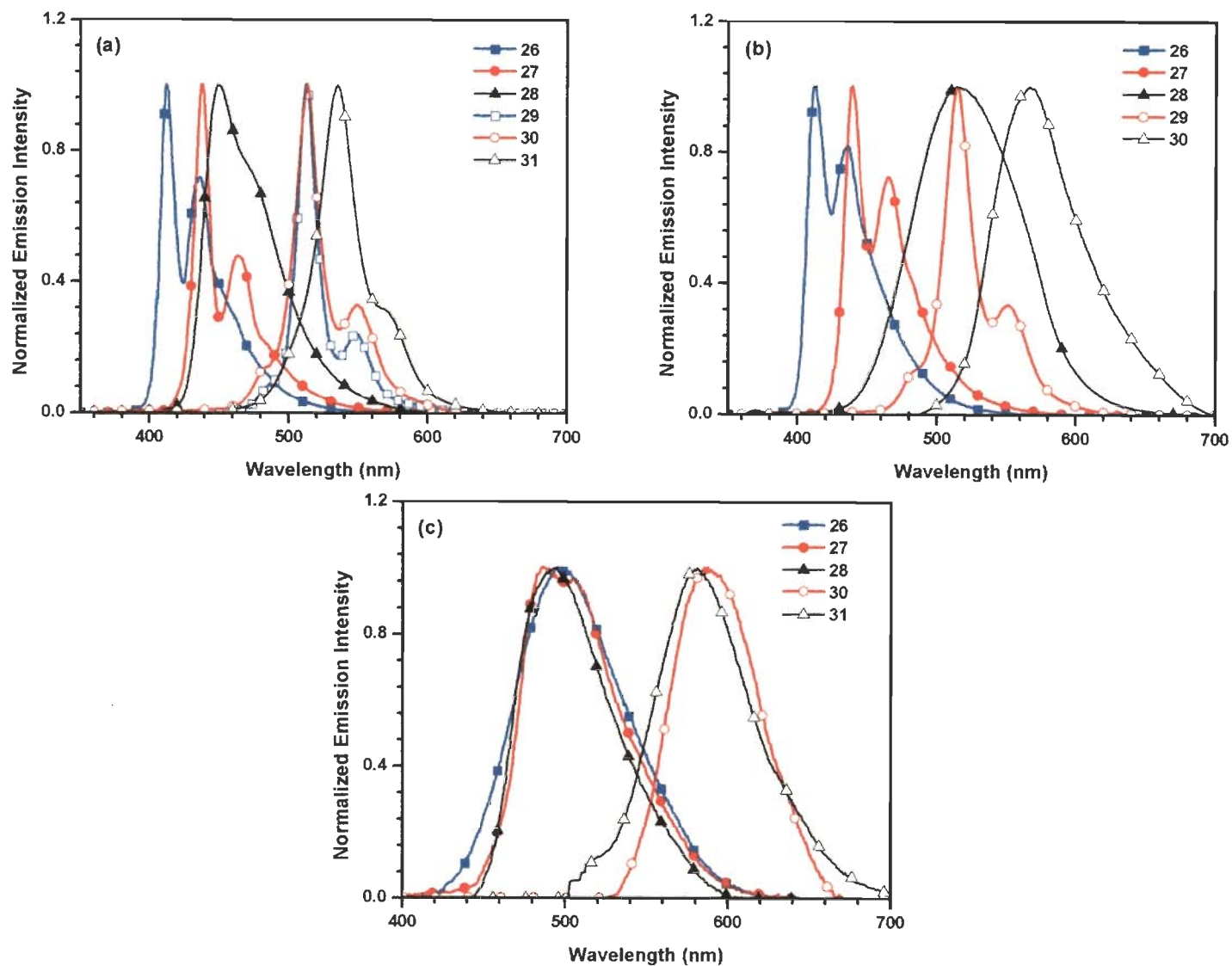


Figure 4.11 Emission spectra of the compounds (26-31) recorded (a) in toluene, (b) in dichloromethane, (c) thin solid film.

relaxation in the excited state or may be the tetrasubstituted derivatives are more solvated. Moorthy et al. have shown that tetraarylpyrene act as inclusion host for binding solvent molecules through its different binding sites.⁴⁹ Thus solvent interaction relaxes the excited state of tetrasubstituted derivative more, leading to larger Stokes' shifts. Among **28** and **31**, compound **31** attribute lower Stokes' shift due to more rigid system as compared to **28**.

The value of Stokes' shift has increases on changing the polarity from less polar toluene to high polar dichloromethane which is due to more solvation in more polar solvent indicating slight polar nature for all the derivatives. The change in Stokes' shift by changing solvent polarity is higher for **28** and **31** indicating the more polar nature in the excited state due to presence of diaryl amine. Thus more dipolar interaction in excited state in more polar solvent results in more relaxation of the molecule and hence larger the Stokes' shift.

All the derivatives showed higher value of quantum yield. The tetrasubstituted derivative presents less quantum yield as compared to monosubstituted due to more nonradiative decay in the excited state (as explained above). Moreover **28** exhibited less quantum yield as compared to **26** due to intramolecular charge transfer (ICT) in the former. ICT decreases the quantum yield due to more relaxation and nonradiative decay in the excited state.⁵⁰

The solvatochromism study has been done for all the compounds in different solvents to confirm the charge transfer character and also to evaluate the effect of solvent polarity on the optical properties of the molecules. The absorption and emission spectra of **26-31** has been recorded in the solvent of different polarity such as cyclohexane (CH), toluene (TOL), chloroform (CHCl₃), ethyl acetate (EA), tetrahydrofuran (THF), dichloromethane (DCM), dimethylformamide (DMF), and acetonitrile (ACN). The absorption and emission spectra of **26-31** in different solvents are shown in Figures 4.12-4.14. The absorption data in different solvents

is collected in Table 4.3 and the emission data is presented in Table 4.4. There is no significant difference in the absorption and emission spectra of **26** and **27** by changing the solvent polarity (only the absorption and emission spectra of **26** showed slight hypsochromic shift in acetonitrile) (Figure 4.12). Compounds **30** & **31** are not soluble in acetonitrile hence the spectra has not been recorded in acetonitrile for these derivatives. The emission spectra of **30** demonstrated slight bathochromic shift by increasing the solvent polarity indicating that excited state is more stabilized than ground state (Figure 4.13(d)).

Diphenylamine derivative **28** exhibited some discrepancy in its absorption spectra like 1) there is a slight blue shift observed by increasing the solvent polarity, 2) a well resolved low energy peak can be seen in nonpolar solvent cyclohexane, but low energy band become broader and less resolved in polar solvents (Figure 4.13(a)). The reason of former can be the stabilization of ground state by polar solvent. The later observation indicates that the low energy band corresponds to two peak one is due to π - π^* transition in pyrene and another due to charge transfer from diarylamine to pyrene core which is well resolved in nonpolar solvent and merged in polar solvent.

The emission spectra of **28** displayed positive solvatochromism suggesting the charge transfer character in the molecule (Figure 4.13(b)). It exhibited structured emission in cyclohexane which is a characteristic of pyrene monomer emission but on increasing the solvent polarity the derivative **28** exhibited broad and red shifted emission band. This observation indicates that comparatively less polar locally excited state (LE) is transformed into more polar charge transfer (CT) excited state in polar solvents. Thus, the bathochromic shift and broadening of emission band in polar solvent is due to more dipole-dipole interaction in the excited state which relaxes the molecule and stabilizes excited state.

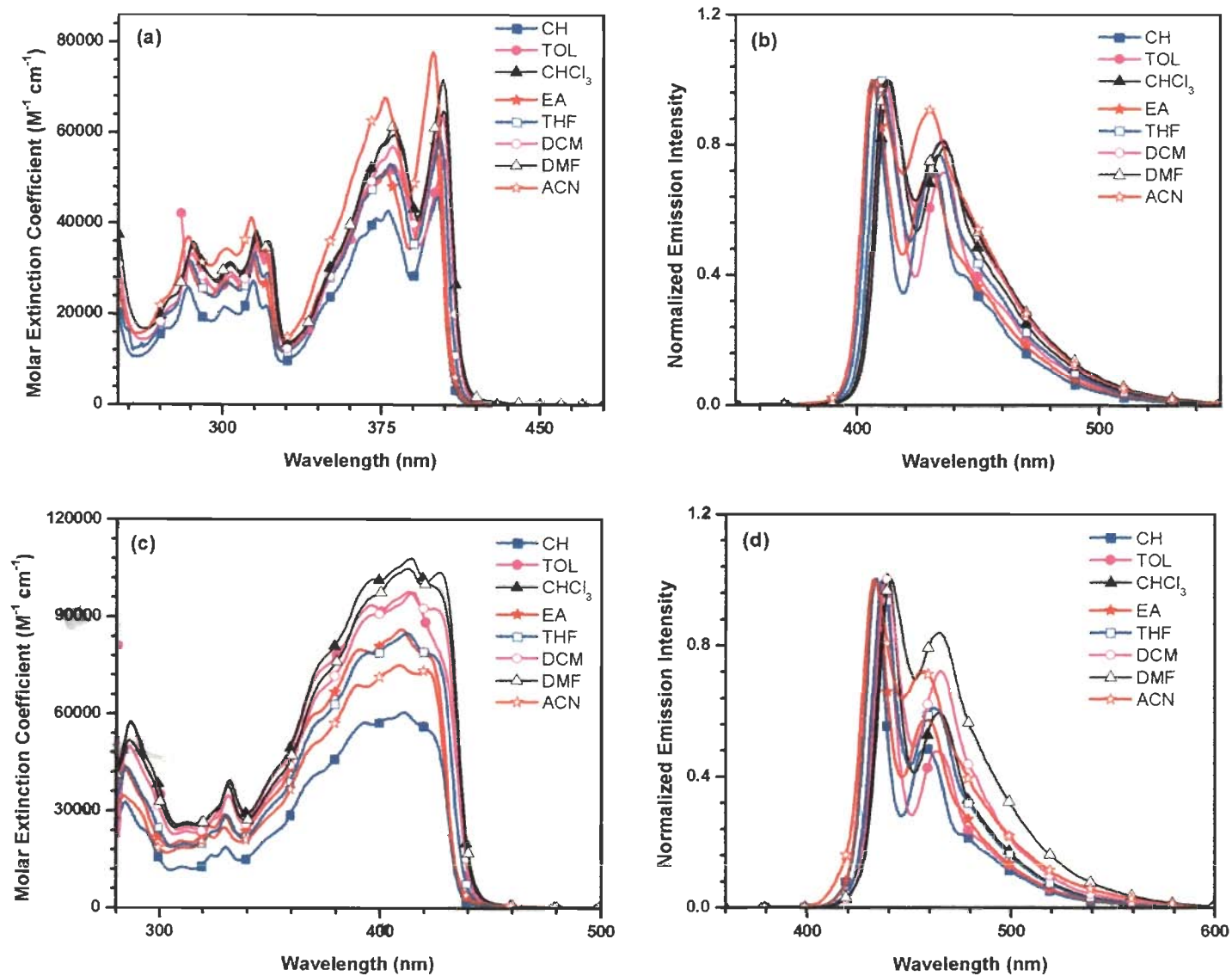


Figure 4.12 Absorption and emission spectra of the compounds 26 (a), (b) and 27 (c), (d) recorded in different solvents.

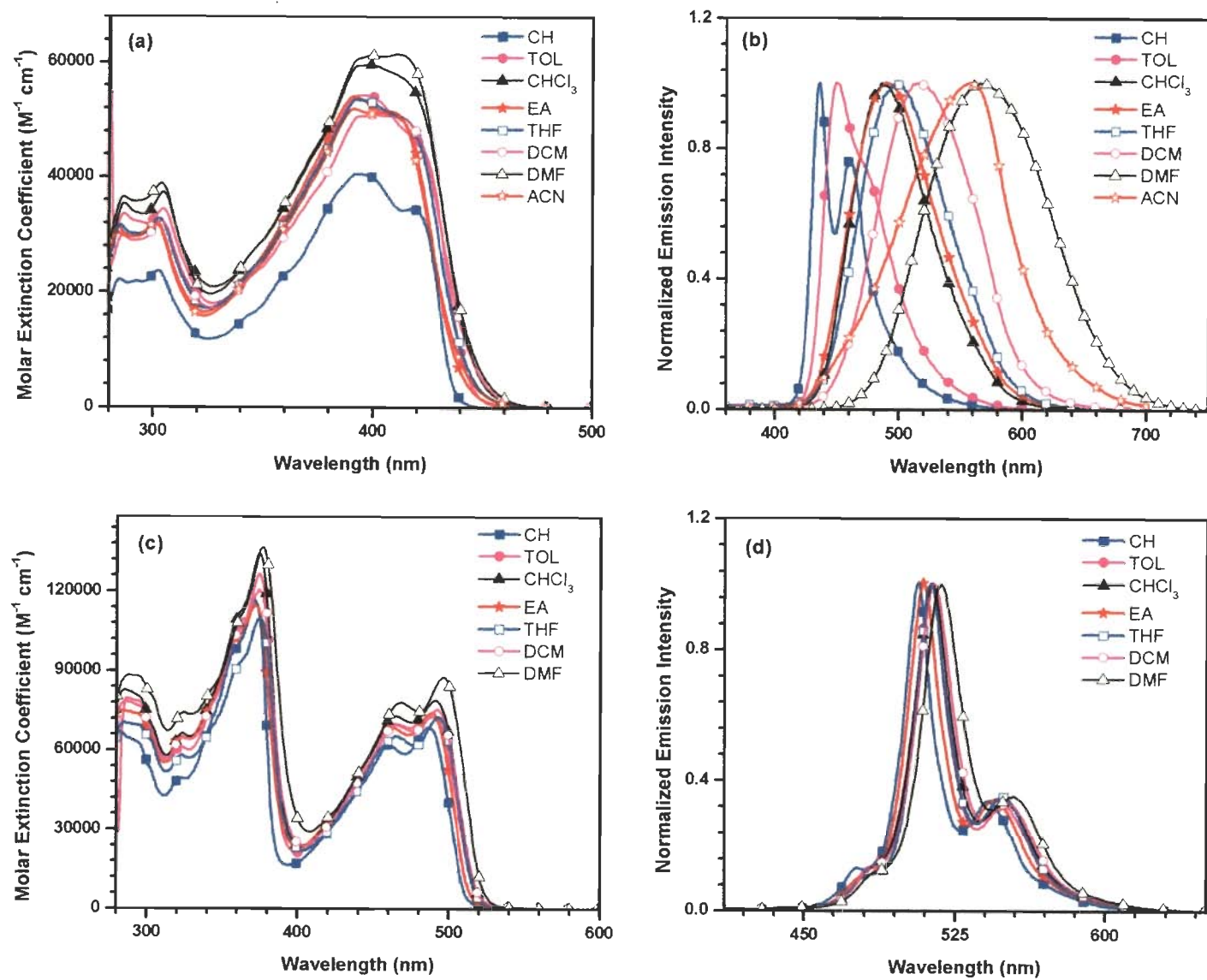


Figure 4.13 Absorption and emission spectra of the compounds 28 (a), (b) and 30 (c), (d) recorded in different solvents.

There is no significant change was observed in absorption spectra of tetrasubstituted diphenylamine derivative **31** by changing the solvent polarity indicating that the ground state is not polar (Figure 4.14(a)). Compound **31** showed positive solvatochromism from cyclohexane to dichloromethane in emission profile (Figure 4.14(b)). But the extent of red shift is lesser than **28**. This indicates that the CT state decrease as the number of peripheral donor substituent increases. The CT state also depends on the molecular symmetry (on the position of donor/acceptor unit).⁵⁰ Thus the comparatively less CT state in **31** is due to its more symmetrical structure.

Additionally, the emission spectrum of **31** is excitation dependant. The emission spectra of **31** were recorded in different solvent at different excitations. Two emission bands were observed at 350 nm excitation. Out of which the intensity of high energy band increase and also possess slight red shift with increasing solvent polarity while the low energy band displayed structured to broad red shifted emission from cyclohexane to dichloromethane same as observed in compound **28**.

The high energy band is similar to the emission of its corresponding acetylene **25c** as shown in Figure 4.14(b). This suggests that the compound is showing dual fluorescence one is due to locally excited (LE) state of diphenylamino fluorene and another is due to intramolecular charge transfer state. The dual fluorescence of pyrene derivative has been reported previously.^{39,51} When the compound was excited at 450 nm then the band due to LE state has disappeared, only ICT band was observed at the same wavelength as excited at 350 nm in all solvents (Figure 4.15(a)). In high polar DMF, a prominent hypsochromic shift was observed and the emission wavelength is different at different excitation when recorded in DMF as shown in Figure 4.15(b). In DMF, the emission due to ICT state is completely quenched, only emission due to LE state was observed at excitation of 350 nm.

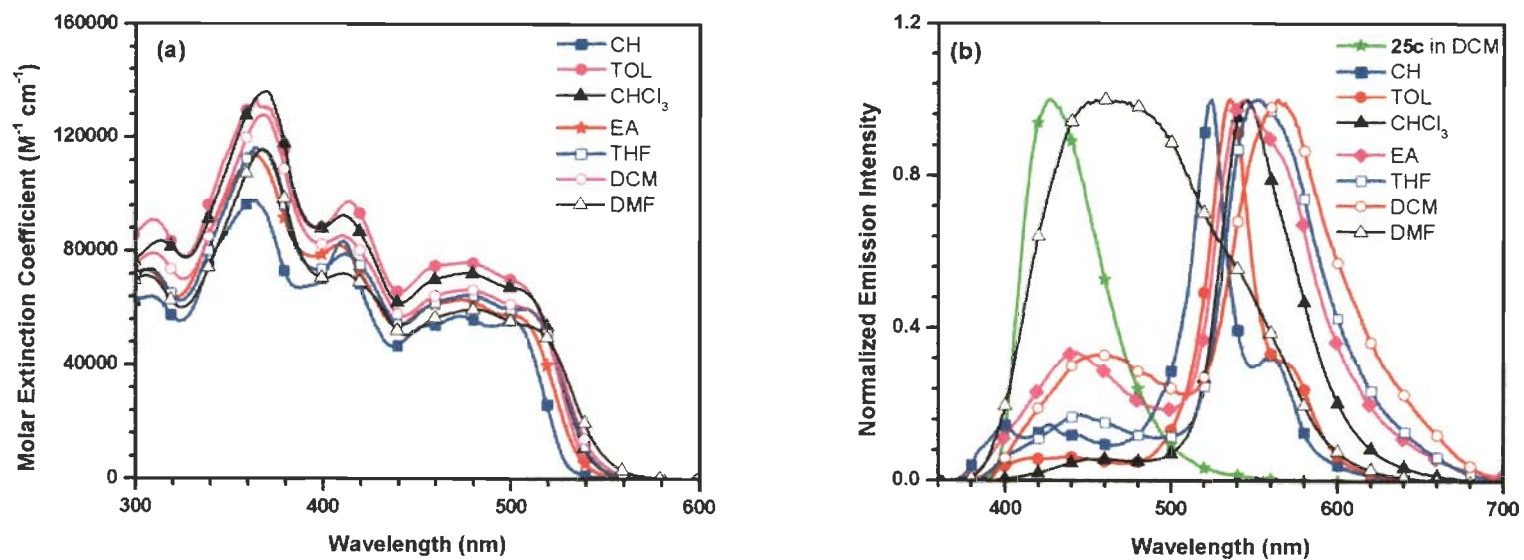


Figure 4.14 Absorption (a) and emission (at 350 nm excitation wavelength) (b) spectra of **31** recorded in different solvents.

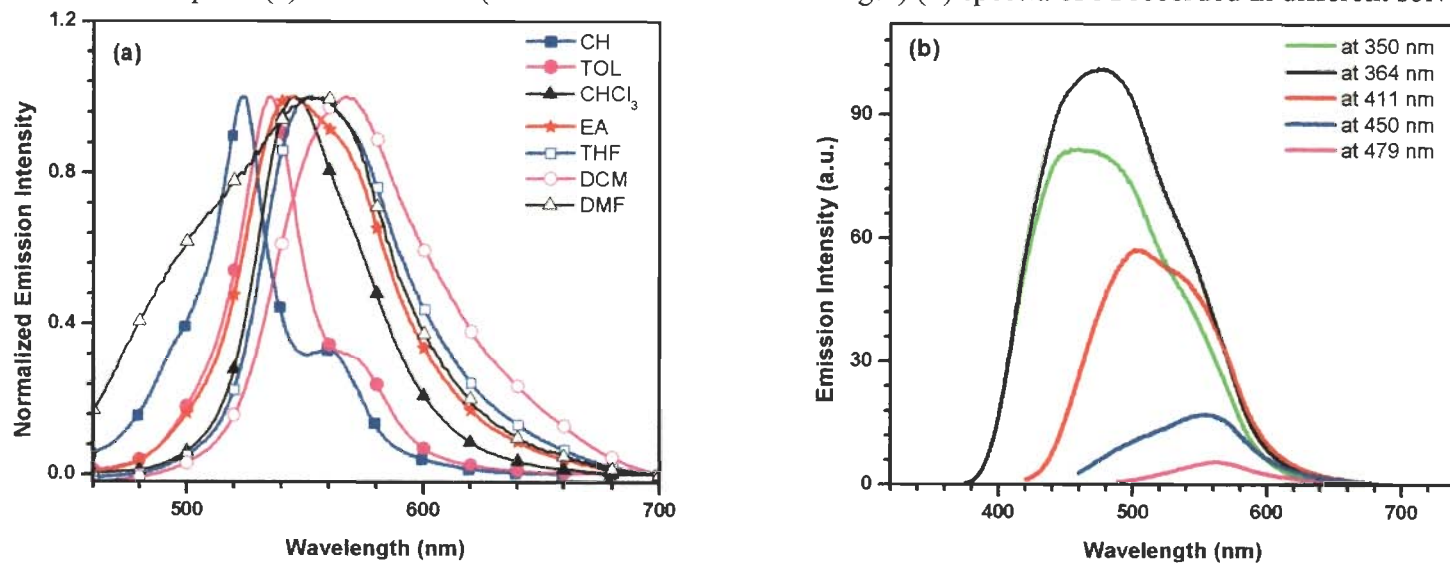


Figure 4.15 Emission spectra of **31** at 450 nm excitation wavelength in different solvents (a) and in DMF at different excitation (b).

Table 4.3 Absorption data of the compounds **26-31** recorded in different solvent.

Compound	λ_{\max} , nm (ϵ_{\max} , $M^{-1}cm^{-1}$) $\times 10^3$							
	Cyclohexane	Toluene	Chloroform	Ethyl acetate	THF	dichloromethane	DMF	acetonitrile
26	283 (26.0),	286 (34.7),	286 (35.9),	283 (31.2),	284 (31.7), 302	285 (33.2), 303	285 (34.6),	283 (36.9),
	301 (21.5),	304 (28.2),	304 (30.7),	301 (26.9),	(26.8), 315	(29.1), 315	304 (31.3),	302 (34.2),
	314 (27.4),	316 (35.3),	316 (37.6),	313 (32.7),	(33.4), 321	(35.4), 321	315 (38.3),	313 (41.1),
	320 (21.9),	322 (33.1),	322 (35.4),	319 (26.9),	(29.0), 379	(32.5), 380	321 (35.9),	320 (34.2),
	378 (42.9),	381 (52.3),	381 (59.6),	377 (51.8),	(53.2), 402	(57.0), 403	381 (61.5),	376 (67.7),
	401 (46.1)	405 (53.9)	404 (64.9)	400 (57.4)	(58.8)	(63.6)	404 (71.7)	399 (77.8)
27	284, 330,	286 (56.9),	286 (57.7),	283 (43.8),	285 (43.3), 330	285 (49.8), 331	286 (51.7),	283 (34.4),
	410, 418	332 (38.5),	332 (39.6),	329 (28.7),	(28.7), 411	(34.7), 412	331 (37.8),	329 (24.8),
		414 (97.5),	414 (108.0),	409 (86.0),	(85.0), 421	(97.5), 424	413 (105.0),	408 (75.1),
		424 (82.1)	421 (100.7)	419 (78.8)	(78.8)	(92.4)	427 (104.0)	420 (73.5)
28	285, 302,	287 (33.5),	287 (35.4),	284 (31.3),	285 (31.7), 303	286 (29.8), 304	287 (36.5),	284 (30.3),
	392, 418	304 (34.4),	305 (37.3),	301 (32.0),	(32.8), 392	(32.3), 400	304 (38.9),	301 (31.9),
		395 (54.2),	399 (59.7),	391 (54.0),	(53.6), 413	(50.8), 410	400 (61.2),	391 (51.9),
		418 (46.8)	412 (57.6)	411 (50.3)	(50.4)	(50.4)	411 (61.4)	407 (51.3)
30	282 (66.9),	287(79.3),	285 (82.7),	283 (74.8),	285 (70.3), 375	285 (78.2), 374	288 (88.3),	-
	371 (116.5),	374 (120.1),	375 (134.0),	372 (114.8),	(109.8), 464	(126.1), 465	377 (136.6),	-
	459 (62.0),	464 (70.0),	465 (72.9),	461 (68.5),	(65.3), 492	(69.2), 492	468 (78.1),	-
	486 (68.5)	488 (72.5)	491 (79.0)	488 (73.9)	(72.4)	(75.1)	496 (87.7)	-
31	308, 364,	310 (90.8),	314 (83.6),	306 (73.1),	306 (73.4), 364	310 (78.9), 368	306 (71.3),	-
	410, 472,	364 (133.8),	370 (136.2),	364 (114.4),	(116.4), 412	(127.8), 410	368 (115.8),	-
	500	413 (97.2),	411 (92.5),	408 (81.9),	(78.9), 477	(85.1), 476	411 (72.0),	-
		476 (75.9),	476 (72.4),	473 (62.8),	(64.5), 506	(66.4), 504	479 (59.6),	-
	503 (69.0)	503 (66.9)	502 (57.2)	(59.7)	(60.7)	506 (54.2)	-	

Table 4.4 Emission data of the compounds **26-31** recorded in different solvent.

Compound	λ_{em} , nm							
	cyclohexane	toluene	chloroform	Ethyl acetate	THF	dichloromethane	DMF	acetonitrile
26	407, 432	412, 436	413, 436	406, 431	410, 434	412, 435	412, 435	408, 430
27	433, 457	438, 463	439, 464	433, 459	437, 462	439, 465	441, 465	433, 457
28	436, 460	449	486	490	498	516	565	557
30	507, 542	513, 549	514, 550	509, 545	513, 549	514, 551	518, 554	-
31	524, 558	535, 568	545	545	552	567	557	-

Table 4.5 Stokes' shift observed for the compounds **26-31** in different solvents and the parameters used for correlation.

Solvents	Orientation polarizability	$E_T(30)$	π^*	Stokes' Shift				
				26	27	28	30	31
Cyclohexane	-0.001	30.9	0	368	829	988	852	916
Toluene	0.0135	33.9	0.54	420	754	1652	999	1189
Chloroform	0.148	39.1	0.58	539	974	3696	911	1532
Ethyl acetate	0.201	38.1	0.55	369	772	3923	845	1572
THF	0.2096	37.4	0.58	485	978	4133	832	1647
dichloromthane	0.219	40.7	0.82	542	806	5010	870	2205
DMF	0.275	43.2	0.88	481	743	6632	856	1810
Acetonitrile	0.306	45.6	0.75	553	715	6617	-	-

It can be clearly seen in Figure 4.15(b) that at 450 nm excitation a less intense ICT band was observed as the excitation wavelength was decreased this ICT band shift towards shorter wavelength and finally merged with the LE state band at 350 nm excitation which appear as single broad band but in actual it is a combination of LE and ICT band. This may be due to the solvation process which causes the emission due to LE state. Since the conversion from the LE to CT state is reversible, the population of the LE state is strongly affected by its solvation dynamics. It might be possible that the rate of the stabilization of CT state of **31** will be slow so that the population of LE state increases which lead to the emission from LE state.

When a fluorophore absorbs light and reach to the excited state, there are several interactions and processes takes place. One of the important interaction is the solvent interaction. When fluorophore comes into the contact of solvent, the solvent stabilize the excited state of fluorophore via non specific (van der Waals interactions operative for molecules in all cases with no exceptions and electrostatic interactions) or specific interactions (pairwise interactions of the chemical nature determined by individual features of the interacting molecules). The estimation of solvent interaction with the fluorophore in excited state is an important tool which gives an idea about the geometry and conformational changes of the fluorophore. Thus general solvent effect was interpreted by Lippert-Mataga plot (Stokes' shift vs orientation polarizability).

The plots Stokes' shifts vs $E_T(30)$ parameter and wave number vs π^* (Kamlet-Taft parameter) for derivatives **26-31** have also been plotted to know the specific interaction of molecules with solvent in the excited state. The Stokes' shift of all the compounds in different solvents is given in Table 4.5. Compound **26** showed no linear relationship in Lippert-Mataga plot (Figure 4.16(a)) indicating some specific interactions are taking place which is confirmed by $E_T(30)$ plot in which it is showing linearity among CH, TOL, CHCl_3 , THF and DCM (Figure

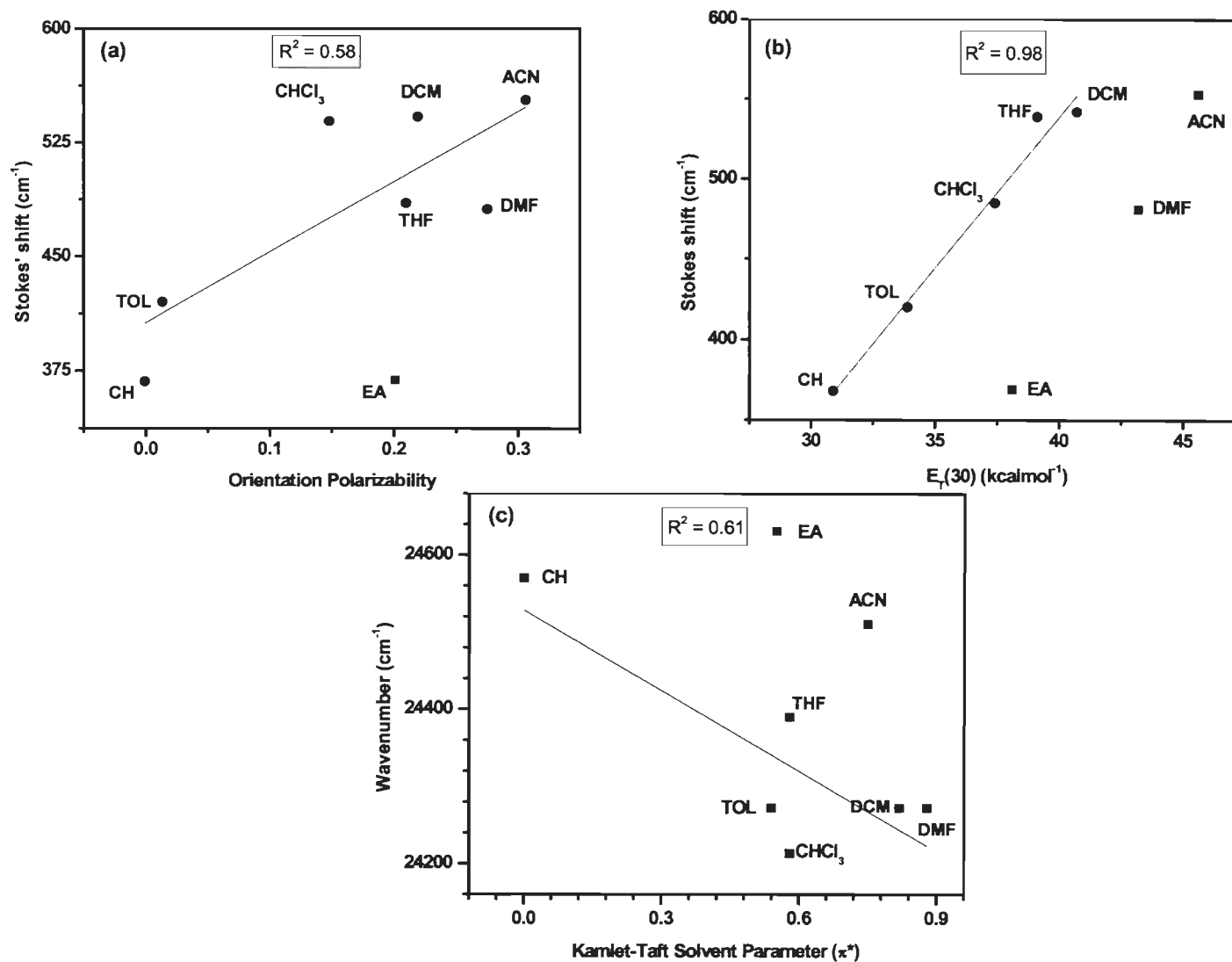


Figure 4.16 Plots for **26** in different solvents (a) Lippert-Mataga plot showing Stokes' shift vs orientation polarizability of the solvents, (b) Stokes' shift vs $E_T(30)$ parameter, (c) emission maxima (in cm^{-1}) vs Kamlet-Taft solvent polarity parameter.

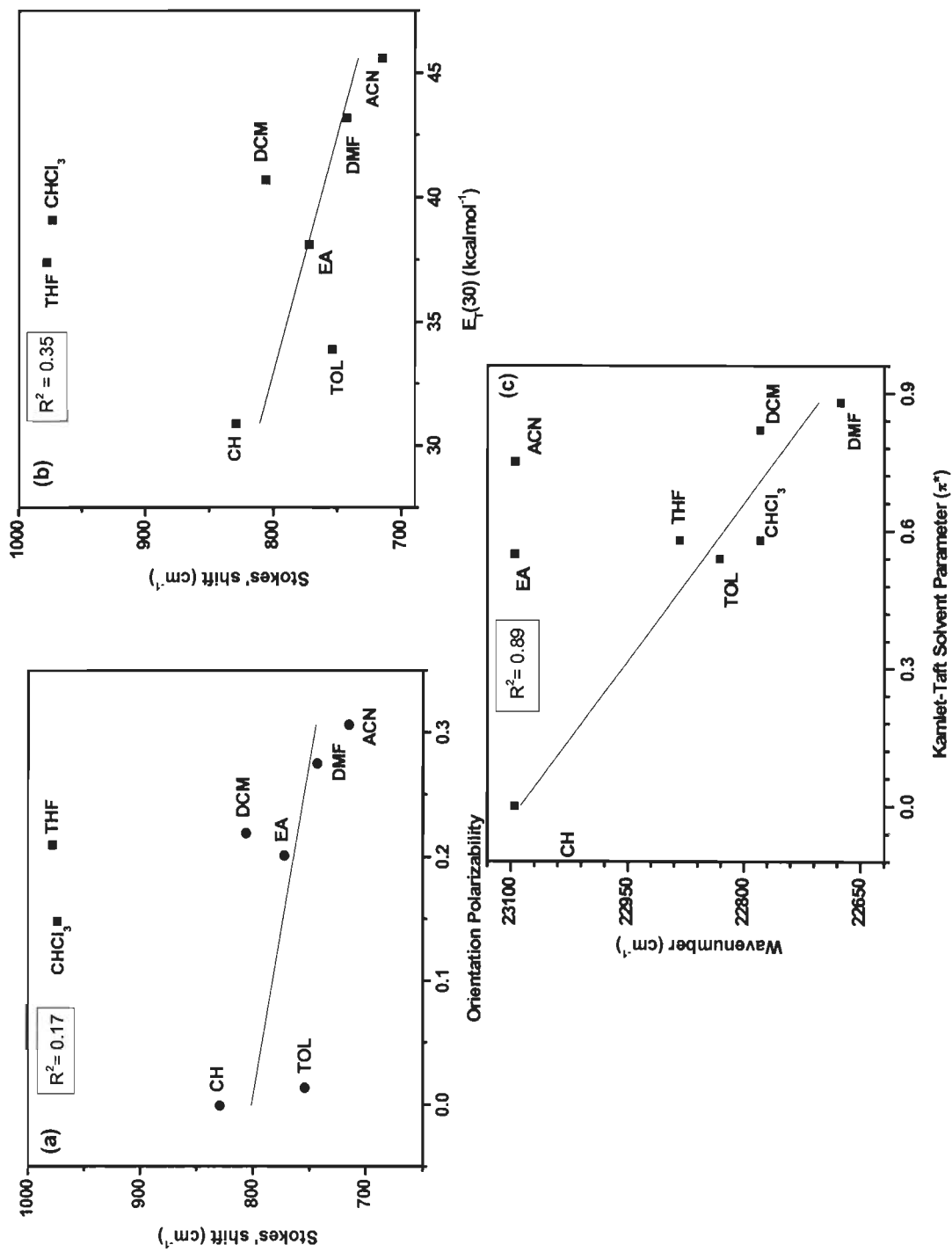


Figure 4.17 Plots for 27 in different solvents (a) Lippert-Mataga plot showing Stokes' shift vs orientation polarizability of the solvents, (b) Stokes' shift vs $E_T(30)$ parameter, (c) emission maxima (in cm⁻¹) vs Kamlet-Taft solvent polarity parameter.

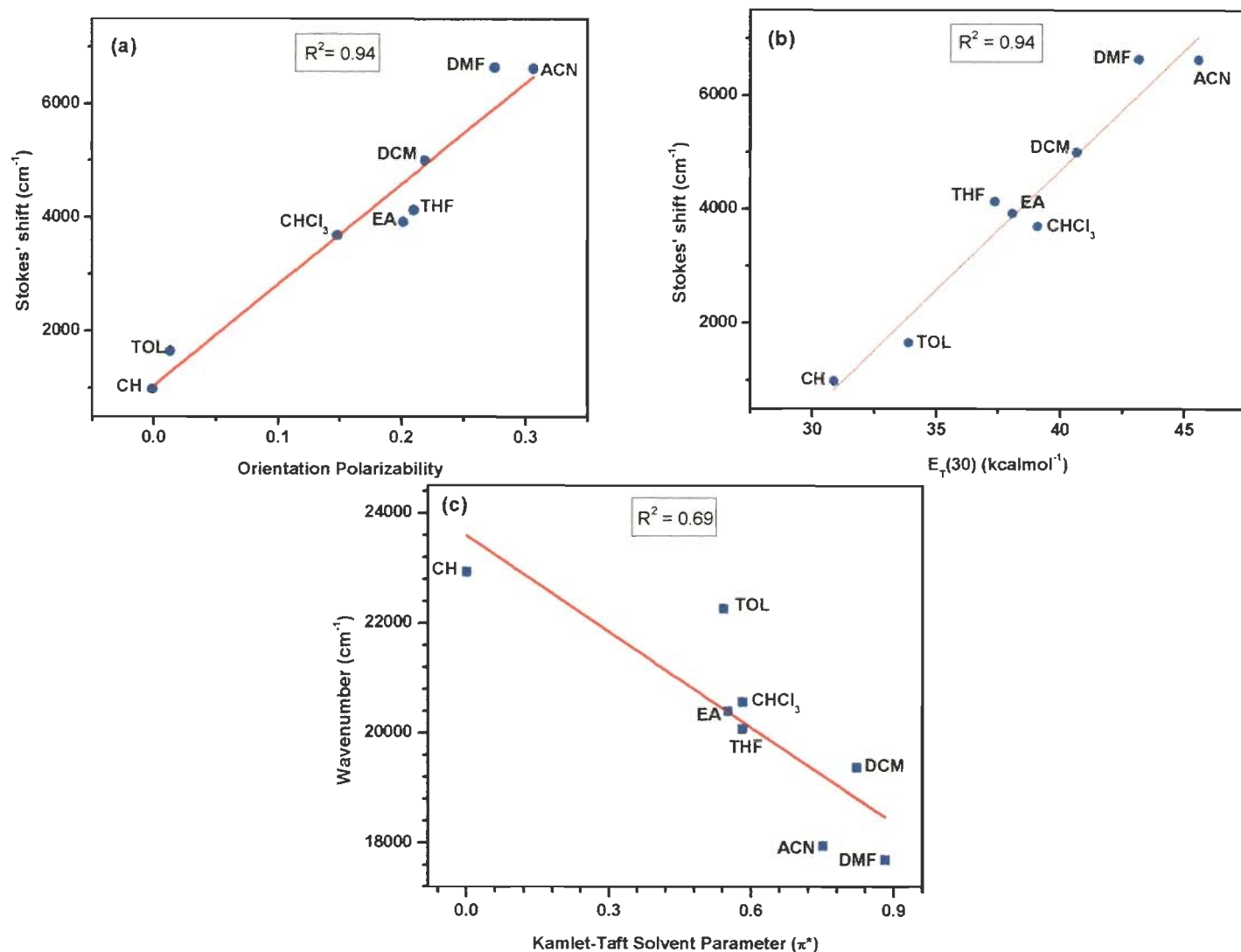


Figure 4.18 Plots for **28** in different solvents (a) Lippert-Mataga plot showing Stokes' shift vs orientation polarizability of the solvents, (b) Stokes' shift vs $E_T(30)$ parameter, (c) emission maxima (in cm^{-1}) vs Kamlet-Taft solvent polarity parameter.

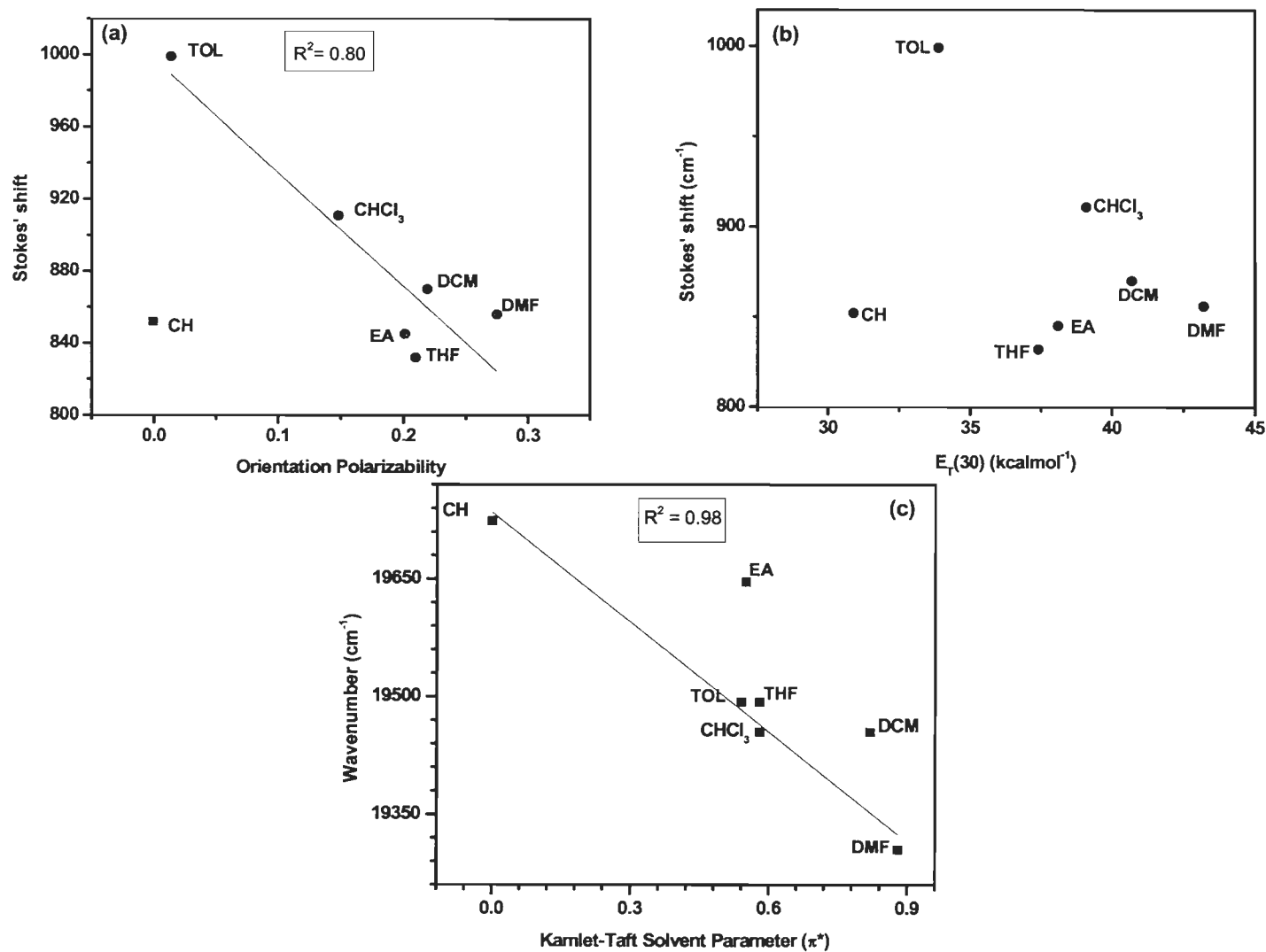


Figure 4.19 Plots for 30 in different solvents (a) Lippert-Mataga plot showing Stokes' shift vs orientation polarizability of the solvents, (b) Stokes' shift vs $E_T(30)$ parameter, (c) emission maxima (in cm⁻¹) vs Kamlet-Taft solvent polarity parameter.

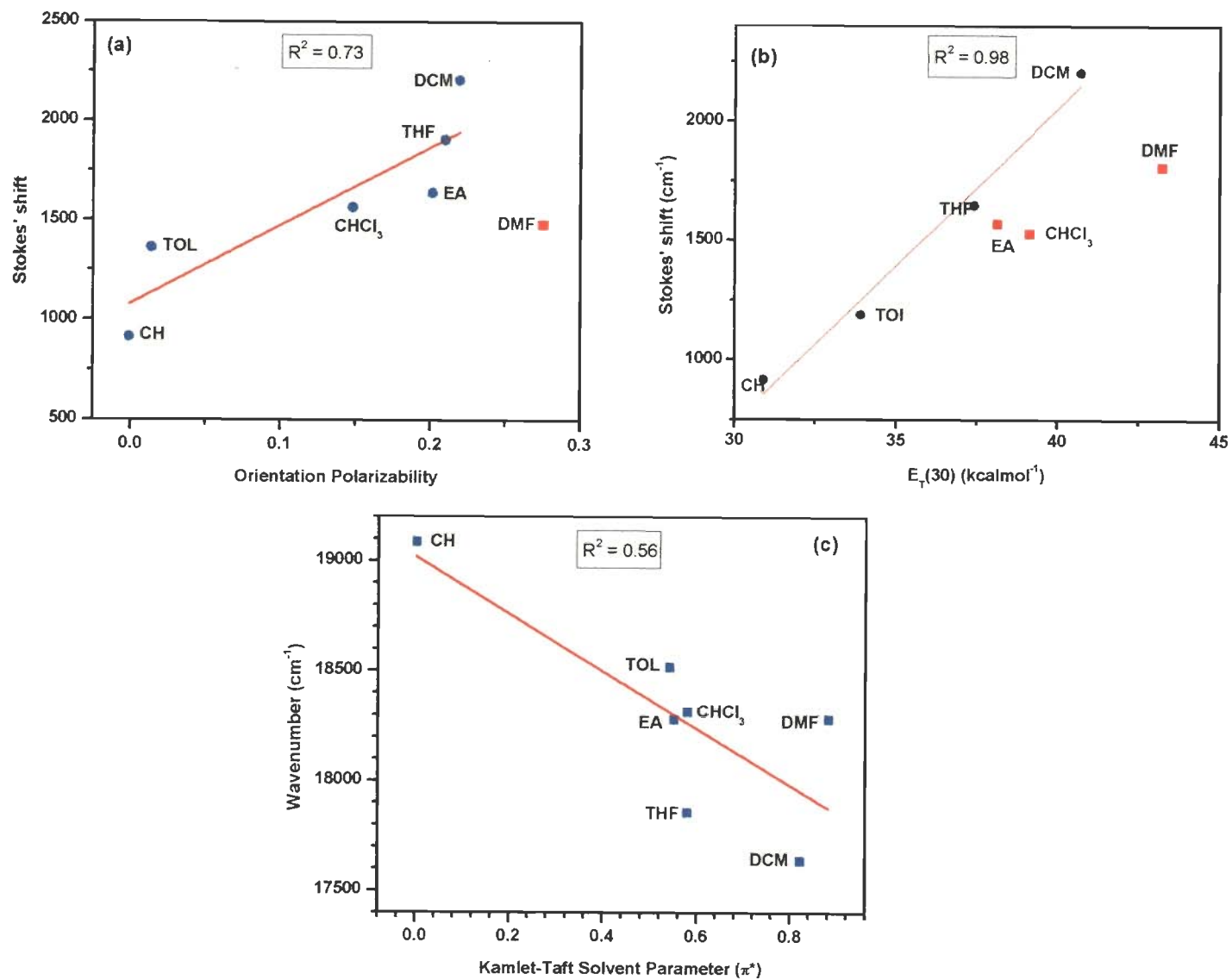


Figure 4.20 Plots for **31** in different solvents (a) Lippert-Mataga plot showing Stokes' shift vs orientation polarizability of the solvents, (b) Stokes' shift vs $E_T(30)$ parameter, (c) emission maxima (in cm⁻¹) vs Kamlet-Taft solvent polarity parameter.

4.16(b). Linearity in $E_T(30)$ indicate some charge transfer character in the excited state which could be due to pyrene which is more electron rich than fluorene. Thus there is a possibility of charge transfer from pyrene to fluorene. No linearity was observed in Kamlet-Taft plot of **26** (Figure 4.16(c)). Compound **27** also show deviation from linearity in Lippert-Mataga, $E_T(30)$ and Kamlet-Taft showing less general and specific interaction taking place (Figure 4.17). Compound **30** displayed linearity in Lippert-Mataga and Kamlet-Taft but exhibited deviation in linearity in $E_T(30)$ (Figure 4.19) suggests the presence of general and hydrogen bonding solvent interaction and the absence of CT state in the excited state.

Monosubstituted diphenyl amine derivative **28** exhibited better linear relationship in Lippert-Mataga and $E_T(30)$ (Figure 4.18). This suggests that both general and specific interactions are taking place in the excited state. Linearity in $E_T(30)$ confirms the specific interaction such as a formation of ICT state in the molecule in its excited state due to the presence of electron donor diphenylamine.

But the tetrasubstituted derivative **31** showed deviation from linearity in Lippert-Mataga as compared to that of **28** which suggest that no general solvent effect is taking place (Figure 4.20 (a)). $E_T(30)$ plot show linearity with CH, TOL, THF and DCM showing charge transfer in the molecule (Figure 4.20(b)). The extent of charge transfer in **31** is less as compared to the derivative having one donor substituent (**28**). Thus the charge transfer decreases as the number of donor substituents increases on the pyrene core and the symmetry increases. Molecular symmetry also play an important role in defining the charge transfer in the excited state.

The absorption spectra of cyanoacrylic acid derivatives (**35a-35d**) were recorded in THF solution ($2 \times 10^{-5}M$) are shown in Figure 4.21. The data was listed in Table 4.6. Compound **35a** showed vibronic absorption pattern due to $\pi-\pi^*$ transition and is more red shifted and broad as

compared to that of pyrene.⁴⁸ This is due to the extended conjugation through ethynyl linkage and also due to some charge transfer character. The partial charge transfer assignment was confirmed by the red shifted and broader absorption as compared to their corresponding aldehydes (Figure 4.22). This suggests that pyrene acts as a weak π -donor and cyanoacrylic acid act as a π -acceptor. It is well known that pyrene can either act as π -donor or π -acceptor according to the substituent present on it.⁴⁰

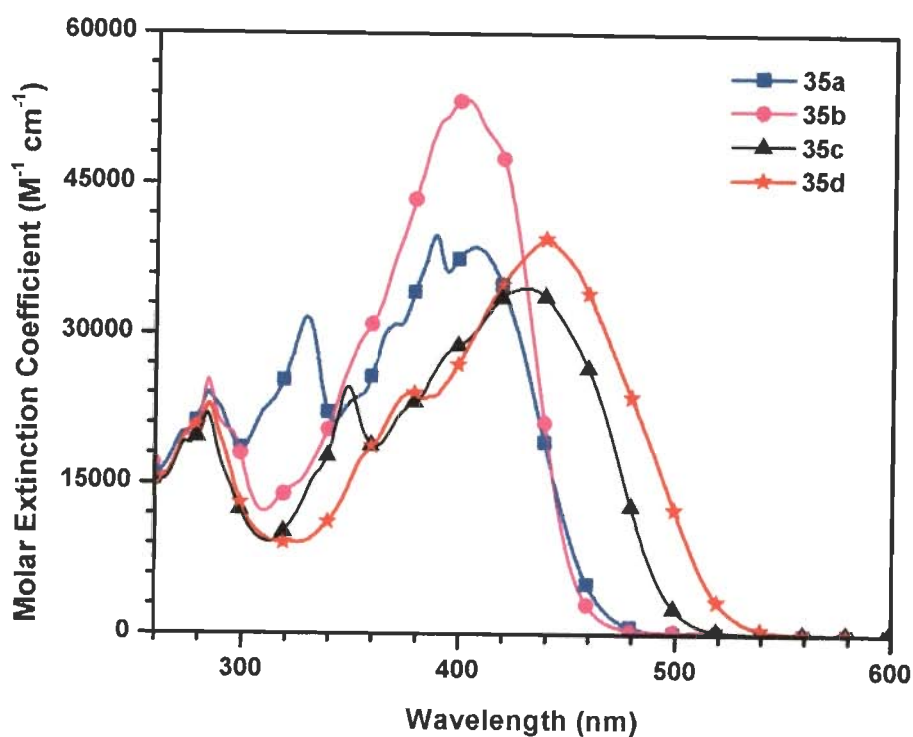


Figure 4.21 Absorption spectra of the dyes **35a-35d** recorded in THF.

By replacing the phenyl spacer with fluorenyl spacer in **35b**, the absorption spectra show red shift and become broader and less resolved pattern. It also exhibits high molar extinction coefficient than **35a**. This is due to presence of fluorene because the fused system of fluorene increases the conjugation and also increases the electronic coupling between pyrene and cyanoacrylic acid which facilitates the electron transfer.

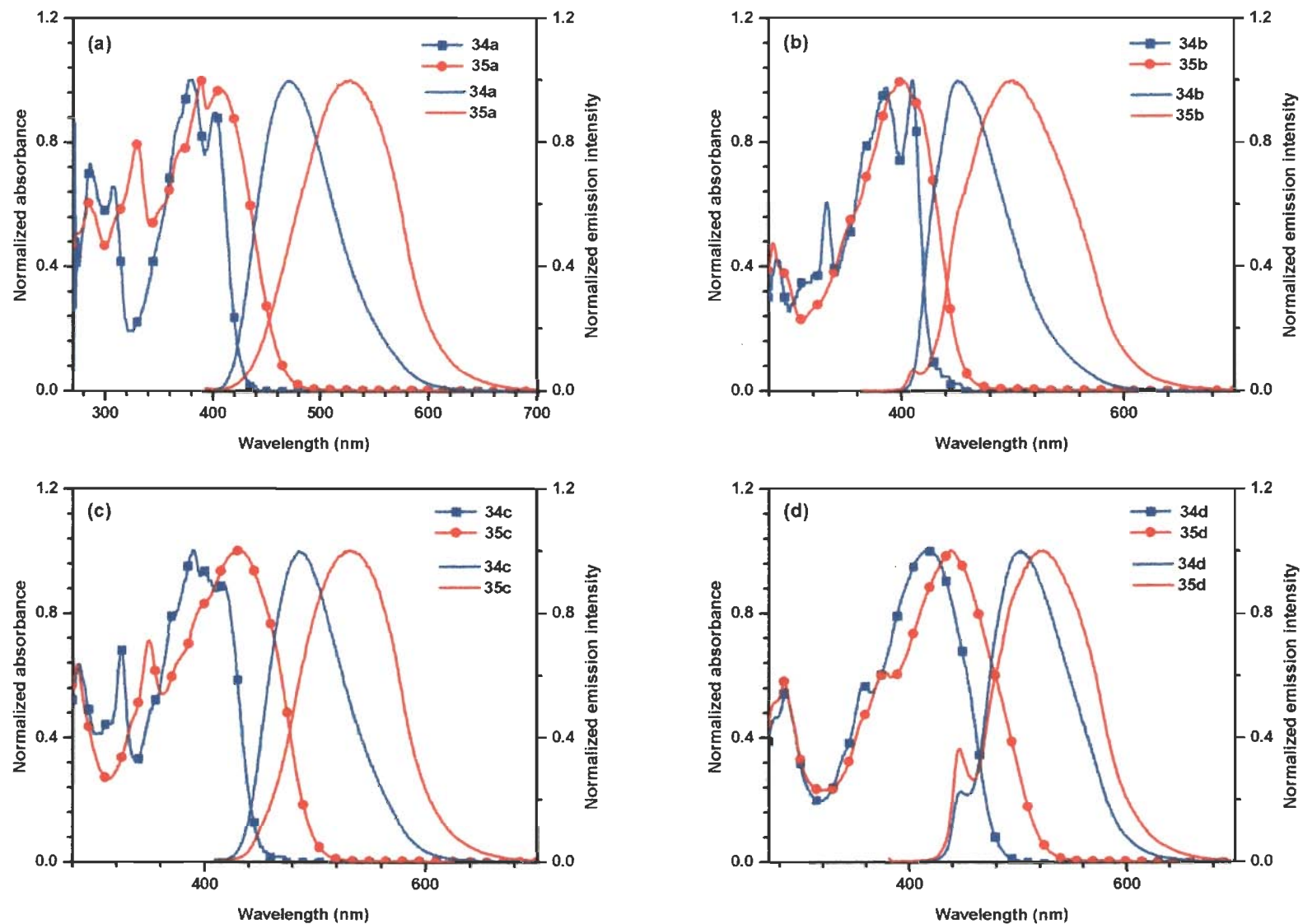
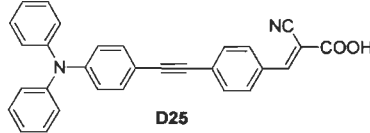
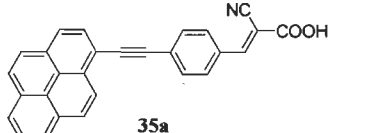
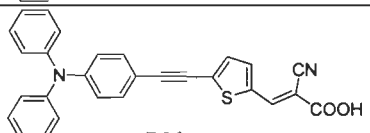
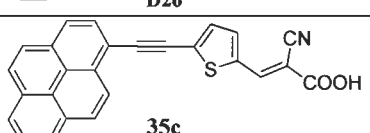


Figure 4.22 Comparison of absorption (filled) and emission (line) spectra of (a) **35a**, (b) **35b**, (c) **35c**, (d) **35d** with their corresponding aldehydes (**34a-35d**) recorded in THF.

Table 4.6 Optical properties of dyes (35a-35d) recorded in THF solution

Dyes	λ_{\max} , nm (ϵ_{\max} , $M^{-1}cm^{-1}$) $\times 10^3$	λ_{em} , nm(Φ_F)	Stokes' shift, cm^{-1}
34a	308, 379, 402	471	3644
34b	387, 410	451	2217
34c	324, 389, 415	485	3478
34d	357, 416	447 (sh), 503	4158
35a	329 (31.6), 370 (31.0), 388 (39.8), 407 (38.7)	527	5595
35b	390 (51.2), 401 (53.5), 411 (50.4)	501	4371
35c	349 (24.6), 430 (34.6)	531 (0.17)	4423
35d	377 (24.0), 439 (39.5)	446 (sh), 523 (0.27)	3659

Table 4.7 Comparison of optical and electrochemical properties of 35a, 35c with D25 and D26.

Dyes	λ_{\max} , nm, ϵ_{\max} , $M^{-1}cm^{-1} \times 10^3$		λ_{em} , nm		E_{0-0} , eV	E_{ox} , eV vs NHE	E_{LUMO} , eV vs NHE	Ref.
	THF	DCM	THF	DCM				
 D25	399 (29.6)	438 (26.0)	579	646	2.59/2.48 (ACN/DMF)	1.13/1.22 (ACN/DMF)	-1.46/-1.26 (ACN/DMF)	12
 35a	407 (38.7)	417	527	572	2.75	1.69	-1.06	This work
 D26	-	457 (17.6)	-	640	2.32	1.23	-1.09	11
 35c	430 (34.6)	454	531	573	2.60	1.73	-0.87	This work

The absorption pattern of **35c** exhibited similar pattern but red shifted as compared to **35a**. The lowest energy band is more red shifted due to the presence of thiophene which increases the conjugation and donor capacity being an electron rich moiety. We have compared **35a** and **35c** with compounds having triphenylamine as a donor instead of pyrene as shown in Table 4.7. **35a** exhibited more red shifted absorption in THF as compared to **D25**¹². This may be due to the reason that coplanarity between pyrene and phenyl ethynyl is more as compared to triphenylamine. Thus more effective conjugation in **35a** red shifts the absorption wavelength than **D25**. The absorption wavelength of **D25** showed 39 nm bathochromic shift in DCM as compared to THF. While **35a** showed only 10 nm red shift in DCM than in THF. This suggests the weak donor nature of pyrene than triphenylamine but its planar nature increase the absorption wavelength in less polar solvent.

There is no significant difference in the absorption wavelength of derivatives with thiophene spacer **D26**¹¹ and **35c** when recorded in dichloromethane. This may be due to the electron richness of thiophene which increases the donor strength of pyrene being more planar with pyrene as compared to triphenylamine in **D26**. The above explanation revealed that pyrene can also be used as donor in organic dyes which can provide more planarity for effective conjugation. Further red shift was observed in absorption profile on introduction bithiophene as a spacer in **35d**. This kind of red shift was observed previously by increasing the thiophene unit.⁵²

The emission spectra of the dyes (**35a-35d**) were recorded in THF solution (2×10^{-5} M) and shown in Figure 4.23. All the derivatives exhibited broad and red shifted emission as compared to pyrene. The red shifted and broad emission band might be due to the intramolecular charge transfer state or excimer formation or molecular aggregation. Dye **35b** showed blue shifted emission as compared to **35a**. This could be due to H-aggregation of dye **35b** in the excited state.

Compound **35d** displayed a hump at lower wavelength which can be attributed to either locally excited state or monomer and the low energy band is either due to intramolecular charge transfer state or excimer. All the derivatives emit in the range of 501-531 nm.

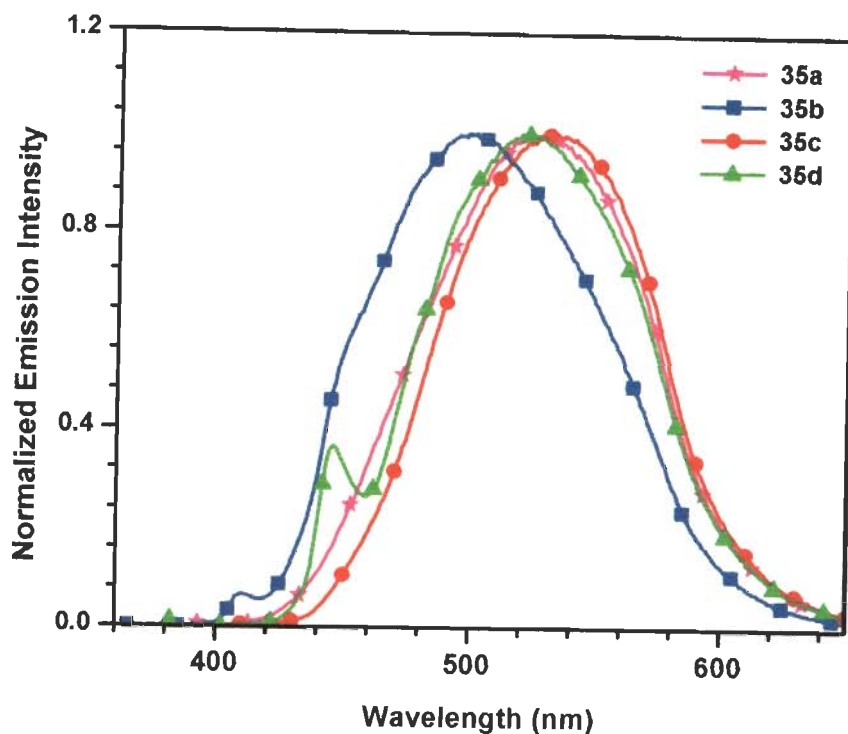


Figure 4.23 Emission spectra of the dyes **35a-35d** recorded in THF.

The solvatochromism study has been done to measure the solvent interaction in ground and excited states. The absorption and emission spectra of **35a-35d** recorded in different solvent polarity are shown in Figures 4.24 & 4.25. The values are collected in Tables 4.8 & 4.9 respectively. The dyes are completely soluble in THF but exhibited poor solubility in other solvents. There was no significant difference observed in absorption wavelength of dyes **35a-35d** in cyclohexane, toluene and dcm. This indicates that the dipole moment of ground state and non polar locally excited state is almost similar. The slight blue shift in THF may be due to hydrogen

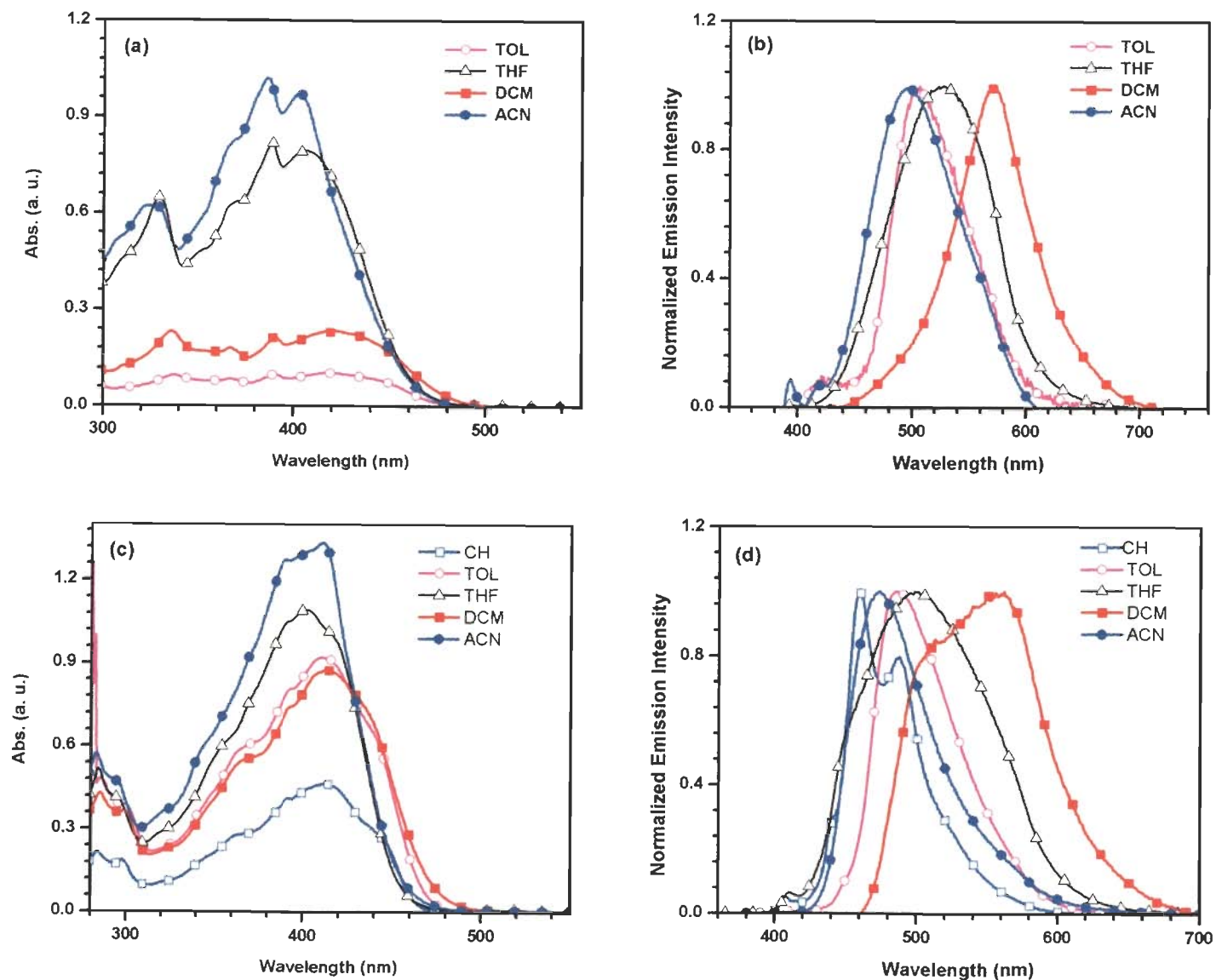


Figure 4.24 Absorption and emission spectra of 35a (a), (b) and 35b (c), (d) recorded in different solvents.

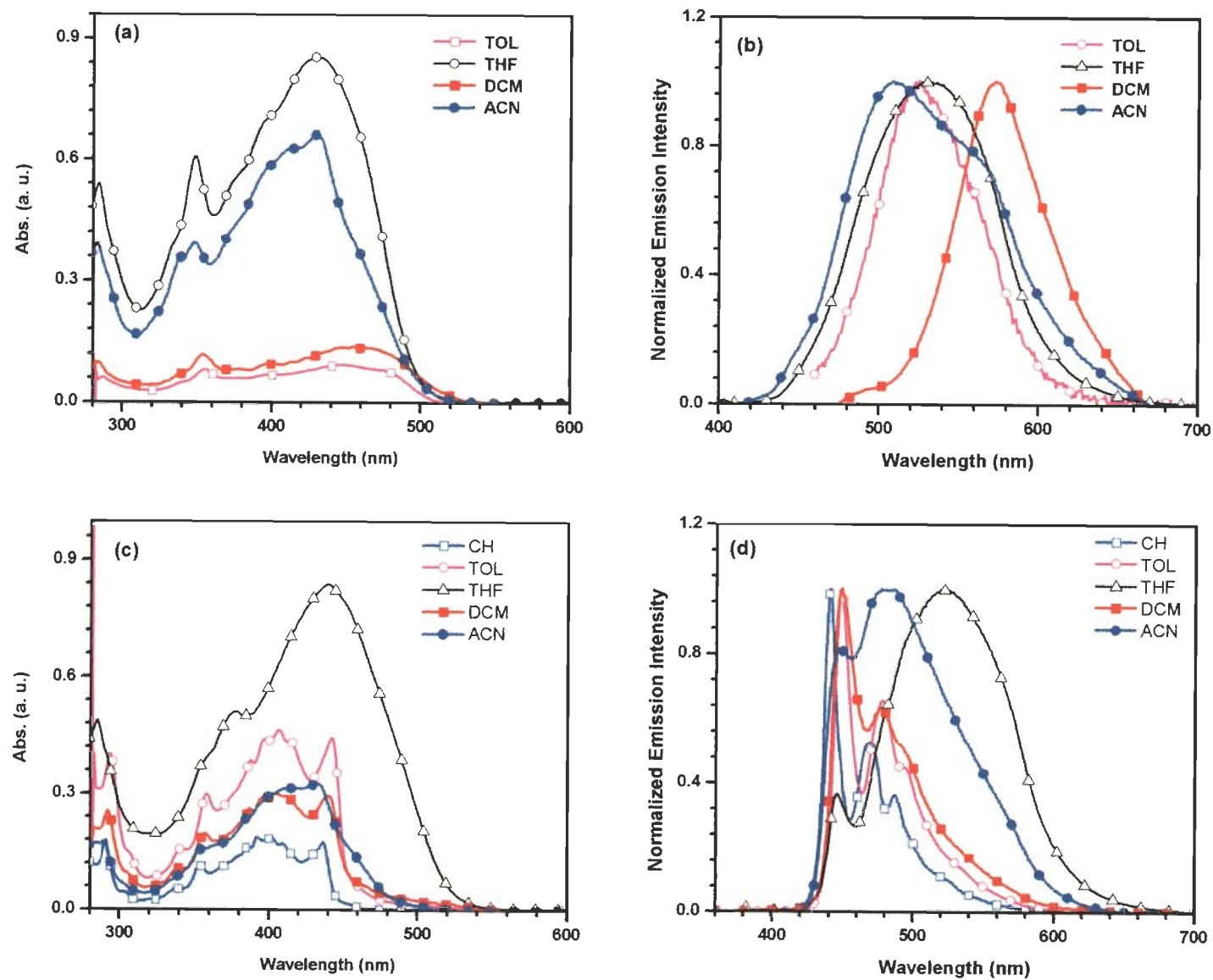


Figure 4.25 Absorption and emission spectra of 35c (a), (b) and 35d (c), (d) recorded in different solvents.

Table 4.6 Absorption data of the dyes **35a-35d** recorded in different solvent.

Dyes	λ_{\max} , nm				
	Cyclohexane	Toluene	THF	Dichloromethane	acetonitrile
35a	-	338, 367, 391, 418	329, 370, 388, 407	336, 367, 390, 417	327, 368, 386, 403
35b	412	392, 410	390, 401, 411	392, 414	390, 411
35c	-	355, 447	349, 430	354, 454	348, 430
35d	354, 401, 436	358, 406, 441	377, 439	357, 405, 439	359, 413, 433

Table 4.7 Emission data of the dyes **35a-35d** recorded in different solvent.

Dyes	λ_{em} , nm				
	cyclohexane	toluene	THF	dichloromethane	acetonitrile
35a		506	527	572	498
35b	459, 487	486	501	561	473
35c		525	531	573	509
35d	441, 469	449, 478	446, 523	449, 477	448, 477

Table 4.10 Stokes' shift observed for the dyes (**35a-35d**) in different solvents and the parameters used for correlation

Solvents	Orientation polarizability	$E_T(30)$	π^*	Stokes' Shift			
				35a	35b	35c	35d
Cyclohexane	-0.001	30.9	0	-	2485	-	260
Toluene	0.0135	33.9	0.54	4161	3814	3324	404
THF	0.2096	37.4	0.58	5595	4371	4423	358
dichloromthane	0.219	40.7	0.82	6498	6329	4574	507
Acetonitrile	0.306	45.6	0.75	4734	3189	3609	773

bonding interaction between the hydrogen of carboxylic acid and oxygen of THF. Blue shift in acetonitrile can be attributed to the partial deprotonation of the dye.

The emission spectra of dyes **35a-35c** displayed positive solvatochromism from cyclohexane, toluene, THF to dichloromethane. The red shift in polar solvent may be due to intramolecular charge transfer state in the excited state. But these dyes showed a blue shift in acetonitrile solution.

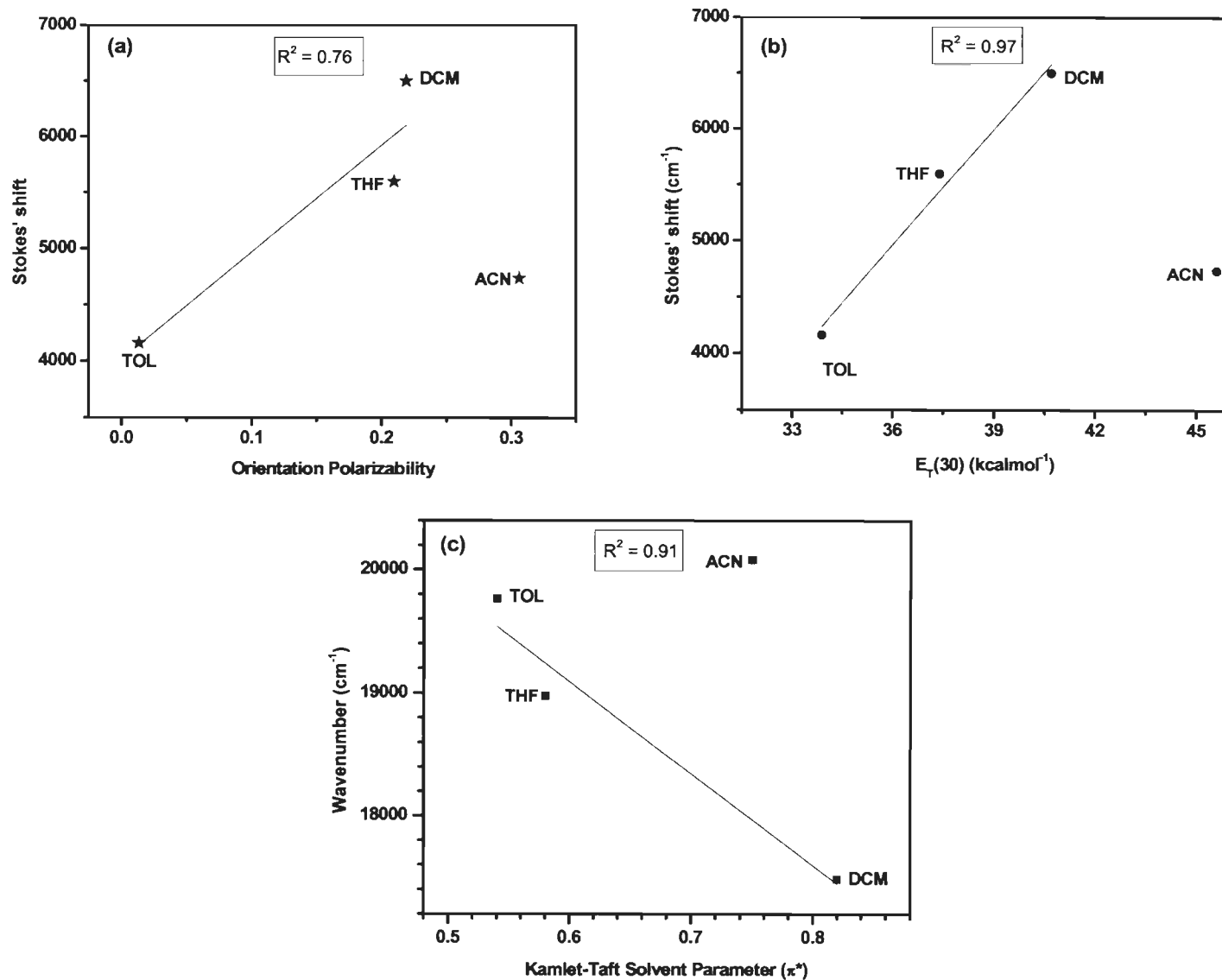


Figure 4.26 Plots for 35a in different solvents (a) Lippert-Mataga plot showing Stokes' shift vs orientation polarizability of the solvents, (b) Stokes' shift vs $E_T(30)$ parameter, (c) emission maxima (in cm⁻¹) vs Kamlet-Taft solvent polarity parameter.

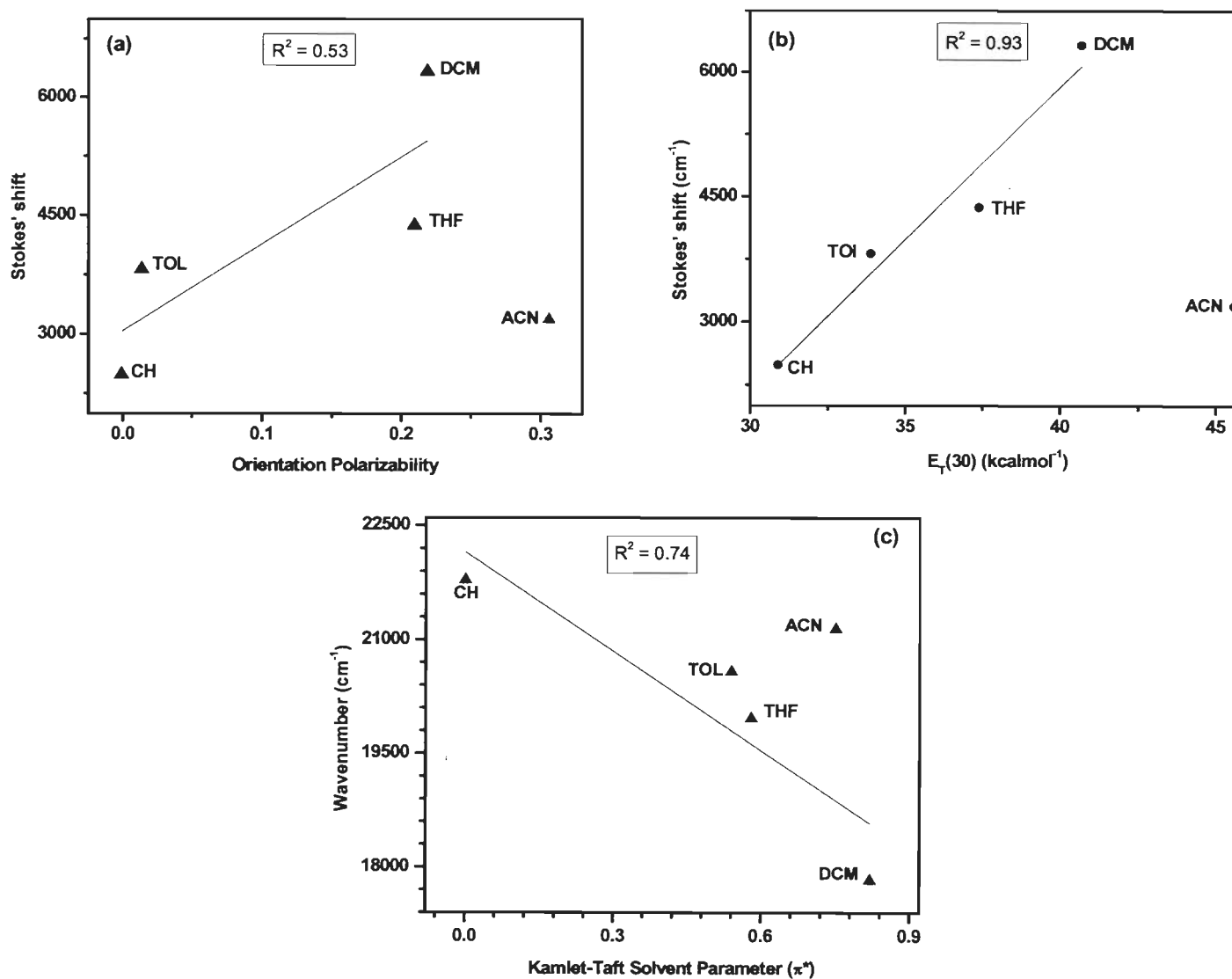


Figure 4.27 Plots for **35b** in different solvents (a) Lippert-Mataga plot showing Stokes' shift vs orientation polarizability of the solvents, (b) Stokes' shift vs $E_T(30)$ parameter, (c) emission maxima (in cm⁻¹) vs Kamlet-Taft solvent polarity parameter.

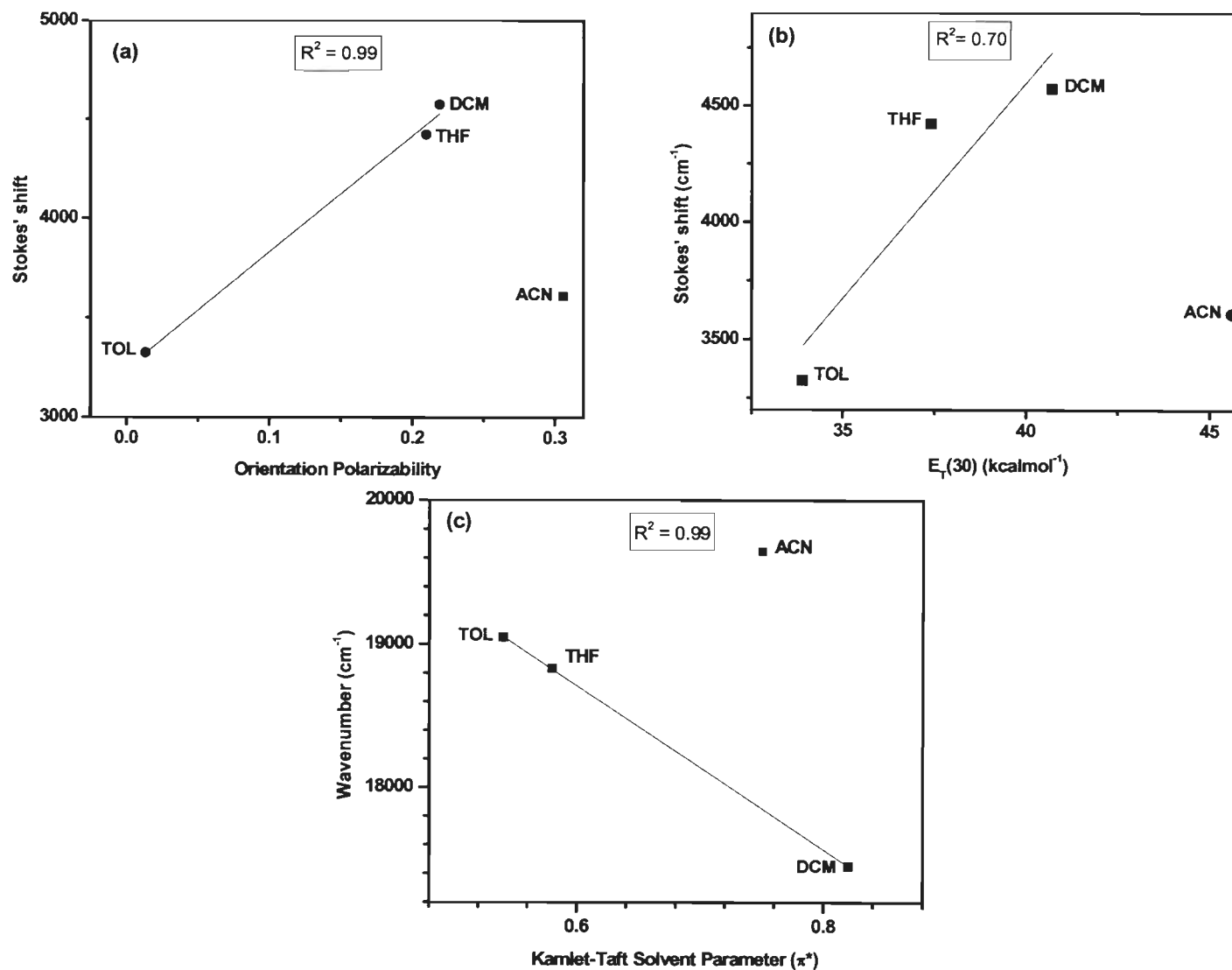


Figure 4.28 Plots for **35c** in different solvents (a) Lippert-Mataga plot showing Stokes' shift vs orientation polarizability of the solvents, (b) Stokes' shift vs $E_T(30)$ parameter, (c) emission maxima (in cm⁻¹) vs Kamlet-Taft solvent polarity parameter.

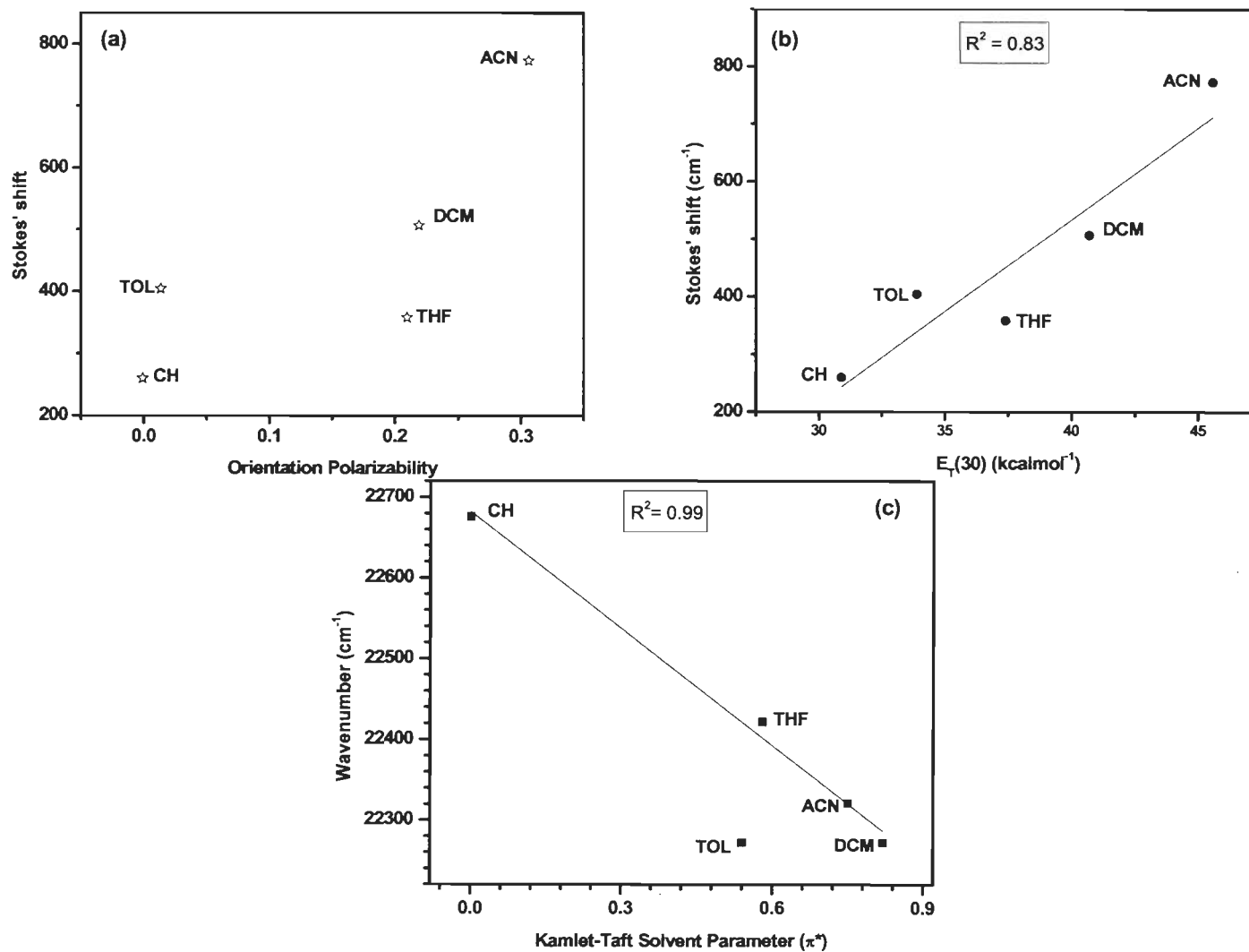


Figure 4.29 Plots for **35d** in different solvents (a) Lippert-Mataga plot showing Stokes' shift vs orientation polarizability of the solvents, (b) Stokes' shift vs E_T(30) parameter, (c) emission maxima (in cm⁻¹) vs Kamlet-Taft solvent polarity parameter.

Dye **35d** exhibited two emission peak in cyclohexane, toluene and dichloromethane solution. The high energy band can be attributed to the emission from locally excited state and the emission at higher wavelength occurred due to intramolecular charge transfer (ICT) state. Figure 4.25(d) indicate that, the intensity of ICT band increases and that of LE state decreases in THF and acetonitrile.

Lippert-Mataga, $E_T(30)$ and Kamlett-Taft plots of all the dyes (**35a-35d**) have shown in Figures 4.26-4.29. Nonlinearity in Lippert-Mataga plots indicates that non specific interactions are not taking place (Figures 4.236a, 4.27a, 4.28a, 4.29a) in the dyes **35a-35d**. On the other hand linearity in $E_T(30)$ and Kamlett-Taft plots of all the dyes indicates that specific interactions like charge transfer and hydrogen bonding interactions are prominent.

4.2.3 Thermal properties

The thermal properties of the compounds **26-31** were studied by TGA/DTA/DTG (See the Table 4.11 for relevant parameters). TGA curves are shown in Figure 4.30. The temperature at 5% wt. loss is in the range of 394-467°C. All the derivatives (**26-31**) exhibited excellent thermal stability and the decomposition temperatures are in the range of 419-735°C. Compound **27** show lower decomposition as compared to **26** due to the presence of butyl chain. The decomposition temperature is least for **30** which is due to the presence of long alkyl chain still it showed higher decomposition temperature than previously reported 1,3,6,8-tetrakis(9,9-dihexyl-9*H*-fluoren-2-yl)pyrene (**T1**).⁴⁸ This shows that ethyne linkage is also responsible for increasing the thermal stability.

Incorporation of diphenylamine increases the thermal stability of **28** and **31**. Decomposition temperature of **28** was found higher than *N,N*-diphenyl-4-(pyren-1-yl)aniline (**PyTPA**)⁵³ which

clearly indicates that fluorene enhances the thermal stability in **28**. Compound **31** exhibited highest decomposition temperature among all. This may be due to presence of four diphenylamine substituents and its rigid structure which increase the thermal stability tremendously. All the derivatives are enough thermally stable for the use in OLEDs and show higher decomposition than other reported blue- and yellow emitting material.^{18,54}

Table 4.11 Thermal data of the compounds **26-31**.

Compound	T _{onset} (°C)	T _d (°C)	T _m (°C)	Ref.
26	435	460	150	This work
27	449	426	264	This work
28	421	473	210	This work
30	394	419	110	This work
31	467	735	274	This work
PyTPA	-	416	160	53
T1	-	377	-	48

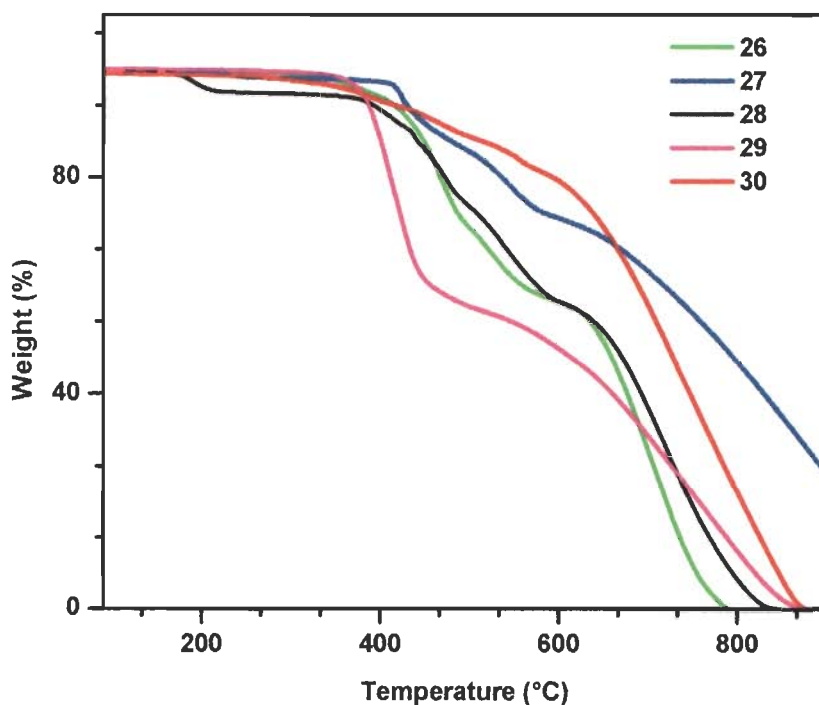


Figure 4.30 TGA curves of the compounds **26-31**

4.2.4 Electrochemical properties

The electrochemistry of the compounds was studied by cyclic voltammetry and differential pulse voltammetry. The results are listed in Table 4.12. Figures 4.31 & 4.32 shows cyclic voltammograms and differential pulse voltammograms of **26**, **27** & **30** and **28** & **31** respectively. Compound **26** showed two oxidation peaks one is reversible and another is irreversible at higher oxidation potential which might be to the formation of cation and dication radical respectively. Compound **27** showed one quasi reversible oxidation peak which is at same potential as in **26**. Tetrasubstituted derivatives (**29** and **30**) exhibited two quasi reversible oxidation peaks which are cathodically shifted as compared to **26**. The cathodic shift may be due to the presence of four fluorene moiety at the periphery which increases the electron density on pyrene and make it more prone to oxidation.

Diphenylamine substituted derivatives (**28** & **31**) show two quasi reversible oxidation peak. The peak at lower oxidation originates due to electron rich diphenylamine while another anodically shifted peak is due to oxidation of pyrene core. The first oxidation of **31** occurs at higher oxidation potential as compared to **28** which indicate more intramolecular donor-acceptor interaction in the molecule. While another oxidation of **31** (due to pyrene) is at low potential as compared to monosubstituted one (**28**) due to the the presence of four fluorene unit which increase the electron density on pyrene as described above. HOMO/LUMO level of the model compounds **26** and **27** is almost similar. While the incorporation of diphenylamine (as **28** & **31**)

Table 4.12 Electrochemical data of the compounds **26-31** measured in dichloromethane.

Compound	E_{ox}^a (ΔE_p) mV	HOMO ^c (eV)	LUMO ^d (eV)	E_{0-0}^e , eV
26	752	5.55	2.50	3.05
27	752	5.55	2.69	2.86
28	396 (65), 792 (66)	5.20	2.44	2.76
30	660 (48), 920 (66)	5.46	3.00	2.46
31	408 (71), 748 (61)	5.21	2.87	2.34

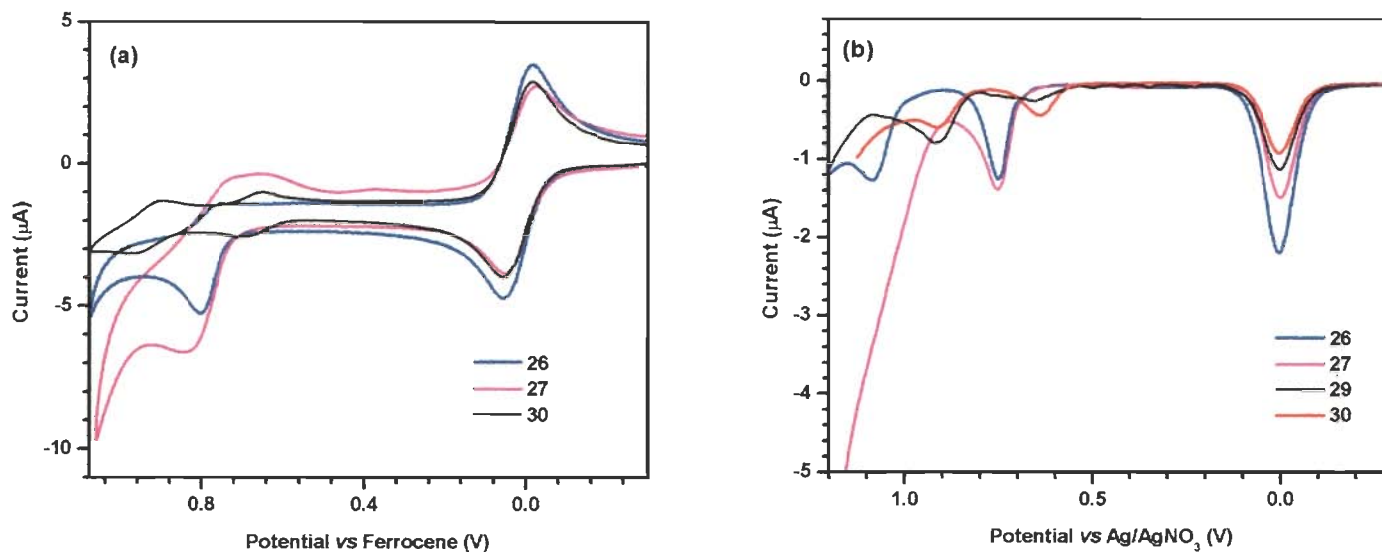


Figure 4.31 Cyclic voltammogram (a) and DPV (b) of **26**, **27** & **30** recorded in dichloromethane solution (2×10^{-5} M) (ferrocene as internal reference).

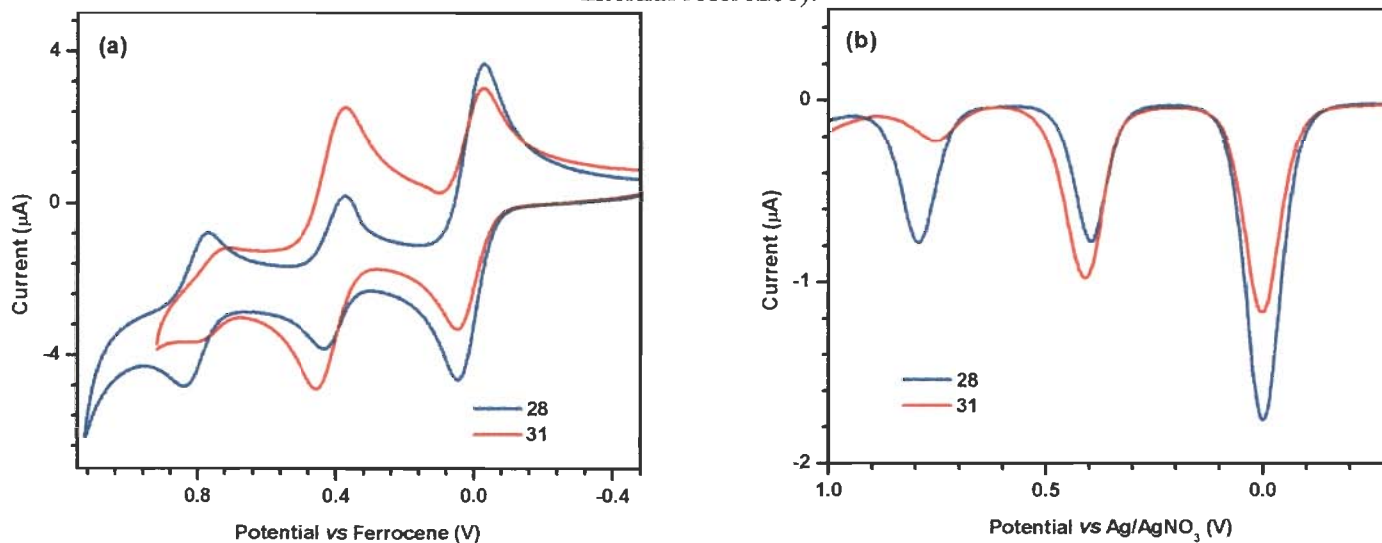


Figure 4.32 Cyclic voltammogram (a) and DPV (b) of **28** & **31** recorded in dichloromethane (ferrocene as internal reference).

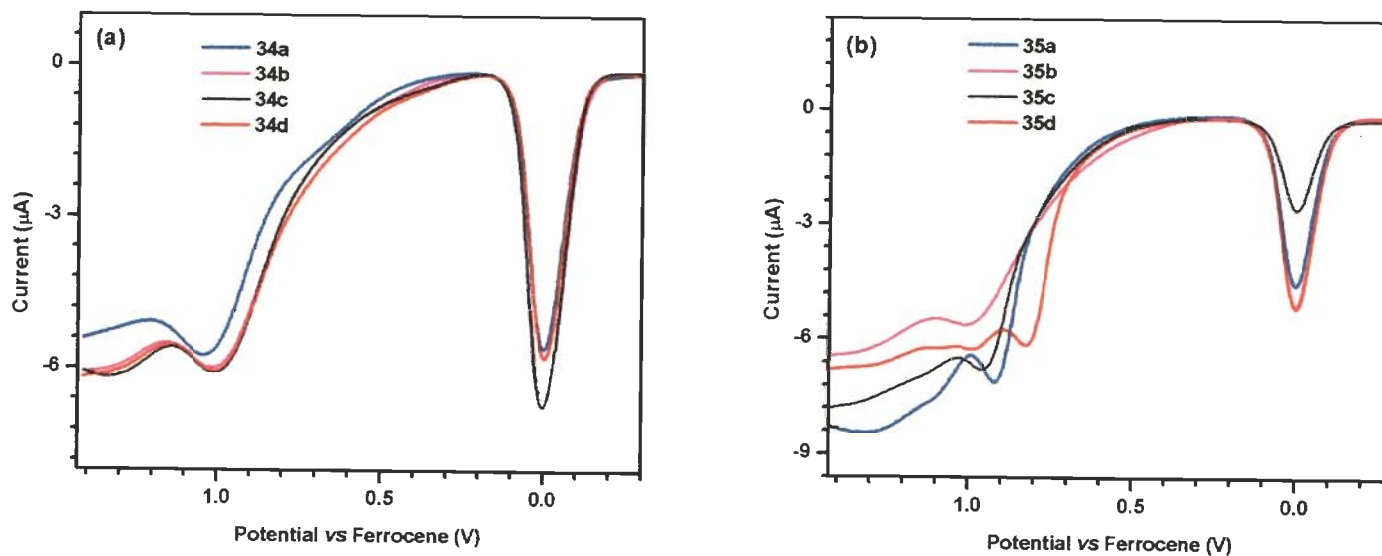


Figure 4.33 DPV of **34a-34d** (a) and **35a-35d** (b) recorded in THF (ferrocene as internal reference).

Table 4.13 Electrochemical data of **34a-34d** and **35a-35d** measured in THF.

Dyes	E_{ox} , mV	HOMO (eV)	LUMO (eV)	E_{0-0} , eV	E_{0-0}^* , V
34a	1040	5.84	2.90	2.94	-
34b	1020	5.82	2.87	2.95	-
34c	1016	5.82	3.00	2.80	-
34d	1004	5.80	3.12	2.68	-
35a	920	5.72	2.97	2.75	-1.060
35b	1016	5.82	3.01	2.81	-1.024
35c	956	5.76	3.16	2.60	-0.874
35d	828	5.63	3.04	2.59	-0.992

increases the HOMO/LUMO levels and lowers the band gap when compared to their corresponding parents (**26** & **30**). Rising of HOMO level may facilitate the transportation of holes.

The differential pulse voltammogram of **35a-35d** along with their corresponding aldehydes (**34a-34d**) are given in Figure 4.33. The DPV were recorded in THF solution (2×10^{-5} M). All the dyes exhibited one irreversible oxidation peak. Electrochemical data (Table 4.13) revealed a favorable ground state potential (1.59-1.78 V) which are more positive than the iodide/triiodide redox couple (~ 0.42 V vs NHE) and suggest facile dye regeneration by the electrolyte. The HOMO/LUMO level raises by increasing the spacer length i.e. **35d** show higher HOMO/LUMO as compared to **35c**. The excited state oxidation potentials, E_{ox}^* , observed for the dyes (-0.87 to -1.06 V versus NHE) are more negative than the conduction band edge energy level of the TiO₂ electrode and favors the electron injection into the conduction band of TiO₂ thermodynamically. Moreover the rod like structure of the dye can be useful for the grafting over semiconductor surface and for increasing the charge injection on the TiO₂ surface. Thus these dyes can be used for fabricating DSSC device.

4.2.5 Electroluminescent properties

Two types of OLED devices were fabricated ITO/PEDOT:PSS/**26**, **27**, **28**, **30** or **31**/TPBI/LiF/Al (Device I) and ITO/PEDOT:PSS/CBP-(**26**, **27**, **28**, **30** or **31**)/TPBI/LiF/Al (Device II). Where ITO act as anode, PEDOT:PSS as hole-injection layer and LiF/Al as cathode. Compounds **26-31** were used as hole transporting and emitting material in Device I while host material 4,4'-Bis(9*H*-carbazol-9-yl)biphenyl (CBP) doped with compounds **26-31** act as hole transporting and emitting layer in Device II (Figure 4.34).

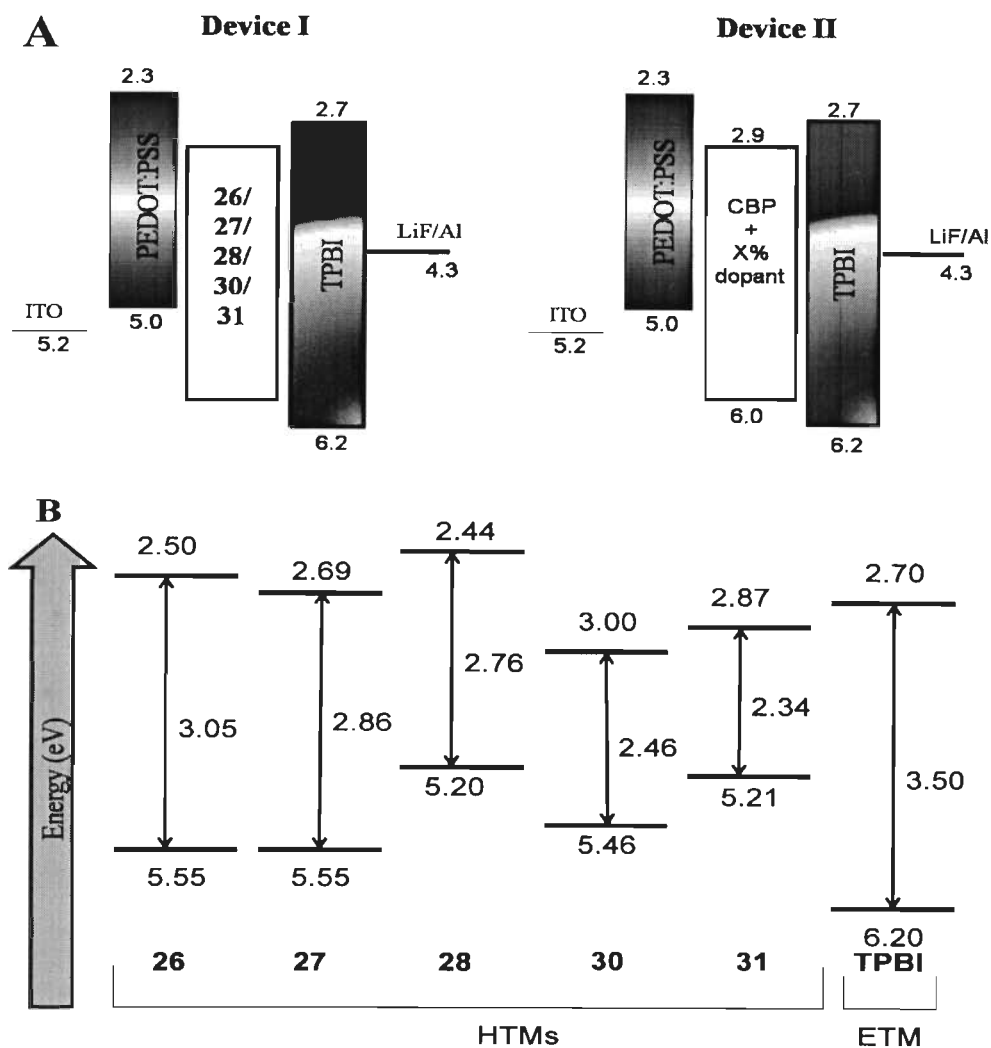


Figure 4.34 Energy level diagram of device I and II (A) and compounds **26-31** with TPBI (B).

Figure 4.35 shows the current density vs voltage curve, luminance vs voltage curve (inset) and current efficiency vs current density curve of device using neat film of **26-31** as hole transporting and emitting layer. Current density vs voltage curve, luminance vs voltage curve, current efficiency vs current density curve and luminance efficiency vs luminance curve of device using **26-31** as a dopant with host material **CBP** have shown in Figure 4.36. The electroluminescent data of both devices are rendered in Table 4.14. When the compounds have been used as dopant, the driving voltage was found low as compared to when the neat film of

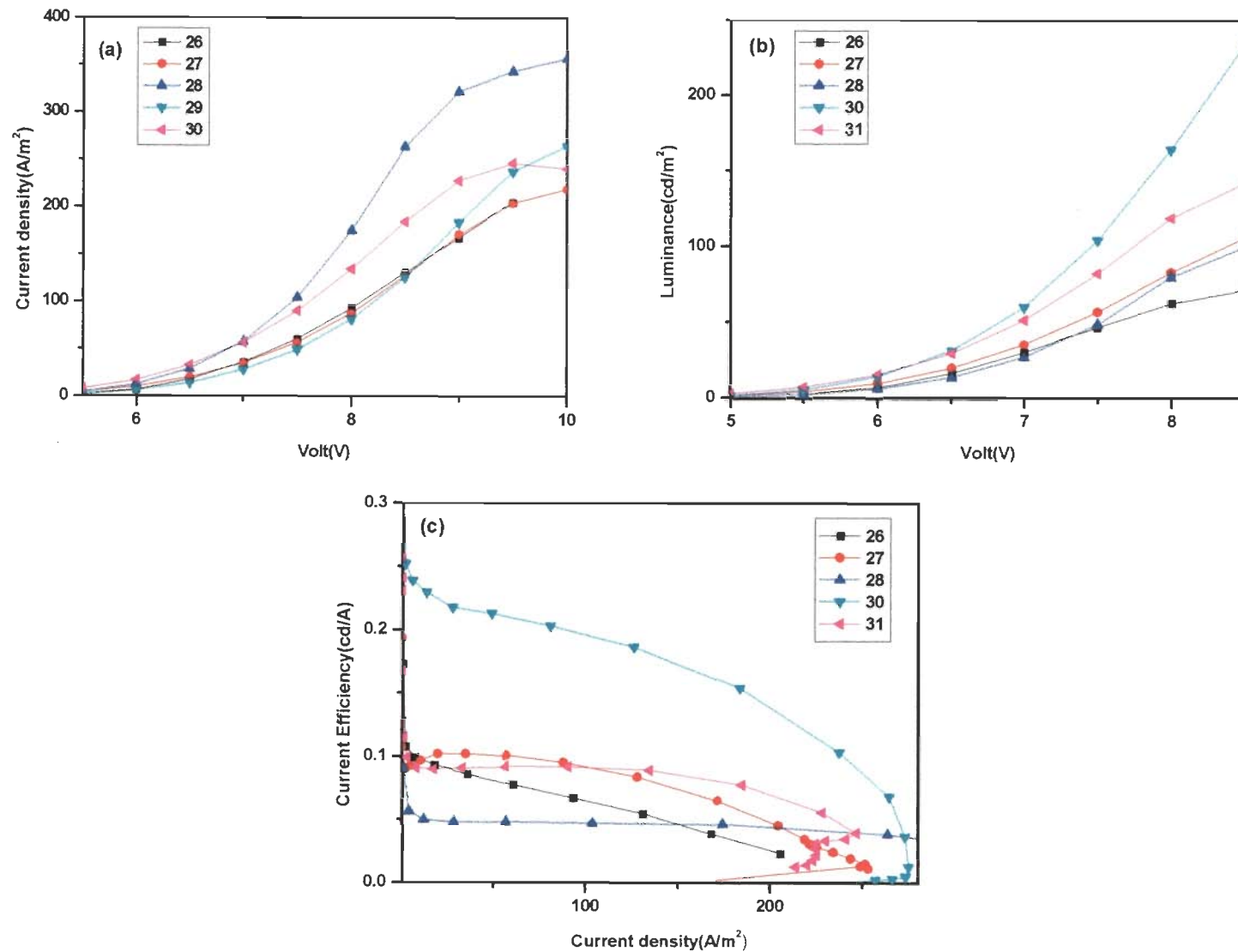


Figure 4.35 Current density vs voltage curve (a), luminance vs voltage curve (b) and current efficiency vs current density curve (c) of device using neat film of **26-31** as hole transporting and emitting layer without **CBP**.

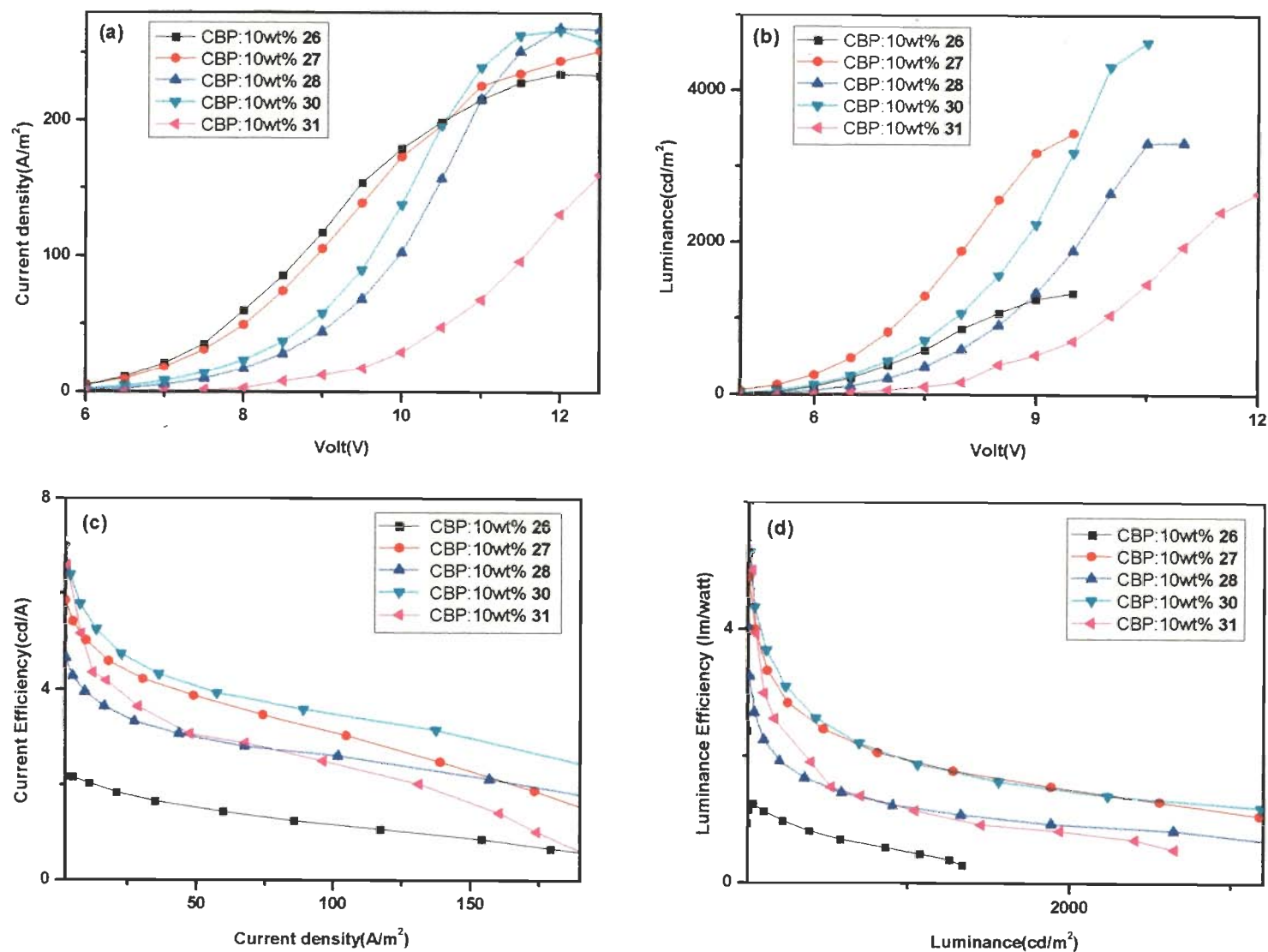


Figure 4.36 Current density vs voltage curve (a), luminance vs voltage curve (b), current efficiency vs current density curve (c) and luminance efficiency vs luminance curve (d) of device using 26-31 as a dopant with host material CBP.

them was used as hole transporting and emitting layer. Device based on dopants **27** and **30** showed low driving voltage. The order for low driving voltage is **31**>**28**>**26**>**30**>**27** when used as dopant. Similarly the trend for external quantum efficiency is **27** (4.5%) >**30** (3.2%) >**26** = **28** (2.6%) >**31** (2.3%) at 100 cd/m². The device based on dopant **30** displayed highest maximum luminescence 4630 cd/m² with power efficiency 3.8 lm/W and current efficiency 7.1 cd/A at 100 cd/m². The reason could be the good film forming property of compound **30**.

Table 4.14 Electroluminescence characteristics of devices I & II based on compounds **26-31**.

Material (neat)	Driving Voltage (V) @ 10 cd/m ²	Power Efficiency (lm/W)	Current Efficiency (Cd/A)	EQE (%)	Max. Luminance (cd/m ²)	CIE
26	6.1	---	---	---	65	(0.19, 0.23)
27	6.0	0.03/0.09	---	---	111	(0.20, 0.34)
28	6.3	---	---	---	99	(0.20, 0.34)
30	6.1	0.09/0.21	---	---	282	(0.48, 0.43)
31	5.9	0.09/0.04	---	---	143	(0.50, 0.46)
26+CBP	5.0	1.1/0.5	2.2/1.3	2.6/1.2	1340	(0.16, 0.23)
27+CBP	4.3	3.6/1.9	6.0/4.4	4.5/3.3	3440	(0.16, 0.21)
28+CBP	5.2	2.3/1.2	4.7/3.3	2.6/1.9	3310	▪ ▪ 脈 ▪ 7,
30+CBP	4.8	3.8/1.9	7.1/4.8	3.2/2.1	4630	(0.52, 0.47)
31+CBP	5.7	3.1/1.2	7.3/3.7	2.3/11	2650	(0.48, 0.51)

Figure 4.37 depicts the EL spectra for devices I and II. EL spectra of device II with compounds **26-31** was recorded at the luminance of 100 cd/m², 1000 cd/m², and 50 mA/m², respectively (Figure 4.37(b)-(d)). In addition, the EL spectra for both devices are almost independent of the driving voltages, with the fwhm remained unchanged over a wide luminance range of 100, 1000 cd/m² and 50 mA/m² (see Table 4.15). It suggests that the hole and electron recombination is well confined within the CBP layer. It is a common phenomenon that the EL spectrum of blue-emitting OLEDs shifts under different electric fields. This is mainly attributed

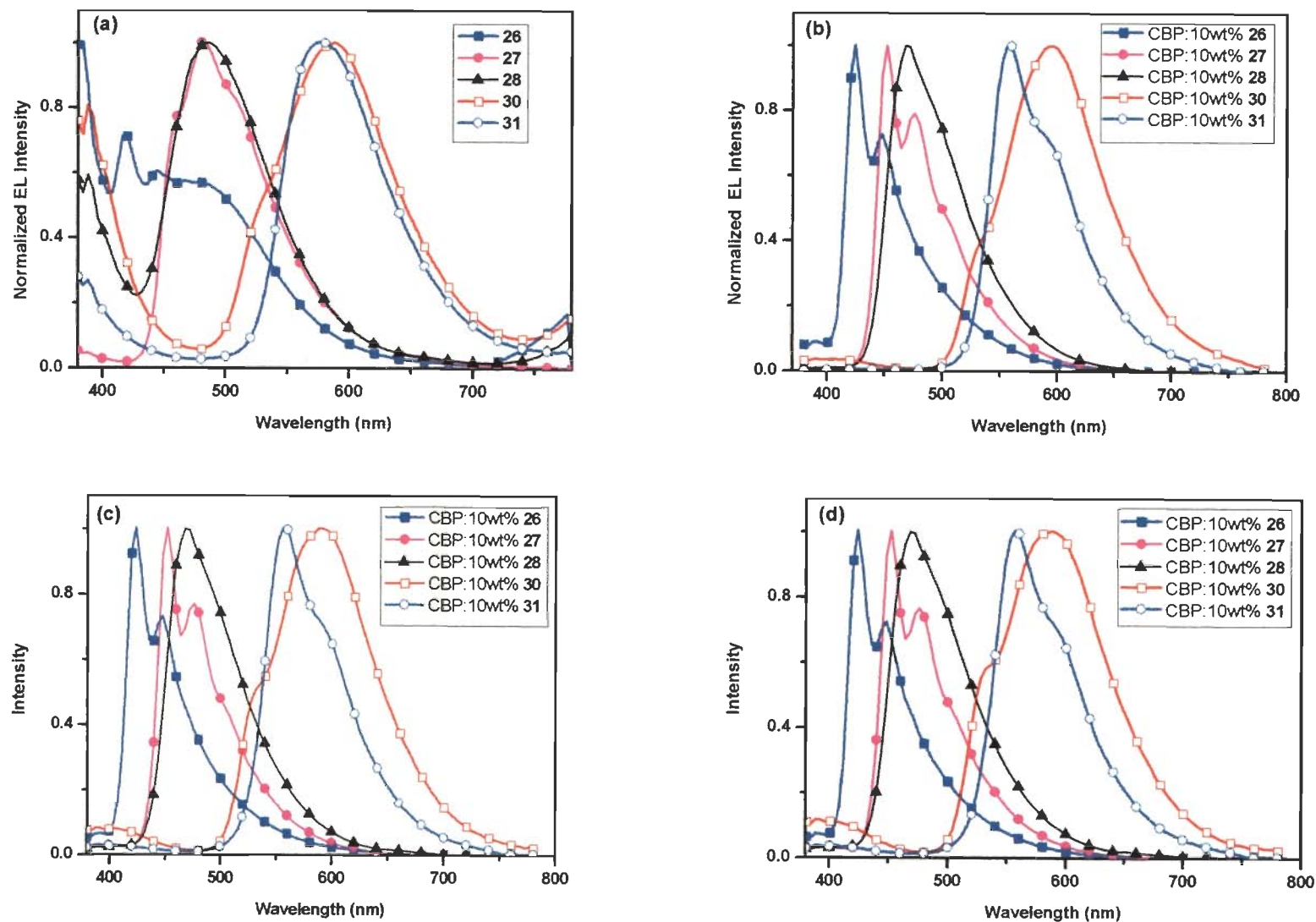


Figure 4.37 EL spectra of the devices with 26-31 without CBP at maximum luminescence (a) and with CBP @100 cd/m² (b), @1000 cd/m² (c), @50 mA/m² (d)

to the difference in the charge carrier mobility in the employed organic layers, resulting in the shift of the emission region. However, it is not the case for the present devices (i.e., the CIE coordinates remain constant over a wide luminance range), which is of particular importance for the commercial full-color applications.

Table 4.15 Emission and electroluminescence spectral data of the compounds **26-31**.

Compound	λ_{em} (nm) ^a		λ_{EL} (nm) ^b			
	dcm	Thin film	@max. luminance ^c	@ ^d 100 cd/m ²	@ ^d 1000 cd/m ²	@ ^d 50 mA/m ²
26	412, 435	496	480	424, 448	424, 448	424, 448
27	439, 465	486, 505	480	452, 476	452, 476	452, 476
28	516	495	484	468	468	468
30	514, 551	587	588	596, 528(sh)	588, 528 (sh)	588, 528 (sh)
31	567	581	576	556, 592(sh)	556, 592 (sh)	556, 592 (sh)

^aEmission wavelength; ^bElectroluminescence wavelength for OLED device; ^cwavelength for device I (without CBP); ^dwavelength for device II (doping with CBP).

4.3 Conclusions

In summary, pyrene ethynyl based derivatives have been emerged out as potential candidate for electronic application. Compounds **26-31** were used for OLED application while **35a-35d** could be used in DSSC application. The derivatives **26-31** exhibited high thermal stability as the decomposition temperature was found in the range of 419-550°C. The absorption and emission spectra of tetraethynyl derivatives (**30**, **31**) showed bathochromic shift as compared to monoethynyl derivative (**26**, **28**). Incorporation of diphenylamine enhances the absorption/emission profile as well as the thermal stability. Compounds **26-31** were used as efficient dopant with the host material CBP which was used as hole transporting layer. Device with **26-28** showed bright blue emission while **30-31** exhibited yellow emission.

Dyes **35a-35d** absorb light in the visible region ca. 400-440 nm in THF solution. They exhibited more negative excited state oxidation potentials, E_{ox}^* (-0.87 to -1.06 V versus NHE) as compared to the conduction band edge energy level of the TiO_2 electrode and favorable HOMO levels (-0.87 to -1.06 V versus NHE) which are more positive than the iodide/triiodide redox couple (~ 0.42 V vs NHE). Thiophene based dyes showed more red shifted absorption and more favourable HOMO/LUMO level. Thus these can be used as organic sensitizer for solar cell devices.

4.4 Experimental section

4.4.1 Materials

All commercial chemicals were used as received. Most of the chemicals were purchased from Sigma Aldrich. Monobromo pyrene and tetrabromopyrene were made by reported procedure. All precursor acetylenes used in synthesis were made by Sonogashira cross coupling reaction followed by cleavage by KOH and toluene. Column chromatography was performed by using silica gel (Rankem, 100-200 mesh) as stationary phase. All solvents used in synthesis and spectroscopic measurements were distilled over appropriate drying and/or degassing reagents.

4.4.2 Physical methods

Physical methods are similar as written in chapter 2.

1-bromopyrene and 1,3,6,8-tetrabromopyrene were made by reported procedure.⁴⁵ Precursor acetylenes **25a-25d** were synthesized by known procedure in literature.¹⁴ We have shown the NMR of **25c** which matches with the reported one. Analytical data of the compounds match with the reported values.

Synthesis of 9,9-diethyl-7-ethynyl-*N,N*-diphenyl-9*H*-fluoren-2-amine (25c) A mixture of 7-bromo-9,9-diethyl-*N,N*-diphenyl-9*H*-fluoren-2-amine (5.0 g, 10.68 mmol), 2-methylbut-3-yn-2-ol (1.07 g, 12.8 mmol), Pd(PPh₃)₂Cl₂ (75 mg, 0.11 mmol), PPh₃ (56 mg, 0.21 mmol), and CuI (21 mg, 0.11 mmol) were mixed in triethylamine (100 mL) under nitrogen atmosphere. The resulting mixture was stirred and heated at 100 °C for 24 h. After completion of the reaction, it was poured into water and extracted with ethyl acetate. The organic extract was washed with brine solution and dried over Na₂SO₄. Finally, the solvent was removed under vacuum to yield a yellow residue. It was purified by column chromatography as yellow liquid (5.2 g, 55%) which further undergo cleavage reaction with KOH and toluene to get the acetylene **2c**. Yellow solid. Yield 3.58 (71%); ¹H NMR (CDCl₃, 500 MHz) δ 7.57-7.55 (m, 2 H), 7.46 (dd, *J* = 6.5, 1.5 Hz, 1 H), 7.42 (d, *J* = 1.0 Hz, 1 H), 7.28-7.25 (m, 4 H), 7.13-7.11 (m, 4 H), 7.09 (d, *J* = 2.0 Hz, 1 H), 7.05-7.01 (m, 3 H), 3.12 (s, 1 H), 1.95-1.87 (m, 4 H), 0.35 (t, *J* = 7.5 Hz, 6 H); ¹³C NMR (CDCl₃, 125 MHz) δ 151.7, 149.9, 147.9, 147.8, 142.2, 135.7, 131.3, 126.5, 123.5, 122.7, 120.8, 119.3, 119.0, 118.9, 84.8, 56.1, 32.6, 8.5.

Synthesis of 2-ethynyl-9,9-di(octan-3-yl)-9*H*-fluorene (25d) Compound **25d** was prepared from 2-bromo-9,9-di(octan-3-yl)-9*H*-fluorene by following a procedure similar to that described above for **25c**. White solid. Yield 77%; ¹H NMR (CDCl₃, 500 MHz) δ 7.68 (d, *J* = 7.5 Hz, 1 H), 7.63 (d, *J* = 7.5 Hz, 1 H), 7.50 (d, *J* = 5.0 Hz, 1 H), 7.48-7.45 (m, 1 H), 7.38-7.35 (m, 1 H), 7.34-7.27 (m, 2 H), 3.10 (s, 1 H), 1.99-1.92 (m, 4 H), 0.92-0.66 (m, 22 H), 0.53-0.45 (m, 8 H).

Compounds **26-31** have been synthesized by Sonogashira cross coupling reaction of mono- or tetra bromo pyrene with their corresponding acetylenes in presence of palladium catalyst. The detailed procedure for **26** has given below.

Synthesis of 1-((9,9-diethyl-9H-fluoren-2-yl)ethynyl)pyrene (26) A mixture of 1-bromopyrene (2.82 g, 10 mmol), 9,9-diethyl-2-ethynyl-9H-fluorene (2.95 g, 12 mmol), Pd(PPh₃)₂Cl₂ (70 mg, 0.1 mmol), PPh₃ (52 mg, 0.2 mmol), and CuI (20 mg, 0.1 mmol) were mixed in triethylamine (100 mL) under nitrogen atmosphere. The resulting mixture was stirred and heated at 100 °C for 24 h. After completion of the reaction, it was poured into water and extracted with ethyl acetate. The organic extract was washed with brine solution and dried over Na₂SO₄. Finally, the solvent was removed under vacuum to yield a yellow residue. It was purified by column chromatography. Yellow solid. Yield 2.2 g (48%); mp 150-152 °C; ¹H NMR (CDCl₃, 500 MHz) δ 8.75 (d, *J* = 9.0 Hz, 1 H), 8.26-8.21 (m, 4 H), 8.17-8.03 (m, 4 H), 7.79-7.70 (m, 4 H), 7.39-7.36 (m, 3 H), 2.12 (q, *J* = 7.5 Hz, 4 H), 0.39 (t, *J* = 7.5 Hz, 6 H); ¹³C NMR (CDCl₃, 125 MHz) δ 150.3, 150.2, 142.1, 140.9, 131.9, 131.3, 131.21, 131.17, 130.9, 129.7, 128.3, 128.1, 127.6, 127.3, 127.0, 126.3, 126.1, 125.7, 125.63, 125.57, 124.62, 124.59, 124.4, 123.0, 121.8, 120.1, 119.8, 118.1, 96.3, 88.7, 32.8, 8.6; IR (KBr, cm⁻¹) *v*_{max} 2954, 2925, 2191 (*v*_{C≡C}), 1450, 825, 771.

Synthesis of 1,1'-((9,9-dibutyl-9H-fluorene-2,7-diyl)bis(ethyne-2,1-diyl)dipyrene (27) Compound **27** was prepared from **23** and **25b** by following a procedure similar to that described above for **26**. Yellow solid. Yield 35%; mp 264-266 °C; ¹H NMR (CDCl₃, 500 MHz) δ 8.76 (d, *J* = 9.0 Hz, 2 H), 8.29-8.22 (m, 8 H), 8.18 (d, *J* = 8.0 Hz, 2 H), 8.13-8.04 (m, 6 H), 7.81 (d, *J* = 8.0 Hz, 2 H), 7.77 (dd, *J* = 1.5, 6.5 Hz, 2 H), 7.73 (s, 2 H), 2.15-2.12 (m, 4 H), 1.21-1.17 (m, 4 H), 0.89-0.69 (m, 10 H); ¹³C NMR (CDCl₃, 125 MHz) δ 151.4, 140.9, 131.9, 131.33, 131.29, 131.2, 131.0, 129.7, 128.4, 128.2, 127.3, 126.3, 126.0, 125.7, 125.6, 124.64, 124.60, 124.4, 122.3, 120.2, 118.0, 96.3, 89.2, 55.4, 40.4, 29.7, 26.0, 23.2, 14.0; IR (KBr, cm⁻¹) *v*_{max} 3037, 2954, 2925, 2187 (*v*_{C≡C}), 1463, 843, 822, 764.

Synthesis of 9,9-diethyl-N,N-diphenyl-7-(pyren-1-ylethynyl)-9H-fluoren-2-amine (28)

Compound **28** was prepared from **23** and **25c** by following a procedure similar to that described above for **26**. Yellow solid. Yield 57%; mp 210-212 °C; ^1H NMR (CDCl_3 , 500 MHz) δ 8.74 (d, $J = 9.0$ Hz, 1 H), 8.25-8.20 (m, 4 H), 8.15 (d, $J = 8.0$ Hz, 1 H), 8.11-8.03 (m, 3 H), 7.71-7.65 (m, 3 H), 7.61 (d, $J = 8.5$ Hz, 1 H), 7.30-7.27 (m, 4 H), 7.17-7.14 (m, 5 H), 7.09-7.03 (m, 3 H), 2.05 (m, 2 H), 1.96 (m, 2 H), 0.44 (t, $J = 7.5$ Hz, 6 H); ^{13}C NMR (CDCl_3 , 125 MHz) δ 151.8, 150.1, 148.0, 147.8, 141.9, 135.9, 131.9, 131.3, 131.18, 131.16, 131.0, 129.6, 129.3, 128.3, 128.1, 127.3, 126.3, 126.0, 125.7, 125.63, 125.57, 124.64, 124.60, 124.4, 124.2, 124.1, 123.6, 122.9, 122.8, 120.9, 120.8, 119.2, 119.1, 118.2, 96.5, 88.7, 56.3, 32.8, 8.7, 8.6; IR (KBr, cm^{-1}) ν_{max} 3033, 2959, 2917, 2195 ($\nu_{\text{C}\equiv\text{C}}$), 1589, 1488, 1462, 818, 755.

Synthesis of 1,3,6,8-tetrakis((9,9-diethyl-9H-fluoren-2-yl)ethynyl)pyrene (29)

Compound **29** was prepared from **24** and **25a** by following a procedure similar to that described above for **26**. Orange solid. Yield 87%; mp >360 °C; ^1H NMR (CDCl_3 , 500 MHz) δ 8.88 (s, 4 H), 8.55 (s, 2 H), 7.81-7.71 (m, 16 H), 7.39-7.38 (m, 12 H), 2.18-2.08 (m, 16 H), 0.40 (t, $J = 7.0$ Hz, 24 H); ^{13}C NMR (CDCl_3 , 125 MHz) δ 149.3, 149.2, 141.3, 139.8, 130.7, 129.9, 126.7, 126.03, 125.96, 125.2, 122.0, 120.4, 119.1, 118.8, 118.2, 99.0, 96.3, 86.9, 55.3, 45.2, 31.8, 7.5. IR (KBr, cm^{-1}) ν_{max} 3057, 2962, 2916, 2195 ($\nu_{\text{C}\equiv\text{C}}$), 1595, 1495, 1452, 828, 769.

Synthesis of 1,3,6,8-tetrakis((9,9-di(octan-3-yl)-9H-fluoren-2-yl)ethynyl)pyrene (30)

Compound **30** was prepared from **24** and **25d** by following a procedure similar to that described above for **26**. Red solid. Yield: 80%; mp: 110-112°C; ^1H NMR (CDCl_3 , 500 MHz): $\delta = 8.87$ (s, 4 H), 8.57-8.55 (m, 2 H), 7.80-7.70 (m, 16 H), 7.47-7.43 (m, 4 H), 7.39-7.31 (m, 8 H), 2.10-2.09 (m, 16 H), 1.02-0.82 (m, 78 H), 0.72-0.80 (m, 10 H), 0.65-0.56 (m, 32 H); ^{13}C NMR (CDCl_3 , 125 MHz): $\delta = 150.89$, 150.85, 150.8, 142.1, 140.61, 140.59, 133.8, 131.8, 130.9, 130.80,

130.75, 129.1, 128.3, 127.4, 127.3, 127.2, 127.1, 127.0, 126.9, 124.4, 124.20, 124.17, 121.0, 120.93, 120.88, 120.1, 119.8, 119.3, 97.4, 87.7, 55.0, 44.8, 44.5, 44.5, 34.7, 33.8, 33.73, 33.66, 33.6, 32.0, 29.73, 29.70, 29.4, 28.2, 27.08, 27.06, 22.8, 22.7, 14.21, 14.15, 14.0, 10.43, 10.41, 10.4. IR (KBr, cm^{-1}) ν_{max} 2956, 2921, 2195 ($\nu_{\text{C}=\text{C}}$), 1494, 1455, 1379, 828, 738.

Synthesis of 7,7',7'',7'''-(pyrene-1,3,6,8-tetrayltetrakis(ethyne-2,1-diyl))tetrakis(9,9-diethyl-*N,N*-diphenyl-9*H*-fluoren-2-amine) (31) Compound **31** was prepared from **24** and **25c** by following a procedure similar to that described above for **26**. Orange solid. Yield 78%; mp 274-276 °C; ^1H NMR (CDCl_3 , 500 MHz) δ 8.85 (s, 4 H), 8.51 (s, 2 H), 7.73-7.65 (m, 11 H), 7.61 (d, $J = 8.5$ Hz, 4 H), 7.29-7.28 (m, 12 H), 7.16-7.13 (m, 22 H), 7.09-7.00 (m, 15 H), 2.09-2.05 (m, 8 H), 1.98-1.94 (m, 8 H), 0.45-0.42 (m, 24 H); ^{13}C NMR (CDCl_3 , 125 MHz) δ 151.8, 150.1, 147.9, 147.8, 142.2, 135.8, 133.7, 131.7, 131.1, 129.2, 126.9, 126.0, 124.3, 123.9, 123.5, 122.7, 120.8, 120.5, 119.22, 119.17, 119.0, 97.5, 87.9, 56.3, 32.7, 29.7, 8.6; IR (KBr, cm^{-1}) ν_{max} 3033, 2962, 2916, 2192 ($\nu_{\text{C}=\text{C}}$), 1592, 1490, 1465, 1276, 818, 752.

Synthesis of 4-(pyren-1-ylethynyl)benzaldehyde (34a) A mixture of 4-bromobenzaldehyde (0.37 g, 2 mmol), 1-ethynylpyrene (0.5 g, 2.2 mmol), $\text{Pd}(\text{PPh}_3)_2\text{Cl}_2$ (14 mg, 0.02 mmol), PPh_3 (10.4 mg, 0.04 mmol), and CuI (4 mg, 0.02 mmol) were mixed in triethylamine (40 mL) under nitrogen atmosphere. The resulting mixture was stirred and heated at 100 °C for 6 h. After completion of the reaction, it was poured into water and extracted with ethyl acetate. The organic extract was washed with brine solution and dried over Na_2SO_4 . Finally, the solvent was removed under vacuum to yield a yellow residue. It was purified by column chromatography. Yellow solid. Yield 0.6 g (91%); ^1H NMR (CDCl_3 , 500 MHz) δ 10.06 (s, 1 H), 8.64 (d, $J = 9.5$ Hz, 1 H), 8.25 (d, $J = 8.0$ Hz, 1 H), 8.23-8.21 (m, 3 H), 8.16-8.12 (m, 2 H), 8.07-8.04 (m, 2 H), 7.93 (d, $J = 8.5$ Hz, 2 H), 7.85 (d, $J = 8.5$ Hz, 2 H); ^{13}C NMR (CDCl_3 , 125 MHz) δ 191.5, 135.4, 132.14,

132.10, 131.8, 131.2, 131.0, 129.8, 129.7, 128.7, 128.6, 127.2, 126.4, 125.92, 125.89, 125.3, 124.6, 124.4, 124.2, 116.8, 94.2, 92.4; IR (KBr, cm^{-1}) ν_{max} 3029, 2730, 2196 ($\nu_{\text{C}=\text{C}}$), 1696 ($\nu_{\text{C}=\text{O}}$), 1597, 1300, 1204, 1160, 847.

Synthesis of 9,9-diethyl-7-(pyren-1-ylethynyl)-9H-fluorene-2-carbaldehyde (34b) Compound

34b was prepared from **33b** by following a procedure similar to that described above for **34a**.

Yellow solid. Yield 65%; ^1H NMR (CDCl_3 , 500 MHz) δ 10.09 (s, 1 H), 8.73 (d, $J = 9.0$ Hz, 1 H), 8.29-8.22 (m, 4 H), 8.17 (d, $J = 8.0$ Hz, 1 H), 8.12 (d, $J = 9.5$ Hz, 1 H), 8.08-8.04 (m, 2 H), 7.91-7.84 (m, 4 H), 7.77 (dd, $J = 1.5, 6.0$ Hz, 1 H), 7.30 (s, 1 H), 2.19-2.15 (m, 4 H), 0.38 (t, $J = 7.5$ Hz, 6 H); ^{13}C NMR (CDCl_3 , 125 MHz) δ 192.3, 151.6, 151.1, 147.2, 140.3, 135.6, 132.0, 131.4, 131.3, 131.2, 131.1, 130.7, 129.7, 128.5, 128.3, 127.3, 126.32, 126.28, 125.7, 125.7, 125.6, 124.63, 124.57, 124.4, 123.8, 123.2, 121.1, 120.3, 117.7, 95.8, 89.9, 56.6, 32.7, 8.5; IR (KBr, cm^{-1}) ν_{max} 3033, 2913, 2195 ($\nu_{\text{C}=\text{C}}$), 1690 ($\nu_{\text{C}=\text{O}}$), 1600, 1462, 1233, 1167, 847.

Synthesis of 5-(pyren-1-ylethynyl)thiophene-2-carbaldehyde (34c) Compound **34c** was

prepared from **33c** by following a procedure similar to that described above for **34a**. Orange

solid. Yield 83%; ^1H NMR (CDCl_3 , 500 MHz) δ 9.91 (s, 1 H), 8.55 (d, $J = 9.0$ Hz, 1 H), 8.29-8.19 (m, 4 H), 8.15-8.13 (m, 2 H), 8.07-8.03 (m, 2 H), 7.75-7.72 (m, 1 H), 7.49-7.47 (m, 1 H); ^{13}C NMR (CDCl_3 , 125 MHz) δ 182.5, 143.9, 136.3, 133.1, 132.5, 132.1, 132.0, 131.2, 130.9, 129.6, 128.9, 128.8, 127.2, 126.5, 126.1, 126.0, 125.1, 124.6, 124.4, 124.1, 116.0, 100.0, 97.6, 87.5; IR (KBr, cm^{-1}) ν_{max} 3033, 2859, 2192 ($\nu_{\text{C}=\text{C}}$), 1686 ($\nu_{\text{C}=\text{O}}$), 1656, 1452, 1224, 1030, 842.

Synthesis of 5'-(pyren-1-ylethynyl)-[2,2'-bithiophene]-5-carbaldehyde (34d) Compound **34d**

was prepared from **33d** by following a procedure similar to that described above for **34a**. Orange

solid. Yield 51%; ^1H NMR (CDCl_3 , 500 MHz) δ 9.90 (s, 1 H), 8.58 (d, $J = 9.0$ Hz, 1 H), 8.26-8.18 (m, 4 H), 8.14 (t, $J = 8.0$ Hz, 2 H), 8.07-8.05 (m, 2 H), 7.69 (d, $J = 4.0$ Hz, 1 H), 7.38 (d, $J =$

4.0 Hz, 1 H), 7.33 (d, $J = 3.5$ Hz, 1 H), 7.30 (d, $J = 4.0$ Hz, 1 H); ^{13}C NMR (CDCl_3 , 125 MHz) δ 182.5, 146.2, 142.1, 137.3, 137.2, 133.1, 131.9, 131.7, 131.2, 131.0, 129.4, 128.7, 128.5, 127.2, 126.4, 126.2, 125.9, 125.8, 125.3, 125.2, 124.6, 124.5, 124.3, 116.8, 95.2, 87.7; IR (KBr, cm^{-1}) ν_{max} 3033, 2917, 2187 ($\nu_{\text{C}=\text{C}}$), 1671 ($\nu_{\text{C}=\text{O}}$), 1655, 1454, 1384, 1226, 1052, 840.

Synthesis of (*E*)-2-cyano-3-(4-(pyren-1-ylethynyl)phenyl)acrylic acid (35a) 4-(pyren-1-ylethynyl)benzaldehyde (0.82 g, 2.06 mmol) was dissolved in 25 ml of glacial acetic acid. To the solution, cyanoacetic acid (0.21 g 2.48 mmol) and ammonium acetate (53 mg, 0.69 mmol) were added. The resulting mixture was refluxed for 12 h. After cooling to room temperature, a precipitate was formed in the solution. The precipitate was filtered out and washed with water. The product was recrystallized by toluene-hexane mixture. Red solid. Yield 85%; mp 263-265 °C; ^1H NMR (CDCl_3 , 500 MHz) δ 8.63 (d, $J = 9.0$ Hz, 1 H), 8.41-8.37 (m, 4 H), 8.33-8.26 (m, 3 H), 8.22 (d, $J = 9.0$ Hz, 1 H), 8.15-8.12 (m, 3 H), 7.94 (d, $J = 8.0$ Hz, 2 H); ^{13}C NMR (CDCl_3 , 125 MHz) δ 163.7, 153.6, 132.6, 132.0, 131.9, 131.8, 131.4, 131.2, 130.9, 130.3, 129.6, 129.2, 127.7, 127.32, 127.28, 126.7, 125.5, 125.3, 124.1, 123.8, 116.6, 116.4, 104.7, 99.9, 95.2, 92.5; IR (KBr, cm^{-1}) ν_{max} 3446, 3037, 2929, 2200 ($\nu_{\text{C}=\text{N}}$), 2179 ($\nu_{\text{C}=\text{C}}$), 1692, 1583, 1420, 1284, 844.

Synthesis of (*E*)-2-cyano-3-(9,9-diethyl-7-(pyren-1-ylethynyl)-9H-fluoren-2-yl)acrylic acid (35b) Dye 35b was prepared from 34b by following a procedure similar to that described above for 35a. Orange solid. Yield 60%; mp 192-194 °C; ^1H NMR (CDCl_3 , 500 MHz) δ 8.69 (d, $J = 9.0$ Hz, 1 H), 8.40-8.37 (m, 4 H), 8.36-8.30 (m, 2 H), 8.28-8.21 (m, 2 H), 8.15-8.12 (m, 2 H), 8.08-8.05 (m, 3 H), 7.93(s, 1 H), 7.82 (dd, $J = 1.5, 6.5$ Hz, 1 H), 2.16-2.06 (m, 4 H), 0.28 (t, $J = 7.5$ Hz, 6 H); ^{13}C NMR (CDCl_3 , 125 MHz) δ 163.9, 151.6, 150.8, 145.1, 140.7, 131.6, 131.54, 131.46, 131.2, 131.0, 130.7, 130.2, 129.3, 128.9, 127.7, 127.2, 126.6, 126.5, 125.6, 125.4, 124.1,

123.9, 122.9, 121.9, 121.5, 117.5, 117.2, 96.5, 89.8, 56.5, 32.0, 8.9; IR (KBr, cm^{-1}) ν_{max} 3438, 3037, 2963, 2216 ($\nu_{\text{C}\equiv\text{N}}$), 2195 ($\nu_{\text{C}\equiv\text{C}}$), 1697, 1583, 1417, 1290, 845.

Synthesis of (*E*)-2-cyano-3-(5-(pyren-1-ylethynyl)thiophen-2-yl)acrylic acid (35c) Dye **35b** was prepared from **34b** by following a procedure similar to that described above for **35a**. Dark brown solid. Yield 64%; mp 266-268 °C; ^1H NMR (CDCl_3 , 500 MHz) δ 8.56-8.53 (m, 2 H), 8.42-8.39 (m, 3 H), 8.34-8.30 (m, 3 H), 8.24 (d, $J = 9.0$ Hz, 1 H), 8.16 (t, $J = 7.5$ Hz, 1 H), 8.07 (d, $J = 4.0$ Hz, 1 H), 7.80 (d, $J = 4.0$ Hz, 1 H); ^{13}C NMR (CDCl_3 , 125 MHz): $\delta = 163.3, 146.0, 140.0, 136.8, 133.6, 131.7, 131.2, 130.7, 130.5, 130.4, 129.7, 129.3, 129.0, 127.2, 126.9, 126.4, 126.3, 125.0, 124.4, 123.5, 123.2, 116.4, 115.2, 97.5, 87.8$; IR (KBr, cm^{-1}) ν_{max} 3440, 2929, 2216 ($\nu_{\text{C}\equiv\text{N}}$), 2175 ($\nu_{\text{C}\equiv\text{C}}$), 1685, 1566, 1412, 1290, 844.

Synthesis of (*E*)-2-cyano-3-(5'-(pyren-1-ylethynyl)-[2,2'-bithiophen]-5-yl)acrylic acid (35d) Dye **35d** was prepared from **34b** by following a procedure similar to that described above for **35a**. Blackish brown solid. Yield 62%; mp 282-284°C; ^1H NMR (CDCl_3 , 500 MHz) δ 8.57-8.55 (m, 1 H), 8.51 (s, 1 H), 8.43-8.39 (m, 3 H), 8.35 (d, $J = 8.0$ Hz, 1 H), 8.31-8.29 (m, 2 H), 8.25 (d, $J = 9.0$ Hz, 1 H), 8.16 (t, $J = 7.5$ Hz, 1 H), 8.02 (d, $J = 4.0$ Hz, 1 H), 3.72-7.69 (m, 3 H); IR (KBr, cm^{-1}) ν_{max} 3449, 3037, 2921, 2216 ($\nu_{\text{C}\equiv\text{N}}$), 2183 ($\nu_{\text{C}\equiv\text{C}}$), 1680, 1572, 1416, 1285, 845. (^{13}C NMR could not be obtained due to solubility problem)

4.5 References

1. Moorthy, J. N.; Venkatakrisnan, P.; Natarajan, P.; Lin, Z.; Chow, T. J. "Nondoped pure-blue OLEDs based on amorphous phenylenevinylene-functionalized twisted bimesitylenes" *J. Org. Chem.* **2010**, *75*, 2599.
2. Braga, D.; Horowitz, G. "High performance organic field-effect transistors" *Adv. Mater.* **2009**, *21*, 1473.

3. Kim, F. S.; Ren, G.; Jenekhe, S. A. "One-dimensional nanostructures of π -conjugated molecular systems: assembly, properties, and applications from photovoltaics, sensors, and nanophotonics to nanoelectronics" *Chem. Mater.* **2011**, *23*, 682.
4. Lee, S.; Thomas, K. R. J.; Thayumanavan, S.; Bardeen, C. J. "Dependence of the two-photon absorption cross section on the conjugation of the phenylacetylene linker in dipolar donor-bridge-acceptor chromophores" *J. Phys. Chem. A* **2005**, *109*, 9767.
5. Kang, H.; Evmenenko, G.; Dutta, P.; Clays, K.; Song, K.; Marks, T. J. "X-shaped electro-optic chromophore with remarkable blue-shifted optical absorption. Synthesis, characterization, linear/nonlinear optical properties, self assembly, and thin film microstructural characteristics" *J. Am. Chem. Soc.* **2006**, *128*, 6194.
6. Wilson, J. N.; Josowicz, M.; Wang, Y.; Bunz, U. H. F. "Cruciform π -systems: hybrid phenylene-ethynylene/phenylene-vinylene oligomers" *Chem. Commun.* **2003**, 2962.
7. Samori, S.; Tojo, S.; Fujitsuka, M.; Spiliter, E. L.; Haley, M. M.; Majima, T. "" *J. Org. Chem.* **2008**, *73*, 3551.
8. Leroy-Lhez, S.; Fages, F. "Synthesis and photophysical properties of a highly fluorescent ditopic ligand based on 1,6-bis(ethynyl)pyrene as central aromatic core" *Eur. J. Org. Chem.* **2005**, 2684.
9. Grisorio, R.; Piliego, C.; Fini, P.; Cosma, P.; Mastroilli, P.; Gigli, G.; Suranna, G. P.; Nobile, C. F. "Influencing the spectral stability and the electroluminescence behavior of new blue-emitting bifluorene-based materials by the 7,7'-functionalization of the core" *J. Phys. Chem. C* **2008**, *112*, 7005.

10. Adhikari, R. M.; Duan, L.; Hou, L.; Qiu, Y.; Neckers, D. C.; Shah, B. K. "Ethyne-phenyl-linked carbazoles as a single-emitting component for white organic light-emitting diodes" *Chem. Mater.* **2009**, *21*, 4638.
11. Teng, C.; Yang, X.; Yang, C.; Tian, H.; Li, S.; Wang, X.; Hagfeldt, A.; Sun, L. "Influence of triple bonds as π -spacer units in metal-free organic dyes for dye-sensitized solar cells" *J. Phys. Chem. C* **2010**, *114*, 11305.
12. Song, J.; Zhang, F.; Li, C.; Liu, W.; Li, B.; Huang, Y.; Bo, Z. "Phenylethyne-bridged dyes for dye-sensitized solar cells" *J. Phys. Chem. C* **2009**, *113*, 13391.
13. Matsunaga, Y.; Takechi, K.; Akasaka, T.; Ramesh, A. R.; James, P. V.; Thomas, K. G.; Kamat, P. V. "Excited-state and photoelectrochemical behavior of pyrene-linked phenyleneethynylene oligomer" *J. Phys. Chem. B* **2008**, *112*, 14539.
14. Ji, S.; Yang, J.; Yang, Q.; Liu, S.; Chen, M.; Zhao, J. "Tuning the intramolecular charge transfer of alkynylpyrenes: Effect on photophysical properties and its application in design of OFF-ON fluorescent thiol probes" *J. Org. Chem.* **2009**, *74*, 4855.
15. Kale, T. S.; Krishnamoorthy, K.; Thelakkat, M.; Thayumanavan, S. "Charge mobility in nonconjugated dendrons with charge transport functionality in every layer" *J. Phys. Chem. Lett.* **2010**, *1*, 1116.
16. Xiao, J.; Xu, J.; Cui, S.; Liu, H.; Wang, S.; Li, Y. "Supramolecular helix of an amphiphilic pyrene derivative induced by chiral tryptophan through electrostatic interactions" *Org. Lett.* **2008**, *10*, 645.
17. Bernhardt, S.; Kastler, M.; Enkelmann, V.; Baumgarten, M.; Müllen, K. "Pyrene as chromophore and electrophore: encapsulation in a rigid polyphenylene shell" *Chem. Eur. J.* **2006**, *12*, 6117.

18. Moorthy, J. N.; Natarajan, P.; Venkatakrisnan, P.; Huang, D.-F.; Chow, T. J. "Steric inhibition of π -stacking: 1,3,6,8-tetraarylpyrenes as efficient blue emitters in organic light emitting diodes (OLEDs)" *Org. Lett.* **2007**, *9*, 5215.
19. Oh, H.-Y.; Lee, C.; Lee, S. "Efficient blue organic light-emitting diodes using newly-developed pyrene-based electron transport materials" *Org. Electron.* **2009**, *10*, 163.
20. Halleux, V.; Calbert, J.-P.; Brocorens, P.; Cornil, J.; Declercq, J.-P.; Brédas, J.-L.; Geerts, Y. "1,3,6,9-Tetraphenylpyrene derivatives: towards fluorescent liquid-crystalline columns?" *Adv. Funct. Mater.* **2004**, *14*, 649.
21. Zhang, H.; Wang, Y.; Shao, K.; Liu, Y.; Chen, S.; Qiu, W.; Sun, X.; Qi, T.; Ma, Y.; Yu, G.; Su, Z.; Zhu, D. "Novel butterfly pyrene-based organic semiconductors for field effect transistors" *Chem. Commun.* **2006**, *42*, 755.
22. Hayer, A.; Halleux, V.; Khler, A.; El-Garouhy, A.; Maijer, E. W.; Barber, J.; Tant, J.; Levin, J.; Lehmann, M.; Gierschner, J.; Cornil, J.; Geerts, Y. H. "Highly fluorescent crystalline and liquid crystalline columnar phases of pyrene-based structures" *J. Phys. Chem. B* **2006**, *110*, 7653.
23. Diring, S.; Camerel, F.; Donnio, B.; Dintzer, T.; Toffanin, S.; Capelli, R.; Muccini, M.; Ziessel, R. "Luminescent ethynyl-pyrene liquid crystals and gels for optoelectronic devices" *J. Am. Chem. Soc.* **2009**, *131*, 18177.
24. Pallas, A.; Palma, C.-A.; Piot, L.; Belbakra, A.; Listorti, A.; Prato, M.; Samori, P.; Armaroli, N.; Bonifazi, D. "Engineering of supramolecular H-bonded nanopolygons via self-assembly of programmed molecular modules" *J. Am. Chem. Soc.* **2009**, *131*, 509.

25. Venkataramana, G.; Sankararaman, S. "Synthesis and spectroscopic investigation of aggregation through cooperative π - π and C-H \cdots O interactions in a novel pyrene octaaldehyde derivative" *Org. Lett.* **2006**, *8*, 2739.
26. Venkataramana, G.; Sankararaman, S. "Synthesis, absorption, and fluorescence-emission properties of 1,3,6,8-tetraethynylpyrene and its derivatives" *Eur. J. Org. Chem.* **2005**, 4162.
27. Hu, J.-Y.; Era, M.; Elsegood, M. R. J.; Yamato, T. "Synthesis and photophysical properties of pyrene-based light-emitting monomers: highly pure-blue-fluorescent, cruciform-shaped architectures" *Eur. J. Org. Chem.* **2010**, 72.
28. Kim, H. M.; Lee, Y. O.; Lim, C. S.; Kim, J. S.; Cho, B. R. "Two-photon absorption properties of alkynyl-conjugated pyrene derivatives" *J. Org. Chem.* **2008**, *73*, 5127.
29. Wong, K.-T.; Chien, Y.-Y.; Chen, R.-T.; Wang, C.-F.; Lin, Y.-T.; Chiang, H.-H.; Hsieh, P.-Y.; Wu, C.-C.; Chou, C. H.; Su, Y. O.; Lee, G.-H.; Peng, S.-M. "Ter(9,9-diarylfluorene)s: highly efficient blue emitter with promising electrochemical and thermal stability" *J. Am. Chem. Soc.* **2002**, *124*, 11576.
30. Setayesh, S; Grimsdale, A. C.; Weil, T.; Enkelmann, V.; Müllen, K.; Meghdadi, F.; List, E. J. W.; Leising, G. "Polyfluorenes with polyphenylene dendron side chains: toward non-aggregating, light-emitting polymers" *J. Am. Chem. Soc.* **2001**, *123*, 946.
31. Morales, A. R.; Belfield, K. D.; Hales, J. M.; Stryland, E. W. V.; Hagan, D. J. "Synthesis of two-photon absorbing unsymmetrical fluorenyl-based chromophores" *Chem. Mater.* **2006**, *18*, 4972.
32. Tang, C.; Liu, F.; Xia, Y.-J.; Lin, J.; Xie, L.-H.; Zhong, G.-Y.; Fan, Q.-L.; Huang, W. "Fluorene-substituted pyrenes-novel pyrene derivatives as emitters in nondoped blue OLEDs" *Org. Electron.* **2006**, *7*, 155.

33. Tang, C.; Liu, F.; Xia, Y.-J.; Xie, L.-H.; Wei, A.; Li, S.-B.; Fan, Q.-L.; Huang, W. "Efficient 9-alkylphenyl-9-pyrenylfluorene substituted pyrene derivatives with improved hole injection for blue light-emitting diodes" *J. Mater. Chem.*, **2006**, *16*, 4074.
34. Liu, F.; Xie, L.-H.; Tang, C.; Liang, J.; Chen, Q.-Q.; Peng, B.; Wei, W.; Cao, Y.; Huang, W. "Facile synthesis of spirocyclic aromatic hydrocarbon derivatives based on *o*-halobiaryl route and domino reaction for deep-blue organic semiconductors" *Org. Lett.* **2009**, *11*, 3850.
35. Zhao, Z.; Xu, X.; Jiang, Z.; Lu, P.; Yu, G.; Liu, Y. "Oligo(2,7-fluorene ethynylene)s with pyrene moieties: synthesis, characterization, photoluminescence, and electroluminescence" *J. Org. Chem.* **2007**, *72*, 8345.
36. Zhao, Z.; Xu, X.; Wang, F.; Yu, G.; Lu, P.; Liu, Y.; Zhu, D. "Synthesis and characterization of light-emitting materials composed of carbazole, pyrene and fluorene" *Synth. Met.* **2006**, *156*, 209.
37. Zhao, Z.; Xu, X.; Wang, H.; Lu, P.; Yu, G.; Liu, Y. "Zigzag molecules from pyrene-modified carbazole oligomers: synthesis, characterization, and application in OLEDs" *J. Org. Chem.* **2008**, *73*, 594.
38. Zhao, Z.; Li, J.-H.; Chen, X.; Wang, X.; Lu, P.; Yang, Y. "Solution-processable stiff dendrimers: synthesis, photophysical, film morphology, and electroluminescence" *J. Org. Chem.* **2009**, *74*, 383.
39. Weigel, W.; Rettig, W.; Dekhtyar, M.; Modrakowski, C.; Beinhoff, M.; Schlüter, A. D. "Dual fluorescence of phenyl and biphenyl substituted pyrene derivatives" *J. Phys. Chem. A* **2003**, *107*, 5941.

40. Yang, S.-W.; Elangovan, A.; Hwang, K.-C; Ho, T.-I. "Electronic polarization reversal and excited state intramolecular charge transfer in donor/acceptor ethynylpyrenes" *J. Phys. Chem. B* **2005**, *109*, 16628.
41. Techert, S.; Schmatz, S.; Wiessner, A.; Staerk, H. "Photophysical characteristics of directly linked pyrene-dimethylaniline derivatives" *J. Phys. Chem. A* **2000**, *104*, 5700.
42. Taratula, O.; Rochford, J.; Piotrowiak, P.; Galoppini, E. "Pyrene-terminated phenylenethynylene rigid linkers anchored to metal oxide nanoparticles" *J. Phys. Chem. B* **2006**, *110*, 15734.
43. Nantalaksakul, A.; Mueller, A.; Klaikherd, A.; Bardeen, C. J.; Thayumanavan, S. "Dendritic and linear macromolecular architectures for photovoltaics: a photoinduced charge transfer investigation" *J. Am. Chem. Soc.* **2009**, *131*, 2727.
44. Coleman, A.; Pryce, M. T. "Synthesis, electrochemistry, and photophysical properties of a series of luminescent pyrene-thiophene dyads and the corresponding $\text{Co}_2(\text{CO})_6$ complexes" *Inorg. Chem.* **2008**, *47*, 10980.
45. Gumprecht, W. H. "3-Bromopyrene" *Org. Syn.* **1973**, *5*, 147.
46. Li, Z. H.; Wong, M. S.; Tao, Y.; Lu, J. "Diphenylamino end-capped oligofluorenes with enhanced functional properties for blue light emission: synthesis and structure-property relationships" *Chem. Eur. J.* **2005**, *11*, 3285.
47. Sun, Y.-P. "Excitation wavelength dependence of pyrene fluorescence in supercritical carbon dioxide. Evidence for a supercritical solvent-assisted solute-solute clustering mechanism" *J. Am. Chem. Soc.* **1993**, *115*, 3340.

48. Liu, F.; Lai, W.-Y.; Tang, C.; Wu, H.-B.; Chen, Q.-Q.; Peng, B.; Wei, W.; Huang, W.; Cao, Y. "Synthesis and characterization of pyrene-centered starburst oligofluorenes" *Macromol. Rapid Commun.* **2008**, *29*, 659.
49. Moorthy, J. N.; Natarajan, P.; Venugopalan, P. "Engineering of ternary co-crystals based on differential binding of guest molecules by a tetraarylpyrene inclusion host" *Chem. Commun.* **2010**, *46*, 3574.
50. Sung, J.; Kim, P.; Lee, Y. O.; Kim, J. S.; Kim, D. "Characterization of ultrafast intramolecular charge transfer dynamics in pyrenyl derivatives: systematic change of the number of peripheral *N,N*-dimethylaniline substituents" *J. Phys. Chem. Lett.* **2011**, *2*, 818.
51. Pereira, R. V.; Gehlen, M. H. "H-bonding assisted intramolecular charge transfer in 1-aminopyrene derivatives" *Chem. Phys. Lett.* **2006**, *426*, 311.
52. Yang, H.-Y.; Yen, Y.-S.; Hsu, Y.-C.; Chou, H.-H.; Lin, J. T. "Organic dyes incorporating the dithieno[3,2-*b*:2',3'-*d*]thiophene moiety for efficient dye-sensitized solar cells" *Org. Lett.* **2010**, *12*, 16.
53. Lai, S.-L.; Tong, Q.-X.; Chan, M.-Y.; Ng, T.-W.; Lo, M.-F.; Lee, S.-T.; Lee, C.-S. "Distinct electroluminescent properties of triphenylamine derivatives in blue organic light-emitting devices" *J. Mater. Chem.*, **2011**, *21*, 1206.
54. Thomas, K. R. J.; Lin, J. T.; Tao, Y.-T.; Chuen, C.-H. "Green and yellow electroluminescent dipolar carbazole derivatives: features and benefits of electron-withdrawing segments" *Chem. Mater.* **2002**, *14*, 3852.

Synthesis and Characterization of Pyrenylamine-Based Organic Dyes as Sensitizers for Dye Sensitized Solar Cells

5.1 Introduction

In this era of industrialization and explosive population growth, there is a higher demand of energy worldwide. All the present resources of energy like coal, petroleum products, thermal, nuclear and hydroelectric energy has one or the other limitations with their use. Most of them are non-renewable and will finish up soon. Hence, there is an urgent need of an energy source which is natural, renewable, cheap, easily available everywhere and easy to use. One such breakthrough is an invention of solar cell as the name suggests, it is a device that uses the solar energy and converts it into electrical energy via photovoltaic effect. In simpler words it recharges itself automatically just by the mere exposure to sunlight. It has got all the qualities described above plus the newer technology solar cells are very efficient and very compact so that they can be installed at each household at different capacities and doesn't need an expensive centralized supply system like thermoelectric and hydroelectric power plants. Moreover, it is totally pollution free and has zero carbon emission. Hence, it is a great boom in reducing global warming.

Now-a-days solar cells are very popular in household products such as solar panel, solar heater, solar invertors, solar fountain, solar lighting, solar batteries and chargers. Not only for

household use, but it is also being commercialized in industries and space organizations. The conventional material for currently available solar cells is silicon but due to its high cost and requirement of thick layer, the researchers were forced to think about other alternatives. In this direction, a cheaper and easily handled concept for this purpose was fulfilled by dye sensitized solar cells (DSSC). DSSC is a thin film solar cell and comprises a class of low-cost materials. The flexibility in shape, color, transparency and their better performance under diffuse light condition and at higher temperature, make them attractive and promising for commercialization.

The dye sensitized solar cell was invented by Michael Grätzel and Brian O'Regan at the Ecole Polytechnique Fédérale de Lausanne in 1991.¹ On the name of inventor, these cells are also known as Grätzel cells. The conventional ruthenium-based sensitizers such as the N3, N719 and the black dye have been intensively investigated for DSSC.^{2,3} These Ru-based dyes have achieved solar-energy-to-electricity conversion efficiencies up to 11% under AM 1.5 irradiation.⁴ The structures of these dyes are shown in Figure 5.1. But due to the rarity and high cost of ruthenium, organic sensitizers came into consideration and have many advantages over conventional Ru-complexes. Organic dyes are cost effective, eco-friendly, having high molar extinction coefficient and can be easily designed and synthesized as compared to Ru-complexes.

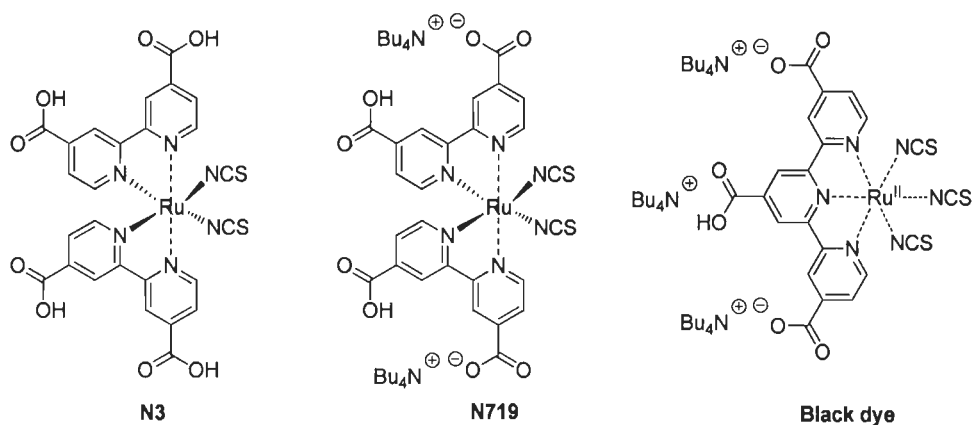


Figure 5.1 Structures of the Ru-complexes used as photosensitizer for DSSC.

DSSC works on the concept of charge separation in which light is absorbed by the dye anchored on the TiO_2 surface.⁵ Then electrons from the excited state of dye inject into the conduction band of the TiO_2 , generating an electric current. At the same time, the oxidized state of the dye is regenerated by the electrolyte to give efficient charge separation. In the meanwhile electrons are transported through TiO_2 conduction band to the counter electrode where the reduction of electrolyte occurs. In this way the circuit is completed and a voltage is generated which is equal to the difference between the fermi level of the electron in the solid TiO_2 and the redox potential of the electrolyte. The voltage generated is known as open circuit voltage (V_{oc}).

During the operation of DSSC some destructive processes may also take place like 1) recombination of oxidized dye by the excited state decay which depend on the excited state lifetime, 2) the second one is the recombination of the electrons in conduction band of TiO_2 with oxidized dye or electrolyte species. The recombination of electrons in TiO_2 with electrolyte species is referred as electron lifetime. Thus, a dye sensitizer needs to have efficient charge injection with photoexcitation. To obtain high conversion efficiencies, the photogenerated electrons must flow into the oxide film with minimal losses to interfacial recombination. Thus, the dye in DSSC is essential for efficient light harvesting and electron generation/transfer.

The common architecture of organic sensitizer used for DSSC is mainly comprised of a donor unit and an acceptor unit linked by a spacer (Figure 5.2). Electrons move from donor to acceptor *via* spacer after photoexcitation. Several dipolar organic dyes have been reported as

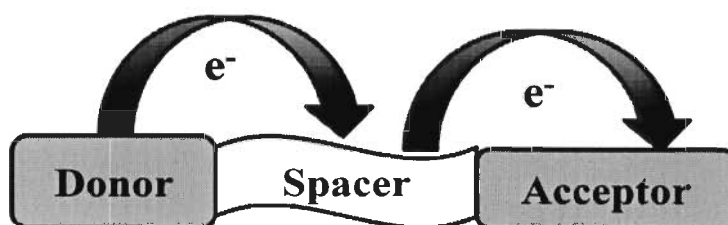


Figure 5.2 A general design of organic dyes.

sensitizers in DSSC, mainly developed using coumarin-⁶, perylene-⁷, carbazole-⁸, thiophene-⁹, oligoene-¹⁰, indoline-¹¹, and triarylamine-¹² building blocks. The structures of the organic dyes having different donor-acceptor systems are shown in Figure 5.3. Out of which coumarin based dye (**E1**) showed better efficiency (6.5%).¹³ The more common and efficient acceptor unit is cyanoacrylic acid in most of the organic dyes applicable in DSSC. The phenothiazine-based dye **E2-a** with cyanoacrylic acid unit as acceptor were found to show better performance in DSSC as compared to the same dye **E2-b** with rhodamine-3-acetic acid group as an acceptor.¹⁴ The former showed solar energy to electricity conversion efficiency 5.5% while the later one showed only 1.9%.

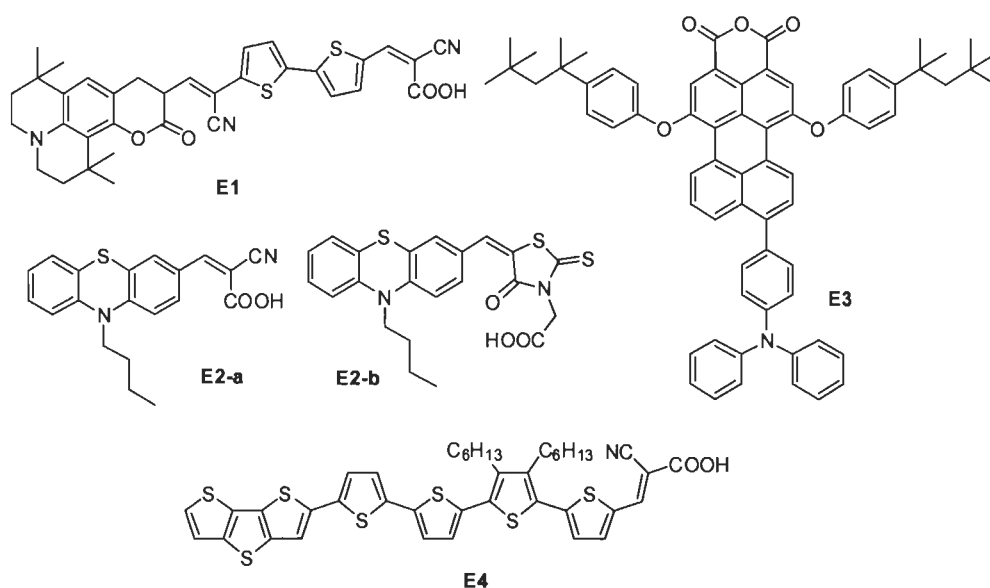


Figure 5.3 Structures of organic dyes having different donor-acceptor systems.

The perylene based dye **E3** showed very less efficiency upto 2.2%.¹⁵ **E4** is the example for the class of organic dyes having triarylamine free donor such as dithienothiophene and this displayed device efficiency of 5.02%.¹⁶ Thus the properties of the dye can be tuned either by changing acceptor or donor or spacer.

Most of the DSSC-based organic dyes have di- or triarylamines as the donor because of the good donor capability and transporting properties.¹⁷ Figure 5.4 shows some examples of organic dyes (**E5-E10**) which have triarylamine as a donor and cyanoacrylic acid as an acceptor linked by thiophene-based spacer. The optical and device data are given in Table 5.1. These examples can be divided into two series one is having diphenylamine as a donor and in other series difluorenylamine as a donor while the acceptor and spacer unit remain same. The solar energy-to-electricity conversion efficiency of **E5** was reported as 5.20% while that of **E8** was 7.2%.^{18,19} Thus, by incorporating the polyaromatic hydrocarbon in place of phenyl increase the performance of device due to red shift in absorption profile and electronic coupling with the electrolyte system.

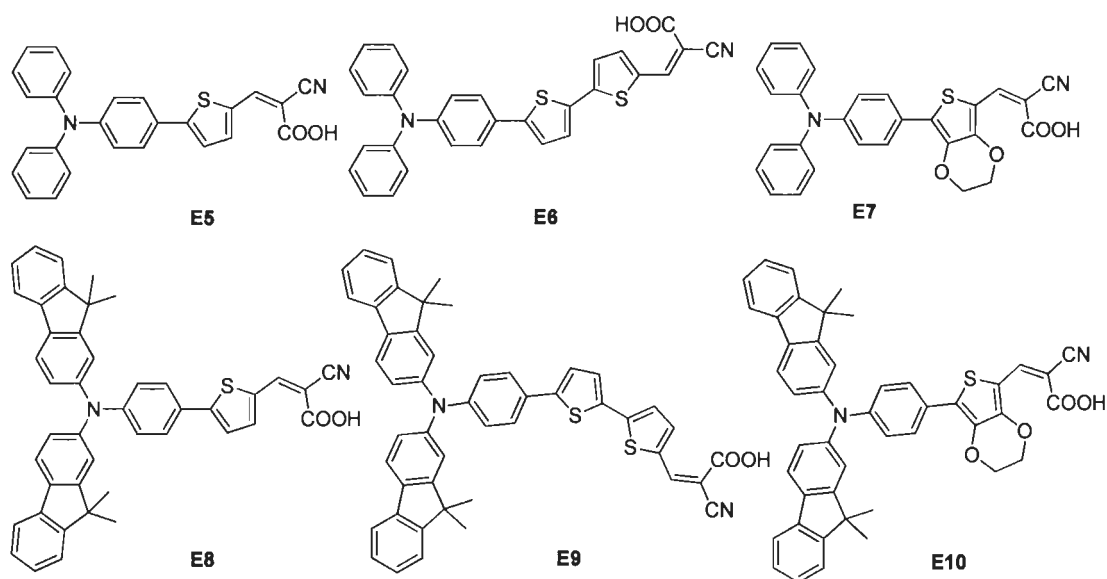


Figure 5.4 Structures of triarylamine-based organic dyes for DSSC.

Similarly the efficiency has increased by increasing the length of spacer unit as dye **E6** showed 6.17% efficiency²⁰, whereas **E9** exhibited 8.01%¹⁹. **E7** displayed overall efficiency 7.30%¹⁸ while replacing the phenyl by fluorene hydrocarbon (**E10**)²¹ increased the overall efficiency upto 7.92%. Thus by changing the substituent on diarylamine or increasing the spacer

Table 5.1 Optical and device data for the compounds **E5-E10**.

S.N.	λ_{abs} , nm	λ_{em} , nm	V_{oc} , V	J_{sc} , mAcm ⁻¹	FF	η , %	Ref.
E5	410	549	0.62	12.8	0.66	5.20	18
E6	461	NA	0.66	16.26	0.58	6.17	20
E7	426	548	0.69	15.5	0.68	7.30	18
E8	436	657	0.76	12.20	0.77	7.20	19
E9	452	670	0.75	14.0	0.77	8.01	19
E10	525	688	0.76	13.82	0.75	7.92	21

length can tune photo harvesting and charge transfer properties of the dye. The above illustration indicates that the incorporation of fluorene increases the donor strength of amine due to its electron richness which increases the donor-acceptor interaction. This facilitates the charge injection to the TiO₂ surface which results in high efficiency.

Pyrene, a flat polyaromatic hydrocarbon have excellent fluorescence properties, carrier mobilities and much improved hole injection ability than fluorene. For instance pyrene was incorporated to increase the hole transporting properties due to its electron richness by Tang et al.²² Moreover pyrene have exceptionally long fluorescence lifetime (τ is up to 400 ns in deaerated solution, compared to $\tau < 10$ ns for most organic fluorophores).²³ Prolongation of excited state lifetime will be beneficial for excited state electron transfer reactions. Although numerous pyrene derivatives are known as efficient material for OFET and OLED.^{24,25} Their use in dye sensitized solar cells is limited. For instance, pyrenylphenylamine has been extensively used as a donor in OLEDs.²⁶ Very few pyrene containing triarylamine as a donor in organic dyes for solar cell has been reported so far.^{27,28} Thayumanavan and co-workers have used pyrenylamino moiety as donor in dendritic macromolecular architecture which enhance the photoinduced charge transfer for photovoltaic application.^{29,30} Our motivation of using pyrene phenylamino unit as a donor due to electron richness and high lifetime of pyrene which can be

increase the donor strength and charge injection ability. Additionally, high lifetime will inhibit the chance of back electron transfer which is the requirement of good performance of device.

Figure 5.5 shows some examples of organic dyes (E11-E16) having two donor system by which the donor acceptor interaction is increasing, resulting in more charge transfer.³¹⁻³⁶ All the

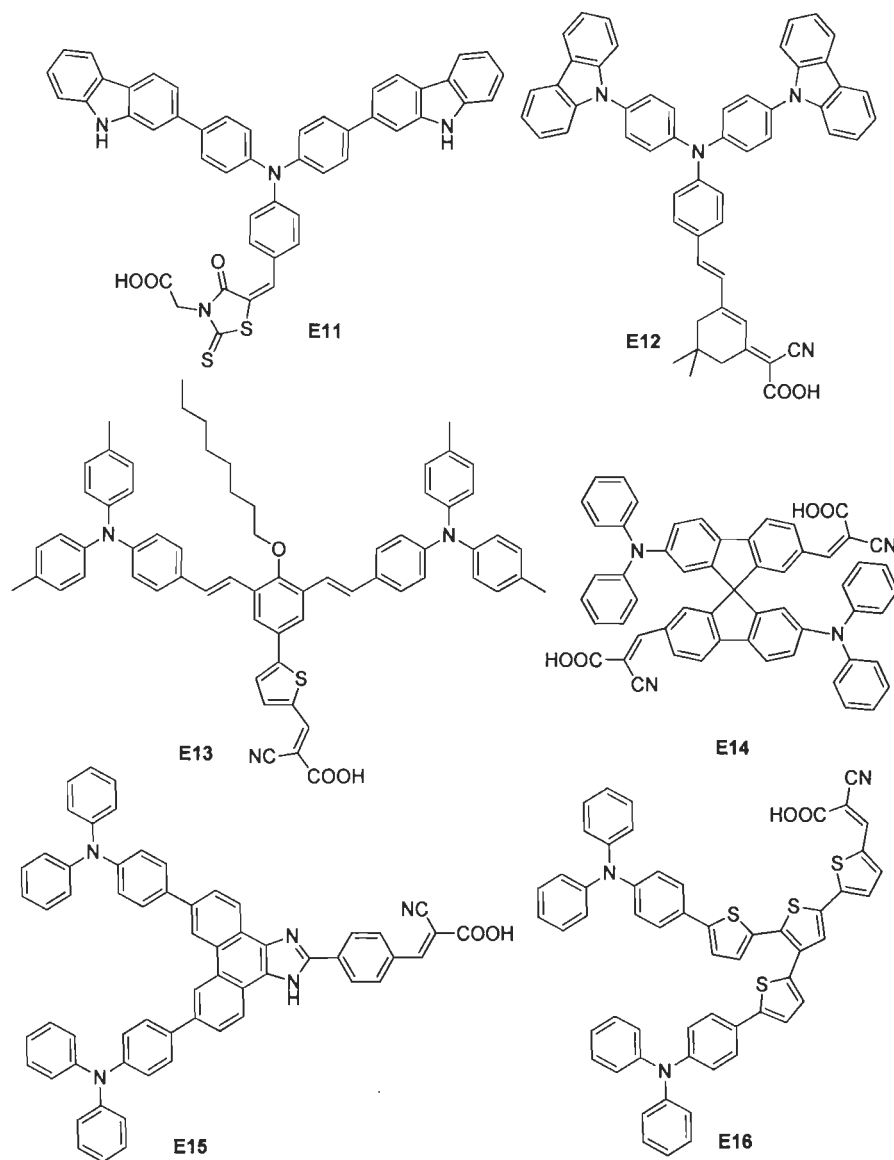


Figure 5.5 Structures of organic dyes containing two donor systems.

dyes showed good solar energy-electricity conversion efficiency. Recently Xu et al.³⁷ have done the DFT studies on the triphenylamine based dye and demonstrated how the incorporation of one

more diphenylamino moiety into the diphenylamine based dye increased the donor strength as well as the conversion efficiency of DSSC. Zhang et al. have also achieved higher conversion efficiency by inserting *N,N*-dimethylarylamine as secondary electron donating group in triarylamine derivatives.³⁸

Many researchers have attempted to achieve all the qualities which are required for increasing the efficiency of DSSC in an organic dye. These requirements are, (1) a dye must carry attachment group such as carboxylate or phosphonate to graft it on TiO₂ surface, (2) it should inject electron to the conduction band of TiO₂ upon excitation with a quantum yield of unity, (3) the energy level of the excited state should be well matched to the conduction band of TiO₂, and (4) its redox potential should be sufficiently high that it can be regenerated by the electrolyte rather than other back electron transfer processes.

By keeping all the things in mind which are described above, I have synthesized three bipolar materials (**43a-43c**) having donor- π -spacer-donor- π -acceptor system using phenyl, biphenyl and 9,9-diethylfluorene as spacer. The dyes have one pyrenylphenylamine as a donor, another as additional chromophore and cyanoacrylic acid as an acceptor. Additionally, I have also synthesized two control molecules **39a** and **39b** to see the effect of incorporation of another donor between the spacer and acceptor. The structures of the dyes are shown in Figure 5.6 (Dye **E17** is shown here to compare the optical properties)

The major idea for the synthesis of above compounds was to exploit the excellent light harvesting properties of pyrene but due to its tendency of aggregation, I have incorporated it through diarylamine segment which inhibit the molecular aggregation due to its non planar structure. Moreover, further introduction of another diarylamine can tune the oxidation potential by increasing the donor strength.

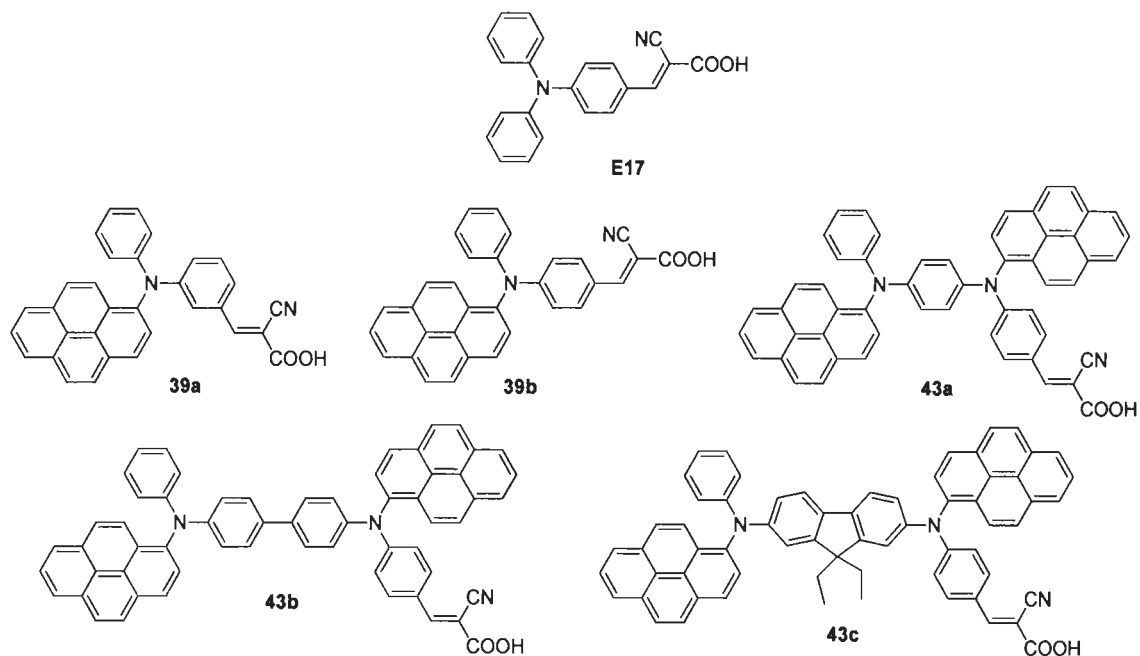


Figure 5.6 Structures of the dyes **39a**, **39b** and **43a-43c**.

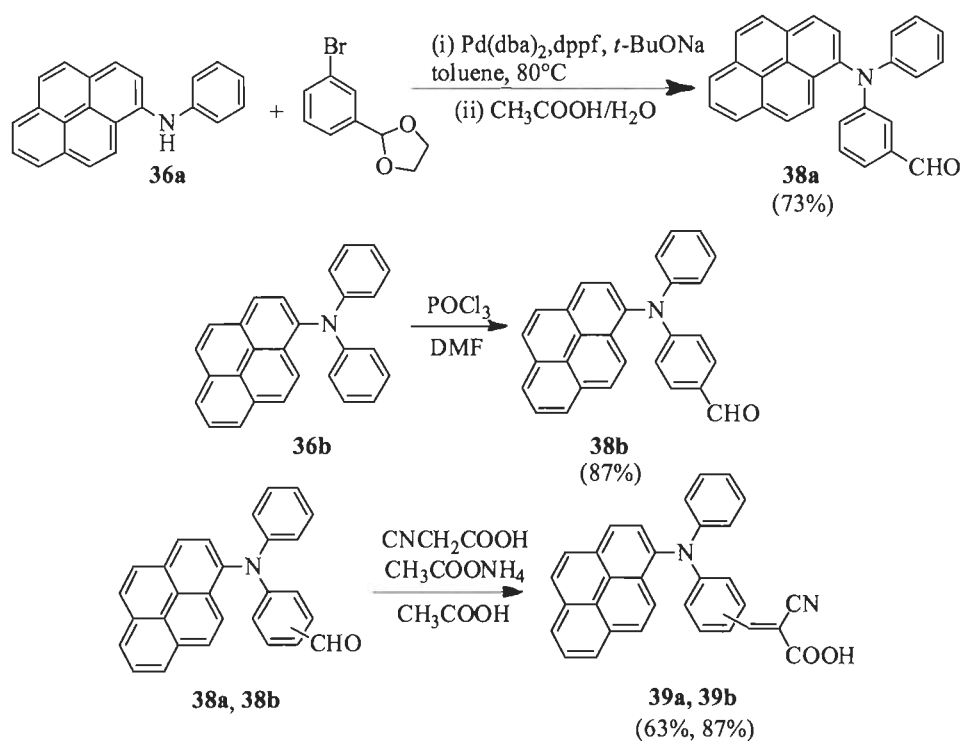
All the compounds were well characterized by ^1H NMR and ^{13}C NMR spectral studies. The absorption and emission spectra have been recorded for all the dyes, their precursor amines and aldehydes. The molar extinction coefficient was found high for the dyes **43a-43c** as compared to the dyes **39a-39b** due to the presence of two cascade donor systems. Protonation-deprotonation study was also performed by recording absorption spectra in the presence of trifluoroacetic acid, triethylamine and sodium hydroxide. The redox potentials of the compounds were calculated from cyclic voltamograms. The DSSC fabrication was done for all the five dyes, out of which the dyes **43b** and **43c** showed the highest solar energy to electricity conversion efficiency.

5.2 Result and discussion

5.2.1 Synthesis

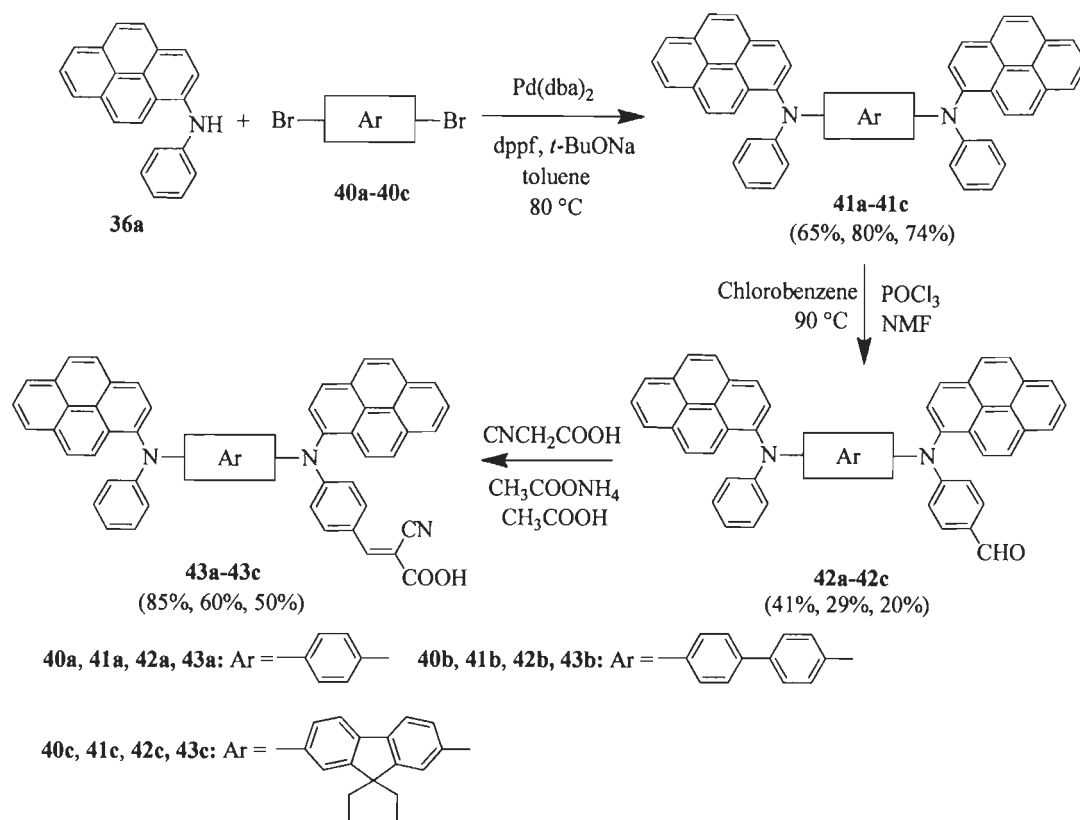
All the dyes have been synthesized by a Knoevenagel condensation reaction of cyanoacetic acid with corresponding aldehyde in presence of ammonium acetate. Dyes **39a** and **39b** have one

donor and one acceptor system separated by a phenyl spacer. The only difference between these two dyes is the position of acceptor group. It is present on the meta- and para- to phenyl in **39a** and **39b** respectively. The synthetic route is somewhat different for both control dyes as displayed in Scheme 5.1.



Scheme 5.1 Synthetic route of the dye **39a** & **39b**.

The dye **39a** has been synthesized by the precursor aldehyde **38a**. To synthesize **38a**, I have started with the 3-bromo benzaldehyde as reported in the literature³⁰ while **38b** which is the precursor aldehyde of **39b**, has been synthesized by formylation of *N,N*-diphenylpyren-1-amine in presence of POCl_3 and DMF. The Dyes (**43a-43c**) have two donor one acceptor (D- π '-D- π -A) systems. The three different spacer unit such as 1,4-phenyl, 1,6-biphenyl and 2,7-(9,9-diethyl-9*H*-fluorene) between two donors has been used in **43a**, **43b** and **43c** respectively. While a common phenyl spacer is present between donor and acceptor **39a** & **39b**. The synthetic route of these three dyes (**43a-43c**) is given in Scheme 5.2.



Scheme 5.2 Synthesis of the pyrenylamine-based organic dyes **43a**, **43b** & **43c** containing aromatic linkers.

Their precursor aldehydes were formed by two step reaction which include Buchward Hartwig C-N coupling reaction³⁹ between pyrenylphenylamine and corresponding 1,4-dibromo derivatives followed by Vilsmeier-Haack formylation⁴⁰ by POCl_3 in NMF and chlorobenzene. All the intermediate amines, aldehydes and dyes were well characterized by ^1H and ^{13}C NMR which confirms the formation of them. To the best of our knowledge all the dyes are novel. The aldehyde **38b** is reported in patents for its electrophotographic photoreceptor properties. But aldehydes (**42a-42c**) are not reported. Their corresponding amine **41a** and **41b** is only reported in the patents in which light emitting properties in OLEDs has been described. Fluorene containing amine **41c** is not reported.

5.2.2 Optical properties

The absorption spectra of the dyes (**39a**, **39b** and **43a-43c**) recorded in dichloromethane solution ($2 \times 10^{-5} \text{M}$) is shown in Figure 5.7. The data are compiled in Table 5.2. All the dyes showed three absorption bands. The higher energy band appears at same wavelength (276 nm) for all the dyes. This band arises due to a $\pi-\pi^*$ transition localized within the aromatic segment. The middle and higher wavelength bands in **39a** are blue shifted than other dyes and arise due to $\pi-\pi^*$ or $n-\pi^*$ transitions localized on pyrene unit. The intensity of this band is suppressed in **39b** and appeared as a hump at longer wavelength than in **39a**.

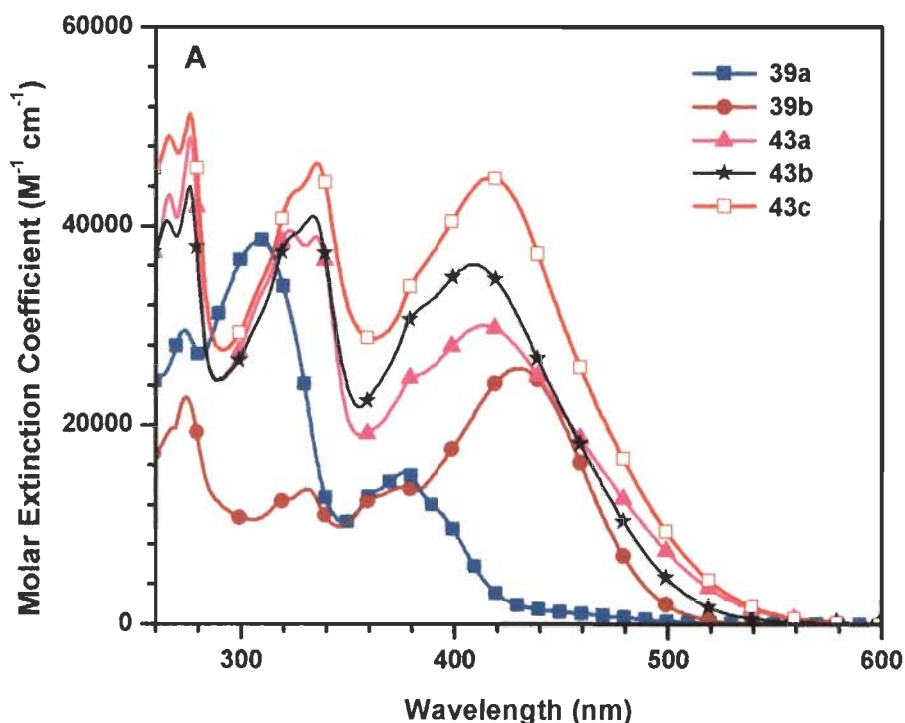


Figure 5.7 Absorption spectra of the dyes **39a**, **39b** and **43a-43c** recorded in dichloromethane.

When I compare the absorption spectra of the dyes **39b**, **43a-43c** with **39a**, there is an additional band in the range of 400-550 nm which is due to intramolecular charge transfer from amine donor to cyanoacrylic acid acceptor present on the para position to the phenyl spacer. While this charge transfer band does not appear in **39a** because the acceptor moiety is present on

meta- position to phenyl ring which is not in the direct conjugation to the donor. This confirms the unfavorability of the meta- position in increasing the conjugation of molecule.

The absorption maximum observed for the dye **39b** (431 nm) is bathochromically shifted when compared to the previously reported dye (*E*)-2-cyano-3-(4-(diphenylamino)phenyl)acrylic acid (**E17**, 391 nm).⁴¹ This clearly indicates the electron-richness of the pyrene unit, which enhances the donor strength of the amine segment to result in a pronounced donor-acceptor interaction.

Table 5.2 Optical data of precursor amines (**38a**, **41a-41c**), aldehydes (**38b**, **42a-42c**) and dyes (**39b**, **43a-43c**) measured in dichloromethane solution.

Compound	λ_{\max} , nm (ϵ_{\max} , $M^{-1} \text{cm}^{-1} \times 10^3$)	λ_{em} , nm	Stokes' shift, cm^{-1}
36b	300 (25.7), 381 (14.1)	469	4925
41a	323 (55.5), 335 (54.2), 413 (22.5)	562	6419
41b	334 (76.3), 406 (37.0)	503	4750
41c	337 (47.7), 362 (37.8), 418 (30.4)	542	5473
38b	329 (27.0), 349 (26.9), 378 (23.5)	467	5042
42a	336 (49.8), 381 (33.7)	559	8358
42b	332 (50.7), 376 (47.7)	497	6475
42c	335 (50.2), 390 (52.2)	513	6148
39a	274 (29.5), 309 (38.6), 377 (15.4)	461	4833
39b	274 (22.9), 331 (13.6), 376 (13.8), 431 (25.7)	484	2541
43a	276 (49.0), 323 (39.5), 335 (38.9), 414 (30.0)	561	6329
43b	276 (44.0), 334 (40.9), 409 (36.1)	510	4664
43c	276 (51.3), 335 (46.3), 417 (44.8)	545	5632

The broadening of low energy absorption band of **43a-43c** as compared to **39b** in dichloromethane solution is due to the merging of charge transfer band with the π - π^* transition in the former. The splitting of low energy band into three bands can be clearly seen by addition of TFA in dichloromethane of which the first two are originating from their corresponding amines (see Figure 5.7). The third low energy part of this band is due to charge transfer from amine donor to cyanoacrylic acid acceptor because only the third part is shifted towards the longer wavelength on addition of TFA (*vide infra*).

Dyes **43a-43c** possess high molar extinction coefficients for the longer wavelength in absorption which is due to presence of two adjacent donor moiety, increasing the transition probability. High molar extinction coefficient makes these dyes more promising for light harvesting capacity. Among the dyes **43a-43c**, the dye containing fluorene as spacer show highest molar extinction coefficient providing more planarity for the charge transfers.

The influence of the donor-acceptor interactions on the absorption spectra is clearly evident on comparing the absorption maxima of the precursor amines (**36b**, **41a-41c**) and aldehydes (**38b**, **42a-42c**) with that of the dyes **39b**, **43a-43c**. The dyes **39b**, **43a-43c** exhibited bathochromic shift in absorption as compared to parent amines and aldehydes as shown in Figure 5.8. The data are displayed in Table 5.2. The absorption pattern of amines consist of two absorption band out of which the highest energy band is due to $\pi-\pi^*$ transition and another band at higher wavelength is due to $\pi-\pi^*$ transition of pyrene. The amines show vibronic pattern in absorption due to the presence of pyrene. The absorption pattern of *N,N*-diphenylpyren-1-amine (**36b**) was found to be very similar to that reported for pyrene-dimethylaniline derivative by Techert et al.⁴² The slight red shift for **36b** as compared to pyrene-dimethylaniline is due to the directly linked nitrogen to the pyrene which results in more electronic coupling with π -electrons of pyrene.

The absorption profile of **41a-41c** is red shifted as compared to **36b**. This is due to the increase in conjugation by inserting spacer between two donor systems. The molar extinction coefficient is also high for **41a-41c** as compared to **36b**. This is due to the presence of two donor systems which increase the donor strength and hence the transition probability. Another observation is that the amine (**41b**) having biphenyl between the two pyrenylphenylamine, showed hypsochromic shift as compared to phenyl (**41a**) and fluorene containing amines (**41c**).

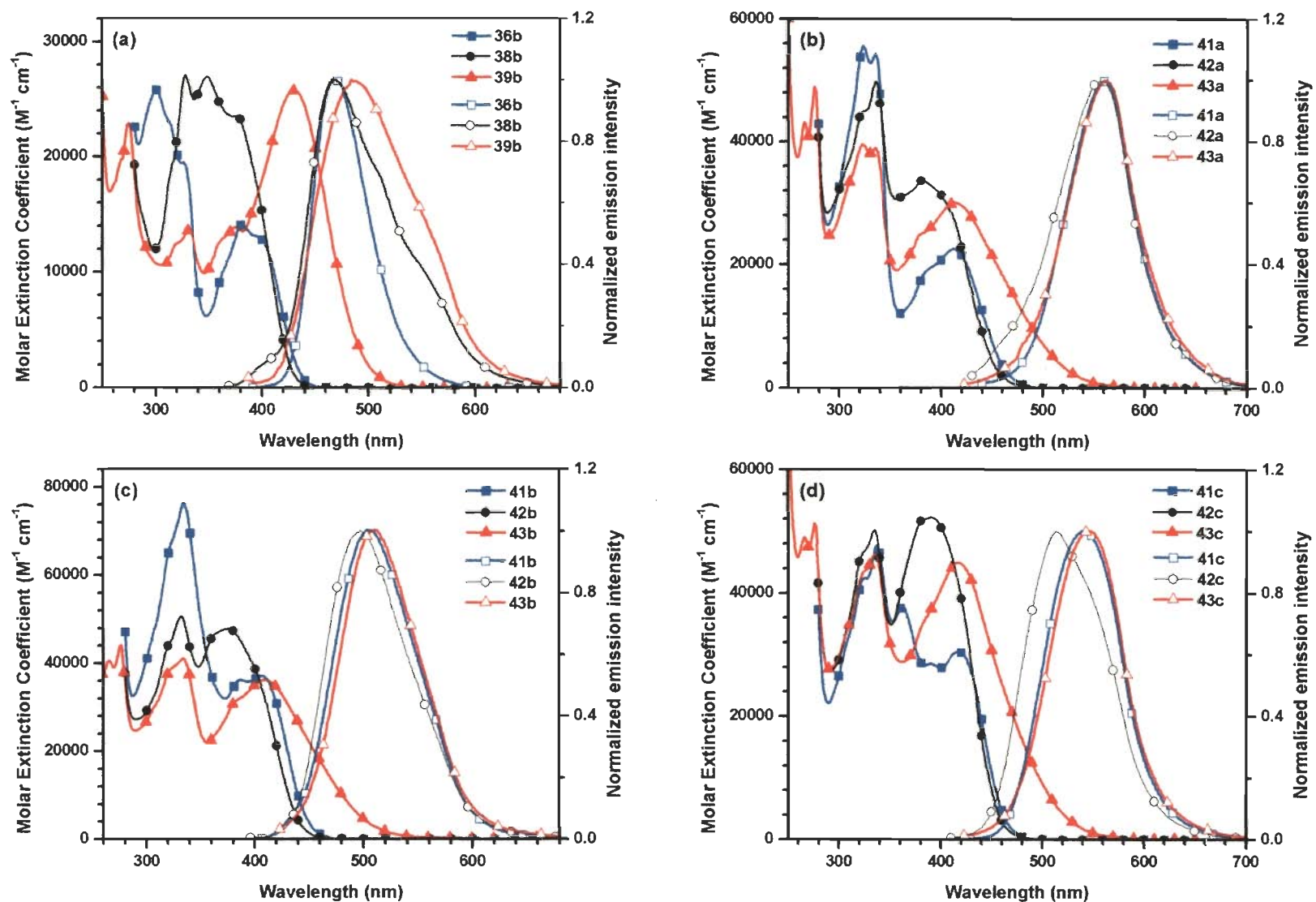


Figure 5.8 Comparison of absorption (filled) and emission (unfilled) spectra of (a) 39b, (b) 43a, (c) 43b, (d) 43c with their corresponding amines (36b, 41a-41c) and aldehydes (38b, 42a-42c) recorded in dichloromethane.

This is because of the twisting nature of biphenyl which decreases the electronic coupling between two donor systems. The fluorene containing amine (**41c**) showed red shifted absorption among all amines but the molar extinction coefficient was found higher for **41b**. Another interesting thing is red shift for **41b** in the absorption spectra when compared to previously reported *N,N'*-bis-(1-naphthyl)-*N,N'*-diphenyl-1,1'-biphenyl-4,4'-diamine (**NPB**)⁴³ which showed absorption peak at 340 nm. The new peak appearing at 406 nm on replacement of pyrene instead of naphthalene, is due to the presence of electron rich pyrene which increase the donor strength and charge transporting properties of amine or amine to pyrene charge transfer.

In comparison to amines (**36b**, **41a-41c**), the absorption spectra of the aldehydes (**38b**, **42a-42c**) showed higher molar extinction coefficient with slight blue shift in the higher wavelength absorption. Aldehyde group being an acceptor may cause the charge transfer from amine to aldehyde, which competes with the charge transfer from amine to pyrene. But the intensity of absorption band for aldehydes has increased because the higher wavelength absorption in the aldehydes probably originates from two transitions one is amine to pyrene and another amine to aldehyde electronic transition. Moreover, the intensity of charge transfer band increases on going from phenyl (**42a**) to fluorene (**42c**). In case of **38b** only one band with vibronic pattern was observed because the charge transfer band was merged with the π - π^* transition band. The absorption profile of the dyes (**39b**, **43a-43c**) is red shifted and broader as compared to their corresponding amines and aldehydes due to the origin of charge transfer transition from amine donor to cyanoacrylic acid acceptor.

The absorption spectra of all the dyes were recorded in the solvent of different polarity viz toluene, tetrahydrofuran, dichloromethane, acetonitrile and methanol to identify the effect of solvent polarity. The absorption spectrum of dye **39a** was not affected by solvent polarity while

that of **39b** showed a prominent negative solvatochromism for the low energy band by increasing the solvent polarity (Figure 5.9). This could be due to more solvation of **39b** in polar solvent. This also reasserts the charge transfer nature for this band in **39b**. Following changes were observed in the absorption wavelength of dye **39b** by changing solvent polarity.

(1) The trend of blue shift was observed as (MeOH>CH₃CN>DCM) which is according to the ionizing power of solvent. More ionizable solvent causes the deprotonation of the dye resulting in less donor-acceptor interaction and hence more blue shifted absorption was observed in case of methanol. Another reason for blue shift in methanol could be the hydrogen bonding possibility of the protic polar solvent methanol with the carbonyl of dye. (2) The unusual blue shift in THF may also be due to hydrogen bonding interaction between oxygen of THF and carboxylic acid of dye. The hydrogen bonding interaction leads to reduce donor-acceptor interactions which result in blue shifted absorption. For further confirmation the absorption and emission spectra of **39b** was recorded in acetonitrile (1×10^{-5} M) and the change was observed after addition of different amount of methanol (Figure 5.10). The trend of blue shift in methanol is showing that the equilibrium is completely shifted towards the deprotonated side. In ground state **39b** is present in deprotonated form in methanol. In Figure 5.10B, the blue shift in emission wave length after addition of methanol is due to methanol induced relaxation of the dye in the excited state.

The absorption spectra of the dyes **43a-43c** showed no significant difference by changing the solvent polarity (Figure 5.11). Only slight blue shift was observed in methanol. The reason could be the less chance of deprotonation in the dyes **43a-43c** due to presence of two donor systems which increases the donor strength and hence strengthens O-H bond of carboxylic acid. Thus the donor-acceptor interaction was not affected by changing the solvent polarity resulting

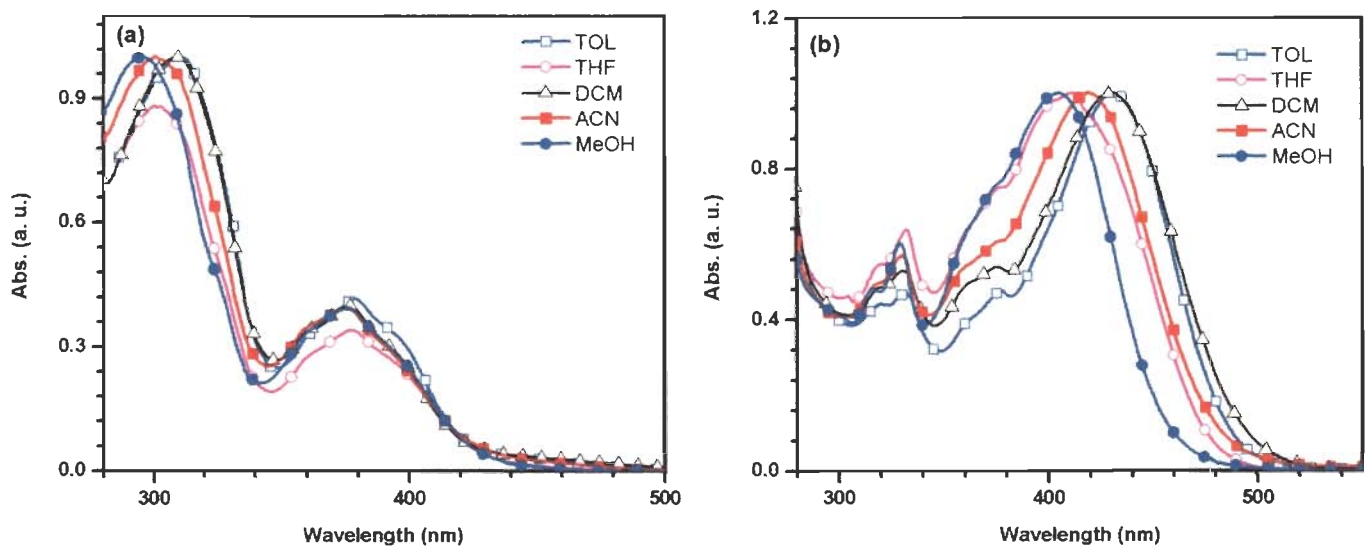


Figure 5.9 Absorption spectra of (a) 39a and (b) 39b in toluene, tetrahydrofuran, dichloromethane, acetonitrile and methanol.

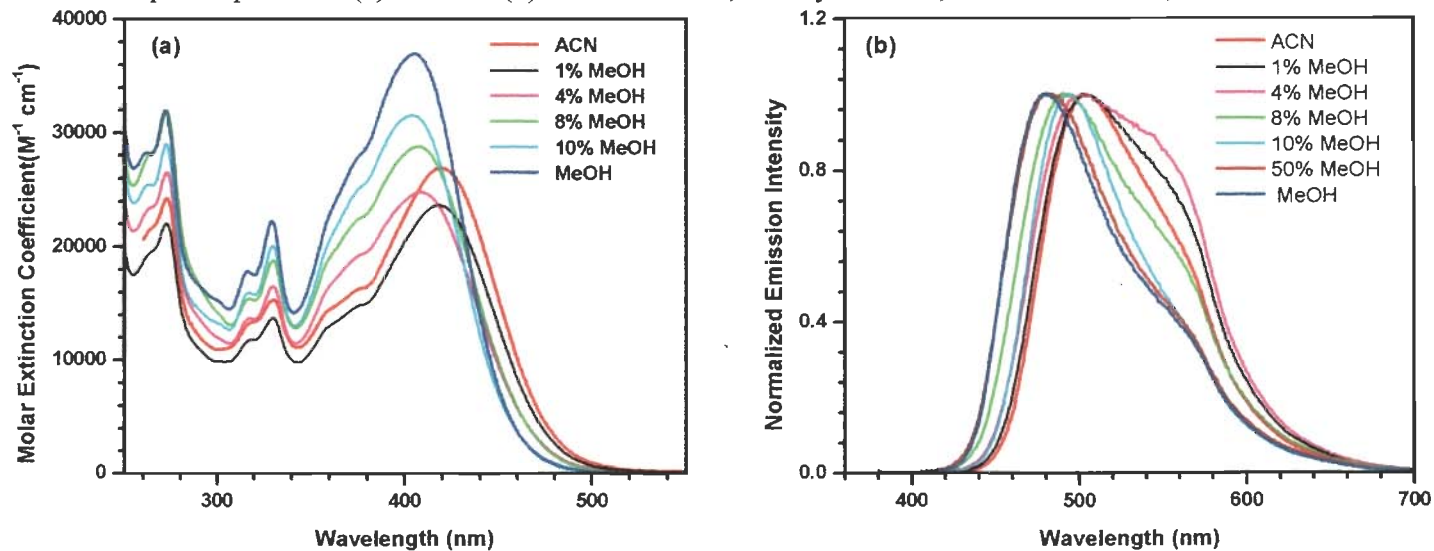


Figure 5.10 Absorption (a) and emission (b) spectra of 39b in acetonitrile and methanol.

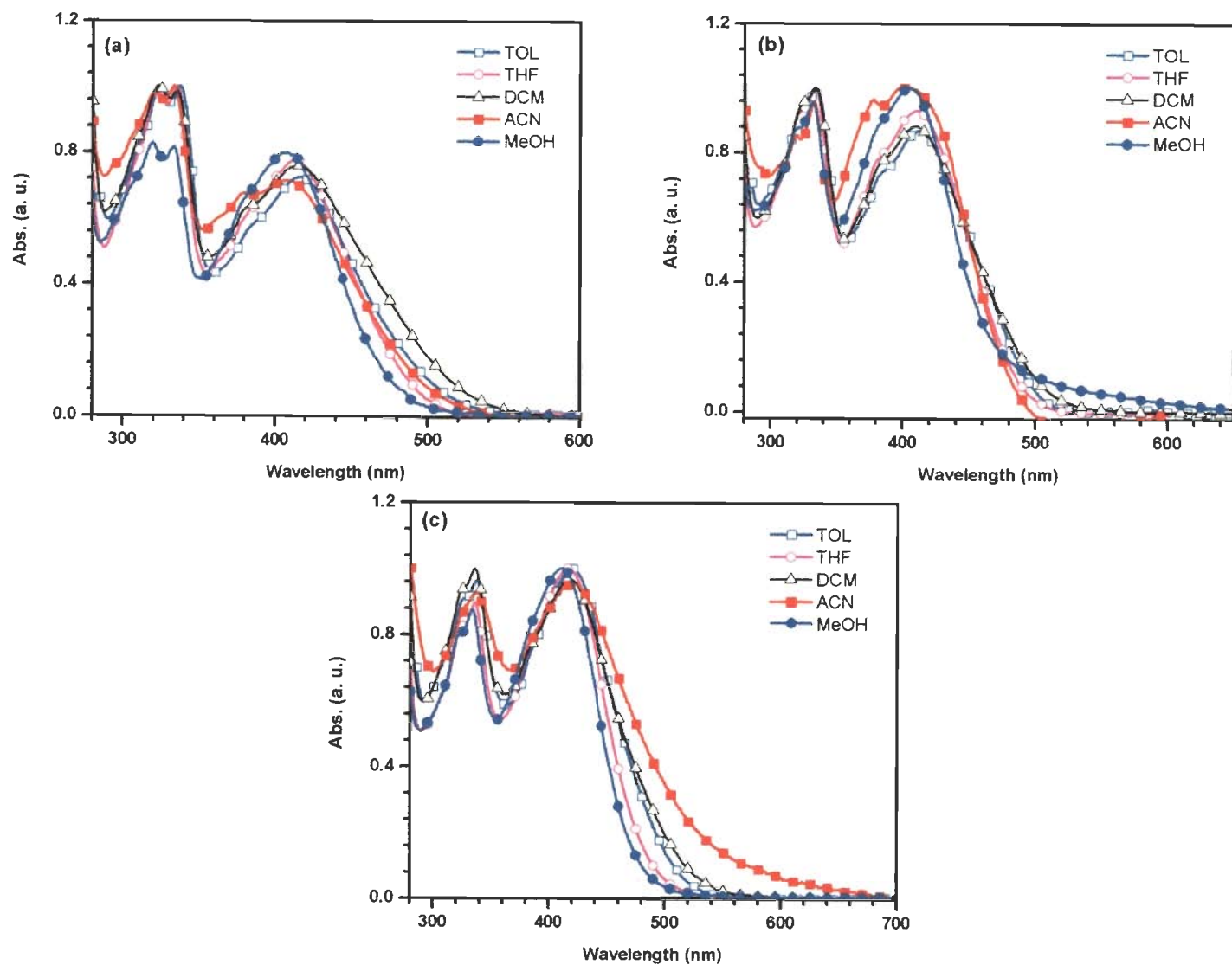


Figure 5.11 Absorption spectra of **43a** (a), **43b** (b) and **43c** (c) in toluene, tetrahydrofuran, dichloromethane, acetonitrile and methanol.

Table 5.3 Absorption data of the dyes **39a**, **39b** and **43a–43c** recorded in different solvents.

Dyes	λ_{\max} , nm (ϵ_{\max} , $M^{-1}cm^{-1} \times 10^3$)								
	TOL	THF	DCM	DCM + TFA	DCM + TEA	MeOH	MeOH + TFA	MeOH + NaOH	ACN
39a	309, 379	300, 377	274 (29.5), 309 (38.6), 377 (15.4)	273 (30.3), 311 (42.4), 376 (17.1)	296 (35.6), 377 (15.2)	272 (36.9), 296 (40.5), 376 (16.0)	273 (32.4), 303 (40.6), 376 (16.9)	272 (35.2) 296 (38.9) 376 (15.6)	376, 300
39b	332, 375, 431	332, 376, 411	274 (22.9), 331 (13.6), 376 (13.8), 431 (25.7)	274 (23.9), 327 (13.6), 360 (12.9), 448 (31.4)	332 (16.1), 402 (23.2)	272 (31.9), 329 (22.2), 405 (36.9)	271 (32.5), 329 (19.3), 423 (41.3)	272 (25.5) 329 (18.1) 403 (29.6)	330, 374, 420
43a	324, 337, 415	322, 335, 413	276 (49.0), 323 (39.5), 335 (38.9), 414 (30.0)	276 (58.6), 322 (43.9), 381 (29.5), 408 (30.9), 460 (28.1)	276 (48.9), 322 (39.9), 336 (39.9), 410 (33.9)	274, 319, 333, 407	274, 319, 332, 412	274, 319, 333, 406	320, 333, 406
43b	334, 411	333, 410	276 (44.0), 334 (40.9), 409 (36.1)	275 (51.3), 331 (47.0), 378 (32.3), 401 (29.6), 460 (36.3)	276 (44.0), 335 (42.4), 405 (42.8)	273, 331, 403	273, 330, 411	273, 331, 403	332, 400
43c	337, 419	335, 415	276 (51.3), 335 (46.3), 417 (44.8)	276 (54.6), 334 (48.2), 380 (36.2), 416 (40.9), 463 (33.2)	322 (38.6), 336 (38.7), 409 (32.8)	274, 333, 410	274, 332, 412	274, 333, 410	336, 420

in unaffected absorption spectra.

The protonation-deprotonation study was done by the addition of acid TFA and base (TEA and NaOH) to the dye solutions dichloromethane and methanol. All the dyes except **39a** showed a red shift after addition of TFA in dichloromethane solution. The reason could be the equilibrium between the protonated and deprotonated form of the dye in solution (Figure 5.12).

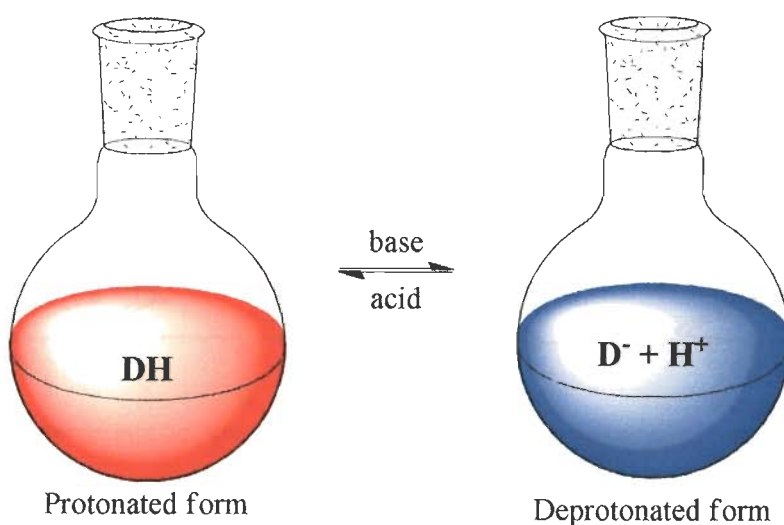


Figure 5.12 Illustration of acid-base equilibria of the dyes.

This indicates that dyes are partially deprotonated in dichloromethane solution which would diminish the electron accepting ability of acceptor resulting in less donor-acceptor interaction. But after addition of TFA the equilibrium shifted towards protonated form due to which the charge transfer interaction increases that lead to red shift in absorption wavelength.

The lower energy band of the dye **39b** exhibited 17 nm bathochromic shift after addition of TFA in dichloromethane. Whereas the higher wavelength band of the dyes **43a-43c** split into three bands after addition of TFA. Out of the three band, the band at higher wavelength region showed red shift in TFA, while other two bands remain at the same position. This clearly indicates that the low energy absorption band of the dyes **43a-43c** consists of three bands, out of

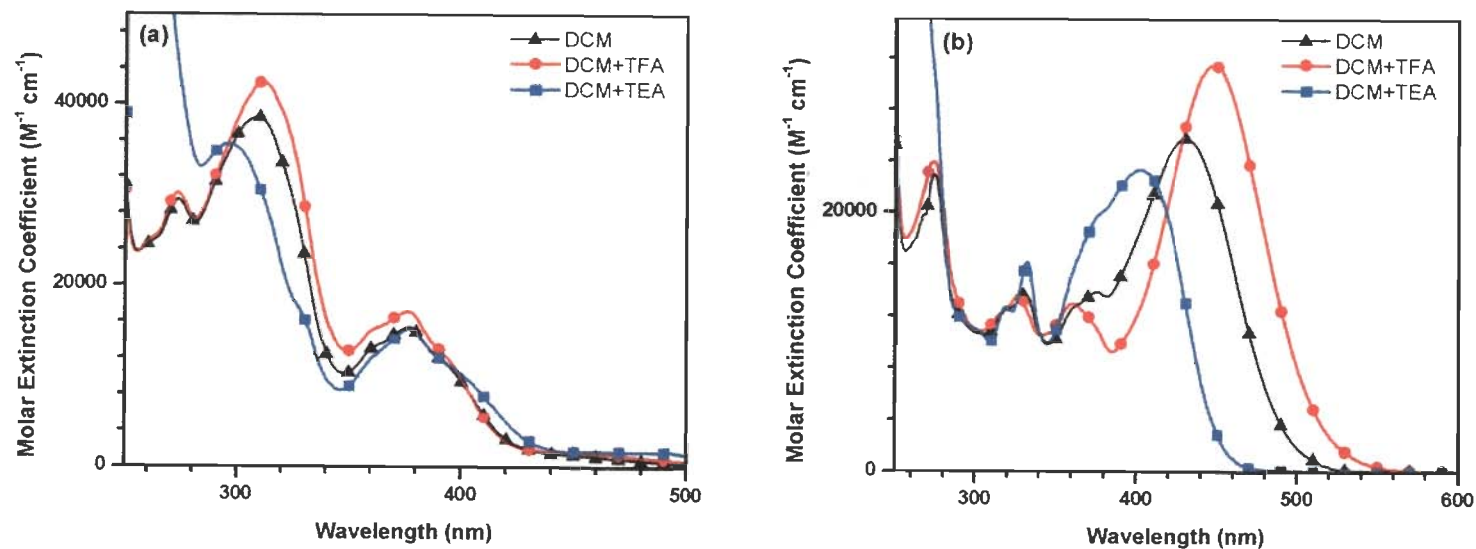


Figure 5.13 Absorption spectra of **39a** (a) and **39b** (b) in dichloromethane before and after addition of TFA or TEA.

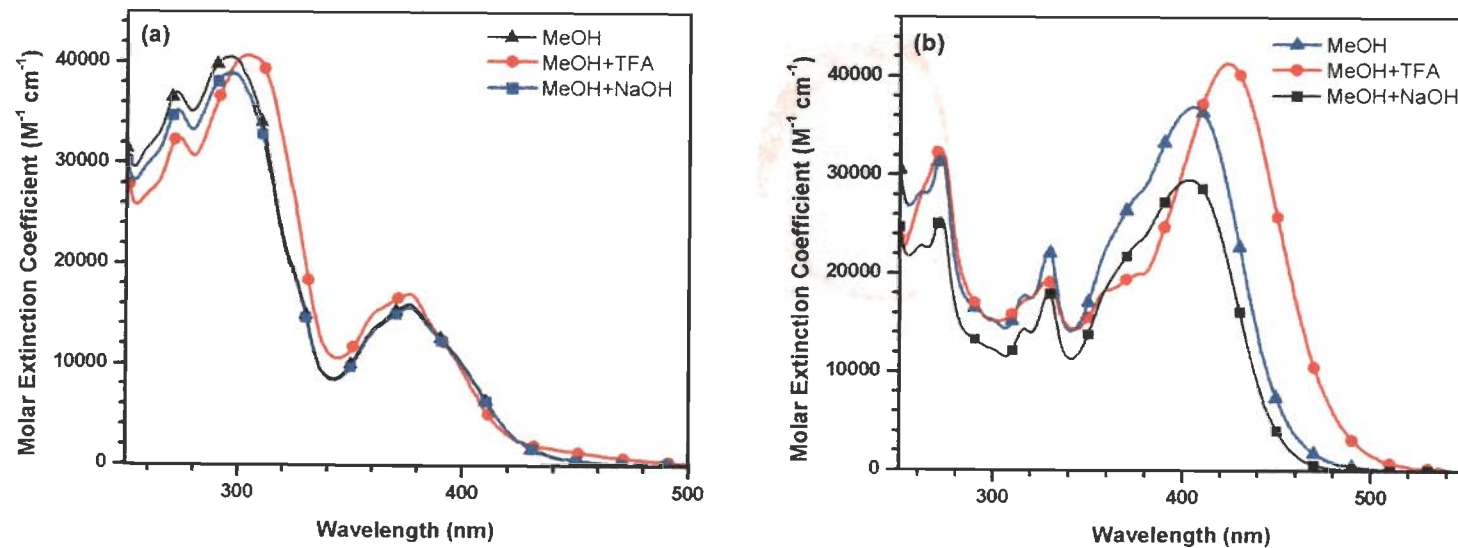


Figure 5.14 Absorption spectra of **39a** (a) and **39b** (b) in methanol before and after addition of TFA or TEA.

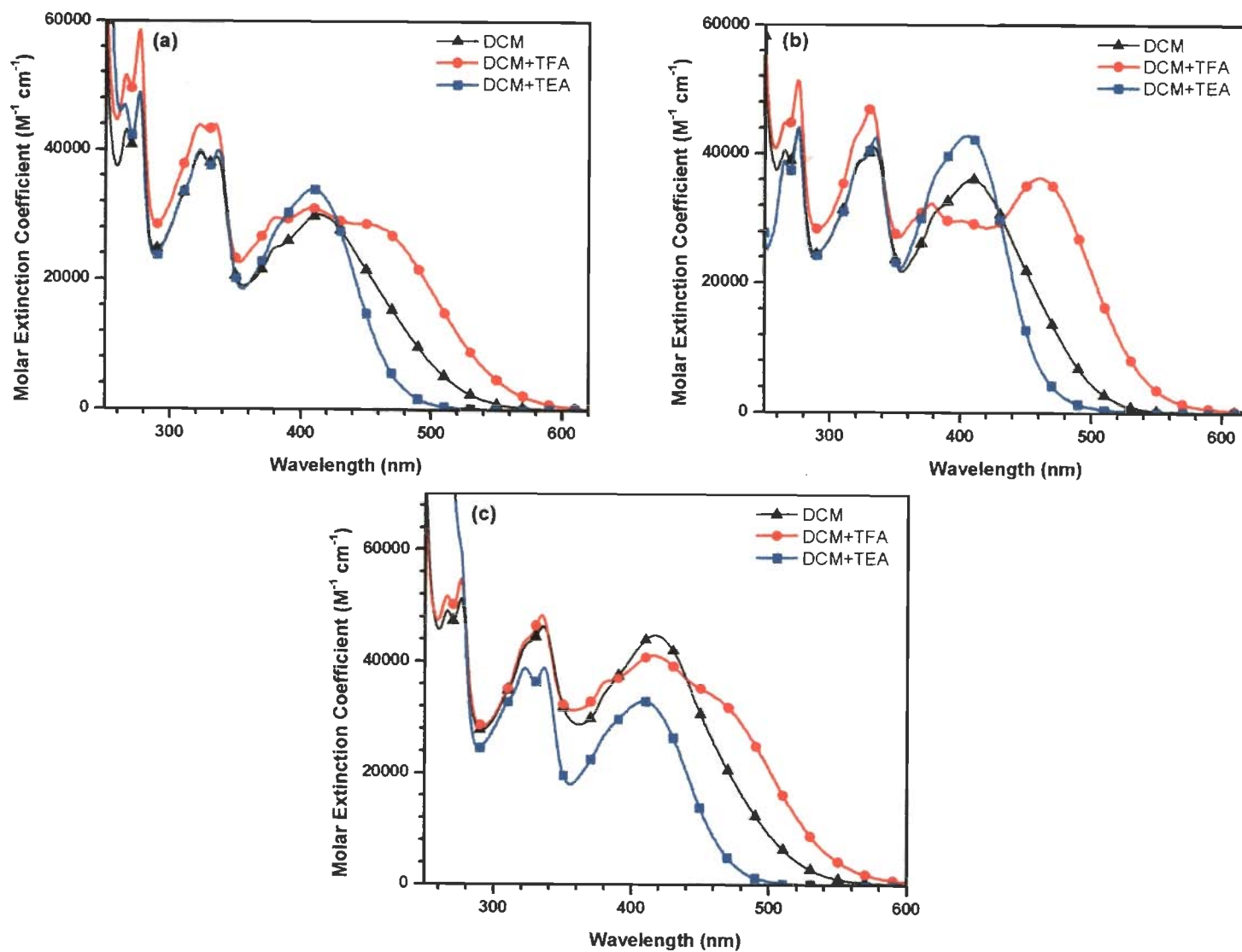


Figure 5.15 Absorption spectra of 43a (a), 43b (b) and 43c (c) in dichloromethane before and after addition of TFA or TEA.

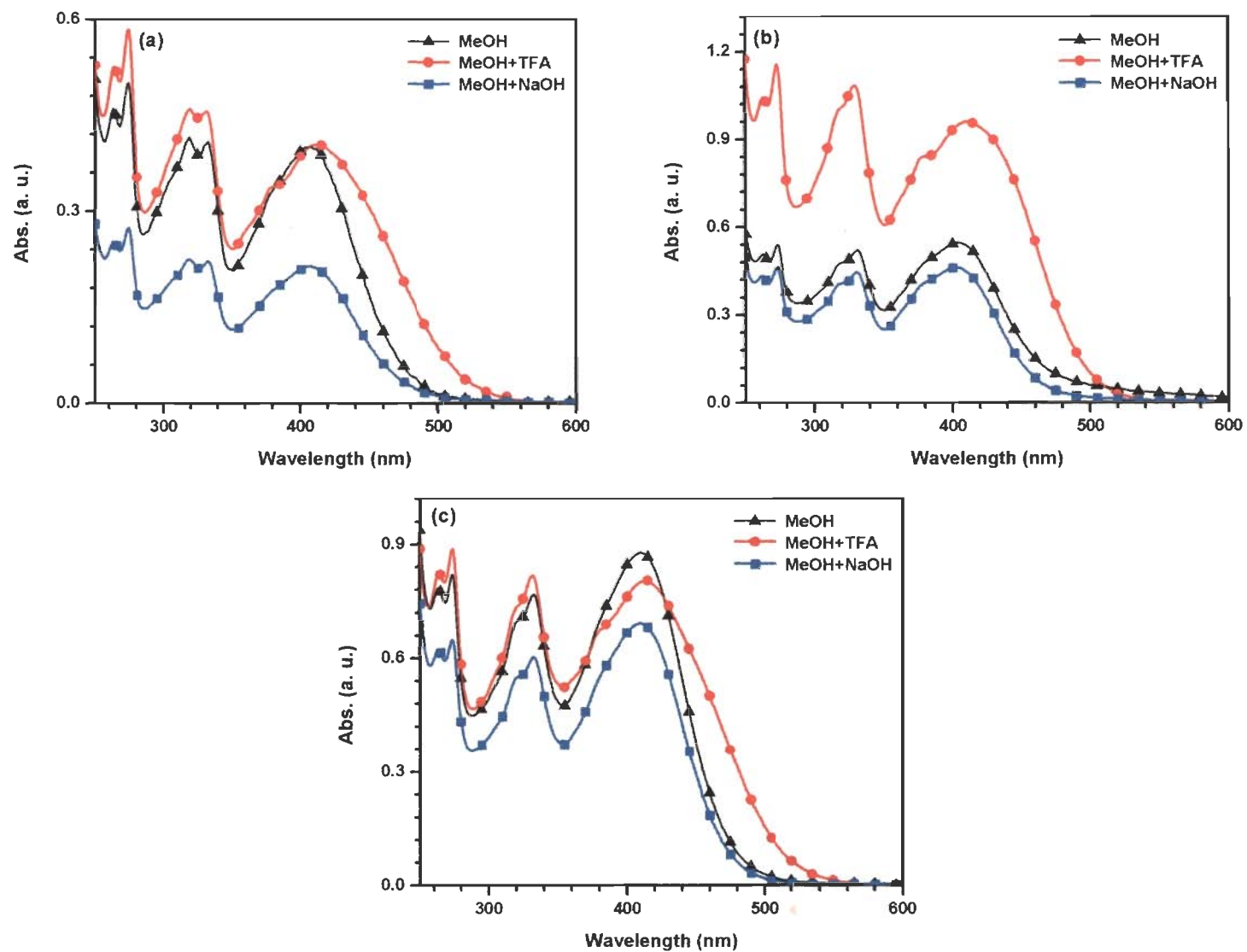


Figure 5.16 Absorption spectra of 43a (a), 43b (b) and 43c (c) in methanol before and after addition of TFA or TEA.

which the band at higher wavelength arises due to charge transfer from amine to cyanoacrylic acid and other two originates from their corresponding amine.

The equilibrium between protonated and deprotonated form was further confirmed when we have added triethylamine (TEA) to the dichloromethane solution. The blue shift was observed after addition of TEA. However, there is no change in absorption profile of **39a** by the addition of TEA. While in other dyes, the lowest energy band shows a prominent blue shift and also shrinks after addition of TEA. This is due to deprotonation of $-\text{COOH}$ group of the dye in the presence of a base which decreases the acceptor strength. (see Figures 5.13 and 5.15).

The dyes showed red shift in longer wavelength of absorption spectra after addition of TFA in methanol solution (Figures 5.14 and 5.16). This suggests that the dyes are present in deprotonated form in methanol solution and after addition of TFA equilibrium shifts towards protonated form leading to red shift. The dyes are present completely in deprotonated form in methanol which is confirmed by addition of a base NaOH which is showing no change in absorption wavelength. Methanol is an ionizable solvent whereas dichloromethane is not. The chance of deprotonation is more in case of methanol due to anionic species of solvent. Therefore the dyes are present in more deprotonated form in methanol as compared to dichloromethane.

There was more red shift (18 nm) observed in case of **39b** after the addition of TFA in methanol solution while in the dyes **43a-43c** showed only 2-8 nm red shift after addition. This observation is showing more deprotonated form in methanol in case of **39b** but the presence of two donor system in the dyes **43a-43c** make more stronger O-H bond of $-\text{COOH}$. Thus the chance of deprotonation is comparatively less for the dyes **43a-43c** as compared to **39b**. The pictorial presentation is shown in Figure 5.17. This suggests that another donor unit increases the

donor as well as acceptor strength of the dyes **43a-43c** which was also assumed in the absorption studies of **39b** and **43a-43c** dyes in different solvents (*vide supra*).

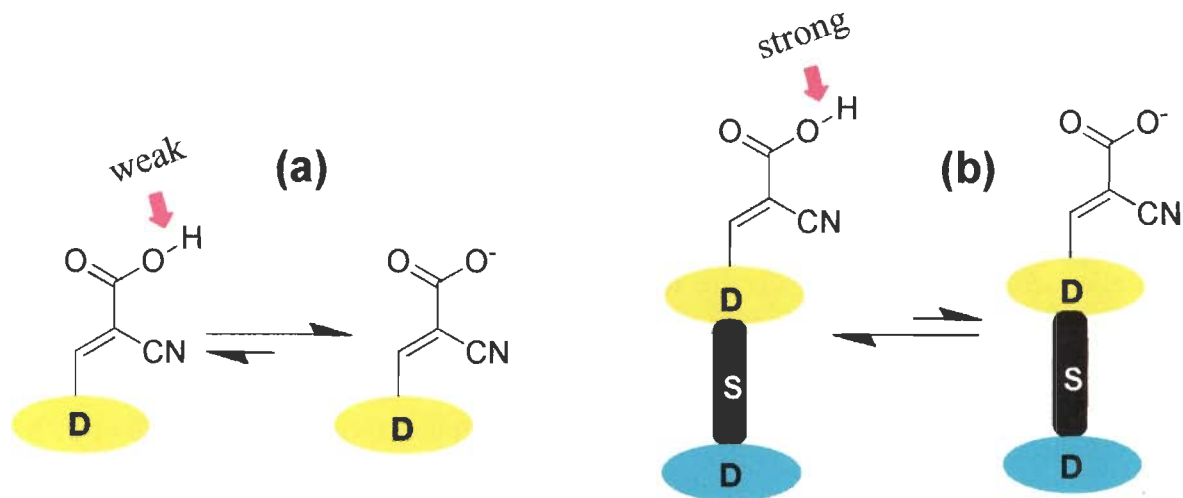


Figure 5.17 Possibility of deprotonation in system having (a) one donor, (b) two donor units.

The absorption spectra were recorded for the dyes (**39a-39b** & **43a-43c**) adsorbed on TiO_2 and displayed in Figure 5.18. The dyes showed broad and red shifted absorption on TiO_2 surface.

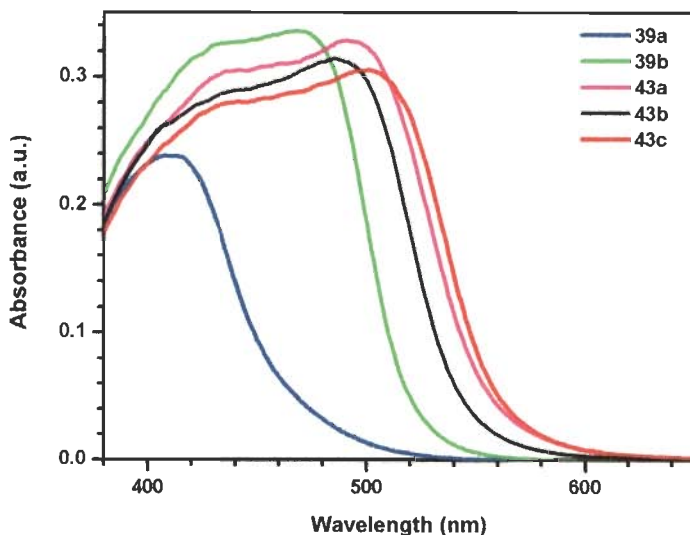


Figure 5.18 Absorption spectra of the dyes **39a**, **39b** and **43a-43c** on TiO_2 layer.

The red shift may be due to the formation of J-aggregates on TiO₂ surface. The red shift in absorption wavelength for the dye adsorbed on TiO₂ has also been previously reported.^{15,31}

The emission spectra of the dyes were recorded in dichloromethane and methanol. As displayed in Figure 5.19. The emission data are given in Table 5.3. All the dyes emit very weakly. The emission range for all the dyes are 461-561 nm in dichloromethane solution. There was no change observed for all the dyes after addition of TFA in emission wavelength except **39b**. The emission wavelength of **39b** is red shifted after addition of TFA. The charge transfer character is evidenced by the red shift of dyes as compared to their corresponding amines and aldehydes.

The amines exhibited the emission wavelength in the range of 469-562 nm. The observed trend of emission wavelength was **36b** < **41b** < **41c** < **41a**. On comparing the emission of **36b**, that of **41a-41c** showed bathochromic shift due to the presence of two donor system separated by a spacer. The amine containing smaller phenyl spacer (**41a**) exhibited the highest red shifted emission. The aldehydes showed hypsochromic shift than the amine due to competitive delocalization of electrons (*vide supra*). The Stokes' shift was found higher for aldehydes as compared to amines showing the more planarity and rigidity of amines in the excited state.

Table 5.4 Emission properties of the dyes **39a**, **39b** and **43a-43b**.

Dyes	λ_{em} , nm		Stokes shift, cm ⁻¹	
	dichloromethane	methanol	dichloromethane	methanol
39a	461	469	4833	5274
39b	484	475	2541	3639
43a	561	572	6329	7088
43b	510	499	4664	4774
43c	545	542	5632	5940

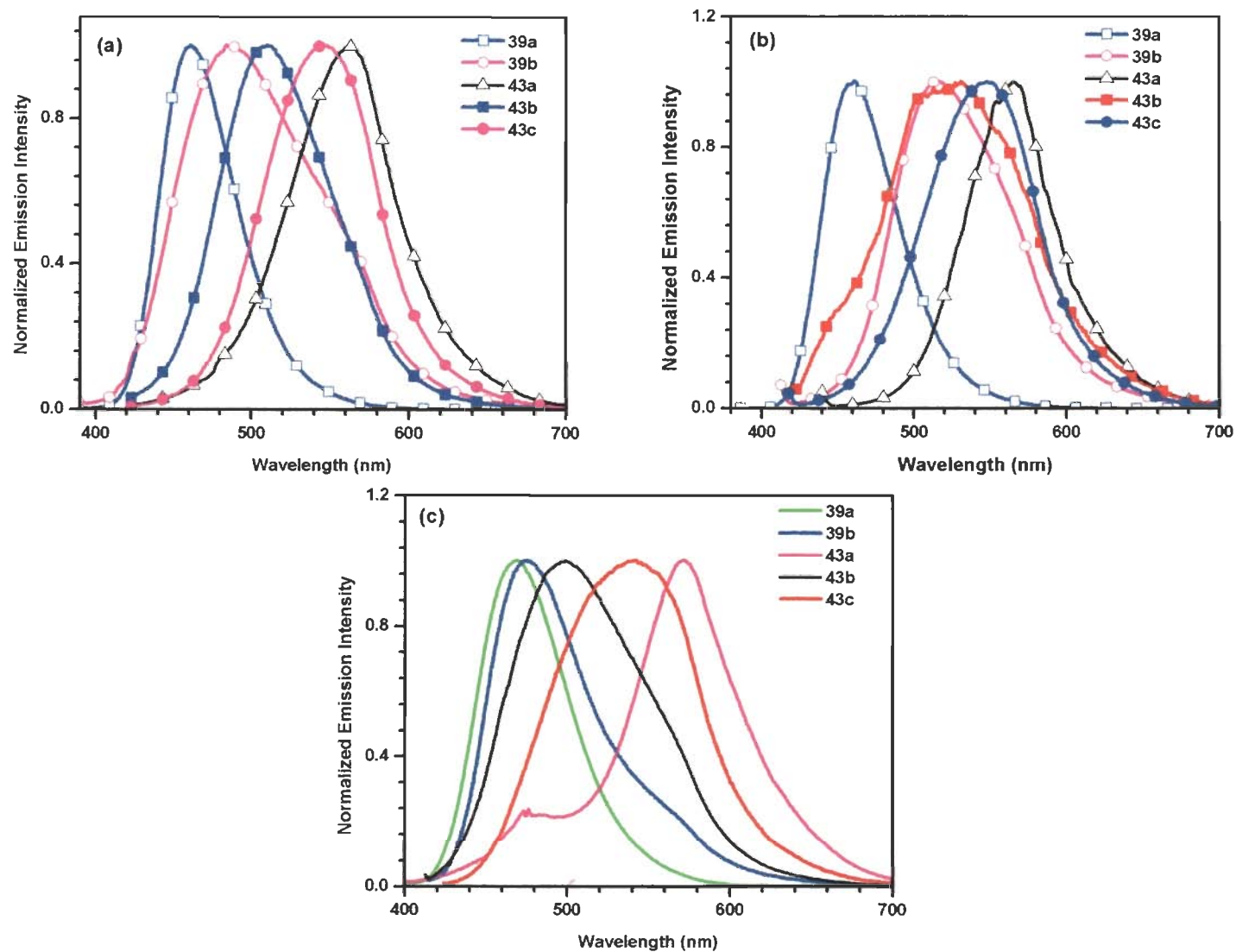


Figure 5.19 Absorption spectra of dyes **39a**, **39b** and **43a-43c** recorded in dichloromethane before (a), after (b) addition of TFA, (c) in methanol.

5.2.3 Electrochemical properties

The possibility of electron transfer from the excited dye molecule to the conductive band of TiO₂ and the dye regeneration can be best understood by cyclic voltammetric (CV) method. The electrochemical analysis was done in dichloromethane solution (2×10^{-5} M) using tetrabutylammonium hexafluorophosphate as a supporting electrolyte. The cyclic voltammograms of the dyes **43a-43c** with precursor amines, and aldehydes are shown in Figure 5.20 and the electrochemical data are given in Table 5.7. Compounds **36b** and **38b** exhibited one quasi reversible oxidation couple, whereas **41a-41c** and **42a-42c** exhibit two quasi reversible oxidation couple indicating the presence of one and two donor amines respectively.

The dyes **39a-39b** showed one quasi reversible oxidation peak while two oxidation peaks were observed for the dyes **43a-43c** which confirms the presence of two amine donor moieties. The oxidation potential of **39b** is anodically shifted as compared to **39a**. The reason may be the more pronounced interaction between donor and acceptor in **39b** which make the amine donor less prone to oxidize. In general, high oxidation potential show a strong intramolecular charge transfer interaction between donor and acceptor due to which lone pair of donor is less available for oxidation. The donor-acceptor interactions can be verified by comparing the oxidation potential of the dyes to that of their corresponding amines and aldehyde. The dyes showed higher oxidation potential than their amines and aldehyde, which confirms the presence of intramolecular charge transfer interactions between donor and acceptor. Among the dyes **43a-43c**, dye **43b** exhibited high oxidation potential as compared to **43a** and **43c** showing more intramolecular charge transfer interaction.

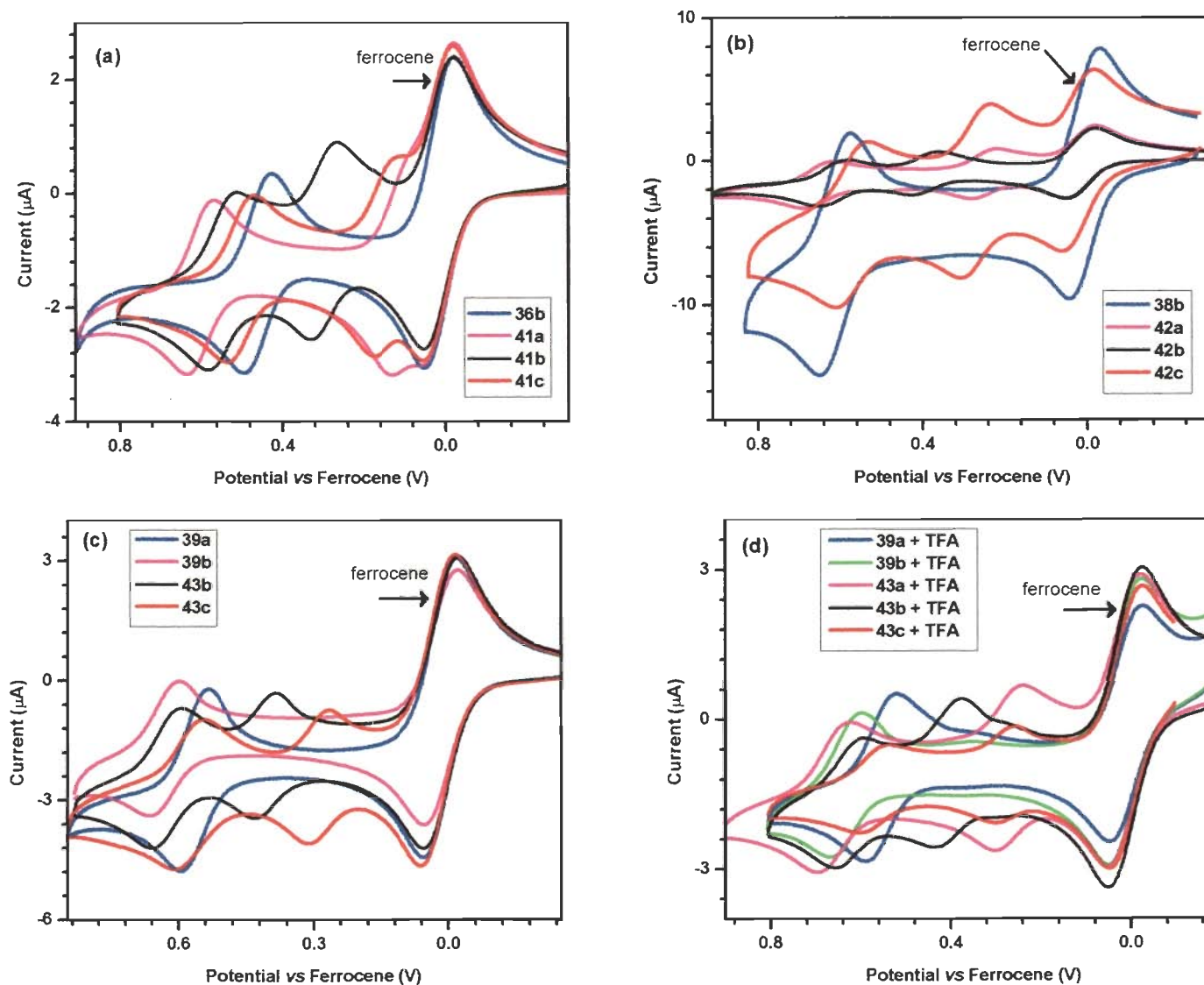


Figure 5.20 Cyclic voltammograms of (a) the precursor amines (36b, 41a-41c), (b) aldehydes (38b, 42a-42c) and dyes (39a, 39b & 43a-43c) (c) before and (d) after addition of TFA.

The cyclic voltammograms of dyes in the presence of TFA has shown in Figure 5.20(d). When the cyclic voltammetry was done in presence of TFA, the oxidation potential increases slightly confirming our above explanation of protonation-deprotonation in absorption spectra. **43c** showed no change in oxidation potential after addition of TFA, indicating the O-H bond of -COOH is comparatively stronger due to which there is less chance of deprotonation in **43c**. This may be due to the presence of fluorene.

To evaluate the possibility of electron transfer from the excited dye molecule to the conductive band of TiO₂ and the dye regeneration, we have calculated the ground-state oxidation potentials correspond to the HOMO levels of the dyes, ranging from 1.31 to 1.38 V vs NHE for DC dyes while 1.01-1.16 V vs NHE for **43a-43c** dyes. The values are more positive than the iodide/ triiodide redox couple (~0.42 V vs NHE). That ensures the efficient regeneration of the dye by receiving the electron from electrolyte and prevents the chance of charge recombination. The values of redox potential of **43a-43c** dyes are well matching with that of electrolyte as compared to **39a, 39b** dyes due to the presence of extra pyrenylphenylamine donor which decrease the HOMO energy level of the dye. **43b** show more positive ground state potential than **43a & 43c** due to more charge transfer character.

We have also estimated the excited-state redox potential (E_{ox}^*) of the sensitizers which corresponds to LUMO levels of the dyes to identify the feasibility of electron injection from the dye to TiO₂. The excited state potential was calculated from the first oxidation potential (E_{ox}) at the ground state and the zero-zero electronic transition energy (E_{0-0}) as given below

$$E_{ox}^* = E_{ox} - E_{0-0}$$

The optical band gap was derived from the absorption edge which is the transition wavelength of the normalized absorption and emission spectra. A dye must possess more

negative excited state potential than the energy level of TiO₂ conduction band edge (-0.5 V vs NHE) for energetically favorable downhill electron injection to TiO₂ conduction band. The E_{ox}* values observed for the dyes (-1.32 to -1.63 V versus NHE) are more negative than the conduction band edge energy level of the TiO₂ electrode. Thus these dyes are suitable for the injection of electron to the TiO₂ conduction band. The energy level diagram of dyes is shown in Figure 5.21.

Table 5.5 Electrochemical properties of amines (36b, 41a-41c), aldehydes (38b, 42a-42c) and dyes (39a, 39b, 43a-43c)

Dyes	E _{ox} ^a (ΔE _p) mV	E _{ox} ^b , mV	HOMO ^c (eV)	LUMO ^d (eV)	E ₀₋₀ ^e , eV	E ₀₋₀ * ^f , V
36b	444 (69), 940	-	5.24	2.36	2.88	-
41a	96 (48), 588 (64), 1128	-	4.90	2.25	2.65	-
41b	280 (64), 532 (70), 992	-	5.08	2.28	2.80	-
41c	140 (66), 492 (67), 1040	-	4.94	2.28	2.66	-
38b	604 (76), 976	-	5.40	2.45	2.95	-
42a	236 (65), 644 (71), 1124	-	5.04	2.28	2.76	-
42b	380 (63), 604 (69), 992	-	5.18	2.36	2.82	-
42c	260 (76), 556 (80), 964	-	5.06	2.33	2.73	-
39a	544 (62), 972	544, 956	5.34	2.40	2.94	-1.626
39b	612 (65), 968	620, 968	5.41	2.71	2.70	-1.318
43a	244 (48), 636 (48), 1108	260, 648, 1120	5.04	2.51	2.53	-1.516
43b	392 (44), 608 (64), 1004	400, 616, 1008	5.19	2.52	2.67	-1.508
43c	276 (47), 556 (64), 1060	272, 556, 1024	5.07	2.51	2.56	-1.518

^a measured in dichloromethane (2 x 10⁻⁵M); ^b measured in dichloromethane in the presence of TFA; ^c derived from oxidation potential using the formula E_{HOMO} = E_{ox} + 4.8 eV; ^d deduced using the formula E_{LUMO} = E_{HOMO} - E₀₋₀ (Band Gap); ^e calculated from absorption edge; ^f excited state oxidation potential vs NHE.

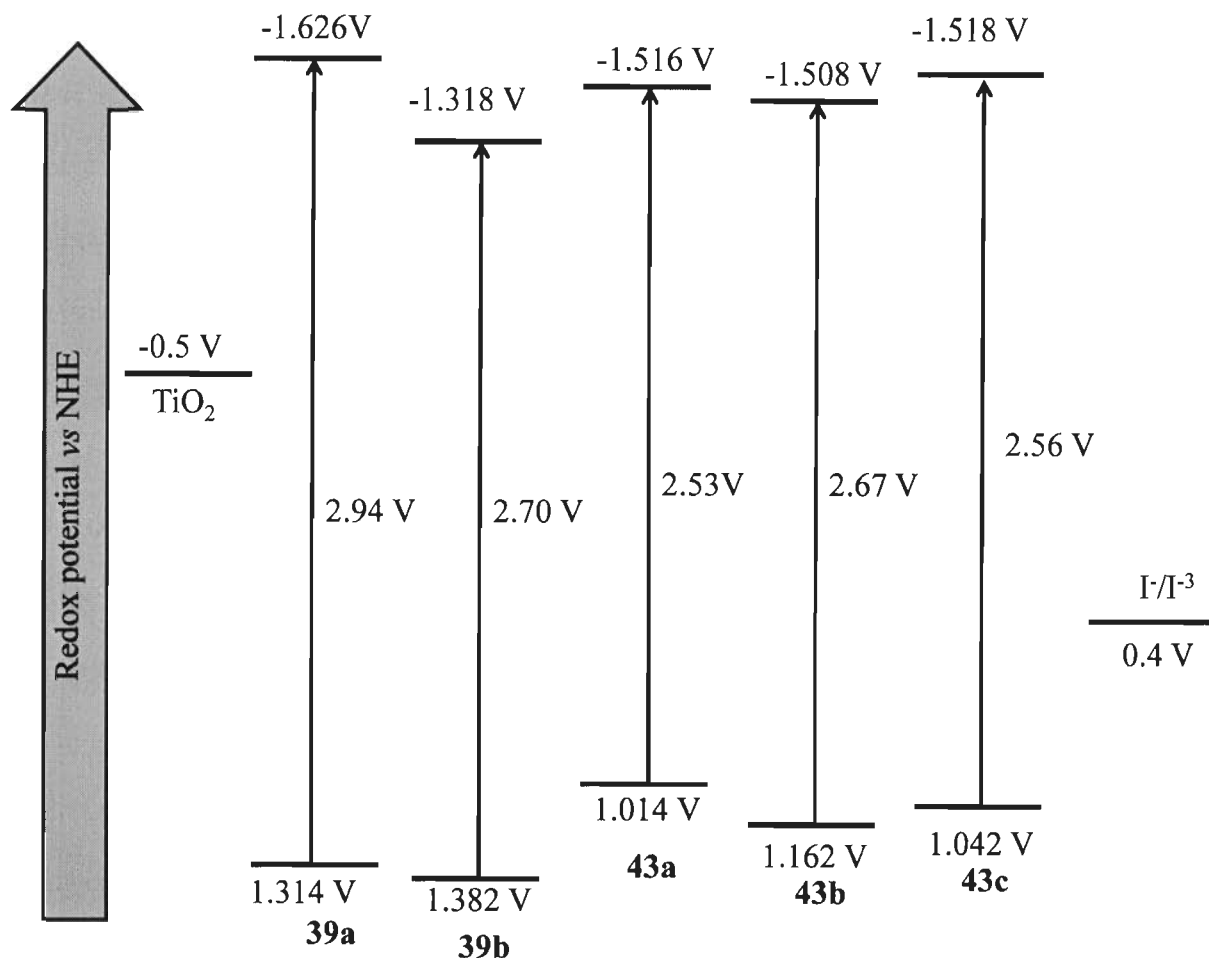


Figure 5.21 Energy level diagram of the dyes 39a, 39b and 43a-43c.

5.2.4 Theoretical investigations

Density functional theory (DFT) calculations have been employed to investigate the structures and absorption spectra of the dyes 39a, 39b and 43a-43c. The ground-state geometries were fully optimized without any symmetry constraints at the DFT level with Becke's⁴⁴ three parameters hybrid functional and Lee, Yang and Parr's correlational functional B3LYP⁴⁵ using a standard 6-31g(d,p) basis set on all atoms. The prominent higher wavelength vertical transitions, dipole moments and their oscillator strength (f) predicted by the theory is collected in Table 5.6. The dyes are not coplanar. These are more tilted due to the presence of bulky pyrene. The π -electron delocalization can be best understood by the frontier molecular orbital diagram.

Frontier molecular orbital diagram give very important information regarding the charge separation and intramolecular charge transfer (ICT) among the organic sensitizer which is an important tool to know the electron injection capability and the overall conversion efficiency. For understanding the distribution of HOMO and LUMO of **39a-39b** and **43a-43c** dyes, we are defining the units present in the molecule. **39a-39b** dyes have pyrene phenyl aniline as donor and cyanoacrylic acid as acceptor. **43a-43c** dye contain donor (D1)- π' -donor (D2)- π -acceptor system. Pyrenylamino donors (D1 & D2) are linked by 1,4-phenyl, 1,6-biphenyl and 2,7-(9,9-diethylfluorenyl) linkers in **43a**, **43b** & **43c** respectively. All the **43a-43c** dyes have cyanoacrylic acid as an acceptor.

The molecular orbital diagram of the dyes (**39a-39b** & **43a-43c**) has been shown in Figures 5.22 and 5.23. In **39a**, HOMO and HOMO-1 is located on the pyrene phenyl aniline while in **39b**, HOMO and HOMO-1 is π -orbital delocalized over the entire molecule. The LUMO is located on the cyanoacrylic group through the phenyl ring of pyrenepheryl aniline and LUMO+1 is located through pyrene phenyl aniline with major contribution of pyrene in both the dyes. This suggests that there is an electron transfer from amine donor to cyanoacrylic acid acceptor but lone pair of nitrogen is also competitively delocalized on pyrene in **39b**. Therefore pyrene is increasing the conjugation of the dye and not taking part in increasing the donor strength.

There is a difference in the distribution of HOMO, HOMO-1, LUMO and LUMO+1 by changing the linker between two donor. In **43a** the HOMO is localized over entire molecule while the HOMO of **43b** and **43c** localized with major contribution of D1- π' and very less contributed by cyanoacrylic acid through phenyl of D2. LUMO of **43a** and **43c** is lying on the cyanoacrylic group with the phenyl ring attached to D2 with less contribution by pyrene of D2 while LUMO of **43b** is mainly on the cyanoacrylic acid unit through phenyl of D2. This suggest

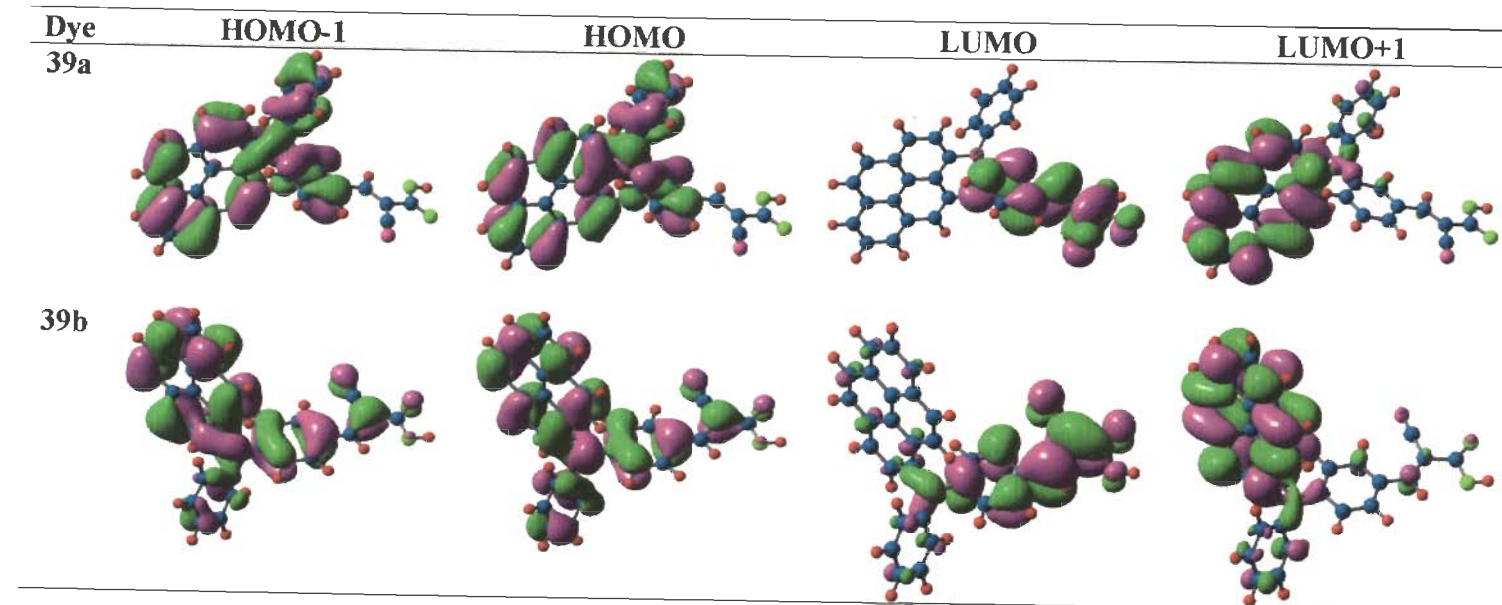
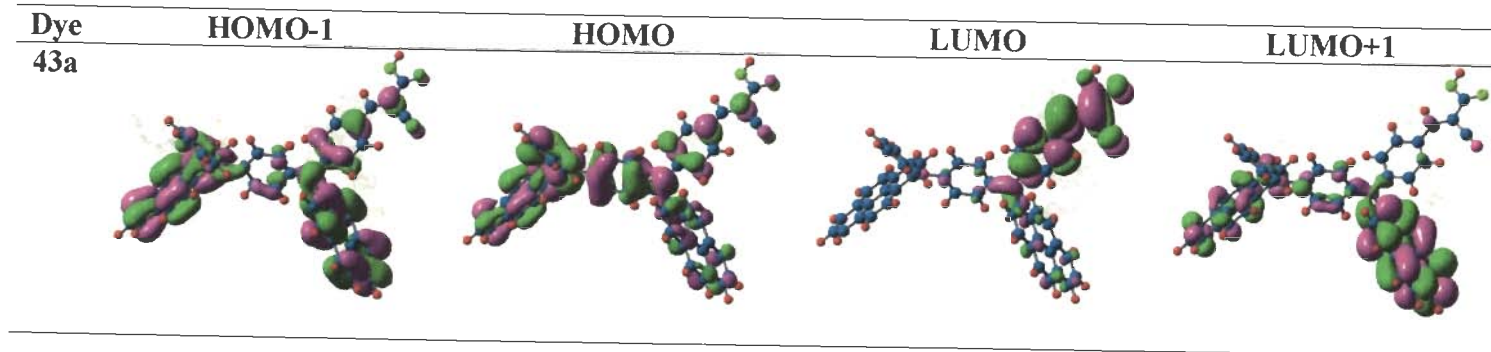


Figure 5.22 Electronic distribution in the frontier molecular orbital diagrams of the dyes 39a and 39b.



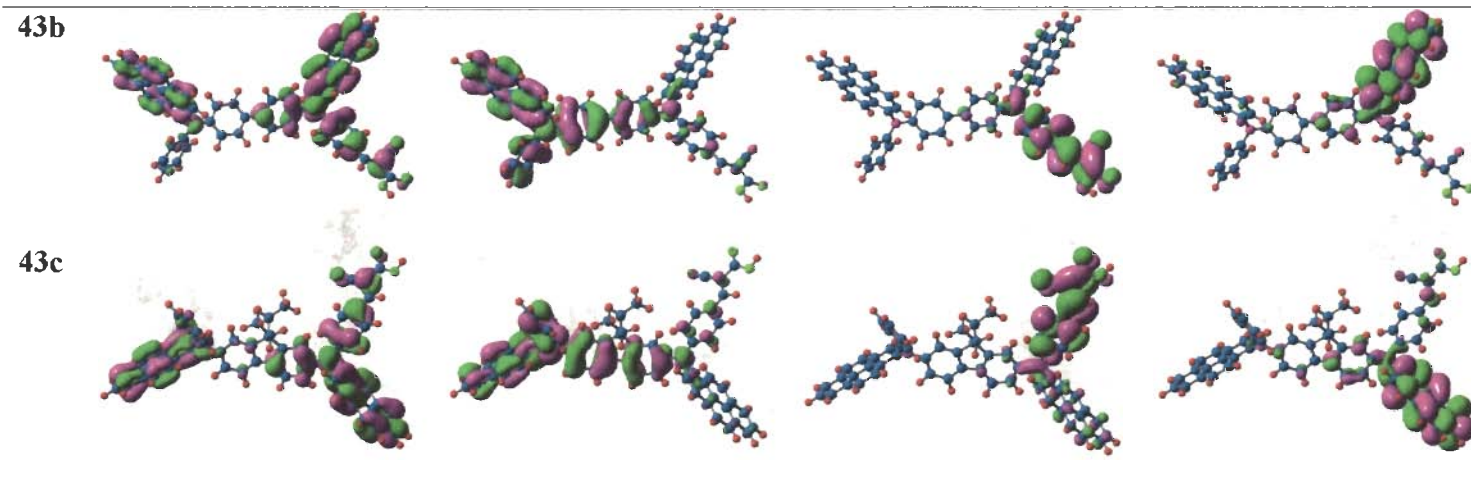


Figure 5.23 Electronic distribution in the frontier molecular orbital diagrams of the dyes **43a-43c**.

Table 5.6 Predicted (TDDFT B3LYP/6-31G(d,p)) vertical transitions and their assignments.

compound	λ_{abs} (nm)	μ	f	Assignment
39a	408.6	7.33	0.26	HOMO→LUMO+1 (+77%), HOMO-1→LUMO (13%), HOMO-1→LUMO+1 (+8%)
	326.4		0.17	HOMO-1→LUMO+1 (+73%), HOMO-2→LUMO+1 (6%), HOMO→LUMO+1 (6%), HOMO-2→LUMO+2 (+6%), HOMO→LUMO+2 (5%)
	310.0		0.19	HOMO→LUMO+3 (+62%), HOMO-2→LUMO+1 (11%), HOMO→LUMO+2 (+9%), HOMO-1→LUMO+2 (+9%)
	305.5		0.36	HOMO-3→LUMO (54%), HOMO-4→LUMO (41%)
39b	440.2	8.19	0.43	HOMO→LUMO (+95%)
	407.0		0.11	HOMO→LUMO+1 (+78%), HOMO-1→LUMO (13%), HOMO-1→LUMO+1 (+7%)
	368.1		0.48	HOMO-1→LUMO (+81%), HOMO-1→LUMO+1 (+7%), HOMO→LUMO+1 (+7%)
	333.3		0.21	HOMO-1→LUMO+1 (+72%), HOMO→LUMO+1 (8%), HOMO-2→LUMO+2 (6%)
43a	489.1	9.58	0.40	HOMO→LUMO (+98%)

	451.2	0.31	HOMO→LUMO+1 (+92%)
	420.3	0.12	HOMO-1→LUMO (+94%), HOMO-2→LUMO (5%)
	382.4	0.15	HOMO-1→LUMO+1 (56%), HOMO-2→LUMO (+32%)
	369.4	0.12	HOMO-2→LUMO (59%), HOMO-1→LUMO+1 (24%)
	351.0	0.23	HOMO-3→LUMO (+48%), HOMO→LUMO+4 (18%), HOMO-2→LUMO+1 (10%), HOMO→LUMO+3 (+10%)
	348.2	0.26	HOMO-3→LUMO (+35%), HOMO→LUMO+3 (26%)
43b	487.1	9.59	0.31 HOMO→LUMO (+98%)
	446.5	0.41	HOMO→LUMO+1 (+71%), HOMO→LUMO+2 (+21%),
	434.8	0.41	HOMO-1→LUMO (+68%), HOMO→LUMO+2 (+20%)
	378.7	0.29	HOMO-2→LUMO (+73%), HOMO-3→LUMO (11%), HOMO-1→LUMO+1 (+7%)
	362.8	0.38	HOMO-1→LUMO+2 (+43%), HOMO-3→LUMO (+35%), HOMO-2→LUMO (+9%)
	347.9	0.35	HOMO→LUMO+3 (+51%), HOMO-2→LUMO+1 (14%)
43c	516.3	8.31	0.21 HOMO→LUMO (+99%)
	468.6	0.48	HOMO→LUMO+1 (+88%), HOMO→LUMO+2 (+7%)
	444.2	0.28	HOMO→LUMO+2 (+75%), HOMO-1→LUMO (+14%)
	435.6	0.24	HOMO-1→LUMO (+81%), HOMO→LUMO+2 (+12%)
	368.9	0.51	HOMO-3→LUMO (+58%), HOMO→LUMO+4 (+26%), HOMO-2→LUMO (+8%)
	362.4	0.11	HOMO-1→LUMO+2 (+82%), HOMO→LUMO+4 (7%), HOMO→LUMO+5 (+7%)
	356.5	0.16	HOMO→LUMO+3 (+34%), HOMO→LUMO+4 (+24%), HOMO-2→LUMO+1 (+13%), HOMO-1→LUMO+3 (+11%), HOMO-3→LUMO (+6%)

that by increasing the linker length between D1 & D2, the extent of ICT increases which will lead to efficient photoexcitation of electron and therefore electron injection from excited dye sensitizer to conduction band of TiO₂. The HOMO-1 of **43a** is majorly contributed by D1 and D2- π -A while that of **43b** and **43c** is occupied pyrene of D1 and one phenyl of biphenyl or fluorene with D2- π -A respectively. LUMO+1 of **43a** is located on D1- π' -D2 with major contribution from pyrene of D2 while LUMO+1 of **43b** and **43c** is mainly located on pyrene of D2 and very less contribution by one phenyl of spacer and cyanoacrylic part through phenyl of D2.

From the theoretical electronic transition data, the dipole moment is higher for the **43a-43c** dyes as compared to **39a-39b** dyes which show the more polar nature due to the presence of two donor system. Among the dyes **43a-43c**, dye **43b** have higher dipole moment than other dyes.

The higher transition in **39a** is due to HOMO \rightarrow LUMO+1, HOMO-1 \rightarrow LUMO+1 and HOMO-1 \rightarrow LUMO clearly indicate that it is due to π - π^* or n- π^* transition in pyrene. The higher transition in **39b** is HOMO \rightarrow LUMO which is an π - π^* transition with some ICT character. Our assumption in assigning the higher wavelength band in experimentally calculated absorption spectra that it comprises of three merged band. It is clearly indicated in the theoretically calculated data. For **43a-43c** dyes the higher three vertical transition bands (Table 5.5) corresponds to these three merged bands (experimentally) which are due to HOMO \rightarrow LUMO, HOMO \rightarrow LUMO-1 and HOMO-1 \rightarrow LUMO respectively. The explanation regarding experimental absorption bands are in accordance to theoretical data.

HOMO-LUMO transition in **43a** is due to π - π^* transition with some ICT character. But in case of **43b** and **43c**, it is due to ICT from donor D1 to cyanoacrylic acid acceptor because the HOMO and LUMO is located on the donor D1 and acceptor respectively and there is a

possibility for electron transfer from donor to acceptor. HOMO to LUMO+1 transition in **43a** is dye to the π - π^* transition in pyrene units. In the dyes **43b** and **43c**, there is an ICT from electron donor D1- π' to electron acceptor pyrene of D2. HOMO-1 to LUMO transition is due to π - π^* transition. Thus **43b** and **43c** exhibited more charge separation as compared to **43a** which enhance the electron injection from dye to TiO₂ surface.

5.2.5 Photovoltaic performance of the dyes

The dye-sensitized solar cells were constructed by using the dyes **39a-39b** and **43a-43c** as the sensitizer for nanocrystalline anatase TiO₂. Typical solar cells, with an effective area of 0.25 cm², were fabricated with an electrolyte composed of 0.05 M I₂/0.5 M LiI/0.5 M *tert*-butylpyridine in acetonitrile solution. The device performance statistics was done under AM 1.5 illumination solar irradiation. The I-V curves of the DSCs sensitized by all the dyes are shown in Figure 5.24 while the IPCE spectra are displayed in Figure 5.25. The detailed photovoltaic parameters are summarized in Table 5.7.

The dye **39b** exhibits maximum IPCE (>70%) between 400 and 550 nm while **43a-43c** display broader IPCE spectra which extends to 620 nm. The broadening is due to the incorporation of additional diarylamine unit which is consistent with the bathochromic shift observed for these dyes in the absorption spectra of the dyes adsorbed on TiO₂ (Figure 5.18). The broadening of the IPCE spectra is desired for a larger photocurrent and better light harvesting which explains the higher efficiency observed for the dyes **43a-43c** when compared to **39a-39b**. Current density J_{SC} increased in the order of **39a** < **39b** < **43a** < **43c** < **43b** as a result of the broadening of the IPCE spectra.

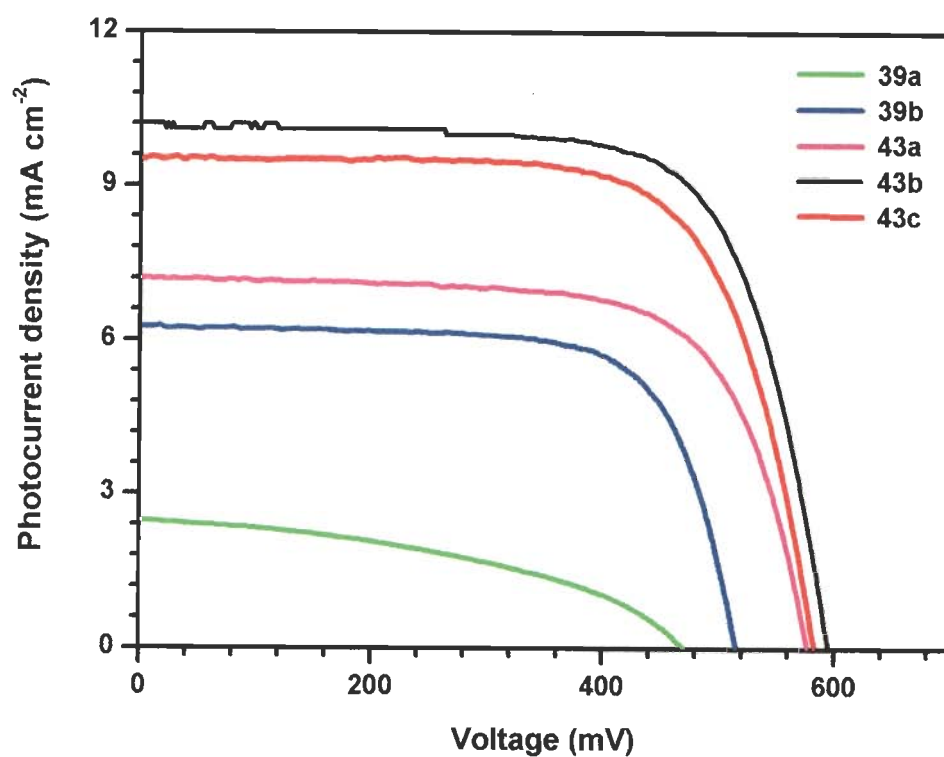


Figure 5.24 I-V characteristics of the DSSC fabricated using the dyes 39a-39b and 43a-43c.

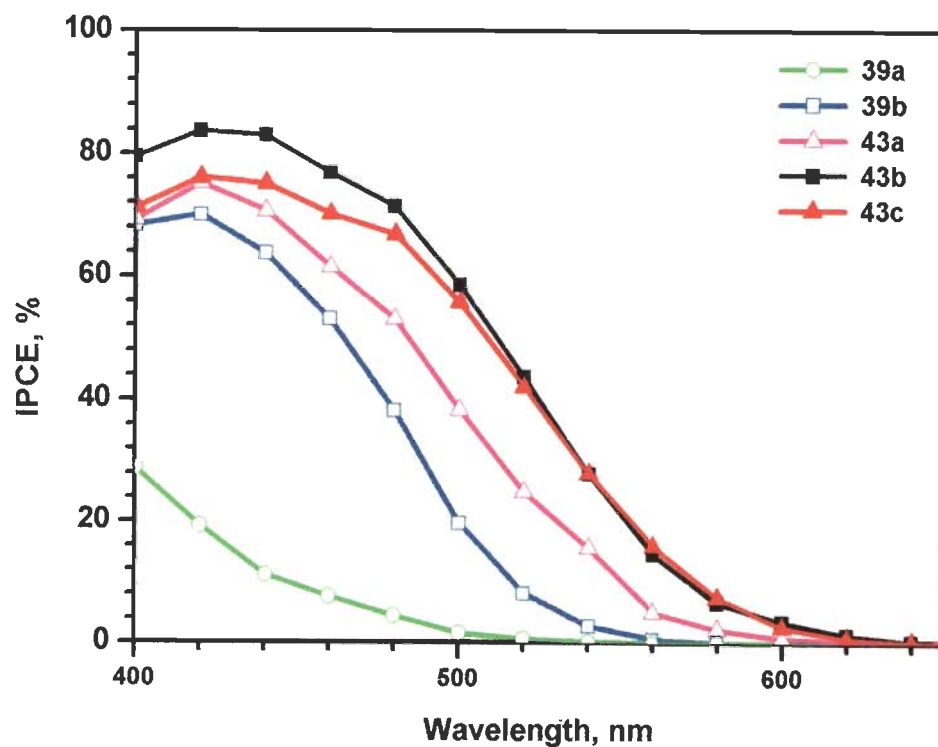


Figure 5.25 IPCE plots of the DSSC devices fabricated using the dyes 39a, 39b and 43a-43c.

The dyes **43a-43c** showed higher current conversion efficiency than control **39a-39b** dyes due to increase in the donor strength by inserting two donor system. Moreover by increasing the linker length between two donors further increase the device efficiency. The DSSCs sensitized by the dyes **43b** and **43c** obtained the higher η values 4.28% ($J_{sc} = 10.2 \text{ mA cm}^{-2}$, $V_{oc} = 0.595 \text{ V}$, $ff = 0.71$) and 3.89% ($J_{sc} = 9.51 \text{ mA cm}^{-2}$, $V_{oc} = 0.583 \text{ V}$, $ff = 0.70$) respectively. The highest device efficiency with **43b** sensitizer is due to the more ICT character as explained in theoretical calculation (*vide supra*). The lower value of J_{sc} for **39a** is due to the absence of electron delocalization from donor to acceptor resulting in lower charge injection from dye to TiO_2 and hence lower efficiency.

Table 5.7 Photovoltaic performance and other parameters extracted from EIS of DSSC sensitized by the dyes **39a**, **39b** and **43a-43c**.

Dyes	J_{sc} (mA cm^{-2})	V_{oc} (mV)	Ff	η (%)	R_{ct2} (ohm)	f_{max}	Electron life time, τ_e (ms)
39a	2.48	472	0.43	0.51	86.36	34.36	4.63
39b	6.27	516	0.71	2.29	19.84	112.98	1.41
43a	7.20	577	0.69	2.88	27.93	92.68	1.72
43b	10.2	595	0.71	4.28	17.50	7.01	22.69
43c	9.51	583	0.70	3.89	17.24	8.55	18.61

Electrochemical impedance spectroscopy (EIS) analysis was performed to study the interfacial charge transfer processes in DSSC sensitized by the dyes. The electrochemical impedance of the cells was measured over the frequency range of 10 mHz to 65 kHz under illumination at the applied bias voltage set at the open-circuit voltage of the DSSCs with an ac amplitude of 10 mV. In general, the EIS spectrum of a dye-sensitized solar cell having a configuration FTO/ TiO_2 /dye/electrolyte/Pt/ITO displays three semicircles in the frequency range of 10 mHz to 65 kHz. The first and second semicircles correspond to the charge-transfer

resistances at the counter electrode (R_{ct1}) and the TiO_2 /dye/electrolyte interface (R_{ct2}), respectively. The Warburg diffusion process of I^-/I^{3-} in the electrolyte (Z_w) is associated with the third semicircle. However, in this work the conventional diffusion resistance of the redox couple is apparently greatly overlapped by R_{ct2} because of a short length for I^- ion diffusion available with the thin spacer used (25 μm thick) and owing to the low viscosity of the solvents used in our electrolyte (viscosities of ACN and MPN are 0.37 and 1.60 cP, respectively).

The Nyquist plots displayed in Figure 5.26 show two semicircles which correspond to the charge-transfer resistances at the counter electrode and TiO_2 /dye/electrolyte interface, respectively. The radius of the bigger semicircle of the dye **43a** is significantly larger than the other dyes, indicating the enlarged charge-transfer resistance for this dye. The charge-transfer resistance assumes the order **43b** < **43c** < **39b** < **43a**. Though the charge-transfer resistance of **43b** and **43c** is smaller than that of other dyes, the V_{oc} is larger.

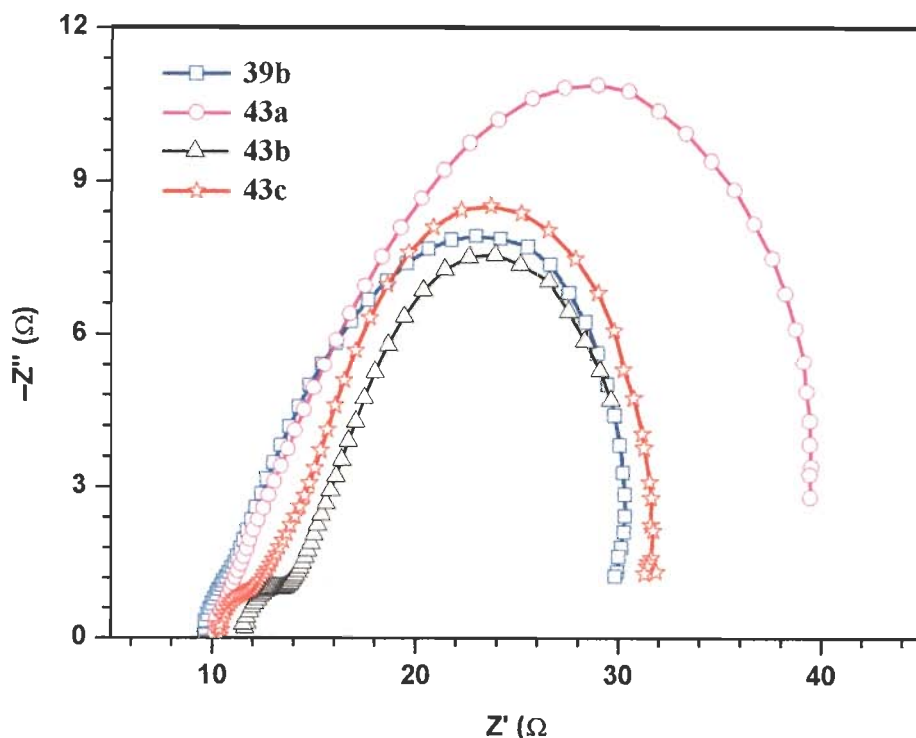


Figure 5.26 Nyquist plots of the DSSC fabricated using the dyes **39b**, **43a-43c**.

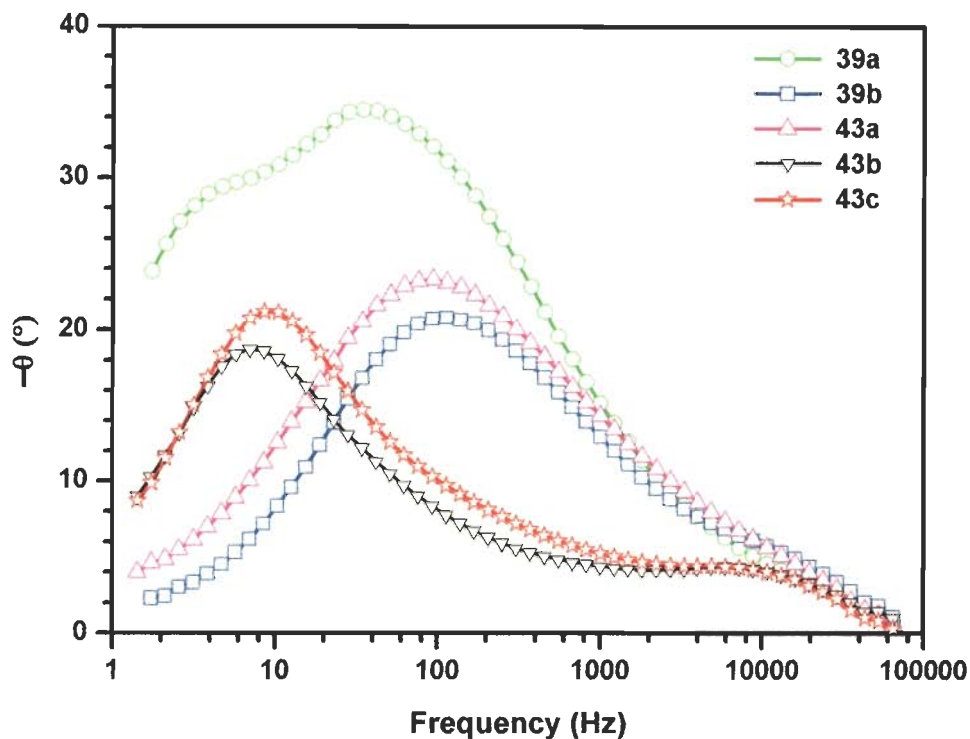


Figure 5.27 Bode phase plots of the DSSC fabricated using the dyes **39a**, **39b** and **43a-43c**.

In the Bode phase plot (Figure 5.27) the semicircle of the dye **39b** and **43a** is shifted to higher frequency when compared to those of **43b** and **43c**. This corresponds to a decrease in the electron lifetime for the **39b** and **43a** sensitized DSSC. The electron lifetime can be extracted from the angular frequency (ω_{\min}) at the mid frequency peak in the Bode phase plot using $\tau_e = 1/\omega_{\min}$.⁴⁶ The electron lifetime follows the trend, **43a** < **39b** < **43c** < **43b**. The increase in electron lifetime reduce of the chance of back reaction of the injected electrons with the I^{3-} in the electrolyte by alternation of HOMO of the sensitizer, which leads to the improvement in the photocurrent and photovoltage and to the significant enhancement of the device efficiency. Since the electron lifetime was found higher for the dye **43b**, it displayed the higher V_{oc} and device efficiency.

5.3 Conclusions

In summary, I have synthesized three dyes (**43a-43c**) containing two cascade 1-pyrenylphenyl amino donor system and one cyanoacrylic acid acceptor. Additionally we have synthesized two control dyes (**39a** & **39b**) having one donor-acceptor system. The incorporation of two donor system red shifts the absorption as well as emission profile. The molar extinction coefficient also increases in case of the dyes **43a-43c** which increase the light harvesting properties of these dyes. The chance of deprotonation of dyes is less in **43a-43c** which makes these dyes more stable than the control dye **39b**. The oxidation potential of the dyes was found higher than their corresponding amines indicating the more charge transfer character due to the presence of donor-acceptor interaction. Electrochemical data reveal that all the dyes have more negative excited state potential than the energy level of TiO₂ conduction band edge (-0.5 V vs NHE) which favour efficient downhill electron injection to TiO₂ conduction band. All the dyes showed more positive ground state oxidation potential than the iodide/ triiodide redox couple (~0.42 V vs NHE). That ensures the efficient regeneration of the dye by receiving electron from electrolyte and prevents the chance of charge recombination. Theoretical calculation reveals that two cascade donor systems increases the donor strength and also increases the donor-acceptor interaction which increase the efficient electron injection from dye to TiO₂ surface. The species having more charge separation is beneficial for generating high current density and hence high efficiency. The dye having biphenyl as spacer between two donors (**43b**) have shown higher photocurrent conversion efficiency $\eta = 4.28\%$ ($J_{sc} = 10.2 \text{ mA cm}^{-2}$, $V_{oc} = 0.595 \text{ V}$, $ff = 0.71$).

5.4 Experimental section

5.4.1 Materials

All commercial chemicals were used as received. Most of the chemicals were purchased from Sigma Aldrich. Diarylamine derivatives have been made by Buchwald-Hartwig CN coupling reaction as reported in the literature. Formylation was done by Vilsmeier-Hack reaction. Cyanoacrylic acid derivatives were made by Knoevenagel condensation reaction. Column chromatography was performed by using silica gel (Rankem, 100-200 mesh) as stationary phase. All solvents used in synthesis and spectroscopic measurements were distilled over appropriate drying and/or degassing reagents.

5.4.2 Physical methods

Physical methods are similar as written in chapter 2.

5.4.3 DSSC fabrication and characterizations

For the TiO₂ colloid solution, the TiO₂ precursor was prepared by the sol-gel method as described below. Titanium(IV) tetraisopropoxide (72mL) was added to 430mL of a 0.1M nitric acid aqueous solution with constant stirring and heated to 85 °C simultaneously for 8 h. When the mixture was cooled to room temperature, the resultant colloid was transferred to an autoclave and then heated at 240 C for 12 h in order to allow the TiO₂ particles to grow uniformly (ca. 20 nm). Consequently, the TiO₂ colloid was concentrated to 10 wt % (with respect to the TiO₂). The first type of TiO₂ paste (for transparent layer) was prepared by the addition 25 wt % (with respect to the TiO₂) of poly(ethylene glycol) (PEG, MW ~20000) to the above solution in order to control the pore diameters and to prevent the film from cracking during drying. For the second one (for scattering layer), the first type of TiO₂ paste was incorporated with 50 wt % of light scattering TiO₂ particles for reducing the light loss by back scattering.

A fluorine-doped SnO₂ conducting glass (FTO, 7 Ω sq, transmittance ~80%) was first cleaned with a neutral cleaner and then washed with deionized water, acetone, and isopropyl alcohol, sequentially. The conducting surface of the FTO was treated with a solution of titanium tetraisopropoxide (1 g) in 2-methoxyethanol (3 g) to obtain a good mechanical contact between the conducting glass and TiO₂ film, as well as to isolate the conducting glass surface from the electrolyte. TiO₂ pastes were coated onto the treated conducting glass by using the doctor blade technique. To coat each TiO₂ layer, the dried TiO₂ film was gradually heated to 450 °C in an oxygen atmosphere and subsequently sintered at that temperature for 30 min. The TiO₂ photoanodes of the DSSCs employed in the experiments were composed of a 14 μm thick transparent TiO₂ layer and with a scattering layer of 4.5 μm thickness. After sintering at 450 °C and cooling to 80 °C, the TiO₂ film was immersed in a 3x10⁻⁴M solution of dye at room temperature for 24 h. Various organic dye solutions were prepared in a mixing solvent containing ACN, tert-butyl alcohol, and dimethyl sulfoxide (DMSO) (volume ratio of 1:1:3). The thus prepared TiO₂/dye electrode was placed on a platinum-sputtered conducting glass electrode (ITO, 7Ωsq), keeping the two electrodes separated by a 25 μm thick Surlyn. The two electrodes were then sealed by heating. A mixture of 0.1 M LiI, 0.6 M DMPII, 0.05 M I₂, and 0.5 M TBP in 3-methoxypropionitrile (MPN)/ACN (volume ratio of 1:1) was used as the electrolyte. The electrolyte was injected into the gap between the electrodes by capillarity; the electrolyte-injecting hole was previously made in the counter electrode with a drilling machine, and the hole was sealed with hot-melt glue after the injection of the electrolyte.

The surface of the DSSC was covered by a mask with a light-illuminated area of 0.16 cm² and then illuminated by a class A quality solar simulator. Incident light intensity (100 mW cm⁻²) was calibrated with a standard silicon cell. Photocurrent-voltage curves of the DSSCs were

obtained with a potentiostat/galvanostat. The thickness of the TiO₂ film was judged by scanning electron microscopic images (SEM). For UV absorption spectra, dye molecules were coated on the TiO₂ films, and the corresponding spectra were obtained using an UVvis spectrophotometer equipped with an integrating sphere. Electrochemical impedance spectra (EIS) were obtained from the potentiostat/galvanostat, equipped with an FRA2 module, under a constant light illumination of 100 mW cm⁻². The frequency range explored was 10 mHz to 65 kHz. The applied bias voltage was set at the open-circuit voltage of the DSSC between the ITOPt counter electrode and the FTO-TiO₂ dye working electrode, starting from the short-circuit condition; the corresponding AC amplitude was 10mV. The impedance spectra were analyzed using an equivalent circuit model. Incident phototo-current conversion efficiency (IPCE) curves were obtained under short-circuit conditions. The light source was a class A quality solar simulator (PEC-L11, AM 1.5 G); light was focused through a monochromator onto the photovoltaic cell. The monochromator was incremented through the visible spectrum to generate the IPCE (λ) as defined by $IPCE(\lambda) = 1240 (J_{sc}/\lambda\phi)$, where λ is the wavelength, J_{sc} is the short-circuit photocurrent density (mA cm⁻²) recorded with a potentiostat/galvanostat, and j is the incident radiative flux (W m⁻²) measured with an optical detector and a power meter.

Synthesis of *N,N*-diphenylpyren-1-amine (36b) A mixture of 1-bromopyrene (5.5 g, 19.5 mmol), diphenylamine (3.95 g, 23.4 mmol), Pd(dba)₂ (224 mg, 39 mmol), dppf (216 mg, 39 mmol), sodium *tert*-butoxide (2.8 g, 29.25 mmol), and toluene (40 ml) was taken in a pressure tube. It was heated at 80°C and stirred for 48 h. After completion of reaction, it was quenched by the addition of water and extracted with dichloromethane. The combined extracts were washed with brine solution and dried over anhydrous Na₂SO₄. Rotary evaporation of the extracts gave

the crude product which on column chromatography purification using 1:4 hexane-dichloromethane mixtures produced a yellow solid. Yield 2.8 g (40%); ^1H NMR (CDCl_3 , 500 MHz) δ 8.21-8.14 (m, 3 H), 8.11 (d, $J = 7.5$ Hz, 1 H), 8.06 (s, 2 H), 7.99 (t, $J = 7.5$ Hz, 1 H), 7.94 (d, $J = 9.0$ Hz, 1 H), 7.84 (d, $J = 8.5$ Hz, 1 H), 7.22-7.19 (m, 4 H), 7.09-7.07 (m, 4 H), 6.95 (t, $J = 7.5$ Hz, 2 H).

Synthesis of N^1, N^4 -diphenyl- N^1, N^4 -di(pyren-1-yl)benzene-1,4-diamine (41a) Derivative **41a** was prepared from **40a** and **36a** by following a procedure similar to that described above for **36b**. Yellow solid. Yield 65%; mp 320-322 °C; ^1H NMR (CDCl_3 , 500 MHz) δ 8.17-8.16 (m, 6 H), 8.12 (d, $J = 7.5$ Hz, 2 H), 8.04 (s, 4 H), 7.98 (t, $J = 7.8$ Hz, 3 H), 7.95 (d, $J = 9.5$ Hz, 1 H), 7.87-7.85 (m, 2 H), 7.18-7.14 (m, 4 H), 7.01-6.98 (m, 8 H), 6.89-6.86 (m, 2 H); ^{13}C NMR (CDCl_3 , 125 MHz) δ 143.0, 131.1, 130.9, 129.2, 128.9, 127.6, 127.3, 127.0, 126.8, 126.1, 126.0, 125.8, 125.0, 124.8, 124.6, 123.7, 123.2, 120.7, 120.6.

Synthesis of $N^4, N^{4'}$ -diphenyl- $N^4, N^{4'}$ -di(pyren-1-yl)biphenyl-4,4'-diamine (41b) Derivative **41b** was prepared from **40b** and **36a** by following a procedure similar to that described above for **36b**. Yellow solid. Yield 80%; mp 310-312 °C; ^1H NMR (CDCl_3 , 500 MHz) δ 8.17 (d, $J = 8.5$ Hz, 5 H), 8.14 (s, 1 H), 8.11 (d, $J = 7.5$ Hz, 2 H), 8.06 (s, 4 H), 7.99-7.97 (m, 2 H), 7.93 (d, $J = 8.0$ Hz, 2 H), 7.86 (d, $J = 8.0$ Hz, 2 H), 7.39-7.37 (m, 4 H), 7.23-7.19 (m, 4 H), 7.12-7.07 (m, 8 H), 6.96 (t, $J = 7.0$ Hz, 2 H); ^{13}C NMR (CDCl_3 , 125 MHz) δ 147.5, 146.4, 139.7, 132.8, 130.2, 130.0, 128.7, 128.5, 128.2, 127.7, 127.6, 127.1, 126.9, 126.6, 126.2, 126.14, 126.08, 125.5, 125.3, 125.2, 125.0, 124.2, 124.1, 123.8, 122.3, 121.3, 121.2, 121.1, 120.8.

Synthesis of 9,9-diethyl- N^2, N^7 -diphenyl- N^2, N^7 -di(pyren-1-yl)-9H-fluorene-2,7-diamine (41c) Derivative **41c** was prepared from **40c** and **36a** by following a procedure similar to that described above for **36b**. Yellow solid. Yield 74%; mp 250-253 °C; ^1H NMR (CDCl_3 , 500 MHz)

δ 8.17-8.13 (m, 6 H), 8.09 (d, $J = 7.5$ Hz, 2 H), 8.05 (s, 4 H), 8.00-7.97 (m, 2 H), 7.89 (d, $J = 9.0$ Hz, 2 H), 7.83 (d, $J = 8.5$ Hz, 2 H), 7.39 (d, $J = 8.5$ Hz, 2 H), 7.22-7.16 (m, 4 H), 7.10 (d, $J = 2.0$ Hz, 2 H), 7.07-7.05 (m, 4 H), 6.96-6.94 (m, 4 H), 1.69 (q, $J = 7.5$ Hz, 4 H), 0.34 (t, $J = 7.5$ Hz, 6 H); ^{13}C NMR (CDCl_3 , 125 MHz) δ 151.0, 149.0, 147.3, 141.2, 135.8, 131.1, 130.9, 129.1, 129.0, 128.1, 127.6, 127.4, 127.1, 126.7, 126.2, 126.0, 125.8, 124.9, 124.8, 124.7, 123.4, 121.9, 121.6, 121.2, 119.5, 117.3, 55.9, 32.4, 8.3.

Synthesis of 4-(phenyl(pyren-1-yl)amino)benzaldehyde (38b) *N,N*-diphenylpyren-1-amine (1.85 g, 5 mmol) was dissolved in chlorobenzene (30 mL) and DMF (15 mL). POCl_3 (2.8 mL, 30 mmol) was added dropwise to it at room temperature. The reaction mixture was stirred and heated at 65°C for 8 h. After completion of reaction as evidenced by disappearance of aldehyde, the reaction mixture was poured into ice water and neutralized by sodium bicarbonate. The solution was extracted with dichloromethane, washed with brine solution, dried over Na_2SO_4 followed by evaporation of solvent. The desired product was purified by column chromatography eluting with 10% dcm-ethylacetate mixture. The obtained product was further recrystallized by dichloromethane and methanol. Yellow solid. Yield 1.74 g (87%); ^1H NMR (CDCl_3 , 500 MHz) δ 9.78 (s, 1 H), 8.23-8.20 (m, 2 H), 8.16 (d, $J = 7.0$ Hz, 1 H), 8.12-8.07 (m, 3 H), 8.04-7.99 (m, 2 H), 7.86 (d, $J = 8.5$ Hz, 1 H), 7.66-7.64 (m, 2 H), 7.33-7.28 (m, 4 H), 7.15-7.11 (m, 1 H), 6.94 (dd, $J = 2.5, 8.5$ Hz, 2 H); ^{13}C NMR (CDCl_3 , 125 MHz) δ 190.3, 153.9, 146.3, 138.7, 131.4, 131.0, 130.7, 130.2, 129.6, 129.5, 128.6, 128.1, 127.6, 127.4, 126.9, 126.3, 126.1, 126.0, 125.5, 125.4, 124.8, 124.5, 122.4, 118.0, 117.8; IR (KBr, cm^{-1}) ν_{max} 3037, 1684 ($\nu_{\text{C=O}}$), 1584, 1487, 1264, 1163, 843.

Synthesis of 4-((4-(phenyl(pyren-1-yl)amino)phenyl)(pyren-1-yl)amino)benzaldehyde (42a) N^1,N^4 -diphenyl- N^1,N^4 -di(pyren-1-yl)benzene-1,4-diamine (0.66 g, 1 mmol) was dissolved in

chlorobenzene (20 mL) and NMF (0.2 mL, 1.5 mmol). POCl₃ (0.14 mL, 1.5 mmol) was added dropwise to it at room temperature. The reaction mixture was stirred and heated at 90°C for 12 h. After completion of reaction as evidenced by disappearance of aldehyde, the reaction mixture was poured into ice water and neutralized by sodium bicarbonate. The solution was extracted with dichloromethane, washed with brine solution, dried over Na₂SO₄ followed by evaporation of solvent. The desired product was purified by column chromatography eluting with 10% dcm-ethylacetate mixture. The obtained product was further recrystallized by dichloromethane and methanol. Yellow solid. Yield 0.28 g (41%); mp 192-194 °C; ¹H NMR (CDCl₃, 500 MHz) δ 9.75 (s, 1 H), 8.23-8.21 (m, 2 H), 8.18-8.16 (m, 3 H), 8.14-8.12 (m, 2 H), 8.10-8.08 (m, 3 H), 8.05 (d, *J* = 1.5 Hz, 2 H), 8.04-7.99 (m, 3 H), 7.95 (d, *J* = 9.5 Hz, 1 H), 7.90-7.85 (m, 2 H), 7.63 (d, *J* = 9.0 Hz, 2 H), 7.21-7.15 (m, 4 H), 7.07 (dd, *J* = 1.0, 7.5 Hz, 2 H), 7.03-7.01 (m, 2 H), 6.95-6.94 (m, 1 H), 6.87 (d, *J* = 8.5 Hz, 2 H); ¹³C NMR (CDCl₃, 125 MHz) δ 190.4, 154.3, 148.3, 145.8, 140.4, 139.8, 138.8, 131.6, 131.24, 131.17, 131.0, 130.9, 130.4, 129.7, 129.3, 128.7, 128.3, 128.20, 128.16, 128.1, 127.8, 127.6, 127.4, 127.3, 127.2, 127.1, 126.5, 126.4, 126.3, 126.23, 126.19, 126.1, 125.7, 125.5, 125.4, 125.2, 124.8, 124.7, 123.2, 122.8, 122.7, 122.0, 117.0, 112.4; IR (KBr, cm⁻¹) *v*_{max} 3029, 1686 (*v*_{C=O}), 1593, 1499, 1264, 1163, 843.

Synthesis of 4-((4'-(phenyl(pyren-1-yl)amino)biphenyl-4-yl)(pyren-1-yl)amino)benzaldehyde (42b) *N*⁴,*N*^{4'}-diphenyl-*N*⁴,*N*^{4'}-di(pyren-1-yl)biphenyl-4,4'-diamine (1.0 g, 1.36 mmol) was dissolved in chlorobenzene (30 mL) and NMF (0.34 mL, 2.72 mmol). POCl₃ (0.25 mL, 2.72 mmol) was added dropwise to it at room temperature. The reaction mixture was stirred and heated at 90°C for 12 h. After completion of reaction as evidenced by disappearance of aldehyde, the reaction mixture was poured into ice water and neutralized by sodium bicarbonate. The solution was extracted with dichloromethane, washed with brine solution, dried

over Na₂SO₄ followed by evaporation of solvent. The desired product was purified by column chromatography eluting with 10% dcm-ethylacetate mixture. The obtained product was further recrystallized by dichloromethane and methanol. Yellow solid. Yield 0.3 g (29%); mp 196-198 °C; ¹H NMR (CDCl₃, 500 MHz) δ 9.79 (s, 1 H), 8.22 (d, *J* = 8.0 Hz, 2 H), 8.19-8.15 (m, 4 H), 8.13-8.02 (m, 6 H), 8.01-7.99 (m, 3 H), 7.94 (d, *J* = 9.5 Hz, 1 H), 7.88 (d, *J* = 8.0 Hz, 1 H), 7.86 (d, *J* = 8.0 Hz, 1 H), 7.67-7.65 (m, 2 H), 7.49-7.47 (m, 2 H), 7.40-7.38 (m, 2 H), 7.30-7.28 (m, 2 H), 7.24-7.21 (m, 2 H), 7.13-7.12 (m, 2 H), 7.09-7.08 (m, 2 H), 6.99-6.97 (m, 3 H); ¹³C NMR (CDCl₃, 125 MHz) δ 190.5, 153.9, 148.3, 148.0, 145.1, 140.6, 138.8, 136.9, 133.2, 131.6, 131.24, 131.16, 131.1, 130.9, 130.5, 129.7, 129.3, 128.80, 128.75, 128.3, 128.2, 128.0, 127.8, 127.7, 127.6, 127.5, 127.4, 127.2, 127.1, 126.5, 126.4, 126.3, 126.2, 126.1, 125.7, 125.6, 125.3, 125.2, 125.1, 124.8, 124.7, 123.3, 122.6, 122.5, 122.2, 121.9, 118.2; IR (KBr, cm⁻¹) ν_{max} 3033, 1685 (ν_{C=O}), 1591, 1462.

Synthesis of 4-((9,9-diethyl-7-(phenyl(pyren-1-yl)amino)-9H-fluoren-2-yl)(pyren-1-yl)amino)benzaldehyde (42c) 9,9-diethyl-*N*²,*N*⁷-diphenyl-*N*²,*N*⁷-di(pyren-1-yl)-9H-fluorene-2,7-diamine (2.5 g, 3.1 mmol) was dissolved in chlorobenzene (25 mL) and NMF (0.76 mL, 6.2 mmol). POCl₃ (0.56 mL, 6.2 mmol) was added dropwise to it at room temperature. The reaction mixture was stirred and heated at 90°C for 10 h. After completion of reaction as evidenced by disappearance of aldehyde, the reaction mixture was poured into ice water and neutralized by sodium bicarbonate. The solution was extracted with dichloromethane, washed with brine solution, dried over Na₂SO₄ followed by evaporation of solvent. The desired product was purified by column chromatography eluting with 10% dcm-ethylacetate mixture. The obtained product was further recrystallized by dichloromethane and methanol. Yellow solid. Yield 0.52 g (20%); mp 220-222 °C; ¹H NMR (CDCl₃, 500 MHz) δ 9.78 (s, 1 H), 8.22-8.20 (m, 2 H), 8.18-8.15 (m, 3

H), 8.13-8.08 (m, 5 H), 8.06 (s, 2 H), 8.02-7.97 (m, 3 H), 7.89-7.83 (m, 3 H), 7.65 (d, $J = 8.5$ Hz, 2 H), 7.47 (d, $J = 8.0$ Hz, 1 H), 7.42 (d, $J = 8.5$ Hz, 1 H), 7.28 (d, $J = 1.5$ Hz, 1 H), 7.21 (t, $J = 7.5$ Hz, 2 H), 7.10-7.07 (m, 4 H), 6.96-6.93 (m, 4 H), 1.81-1.72 (m, 4 H), 0.35 (t, $J = 7.25$ Hz, 6 H); ^{13}C NMR (CDCl_3 , 125 MHz) δ 190.5, 154.4, 151.53, 151.46, 148.9, 148.2, 144.9, 141.2, 139.2, 138.5, 131.6, 131.3, 131.2, 131.1, 130.9, 130.2, 129.4, 129.2, 128.54, 128.47, 127.9, 127.8, 127.7, 127.32, 127.25, 127.2, 127.0, 126.5, 126.4, 126.3, 126.23, 126.15, 126.0, 125.7, 125.5, 125.2, 125.1, 124.9, 124.4, 123.5, 122.8, 122.1, 121.7, 120.2, 120.0, 119.8, 118.0, 117.1, 56.2, 32.6, 8.6; IR (KBr, cm^{-1}) ν_{max} 3031, 1685 ($\nu_{\text{C=O}}$), 1589, 1488, 1160, 843.

The cyanoacrylic acid derivatives (**39a**, **39b**, **43a-43c**) were synthesized by the same procedure from their corresponding aldehydes (**38a**, **38b**, **42a-42c**) respectively. The procedure for the synthesis of (*E*)-2-cyano-3-(3-(phenyl(pyren-1-yl)amino)phenyl)acrylic acid (**39a**) is given below.

Synthesis of (*E*)-2-cyano-3-(3-(phenyl(pyren-1-yl)amino)phenyl)acrylic acid (39a**)** 3-(phenyl(pyren-1-yl)amino)benzaldehyde (**38a**) (0.82 g, 2.06 mmol) was dissolved in 25 ml of glacial acetic acid. To the solution, cyanoacetic acid (0.21 g, 2.48 mmol) and ammonium acetate (53 mg, 0.69 mmol) were added. The resulting mixture was refluxed for 12 h. After cooling to room temperature, the desired product was crystallized from the solution. The precipitate was filtered and washed with water. The product was recrystallized by toluene-hexane mixture. Orange solid. Yield 0.6 g (63%); mp 196-198 °C; ^1H NMR (CDCl_3 , 500 MHz) δ 8.36 (d, $J = 8.0$ Hz, 1 H), 8.32 (d, $J = 7.5$ Hz, 1 H), 8.24 (d, $J = 7.5$ Hz, 1 H), 8.20 (s, 2 H), 8.15 (s, 1 H), 8.11-8.06 (m, 3 H), 7.89 (d, $J = 8.0$ Hz, 1 H), 7.64 (s, 1 H), 7.56 (d, $J = 7.5$ Hz, 1 H), 7.38 (t, $J = 8.0$ Hz, 1 H), 7.28-7.23 (m, 2 H), 7.11-7.06 (m, 3 H), 7.01 (t, $J = 7.5$ Hz, 1 H); ^{13}C NMR (CDCl_3 , 125 MHz) δ 163.7, 154.2, 149.3, 147.6, 139.9, 133.3, 131.2, 130.9, 130.6, 130.1, 130.0, 128.8,

128.6, 128.2, 128.1, 127.8, 127.7, 127.1, 127.0, 126.1, 125.8, 125.1, 124.4, 123.7, 123.2, 122.9, 122.8, 122.4, 116.5, 105.2; IR (KBr, cm^{-1}) ν_{max} 3440, 2923, 2216 ($\nu_{\text{C}\equiv\text{N}}$), 1682, 1577, 1504, 1384, 1184; HRMS calcd for $\text{C}_{32}\text{H}_{20}\text{N}_2\text{O}_2$ [M + Na] m/z 487.1422, found 487.1423.

Synthesis of (*E*)-2-cyano-4-(3-(phenyl(pyren-1-yl)amino)phenyl)acrylic acid (39b) Yellow solid. Yield 87%; mp 154-156 °C; ^1H NMR (CDCl_3 , 500 MHz) δ 8.41-8.39 (m, 1 H), 8.37-8.36 (m, 1 H), 8.28-8.26 (m, 1 H), 8.24 (d, $J = 2.5$ Hz, 2 H), 8.17-8.15 (m, 1 H), 8.13-8.04 (m, 3 H), 7.99 (d, $J = 8.0$ Hz, 1 H), 7.87 (d, $J = 9.5$ Hz, 2 H), 7.39-7.32 (m, 4 H), 7.17 (t, $J = 7.0$ Hz, 1 H), 6.81 (d, $J = 9.0$ Hz, 2 H); ^{13}C NMR (CDCl_3 , 125 MHz) δ 164.6, 152.8, 146.0, 138.7, 133.3, 131.1, 130.8, 130.6, 130.4, 129.3, 128.2, 128.1, 127.7, 127.3, 127.0, 126.4, 126.1, 125.8, 125.5, 124.3, 123.4, 122.6, 117.9, 117.8. IR (KBr, cm^{-1}) ν_{max} 3440, 2921, 2220 ($\nu_{\text{C}\equiv\text{N}}$), 1688, 1588, 1488, 1271; IR (KBr, cm^{-1}) ν_{max} 3440, 2923, 2216 ($\nu_{\text{C}\equiv\text{N}}$), 1682, 1577, 1504, 1384, 1184; HRMS calcd for $\text{C}_{32}\text{H}_{20}\text{N}_2\text{O}_2$ [M + Na] m/z 487.1422, found 487.1421.

Synthesis of (*E*)-2-cyano-3-(4-((4-(phenyl(pyren-1-yl)amino)phenyl)(pyren-1-yl)amino)phenyl)acrylic acid (43a) Red solid. Yield 85%; mp 220-222 °C; ^1H NMR (CDCl_3 , 500 MHz) δ 8.39 (d, $J = 8.0$ Hz, 1 H), 8.35-8.32 (m, 2 H), 8.29 (t, $J = 7.75$ Hz, 2 H), 8.24-8.22 (m, 3 H), 8.17-8.15 (m, 3 H), 8.11-8.04 (m, 6 H), 7.99 (d, $J = 8.0$ Hz, 2 H), 7.88 (d, $J = 8.0$ Hz, 1 H), 7.81 (d, $J = 9.0$ Hz, 2 H), 7.25-7.20 (m, 4 H), 6.98 (d, $J = 9.0$ Hz, 4 H), 6.94 (t, $J = 7.5$ Hz, 1 H), 6.76 (d, $J = 9.0$ Hz, 2 H); ^{13}C NMR (CDCl_3 , 125 MHz) δ 152.3, 148.3, 145.5, 140.4, 139.8, 138.8, 132.7, 131.14, 131.09, 130.9, 130.8, 130.3, 129.9, 129.7, 129.1, 128.5, 128.1, 128.02, 127.96, 127.6, 127.2, 127.1, 127.0, 126.9, 126.3, 126.0, 125.8, 125.7, 124.4, 124.3, 123.1, 123.0, 122.7, 122.4, 121.9, 117.3; IR (KBr, cm^{-1}) ν_{max} 3432, 2920, 2208 ($\nu_{\text{C}\equiv\text{N}}$), 1628, 1593, 1498, 1384, 1181, 844.

Synthesis of (E)-2-cyano-3-(4-((4'-(phenyl(pyren-1-yl)amino)biphenyl-4-yl)(pyren-1-yl)amino)phenyl)acrylic acid (43b) Brown solid. Yield 60%; mp 257-262 °C; ^1H NMR (CDCl_3 , 500 MHz) δ 8.36-8.28 (m, 4 H), 8.23-8.17 (m, 6 H), 8.11-8.01 (m, 6 H), 7.92 (d, $J = 8.0$ Hz, 2 H), 7.85 (d, $J = 8.5$ Hz, 1 H), 7.77 (d, $J = 8.5$ Hz, 2 H), 7.49 (d, $J = 8.5$ Hz, 2 H), 7.42 (d, $J = 8.5$ Hz, 2 H), 7.25-7.18 (m, 4 H), 7.01 (d, $J = 8.0$ Hz, 2 H), 6.98-6.92 (m, 3 H), 6.87 (d, $J = 8.5$ Hz, 2 H); ^{13}C NMR (CDCl_3 , 125 MHz) δ 148.1, 140.5, 132.1, 131.1, 130.9, 130.0, 129.8, 128.6, 128.2, 128.1, 127.7, 127.2, 127.1, 126.9, 126.0, 125.8, 124.7, 124.3, 123.1, 122.7, 122.5, 121.7, 119.0; IR (KBr, cm^{-1}) ν_{max} 3429, 2922, 2216 ($\nu_{\text{C}\equiv\text{N}}$), 1625, 1592, 1490, 1384, 1182, 844; HRMS calcd for $\text{C}_{60}\text{H}_{37}\text{N}_3\text{O}_2$ [$\text{M} + \text{Na}$] m/z 854.2783, found 854.2932.

Synthesis of (E)-2-cyano-3-(4-((9,9-diethyl-7-(phenyl(pyren-1-yl)amino)-9H-fluoren-2-yl)(pyren-1-yl)amino)phenyl)acrylic acid (43c) Red solid. Yield 50%; mp 277-279 °C; ^1H NMR (CDCl_3 , 500 MHz) δ 8.36-8.26 (m, 4 H), 8.23-8.15 (m, 6 H), 8.07-7.95 (m, 8 H), 7.83 (d, $J = 8.5$ Hz, 1 H), 7.78 (d, $J = 7.0$ Hz, 2 H), 7.58-7.52 (m, 2 H), 7.36 (s, 1 H), 7.23-7.20 (m, 2 H), 7.08-7.06 (m, 2 H), 6.97-6.92 (m, 3 H), 6.85-6.81 (m, 3 H), 1.69-1.62 (m, 4 H), 0.23-0.20 (m, 6 H); ^{13}C NMR (CDCl_3 , 125 MHz) δ 156.7, 156.2, 153.6, 152.7, 145.8, 144.1, 142.7, 140.0, 136.0, 135.9, 135.6, 134.9, 134.6, 134.2, 132.4, 132.2, 131.8, 130.8, 130.7, 130.4, 129.2, 129.1, 127.0, 126.7, 125.8, 125.6, 123.2, 60.8, 36.8, 13.6; IR (KBr, cm^{-1}) ν_{max} 3432, 2924, 2212 ($\nu_{\text{C}\equiv\text{N}}$), 1628, 1594, 1503, 1463, 1383, 1183, 844; LRMS calcd for $\text{C}_{65}\text{H}_{45}\text{N}_3\text{O}_2$ [$\text{M} + \text{Na}$] m/z 922.3, found 922.2.

5.5 References

1. O'Regan, B.; Grätzel, M. "A low-cost, high-efficiency solar cell based on dye-sensitized colloidal TiO_2 films" *Nature* **1991**, 353, 737.
2. Grätzel, M. "Dye sensitized solar cells" *J. Photochem. Photobiol., C* **2003**, 4, 145.

3. Fredin, K.; Anderson, K. F.; Duffy, N. W.; Wilson, G. J.; Fell, C. J.; Hagberg, D. P.; Sun, L.; Bach, U.; Lindquist, S.-E. "Effect of cell efficiency following thermal degradation of dye-sensitized mesoporous electrodes using N719 and D5 sensitizers" *J. Phys. Chem. C* **2009**, *113*, 18902.
4. Nazeeruddin, M. K.; Péchy, P.; Renouard, T.; Zakeeruddin, S. M.; Humphry-Baker, P.; Comte, P.; Liska, P.; Cevey, L.; Costa, E.; Shklover, V.; Spiccia, L.; Deacon, G. B.; Bignozzi, C. A.; Grätzel, M. "Engineering of efficient panchromatic sensitizers for nanocrystalline TiO₂-based solar cells" *J. Am. Chem. Soc.* **2001**, *123*, 1613.
5. Hagfeldt, A.; Boschloo, G.; Sun, L.; Kloo, L.; Pettersson, H. "Dye-sensitized solar cells" *Chem. Rev.* **2010**, *110*, 6595.
6. Hara, K.; Wang, Z.-S.; Sato, T.; Furube, A.; Katoh, R.; Sugihara, H.; Dan-oh, Y.; Kasada, C.; Shinpo, A.; Suga, S. "Oligothiophene-containing coumarin dyes for efficient dye-sensitized solar cells" *J. Phys. Chem. B* **2005**, *109*, 15476.
7. Shibano, Y.; Umeyama, T.; Matano, Y.; Imahori, H. "Electron-donating perylene tetracarboxylic acids for dye-sensitized solar cells" *Org. Lett.* **2007**, *9*, 1971.
8. Kim, D.; Lee, J. K.; Kang, S. O.; Ko, J. "Molecular engineering of organic dyes containing *N*-aryl carbazole moiety for solar cell" *Tetrahedron* **2007**, *63*, 1913.
9. Xia, P. F.; Lu, J.; Kwok, C. H.; Fukutani, H.; Wong, M. S.; Tao, Y. "Synthesis and properties of monodisperse multi-triarylamine-substituted oligothiophenes and 4,7-bis(2'-oligothienyl)-2,1,3-benzothiadiazoles for organic solar cell applications" *J. Polym. Sci., Part A: Polym. Chem.* **2009**, *47*, 137.

10. Kitamura, T.; Ikeda, M.; Shigaki, K.; Inoue, T.; Anderson, N. A.; Ai, X.; Lian, T.; Yanagida, S. "Phenyl-conjugated oligoene sensitizers for TiO₂ solar cells" *Chem. Mater.* **2004**, *16*, 1806.
11. Dentani, T.; Kubota, Y.; Funabiki, K.; Jin, J.; Yoshida, T.; Minoura, H.; Miura, H.; Matsui, M. "Novel thiophene-conjugated indoline dyes for zinc oxide solar cells" *New. J. Chem.* **2009**, *33*, 93.
12. Tian, H.; Yang, X.; Pan, J.; Chen, R.; Liu, M.; Zhang, Q.; Hagfeldt, A.; Sun, L. "A triphenylamine dye model for the study of intramolecular energy transfer and charge transfer in dye-sensitized solar cells" *Adv. Funct. Mater.* **2008**, *18*, 3461.
13. Wang, Z.-S.; Cui, Y.; Hara, K.; Dan-oh, Y.; Kasada, C.; Shinpo, A. "A high-light harvesting-efficiency coumarin dye for stable dye-sensitized solar cells" *Adv. Mater.* **2007**, *19*, 1138.
14. Tian, H.; Yang, X.; Chen, R.; Pan, Y.; Li, L.; Hagfeldt, A.; Sun, L. "Phenothiazine derivatives for efficient organic dye-sensitized solar cells" *Chem. Commun.* **2007**, *43*, 3741.
15. Edvinsson, T.; Li, C.; Pschirer, N.; Schöneboom, J.; Eickemeyer, F.; Sens, R.; Boschloo, G.; Herrmann, A.; Müllen, K.; Hagfeldt, A. "Intramolecular charge-transfer tuning of perylenes: spectroscopic features and performance in dye-sensitized solar cells" *J. Phys. Chem. C* **2007**, *111*, 15137.
16. Yang, H.-Y.; Yen, Y.-S.; Hsu, Y.-C.; Chou, H.-H.; Lin, J. T. "Organic dyes incorporating the dithieno[3,2-*b*:2',3'-*d*]thiophene moiety for efficient dye-sensitized solar cells" *Org. Lett.* **2010**, *12*, 16.
17. Liang, M.; Xu, W.; Cai, F.; Chen, P.; Peng, B.; Chen, J.; Li, Z. "New triphenylamine-based organic dyes for efficient dye-sensitized solar cells" *J. Phys. Chem. C* **2007**, *111*, 4465.

18. Kim, S.; Lee, J. K.; Kang, S. O.; Ko, J.; Yum, J.-H.; Fantacci, S.; Angelis, F. D.; Censo, D. D.; Nazeeruddin, M. K.; Grätzel, M. "Molecular engineering of organic sensitizers for solar cell applications" *J. Am. Chem. Soc.* **2006**, *128*, 16701.
19. Chang, Y. J.; Chow, T. J. "Dye-sensitized solar cell utilizing organic dyads containing triarylene conjugates" *Tetrahedron* **2009**, *65*, 4726.
20. Liu, W.-H.; Wu, I.-C.; Lai, C.-H.; Lai, C.-H.; Chou, P.-T.; Li, Y.-T.; Chen, C.-L.; Hsu, Y.-Y.; Chi, Y. "Simple organic molecules bearing a 3,4-ethylenedioxythiophene linker for efficient dye-sensitized solar cells" *Chem. Commun.* **2008**, 5152.
21. Xu, M.; Wenger, S.; Bala, H.; Shi, D.; Li, R.; Zhou, Y.; Zakeeruddin, S. M.; Grätzel, M.; Wang, P. "Tuning the energy level of organic sensitizers for high-performance dye-sensitized solar cells" *J. Phys. Chem. C* **2009**, *113*, 2966.
22. Tang, C.; Liu, F.; Xia, Y.-J.; Xie, L.-H.; Wei, A.; Li, S.-B.; Fan, Q.-L.; Huang, W. "Efficient 9-alkylphenyl-9-pyrenylfluorene substituted pyrene derivatives with improved hole injection for blue light-emitting diodes" *J. Mater. Chem.* **2006**, *16*, 4074.
23. Ji, S.; Yang, J.; Yang, Q.; Liu, S.; Chen, M.; Zhao, J. "Tuning the intramolecular charge transfer of alkynylpyrenes: Effect on photophysical properties and its application in design of OFF-ON fluorescent thiol probes" *J. Org. Chem.* **2009**, *74*, 4855.
24. Zhang, H.; Wang, Y.; Shao, K.; Liu, Y.; Chen, S.; Qiu, W.; Sun, X.; Qi, T.; Ma, Y.; Yu, G.; Su, Z.; Zhu, D. "Novel butterfly pyrene-based organic semiconductors for field effect transistors" *Chem. Commun.* **2006**, 42, 755.
25. Lai, S.-L.; Tong, Q.-X.; Chan, M.-Y.; Ng, T.-W.; Lo, M.-F.; Lee, S.-T.; Lee, C.-S. "Distinct electroluminescent properties of triphenylamine derivatives in blue organic light-emitting devices" *J. Mater. Chem.* **2011**, *21*, 1206.

26. Thomas, K. R. J.; Velusamy, M.; Lin, J. T.; Chuen, C. H.; Tao, Y.-T. "Hexaphenylphenylene dendronised pyrenylamines for efficient organic light-emitting diodes" *J. Mater. Chem.* **2005**, *15*, 4453.
27. Matsunaga, Y.; Takechi, K.; Akasaka, T.; Ramesh, A. R.; James, P. V.; Thomas, K. G.; Kamat, P. V. "Excited-state and photoelectrochemical behavior of pyrene-linked phenyleneethynylene oligomer" *J. Phys. Chem. B* **2008**, *112*, 14539.
28. Thomas, K. R. J.; Lin, J. T.; Hsu, Y.-C.; Ho, K.-C. "Organic dyes containing thienylfluorene conjugation for solar cells" *Chem. Commun.* **2005**, *41*, 4098.
29. Nantalaksakul, A.; Mueller, A.; Klaikherd, A.; Bardeen, C. J.; Thayumanavan, S. "Dendritic and linear macromolecular architectures for photovoltaics: a photoinduced charge transfer investigation" *J. Am. Chem. Soc.* **2009**, *131*, 2727.
30. Thomas, K. R. J.; Thompson, A. L.; Sivakumar, A. V.; Bardeen, C. J.; Thayumanavan, S. "Energy and electron transfer in bifunctional non-conjugated dendrimers" *J. Am. Chem. Soc.* **2005**, *127*, 373.
31. Yang, C.-H.; Liao, S.-H.; Sun, Y.-K.; Chuang, Y.-Y.; Wang, T.-L.; Shieh, Y.-T.; Lin, W.-C. "Optimization of multiple electron donor and acceptor in carbazole-triphenylamine-based molecules for application of dye-sensitized solar cells" *J. Phys. Chem. C* **2010**, *114*, 21786.
32. Ning, Z.; Zhang, Q.; Wu, W.; Pei, H.; Liu, B.; Tian, H. "Starburst triarylamine based dyes for efficient dye-sensitized solar cells" *J. Org. Chem.* **2008**, *73*, 3791.
33. Chen, H.; Huang, H.; Huang, X.; Clifford, J. N.; Forneli, A.; Palomares, E.; Zheng, X.; Zheng, L.; Wang, X.; Shen, P.; Zhao, B.; Tan, S. "High molar extinction coefficient branchlike organic dyes containing di(*p*-tolyl)phenylamine donor for dye-sensitized solar cells applications" *J. Phys. Chem. C* **2010**, *114*, 3280.

34. Heredia, D.; Natera, J.; Gervaldo, M.; Otero, L.; Fungo, F.; Lin, C.-H.; Wong, K.-T. "Spirobifluorene-bridged donor/acceptor dye for organic dye-sensitized solar cells" *Org. Lett.* **2010**, *12*, 12.
35. Tsai, M.-S.; Hsu, Y.-C.; Lin, J. T.; Chen, H.-C.; Hsu, C.-P. "Organic dyes containing 1*H*-phenanthro[9,10-*d*]imidazole conjugation for solar cells" *J. Phys. Chem. C* **2007**, *111*, 18785.
36. Thomas, K. R. J.; Hsu, Y.-C.; Lin, J. T.; Lee, K.-M.; Ho, K.-C.; Lai, C.-H.; Cheng, Y.-M.; Chou, P.-T. "2,3-disubstituted thiophene-based organic dyes for solar cells" *Chem. Mater.* **2008**, *20*, 1830.
37. Xu, J.; Wang, L.; Liang, G.; Bai, Z.; Wang, L.; Xu, W.; Shen, X. "Density functional theory study on triphenylamine-based dye sensitizers containing different donor moieties" *Bull. Korean Chem. Soc.* **2010**, *31*, 2531.
38. Zhang, L.; Liu, Y.; Wang, Z.; Liang, M.; Sun, Z.; Xue, S. "Synthesis of sensitizers containing donor cascade of triarylamine and dimethylarylamine moieties for dye-sensitized solar cells" *Tetrahedron* **2010**, *66*, 3318.
39. Hartwig, J. F. "Transition metal catalyzed synthesis of arylamines and aryl ethers from aryl halides and triflates: scope and mechanism" *Angew. Chem. Int. Ed.* **1998**, *37*, 2046.
40. Drewry, D. T.; Scrowston, R. M. "Bromination and Vilsmeier-Haack formylation of 6,7-dihydrobenzo[*b*]-thiophen-4(5*H*)-one" *J. Chem. Soc. C* **1969**, 2750.
41. Teng, C.; Yang, X.; Yang, C.; Tian, H.; Li, S.; Wang, X.; Hagfeldt, A.; Sun, L. "Influence of triple bonds as π -spacer units in metal-free organic dyes for dye-sensitized solar cells" *J. Phys. Chem. C* **2010**, *114*, 11305.

42. Techert, S.; Schmatz, S.; Wiessner, A.; Staerk, H. "Photophysical characteristics of directly linked pyrene-dimethylaniline derivatives" *J. Phys. Chem. A* **2000**, *104*, 5700.
43. Koene, B. E.; Loy, D. E.; Thompson, M. E. "Asymmetric triaryldiamines as thermally stable hole transporting layers for organic light-emitting devices" *Chem. Mater.* **1998**, *10*, 2235.
44. Becke, A. D. "Density-functional thermochemistry. III. The role of exact exchange" *J. Chem. Phys.* **1993**, *98*, 5648.
45. Lee, C.; Yang, W.; Parr, R. G. "Development of the cole-salvetti correlation-energy formula into a functional of the electron density" *Phys. Rev. B* **1988**, *37*, 785.
46. van de Lagemaat, J.; Park, N.-G.; Frank, A. J. "Influence of electrical potential distribution, charge transport, and recombination on the photopotential and photocurrent conversion efficiency of dye-sensitized nanocrystalline TiO₂ solar cells: a study by electrical impedance and optical modulation techniques" *J. Phys. Chem. B* **2000**, *104*, 2044.

Summary and Outlook

Polyaromatic hydrocarbons (PAH) are considered as a promising building block for the design of molecular materials suitable for application in electro-optical devices because of their unique optical, charge transporting, liquid crystalline and thermal properties. And the key to these favorable properties is the planar and rigid backbone. In this I have demonstrated the use of PAH such as pyrene, fluoranthene, triphenylene and fluorene for the development of organic materials suitable for electroluminescent devices and dye-sensitized solar cells. I have also explored the structure-property relationship in the newly synthesized compounds. Molecular aggregation a detrimental property of PAH has been avoided in most of the derivatives due to the incorporation bulkier and non-planar chromophores. A summary of the research outcome is presented in this chapter.

In chapter 2, I have described the synthesis, photophysical and electrochemical properties of electroluminescent materials based on fluoranthene and triphenylene core which contain multiple phenyl groups and an amine donor featuring an additional aromatic segment such as pyrene or naphthalene or carbazole. These derivatives exhibited tunable optical and electrochemical properties. Some of the salient observations are:

- (a) Introduction of the amino group on the fluoranthene or triphenylene core red shifts the absorption/emission profiles. It also enhances the charge transporting and thermal properties and inhibits the crystallization. Presence of diarylamine is also found to be beneficial to retard the molecular aggregation to some extent in the fluoranthene-based derivatives.

- (b) Use of pyrenylamine as an amino donor helped to improve the optical and thermal properties. The pyrenylamine-based derivatives exhibited bathochromically shifted optical properties and enhanced thermal stability.
- (c) Triphenylene-based derivatives exhibited hypsochromically shifted absorption/emission, higher thermal stability, comparatively wider band gap, and higher HOMO/LUMO levels when compared to fluoranthene-based materials. Carbazole unit has been found to impart good thermal stability to the compound than the diarylamine units.
- (d) Fluoranthene-based diarylamine derivatives (**7c** and **7d**) displayed good performance when used as hole-transporting and emitting materials in multi-layered organic light-emitting diodes. They displayed greenish-yellow or yellow color. However the electroluminescent devices of triphenylene-based derivatives (**14a-14d**) showed promising blue electroluminescence only when used as dopants in OLED devices.

Fluorene-based quinoxaline, pyrazine and thienopyrazine derivatives have been described in Chapter 3. They were obtained by following a series of reactions such as Sonogashira coupling reaction, oxidation of acetylene unit to 1,2-diketone and condensation reaction of diamines with 1,2-diketones. These compounds were thoroughly characterized by various spectroscopic methods. The effects of introduction of electron-withdrawing and electron-donating groups on the pyrazine segment on the optical and electrochemical properties have been analyzed. The important points those emerge from the photophysical and electrochemical measurements are:

- (a) The presence of electron withdrawing group (-CN) enhances the electron-accepting propensity of the pyrazine unit and contributes to the red shifts in the absorption and emission profiles, increases the fluorescence quantum yields and glass transition temperatures.

- (b) Thienopyrazine derivatives (**22a**, **22b**) exhibited an additional absorption peak at higher wavelength (ca. 556 nm) corresponding to the charge transfer transition originating due to presence of donor/acceptor (thiophene/pyrazine) system and emit in the range of 661-663 nm.
- (c) All the derivatives are thermally stable with thermal decomposition temperature in the range 398-451 °C. The promising thermal stability is attributed to the presence of fused aromatic segments.
- (d) Presence of terthiophene unit decreases the band gap of compounds **22a** and **22b** dramatically and they were found to undergo electropolymerization.
- (e) The results reveal that pyrazine and quinoxaline derivatives can be exploited in blue OLED, whereas thienopyrazines can be suggested as suitable monomer for the development of polymers useful for fabrication in bulk-heterojunction solar cell.

We have also explored the use of pyrene for the development of functional materials for applications in electronic devices such as OLED and DSSC. The findings have been presented in the chapters 4 and 5. In the chapter 5, I have collected the pyrene derivatives containing acetylene linkers and fluorene-based chromophores. Both mono- and tetra-substituted derivatives were synthesized and characterized by spectral, electrochemical and thermal methods. Use of acetylene linkage between fluorene and pyrene not only increases the conjugation but also attenuates the electronic coupling between pyrene and fluorene which leads to enhanced charge transporting properties. The results are summarized in following points:

- (a) Tetrasubstituted pyrene derivatives (**29-31**) displayed broader absorption and lower energy band than the corresponding monosubstituted compound (**26**) due to the presence of elongated conjugation pathway.

- (b) Further, incorporation of diphenylamine red shifts the absorption/emission profile and also enhances thermal stability.
- (c) The diphenylamine derivatives (**28** & **31**) showed positive solvatochromism in emission profile. But the extent of red shift in **31** is lesser than **28**. This indicates that the energy of the charge transfer state increases as the number of peripheral donor substituents increase.
- (d) Compounds **26-31** were used as efficient dopant with the host material CBP which was used as hole-transporting layer. Electroluminescent devices derived from the monosubstituted compound **26-28** showed bright blue emission while the tetrasubstituted derivatives **30** and **31** exhibited yellow emission.
- (e) Incorporation of thiophene red shifts the absorption and displays more favorable HOMO/LUMO level.

In the chapter 5, I have described the synthesis and characterization of pyrenylamine-based organic dyes as sensitizers for dye-sensitized solar cells. The important results are summarized below:

- (a) Polyaromatic segment such as pyrene on amine donor increases the donor strength.
- (b) The incorporation of two donor system red shifts the absorption as well as emission profile and also increases molar extinction coefficient which lead to improved light harvesting properties of these dyes.
- (c) Theoretical calculations reveal that two cascade donors present in the dyes enhance the donor strength and also improve the donor-acceptor interaction which tunes the electron injection from the dye to TiO₂ surface.
- (d) The dye possessing biphenyl spacer between the two donors (**43b**) has shown better DSSC performance.

In summary, we have developed functional materials by exploiting the unique optical and thermal properties of PAHs such as pyrene, fluorene, fluoranthene and triphenylene. Introduction of chromophores such as cyano or diarylamines into the backbone of PAH, tuned their photophysical and electrochemical properties. Further incorporation of heterocycles such as pyrazine and thiophene modulated the interaction between the chromophores due to electron-accepting and electron-donating properties respectively. Fluoranthene was found as the promising core for the stable emission and displayed thermal and electroluminescent properties. Though, triphenylene-based derivatives have been intensively studied as liquid-crystalline materials, their use in electro-optical materials is limited. More functional materials need to be developed using triphenylene core to unravel the structure-property relationship in the new class of compounds. We have used pyrene as a core or as peripheral segment in a triarylamine to construct the molecular materials. Pyrene can also be used as linker to obtain π -conjugated materials. Such architectures may be beneficial to favorably tune the energy levels of the molecular orbitals.

*Supporting
Information*

	Page No.
Figure S1	¹ H NMR Spectra of 6 . S1
Figure S2	¹³ C NMR Spectra of 6 . S1
Figure S3	¹ H NMR Spectra of 7a . S2
Figure S4	¹³ C NMR Spectra of 7a . S2
Figure S5	¹ H NMR Spectra of 7b . S3
Figure S6	¹³ C NMR Spectra of 7b . S3
Figure S7	¹ H NMR Spectra of 7c . S4
Figure S8	¹³ C NMR Spectra of 7c . S4
Figure S9	¹ H NMR Spectra of 7d . S5
Figure S10	¹³ C NMR Spectra of 7d . S5
Figure S11	¹ H NMR Spectra of 13 . S6
Figure S12	¹³ C NMR Spectra of 13 . S6
Figure S13	¹ H NMR Spectra of 14a . S7
Figure S14	¹³ C NMR Spectra of 14a . S7
Figure S15	¹ H NMR Spectra of 14b . S8
Figure S16	¹³ C NMR Spectra of 14b . S8
Figure S17	¹ H NMR Spectra of 14c . S9
Figure S18	¹³ C NMR Spectra of 14c . S9
Figure S19	¹ H NMR Spectra of 14d . S10
Figure S20	¹³ C NMR Spectra of 14d . S10
Figure S21	¹ H NMR Spectra of 19a . S11
Figure S22	¹³ C NMR Spectra of 19a . S11
Figure S23	¹ H NMR Spectra of 19b . S12
Figure S24	¹³ C NMR Spectra of 19b . S12
Figure S25	¹ H NMR Spectra of 20a . S13
Figure S26	¹³ C NMR Spectra of 20a . S13
Figure S27	¹ H NMR Spectra of 21a . S14
Figure S28	¹³ C NMR Spectra of 21a . S14
Figure S29	¹ H NMR Spectra of 22a . S15
Figure S30	¹³ C NMR Spectra of 22a . S15
Figure S31	¹ H NMR Spectra of 20b . S16
Figure S32	¹³ C NMR Spectra of 20b . S16
Figure S33	¹ H NMR Spectra of 21b . S17
Figure S34	¹³ C NMR Spectra of 21b . S17
Figure S35	¹ H NMR Spectra of 22b . S18
Figure S36	¹³ C NMR Spectra of 22b . S18
Figure S37	¹ H NMR Spectra of 26 . S19
Figure S38	¹³ C NMR Spectra of 26 . S19
Figure S39	¹ H NMR Spectra of 27 . S20

Figure S40	^{13}C NMR Spectra of 27 .	S20
Figure S41	^1H NMR Spectra of 28 .	S21
Figure S42	^{13}C NMR Spectra of 28 .	S21
Figure S43	^1H NMR Spectra of 29 .	S22
Figure S44	^{13}C NMR Spectra of 29 .	S22
Figure S45	^1H NMR Spectra of 30 .	S23
Figure S46	^{13}C NMR Spectra of 30 .	S23
Figure S47	^1H NMR Spectra of 31 .	S24
Figure S48	^{13}C NMR Spectra of 31 .	S24
Figure S49	^1H NMR Spectra of 34b .	S25
Figure S50	^{13}C NMR Spectra of 34b .	S25
Figure S51	^1H NMR Spectra of 34c .	S26
Figure S52	^{13}C NMR Spectra of 34c .	S26
Figure S53	^1H NMR Spectra of 34d .	S27
Figure S54	^{13}C NMR Spectra of 34d .	S27
Figure S55	^1H NMR Spectra of 35a .	S28
Figure S56	^{13}C NMR Spectra of 35a .	S28
Figure S57	^1H NMR Spectra of 35b .	S29
Figure S58	^{13}C NMR Spectra of 35b .	S29
Figure S59	^1H NMR Spectra of 35c .	S30
Figure S60	^{13}C NMR Spectra of 35c .	S30
Figure S61	^1H NMR Spectra of 35d .	S31
Figure S62	^1H NMR Spectra of 41a .	S32
Figure S63	^{13}C NMR Spectra of 41a .	S32
Figure S64	^1H NMR Spectra of 41b .	S33
Figure S65	^{13}C NMR Spectra of 41b .	S33
Figure S66	^1H NMR Spectra of 41c .	S34
Figure S67	^{13}C NMR Spectra of 41c .	S34
Figure S68	^1H NMR Spectra of 38b .	S35
Figure S69	^{13}C NMR Spectra of 38b .	S35
Figure S70	^1H NMR Spectra of 42a .	S36
Figure S71	^{13}C NMR Spectra of 42a .	S36
Figure S72	^1H NMR Spectra of 42b .	S37
Figure S73	^{13}C NMR Spectra of 42b .	S37
Figure S74	^1H NMR Spectra of 42c .	S38
Figure S75	^{13}C NMR Spectra of 42c .	S38
Figure S76	^1H NMR Spectra of 39a .	S39
Figure S77	^{13}C NMR Spectra of 39a .	S39
Figure S78	^1H NMR Spectra of 39b .	S40
Figure S79	^{13}C NMR Spectra of 39b .	S40

Figure S80	^1H NMR Spectra of 43a .	S41
Figure S81	^{13}C NMR Spectra of 43a .	S41
Figure S82	^1H NMR Spectra of 43b .	S42
Figure S83	^{13}C NMR Spectra of 43b .	S42
Figure S84	^1H NMR Spectra of 43c .	S43
Figure S85	^{13}C NMR Spectra of 43c .	S43

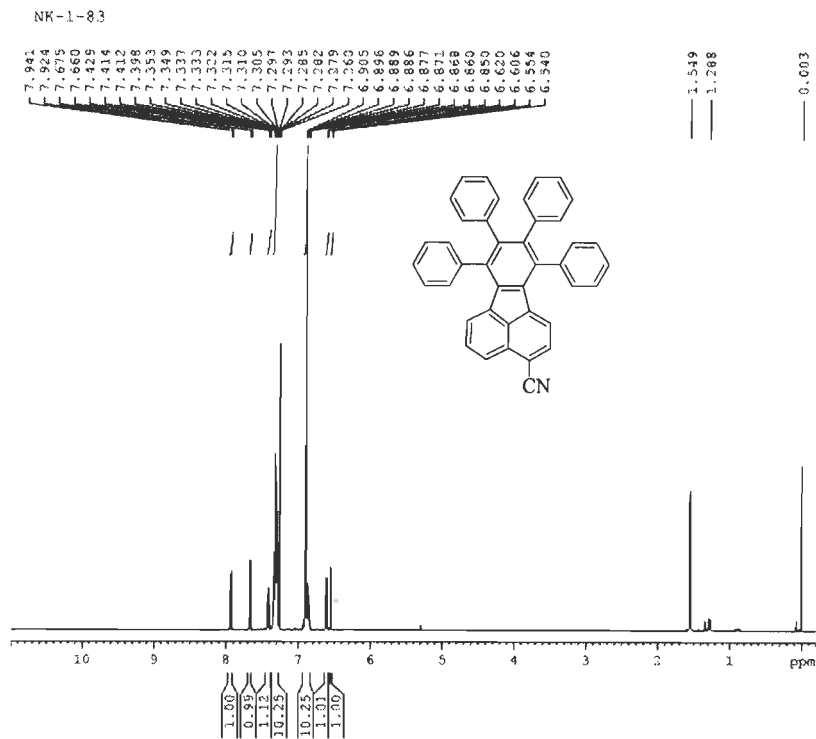


Figure S1. ¹H NMR spectra of 6.

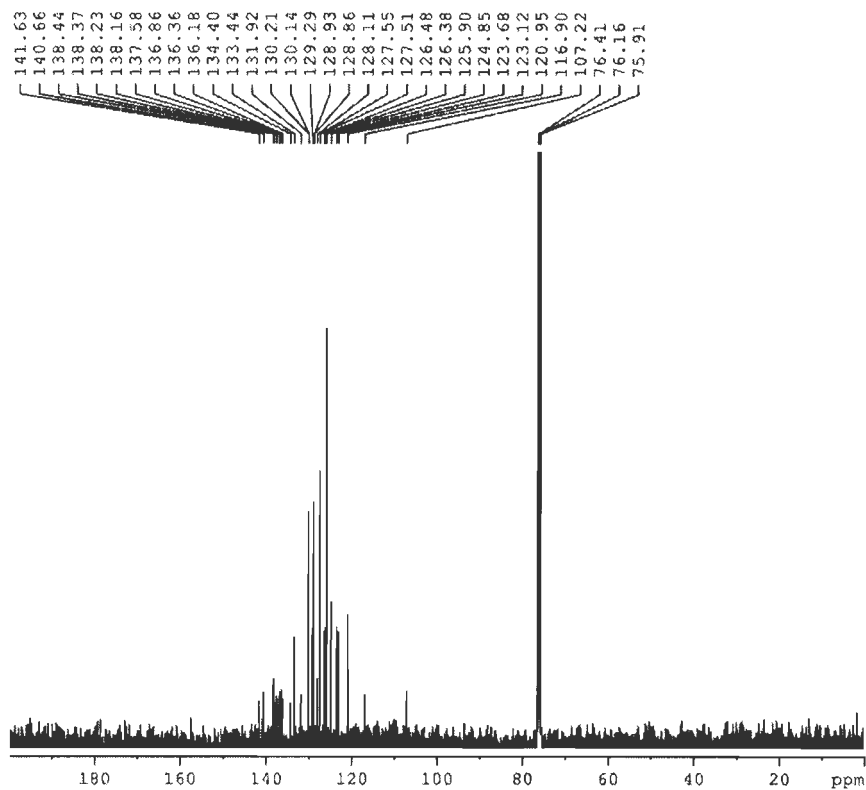
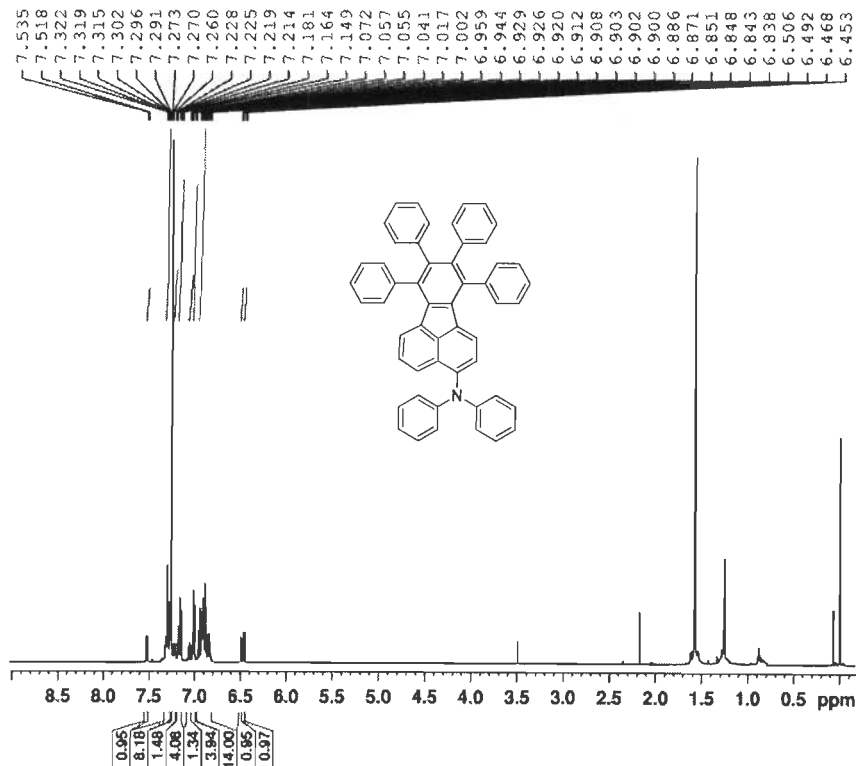


Figure S2. ¹³C NMR spectra of 6.

NK-1-89



```

Current Data Parameters
NAME      NK-1-89
EXPNO    1
PROCNO   1

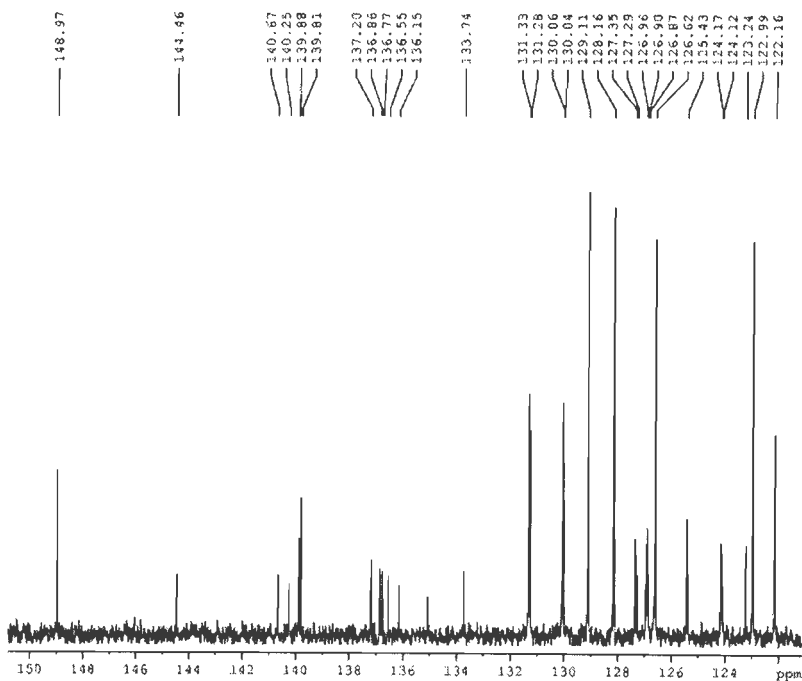
F2 - Acquisition Parameters
Date_    20090910
Time     14.59
INSTRUM  spect
PROBHD   5 mm PABBO BBO
PULPROG  zgpg30
TD       65536
SOLVENT  CDCl3
NS       16
DS       2
SWH      10030.578 Hz
FIDRES   0.157672 Hz
AQ       3.1720407 sec
RG       524
DM       48.600 umsec
DE       6.00 umsec
TE       297.4 K
D1       1.0000000 sec
TDO      1

----- CHANNEL f1 -----
NUC1     1H
P1       14.80 umsec
PL1      0.00 dB
SFO1     500.130480 MHz

F2 - Processing parameters
SI       32768
SF       500.1299214 MHz
WDW      EM
SSB      0
LB       0.30 Hz
GB       0
PC       1.00
  
```

Figure S3. ¹H NMR spectra of 7a.

NK-1-89



```

Current Data Parameters
NAME      NK-1-89b
EXPNO    2
PROCNO   1

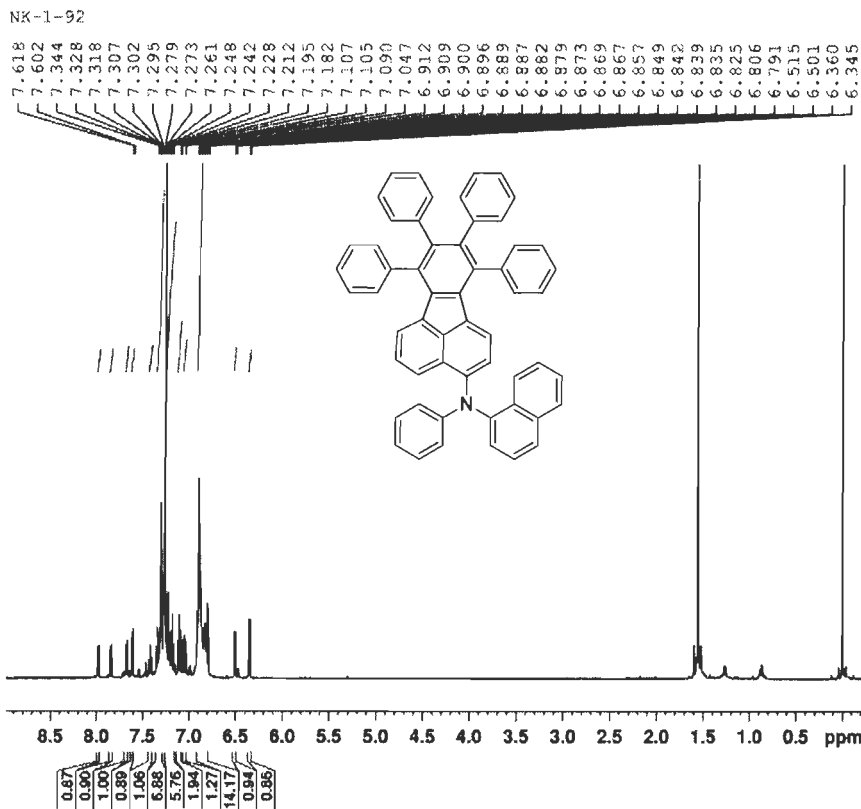
F2 - Acquisition Parameters
Date_    20090910
Time     21.92
INSTRUM  spect
PROBHD   5 mm PABBO BBO
PULPROG  zgpg30
TD       65536
SOLVENT  CDCl3
NS       112
DS       2
SWH      80360.000 Hz
FIDRES   0.158122 Hz
AQ       1.912410 sec
RG       375
DM       16.650 umsec
DE       6.00 umsec
TE       296.7 K
D1       2.0000000 sec
d11      0.0100000 sec
DELTA    1.9999999 sec
TDO      1

----- CHANNEL f1 -----
NUC1     13C
P1       9.00 umsec
PL1      1.00 dB
SFO1     125.767890 MHz

----- CHANNEL f2 -----
CPDPRG2  waltz16
NUC2     1H
PCPD2    60.00 umsec
PL2      2.00 dB
PL12     16.60 dB
PL13     20.00 dB
SFO2     500.130480 MHz

F2 - Processing parameters
SI       32768
SF       125.767890 MHz
WDW      EM
SSB      0
LB       1.00 Hz
GB       0
PC       1.00
  
```

Figure S4. ¹³C NMR spectra of 7a.



```

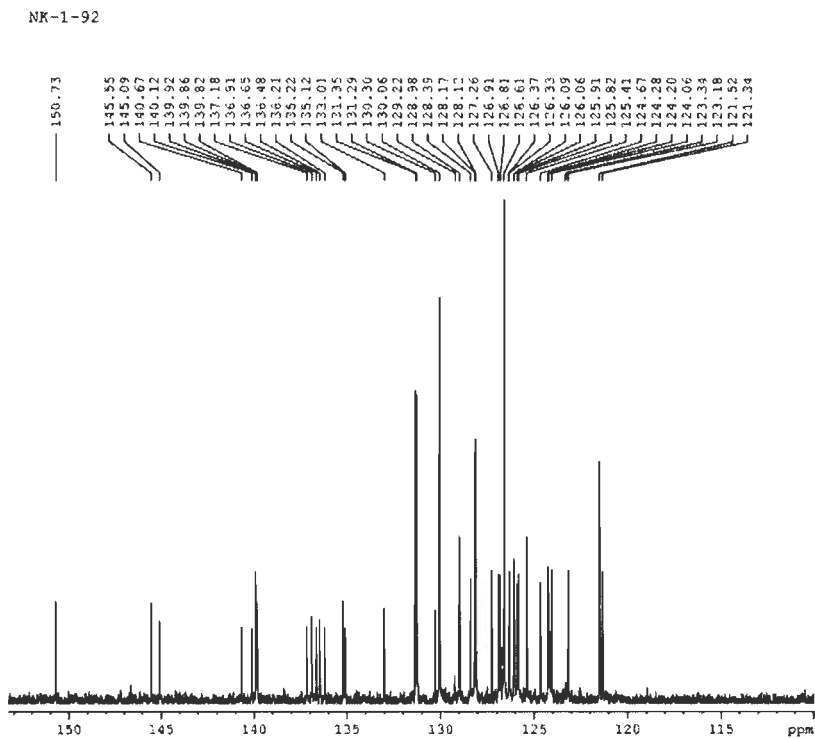
Current Data Parameters
NAME      NK-1-92F34
EXPNO    1
PROCNO    1

F2 - Acquisition Parameters
Date_     20070113
Time      12.50
INSTRUM   avn500
PROBHD    5 mm PABBO BB-
PULPROG   zgpg30
TD         65536
SOLVENT   CDCl3
NS         16
DS         2
SWH        10210.578 Hz
FIDRES     0.131634 Hz
AQ         3.1720403 sec
RG         724
IN         65.400 umm
QE         6.00 umm
TE         290.4 K
D1         1.00000000 sec
TD0        1

----- CHANNEL f1 -----
NUC1       1H
P1         14.70 umm
PL1        2.00 dB
SFO1       500.1326800 MHz

F2 - Processing parameters
SI         32768
SF         500.1299534 MHz
WDW        EM
SSB        0
LB         0.10 Hz
GB         0
PC         1.00
  
```

Figure S5. ¹H NMR spectra of 7b.



```

Current Data Parameters
NAME      NK-1-92F0
EXPNO    2
PROCNO    1

F2 - Acquisition Parameters
Date_     20090221
Time      22.41
INSTRUM   avn500
PROBHD    5 mm PABBO BB-
PULPROG   zgpg30
TD         65536
SOLVENT   CDCl3
NS         312
DS         4
SWH        30030.029 Hz
FIDRES     0.489227 Hz
AQ         1.6517410 sec
RG         1040
IN         14.450 umm
QE         6.00 umm
TE         300.4 K
D1         1.00000000 sec
D11       1.00000000 sec
DELTA     1.89999998 sec
TD0        1

----- CHANNEL f1 -----
NUC1       13C
P1         9.80 umm
PL1        1.00 dB
SFO1       125.7705447 MHz

----- CHANNEL f2 -----
CPDPRG2   waltz16
NUC2       1H
PCPD2     80.00 umm
PC2       2.00 dB
PL12      19.00 dB
PL13      19.00 dB
RFOC      500.1299534 MHz

F2 - Processing parameters
SI         32768
SF         125.7705447 MHz
WDW        EM
SSB        0
LB         0.10 Hz
GB         0
PC         1.00
  
```

Figure S6. ¹³C NMR spectra of 7b.

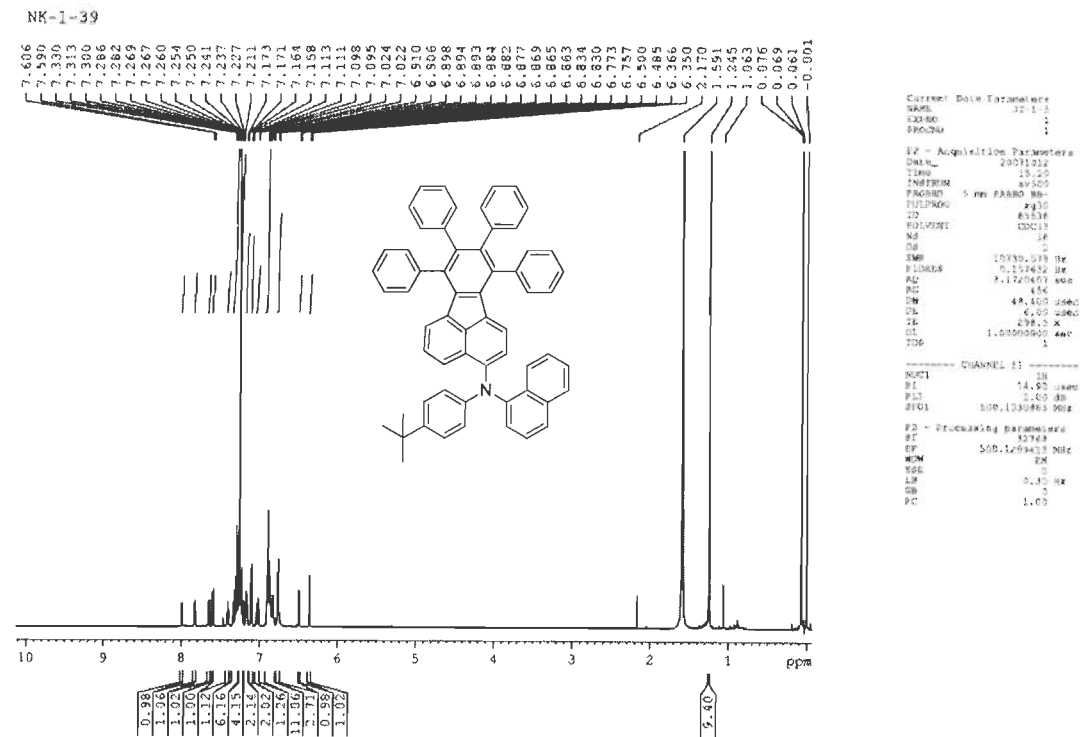


Figure S7. ¹H NMR spectra of 7c.

NK-1-39

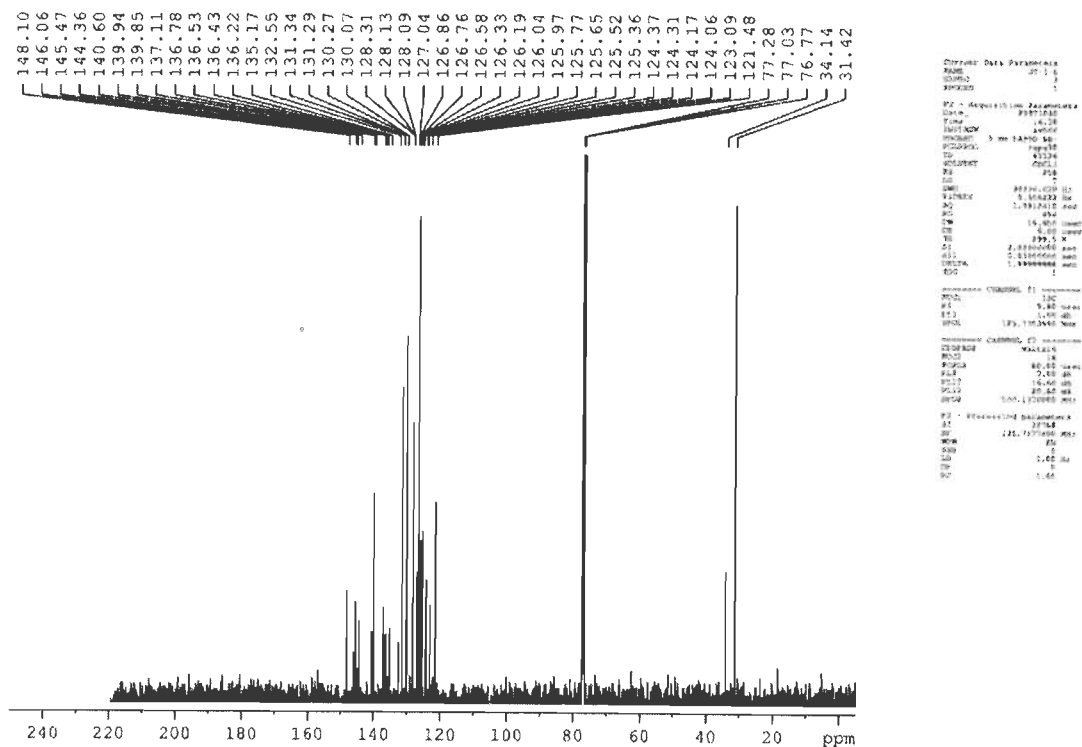
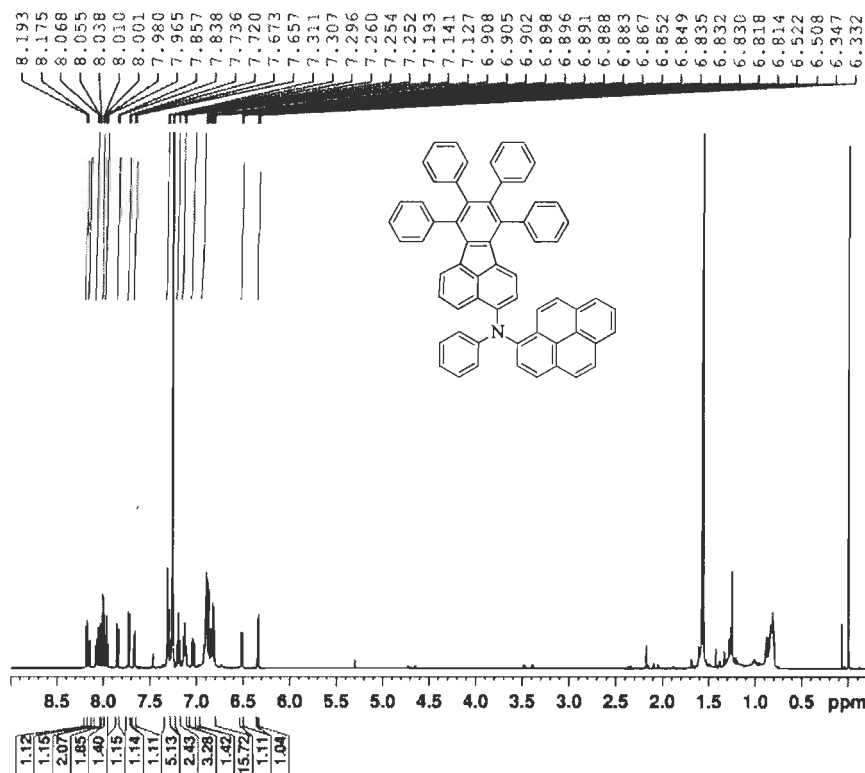


Figure S8. ¹³C NMR spectra of 7c.

NK-1-91



```

Current Data Parameters
NAME      NK-1-91
EXPNO    1
PROCNO   1

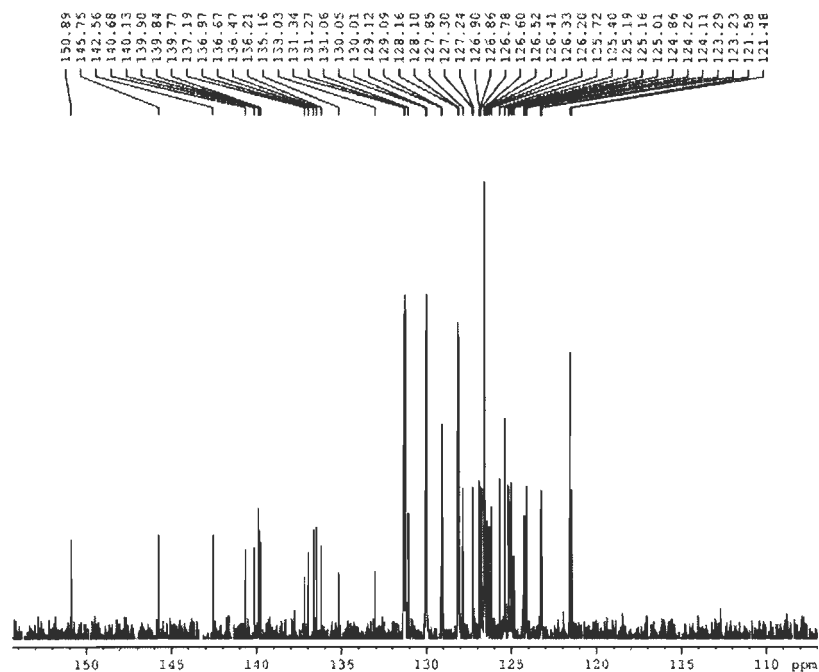
F2 - Acquisition Parameters
Date_    20090917
Time     13.32
INSTRUM  av500
PROBHD   5 mm PACT1 1H/
PULPROG  zgpg30
TD        65536
SOLVENT  DMSO-D
NS        512
DS        4
SWH       10150.578 Hz
FIDRES    0.157630 Hz
AQ        1.1725407 sec
RG         515
DN         48.405 umax
TE        4.00 umax
DE        250.0 K
DELTA    1.00000000 sec
TD0       1

===== CHANNEL f1 =====
NUC1      1H
P1        7.70 umax
PC1       2.00 dB
SFO1      500.136093 MHz

F2 - Processing parameters
SI         32768
SF         500.136093 MHz
WDW        EM
SSB        0
LB         0.35 Hz
GB         0
PC         1.00
  
```

Figure S9. ¹H NMR spectra of 7d.

NK-1-91



```

Current Data Parameters
NAME      NK-1-91
EXPNO    1
PROCNO   1

F2 - Acquisition Parameters
Date_    20090222
Time     0.15
INSTRUM  av500
PROBHD   5 mm PABBO-9B
PULPROG  zgpg30
TD        65536
SOLVENT  DMSO-D
NS        512
DS        4
SWH       30070.729 Hz
FIDRES    0.354223 Hz
AQ        1.0314419 sec
RG         575
DN         16.650 umax
TE        4.00 umax
DE        300.0 K
DELTA    2.07390300 sec
DELTA    0.03090300 sec
DELTA    1.87999990 sec
TD0       1

===== CHANNEL f1 =====
NUC1      13C
P1        9.40 umax
PC1       1.00 dB
SFO1      125.7703643 MHz

===== CHANNEL f2 =====
NUC2      13C
P2        9.40 umax
PC2       1.00 dB
SFO2      125.7703643 MHz

F2 - Processing parameters
SI         32768
SF         125.770364 MHz
WDW        EM
SSB        0
LB         1.00 Hz
GB         0
PC         1.00
  
```

Figure S10. ¹³C NMR spectra of 7d.

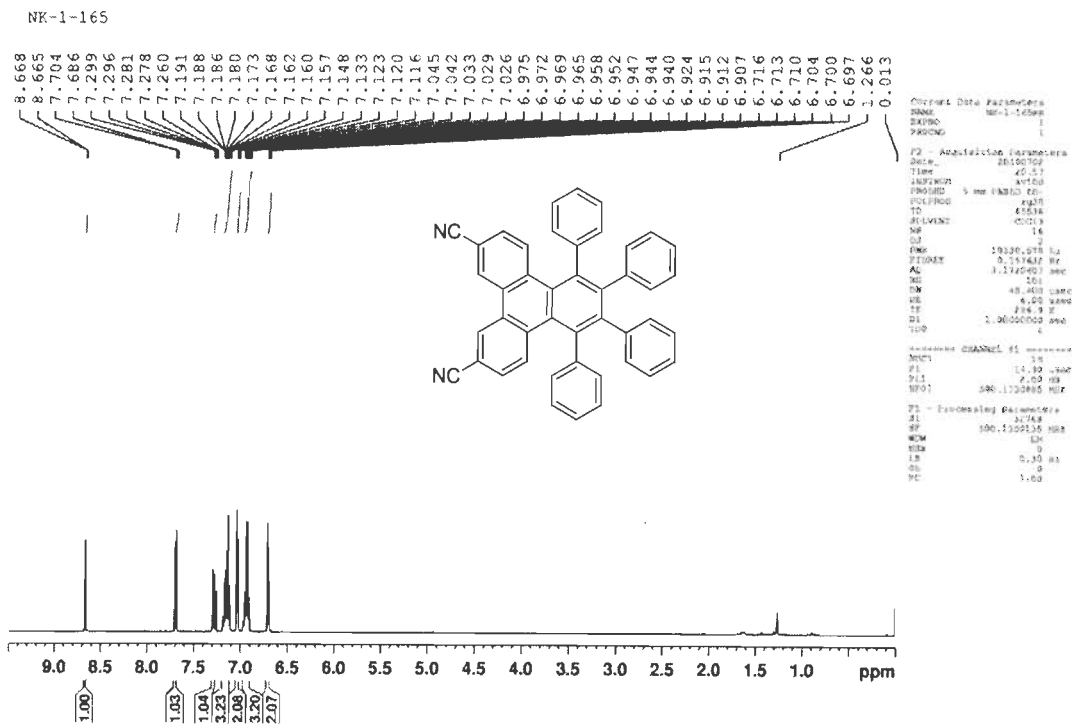


Figure S11. ¹H NMR spectra of 13.

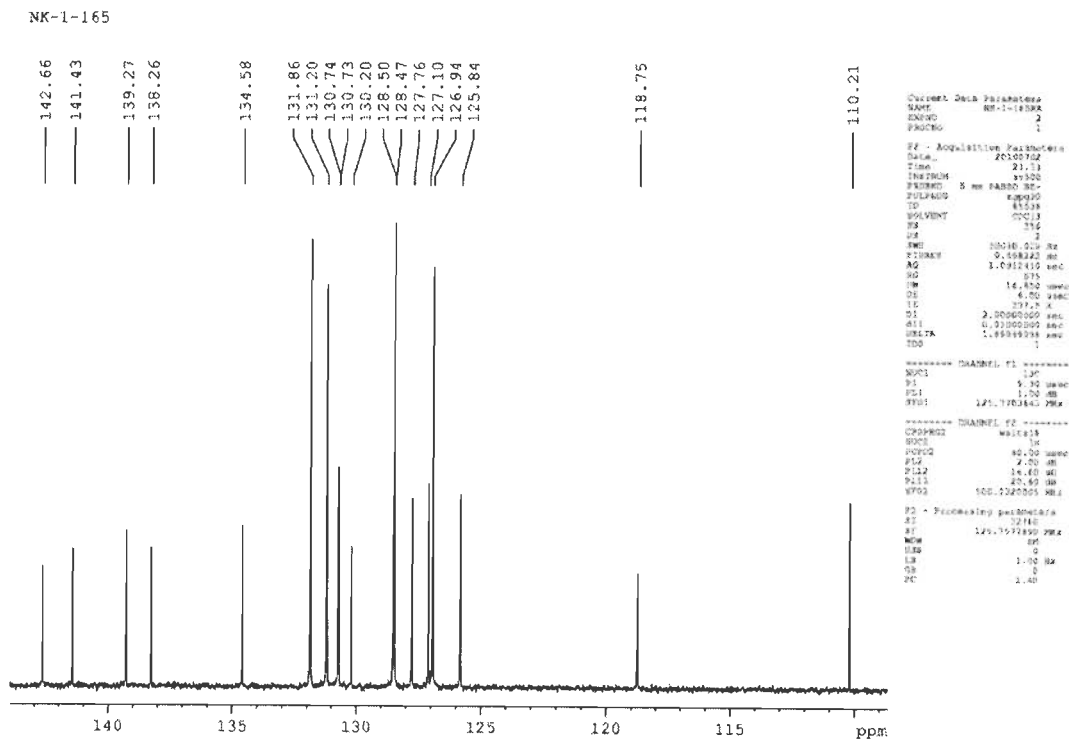


Figure S12. ¹³C NMR spectra of 13.

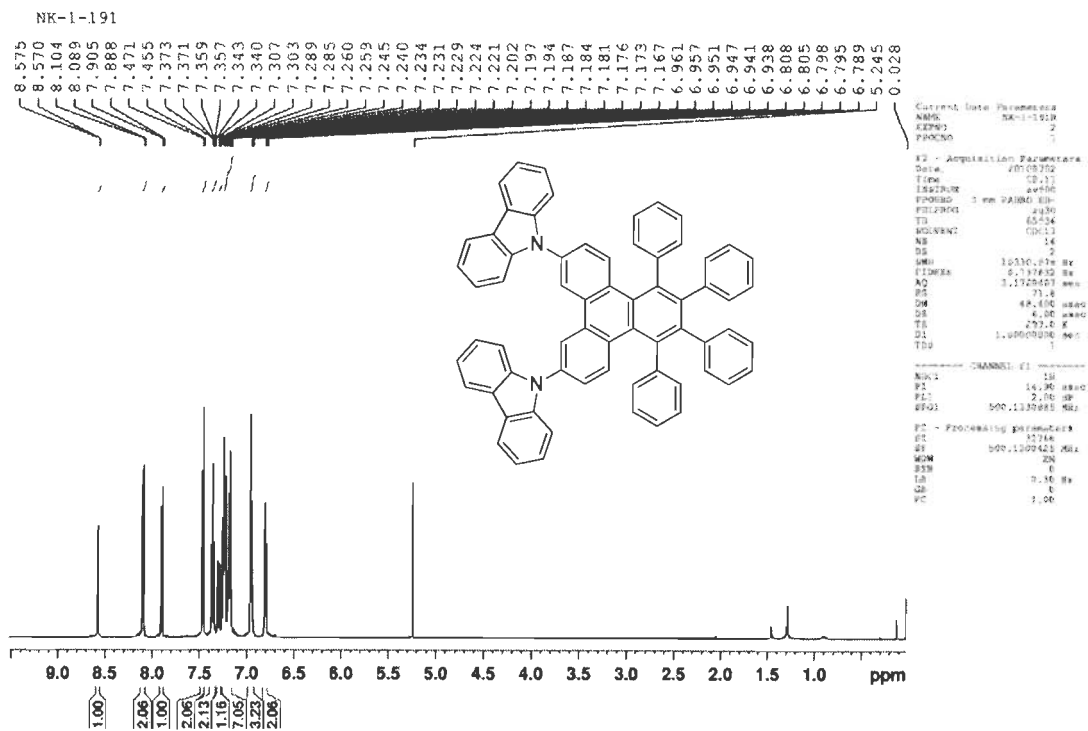


Figure S13. ^1H NMR spectra of 14a.

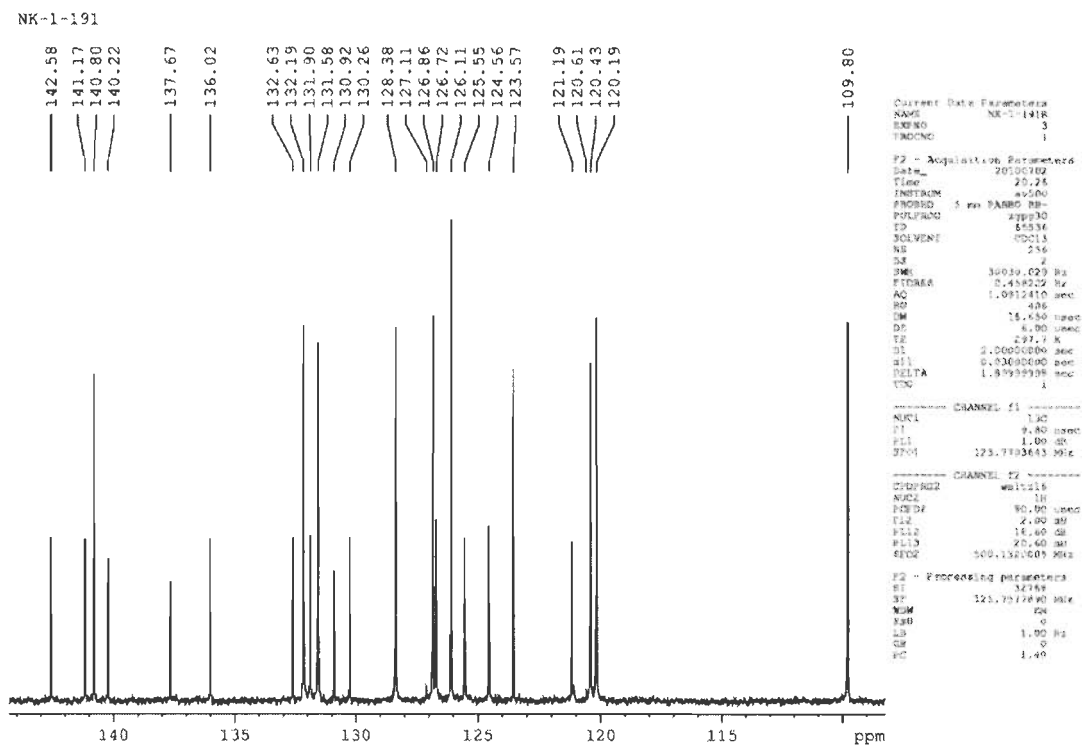


Figure S14. ^{13}C NMR spectra of 14a.

NK-1-123

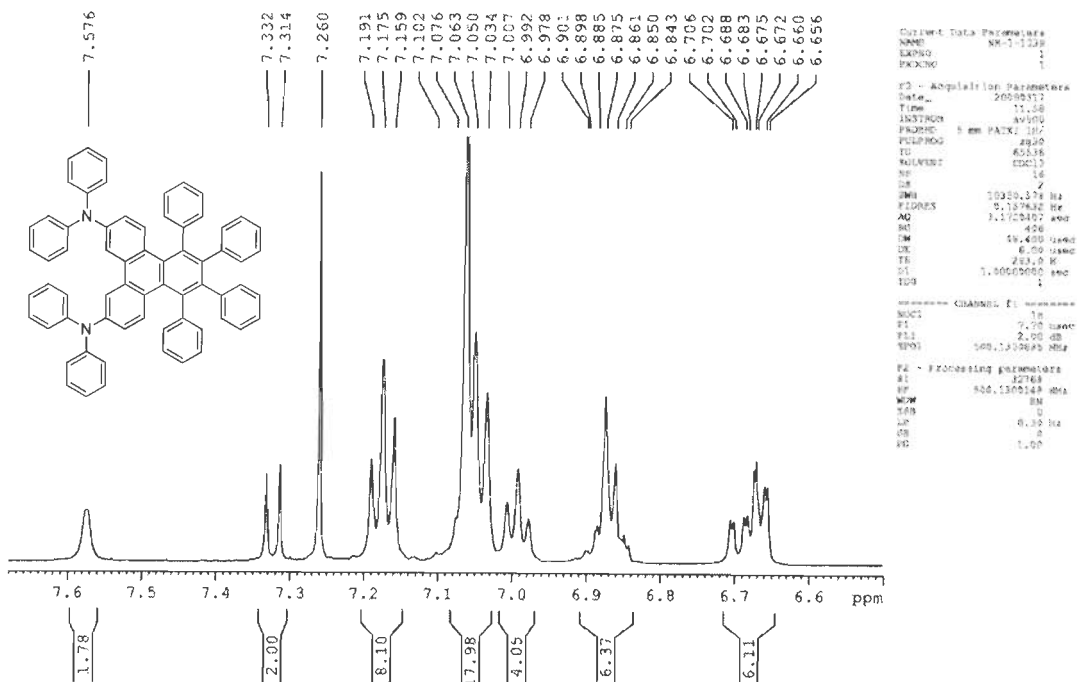


Figure S15. ¹H NMR spectra of 14b.

NK-1-123

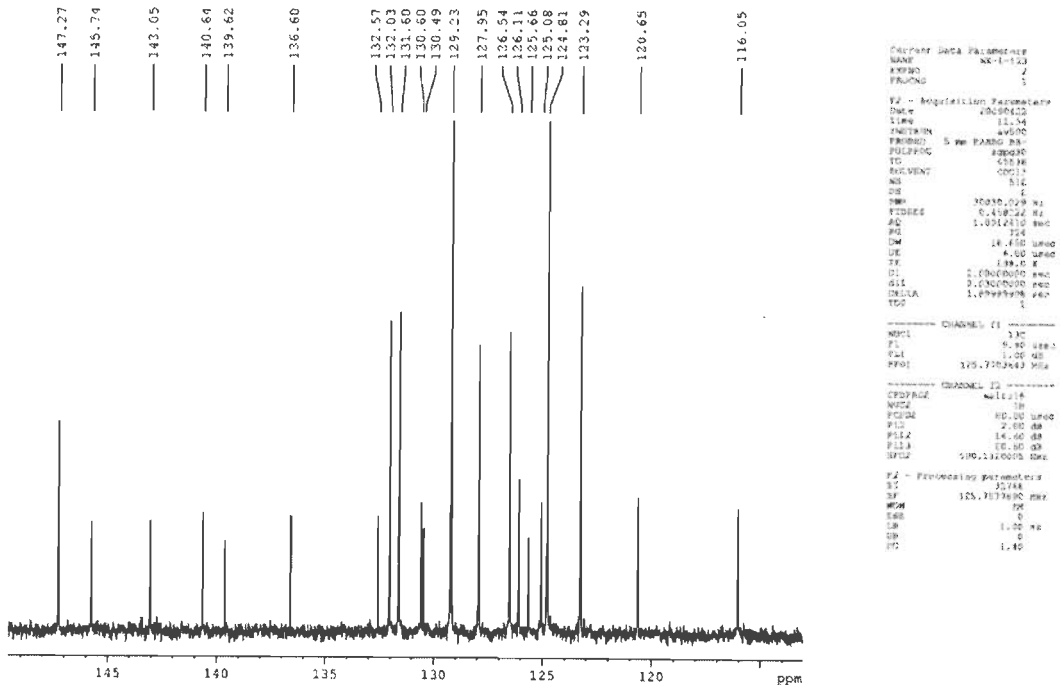


Figure S16. ¹³C NMR spectra of 14b.

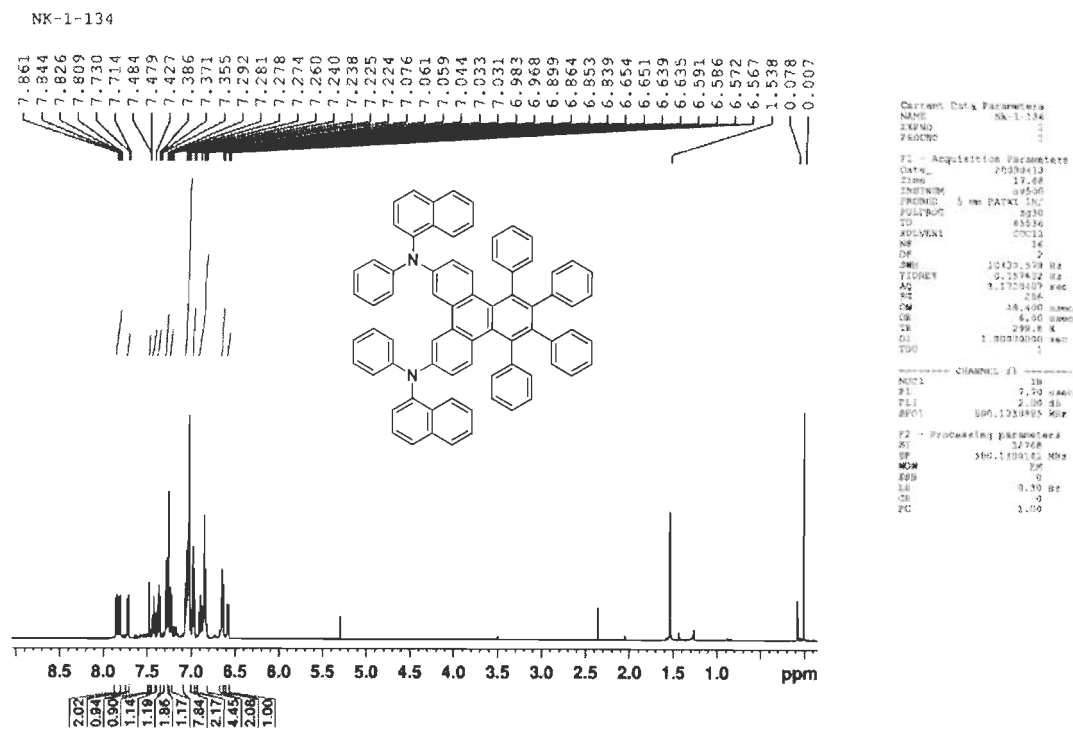


Figure S17. ^1H NMR spectra of 14c.

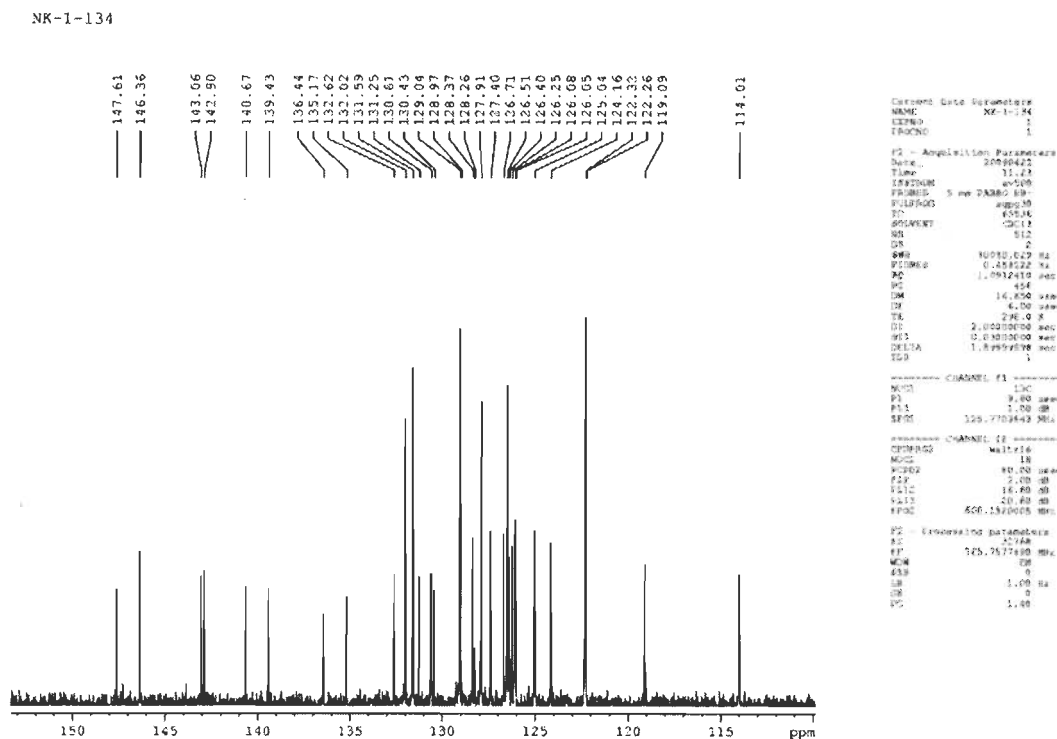


Figure S18. ^{13}C NMR spectra of 14c.

NK-1-136

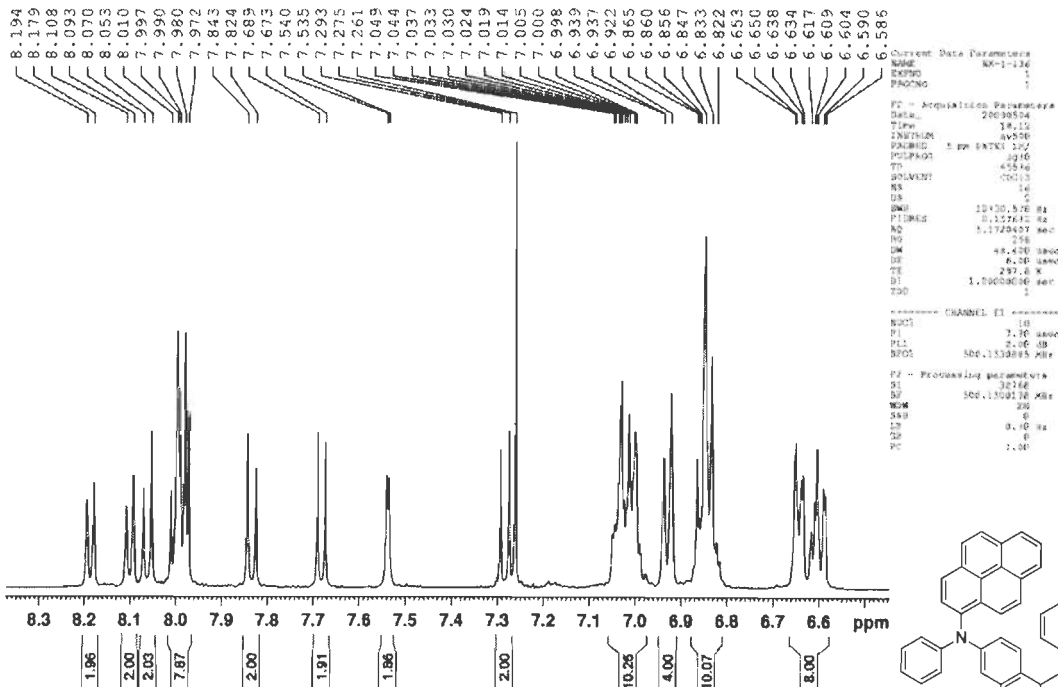


Figure S19. ¹H NMR spectra of 14d.

NK-1-136

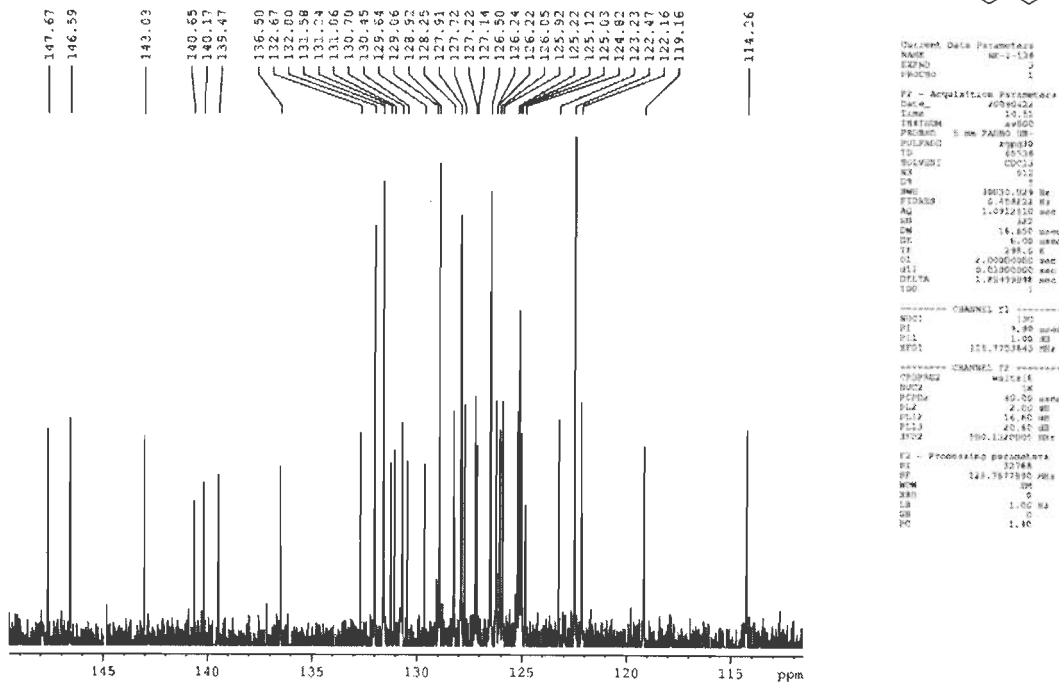


Figure S20. ¹³C NMR spectra of 14d.

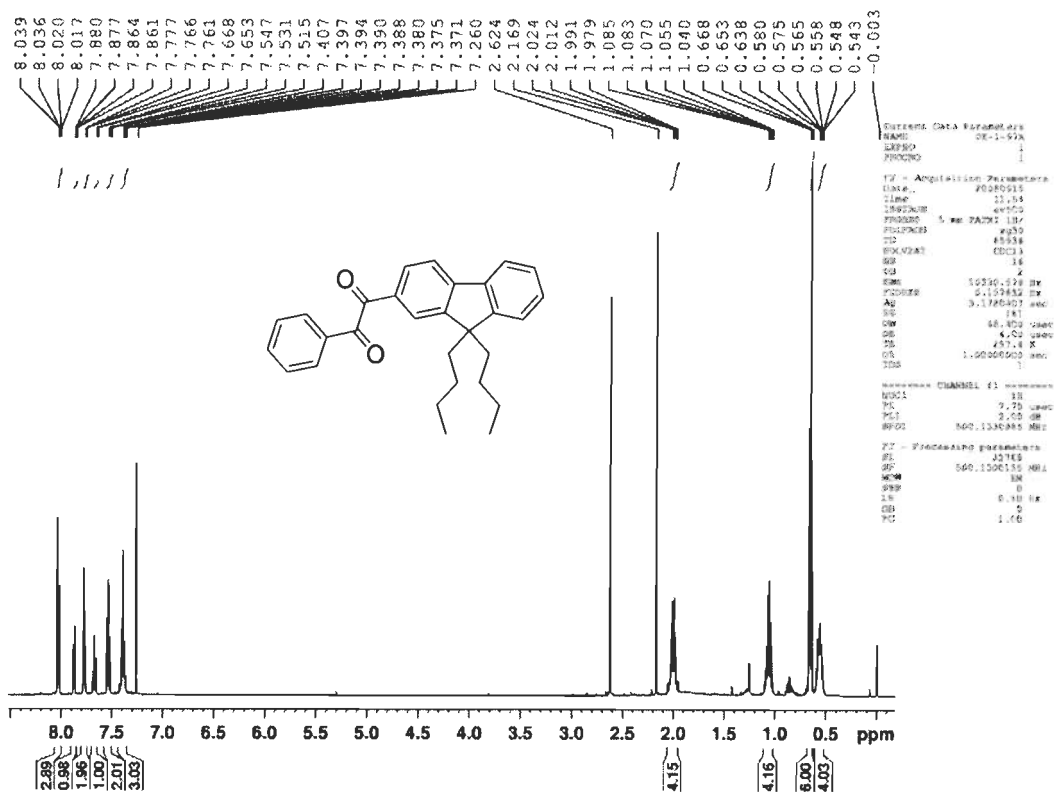


Figure S21. ¹H NMR spectra of 19a.

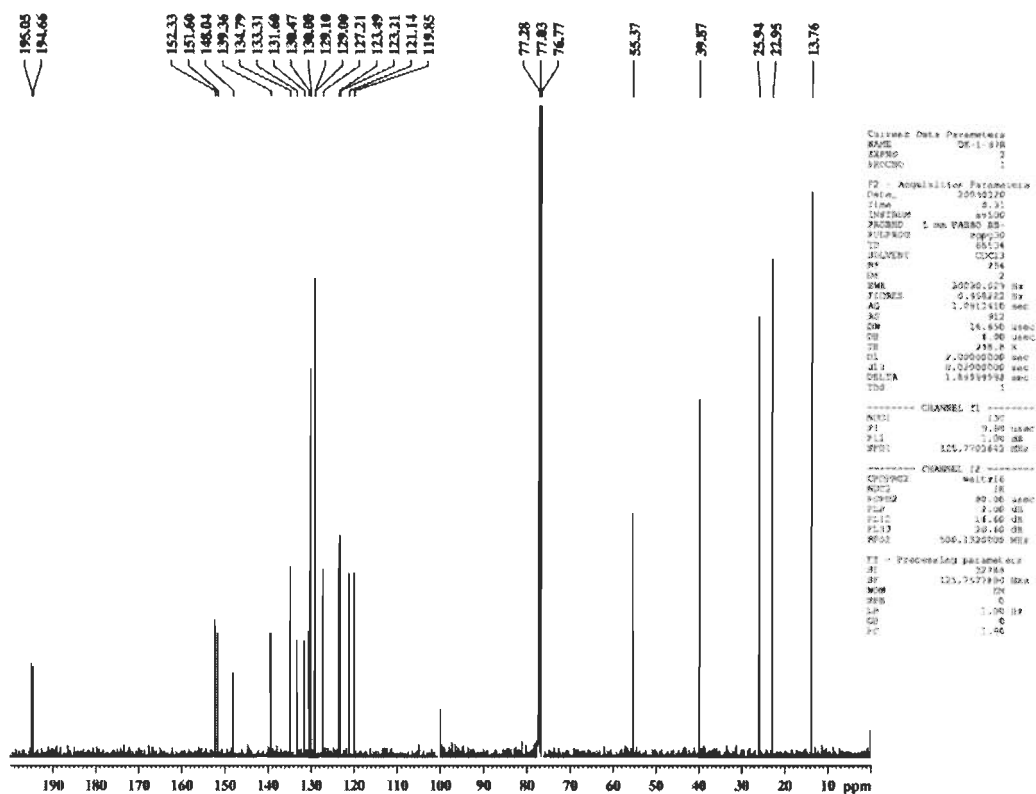


Figure S22. ¹³C NMR spectra of 19a.

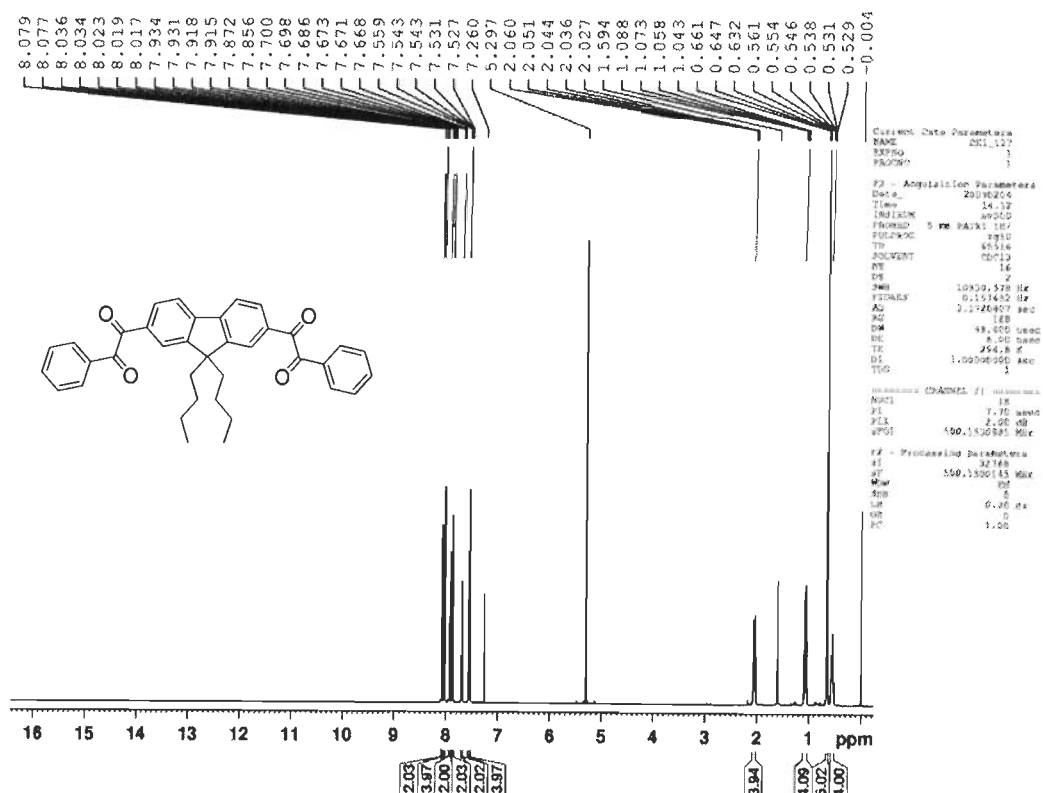


Figure S23. ¹H NMR spectra of 19b.

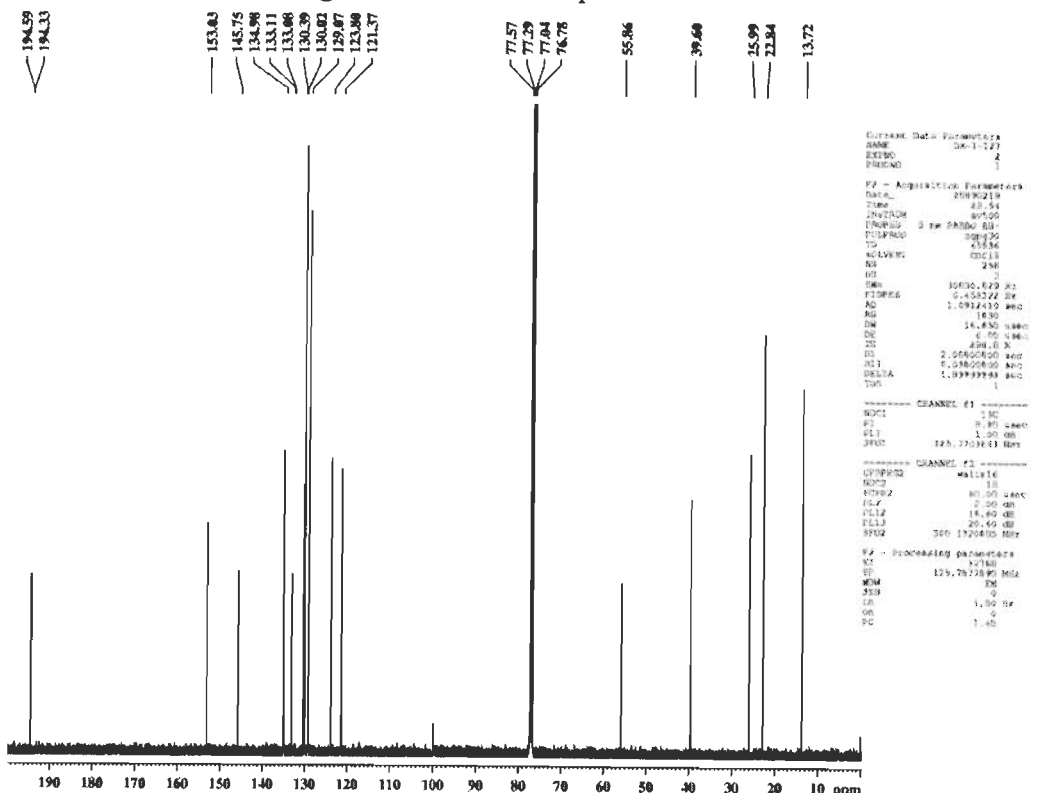


Figure S24. ¹³C NMR spectra of 19b.

NK-1-106

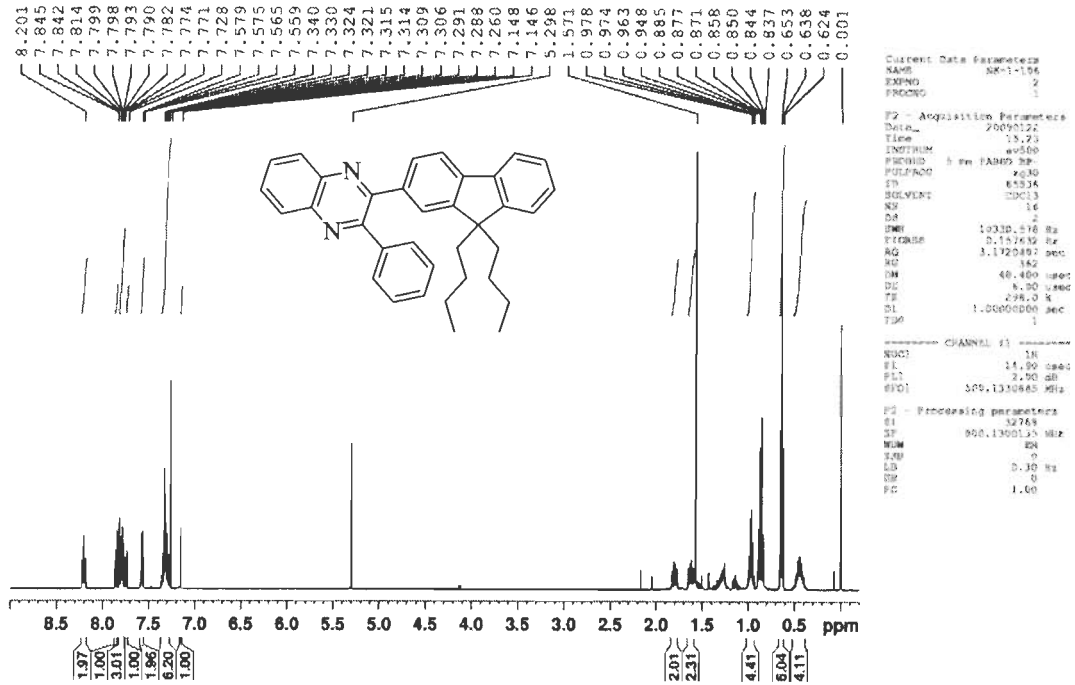


Figure S25. ¹H NMR spectra of 20a.

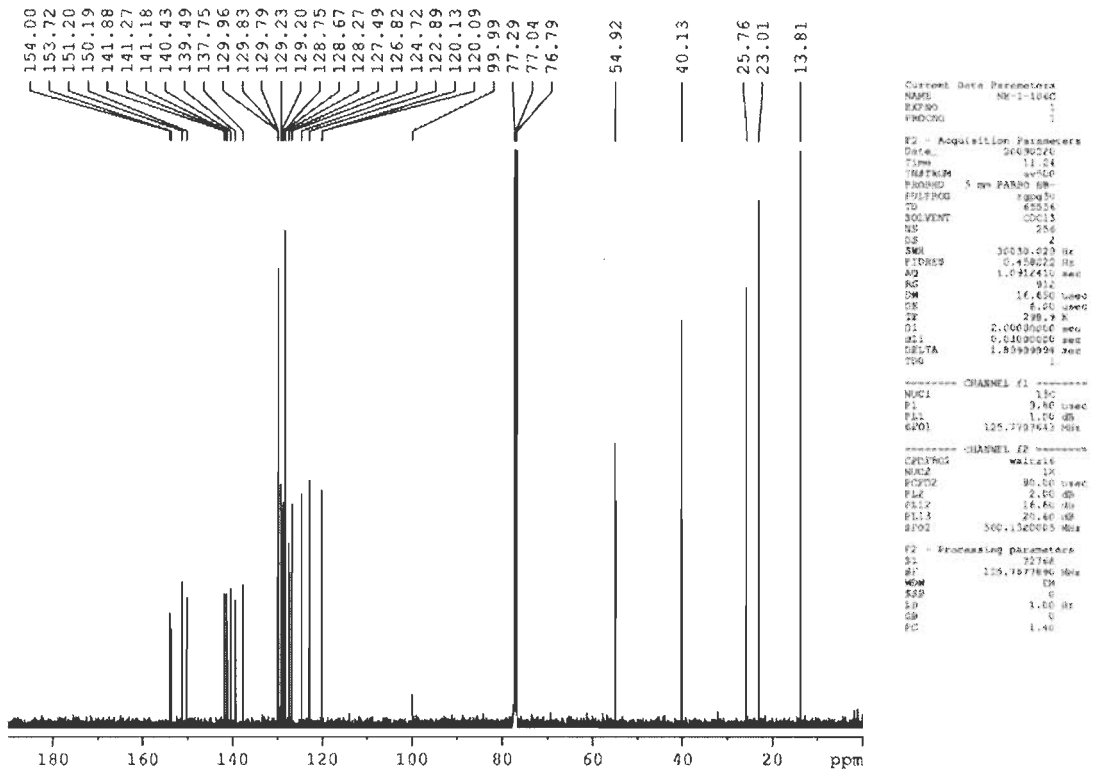


Figure S26. ¹³C NMR spectra of 20a.

NK-1-107

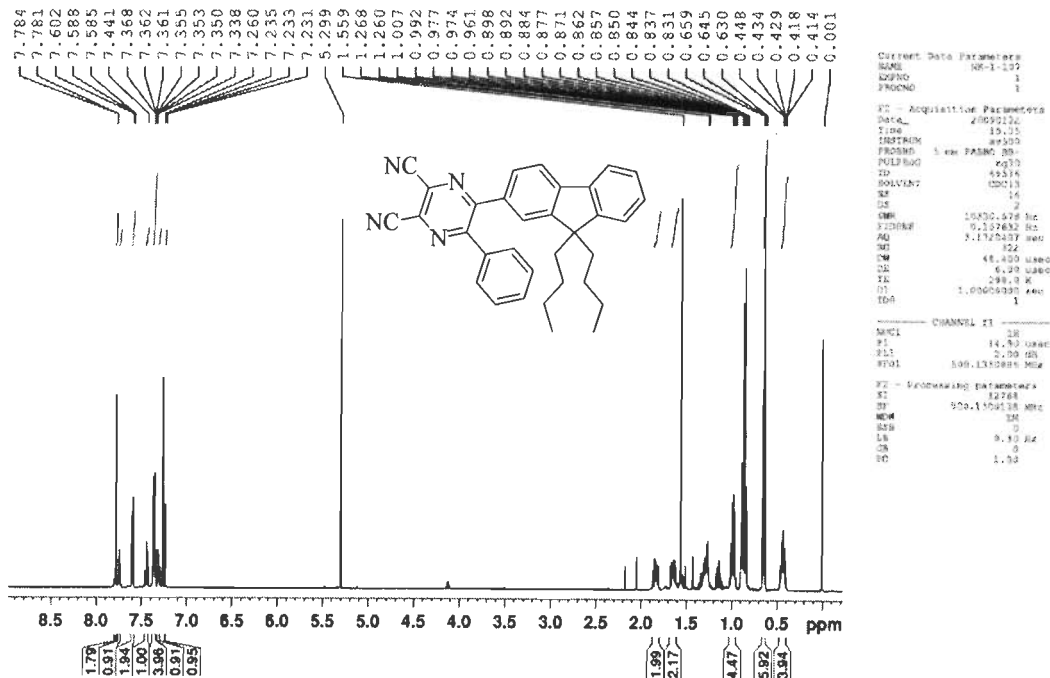


Figure S27. ¹H NMR spectra of 21a.

NK-1-107

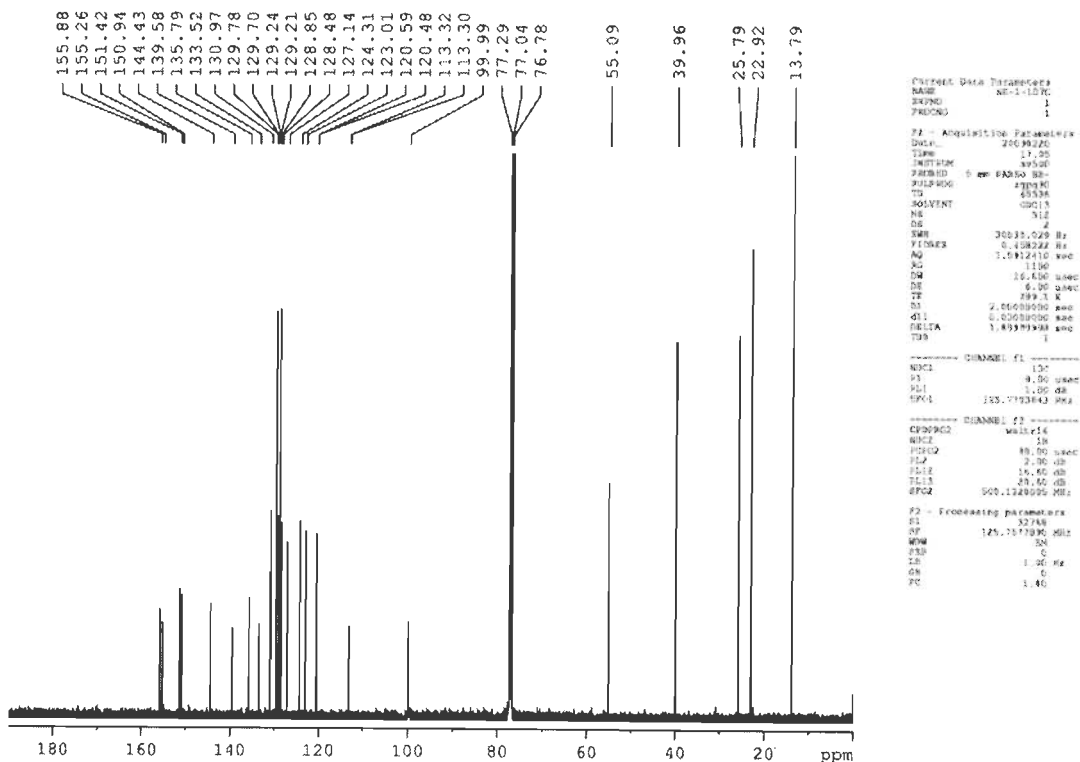


Figure S28. ¹³C NMR spectra of 21a.

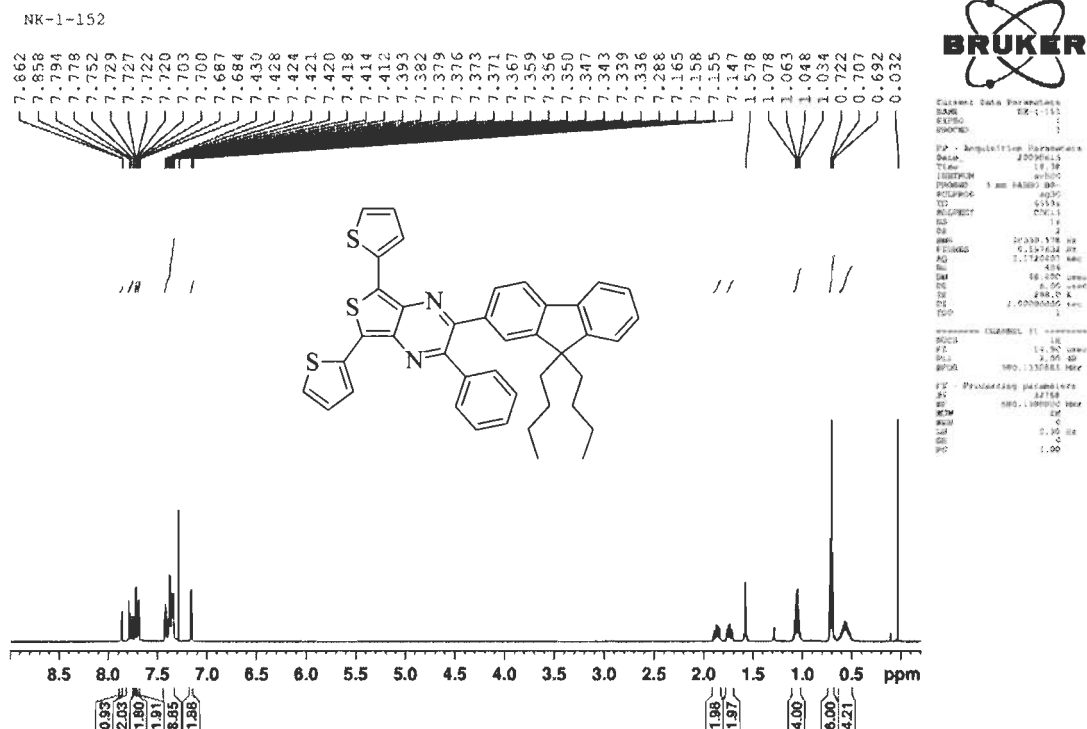


Figure S29. ¹H NMR spectra of 22a.

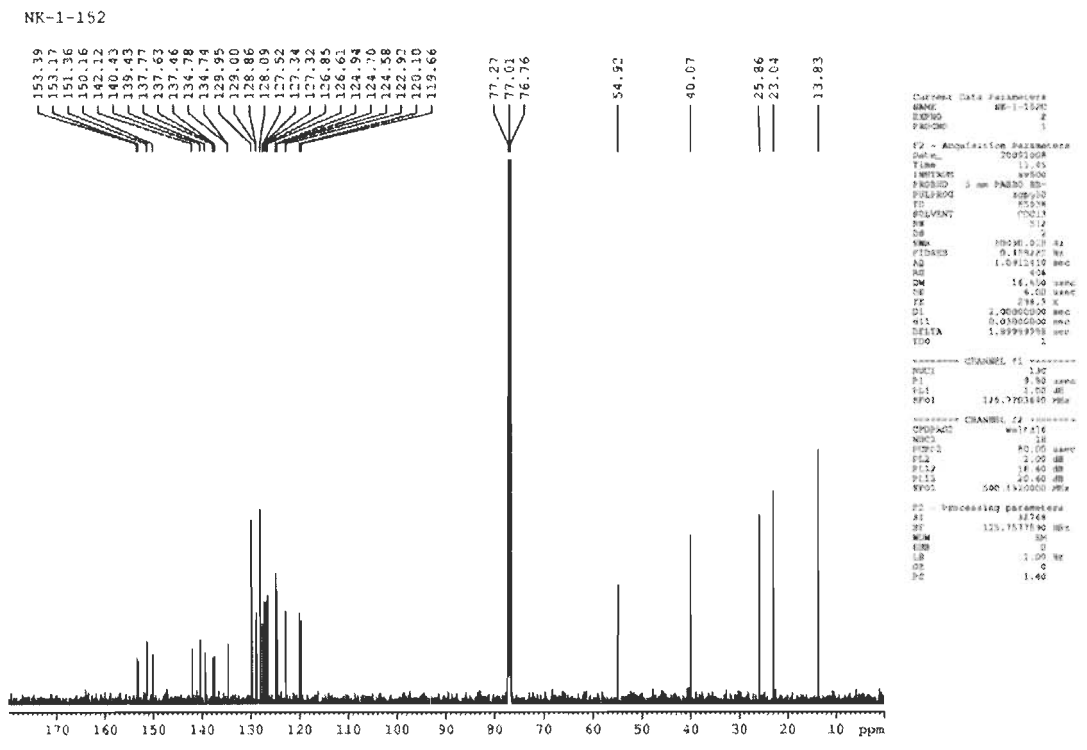


Figure S30. ¹³C NMR spectra of 22a.

NK-1-113

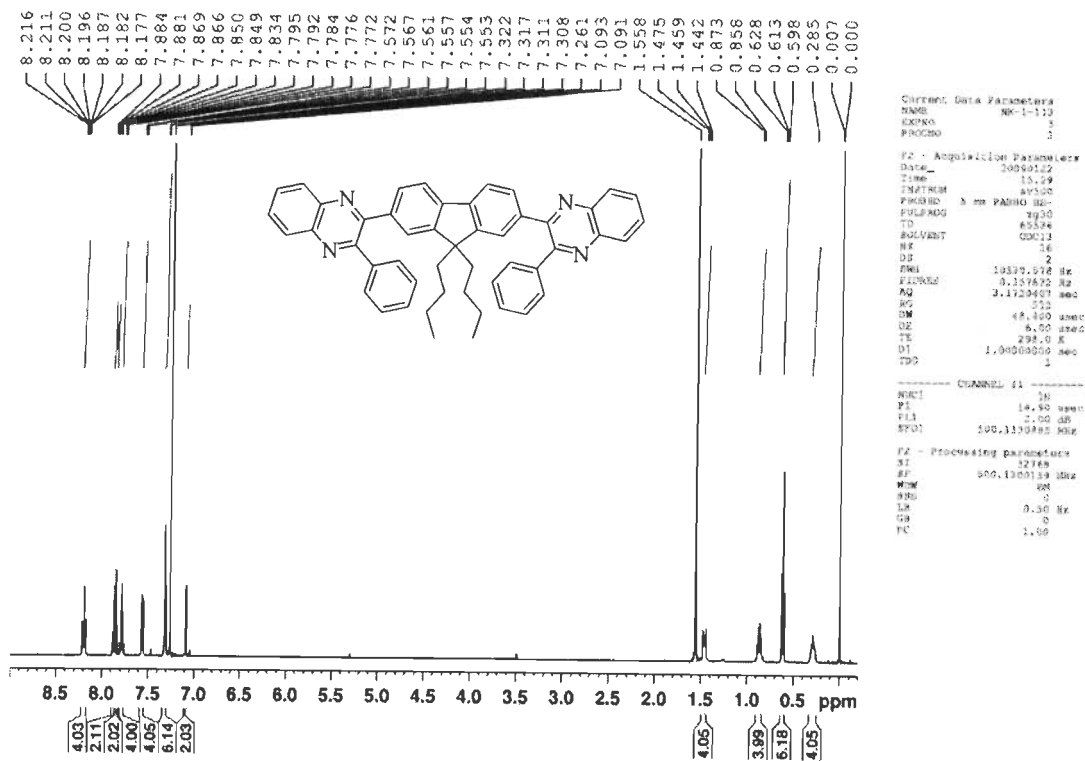


Figure S31. ¹H NMR spectra of 20b.

NK-1-113

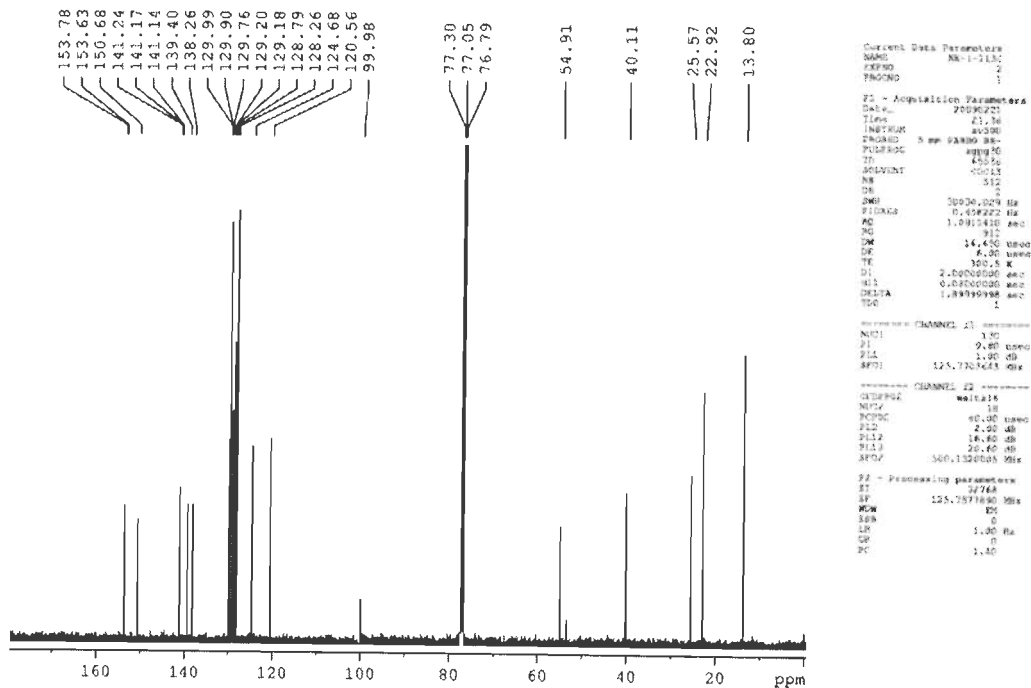
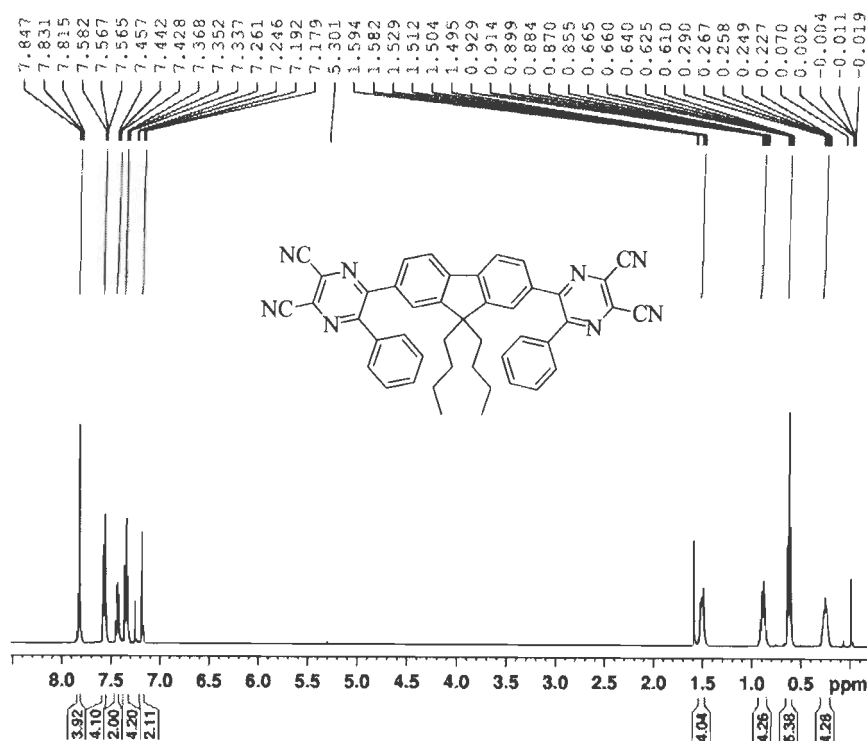


Figure S32. ¹³C NMR spectra of 20b.



```

Current Data Parameters
NAME      NK-1-114
EXPNO    1
PROCNO   1

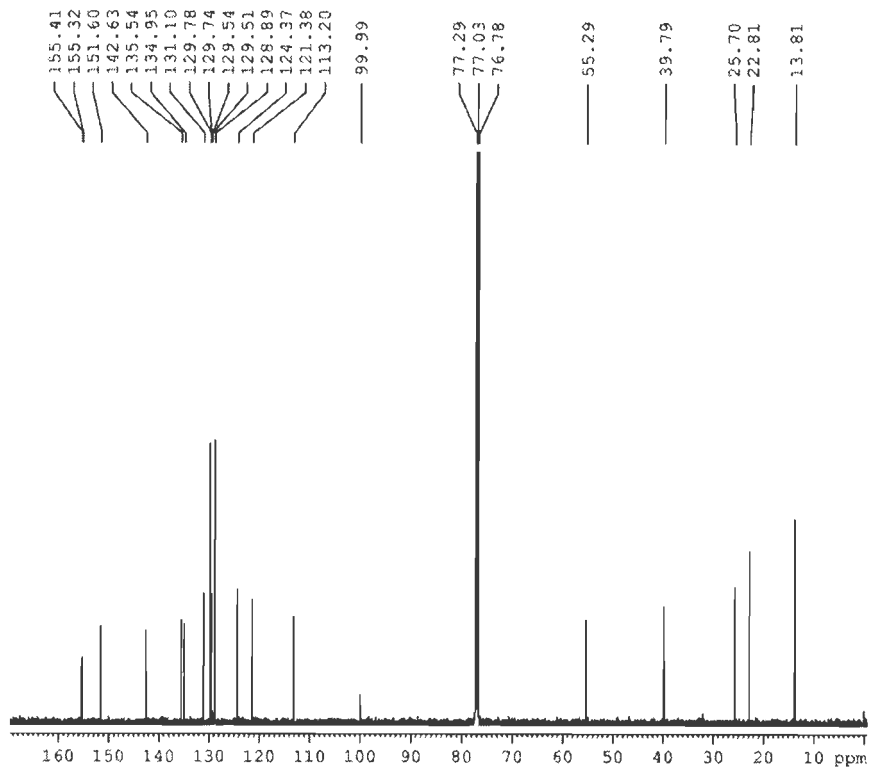
F2 - Acquisition Parameters
Date_    20080310
Time     17.17
INSTRUM  Av500
PROBHD   5 mm PABBI 1H/
PULPROG  zgpg30
TD       65536
SOLVENT  CDCl3
AQ       16
RG       2
DS       2
SWH      10180.575 Hz
FIDRES   0.157632 Hz
AQ       1.122057 sec
RG       514
DM       69.600 sec
DE       6.00 umol
TE       299.6 K
DQ       1.0000000 sec
TD0      1

===== CHANNEL f1 =====
NUC1      1H
P1        12.00 nsec
PC1       0.00 dB
NUC2      13C
P2        1.00 nsec
PC2       0.00 dB
SFO1      500.1324900 MHz

F2 - Processing parameters
SI        32768
SF        125.7679000 MHz
WDW       EM
SSB       0
LB        1.00 Hz
GB        0
PC        1.00
  
```

Figure S33. ¹H NMR spectra of 21b.

NK-1-114C



```

Current Data Parameters
NAME      NK-1-114C
EXPNO    1
PROCNO   1

F2 - Acquisition Parameters
Date_    20080220
Time     11.04
INSTRUM  Av500
PROBHD   5 mm PABBI 1H-
PULPROG  zgpg30
TD       65536
SOLVENT  CDCl3
AQ       16
RG       2
DS       2
SWH      10180.575 Hz
FIDRES   0.157632 Hz
AQ       1.122057 sec
RG       514
DM       69.600 sec
DE       6.00 umol
TE       299.6 K
DQ       1.0000000 sec
TD0      1

===== CHANNEL F1 =====
NUC1      13C
P1        1.00 nsec
PC1       0.00 dB
SFO1      125.7679000 MHz

===== CHANNEL F2 =====
NUC2      1H
P2        12.00 nsec
PC2       0.00 dB
SFO2      500.1324900 MHz

F2 - Processing parameters
SI        32768
SF        125.7679000 MHz
WDW       EM
SSB       0
LB        1.00 Hz
GB        0
PC        1.00
  
```

Figure S34. ¹³C NMR spectra of 21b.

NK-1-148

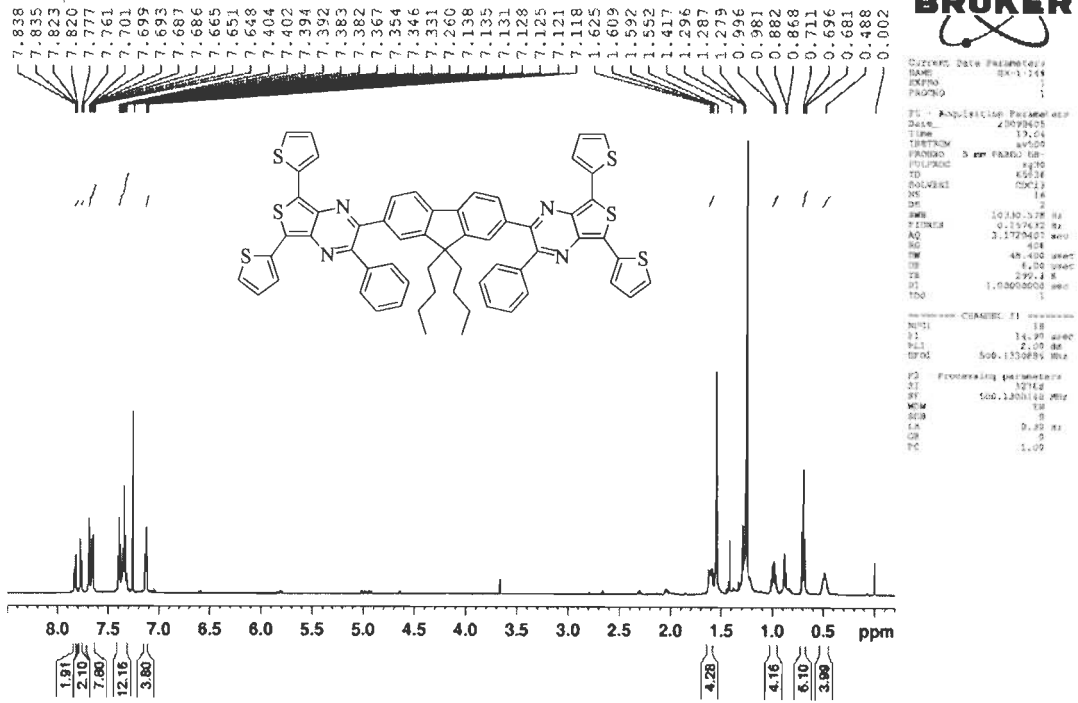


Figure S35. ¹H NMR spectra of 22b.

NK-1-148C

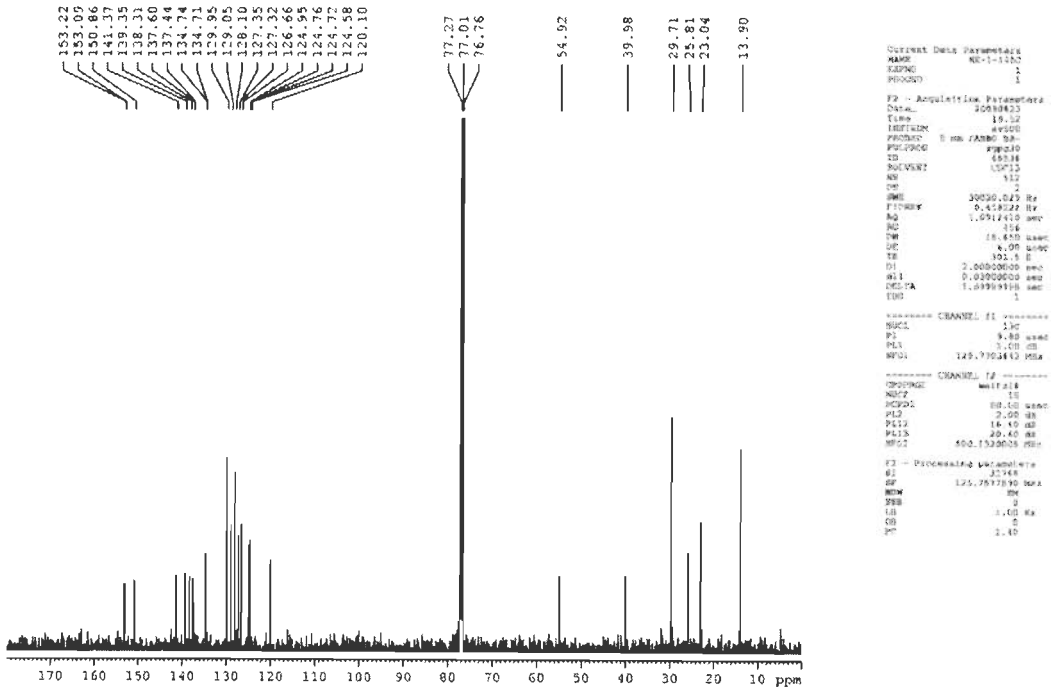


Figure S36. ¹³C NMR spectra of 22b.

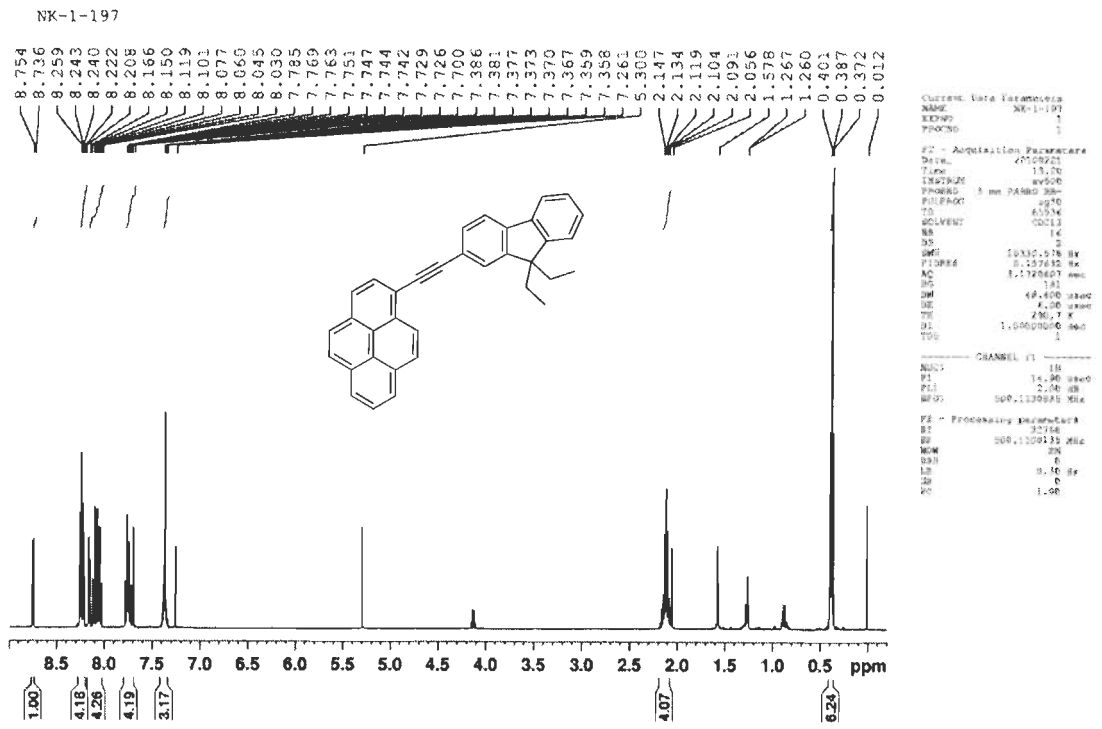


Figure S37. ¹H NMR spectra of 26.

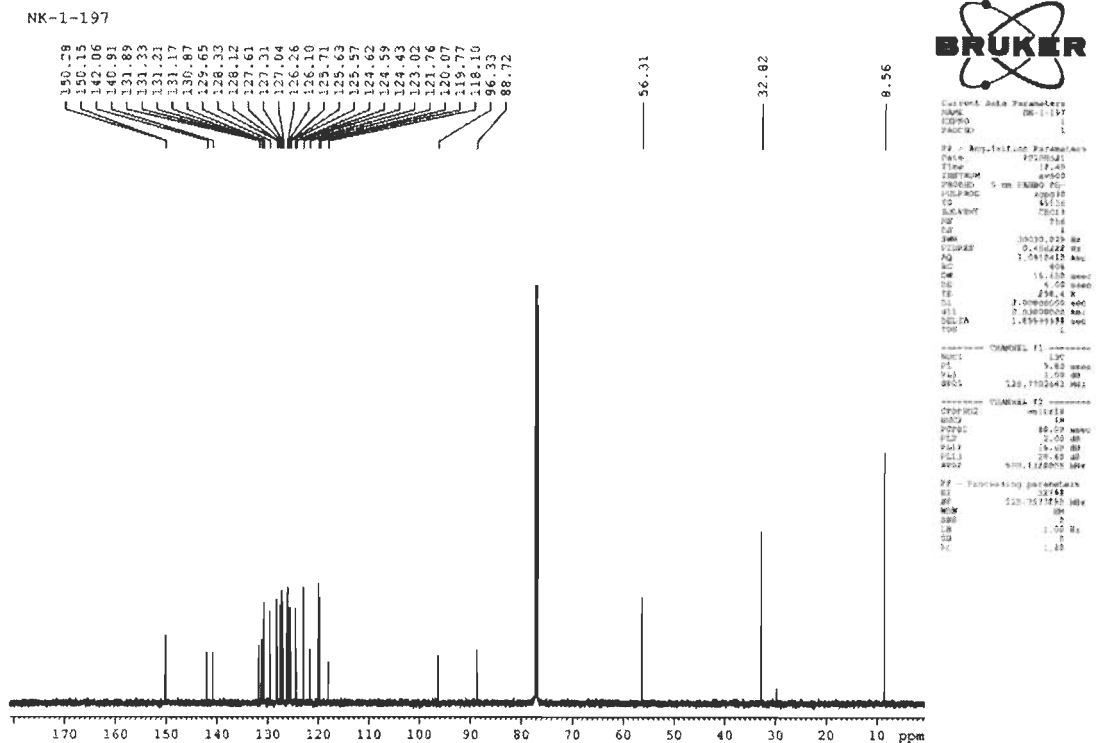


Figure S38. ¹³C NMR spectra of 26.

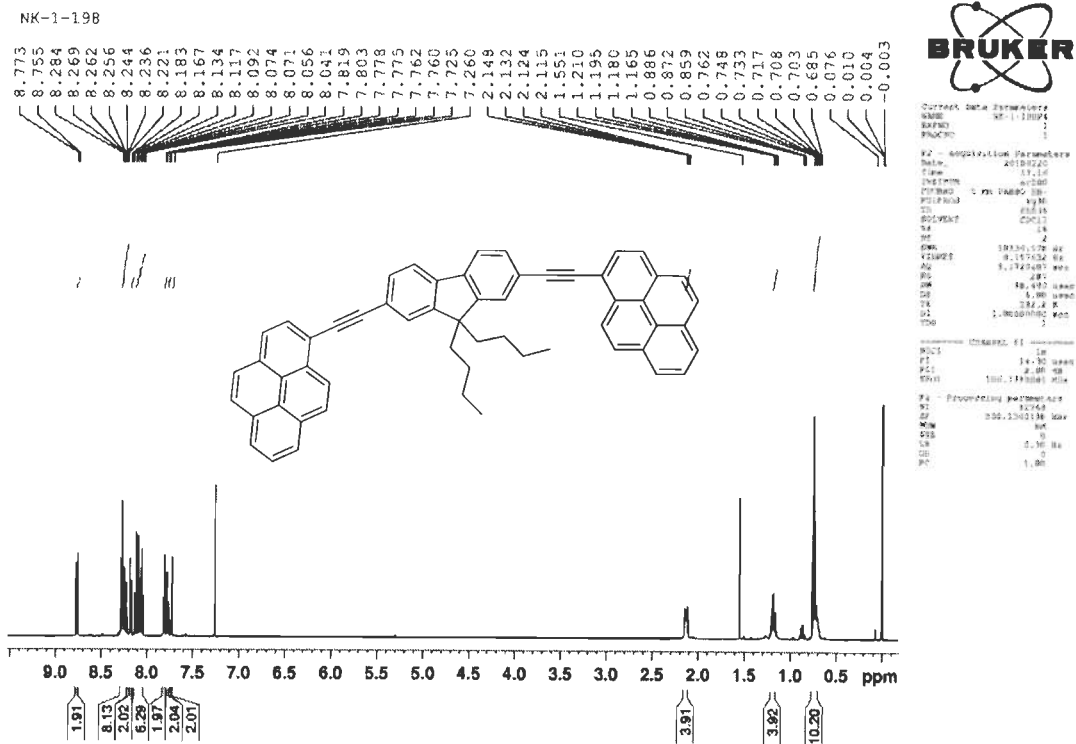


Figure S39. ¹H NMR spectra of 27.

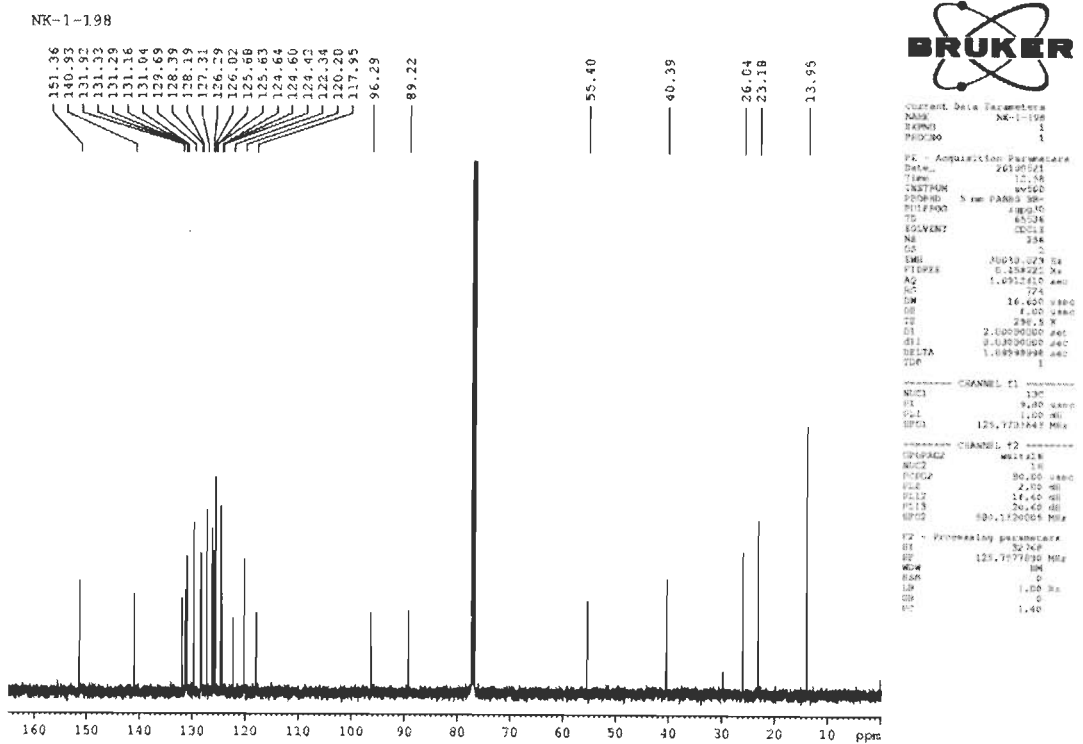


Figure S40. ¹³C NMR spectra of 27.

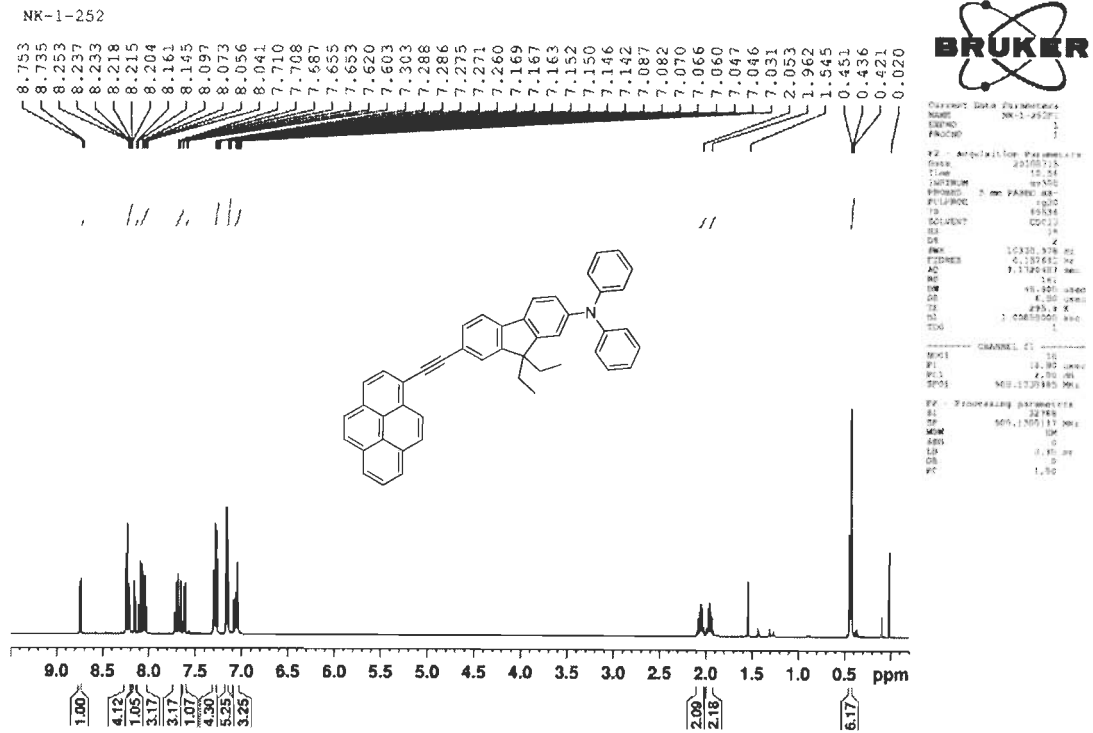


Figure S41. ¹H NMR spectra of 28.

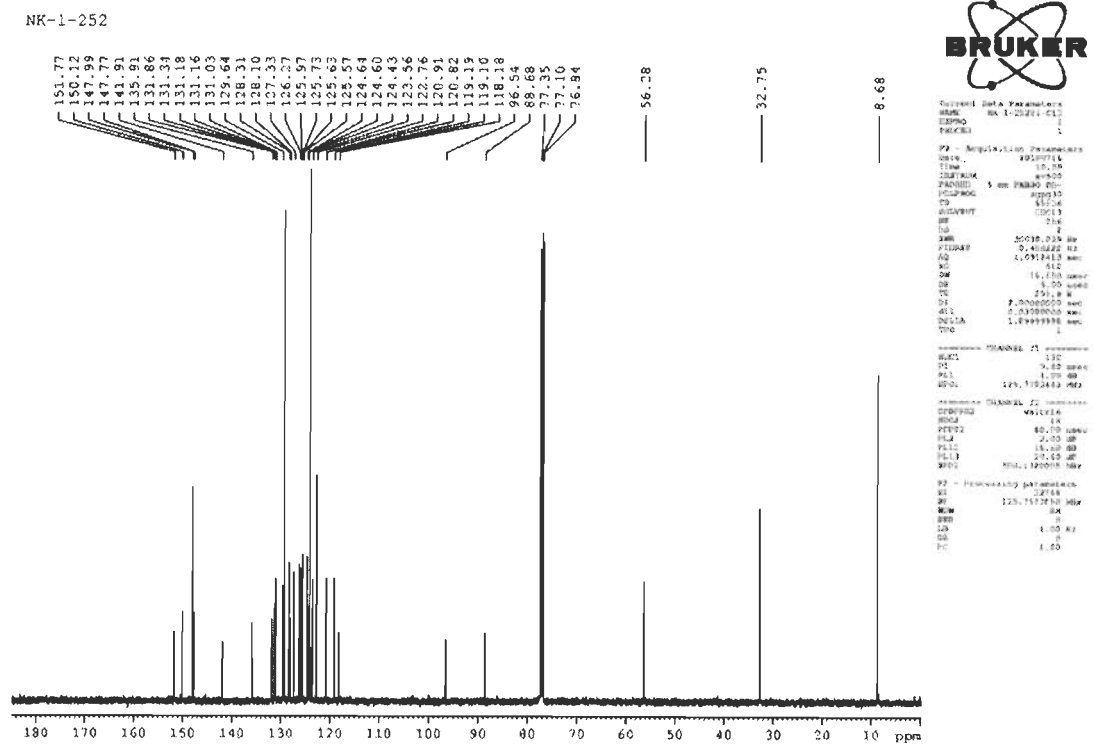


Figure S42. ¹³C NMR spectra of 28.

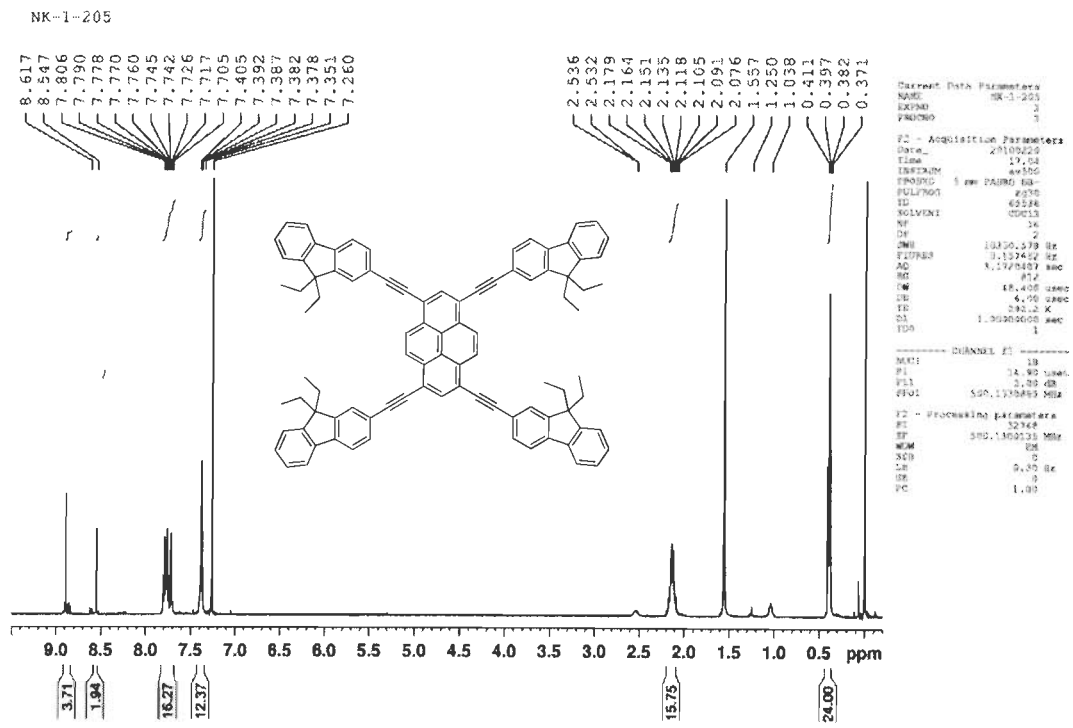


Figure S43. ¹H NMR spectra of 29.

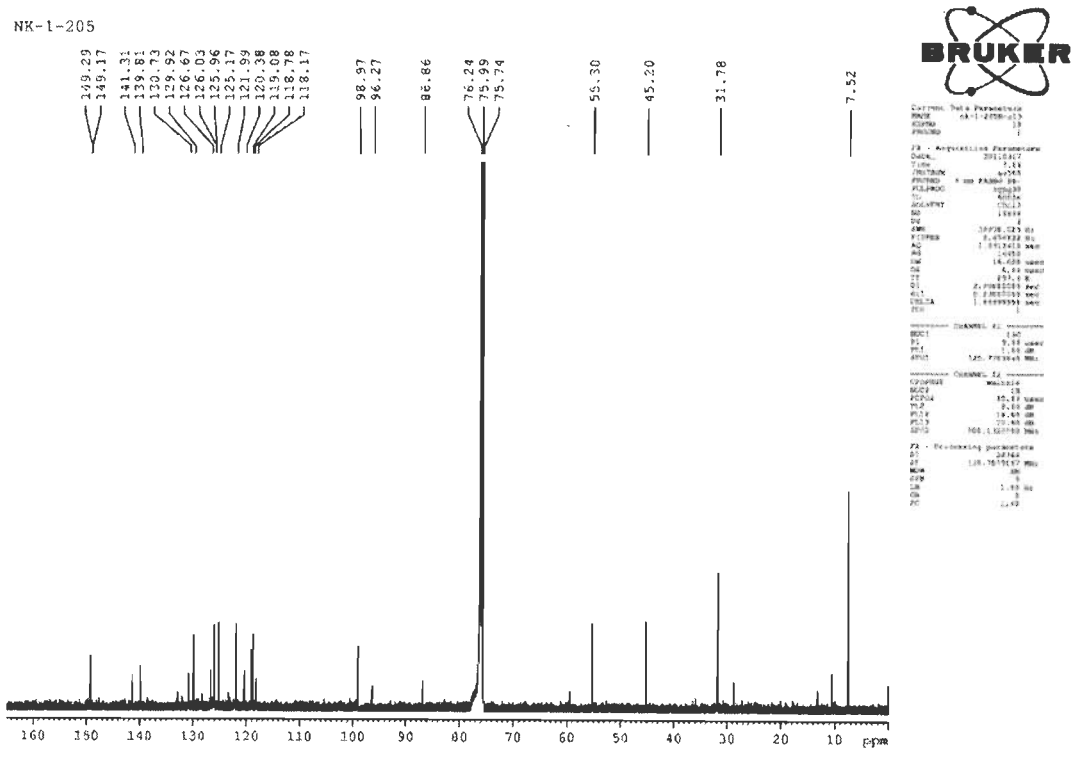
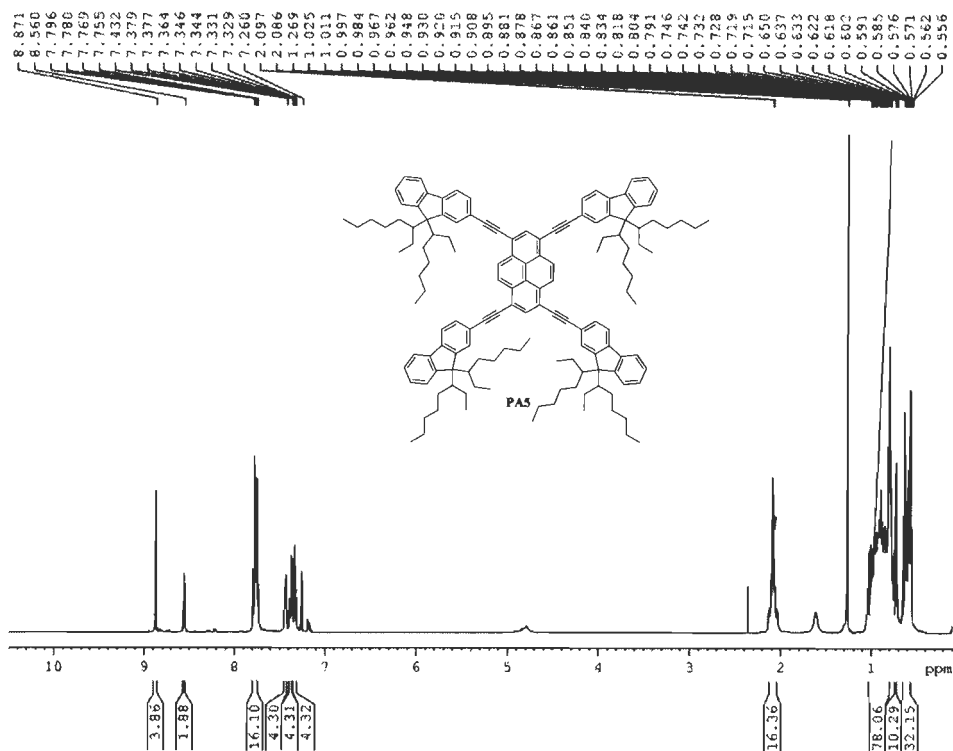


Figure S44. ¹³C NMR spectra of 29.

NK-1-216

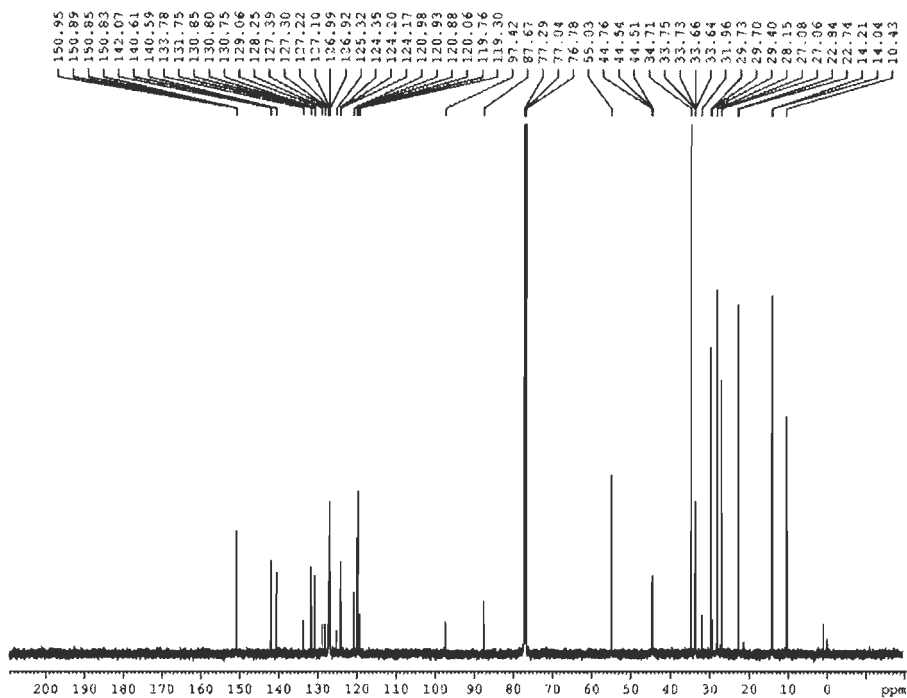


Current Data Parameters
 NAME NK-1-216
 EXPNO 1
 PROCNO 1

F2 - Acquisition Parameters
 Date_ 20160211
 Time 19.19
 INSTRUM spect
 PULPROG zgpg30
 F2 - Processing parameters
 SI 500.135095 MHz
 SF 500.135095 MHz
 MDW 32
 EQ 4
 LB 0.20 Hz
 GB 0
 VC 1.00

Figure S45. ¹H NMR spectra of 30.

NK-1-216



Current Data Parameters
 NAME NK-1-216
 EXPNO 1
 PROCNO 1

F2 - Acquisition Parameters
 Date_ 20160211
 Time 19.17
 INSTRUM spect
 PULPROG zgpg30
 F2 - Processing parameters
 SI 125.761443 MHz
 SF 125.761443 MHz
 MDW 32
 EQ 4
 LB 1.00 Hz
 GB 0
 VC 1.00

Figure S46. ¹³C NMR spectra of 30.

NK-1-255

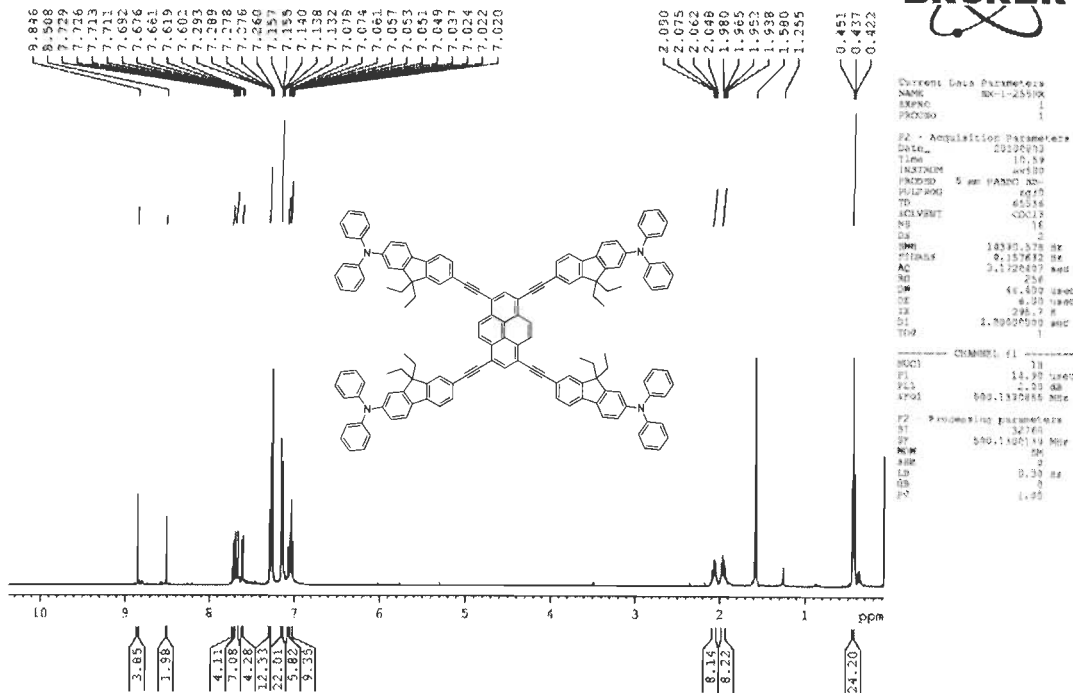


Figure S47. ¹H NMR spectra of 31.

NK-1-255

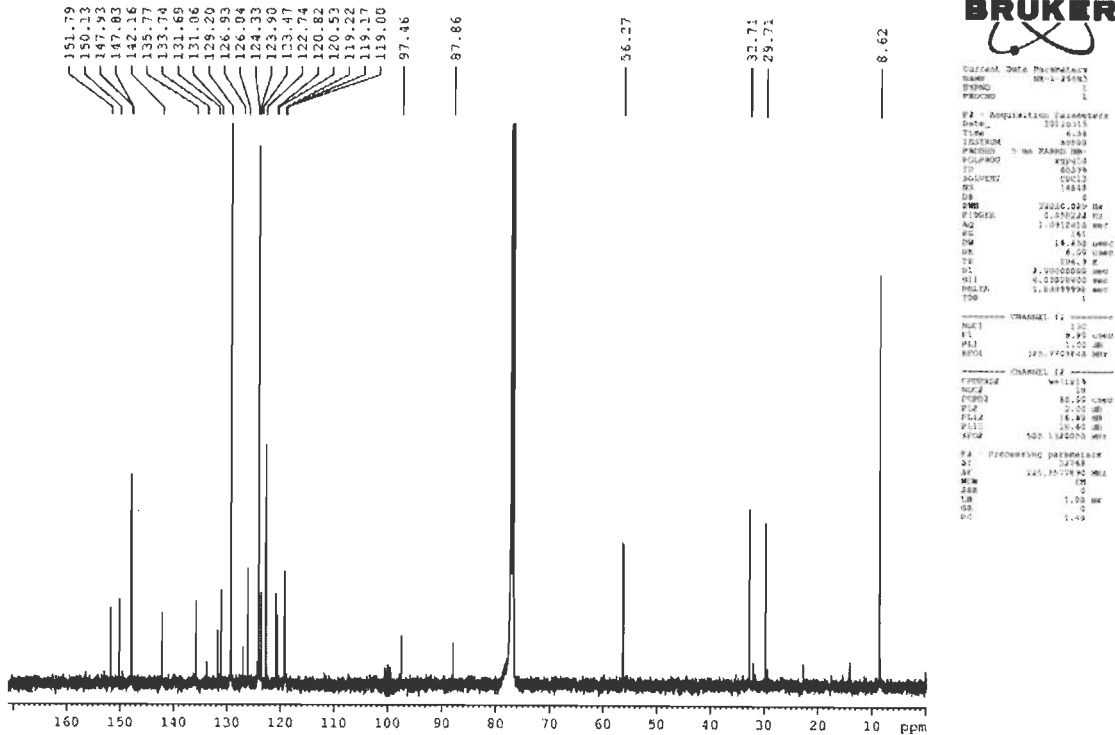
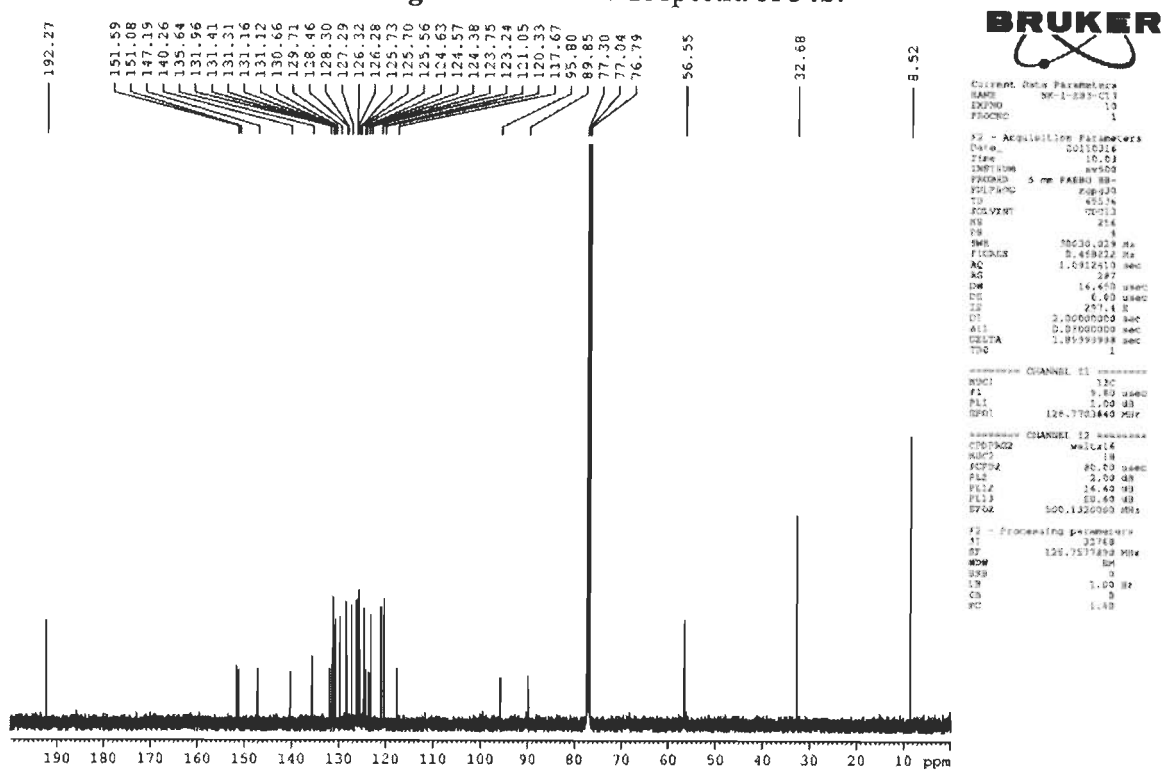
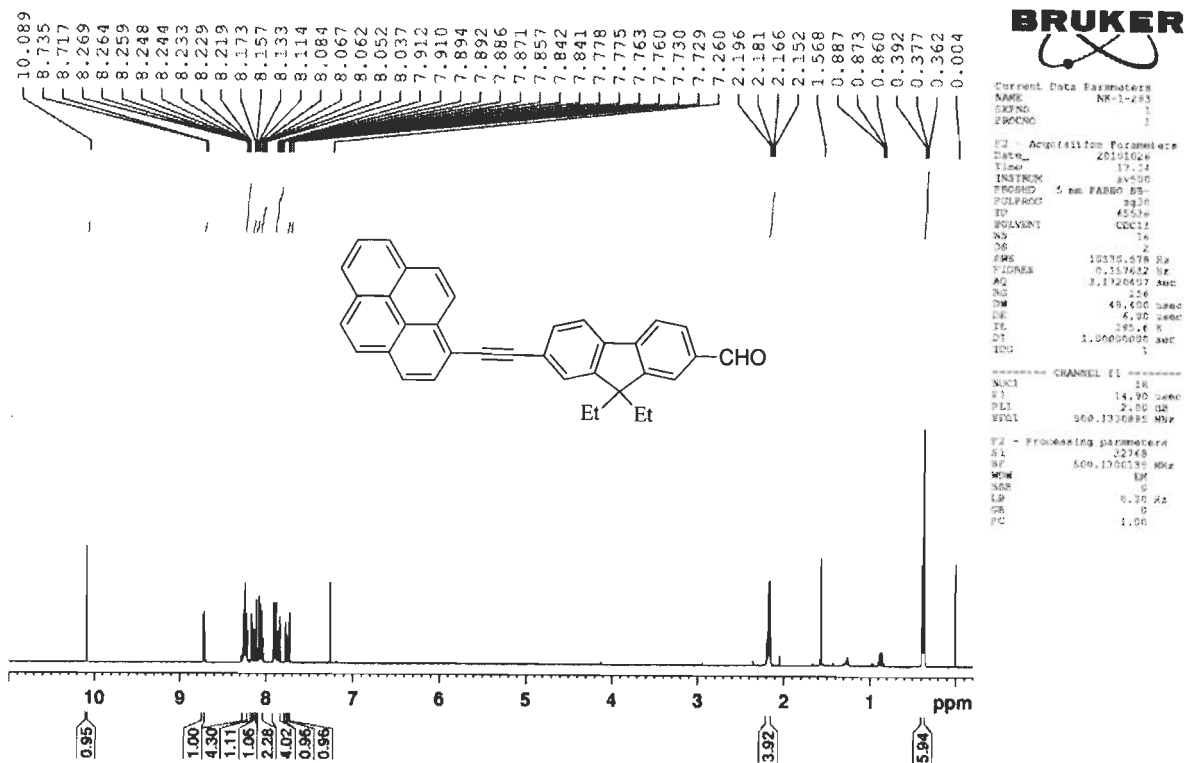
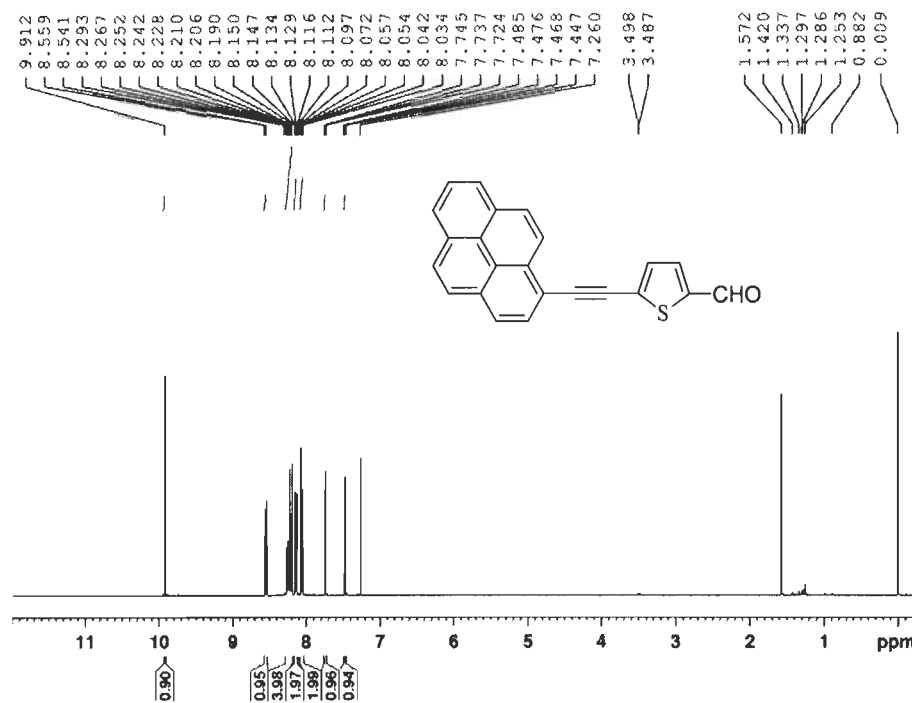
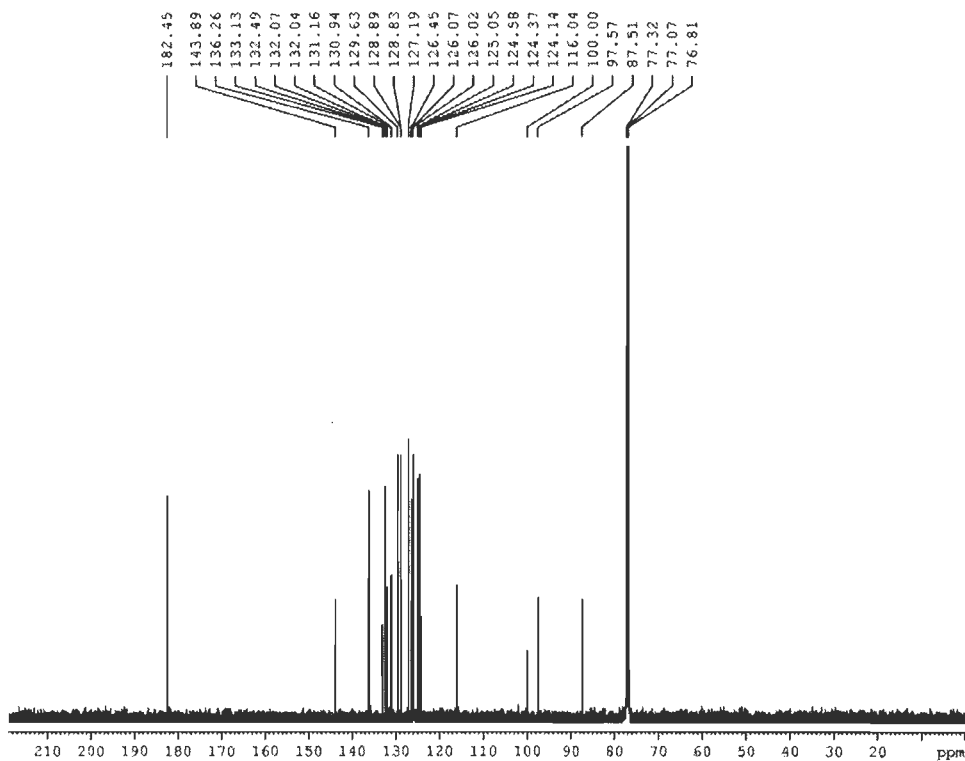


Figure S48. ¹³C NMR spectra of 31.



BRUKERFigure S51. ¹H NMR spectra of 34c.

NO-17474-130

Figure S52. ¹³C NMR spectra of 34c.

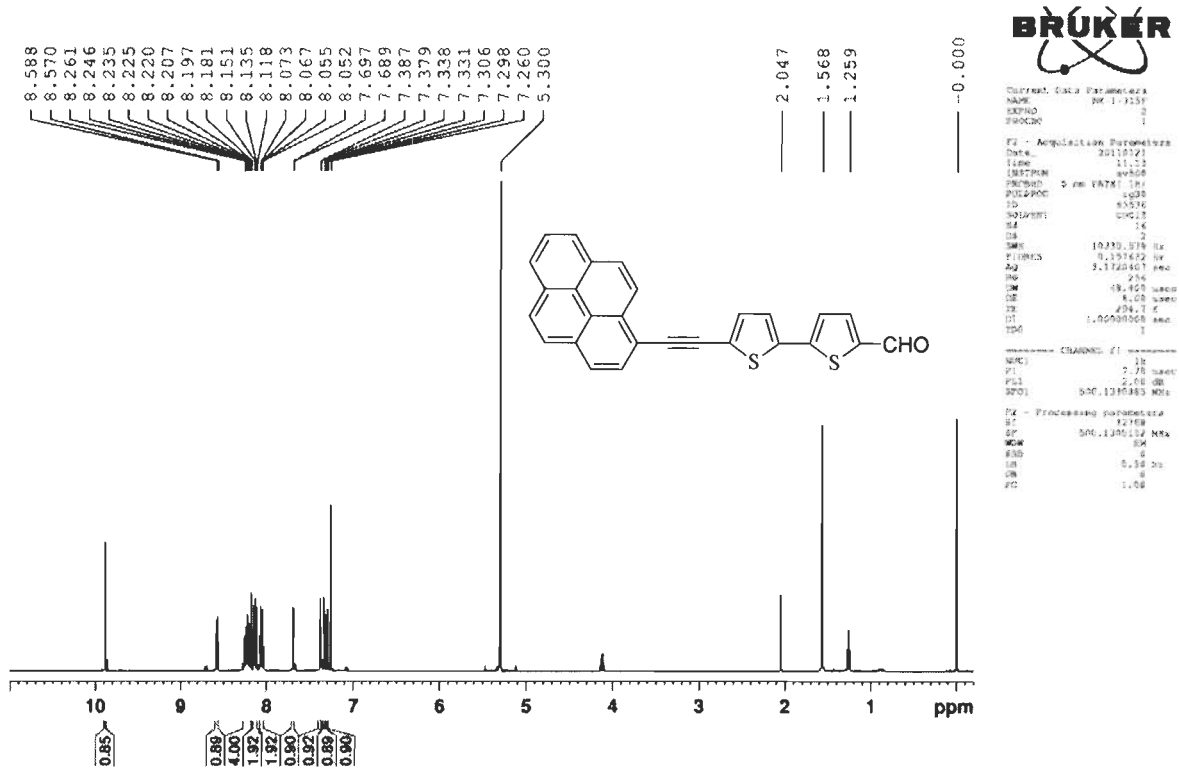


Figure S53. ¹H NMR spectra of 34d.

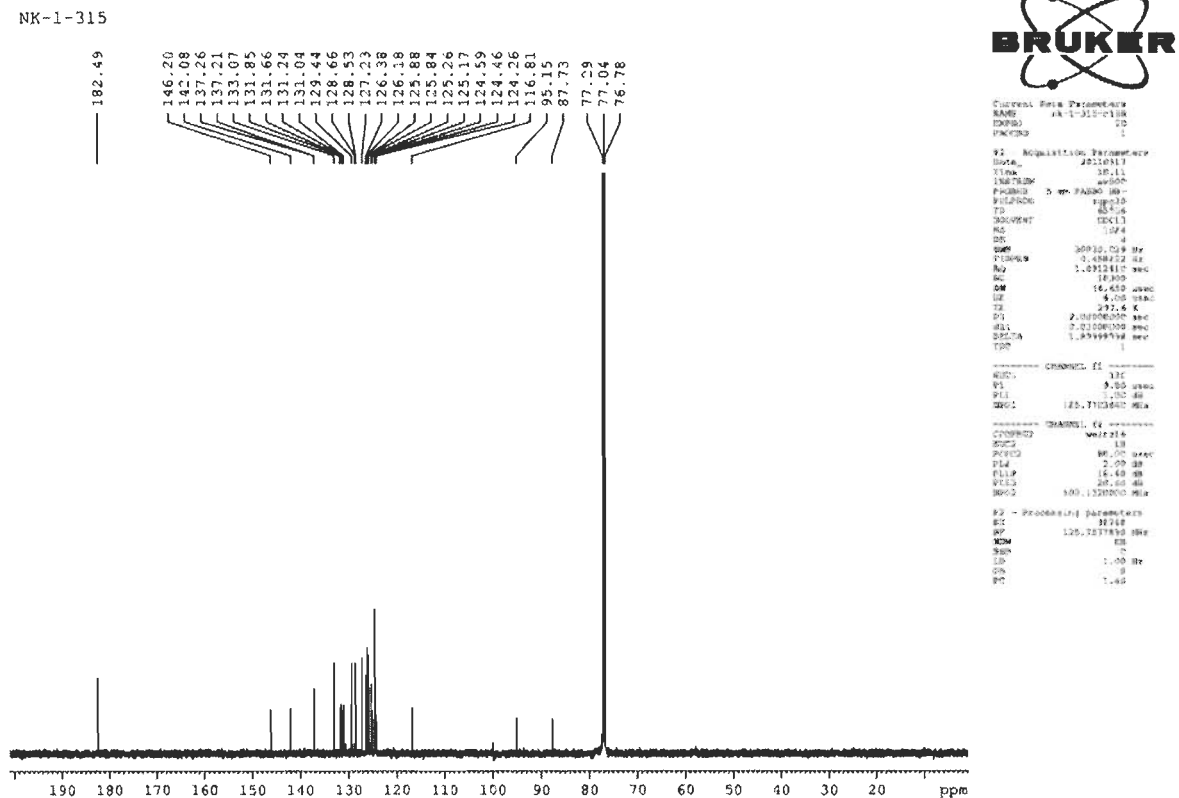
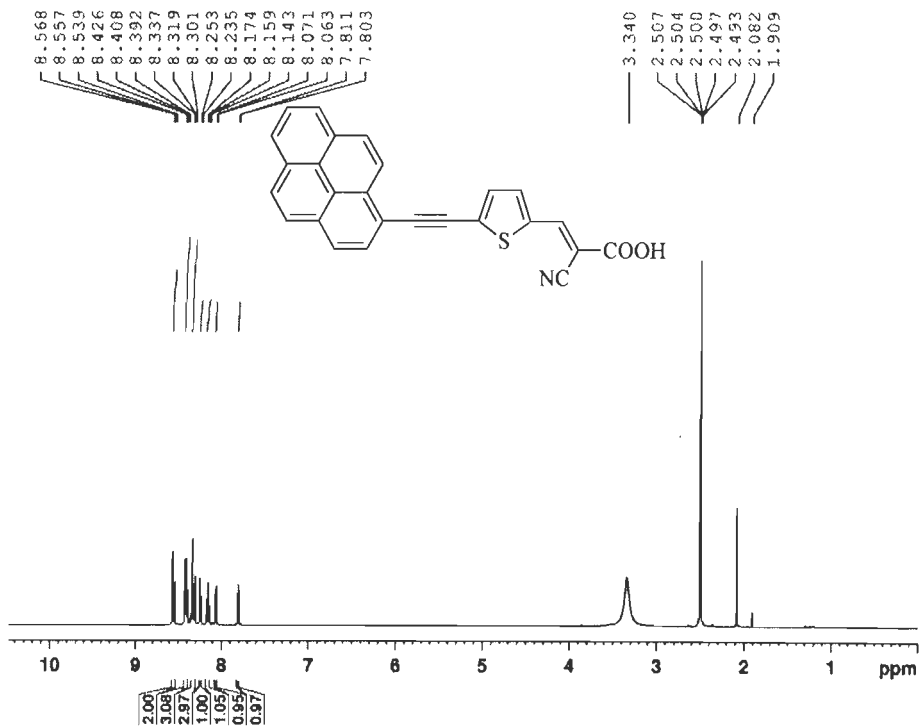


Figure S54. ¹³C NMR spectra of 34d.

NK-1-27



Current Data Parameters
 NAME: nk-1-277rec
 EXNO: 1
 F2NAME: 1

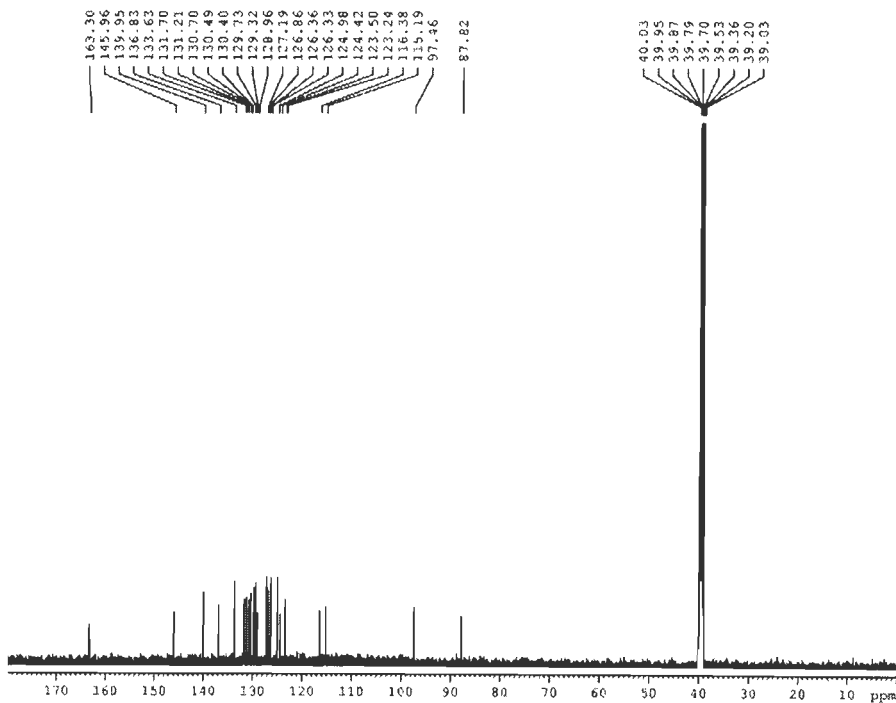
F2 - Acquisition Parameters
 Date_: 20110828
 Time: 10.21
 INSTRUM: avn60
 FREQBBD: 5 mm PATA1 1H
 PULPROG: zg30
 TD: 65536
 SOLVENT: DMSO
 NS: 2
 DS: 2
 SWH: 10390.558 Hz
 FWHZ: 0.151662 Hz
 AQ: 3.1120197 sec
 RG: 322
 DM: 18.000 usec
 DE: 2.00 dB
 TE: 296.9 K
 D1: 1.00000000 sec
 TSD: 1

===== CHANNEL f1 =====
 NUC1: 1H
 P1: 4.70 usec
 PL1: 2.00 dB
 SFO1: 500.1330000 MHz

F2 - Processing parameters
 SI: 32768
 SF: 500.1330000 MHz
 WDM: 64
 SSB: 0
 LB: 0.30 Hz
 GB: 0
 PC: 1.00

Figure S59. ¹H NMR spectra of 35c.

NK-1-277



Current Data Parameters
 NAME: nk-1-277
 EXNO: 1
 F2NAME: 1

F2 - Acquisition Parameters
 Date_: 20110829
 Time: 11.36
 INSTRUM: avn60
 FREQBBD: 5 mm PATA1 1H
 PULPROG: zgpg30
 TD: 65536
 SOLVENT: DMSO
 NS: 2
 DS: 2
 SWH: 10390.029 Hz
 FWHZ: 0.148022 Hz
 AQ: 1.0912810 sec
 RG: 3768
 DM: 18.000 usec
 DE: 8.00 usec
 TE: 296.9 K
 D1: 2.00000000 sec
 D11: 0.03000000 sec
 MDELTA: 1.00000000 sec
 TSD: 1

===== CHANNEL f1 =====
 NUC1: 13C
 P1: 11.40 usec
 PL1: 0.00 dB
 SFO1: 125.7703440 MHz

===== CHANNEL f2 =====
 NUC2: 1H
 P2: 80.00 usec
 PL2: 2.00 dB
 PL12: 27.00 dB
 PL13: 29.00 dB
 SFO2: 500.1330000 MHz

F2 - Processing parameters
 SI: 32768
 SF: 125.7703440 MHz
 WDM: 64
 SSB: 0
 LB: 1.00 Hz
 GB: 0
 PC: 1.00

Figure S60. ¹³C NMR spectra of 35c.



Current Data Parameters
 NAME: nk-1-320
 EXPNO: 1
 PROCNO: 1
 F2 - Acquisition Parameters
 Date_ : 201006
 Time : 10
 INSTRUM : MVS00
 PROBMOD : 5 mm BBTX1 H/
 PULPROG : zg30
 TD : 65536
 SOLVENT : DMSO
 NS : 16
 DS : 2
 SWH : 10350.578 Hz
 FWHM : 0.1720007 Hz
 AQ : 3.1720007 sec
 RG : 322
 DM : 48,400 USE
 DE : 2,000 USE
 TE : 300.2 K
 D1 : 1.00000000 sec
 TDO : 1
 CHANNEL f1
 NUC1 : ¹H
 P1 : 7.70 dB
 PL1 : 7.00 dB
 SFO1 : 500.130065 MHz
 F2 - Processing parameters
 SI : 32768
 SF : 500.130065 MHz
 DSF : 0
 SSB : 0
 LB : 0
 GB : 0
 PC : 1.00

8.570
8.552
8.546
8.512
8.431
8.421
8.416
8.403
8.390
8.357
8.341
8.313
8.300
8.295
8.285
8.257
8.239
8.177
8.161
8.146
8.026
8.018

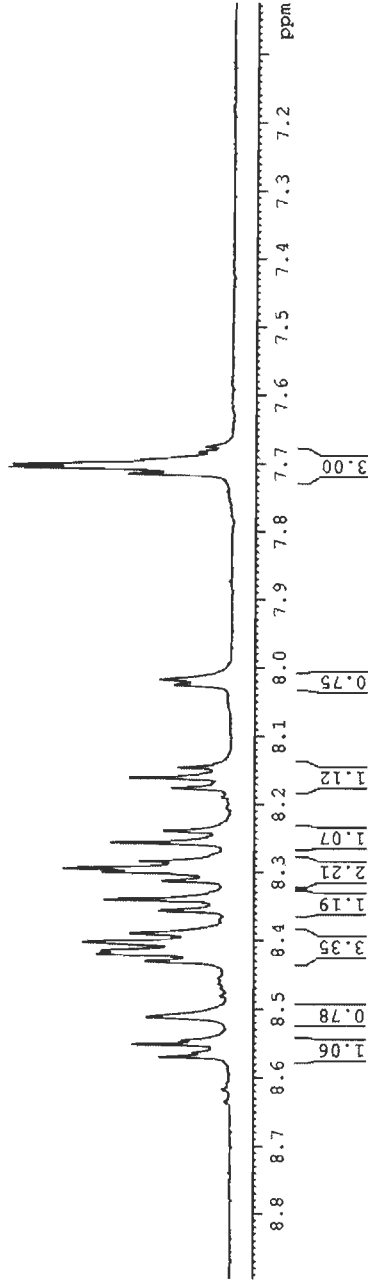
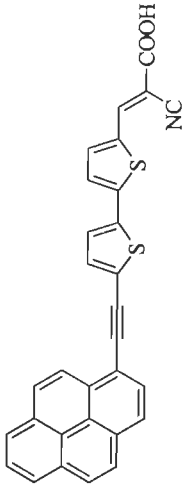


Figure S61. ¹H NMR spectra of 35d.

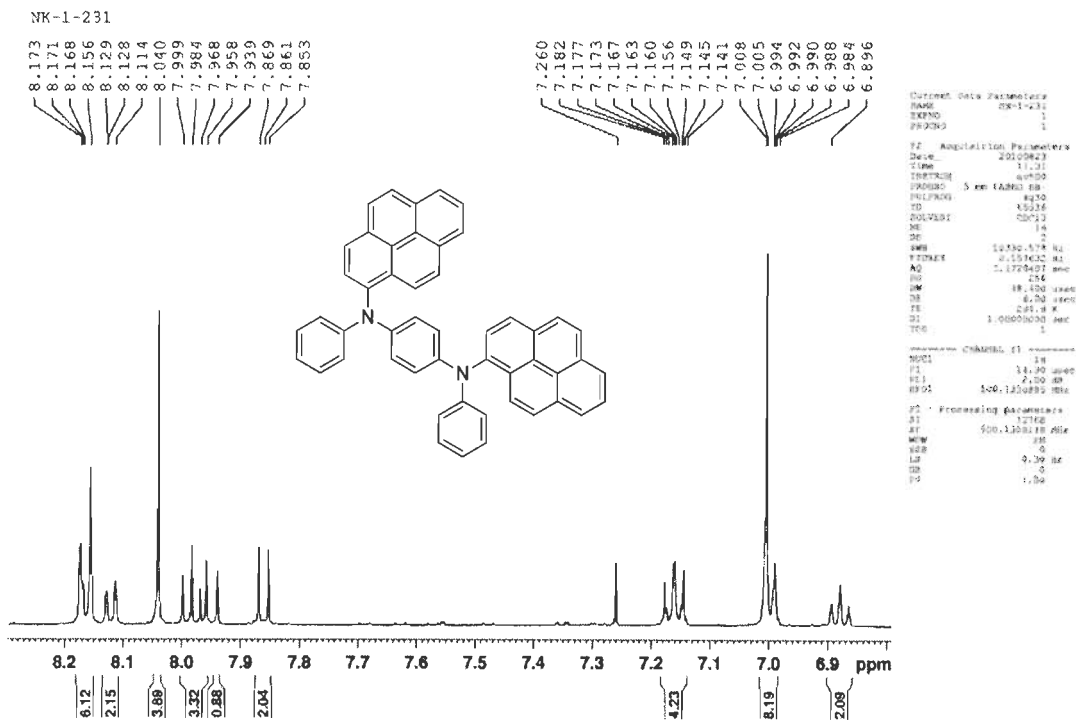


Figure S62. ¹H NMR spectra of 41a.

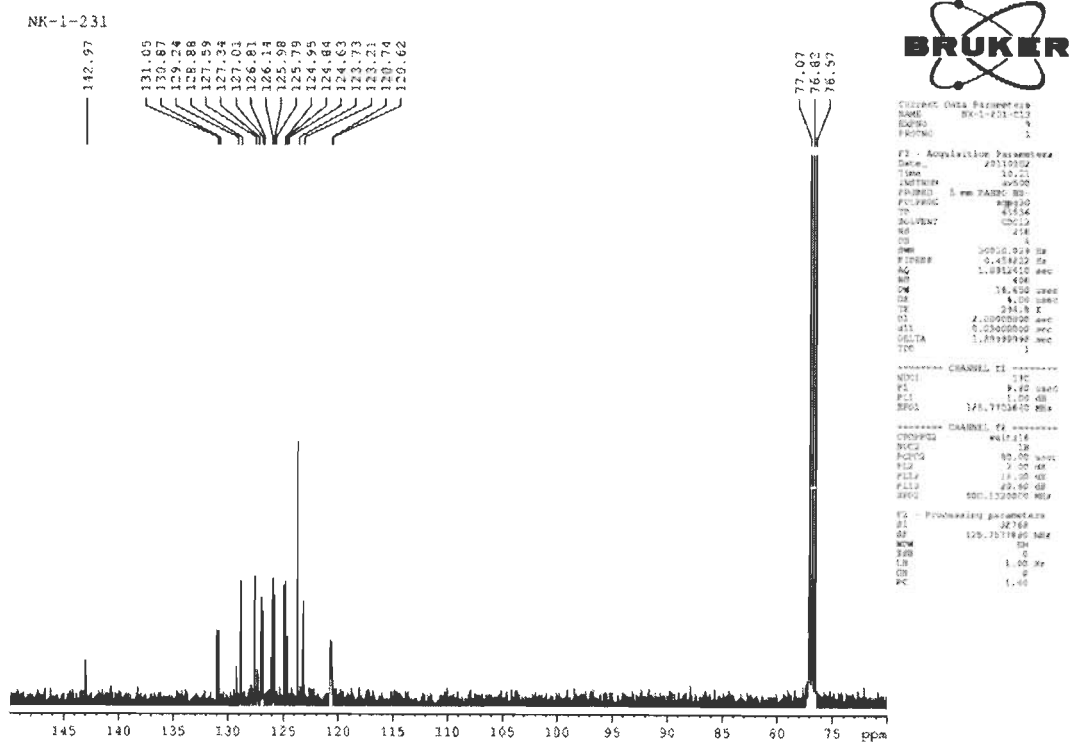
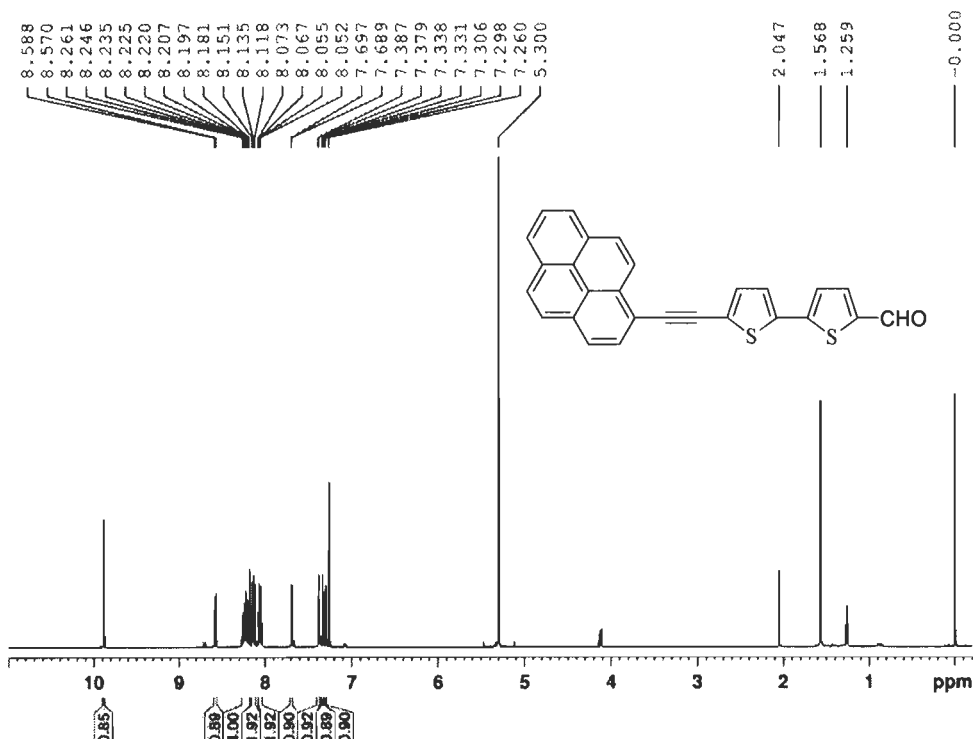


Figure S63. ¹³C NMR spectra of 41a.



BRUKER

Current Data Parameters
NAME nk-1-315
EXPNO 2
PROCNO 1

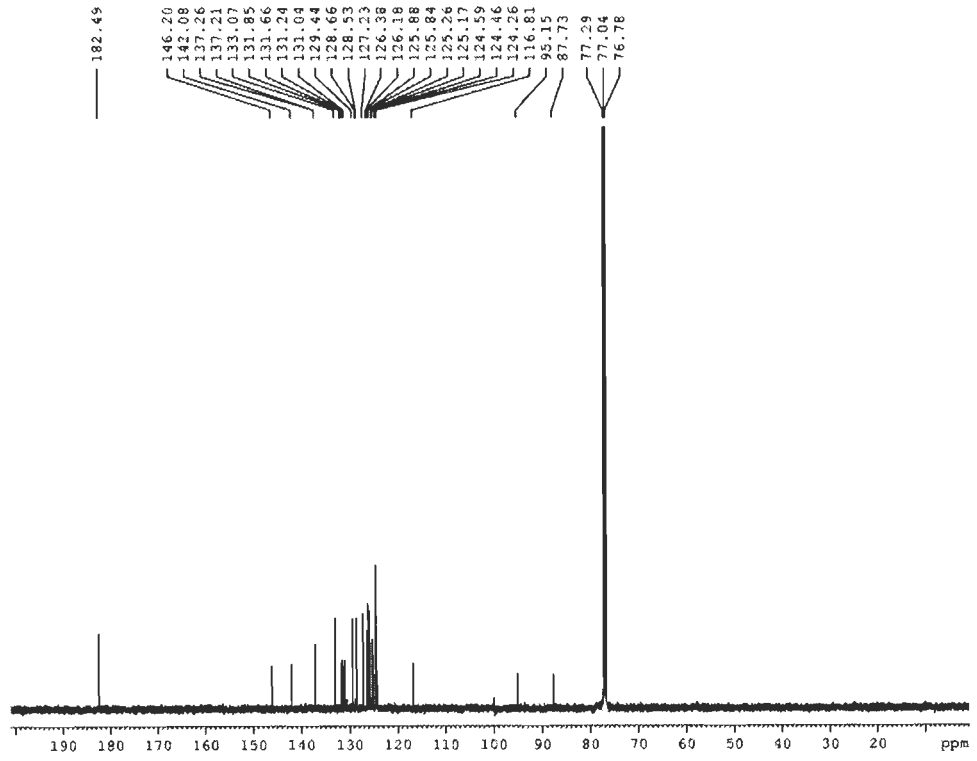
F2 - Acquisition Parameters
Date_ 2018121
Time 21.12
INSTRUM spect
PROBHD 5 mm VARI 1H
PULPROG zgpg30
TD 65536
SOLVENT cdcl3
NS 16
DS 2
SWH 19230.378 Hz
FIDRES 0.151432 Hz
AQ 2.172467 sec
RG 256
DM 48.401 usec
DC 8.00 usec
TE 297.2 K
DT 1.0000000 sec
TD0 1

----- CHANNEL f1 -----
NUC1 13
P1 2.70 usec
PL1 2.00 dB
SFO1 500.135065 MHz

F2 - Processing parameters
SI 32768
SF 500.135117 MHz
WDW EM
SSB 0
GB 0.50 Hz
CB 0
PC 1.00

Figure S53. ¹H NMR spectra of 34d.

NK-1-315



BRUKER

Current Data Parameters
NAME nk-1-315-13c
EXPNO 10
PROCNO 1

F2 - Acquisition Parameters
Date_ 2018117
Time 18.11
INSTRUM spect
PROBHD 5 mm PABBO 1H-
PULPROG zgpg30
TD 65536
SOLVENT cdcl3
NS 1074
DS 4
SWH 30910.008 Hz
FIDRES 0.458722 Hz
AQ 1.0915117 sec
RG 68000
DM 18.610 usec
DC 8.00 usec
TE 297.2 K
DT 1.0000000 sec
SFO1 125.767800 MHz
SFO2 100.628150 MHz

----- CHANNEL f1 -----
NUC1 13C
P1 9.00 usec
PL1 1.00 dB
SFO1 125.767800 MHz

----- CHANNEL f2 -----
CPDPRG2 waltz16
NUC2 1H
PULPROG zgpg30
P2 90.00 usec
PL2 2.00 dB
PL12 14.00 dB
PL13 20.00 dB
SFO2 500.135065 MHz

F2 - Processing parameters
SI 32768
SF 125.767800 MHz
WDW EM
SSB 0
GB 1.00 Hz
CB 0
PC 1.00

Figure S54. ¹³C NMR spectra of 34d.

NK-1-280

8.637
8.619
8.410
8.395
8.382
8.375
8.367
8.329
8.313
8.296
8.281
8.264
8.225
8.207
8.151
8.135
8.117
7.979
7.944
7.928

3.543
3.167
3.090
2.500
1.910

```

Current Data Parameters
NAME      NK-1-280-180208
EXPNO    1
PROCNO   1

F2 - Acquisition Parameters
Date_    20101223
Time     15.58
INSTRUM  spect
PULPROG  zgpg30
SOLVENT  DMSO
NS       18
DS       2
SWH      10000.810 Hz
FIDRES   0.151642 Hz
AQ       2.1727403 sec
RG       381
SQ       181
DM       48.100 cmhz
DE       6.00 umhz
TE       295.2 K
D1       1.00000000 sec
DELTA    1
TD       1

===== CHANNEL f1 =====
NUC1      1H
P1        12.00 umhz
PC1       2.00 nA
SFO1     500.1360000 MHz

F2 - Processing parameters
SI        32768
SF        500.1360000 MHz
WDW       EM
SSB       0
GB        0.00 Hz
PC        1.00
  
```

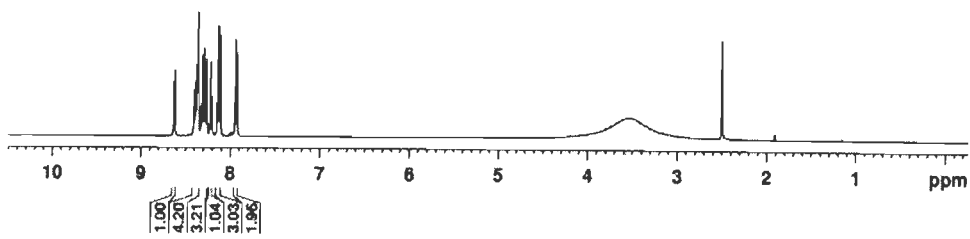
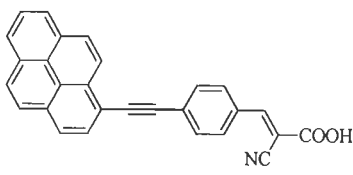


Figure S55. ¹H NMR spectra of 35a.

NK-1-280

165.67
151.61
151.00
132.00
131.89
131.84
131.40
131.19
130.92
130.34
129.60
129.23
127.65
127.32
127.28
126.68
125.46
125.22
123.75
123.75
116.60
116.43
104.71
99.39
95.17
92.45

40.43
40.35
40.26
40.18
39.09
38.72
38.59
38.42

```

Current Data Parameters
NAME      NK-1-280-211
EXPNO    1
PROCNO   1

F2 - Acquisition Parameters
Date_    20101223
Time     11.02
INSTRUM  spect
PULPROG  zgpg30
SOLVENT  DMSO
NS       256
DS       2
SWH      20000.822 Hz
FIDRES   0.448222 Hz
AQ       1.002410 sec
RG       3700
SQ       18.450 umhz
DM       292.0 K
DE       6.00 umhz
TE       295.2 K
D1       0.03000000 sec
DELTA    1.89999999 sec
TD       1

===== CHANNEL f1 =====
NUC1      13C
P1        8.00 umhz
PC1       1.00 nA
SFO1     125.7603441 MHz

===== CHANNEL f2 =====
NUC2      1H
P2        60.00 umhz
PC2       2.00 nA
SFO2     500.1360000 MHz

F2 - Processing parameters
SI        32768
SF        125.7677860 MHz
WDW       EM
SSB       0
GB        0.00 Hz
PC        1.00
  
```

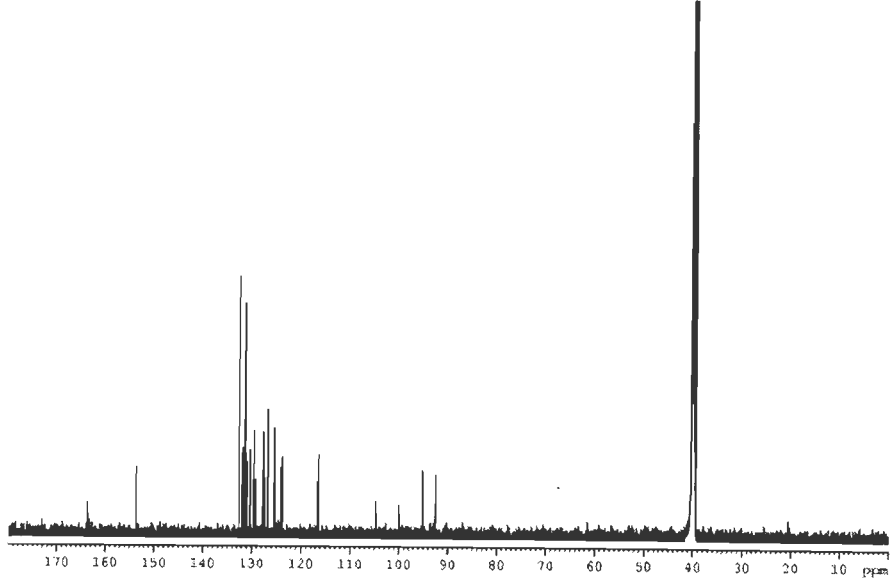


Figure S56. ¹³C NMR spectra of 35a.

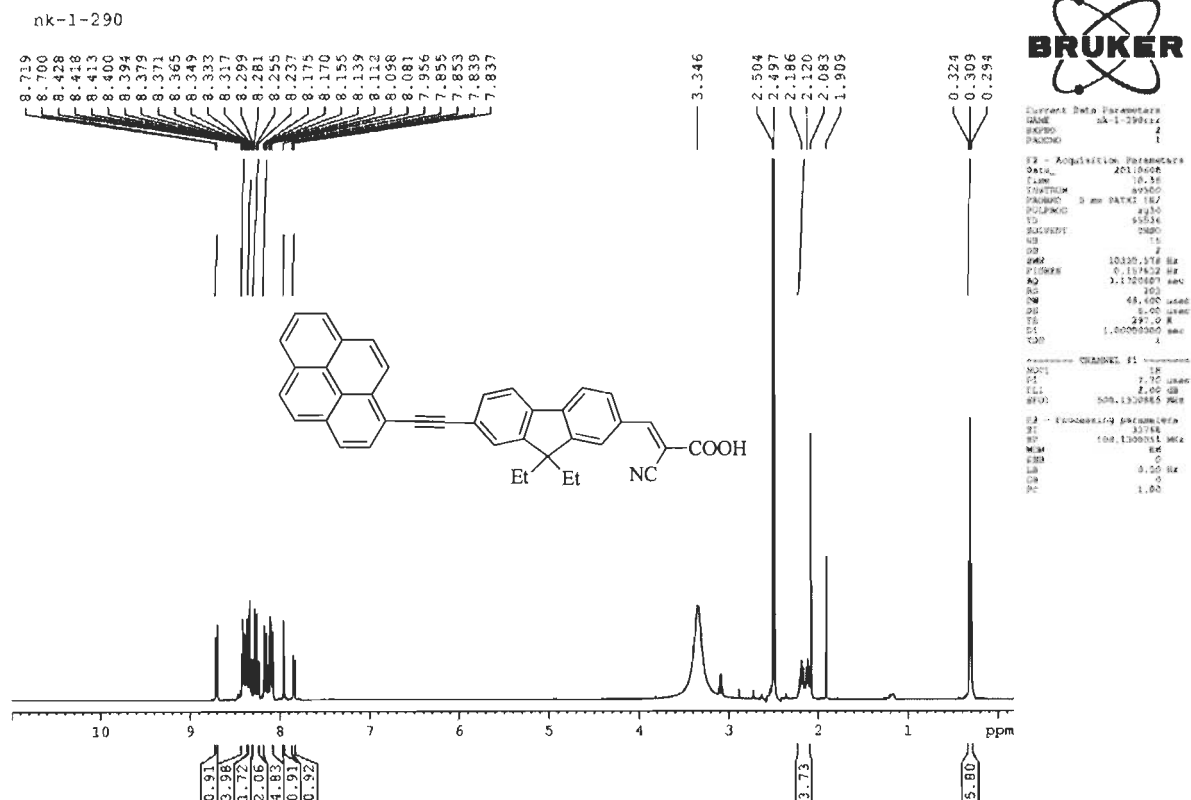


Figure S57. ¹H NMR spectra of 35b.

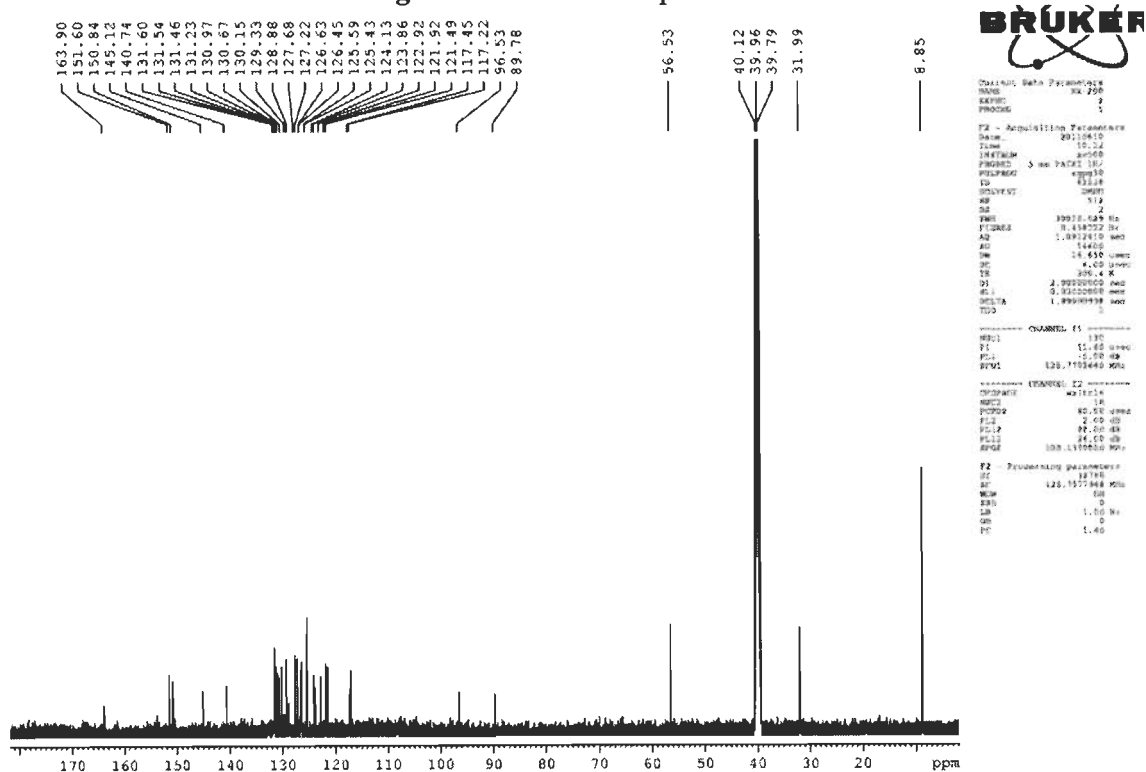
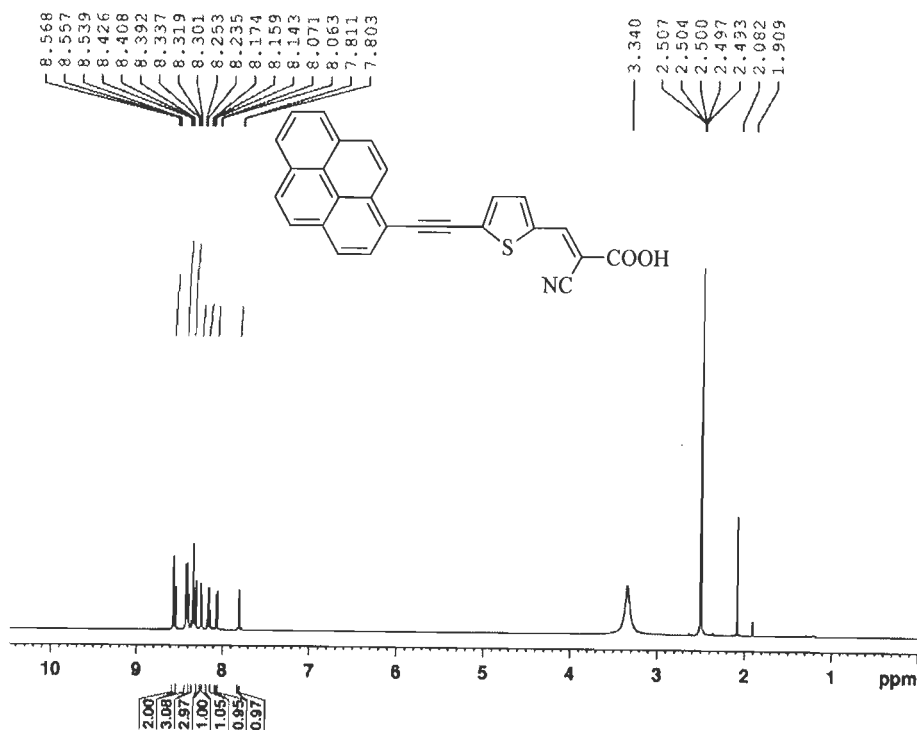


Figure S58. ¹³C NMR spectra of 35b.

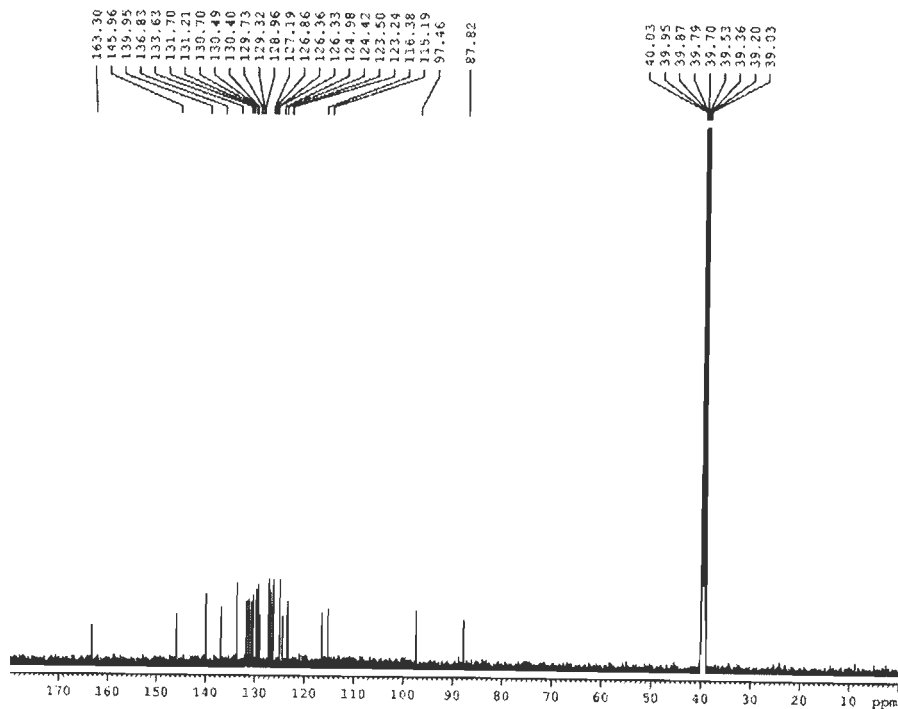
NK-1-277



Current Data Parameters
 NAME nk-1-277res
 EXPNO 1
 PROCNO 1
 F2 - Acquisition Parameters
 Date_ 20110608
 Time 10.51
 INSTRUM av650
 PUSHD 5 mm PATAI 135
 FULPRG 4030
 TD 65536
 SOLVENT DMF0
 NS 14
 DS 2
 SWH 10330.578 Hz
 FIDRES 0.157632 Hz
 AQ 3.172019 sec
 RG 321
 DW 18.400 usec
 DE 6.00 usec
 TE 300.2 K
 D1 1.0000000 sec
 TSD 0
 ===== CHANNEL f1 =====
 NUC1 1H
 P1 7.70 usec
 PL1 2.00 dB
 SFO1 500.130000 MHz
 F2 - Processing parameters
 SI 32768
 SF 500.130000 MHz
 WDM 0
 SSB 0
 LB 0.30 Hz
 GB 0
 PC 1.00

Figure S59. ¹H NMR spectra of 35c.

NK-1-277



Current Data Parameters
 NAME nk-1-277
 EXPNO 1
 PROCNO 1
 F2 - Acquisition Parameters
 Date_ 20110609
 Time 11.26
 INSTRUM av650
 PUSHD 5 mm PATAI 135
 FULPRG 4030
 TD 65536
 SOLVENT DMF0
 NS 14
 DS 2
 SWH 10330.029 Hz
 FIDRES 0.159122 Hz
 AQ 3.172019 sec
 RG 321
 DW 14.450 usec
 DE 6.00 usec
 TE 300.2 K
 D1 2.0000000 sec
 D11 0.0200000 sec
 DELTA 1.0000000 sec
 TSD 0
 ===== CHANNEL f1 =====
 NUC1 13C
 P1 11.40 usec
 PL1 5.00 dB
 SFO1 125.761410 MHz
 ===== CHANNEL f2 =====
 NUC2 1H
 P2 7.70 usec
 PL2 2.00 dB
 SFO2 500.130000 MHz
 F2 - Processing parameters
 SI 32768
 SF 125.761410 MHz
 WDM 0
 SSB 0
 LB 1.00 Hz
 GB 0
 PC 1.40

Figure S60. ¹³C NMR spectra of 35c.

NK-1-238

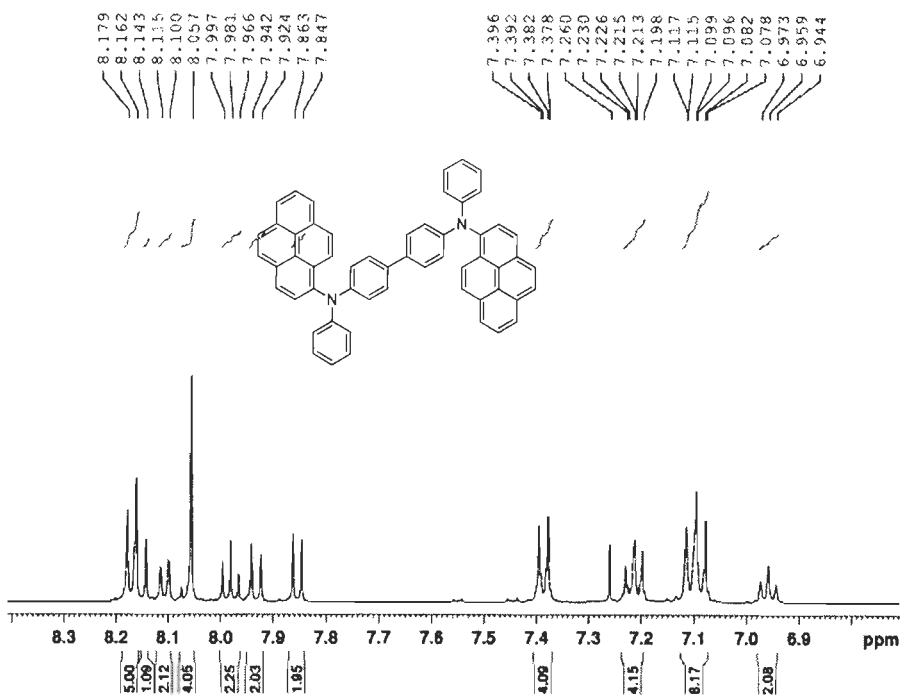


Figure S64. ¹H NMR spectra of 41b.



```

Current Data Parameters
NAME      NK-1-238
EXPNO    1
PROCNO   1

F2 - Acquisition Parameters
Date_    201002
Time     10.26
INSTRUM  spect
PROBHD   1 mm ZAMC 5Q
PULPROG  zgpg
PCPDPRG2 4
AQ       4.159
RG        64
SOLVENT  CDCl3
NS        16
DS        2
SWH       10338.116 Hz
FREQ      251.1622 MHz
AQ        4.159
RG         64
SOLVENT   CDCl3
NS         16
DS         2
SWH        10338.116 Hz
FREQ        251.1622 MHz
===== CHANNEL f1 =====
NUC1      13C
P1        14.00 usec
PL1       0.00 dB
PL12      0.00 dB
SFO1      101.625390 MHz

F2 - Processing parameters
SI        32768
SF        500.136199 MHz
WDW        EM
SSB        0
LB         0.300 Hz
GB         0
PC         1.50
  
```

NK-1-238

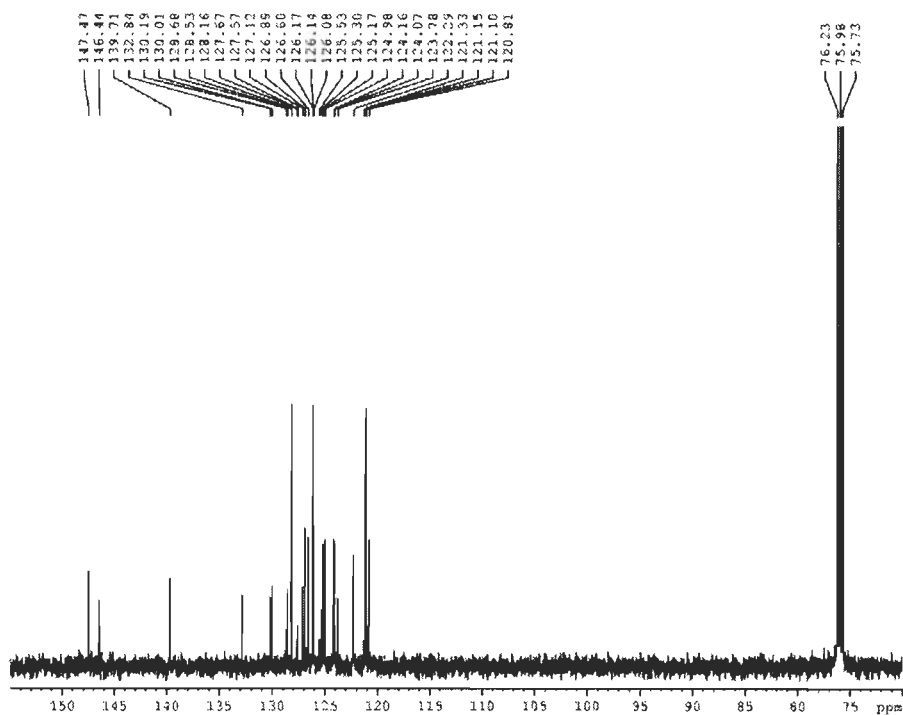


Figure S65. ¹³C NMR spectra of 41b.



```

Current Data Parameters
NAME      NK-1-238-F13
EXPNO    1
PROCNO   1

F2 - Acquisition Parameters
Date_    201002
Time     10.12
INSTRUM  spect
PROBHD   5 mm PABBO 5Q
PULPROG  zgpg
PCPDPRG2 4
AQ       4.159
RG        64
SOLVENT  CDCl3
NS        16
DS        2
SWH       10338.116 Hz
FREQ      251.1622 MHz
===== CHANNEL f1 =====
NUC1      13C
P1        14.00 usec
PL1       0.00 dB
PL12      0.00 dB
SFO1      101.625390 MHz

F2 - Processing parameters
SI        32768
SF        500.136199 MHz
WDW        EM
SSB        0
LB         0.300 Hz
GB         0
PC         1.50
  
```

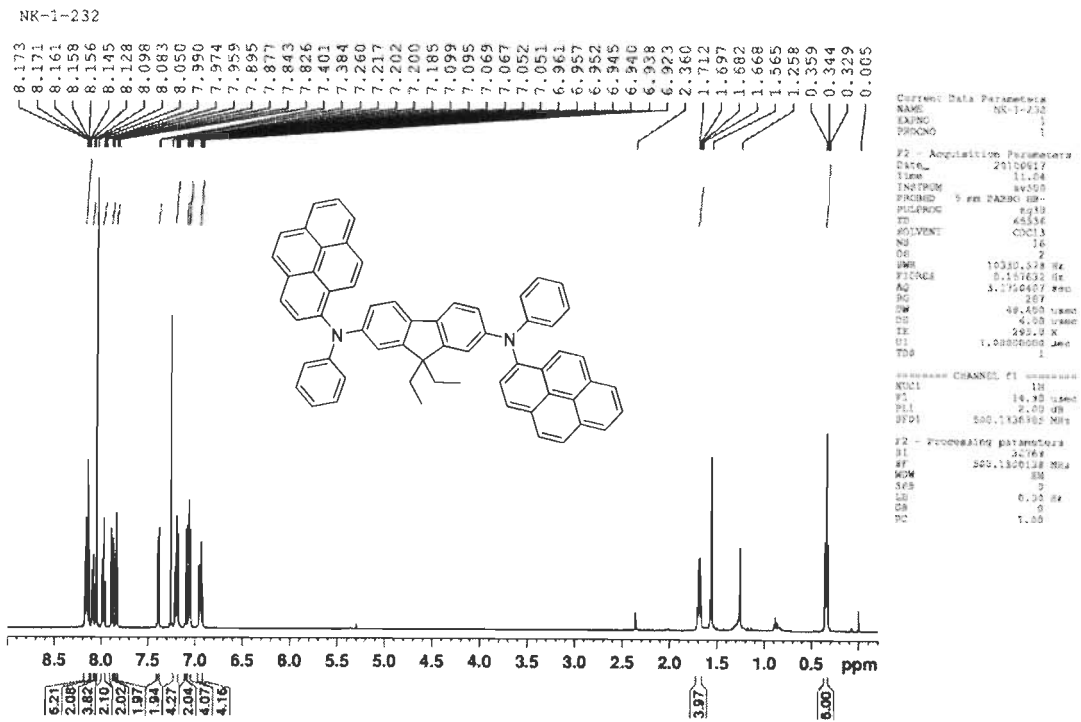



Figure S66. ¹H NMR spectra of 41c.

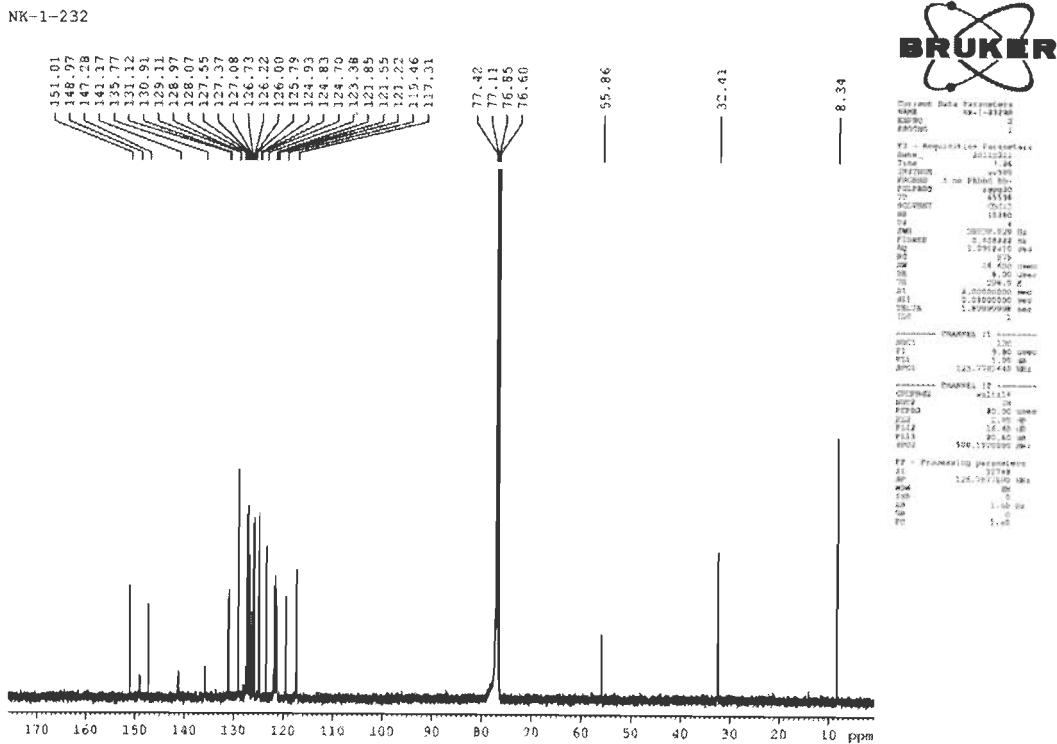


Figure S67. ¹³C NMR spectra of 41c.

NK-1-233

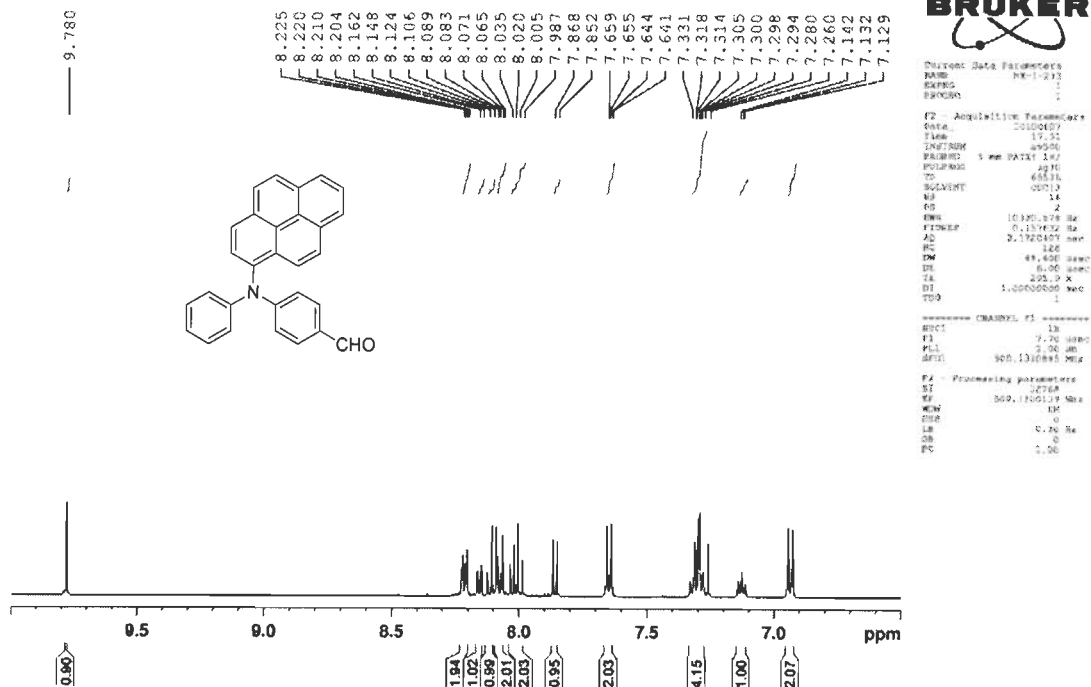


Figure S68. ¹H NMR spectra of 38b.

NK-1-233

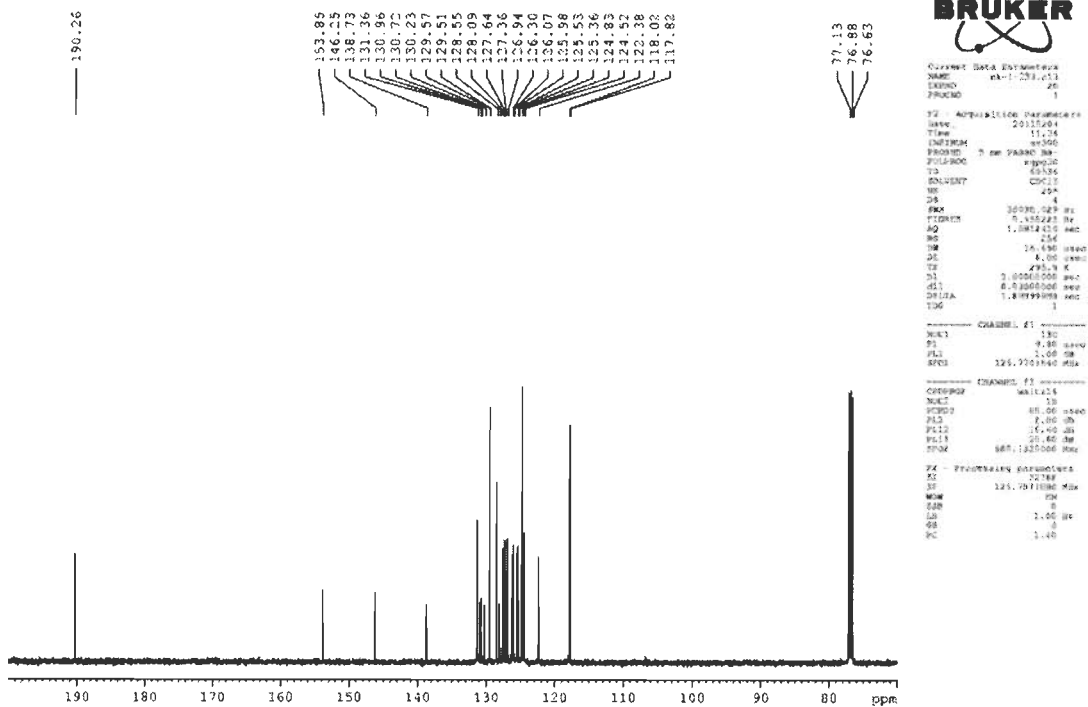
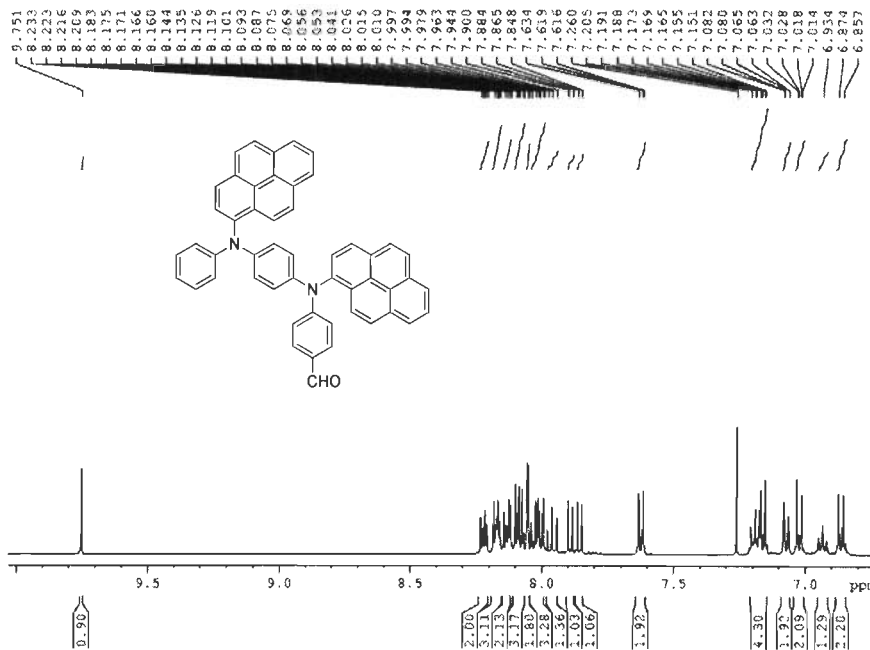


Figure S69. ¹³C NMR spectra of 38b.

NK-1-234



Current Data Parameters
 NAME NK-1-234
 EXPNO 1
 PROCNO 1

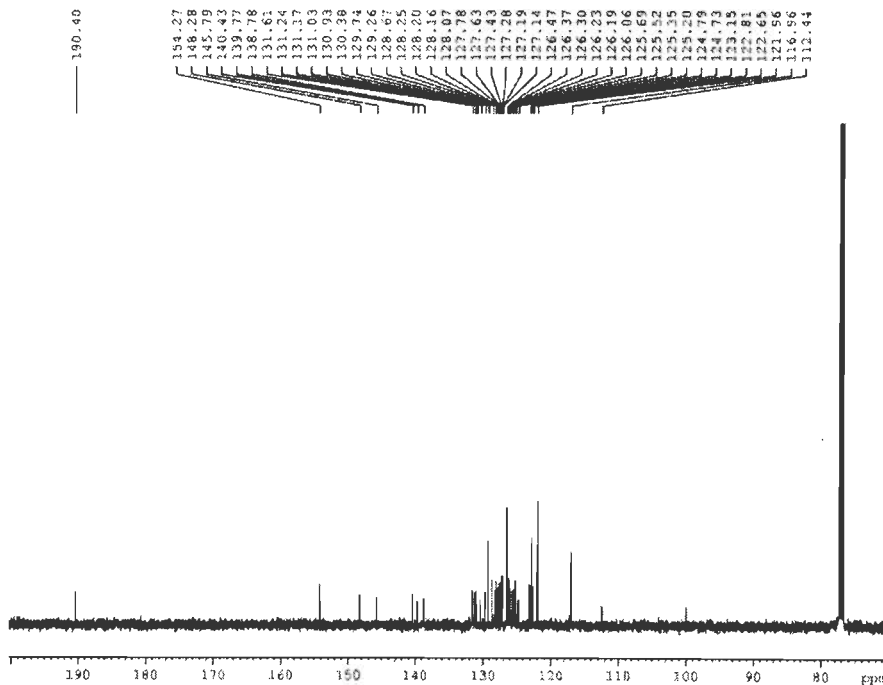
F2 - Acquisition Parameters
 Date_ 201004
 Time 19.21
 INSTRUM spect
 PULPROG zgpg30
 TD 65536
 SOLVENT CDCl3
 NS 16
 DS 2
 SWH 10001.578 Hz
 FIDRES 0.1707634 Hz
 AQ 0.1747019 sec
 RG 327
 SFO 400.146400 MHz
 DE 4.00 umm
 TE 300.2 K
 D1 1.0000000 sec
 TSD 1

===== CHANNEL f1 =====
 NUC1 13C
 P1 14.90 umm
 PL 0.00 dB
 REG1 500.1300130 MHz

F2 - Processing parameters
 SI 32768
 SF 500.1300130 MHz
 WHW 500.1300130 MHz
 SSB 0
 LB 0.30 Hz
 GB 0
 PC 1.00

Figure S70. ¹H NMR spectra of 42a.

NK-1-234



Current Data Parameters
 NAME NK-1-234-013
 EXPNO 1
 PROCNO 1

F2 - Acquisition Parameters
 Date_ 201010
 Time 19.16
 INSTRUM spect
 PULPROG zgpg30
 TD 65536
 SOLVENT CDCl3
 NS 16
 DS 2
 SWH 1001.458 Hz
 FIDRES 0.448332 Hz
 AQ 0.1747019 sec
 RG 327
 SFO 400.146400 MHz
 DE 4.00 umm
 TE 300.2 K
 D1 1.0000000 sec
 D11 0.0500000 sec
 DELTA 1.8500000 sec
 TSD 1

===== CHANNEL f1 =====
 NUC1 13C
 P1 9.80 umm
 PL 0.00 dB
 REG1 125.7773450 MHz

===== CHANNEL f2 =====
 NUC2 1H
 P2 0.00 umm
 PL2 0.00 dB
 PL12 0.00 dB
 PL11 0.00 dB
 REG2 500.1300130 MHz

F2 - Processing parameters
 SI 32768
 SF 125.7773450 MHz
 WHW 125.7773450 MHz
 SSB 0
 LB 1.00 Hz
 GB 0
 PC 1.00

Figure S71. ¹³C NMR spectra of 42a.

NK-1-241

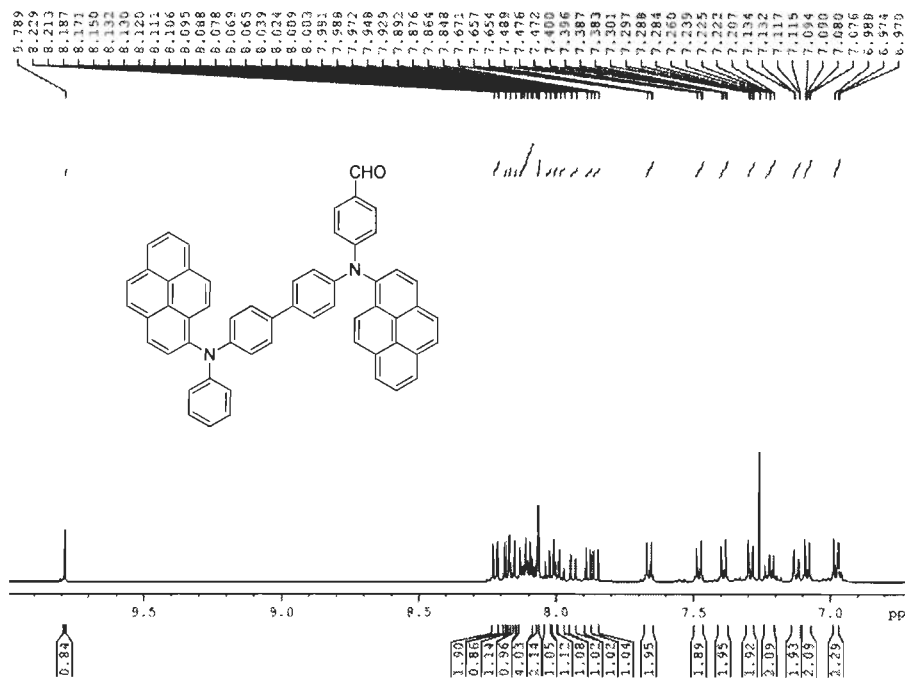


Figure S72. ¹H NMR spectra of 42b.

NK-1-241

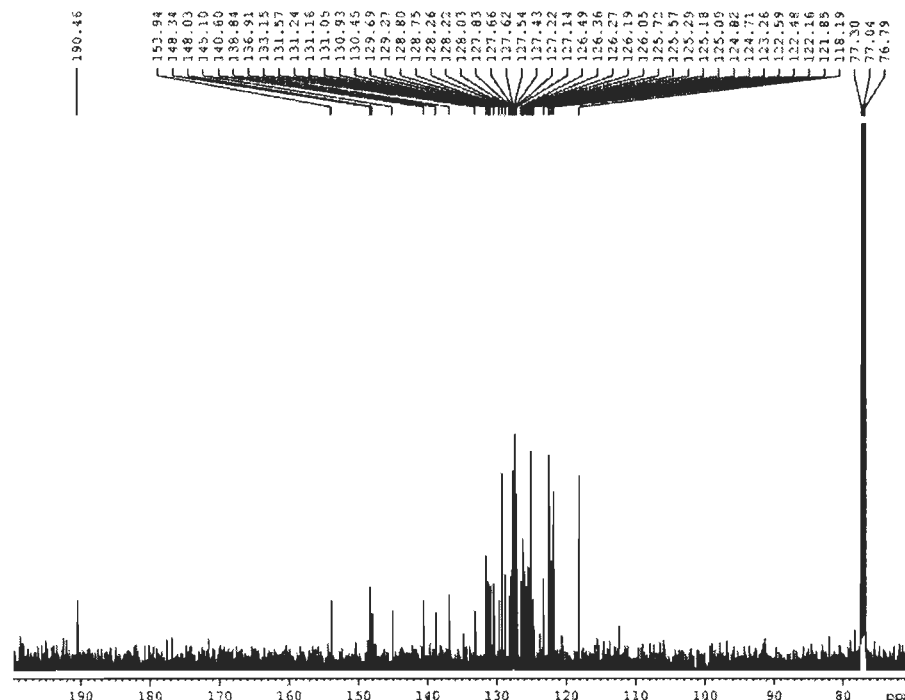


Figure S73. ¹³C NMR spectra of 42b.

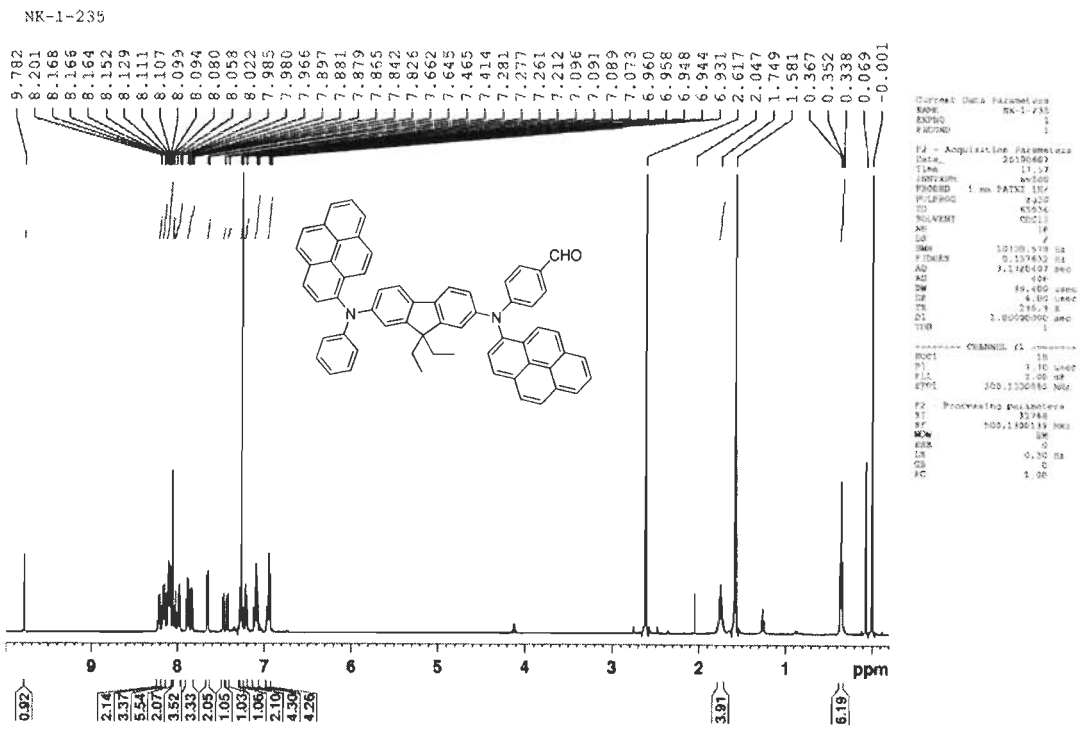


Figure S74. ¹H NMR spectra of 42c.

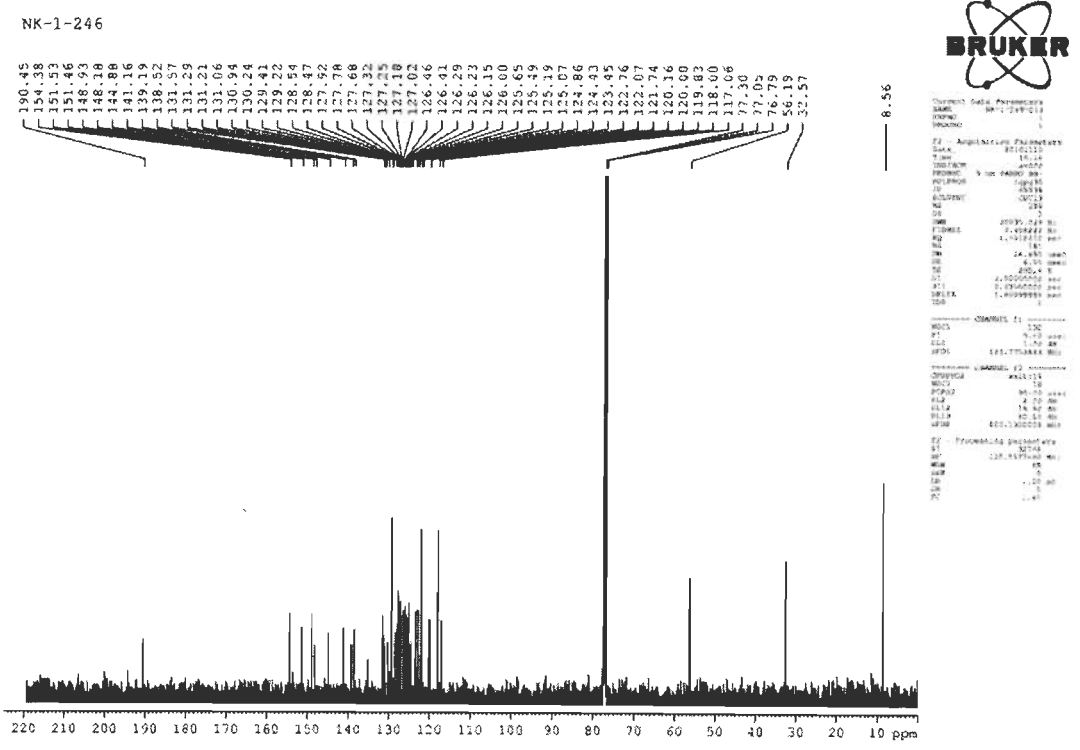


Figure S75. ¹³C NMR spectra of 42c.

NK-1-223

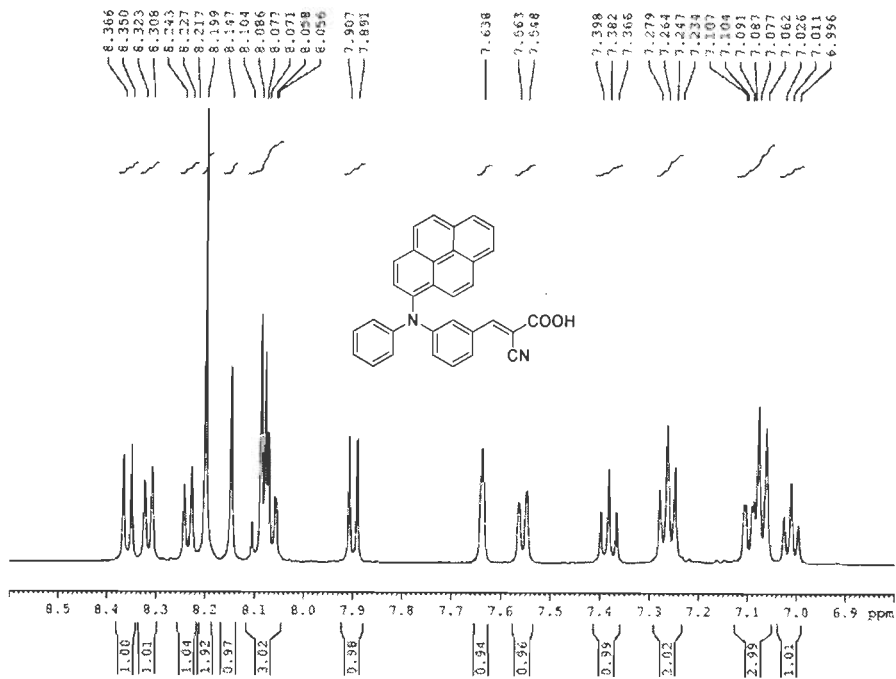


Figure S76. ¹H NMR spectra of 39a.



```

Current Data Parameters
NAME NK-1-223
EXPNO 1
PROCNO 1
F2 - Acquisition Parameters
Date_ 20160428
Time 17.02
INSTRUM spect
PROBHD 5 mm PABY 201
PULPROG zgpg30
TD 65536
SOLVENT DMSO
NS 16
DS 2
SWH 10320.578 Hz
FIDRES 0.152638 Hz
AQ 3.1168401 sec
RG 31.8
DM 48.400 umet
DE 4.00 umet
TE 298.2 K
D1 1.0000000 sec
D11 1
===== CHANNEL f1 =====
NUC1 13
P1 3.00 umet
PC1 7.00 dB
SFO1 100.125085 MHz
F2 - Processing parameters
SI 32768
SF 100.125085 MHz
WDW EM
SSB 0
LB 0.35 Hz
GB 0
PC 1.00
  
```

NK-1-223

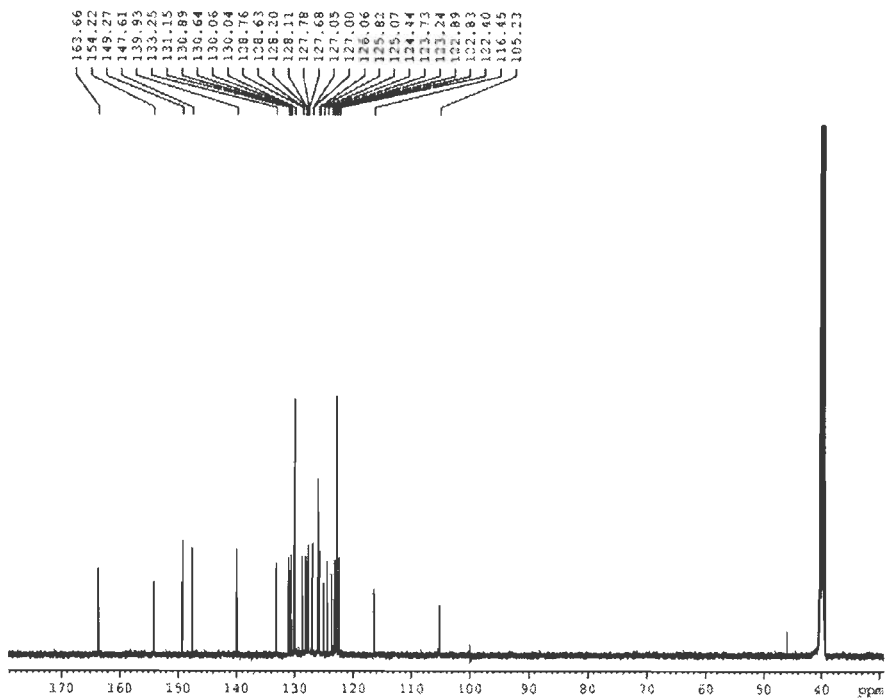


Figure S77. ¹³C NMR spectra of 39a.



```

Current Data Parameters
NAME NK-1-223
EXPNO 1
PROCNO 1
F2 - Acquisition Parameters
Date_ 20160428
Time 18.57
INSTRUM spect
PROBHD 5 mm PABY 201
PULPROG zgpg30
TD 65536
SOLVENT DMSO
NS 16
DS 2
SWH 35038.029 Hz
FIDRES 0.478222 Hz
AQ 1.7932410 sec
RG 345
DM 14.400 umet
DE 4.00 umet
TE 298.2 K
D1 2.0000000 sec
D11 0.2000000 sec
DELTA 1.1991999 sec
TSC 1
===== CHANNEL f1 =====
NUC1 13C
P1 3.00 umet
PC1 1.00 dB
SFO1 125.7695401 MHz
===== CHANNEL f2 =====
INSTRUM spect
PROBHD 5 mm PABY 201
PULPROG zgpg30
TD 65536
SOLVENT DMSO
NS 16
DS 2
SWH 100.125085 MHz
F2 - Processing parameters
SI 32768
SF 100.125085 MHz
WDW EM
SSB 0
LB 0.35 Hz
GB 0
PC 1.00
  
```

NK-1-236

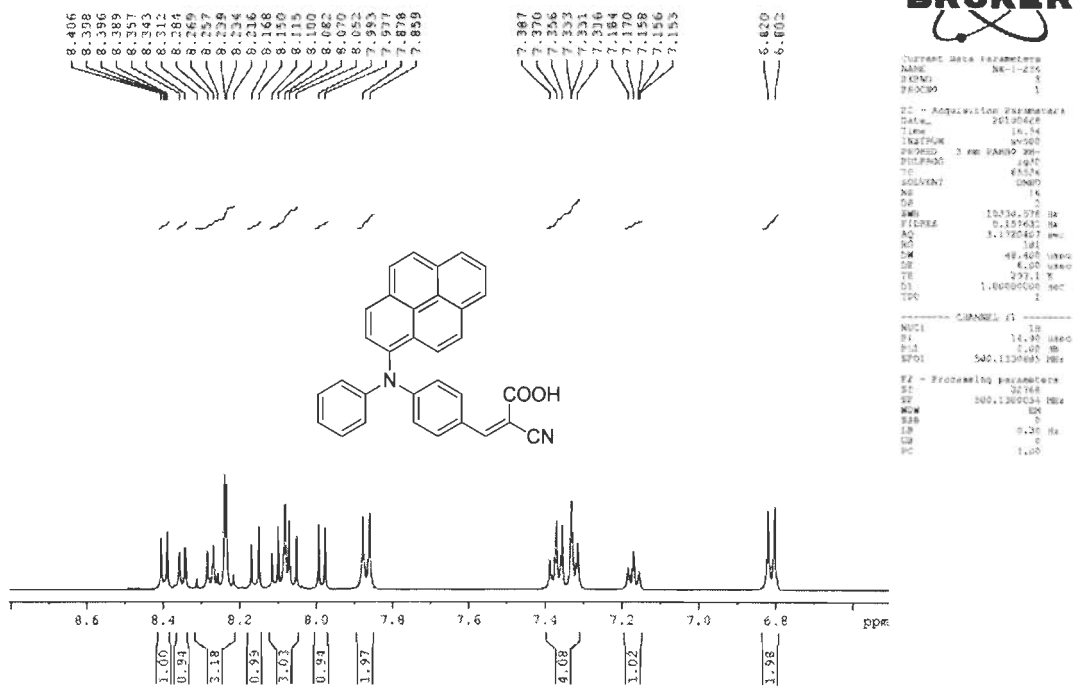


Figure S78. ¹H NMR spectra of 39b.

NK-1-236

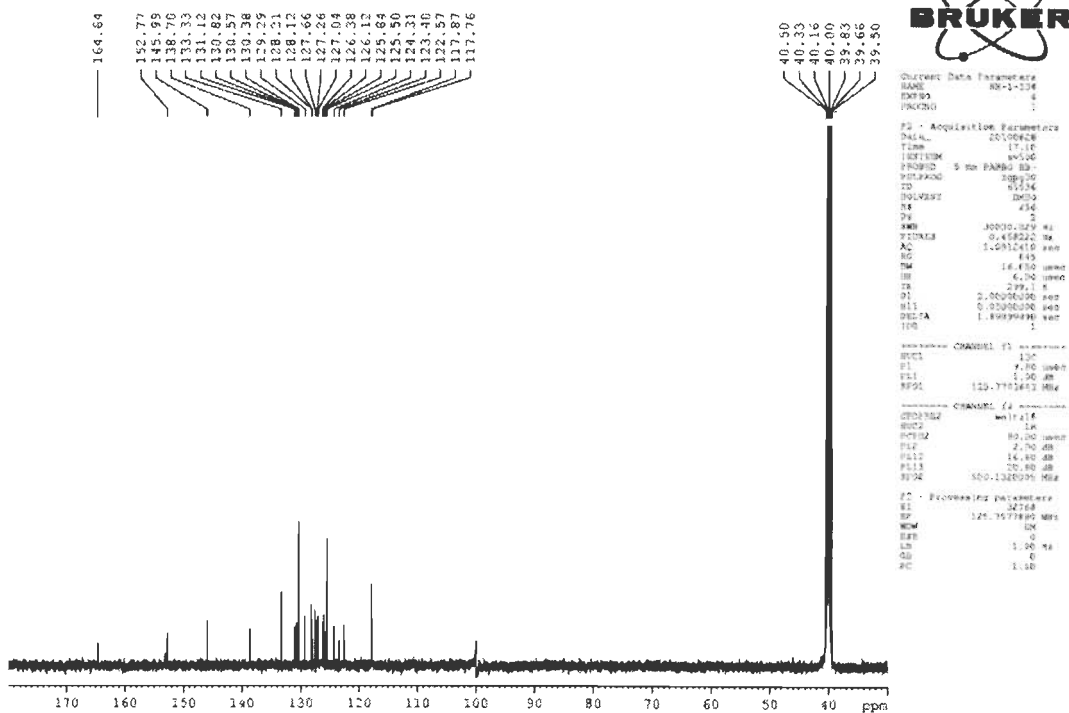


Figure S79. ¹³C NMR spectra of 39b.

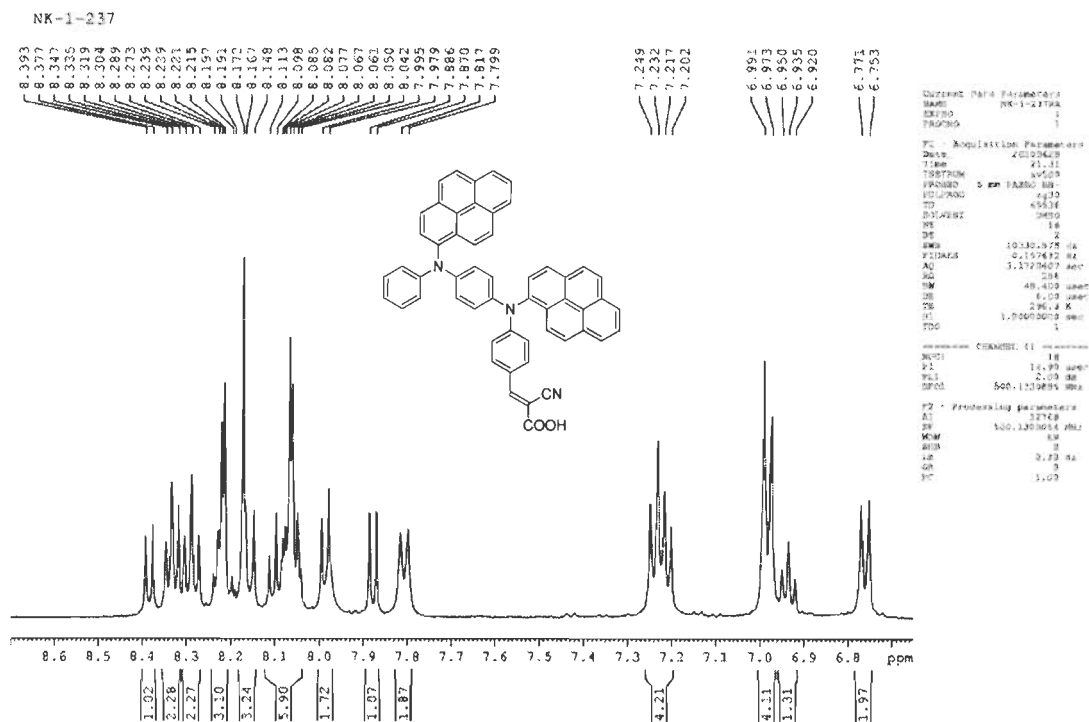


Figure S80. ¹H NMR spectra of 43a.

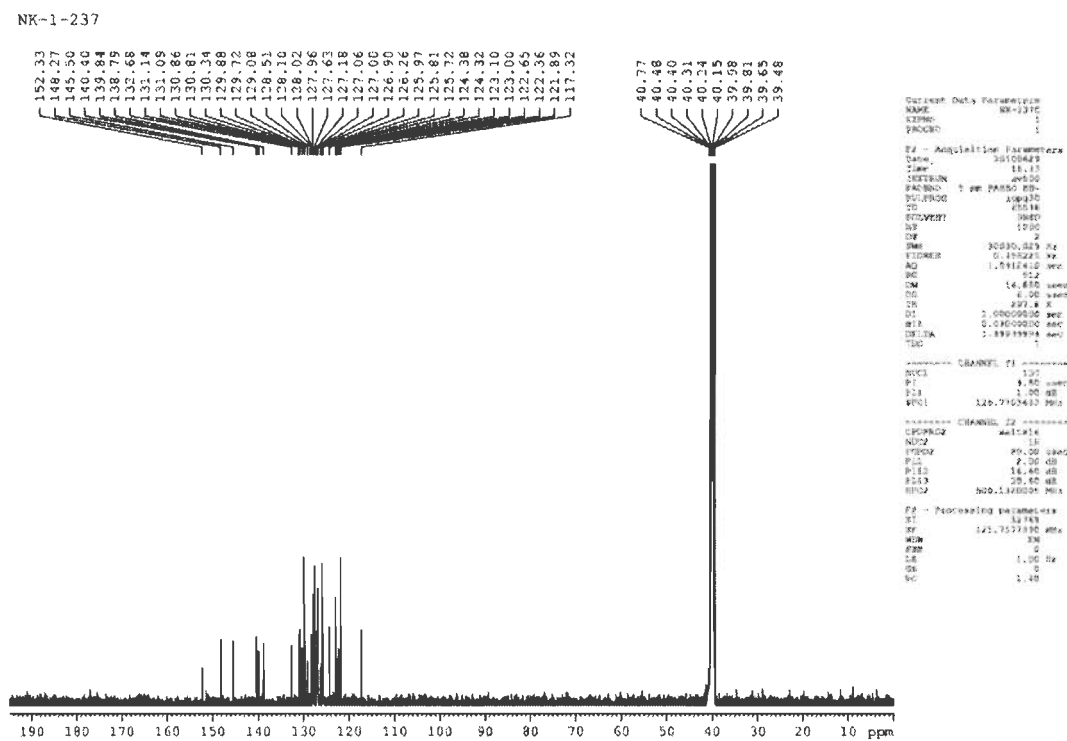
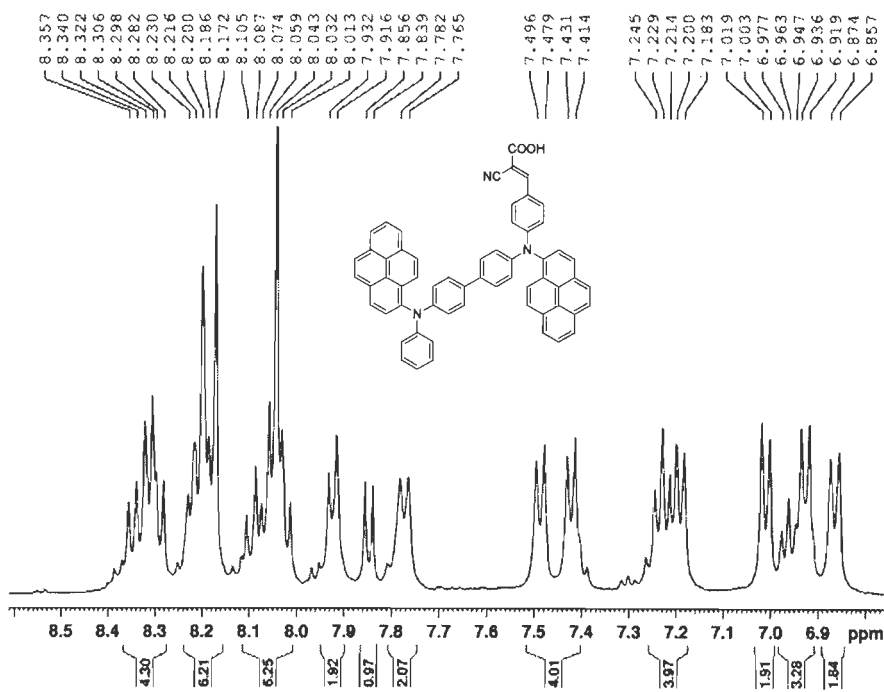


Figure S81. ¹³C NMR spectra of 43a.

NK-1-275

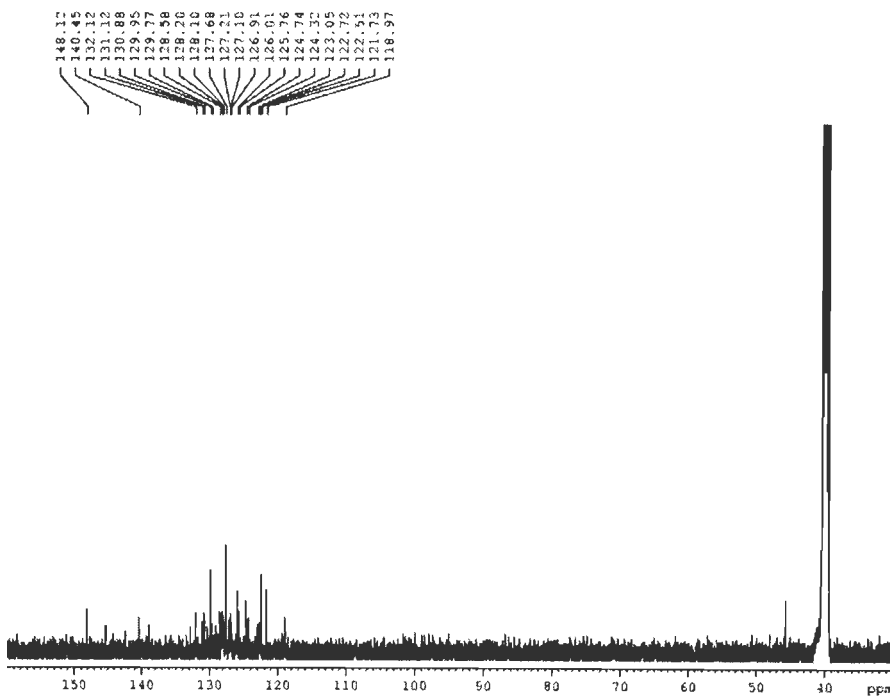


```

Current Data Parameters
NAME 20110111
EXPNO 1
PROCNO 1
F2 - Acquisition Parameters
DATE_ 20110111
TIME 10.24
INSTRUM aw500
PROBHD 5 mm VNP01ZB-HS
PULPROG zgpg30
TD 65536
SOLVENT CDCl3
NS 2
DS 2
SWH 10370.575 Hz
FIDRES 0.137632 Hz
AQ 3.1770007 sec
RG 181
SQ 48.600 umm
DE 6.30 umm
TE 296.2 K
D1 1.00000000 sec
D2 0
===== CHANNEL f1 =====
NUC1 13
PC 14.20 umm
P1 2.00 umm
SFO1 500.1310000 MHz
F2 - Processing parameters
SI 32768
SF 500.1310000 MHz
WDW EM
SSB 0
LB 0.30 Hz
GB 0
PC 1.00
  
```

Figure S82. ¹H NMR spectra of 43b.

NK-1-275



```

Current Data Parameters
NAME 20110111
EXPNO 1
PROCNO 1
F2 - Acquisition Parameters
DATE_ 20110111
TIME 20.54
INSTRUM aw500
PROBHD 5 mm VNP01ZB-HS
PULPROG zgpg30
TD 65536
SOLVENT CDCl3
NS 2
DS 2
SWH 70020.028 Hz
FIDRES 0.446224 Hz
AQ 3.0914100 sec
RG 375
SQ 11.850 umm
DE 6.30 umm
TE 296.2 K
D1 1.00000000 sec
D2 0.00000000 sec
D3 0.00000000 sec
D4 0.00000000 sec
D5 0
===== CHANNEL f1 =====
NUC1 13
PC 9.00 umm
P1 1.00 umm
SFO1 125.7613500 MHz
F2 - Processing parameters
SI 32768
SF 125.7613500 MHz
WDW EM
SSB 0
LB 1.00 Hz
GB 0
PC 1.00
  
```

Figure S83. ¹³C NMR spectra of 43b.

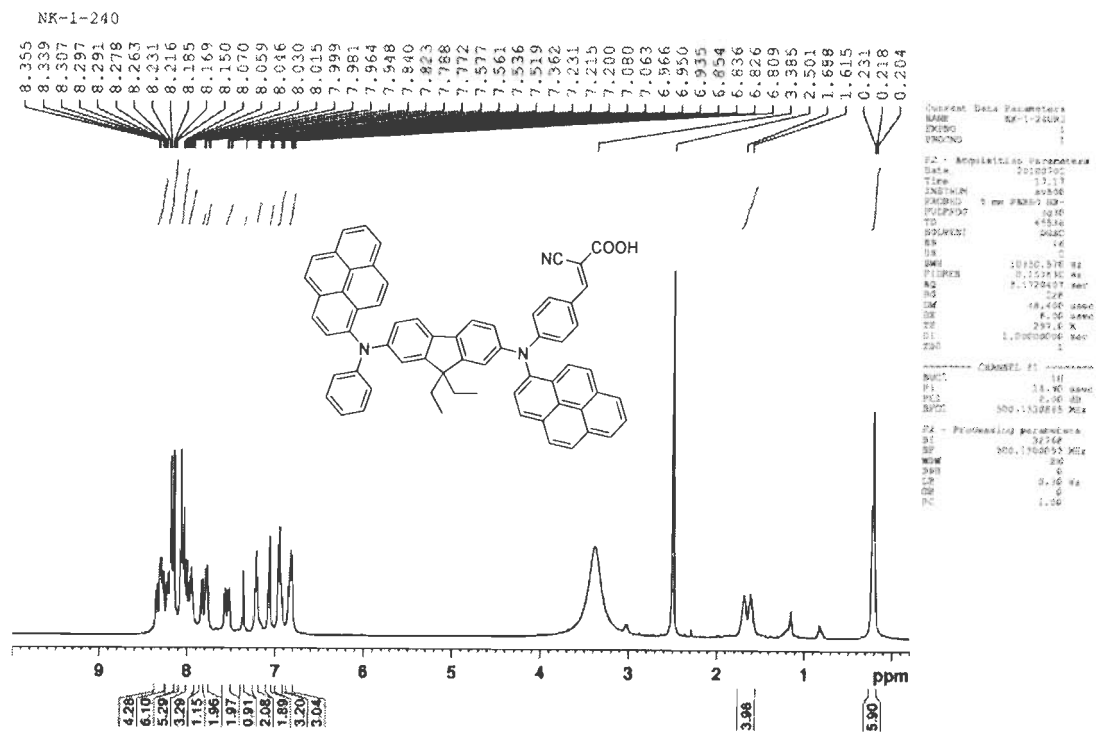


Figure S84. ^1H NMR spectra of 43c.

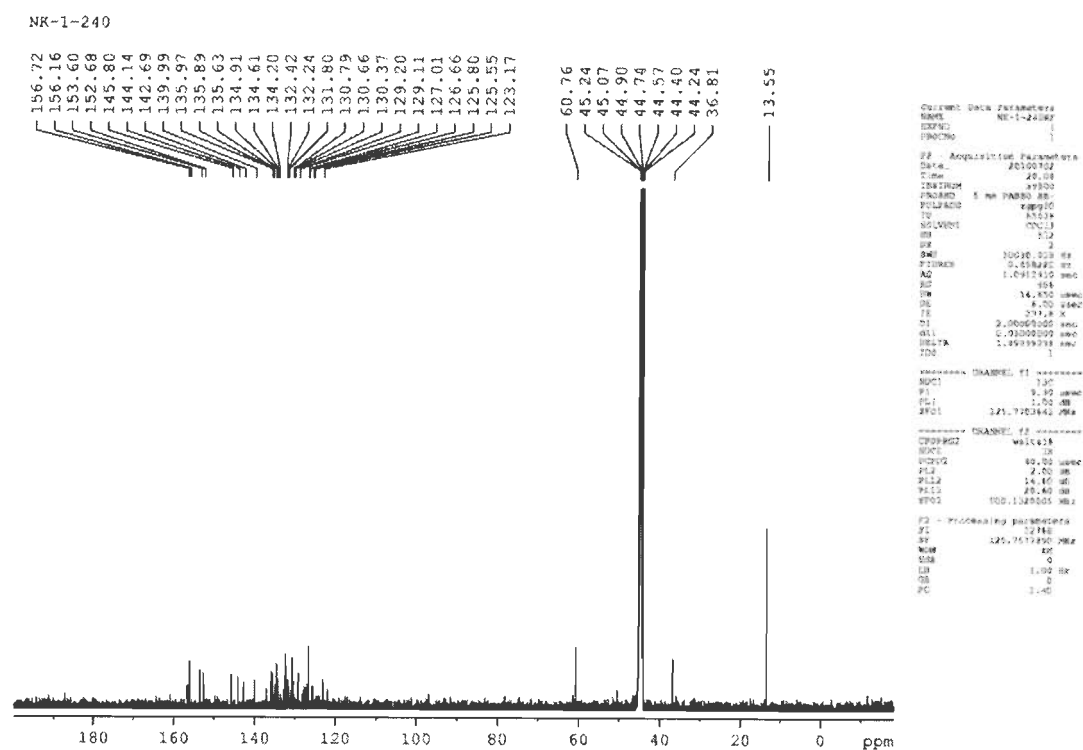


Figure S85. ^{13}C NMR spectra of 43c.

PUBLICATIONS

1. Fluoranthene-based triarylamines as hole-transporting and emitting materials for efficient electroluminescent devices.
Neha Kapoor and K. R. Justin Thomas
New J. Chem., **2010**, *34*, 2739.
2. Pyrenylamine-based organic dyes for dye-sensitized solar cells: Effect of linkers and auxiliary donors on optical and electrochemical properties.
Neha Kapoor, K. R. Justin Thomas, Chuan-Pei Lee and Kuo-Chuan Ho
Submitted for publication
3. Triphenylene-based triarylamines as efficient blue-electroluminescent materials: Synthesis and optical properties.
Neha Kapoor, K. R. Justin Thomas and Jwo-Huei Jou
Manuscript under preparation
4. Fluorene containing quinoxalines: Synthesis and optical properties.
Neha Kapoor and K. R. Justin Thomas
Manuscript under preparation
5. Acetylene-linked pyrene-fluorene conjugates as color-tunable emitting materials for OLEDs.
Neha Kapoor, K. R. Justin Thomas, and Jwo-Huei Jou
Manuscript under preparation

CONFERENCE PUBLICATION

6. Synthesis, photophysical and electrochemical properties of fluoranthene derivatives, Neha Kapoor and K. R. Justin Thomas, International Conference on "Functional Materials: Controlled Synthesis, Discrete Molecular Processes and Engineering", IIT Madras, Chennai, India, November 27-29, 2008.